
INTERNAL FLOW STUDIES FOR THE
CHARACTERISATION AND OPTIMISATION OF AN
EFFERVESCENT ATOMISER

Thesis submitted for the
Degree of Doctor of Philosophy
of Cardiff University, School of Engineering

by
Andrew Niland

September 2017

Abstract

This thesis is concerned with the study of effervescent atomisation, a two-phase gas-liquid spray generation technique that offers many advantages over conventional atomisers. Following a thorough literature review, it was found that the effects of various parameters were disputed between studies or untested with many reports presenting findings without internal flow regime study – in fact, the quantification of gas injection at the aerator was completely unrepresented throughout the literature.

Hence, two purpose-built transparent experiment systems were designed and commissioned at Cardiff School of Engineering to characterise the complete effervescent atomisation, from gas injection to spray generation, and to investigate the effect of various design and operating parameters on the internal two-phase flow. All investigations were performed from unbled start-up conditions, to best simulate industrial applications.

The results of this work identified that the droplet size decreases with an increase in the mass ratio of input air to liquid (ALR) and a homogenous flow of bubbles within the mixing chamber (bubbly flow) generates a stable spray compared to alternative heterogeneous flow regimes, due to a regular and consistent atomisation process. Hence, an optimal effervescent atomiser configuration would enable a homogenous bubbly flow at the highest ALRs.

Further work was performed to quantify the bubbly flow operating range for various independent parameters. It was determined that bubbling at the aerator was encouraged by the injection of an unstable gas-phase into a strong liquid cross-flow, suiting low ALRs, high liquid flow rates (e.g. large exit orifice diameters, high operating pressures), small aerator orifice diameters, high aeration areas and small mixing chamber diameters.

However, a conventional flat-end aerator body design was found to be unsuitable for inside-out effervescent atomisation in a vertically downwards orientation, due to the formation of a gas void in the aerator wake – this was found to be a result of aerator bluff body recirculation and gas-phase buoyancy effects. Hence, bubbly flow was only enabled in a vertically upwards orientation or with a streamlined aerator body profile.

Published Outcomes

The published outcomes of the current work are presented in Appendix 1:

- Niland, A. et al. 2016. A Refraction Reduced Optical Study of Effervescent Atomiser Internal Flow. In: ILASS – Europe 2016, 27th Annual Conference on Liquid Atomization and Spray Systems. Brighton, UK.

Acknowledgements

This work would not have been possible without the contribution of many individuals, to whom I owe a huge debt of gratitude.

Firstly, I would like to thank my supervisors, Dr Richard Marsh and Prof Phil Bowen, for initiating this project and for their continued support and guidance throughout. Thanks also to all my research colleagues at Cardiff School of Engineering who have consistently and unwaveringly exceeded my expectations for help – my gratitude in particular to: Dr Anthony Giles and the Gas Turbine Research Centre (GTRC) for their assistance with Phase Doppler Anemometry and instrumentation; Dr Rhys Pullin and the Cardiff University Structural Performance group for their provision of experimental apparatus; Prof Tim O’Doherty for the donation of a suitable laboratory space; and, Andrew Hopkins and my ASTUTE 2020 colleagues for accommodating my research.

This research would not have been possible without the invaluable technical advice and support of Paul Malpas, Malcolm Seaborne, Steve Rankmore and the remaining workshop technicians – in particular, during the design and commissioning of the experimental rigs.

Greatly acknowledged is the financial support generously afforded by Stork Thermeq B.V. and the advice of Dr Marco Derksen and Joris Koomen.

A special thanks to my family, especially my parents, and friends for their support and encouragement throughout the trials and tribulations of this research project. Finally, my eternal gratitude to my loving partner Hannah, who has not only sustained my drive but, somehow, endured my persistent mumbling about bubbles – your compromise and sacrifice has enabled this effort and so, to you, I dedicate this thesis.

Nomenclature

Roman Characters

Symbol	Definition	Unit
A_a	Aeration area	m^2
a_b	Bubble acceleration	m/s^2
A_{MC}	Mixing chamber cross-sectional area	m^2
A_o	Exit orifice area	m^2
C_D	Drag coefficient	-
C_d	Discharge coefficient	-
C_m	Added mass coefficient	-
D10	Arithmetic mean diameter, AMD	m
D32	Sauter mean diameter, SMD	m
d_a	Aerator orifice diameter	m
d_b	Bubble diameter	m
d_d	Droplet diameter	m
d_{MC}	Mixing chamber diameter	m
d_o	Exit orifice diameter	m
e_b	Bubble expansion energy	J
F	Force	N
G_g	Gas mass flux	kg/m^2s
G_l	Liquid mass flux	kg/m^2s
l_m	Mixing length	m
l_o	Exit orifice length	m
\dot{m}_g, m_g	Gas mass flow rate	kg/s
\dot{m}_l, m_l	Liquid mass flow rate	kg/s
M_W	Molecular weight	g/mol
n_d	Droplet counter	-
OR	Operating range	g^2/s^2
P_{amb}	Ambient pressure	bar
P_{op}	Operating pressure (i.e. differential pressure between mixing chamber and atmosphere)	bar
Q_g	Gas volumetric flow rate	m^3/s
Q_l	Liquid volumetric flow rate	m^3/s
R^2	Statistical, regression analysis	-
T	Temperature	K
U_b	Bubble velocity	m/s
$U_{g,a}$	Gas injection velocity through aerator orifice	m/s
$U_{l,a}$	Liquid cross-flow velocity across the aerator	m/s
V_b	Bubble volume	m^3
X, x	Radial displacement	m
Y, y	Axial displacement	m

Greek Symbols

Symbol	Definition	Unit
α	Spray cone angle	°
σ	Surface tension	kg/s ²
θ_A	Advancing contact angle between bubble and aerator orifice	°
θ_R	Receding contact angle between bubble and aerator orifice	°
ρ_g	Gas density, where ρ_a is air density	kg/m ³
ρ_l	Liquid density, where ρ_w is water density	kg/m ³
μ_l	Liquid dynamic viscosity, where μ_w is water dynamic viscosity	kg/ms
ν_l	Liquid kinematic viscosity, where ν_w is water kinematic viscosity	m ² /s
β	Exit orifice convergence angle	°
ψ	$\left(\frac{\sigma_l}{\sigma_w}\right)^{-1} \left(\frac{\rho_l}{\rho_w}\right)^{-2.3} \left(\frac{\mu_l}{\mu_w}\right)^{1.3}$	-
λ	$\sqrt{\left(\frac{\rho_g}{\rho_a}\right) \left(\frac{\rho_l}{\rho_w}\right)}$	-

Constants

Symbol	Definition	Value	Unit
g	Gravitational acceleration	9.81	m/s ²
R	Universal gas constant	8.314	J/mol K

Acronyms

Acronym	Definition
ADARPA	DARPA SUBOFF afterbody [1]
ALR	Air-to-liquid mass ratio
AMD	Arithmetic mean diameter (D10)
IFOR	Internal flow optimisation rig, system developed for research
OEA	Optical effervescent atomiser, system developed for research
PDA	Phase Doppler Anemometry
SMD	Sauter mean diameter (D32)

Dimensionless Parameters

Parameter	Definition
Re	Reynolds number
We	Weber number
Oh	Ohnesorg number

TABLE OF CONTENTS

CHAPTER 1. INTRODUCTION	1
1.1 Background.....	1
1.2 Motivation	4
1.3 Modern Atomisation Technology	5
1.4 Effervescent Atomisation.....	8
1.5 Aims and Objectives.....	9
1.5 Thesis Content	10
CHAPTER 2. THEORY AND LITERATURE REVIEW.....	11
2.1 Gas-Phase Injection at Aerator.....	12
2.1.1 Bubble Formation	12
2.1.2 Gas Injection Regimes in a Liquid Cross-Flow.....	15
2.1.3 Bluff Body Recirculation.....	20
2.2 Stabilised Two-Phase Gas-Liquid Flow in the Mixing Chamber	21
2.2.1 Stabilisation of the Injected Gas-Phase	22
2.2.2 Flow Regimes	23
2.3 Effervescent Atomisation Mechanisms	28
2.3.1 Single-Phase Primary Atomisation.....	28
2.3.4 Two-Phase Primary Atomisation.....	30
2.3.2 Secondary Atomisation.....	34
2.4 Dependent Parameters of Effervescent Atomiser Literature	36
2.4.1 Effervescent Atomiser Characterisation.....	36
2.4.2 Spray Characterisation.....	38
2.4.3 Others.....	41
2.5 Independent Parameters of Effervescent Atomiser Literature	41
2.5.1 Effect of Fluid Flow Rates, including Air-to-Liquid Ratio	42
2.5.2 Effect of Operating Pressure.....	47
2.5.3 Effect of Orientation.....	49
2.5.4 Effect of Aerator Design.....	50
2.5.5 Effect of Mixing Chamber Design	55
2.5.7 Effect of Fluid Properties	61
2.6 Summary	64
CHAPTER 3. DEVELOPMENT OF FACILITIES	65
3.1 Optical Effervescent Atomiser (OEA).....	65
3.2 Internal Flow Optimisation Rig (IFOR)	67
3.3 Auxiliary Systems.....	70
3.4 High-Speed Shadowography	72
3.4.1 Experimental Set-Up	73
3.4.2 Internal Two-Phase Regime Quantification	74
3.4.3 Bubble Sizing and Feature Tracking for Internal Flow	77
3.5 Phase Doppler Anemometry for Spray Characterisation	81
3.5.1 Experimental Set-Up	82
3.5.2 Analysis Techniques.....	84
3.6 Programme of Work	86
3.6.1 Identification of Optimal Internal Flow to Facilitate Stable Effervescent Atomisation (Chapter 4)	86

3.6.2 Internal Flow Studies of Flat-End Aerators to Optimise Bubbly Flow Operation (Chapter 5).....	89
3.6.3 Internal Flow Studies of Streamlined Aerators to Reduce Wake Effect (Chapter 6).....	93
3.6.4 Internal Flow Studies of ADARPA Aerators to Optimise Bubbly Flow Operation (Chapter 7).....	94
CHAPTER 4. IDENTIFICATION OF OPTIMAL INTERNAL FLOW TO FACILITATE STABLE EFFERVESCENT ATOMISATION	97
4.1 Observed Gas Injection Regimes	97
4.1.1 Single Bubbling.....	99
4.1.2 Pulse Bubbling.....	100
4.1.3 Elongated Jetting	102
4.1.4 Atomised Jetting.....	103
4.1.5 Cavity Forming.....	104
4.1.6 Coalesced Jetting.....	105
4.1.7 Evacuated Chamber.....	106
4.2 Observed Internal Flow Regimes.....	108
4.2.1 Bubbly Flow	110
4.2.2 Gas Void Disintegration (Bubbly Flow)	113
4.2.3 Bubbly-Slug Flow	117
4.2.4 Slug Flow.....	119
4.2.5 Gas Void Disintegration (Slug Flow).....	121
4.2.6 Churn Flow	123
4.2.7 Pulsing Flow	125
4.2.8 Annular Flow.....	126
4.2.9 Disrupted Annular Flow	128
4.2.10 Annular Flow (Liquid Droplets).....	130
4.3 Spray Characterisation.....	132
4.4 Summary	140
CHAPTER 5. INTERNAL FLOW STUDIES OF FLAT-END AERATORS TO OPTIMISE BUBBLY FLOW OPERATION.....	141
5.1 Bluff Body Recirculation of Conventional Flat-End Aerators.....	141
5.2 Effect of Fluid Flow Rates, including Air-to-Liquid Ratio	146
5.3 Effect of Aerator Orifice Diameter.....	151
5.4 Effect of Unconventional Aerator Designs.....	156
5.5 Effect of Mixing Chamber Diameter	159
5.6 Effect of Operating Pressure.....	163
5.7 Effect of Orientation	166
5.8 Summary	170
CHAPTER 6. INTERNAL FLOW STUDIES OF STREAMLINED AERATORS TO REDUCE WAKE EFFECT	172
6.1 Bluff Body Recirculation of Streamlined Aerator Designs	172
6.2 Effect of Aerator Body Design	176
6.3 Summary	181
CHAPTER 7. INTERNAL FLOW STUDIES OF ADARPA AERATORS TO OPTIMISE BUBBLY FLOW OPERATION.....	183
7.1 Bluff Body Recirculation of Streamlined ADARPA Aerators.....	183
7.2 Effect of Fluid Flow Rates, including Air-to-Liquid Ratio	186

7.3 Effect of Aerator Orifice Diameter.....	192
7.4 Effect of Aeration Area.....	197
7.5 Effect of Unconventional Aerator Designs.....	202
7.6 Effect of Mixing Chamber Diameter.....	207
7.7 Effect of Operating Pressure.....	213
7.8 Effect of Orientation.....	218
7.9 Summary.....	223
CHAPTER 8. CONCLUSIONS AND FUTURE WORK.....	225
8.1 Conclusions of the Experimental Findings.....	225
8.2 Novelty of the Current Investigation.....	228
8.3 Recommendations for Future Work.....	228
REFERENCES.....	231
APPENDIX 1: PUBLISHED OUTCOMES.....	245
A Refraction Reduced Optical Study of Effervescent Atomiser Internal Flow	246
APPENDIX 2: LITERATURE REVIEW.....	257
A2.1 Experiment Details.....	257
A2.2 Fluid Properties and Operating Conditions.....	261
A2.3 Atomiser Design.....	266
A2.4 Correlations.....	271
APPENDIX 3: ENGINEERING DRAWINGS OF TEST RIGS.....	275
A3.1 Optical Effervescent Atomiser (OEA).....	275
A3.2 Internal Flow Optimisation Rig (IFOR).....	282
APPENDIX 4: MATHWORKS® MATLAB® SCRIPTS.....	313
A4.1 Optimisation of High-Speed Internal Flow Imagery.....	313
A4.2 Bubble Sizing and Feature Tracking for Internal Flow.....	320
APPENDIX 5: REGIME MAPS FOR CONVENTIONAL FLAT-END AERATOR DESIGNS.....	343
A5.1 Effect of Aerator Orifice Diameter.....	343
A5.1.1 1 x 3.0 mm (Aerator A2).....	343
A5.1.2 4 x 2.0 mm (Aerator A3).....	346
A5.1.3 9 x 1.0 mm (Aerator A4).....	348
A5.1.4 16 x 0.75 mm (Aerator A5).....	351
A5.2 Effect of Unconventional Aerator Designs.....	351
A5.2.1 Co-Flow Aerator (Aerator A1).....	351
A5.2.2 Porous Aerator (Aerator A6).....	354
A5.3 Effect of Mixing Chamber Diameter.....	356
A5.3.1 14 mm Diameter.....	356
A5.3.2 20 mm Diameter.....	359
A5.4 Effect of Operating Pressure.....	359
A5.4.1 5 bar _g	359
A5.4.2 3 bar _g	359
A5.4.3 1 bar _g	362
A5.5 Effect of Orientation.....	364
A5.5.1 Vertically Downwards.....	364
A5.5.2 Vertically Upwards.....	364

APPENDIX 6: REGIME MAPS FOR STREAMLINED AERATOR DESIGNS

..... **369**

A6.1 Effect of Aerator Body Design 369

A6.1.1 Circular Arc 369

A6.1.2 Hybrid 372

A6.1.3 Conical 374

A6.1.4 ADARPA 376

A6.1.5 Flat-End 376

APPENDIX 7: REGIME MAPS FOR ADARPA STREAMLINED AERATOR DESIGNS 377

A7.1 Effect of Aerator Orifice Diameter 377

A7.1.1 1 x 3.0 mm (Aerator A2) 377

A7.1.2 4 x 2.0 mm (Aerator A3) 380

A7.1.3 9 x 1.0 mm (Aerator A4) 382

A7.1.4 16 x 0.75 mm (Aerator A5) 385

A7.2 Effect of Aeration Area 385

A7.2.1 1.77 mm² (Aerator A7) 385

A7.2.2 3.53 mm² (Aerator A8) 388

A7.2.3 7.07 mm² (Aerator A5) 390

A7.2.4 14.14 mm² (Aerator A9) 390

A7.3 Effect of Unconventional Aerator Designs 393

A7.3.1 Porous Aerator (Aerator A6) 393

A7.4 Effect of Mixing Chamber Diameter 395

A7.4.1 14 mm Diameter 395

A7.4.2 20 mm Diameter 398

A7.4.3 25 mm Diameter 398

A7.5 Effect of Operating Pressure 401

A7.5.1 5 bar_g 401

A7.5.2 3 bar_g 401

A7.5.3 1 bar_g 404

A7.6 Effect of Orientation 406

A7.6.1 Vertically Downwards 406

A7.6.2 Vertically Upwards 406

CHAPTER 1. INTRODUCTION

1.1 Background

It is a common requirement in many industrial applications, for bulk volumes of liquid to be dispersed into smaller droplets within a gaseous atmosphere. The benefits of this process, termed atomisation, are increased: surface area to volume ratio; liquid spread; fluid mixing; and evaporation. There are many techniques available to atomise liquids and, since every industrial application has its own unique set of atomisation requirements, each atomiser design has unique advantages and limitations. One of the more common uses for an atomiser, and the application for this thesis, is to produce a suitable chemical fuel spray for a combustion system.

A chemical fuel is a substance that combines with oxygen in an exothermic reaction (e.g. combustion). However, for a chemical fuel to be effectively utilised in combustion systems, it must release heat in an acceptable and controllable manner [2] – for this reason, despite also having solid and gaseous forms, liquid fossil fuel is most commonly used in combustion systems. Liquid fossil fuels (typically refined to petroleum or diesel) are hydrocarbon fuels and are one of the highest utilised global energy sources as they are: readily available; relatively cheap to harvest; have excellent combustion properties (e.g. high calorific value, good combustion efficiency); and are easy to transport and store. Therefore, as a global community, the constant availability and supply of these fossil fuels is inherently linked to our economic growth.

Combustion atomisers have been used to inject refined liquid fossil fuels into internal combustion systems for many years and, during this time, their design and performance has been optimised to match a series of requirements – they should: produce a fine, homogenous spray with large spread; and be cost efficient to manufacture and operate. Current combustion atomisers typically have a narrow operating window (i.e. low turndown ratio), with high sensitivity to small variations in the operating conditions or fuel properties. But, due to only minor fluctuations in fuel properties over the life cycle of our combustion

systems, the requirement for a wide operating range has rarely been sought and, as such, a major combustion atomiser redesign has not yet been forced.

However, times are changing. It is well known that fossil fuels are a finite source and will eventually be depleted, whereby fuel production will gradually slow as oil reserves become more difficult to source, until all reserves are exhausted and production ceases. Using Hubbert Peak Theory, it is predicted that the peak oil production is to occur before 2025 [3], from which point fuel supply will be unable to meet demand. As a global community, we have already experienced large fluctuations in oil prices, suggesting that fossil fuel depletion is already beginning to affect our economy.

An additional deterrent to fossil fuel combustion is the detrimental effect that its waste products have on the environment and, consequently, the negative public image they have developed – for example, the unavoidable production of carbon dioxide (CO_2), a potent greenhouse gas. Furthermore, incomplete combustion can produce additional harmful waste products, such as carbon monoxide (CO), sulphur oxide (SO_x), nitrogen oxide (NO_x) and particulates, which are accountable for environmental concerns such as smog, ozone damage and acid rain.

The Department of Energy & Climate Change (DECC), the UK governmental department responsible for energy management, has clearly stated their intention to reduce carbon emissions within their policies – for example: increase the use of low-carbon technologies [4]; reduce the UK's greenhouse gas emissions by 80% by 2050 [5]; and support international action on climate change [6].

Therefore, due to depleting reserves and environmental concerns, the energy industry is facing considerable pressure to revolutionise the current culture of fossil fuel combustion. Perhaps the most convenient solution would be to improve the efficiency of our current systems, to reduce both the fuel intake and combustion emissions, coupled with a carbon capture system, to reduce carbon dioxide emissions. However, despite a typical hydrocarbon combustion system achieving only around 25% efficiency, endeavouring to improve efficiency is a short sighted and risky solution being: costly in research and implementation; far from guaranteed; and achieving only a delay in the inevitable fossil fuel depletion. An alternative approach of preventing the release of harmful bi-products (e.g. carbon capture systems) are typically expensive in resource (i.e. time, money and space).

As a result, the energy industry is investing heavily in the exploration of alternative renewable energy sources, such as nuclear, hydroelectric, geothermal, wind, solar and biofuel [3]. It is imperative the chosen energy source is: technically feasible; economically competitive; environmentally acceptable; readily available; and, in the short term, compatible with existing systems [3, 7, 8]. As a collective, these renewable energy sources appear to be a promising solution for a vast range of applications and, consequently, their use is being increasingly adopted. Figure 1.1 illustrates this impact in the UK over recent years, with 18.5% of the UK energy production coming from renewable sources in 2016, compared to just 3.5% in 1970.

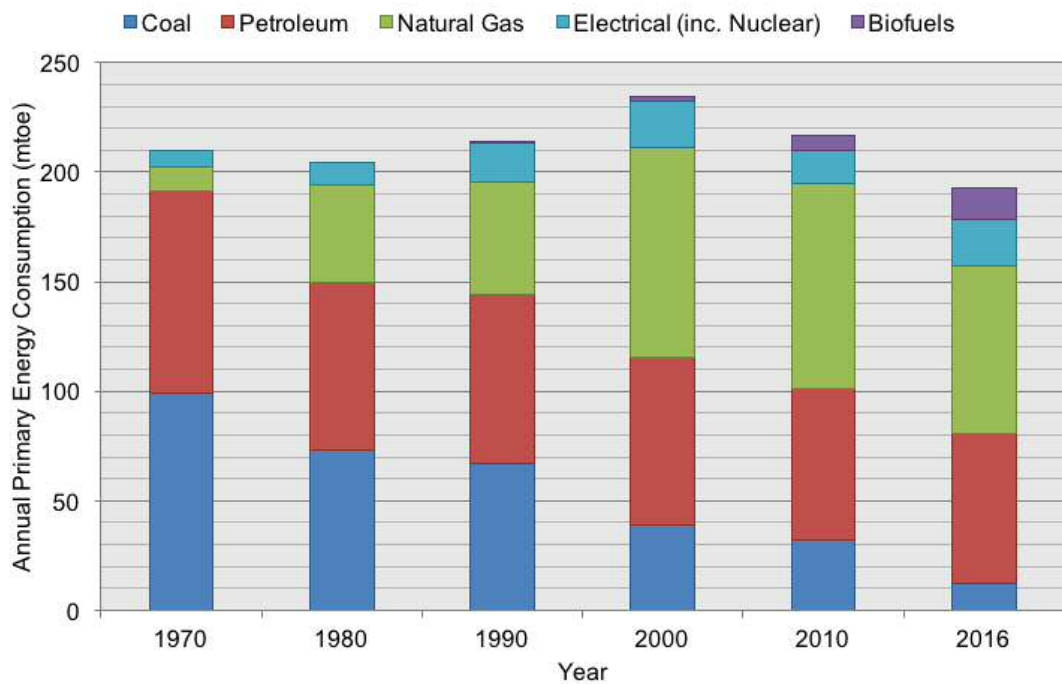


Figure 1.1 Annual primary energy consumption by fuel type, 1970 to 2016. [9]

However, combustion is still required in the interim to maintain compatibility with existing systems and is a necessity for some existing applications (e.g. gas turbines) and, therefore, a renewable combustible fuel is required. Liquid biofuels fulfil this brief and have several major benefits over petroleum [3]:

1. They are an abundant resource, which are typically renewable annually.
2. They can be harvested virtually anywhere, thus promoting greater energy independence as oil scarce countries will no longer be reliant on oil rich states for energy import.

3. Their growth consumes carbon dioxide and, therefore, the complete process from production to combustion can have balanced CO₂ – significantly reducing the net emissions of greenhouse gases compared to fossil fuels.
4. They are generally oxygenated (e.g. bioethanol) allowing for a more complete combustion and further reducing harmful emissions compared to fossil fuels.

An E5 biofuel blend (i.e. 5% bioethanol, 95% petrol), which maintains compatibility with existing combustion systems, is already available in the UK market [8]. Although these small quantities can only have a limited impact on CO₂ emissions, it proves the potential of biofuel as a future energy source and, therefore, it is predicted that the use of biofuels will continue to grow in dominance in the future eventually completely replacing hydrocarbon fuels in combustion systems [7].

1.2 Motivation

Whilst the benefits of combusting biofuel in place of fossil fuel is an attractive proposition, the implementation of pure biofuel into our existing combustion systems could be problematic. One of the main obstacles predicted is difficulty in generating a suitable combustion spray using conventional atomisation techniques. Existing combustion atomisers are finely tuned to deliver a high quality spray, but are typically extremely sensitive to their operating conditions (e.g. liquid mass flow rates, injection pressures, fluid physical properties) and therefore have a relatively narrow operating window. Whilst the properties of pure biofuels can be engineered to be extremely similar to refined liquid fossil fuels, not all are within the necessary operating window and thus compatibility with existing atomisers cannot always be maintained – this presents a significant obstacle to the adoption of biofuels in our existing combustion systems. Furthermore, as time and production processes progress, it is highly likely that the biofuel properties will vary in themselves until an ideal solution is found. Therefore, the use of conventional atomisation techniques would be impracticable, as it would require continual replacement of the combustion atomisers to match the latest blend of biofuel. Consequently, to enable biofuel adoption in combustion systems, it would be incredibly advantageous to develop an atomisation technique that can satisfy the existing spray requirements of a combustion atomiser, but with a much wider operating window.

The development of such an atomiser could also be useful in many alternative spray generation applications – for example, allowing atomisation of various liquids in food or

medical applications, controllable spray properties for fire suppression or incorporation of metallic flecks in spray paints.

A flexible and controllable atomisation method called effervescent atomisation, first proposed by Lefebvre [10], may be the solution. However, this technique is far from optimised. Therefore, the aim of this thesis is to further the scientific understanding of effervescent atomisation with the intention of determining an optimal effervescent atomiser configuration.

1.3 Modern Atomisation Technology

For the purpose of comparison and to aid explanation in the further chapters, it is beneficial to briefly explore the multitude of current atomiser types and discuss their suitability for spraying difficult fuels (e.g. viscous liquids, suspended sediment) for combustion – for example, liquid biofuel. The desired technique should:

1. Generate a high-quality spray (i.e. fine, stable spray with a wide, homogenous spread) in a desired direction.
2. Have low dependence on the properties of difficult fuels (e.g. high viscosity, non-Newtonian fluids, suspended solids).
3. Be cost efficient to manufacture, run and maintain.
4. Be controllable with high turndown ratios.

The most common and simplistic atomisation technique is the pressure atomiser (Figure 1.2), which operates on the principle of forcing high pressure liquid through a small orifice. The turbulence within the liquid is extremely high upon exit from the nozzle, with strong transverse velocity components. If the turbulent energy is sufficient to overcome the restoring action of the liquid (e.g. viscosity, surface tension), then the body of liquid will break up into ligaments and droplets (i.e. atomisation). For the finest sprays, the exit orifice needs to be very small and the operating pressure very high to generate the required level of turbulence [11].



Figure 1.2 Pressure atomiser schematic. [12]

Pressure atomisers have many benefits: they are simple in design; easy to maintain; can be small in size; and are capable of producing very fine spray. However, they have a characteristic narrow operating window being inherently sensitive to any operational changes – the spray quality is strongly affected by the operating pressure, flow rate and liquid properties, leading to poor turndown ratios. In addition, the small exit orifice can easily become clogged with suspended solids. It can be concluded, therefore, that pressure atomisation is a technique well suited to a refined fuel with non-varying properties, but is not appropriate for the atomisation of difficult fuels.

Rotary atomisation (Figure 1.3a) is another technique that generates a spray by increasing the internal energy within the liquid to overcome restoring forces. It operates by injecting liquid at the centre of a rotating surface. The spinning motion of the surface generates centrifugal force, which forces the liquid to the periphery where it is discharged as a spray (Figure 1.3b) [12]. The major benefit of rotary atomisation over pressure atomisation is its insensitivity to the properties of difficult fuels. However, the atomisation process is discontinuous and non-directional, forming an umbrella spray shape around the atomiser. In addition, at very high liquid flow rates the liquid cannot be dissipated at a high enough rate and a thin film is formed at the periphery, which breaks up into a coarse spray. These inherent drawbacks cannot be easily rectified with design and, therefore, rotary atomisation is unsuitable for most combustion systems.

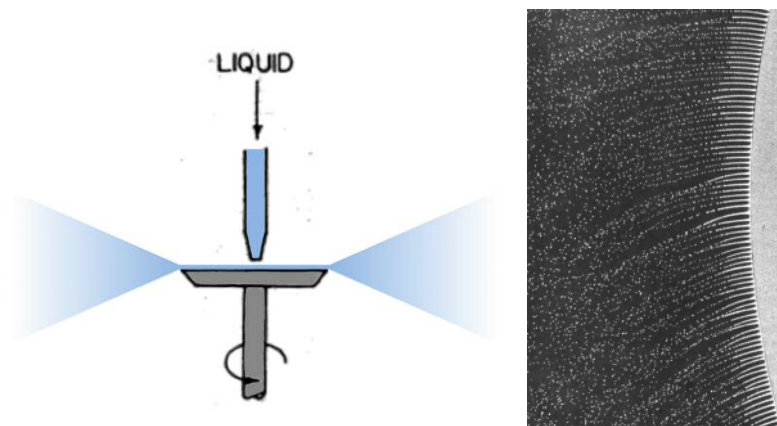


Figure 1.3 Rotary atomiser: a) schematic; b) spray image. [12]

As an alternative to increasing the internal energy within the liquid-phase, as seen in pressure and rotary atomisation, two-phase atomisers induce break up with the addition of a high energy gas-phase. Common examples of this technique are air-assist atomisation and air-blast atomisation (Figure 1.4). Air-assist atomisation produces a spray by shattering a jet of liquid into droplets with a small quantity of high velocity gas, whereas air-blast atomisation

uses a higher flowrate of gas [10]. These techniques produce high quality spray and are insensitive to the liquid properties. However, as they require an auxiliary system capable of providing a stream of high velocity gas, they have high design and operating costs [10, 13]. In addition, they are not very controllable as reducing the gas flow rate significantly reduces atomisation quality and so, for satisfactory atomisation, the process requires high gas flow and is inherently inundated with excess gas. They are therefore not a suitable solution for most difficult fuel combustion systems.

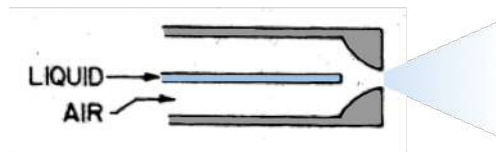


Figure 1.4 Air-assist/air-blast atomiser schematic. [12]

Flashing atomisation (Figure 1.5a) is an alternative two-phase technique, which utilises superheated gaseous bubbles within the internal flow to form a spray. The bubbles are formed in a cavitation/flashing process, when a proportion of the internal flow becomes superheated. These bubbles are discharged from the exit orifice and rapidly expand and explode due to a large pressure drop to the ambient atmosphere, thus shattering the liquid core into droplets and ligaments, as depicted in Figure 1.5b [12]. Flashing atomisation produces a high-quality spray, is suitable for difficult fuels and has low dependence on operating pressure [14]. However, this technique is generally unsuited for combustion as the formation of superheated bubbles is notoriously difficult to control, requiring either nucleation of a dissolved gas within the liquid or superheated cavitation/flashing of the liquid itself [13, 15].

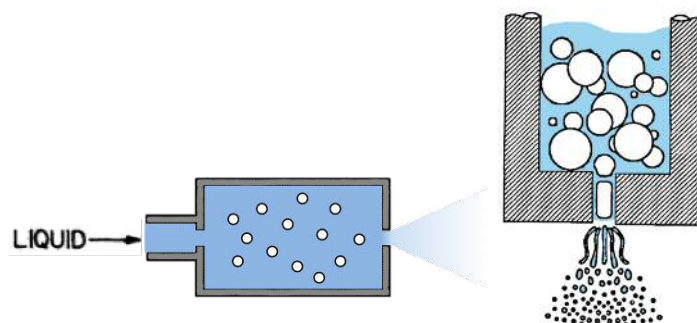


Figure 1.5 Flashing atomiser: a) schematic [12]; b) atomisation principle [16].

1.4 Effervescent Atomisation

In the previous section, the available atomiser types were explored and their suitability for providing combustion sprays of difficult fuels was discussed. Of these techniques, flashing atomisation was established as the most appropriate for generating the required spray but, as it has low controllability and is not cost efficient, it was deemed unsuitable for most combustion systems.

Effervescent atomisation is an alternative technique, with strong similarities to flashing atomisation, that has been widely reported as a promising technique for generating a combustion spray from difficult fuels. A typical effervescent atomiser design is shown in Figure 1.6.

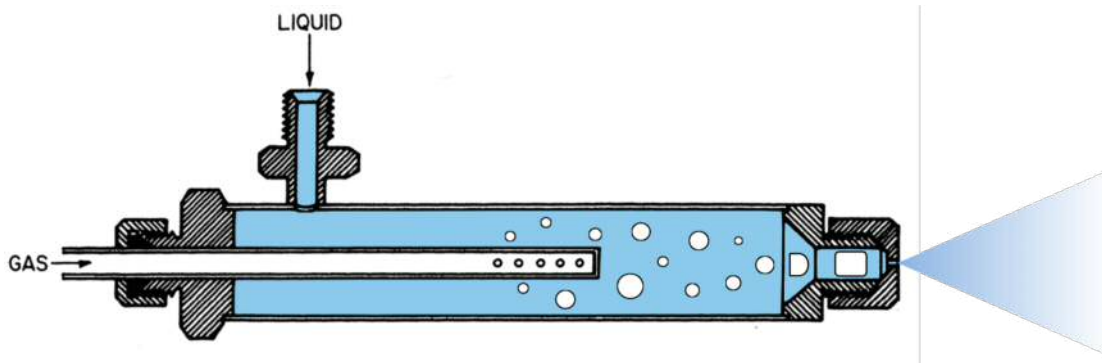


Figure 1.6 Effervescent atomiser schematic, inside-out configuration. [10]

The effervescent atomisation process is well cited within the literature. Firstly, bubbles are injected into a liquid flow through an aerator. These bubbles interact with one another to form two-phase gas-liquid patterns in the flow, termed flow regimes, which are stabilised in the pressurised mixing chamber. Finally, the two-phase flow is forced through a narrow exit orifice, where a substantial pressure drop occurs, causing the gas bubbles to burst and shatter the liquid core into droplets and ligaments, in the same process as depicted in Figure 1.5b.

The advantages of effervescent atomisation are well reported in the literature. It is insensitive to liquid properties, meaning one atomiser can spray a range of liquids without modification [10, 17-19]. Compared to a pressure atomiser: the spray quality is better at low operating pressures [11, 12, 19], reducing operating costs and component wear; and, due to the larger exit orifices [10, 11, 15, 19-21], the likelihood of blockage is reduced. As it utilises a small quantity of low pressure gas for atomisation, it is more efficient than an air-assist or air-blast atomiser [10, 17, 22, 23] and less sensitive to operating pressure [24], reducing operating

costs and increasing controllability with greater turndown ratios. Although similar in principle to flashing atomisation (i.e. using the destructive action of bursting bubbles to aid the atomisation process), effervescent atomisation does not depend on critical thermodynamic conditions to prompt bubble nucleation [13], allowing for greater controllability and eliminating many of the impracticalities (e.g. fluid preheating and high operating pressure). In addition, air can be used as an atomising gas to reduce pollution, such as soot emissions [10, 11, 24].

There are, however, some disadvantages associated with effervescent atomisation. It requires a gas injection system, albeit at reasonably low pressure, which adds to the operation and design costs. Also, due to the discontinuous nature of two-phase internal supply to the exit orifice, effervescent atomisation inherently produces a relatively unstable spray and a large range of droplet sizes, which in the extreme case can cause unwanted combustion characteristics (e.g. combustion instability, droplet clustering, noise and pollution) [11, 25-27]. By fully understanding the effects of the operating parameters on the internal flow and optimising the atomiser design, it is thought possible to minimise these effects and, thus, optimise the effervescent atomiser.

1.5 Aims and Objectives

This thesis aims to further the scientific understanding of effervescent atomisation by studying the internal flow mechanisms at differing operating parameters and atomiser designs, associating these with atomisation quality and, thus, determining an optimal effervescent atomiser configuration. This will be achieved in the following manner:

1. Perform a thorough review of the effervescent atomiser literature, to identify the commonly investigated parameters and understand the existing knowledge of the scientific community.
2. Design, manufacture and commission a state-of-the-art effervescent atomiser, capable of enabling internal flow investigation, spray characterisation and customisability of design parameters.
3. Develop a test matrix to investigate the common independent parameters over a suitable range.
4. Characterise the complete effervescent atomisation process – from gas-injection at the aerator, to the internal two-phase flow generated in the mixing chamber, to the quality of spray produced. Determine the optimal internal two-phase flow for effervescent atomisation.

5. Determine the effect of various common independent parameters on the internal flow performance of an effervescent atomiser and, thus, propose an effervescent atomiser design to enable the greatest range of operating conditions corresponding to the optimal internal flow.

1.5 Thesis Content

- Chapter 2 presents a review of the relevant literature to effervescent atomisation. The physical processes related to the generation of two-phase gas-liquid flow in an effervescent atomiser are summarised, including the formation of bubbles in a liquid cross-flow and their subsequent interaction to form the two-phase flow regimes. The two-phase atomisation mechanisms are described and a thorough literature review specific to effervescent atomisation research is presented.
- Chapter 3 details the development of the two novel experimental systems used for the complete characterisation of an effervescent atomiser and the optimisation of atomiser design to maximise optimal internal flow. The experimental techniques of Shadowgraphy and Phase Doppler Anemometry are explained and justified.
- Chapter 4 reports the findings of a complete effervescent atomiser characterisation study, detailing the gas injection regimes witnessed within the effervescent atomisers, the development into form two-phase flow regimes and the subsequent atomisation processes. The optimal operating criteria for effervescent atomisers are identified.
- Chapters 5, 6 and 7 present findings of internal flow studies in which various independent parameters were investigated. By comparing the results to the optimal internal flow, as identified in the previous chapter, recommendations for optimal effervescent atomiser design are provided.
- Chapter 8 summarises the key findings of the entire investigation and provides recommendations for future work.

CHAPTER 2. THEORY AND LITERATURE REVIEW

This chapter aims to summarise the findings of the scientific publications applicable to effervescent atomisation – this section is a theoretical and literature review study. The relevant theory section encompasses work within numerous research fields to explain the complete effervescent atomisation process – from the initial gas-injection at the aerator, finally through to droplet interactions within the spray. Following this, the literature specific to effervescent atomisation is reviewed, to determine the effect of independent parameters (e.g. fluid flow rates, operating pressure, liquid properties) with respect to dependent parameters (e.g. droplets sizes, droplet velocities, spread of the spray). Finally, the findings are summarised, to inform the further research chapters.

To aid ongoing discussions, it is useful at this stage to introduce the components of an effervescent atomiser (Figure 2.1). The effervescent atomisation process initiates at the aerator where gas is injected into the mixing chamber. There are two main configurations of aerators, where the gas is injected either through orifices located within a central tube (i.e. inside-out; as depicted) or through peripheral holes in the mixing chamber (i.e. outside-in) – this will be important in further discussions. The role of the mixing chamber is to facilitate mixing and stabilise the two fluid phases. This internal gas-liquid two-phase flow is finally supplied to and ejected from the atomiser through an exit orifice. The common independent parameters investigated for the aerator are the orifice diameter, aeration area and atomiser configuration; for mixing chamber are the diameter and mixing length; and for exit orifice are the orifice diameter and length and the convergence angle.

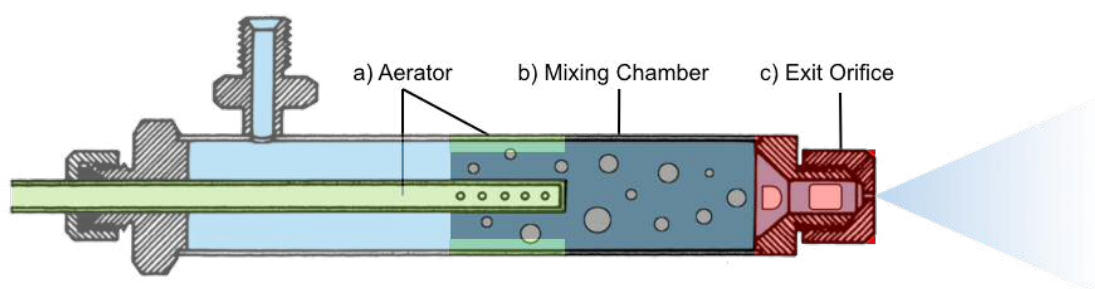


Figure 2.1 Effervescent atomiser common components.

2.1 Gas-Phase Injection at Aerator

This discussion concerns the gas-phase injection phenomena within the aerator region of an effervescent atomiser. For effervescent atomisation, it is a requirement that gas injection must yield a bubbly mixture in the mixing chamber [28, 29] and, therefore, the role of the aerator is to inject the bubbles into a peripheral liquid flow. The vast majority of relevant gas injection theory has been conducted in alternative research fields (e.g. bubble columns), but its applicability is thought to extend to effervescent atomisation.

2.1.1 Bubble Formation

For bubbles to be formed in the liquid, the gas injection pressure must be greater than the capillary pressure of the aerator orifice (i.e. the aerator orifice resistance) [30] and the liquid pressure [10]. The bubble formation process, as depicted in Figure 2.2, is described by Tesař [31]: a) initially, a planar gas-liquid interface exists, with the gas pressure resisting liquid back flow into the aerator; b) Stage 1 bubble growth occurs up to hemi-spherical shape (i.e. bubble radius continually decreasing) and is stable, as a decrease in gas pressure will return the bubble to the planar interface; c) Stage 2 bubble growth follows once the bubble has exceeded hemi-spherical shape (i.e. bubble radius continually increasing) – this is an unstable growth, as there is no mechanism that can restrict the growth of bubble until detachment and, therefore, bubbles can grow to be several magnitudes larger than the aerator orifice. The circumstances leading to bubble detachment can be determined by considering the forces acting on a forming bubble – these are summarised in Table 2.1.

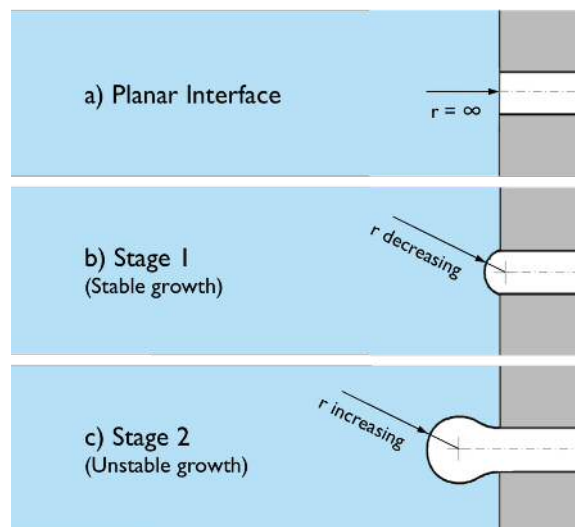


Figure 2.2 Graphical representation of the three bubble growth stages. [31]

In a quiescent (i.e. stagnant) liquid, a forming bubble will detach from an aerator orifice if the detachment forces (i.e. gas momentum and buoyancy force) are great enough to overcome the restoring force of the liquid surface tension (Figure 2.3a-b). However, this is an overly simplified assumption for bubble formation in an effervescent atomiser as the gas is injected, not into quiescent liquid, but into a liquid cross-flow. In this case, several additional viscous detachment mechanisms are generated (i.e. drag, lift and liquid inertia), as shown in Figure 2.3c. Additionally, the liquid flow forces the newly formed bubbles away from the aerator orifice, reducing the frequency of bubble coalescence (i.e. the joining of two bubbles) [32, 33]. Therefore, an increasing liquid cross-flow has the effect of reducing bubble diameter and increasing bubble formation frequency compared to quiescent injection [33, 34].

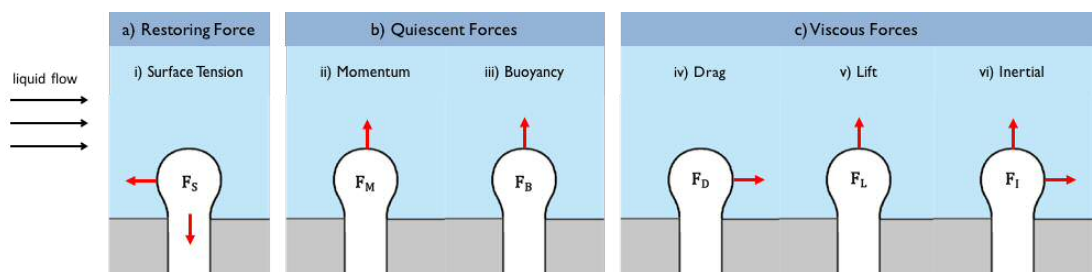


Figure 2.3 Bubble detachment forces in a liquid cross-flow.

Table 2.1 Bubble detachment forces. [30, 33, 35, 36]

Force	Description	Radial Component	Axial Component	Vertical Component
Restoring Force				
Surface Tension	The liquid surface tension acts to keep the bubble attached to the orifice.	$F_{S_x} = -\pi d_o \sigma \times \frac{5}{4} \left[\frac{(\theta_A - \theta_R)(\sin(\theta_A) + \sin(\theta_R))}{\pi^2 - (\theta_A - \theta_R)^2} \right]$	$F_{S_y} = -\pi d_o \sigma \times \left[\frac{\cos(\theta_A) + \cos(\theta_R)}{(\theta_A - \theta_R)^2} \right]$	
Quiescent Forces				
Buoyancy	The difference in density between liquid and gas phase causes a vertical pressure differential across the bubble.	-	-	$F_B = V_b g (\rho_l - \rho_g)$
Gas Momentum	The momentum of the gas emerging through the orifice acts to detach the bubble.	-	$F_M = \frac{4 \rho_g Q_g^2}{\pi d_o^2}$	
Viscous Forces				
Drag	Drag occurs as liquid flows across bubble, generating friction across the surface and a pressure wake.	$F_D = (C_d) \frac{\pi}{8} \rho_l d_b^2 \times (\bar{U}_{l,a} - U_b)^2$	-	
Lift	A vertical pressure differential occurs as liquid passes over the bubble.	-	$F_L = (C_d) \frac{\pi}{8} \rho_l d_b^2 \times (U_b)^2$	
Inertial	The liquid is forced to accelerate as it flows around the bubble. This causes horizontal and vertical inertial forces.	$F_{I_x} = C_m \rho_l (Q_g (\bar{U}_{l,a} - U_b) - V_b a_b)$	$F_{I_y} = C_m \rho_l (Q_g U_b + V_b a_b)$	

2.1.2 Gas Injection Regimes in a Liquid Cross-Flow

Although the purpose of an effervescent atomiser aerator is to inject bubbles into a liquid flow, bubble formation can only occur when the detachment mechanisms are sufficient to separate the bubble from the aerator orifice. Therefore, for any aerator, there exists operating conditions whereby bubbling is not possible and other so called “gas injection regimes” are observed. Curiously, there is no evidence of the gas injection regimes having been investigated within effervescent atomiser literature and so this section explores other research fields.

Considering first the over simplified case of gas injection into a quiescent liquid, multiple gas injection regimes occur with varying gas flow rates [30, 34, 37]. The desired bubbling at the aerator is encouraged by low gas flow rates, where single spherical bubbles are formed directly from the aerator orifice. However, as the gas flow rate increases, the bubble forming process becomes increasingly chaotic due to, for example, the wake effect of detached bubbles. In the extreme case, bubbles are no longer formed at all and the gas injection forms the appearance of a gas jet, whereby discrete bubbles are no longer formed.

Similar gas injection regimes are observed with increasing gas flow rates when a liquid cross-flow is applied [32, 38, 39] – these can be categorised into three distinct gas injection regimes (i.e. single bubbling, pulse bubbling and jetting) with the addition of a unique cavity forming regime.

Single Bubbling

Single bubbling occurs at the lowest gas flow rates and is characterised by the regular formation of individual nearly spherical bubbles of approximately uniform size, which are formed either directly from the aerator orifice or from a small gas filament [32, 39]. The influence of increasing the liquid cross-flow encourages detachment of the forming bubbles, typically before fully expanded [39], and distorts them into a flattened spherical shape [33]. Example observations of single bubbling within the literature are shown in Figure 2.4.

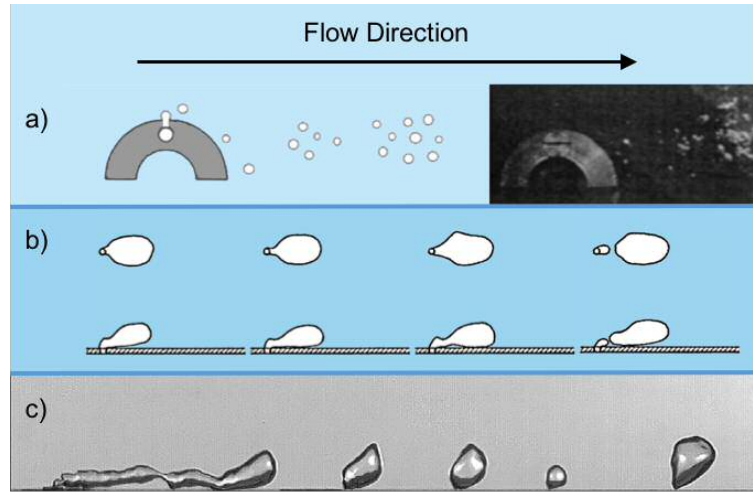


Figure 2.4 Example observations of single bubbling in literature:

a) curved body aerator [32]; b) flat body aerator [38]; c) flat body aerator [39].

Johnson et al. [40] proposed that balancing the viscous drag and the restoring surface tension forces, and neglecting the gas momentum and buoyance forces due to the low gas flow rate, could predict the diameters of the bubbles formed by single bubbling (Equation 2.1). In an investigation of impeller design, Forrester and Rielly [32] found this to correlate well with the trend of their experimental results, but under predict bubble size – this discrepancy could be caused by the wake generated by their aerator design increasing the coalescence of bubbles.

$$d_b = \sqrt{\frac{8d_a\sigma}{C_D U_{l,a}^2 \rho_l}} \quad (\text{m}) \quad (2.1)$$

Furthermore, Sen et al. [41] observed that a pressure wave is generated within the internal two-phase flow as a bubble is discharged from the exit orifice, which was reported to promote bubble formation at the aerator.

Pulse Bubbling

A transition occurs from single bubbling with increased injected gas velocity (i.e. increased mass ratio of air-to-liquid, “ALR”) [32]. Pulse bubbling is the formation of a series of gas entities, interconnected with thin gas necks. The smallest of these necks collapses at some point downstream of the aerator orifice due to the recirculating effect of the internal gas and the drag of the liquid cross-flow. This causes detached bubbles of varying size, relative to single bubbling [32, 39, 42]. Increasing the gas

flow rate within the pulse bubbling regime acts to increase the number of interconnected gas entities, with alternating pulses of jetting [39]. Example observations of pulse bubbling within the literature are shown in Figure 2.5.

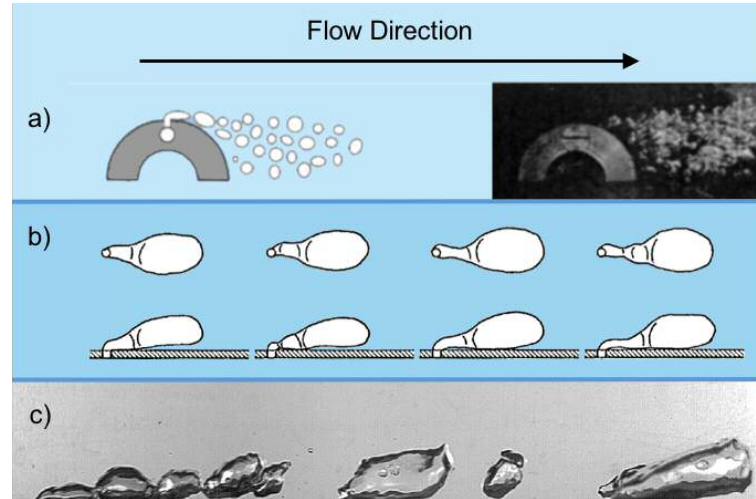


Figure 2.5 Example observations of pulse bubbling in literature:

a) curved body aerator [32]; b) flat body aerator [38]; c) flat body aerator [39].

Jetting

The transition to jetting occurs with increased ALR, where gas injection is no longer seen to bubble at the orifice but takes the appearance of a gas jet [32, 39]. Bubble formation is chaotic, with pockets of gas violently broken off the end of the jet, and consequently the bubble size, shape and frequency are highly irregular [32]. Example observations of pulse bubbling within the literature are shown in Figure 2.6.

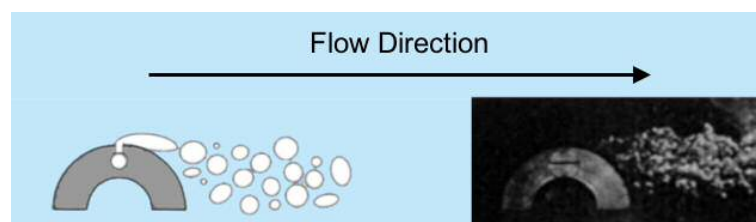


Figure 2.6 Observations of jetting from a curved body aerator [32].

Balzán et al. [39] further divided the jetting regimes into elongated and atomised jetting – an elongated jet was described as “a gas jet whose length is substantially greater than the channel diameter”, whereas for an atomised jet the “bubble formation

is completely disorganized... and detached bubbles are no longer spherical". These regimes are shown in Figure 2.7.

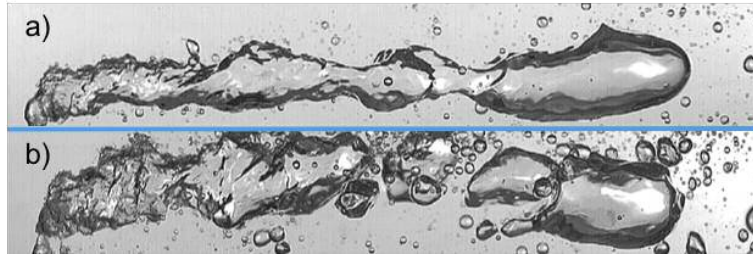


Figure 2.7 Observations by Balzán et al. [39] of:
a) elongated jetting; b) atomised jetting.

It is proposed by Marshall [38] that the transition between bubbling and jetting regimes can be predicted by Equation 2.2 – this was reported to have reasonable agreement with a flat-end aerator [32]. A more general rule reported to describe this transition is when the injection gas velocity ($U_{g,a}$) is one order-of-magnitude larger than the liquid cross-flow velocity ($U_{l,a}$) [32, 42].

$$U_{g,a} = 0.0208d_a^{-0.93} - 0.0190d_a^{-0.75}U_{l,a} \quad (\text{ms}^{-1}) \quad (2.2)$$

for $0.6 \text{ ms}^{-1} \leq U_{l,a} \leq 4.8 \text{ ms}^{-1}$

Forrester and Rielly [32] proposed that the jet break up model, originally presented by Raleigh [43], can be applied to predict the bubble diameter formed in the jetting regime (Equation 2.3). Forrester and Rielly [32] found this model to correlate well with the trend of their experimental results but over predict bubble size in the jetting regime.

$$d_b = 2.4 \sqrt{\frac{Q_g}{U_{l,a}}} \quad (\text{m}) \quad (2.3)$$

Cavity Forming

Cavity forming is observed when a separation bubble forms in the wake of the aerator. The bubble formation is chaotic and irregular bubbles are seen to be violently sheared from the gas cavity [32]. This regime has been observed to occur in the wake of a curved [32] (Figure 2.8) and a flat base aerator [44].

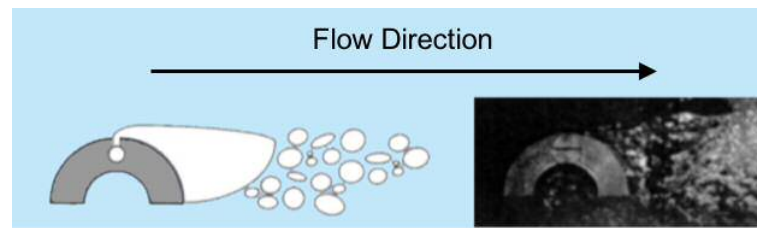


Figure 2.8 Observations of cavity formation from a curved body aerator [32].

N.B. The cavity forming bubbling regime should not be confused with cavitation (i.e. the formation of superheated gas bubbles in a liquid).

In order to quantify an atomiser's response to gas injection, some researchers have produced gas injection regime maps [32, 34, 37] – an example bubbling map is shown in Figure 2.9. These maps allow for interpolation between test points and, therefore, operating regions of gas injection regimes can be identified. These maps provide a measure of aerator performance and can be used to inform studies in which the gas injection regimes cannot be observed. However, care must be taken when applying these to predict internal flow in alternative fields of study as the conditions under which the bubble maps were obtained may be unrepresentative (e.g. long residence time) [29].

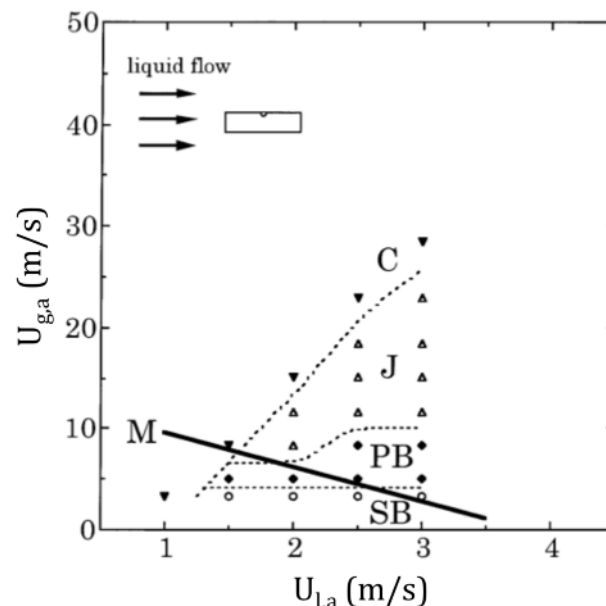


Figure 2.9 An example gas injection regime map for axial liquid cross-flow over a cylinder (SB: Single Bubbling; PB: Pulse Bubbling; J: Jetting; C: Cavity Forming; M: Marshall [38]).

[32]

2.1.3 Bluff Body Recirculation

Bluff body recirculation is the generation of a reduced pressure zone in the downstream region of an aerodynamic body in a fluid flow (Figure 2.10). As previously discussed, there are two main aerator configurations within effervescent atomiser design: inside-out (i.e. gas injection through a central aeration tube), or outside-in (i.e. gas injection through peripheral holes in the mixing chamber). For inside-out configuration, which is the focus of the current work, the aerator tube acts as a bluff body within the axial two-phase flow of the injected fluids. Therefore, bluff body recirculation is thought to be a relevant area of research for inside-out effervescent atomisers and is anticipated to be a major contributing factor to the generation of the cavity forming gas injection regime.

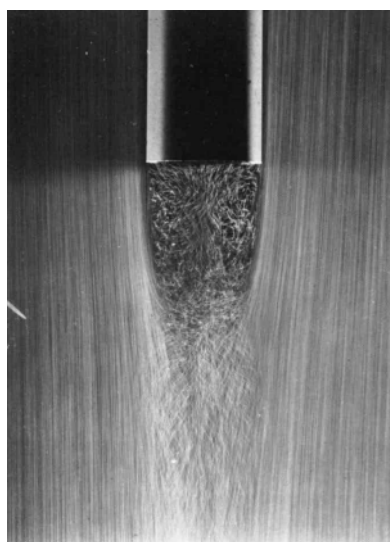


Figure 2.10 Bluff body recirculation for axial liquid cross-flow over a flat-end cylinder. [45]

The study of bluff body recirculation for axial flow across a cylinder applies to a surprisingly few number of scientific fields, being typically reported by research concerning projectiles (e.g. aeroplanes, submarines, torpedoes, missiles) [46]. Within these studies, flat-end cylinders were reported to have a significant wake effect (i.e. high coefficient of drag) compared to alternative drag reduced designs [45, 47]. “Boat-tailing” is an effective streamlining method, in which the cross section of the bluff body is gradual reduced to a tip – example designs referenced in the literature include: conical [48], circular arc [48], circular arc-conical hybrid [49, 50] and other intricate profiles (e.g. DARPA SUBOFF [1, 46, 51-53]). An alternative well-known technique for base drag reduction is base-bleed, which feature a flared base with ventilation cavities to promote axial fluid flow to the wake region [54].

By far the most common aerator body design referenced in effervescent atomiser literature is a flat-end cylinder and therefore it is thought that the majority of inside-out designs are susceptible to significant wake formation and hence cavity forming regimes. The only observation of bluff body recirculation effects in effervescent atomiser literature was in an internal flow visualisation study by Jobehdar [44], in which the formation of a large gas void was observed to form in the wake region of a conventional flat-end aerator (Figure 2.11a) – this effect was reported to be mitigated by installing an arbitrary conical tip to streamline the aerator body (Figure 2.11b). The only other use of a streamlined aerator design is implied within the atomiser design drawings included by Hampel et al. [55], but this is not specifically mentioned nor studied as an independent variable. Therefore, the effect of bluff-body recirculation on inside-out effervescent atomisation is considered to be an under-researched area.

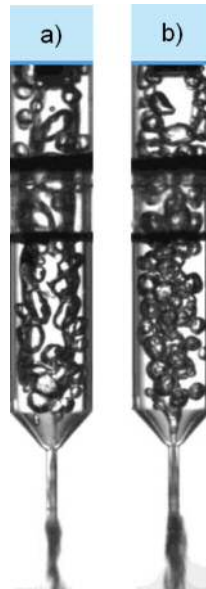


Figure 2.11 Effect of aerator body design on effervescent atomiser internal flow:
 a) a conventional flat-end design enables a gas void to form in the aerator wake;
 b) a transparent conical aerator tip prevents gas void formation. [44]

2.2 Stabilised Two-Phase Gas-Liquid Flow in the Mixing Chamber

This discussion concerns the theory relating to the generation of the two-phase gas-liquid flow within the mixing chamber of an effervescent atomiser. Two-phase flow theory spans many research areas and therefore this discussion covers relevant literature from a variety of fields. An effervescent atomiser is designed such that the newly injected gas-phase is stabilised within the mixing chamber prior to release from the exit orifice. This process is of

particular importance, as the properties of the two-phase flow that supplies the exit orifice is directly linked to the quality of spray produced [19, 20, 56].

2.2.1 Stabilisation of the Injected Gas-Phase

A two-phase flow can only be classed as stable once the spatial distribution of gas entities (e.g. bubbles, slugs, voids) within the liquid flow has no variance with downstream displacement. The gas-phase dynamics (i.e. the coalescence and breakup of gas entities) are therefore important factors affecting the stabilisation of the internal two-phase flow within an effervescent atomiser. The mechanisms affecting these processes are complex and chaotic [57], and therefore the majority of our understanding has come from experimental investigations.

Coalescence is the combining of two or more gas entities upon contact to form a single larger gas void. A popular explanation for the coalescence process is that, upon collision, gas entities will flatten together with their gaseous contents separated by a thin liquid sheet. Given sufficient contact time, this separating liquid ligament will drain under the influence of flow forces and the capillary effect and, when at a critical thickness, it is so unstable that it breaks and the bubbles join to form a single bubble of their combined volume [30, 58-60]. Liao and Lucas [57] state that many investigations have shown that a minority of bubble collisions result in coalescence, with increasing bubble contact time and collision energy encouraging coalescence. Therefore coalescence is promoted by: significant contact time; a high gas void fraction (i.e. high volumetric proportion of gas to liquid); and differing interactions of gas entities with flow gradients (e.g. differing stream paths, wake effects, turbulent fluctuations) [57, 61].

Alternatively, breakup is the splitting of a gas void into two or more entities. This can occur due to: the impact of turbulent eddies; surface instabilities on the gas-liquid interface; solid particle impact; and other shearing forces [30, 61]. A gas entity will breakup when the hydrodynamic forces acting on it are greater than the restoring force of its surface tension [30].

2.2.2 Flow Regimes

Given sufficient residence time, the injected gas-phase is stabilised within the mixing chamber to form patterns in the two-phase flow. In order to quantify the internal two-phase flow, these patterns are typically classified into common groups based on their visual appearance, termed “flow regimes”. The standard flow regimes for vertical pipes are well described throughout two-phase flow literature and are depicted in Figure 2.12.

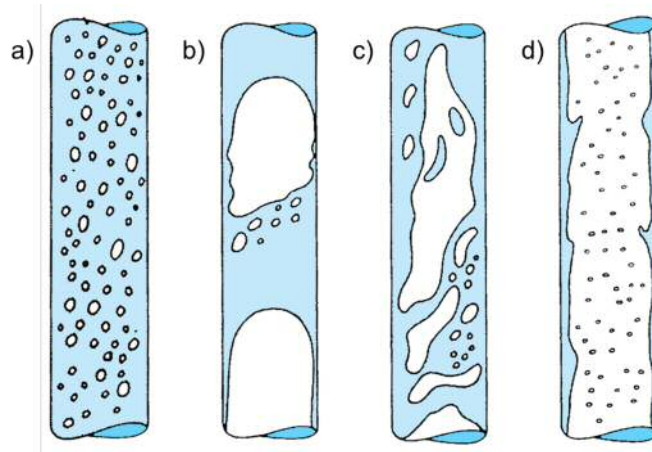


Figure 2.12 Standard gas-liquid two-phase flow regimes for vertical pipes:
a) bubbly flow; b) slug flow; c) churn flow; d) annular flow. [62]

Bubbly Flow

Bubbly flow (Figure 2.13) is characterised by approximately uniformly-sized bubbles in a liquid continuum, which are significantly smaller than the mixing chamber and well dispersed, thus mitigating coalescence [63, 64]. For a study in vertically downwards orientation, Usui and Sato [65] observed that bubbles tend to move towards the centre of the mixing chamber.

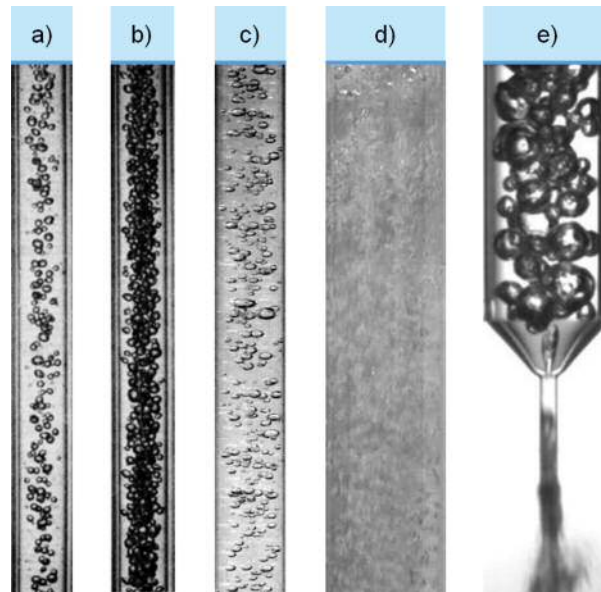


Figure 2.13 Example observations of bubbly flow in literature:

a,b) [65]; c) [66]; d) [64]; e) [44].

Slug Flow

Slug flow (Figure 2.14) is the presence of Taylor bubbles (i.e. hemi-spherical head and blunt tail end) with smooth gas-liquid interface in a liquid continuum and of similar size to the mixing chamber diameter [63, 64, 66]. These large bubbles, commonly termed “slugs”, are typically followed by a frothy wake of bubbles and are widely reported to be generated due to the coalescence of smaller bubbles [64, 65, 67]. As the probability of coalescence increases with bubble size [68], slug flow is thought to be instigated by the injection of sufficiently large gas entities at the aerator.

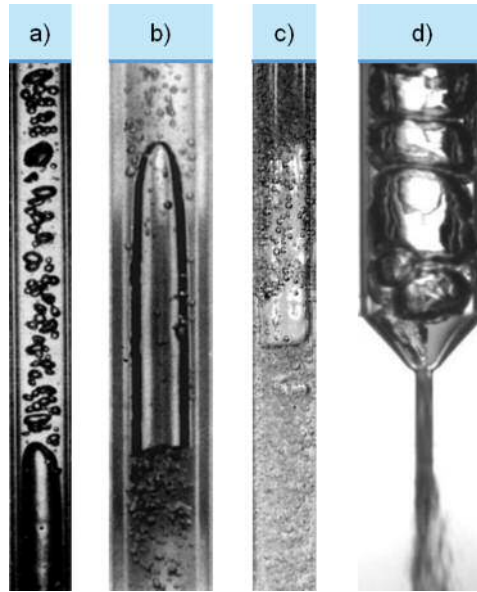


Figure 2.14 Example observations of slug flow in literature:

a) [65]; b) [63]; c) [66]; d) [44].

Churn Flow

Churn flow (Figure 2.15) is a chaotic and oscillating flow regime, featuring disintegrated gas slugs without a hemispherical head shape [64, 65]. The gas slugs are sufficiently large such that a peripheral liquid film is no longer constant and, therefore, neither phase can be considered continuous [64].

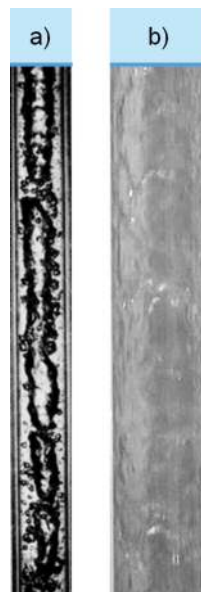


Figure 2.15 Example observations of churn flow in literature:

a) [65]; b) [64].

Annular Flow

Annular flow (Figure 2.16) is characterised by a liquid annulus about the mixing chamber periphery and a central gas core, where both liquid and gas phases are continuous [63, 64]. A small quantity of liquid entrainment may be present within the gas core due to shearing of the internal liquid-gas interface [63].

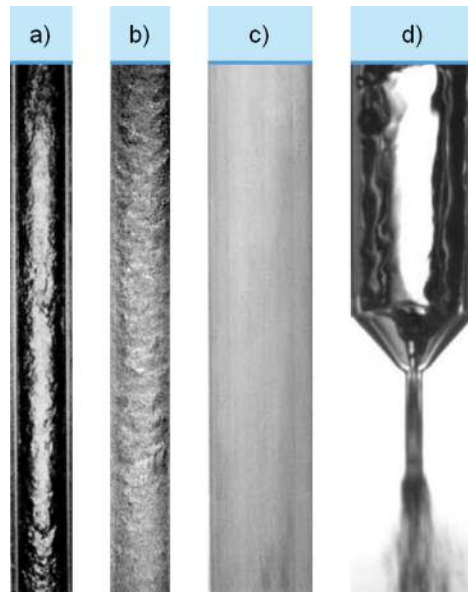


Figure 2.16 Example observations of annular flow in literature:
a) [65]; b) [66]; c) [64]; d) [44].

The transition between any flow regime is not immediate, but rather a gradual process, and therefore the determination of a given flow regime is inherently subjective – particularly in transitional cases. Furthermore, the definitions of these standard flow regimes are sufficiently vague to enable dramatically different internal flows to be grouped under the same flow regime. In order to report these subtle differences, researchers commonly define additional flow regimes to better describe their experimental results. In some cases, these have been transferred between studies – for example, Furukawa and Fukano [63] and Zhou [64] reported a transitional regime between the bubbly flow and slug flow termed bubbly-slug flow, which was defined as the onset of non-uniform bubble sizes prior to the formation of gas slugs through coalescence. In the extreme case, Zhou [64] reported 10 different two-phase flow regimes. It is clear that a compromise exists between categorising internal flow into a sufficient number of flow regimes to aid explanation of the research, whilst lessening the number of transitional regions required such that subjectivity is minimised.

It is also important to acknowledge the role of orientation on the two-phase flow regimes. Unlike vertical flow, in horizontal pipes both the action of buoyancy and gravity works normal to the flow direction. This encourages the separation of phases (i.e. stratified regimes) and, therefore, the flow regimes generated can be dramatically different in visual appearance to an equivalent vertically downwards flow [69, 70]. Phase separation can be prevented with sufficient liquid turbulence due to the bubbles inertial force overcoming the buoyancy effect [71] and, in this case, horizontal flow regimes are akin to the vertical flow regimes.

In any case, the internal two-phase flow regimes are known to vary with differing operating parameters, atomiser designs and fluid properties. Therefore, to quantify internal flow studies there is evidence within effervescent atomiser literature of researchers mapping identified flow regimes across the investigated parameters to produce so-called “flow maps” [20, 72, 73] – for example, Figure 2.17. These flow maps allow interpolation between test points and thus provide a measure of effervescent atomiser internal flow behaviour. However, when applied to an alternative study, care must be taken to ensure that the conditions used to produce the flow maps are representative of the experimental set up [29].

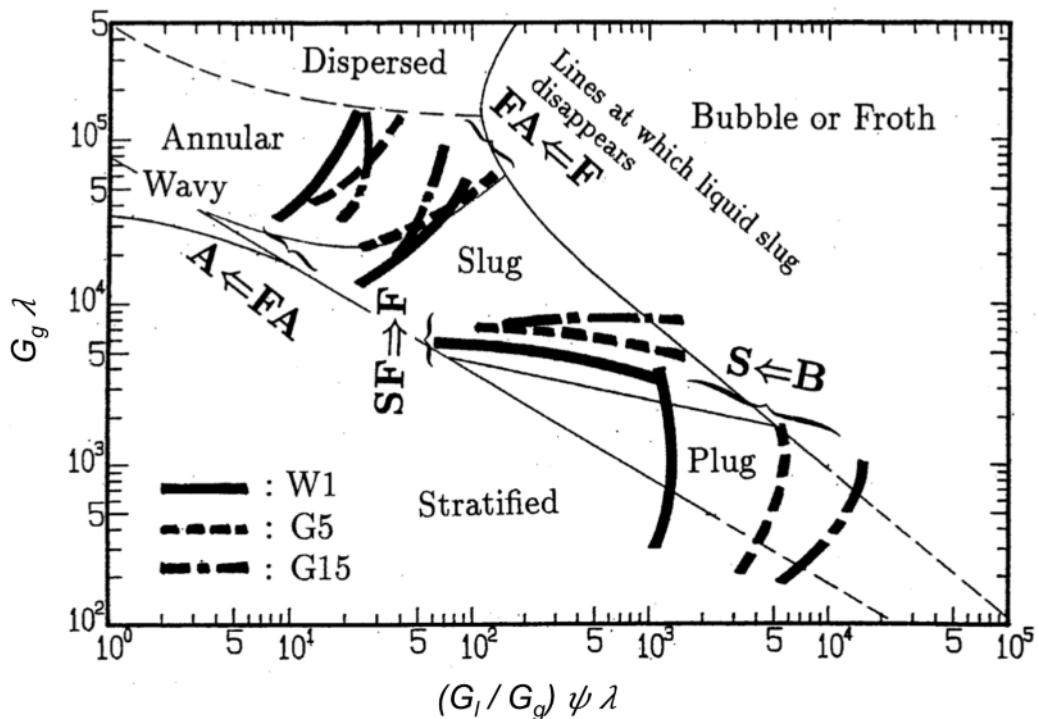


Figure 2.17 An example flow regime map for vertically upward flow. [63]

2.3 Effervescent Atomisation Mechanisms

This discussion concerns the theory of spray formation following the supply of an internal two-phase flow to the exit orifice. The purpose of the exit orifice is to create a restriction to the fluid flow through the atomiser and generate a sudden negative pressure differential due to the Venturi effect [12, 74]. The fundamental understanding of spray formation relies upon the concept that, if the destructive forces acting on the emerging two-phase flow (e.g. turbulence, gas-phase expansion, aerodynamic shear) are sufficient to overcome the restoring force of the surface tension and damping force of the viscosity, then the mass will be broken up into droplets [16].

2.3.1 Single-Phase Primary Atomisation

In a single-phase atomiser, the major destructive mechanism for spray formation is the turbulence of the liquid as it is discharged through the exit orifice. Several dimensionless parameters are cited by atomiser researchers to describe this turbulent break-up process.

Reynolds Number

The dimensionless Reynolds Number describes the velocity profile of an emerging liquid jet (Equation 2.4), where an increased Reynolds number indicates greater turbulence. A fully developed turbulent jet ($Re > 4000$) has greater susceptibility to breakup upon ejection from an orifice than a laminar jet ($Re < 2320$), as the transverse velocity components within the fluid layers (i.e. internal eddies and vortices) exert an internal turbulent force on the jet surface to form instabilities on the gas-liquid interface in a process termed velocity profile relaxation [12] – this aids break-up of the liquid-phase.

$$Re = \frac{\text{Inertia Forces}}{\text{Viscous Forces}} = \frac{\rho_l U_l d_{MC}}{\mu_l} = \frac{U_l d_{MC}}{\nu_l} \quad (2.4)$$

Weber Number

The dimensionless Weber number is a measure of the relative destructive forces applied to the liquid-phase compared to the restoring forces, where a large Weber

number represents greater jet breakup and the production of smaller droplets. For a single-phase atomiser, the destructive forces are generally a combination of: the external frictional force of ambient atmosphere on the emerging liquid-phase (described by the aerodynamic form Weber number, Equation 2.5) and the internal turbulent force (described by the hydrodynamic Weber number, Equation 2.6).

$$We_g = \frac{\text{Aerodynamic Force}}{\text{Restoring Force}} = \frac{\rho_g U_g^2 d_d}{\sigma_l} \quad (2.5)$$

$$We_t = \frac{\text{Turbulent Force}}{\text{Restoring Force}} = \frac{\rho_l U_l^2 d_d}{\sigma_l} \quad (2.6)$$

The critical conditions to generate jet breakup occur when the destructive forces are just enough to overcome the surface tension. This condition is characterised by critical Weber number (We_{crit}), below which breakup does not occur – for liquids with low viscosity (e.g. water) a typical critical Weber number is 9-13.

Ohnesorge Number

The susceptibility of a liquid jet to breakup under the applied disintegration mechanisms is termed stability and is described by the dimensionless Ohnesorge number (Equation 2.7) – where increasing the Ohnesorge number decreases the jet stability and increases its susceptibility to breakup.

$$Oh = \frac{\sqrt{We}}{Re} \quad (2.7)$$

The breakup response of an emerging liquid jet has been shown by researchers to vary with the Reynolds and Ohnesorge numbers (Figure 2.18), which generates differing qualities of spray. The optimal spray is generated at the highest Reynolds and Ohnesorge numbers, whereby the liquid core is shattered into droplets immediately upon ejection from the orifice in a process termed “primary atomisation”. Consequently, single-phase atomisers are reliant on high liquid velocities within the exit orifice to generate sufficient turbulence for primary atomisation to be instigated.

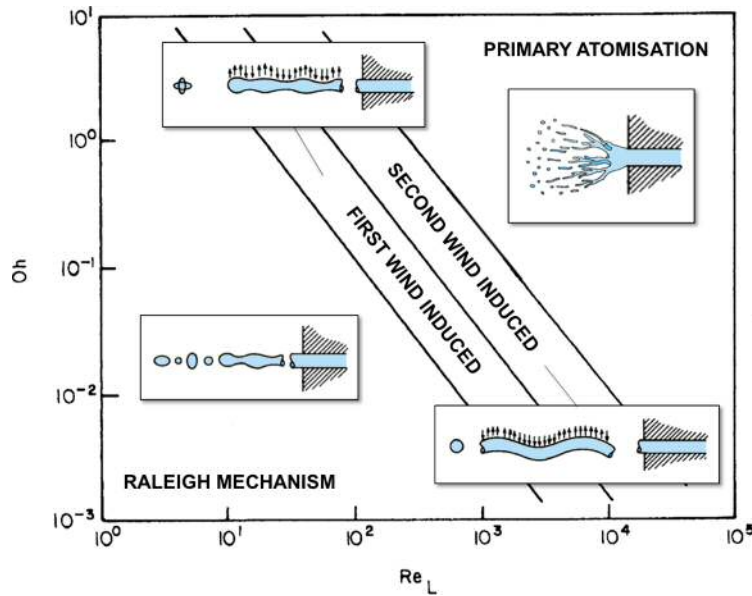


Figure 2.18 Conditions corresponding to the liquid jet breakup regimes. [12]

2.3.4 Two-Phase Primary Atomisation

For effervescent atomisation, a gas-phase is injected into the mixing chamber and, hence, a gas-liquid two-phase flow supplies the exit orifice. The presence of this gas-phase within the exit orifice generates further breakup mechanisms in addition to the single-phase atomisation mechanisms, which allows for forces external to the liquid to play a dominant role over turbulence [13, 75]. This reduces the dependency on high liquid velocities to generate primary atomisation [76] and allows for two-phase atomisers to have a wider operating range with greater turn-down ratios [19]. Therefore, in an effervescent atomiser, the purpose of gas-phase injection is to aid primary atomisation.

The process of two-phase atomisation is initiated by the supply of a two-phase flow to the exit orifice, where the sudden negative pressure differential causes the internal two-phase flow to be “sucked” towards the exit orifice. A photographic study by Catlin and Swithenbank [15] depicts the process for the extremes of internal flow (Figure 2.19). It was observed that individual bubbles taper and deform as they approach the exit orifice (Figure 2.19a), puncturing and expelling their gaseous contents through the nozzle and forcing the liquid-phase into a thin peripheral film. The bubble gradually deflates until it is small enough to pass through the nozzle, where it is succeeded by a period of liquid-phase until the next bubble attaches. This contrasts to an annular flow (Figure 2.19b), where the gas supply does not deflate and, hence, separating liquid ligaments are not present in the exit orifice.

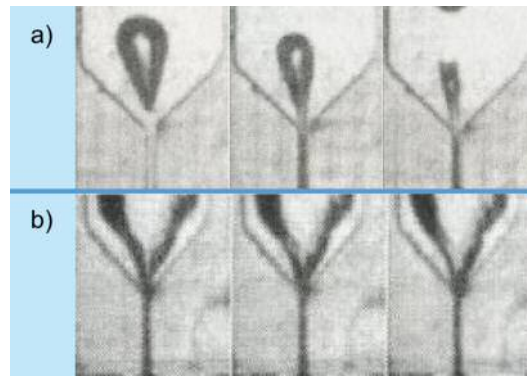


Figure 2.19 Internal flow supply to the exit orifice:
a) individual bubble, b) annular flow. [15]

Gas-Phase Disruption Mechanisms

The presence of the gas-phase within the exit orifice acts to restrict the available flow area for the liquid-phase [74]. This is further exacerbated due to the negative pressure differential across the nozzle, which causes the gas-phase to expand and further reduce the liquid flow area [16]. Consequently, the thin liquid film is less stable than an equivalent jet and more prone to breakup.

Furthermore, as the liquid-phase is forced to flow through a significantly reduced peripheral fraction of the exit orifice [10, 74], the liquid velocity is increased which intensifies the turbulent breakup mechanism (i.e. increased hydrodynamic Weber number). This results in premature choked flow conditions compared to a single-phase liquid supply [13, 14] which allows for sonic velocities to be more easily achieved through the nozzle with lower input energy – Chawla [76], cited in Sovani et al. [74], reported that the sonic velocity of a water/air mixture is 20-30 m/s, whereas independently water and air have sonic velocity 300 and 1500 m/s respectively.

Therefore, the gas-phase disruption has the benefit of increasing the efficiency of the atomiser [12, 77], where the droplet size produced is reported to be proportional to the square root of the liquid annulus thickness in the exit orifice [10, 29]. However, as bubbles smaller than the exit orifice pass through the exit orifice with minimal flow disturbance, only certain internal flow conditions contribute to reduced nozzle chocking [16, 41].

Gas-Phase Expansion Mechanisms

The pressure drop across the exit orifice causes the gas-phase to rapidly expand, generating additional break-up mechanisms on the liquid-phase (i.e. increased aerodynamic Weber number). Two discrete gas-phase expansion mechanisms have been reported in the literature [20, 67, 78-80], with the contribution of each, and hence the properties of spray produced, greatly affected by the two-phase flow regime supplying the exit orifice (Figure 2.20) [19, 20, 56].

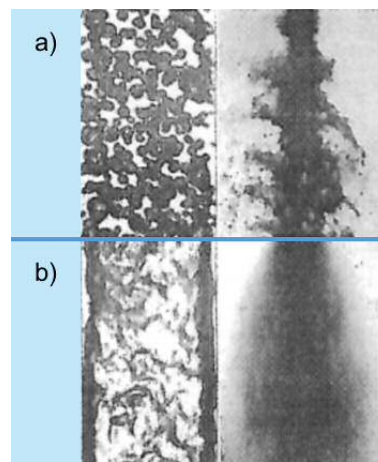


Figure 2.20 Internal flow and near-nozzle observations of:
a) bubbly flow; b) annular flow. [20]

In annular flow, an uninterrupted gas-phase is supplied to the exit orifice. In this case, liquid atomisation is aided by the continuous aerodynamic shearing effect of the expanding gas-phase upon ejection from the exit orifice – this process is termed “tree regime atomisation” (Figure 2.21b) [20, 74, 78, 79]. Certain conditions have been reported to generate a thinner liquid annulus within the nozzle (e.g. increased ALR, decreased operating pressure), which has the effect of decreasing the “trunk” length and generating greater liquid breakup [78]. This compares to bubbly flow, which has the addition of an intermittent liquid-phase separating successive gaseous elements. The rapidly expanding gas upon ejection from the exit orifice has the effect of rupturing of the separating liquid-phase, in a non-continuous, explosion-like event termed “single bubble atomisation” (Figure 2.21a) [15, 20, 78, 79].

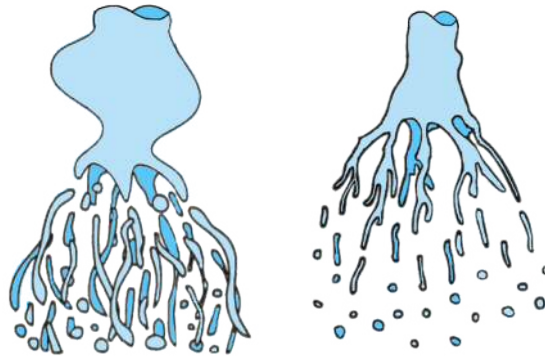


Figure 2.21 Two-phase primary atomisation mechanisms:

a) Single bubble atomisation; b) Tree regime atomisation. [78, 79]

Consequently, the internal two-phase flow regime supplying the exit orifice has a significant effect on the two-phase atomisation processes and hence the spray stability [19, 20, 27, 44, 81, 82]. An unstable spray is undesirable for the majority of considered applications, due to the generation of fluctuating spray properties – this causes a greater range of droplet sizes, whereby fine droplets alternate with the formation of larger ligaments [83]. This can cause unwanted combustion characteristics (e.g. combustion instability, droplet clustering, noise and pollution) [11, 25-27].

The atomisation mechanism for annular flow is a continuous tree regime atomisation, which results in the generation of stable spray [72, 82, 84]. The only spray instability mechanism reported within annular flow was due to variations in the thickness of the internal liquid film created by aerodynamic effects on the internal gas-liquid interface generating Kelvin-Holtzman instabilities [15]. However, when operating in annular flow, an effervescent atomiser behaves akin to an air assist or air blast atomiser and hence adopts its weaknesses [19, 29] – including inefficient use of the atomising gas.

Unlike these alternative two-phase techniques, gas injection in effervescent atomisation is not designed to directly instigate liquid breakup due to the transfer of kinetic energy [29], but rather to generate a bubbly flow to supply the exit orifice [28, 29]. It is widely accepted across the literature that operation within bubbly flow exhibits the most efficient atomisation considering the input energy [23, 67, 80, 83, 85], with numerous bubble expansion energy correlations having been cited in the literature (§A2.4). However, due to the discontinuous nature of single bubble atomisation [15, 20, 72], spray instability is widely reported to be greater compared to annular flow [25, 26, 78]. This disagrees with the findings of Liu et al. [27], who reported greater stability in the bubbly flow regime. Spray stability in bubbly flow can be improved by increasing the homogeneity of the bubbly flow (i.e. increasing the

number of small bubbles) [13, 17, 19, 29, 56, 81, 86] – however a lower limit is reported to exist, where bubbles smaller than the exit orifice play a negligible role in the atomisation process [41].

Operation in a heterogeneous regime (i.e. slug flow, churn flow) produces a highly unstable pulsating spray due to alternating atomisation modes [15, 21, 25, 26, 72, 82, 84, 87-89] – this is considered undesirable for the vast majority of applications.

Additionally, the spread of the spray (i.e. spray cone angle) has been reported to vary with the internal flow regime, increasing with the bubble size in bubbly flow [17], before plateauing in the slug flow region and decreasing in the annular flow regime [90, 91].

2.3.2 Secondary Atomisation

Although initial droplet formation through primary atomisation is hugely influential to the properties of spray produced, the subsequent interaction of the droplets within the discharge atmosphere can also have a significant effect.

“Secondary atomisation” is the further disintegration of ligaments and droplets formed during the primary atomisation process due to the application of external aerodynamic forces in the ambient atmosphere [12]. The secondary atomisation modes are shown in order of increasing aerodynamic Weber number in Figure 2.22. Droplet breakup will continually occur downstream of the near-nozzle section until the consolidating surface tension is great enough relative to the destructive forces to prevent breakup, assuming sufficient residence time.

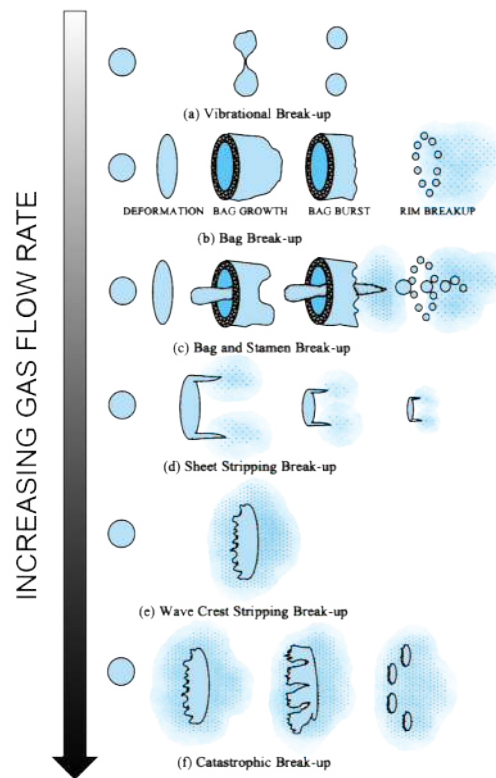


Figure 2.22 Secondary atomisation modes. [92]

In a dense spray, droplets often collide with one another. Given enough collision energy, they may coalesce or repel each other. Kay [92] categorised these interactions into five distinct regimes, as shown in Figure 2.23. Droplet interaction is encouraged by high spray densities and can significantly affect the spray quality, due to an increase in droplet size.

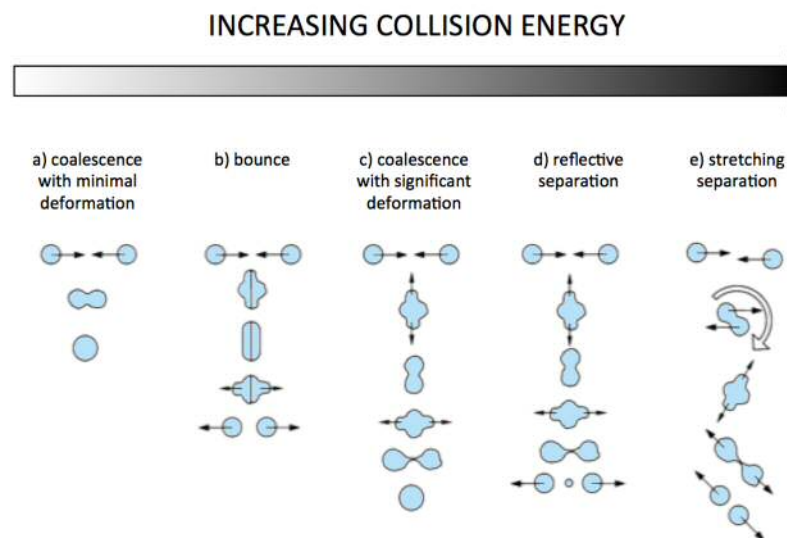


Figure 2.23 Droplet interaction modes. [92]

Droplet evaporation is an important consideration of combustion systems. It is encouraged by high surface area to volume ratios (i.e. small spherical droplets), high temperatures and low atmospheric saturation. However, under ambient conditions (i.e. low temperatures) such as the experimental conditions in the present research, the evaporation process requires significant residence time and, therefore, is not expected to affect the present research.

2.4 Dependent Parameters of Effervescent Atomiser Literature

A thorough survey of the effervescent atomisation literature was performed to identify areas of weakness within the knowledge of the scientific community, with the range of parameters for each publication tabulated in Appendix 2. The aim of the current work is to further the understanding in these areas.

Generally, the aim of effervescent atomisation is to optimise the quality of spray (e.g. smallest droplet size, most stable spray and lowest droplet velocities) with minimum resource (e.g. air supply, operating pressure, weight, cost). The dependent parameters within the effervescent atomisation literature provide a measure of performance and thus allow comparison between investigations. Whilst some of these dependent parameters generate qualitative outcomes (e.g. internal flow determination, near nozzle spray structure), the majority can be quantified with measurement (e.g. bubble size, droplet SMD and velocity). The majority of these dependent parameters have been shown to vary with the independent parameters and some researchers present correlations to describe these relationships (§A2.4).

2.4.1 Effervescent Atomiser Characterisation

As previously discussed, the internal flow is known to have a significant effect on the atomisation mechanisms, where a bubbly flow is a prerequisite for effervescent atomisation [28, 29]. Consequently, it is common within the literature for the internal flow to be investigated as a dependent parameter, usually in relation to an independent parameter (e.g. liquid flow rate, ALR, operating pressure etc.). In most of these cases, the results were quantified by categorising the internal flow behaviour into flow regimes [15, 20, 21, 44, 55, 56, 72, 73, 82, 84, 86-88, 93, 94], with some researchers extending this analysis to produce flow maps [20, 72, 73, 84, 88, 94]. Commonly, published flow maps are referenced between studies as a technique to predict the flow regimes in effervescent atomisers where internal flow measurement may not be possible [19, 56, 73, 93, 95-98]. However, in many cases, the

flow maps used originate from alternative research fields and, therefore, the conditions could be unrepresentative of an effervescent atomiser (e.g. long residence time) – consequently, their reliability for predicting effervescent atomiser internal flow regime could be questioned [29].

The study of the gas injection processes at the aerator is a severely under researched area in effervescent atomisation. Jobehdar [44] performed a basic qualitative assessment of bubble formation at the aerator for an effervescent atomiser, in which only the aerator hole spacing was varied. Sen et al. [41] observed the effects of downstream events on bubble formation at the aerator, but their investigation was limited to a sparse bubbly flow and featured an unrepresentative atomiser design for real-world application (i.e. square cross-section mixing chamber, 1.12 m mixing length, 0.017% ALR). However, no researcher has identified the gas injection regimes at the aerator and, therefore, the relationship between the gas injection regimes at the aerator and the flow regime generated within the mixing chamber has not been established – this restricts comparability between aerator studies in alternative research fields (e.g. nuclear, waste treatment) and effervescent atomisation. Consequently, the fundamental understanding of the independent parameters throughout the effervescent atomiser is incomplete.

The quantification of bubble size is uncommon in effervescent atomisation literature, potentially due to concerns that refraction through a conventional cylindrical atomiser would affect the accuracy of the results and also the difficulties associated with artefact recognition within imaged results. Therefore, of the numerous internal flow studies, only four of the surveyed studies have quantified bubble size [17, 44, 56, 86], in which a large difference in bubble sizes are referenced (0.27-10 mm) – of these studies, only Jobehdar [44] replicates a conventional cylindrical mixing chamber with passive refraction elimination. Rahman et al. [56] and Gomez [86] furthered this work by relating bubbles size to the droplet sizes produced, with both reporting a reduction in droplet size for a decreasing bubble size.

An atomiser is typically required to spray a predetermined liquid mass flow, which is a function of multiple independent parameters and the discharge coefficient (Equation 2.8). The discharge coefficient is the ratio of the actual mass flow rate to the ideal mass flow rate through the exit orifice [99], which is widely reported to vary with the independent parameters [10, 19, 28, 77, 83, 99-103] – notably, it is seen to decrease as gas is added to the two-phase system [10, 19, 28, 83, 99-103], due to gas-phase disruption. There is a large range of discharge coefficients reported in the literature (0.05-1.0), reflecting the wide array

of test conditions undertaken by researchers, and multiple correlations are proposed within the literature (§A2.4).

$$\dot{m}_l = C_d A_o \sqrt{2\rho_l P_{op}} \quad (\text{kg s}^{-1}) \quad (2.8)$$

2.4.2 Spray Characterisation

The near nozzle spray structure is commonly studied in effervescent atomisation literature [11, 15, 17, 20, 56, 73, 81, 88, 93, 94, 104-112] to examine the spray stability, atomisation mechanisms and spray cone half-angle. The spray cone half-angle (i.e. the angle generated between the spray edge and the exit orifice axial centreline) gives a measure of the spread of spray, where a large spray cone half-angle is generally preferred in combustion as it offers a wider spread of fuel and shortened combustion length [113] – the spray cone half-angles range from 6-27° in the literature, with an average value of 16°. The spray cone half-angle can also be determined from droplet data [16, 114] – Konstantinov [16] and Jedelsky et al. [114] report the edge of the spray can be considered to occur when droplet data rates reach 10% of the maximal value at that axial location, although Jedelsky et al. [114] also references a more restrictive case using 25% of the maximal value.

Spray instability is the generation of fluctuating atomisation properties, where fine droplets alternate with larger ligaments to increase the range of droplet sizes [83]. An unstable spray is undesirable for the majority of applications – in particular combustion, where it can cause unwanted combustion characteristics (e.g. combustion instability, droplet clustering, noise and pollution) [11, 25-27]. Effervescent sprays are inherently unstable compared to alternative atomisation techniques, due the chaotic nature of the two-phase atomisation mechanisms, which leads to a greater variations in droplet size [26, 93, 111]. Droplet sizes also vary at different positions within the spray (i.e. radial/axial locations), where effervescent atomisers produce a greater proportion of large droplets: (i) in the near nozzle region [93, 111, 115], likely due to insufficient residence time for secondary atomisation to take effect; and (ii) at the spray periphery, as the droplet momentum due to the expanding gas carries the larger droplets away from the nozzle axis [16, 24, 27, 86, 95] and air entrainment encourages small droplets to the spray centreline [111]. Therefore, effervescent atomisers typically exhibit a bell-shaped droplet size distribution (Figure 2.24a).

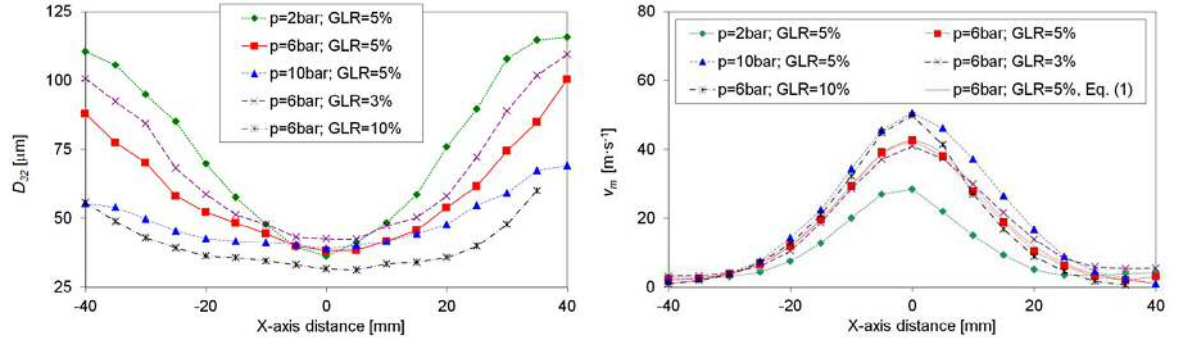


Figure 2.24 Typical effervescent atomiser: a) droplet size and b) velocity distribution.

Measurements taken 152 mm from exit orifice. Spray centreline at 0 mm X-axis distance.

[95]

Whilst droplet distributions give a description of the range of droplet sizes within the spray, it is extremely useful to define an average droplet size in order to quickly and efficiently compare between studies. Typically, effervescent atomisation literature averages the droplet size using the Sauter mean diameter (i.e. SMD, D_{32} ; Equation 2.9), which is defined as the average ratio between the volume and the surface area of droplets in the spray and is highly sensitive to large particles. Figure 2.25 shows the range of droplet SMDs referenced within effervescent atomisation literature. In addition, some researchers use the Arithmetic mean diameter (i.e. AMD, D_{10} ; Equation 2.10), in particular for the measurement of internal flow artefacts.

$$D_{32} = \frac{\sum n_{d,i} d_{d,i}^3}{\sum n_{d,i} d_{d,i}^2} \quad (\text{m}) \quad (2.9)$$

$$D_{10} = \frac{\sum n_{d,i} d_{d,i}}{\sum n_{d,i}} \quad (\text{m}) \quad (2.10)$$

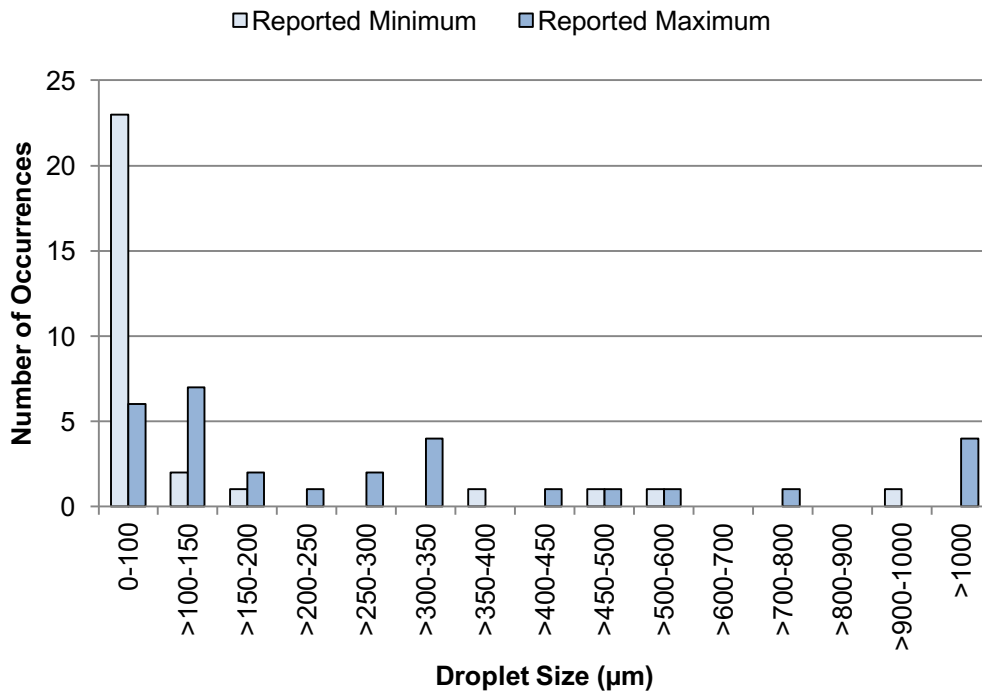


Figure 2.25 Distribution of droplet SMDs reported in effervescent atomiser literature. (SMD_{min} = 2 µm; SMD_{max} = 9000 µm; SMD_{min,med} = 35 µm; SMD_{min,mean} = 123 µm)

Droplet velocity is an additional measure of atomisation performance where, in general, a minimised droplet velocity is preferred – this applies in particular for combustion atomisers, as low droplet velocities promote burnout and enable shorter combustors that reduce capital costs. A typical effervescent atomiser droplet velocity profile is bell-shaped (Figure 2.24b), where droplets on the periphery have lower velocity due to drag of ambient air exposure [86, 95, 114, 116, 117]. Droplet velocity is widely reported to reduce with axial displacement [116, 118], thought to be due to the drag effect of the ambient atmosphere. The droplet velocities referenced within effervescent atomisation are shown in Figure 2.26.

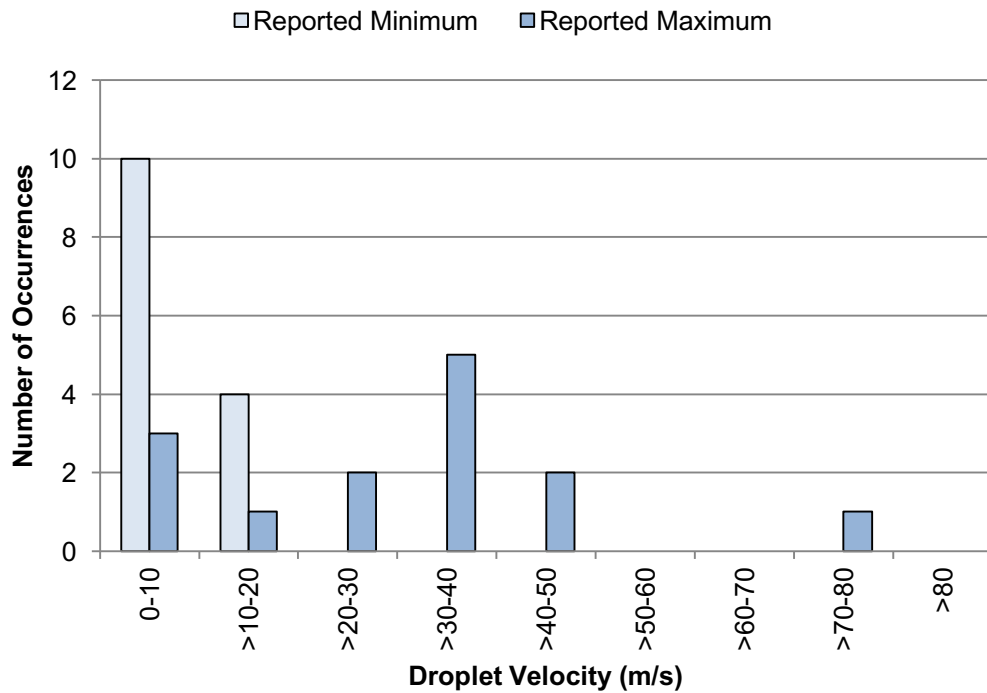


Figure 2.26 Distribution of droplet velocities reported in effervescent atomiser literature.

($Vel_{min} = 0$ m/s; $Vel_{max} = 80$ m/s; $Vel_{max,med} = 36$ m/s; $Vel_{max,mean} = 32$ m/s)

2.4.3 Others

There are numerous other dependent parameters, which lie beyond the scope of the current investigation – for example: combustion testing [119-123], atomiser efficiency [13, 22, 73, 108, 110], patternation [107, 124-127], gas entrainment [16, 111, 128] and spray momentum rate [116, 128, 129].

2.5 Independent Parameters of Effervescent Atomiser Literature

Figure 2.27 shows the distribution of the independent parameters investigated in the effervescent atomisation literature, which are assessed against the dependent parameters to determine their effect on effervescent atomisation performance.

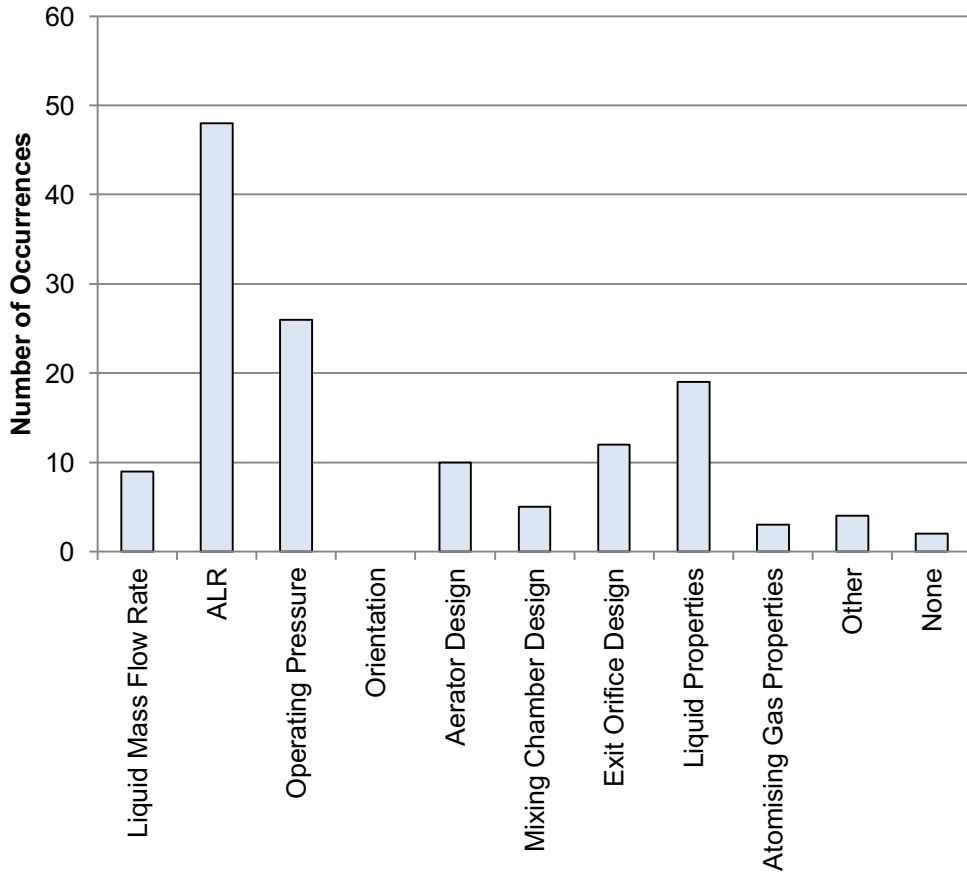


Figure 2.27 Distribution of independent parameters reported in effervescent atomiser literature.

2.5.1 Effect of Fluid Flow Rates, including Air-to-Liquid Ratio

There are a wide range of liquid mass flow rates referenced within effervescent atomisation literature (Figure 2.28). This variation is to be expected, as atomisers are typically designed to spray a predetermined liquid mass flow rate depending on their application [28] – for example, the liquid mass flow rate requirement for an effervescent atomiser intended for fuel injection would be significantly lower than for fire suppression. In addition, since the liquid mass flow rate is a function of various parameters (Equation 2.8), it is generally seen to vary with changes to alternative variables – for example, for a given experimental configuration (i.e. controlled atomiser design, fluid properties and operating pressure), the liquid mass flow rate will decrease with the additional of gas flow.

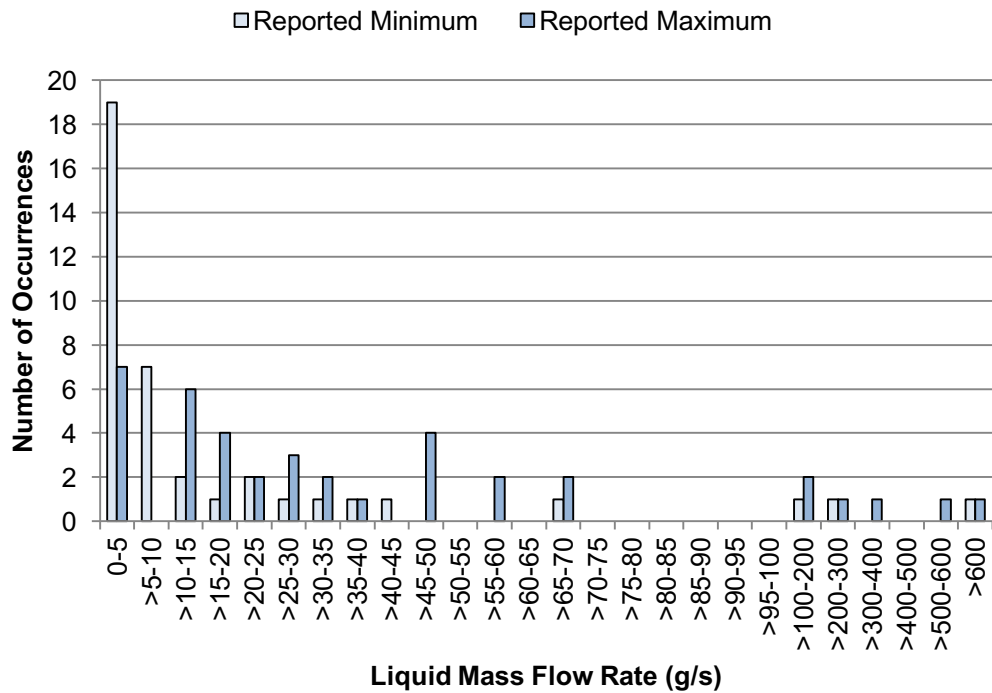


Figure 2.28 Distribution of liquid mass flow rate reported in effervescent atomiser literature.

$$(\dot{m}_{l_{\min}} = 0.2 \text{ g/s}; \dot{m}_{l_{\max}} = 3333 \text{ g/s}; \dot{m}_{l_{\max, \text{med}}} = 25 \text{ g/s}; \dot{m}_{l_{\max, \text{mean}}} = 144 \text{ g/s})$$

To aid comparison between dissimilar studies, researchers commonly reference the mass ratio of the input gas to liquid flow rates, termed the Air-to-Liquid Ratio (ALR). There is consensus across the literature that the ALR has a significant effect on effervescent atomisation [19, 23, 28, 29, 67, 77, 79, 116, 117, 130], affecting both the internal flow and spray quality. Consequently, it is the most common independent parameter examined throughout the literature (Figure 2.27). In almost all of these cases, effervescent atomiser performance is examined at low ALR values in the region of 0-5% and increased to an arbitrary maximum value (Figure 2.29).

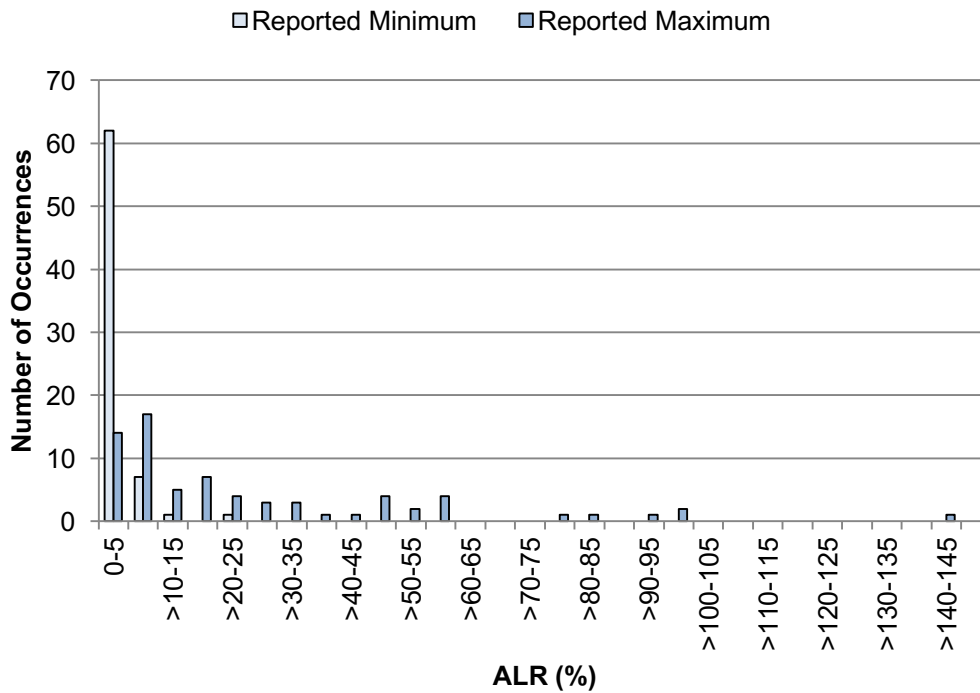


Figure 2.29 Distribution of air-to-liquid ratio reported in effervescent atomiser literature.

($ALR_{min} = 0\%$; $ALR_{max} = 141\%$; $ALR_{max,med} = 15\%$; $ALR_{max,mean} = 27\%$)

The effervescent atomiser literature does not allow a direct correlation to be made between the ALR and the gas-injection regimes at the aerator. However, the response to an increasing ALR can be predicted by considering the previously presented research from alternative scientific fields. It has been discussed that the gas flow rate has a significant effect on the bubbling regime observed at the aerator, where increasing the gas flow rate increases the bubble size and formation frequency and transitions the gas injection phenomena from bubbling to jetting regimes. Similarly, a decrease in liquid flow rate (i.e. liquid velocity) reduces the viscous forces acting on a forming bubble, generating larger bubbles at a reduced frequency. Therefore, increasing the ALR is expected to progressively enlarge the injected bubbles and prompt the transition from bubbling towards jetting gas-injection regimes.

Despite the notable lack of research at the aerator, the effect of ALR on the internal flow regimes within the mixing chamber has been well evidenced within effervescent atomisation literature. Increasing the ALR is widely reported to transition the internal flow regime from bubbly flow, to intermittent regimes (e.g. slug flow, churn flow), and finally to annular flow [29, 44, 72, 84, 85]. Generally, low ALRs are associated with small, discrete bubbles in the mixing chamber (i.e. bubbly flow) [67, 72]. The bubble size and/or number is observed to increase with ALR [29, 44, 85] and hence the frequency of bubble coalescence increases,

eventually forming large gas slugs in the flow and instigating formation of intermittent flow regimes (e.g. slug flow, churn flow). This corresponds to experimental studies that report increased instability at 2% ALR [78], 3% ALR [93] and 5% ALR [82, 106], which is thought to represent the critical ALRs at which transition between bubbly flow and slug flow occurs. At high ALRs, the internal flow transitions to a fully annular flow [56, 72] – this is reported to occur between 5% ALR [78, 82, 106] and 10% ALR [109], with diminishing effects of ALR above 20% ALR [13]. As a result of these differing internal flow regimes, the gas-phase expansion mechanisms have also been shown to vary from single bubbling to tree regime with increasing ALR [15, 20], which corresponds with a decrease in atomiser efficiency [13, 73].

This two-phase flow is then supplied to the exit orifice, where the presence of a gas-phase restricts the liquid flow area – the addition of further gas promotes this restriction and, hence, the coefficient of discharge is reported to decay with an increasing ALR [10, 19, 28, 83, 99-103]. Hence, increasing the atomising gas flow rate to achieve atomiser turndown is most effective at low ALRs.

It is unanimously agreed across the literature that the droplet SMD decreases with increasing ALR [10, 13, 15, 16, 19, 20, 22, 23, 44, 72, 83, 86, 96, 104, 105, 112, 115, 131, 132], particularly in the spray centreline [19, 86] (Figure 2.30). An increase in ALR acts to reduce the liquid film thickness in the exit orifice, as a greater proportion of the nozzle area is occupied by gas – as the droplet size produced is proportional to the square root of the liquid film thickness in the exit orifice [10], the droplet SMD decreases. An increased ALR also increases the volumetric expansion of the emerging two-phase flow and, therefore, the droplet velocity increases [44, 72, 114, 116, 133] and the spray cone half-angle widens [11, 17, 90, 127, 134].

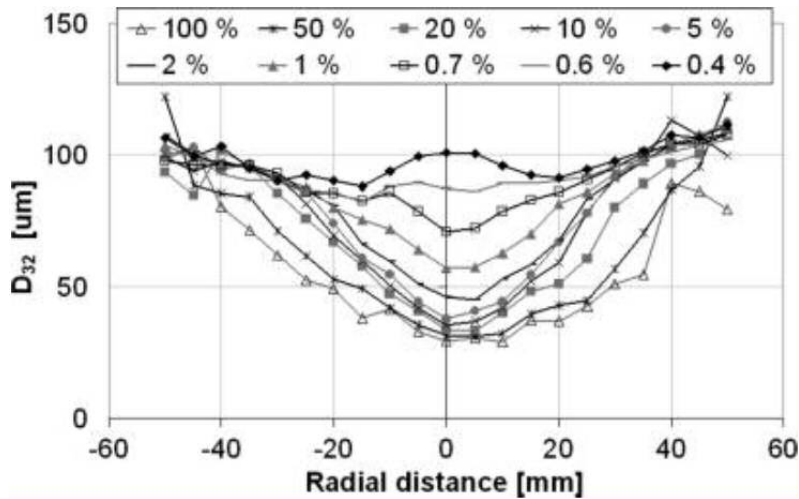


Figure 2.30 The effect of ALR on the spray radial profile. Measurements taken 150 mm from exit orifice [19]

Jedelsky et al. [19] and Ghaemi et al. [81] reported that increased internal flow homogeneity decreased the droplet SMD for equivalent conditions (e.g. ALR, operating pressure). However, alternative evidence suggests that the effect of the internal flow regime has a relatively minor effect on the average droplets size compared to the ALR. Firstly, the droplet SMD is seen to decrease in a smooth decaying profile with increasing ALR, irrespective of the internal flow regime (Figure 2.31) [74, 85, 135]. This is further supported by an ACLR (Air-Core-Liquid-Ring) atomiser investigation by [87] in which it was proven that, despite the constant supply of annular flow throughout the experimentation, the atomiser displayed similar droplet SMD to a conventional effervescent atomiser. Regardless, the supply of a homogenous internal flow to the exit orifice is agreed across the literature to be beneficial for effervescent atomisation.

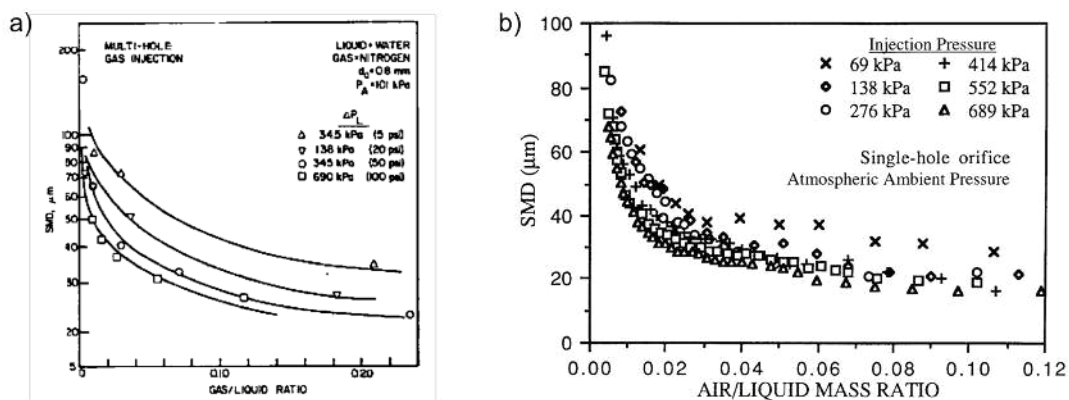


Figure 2.31 The effect of ALR and operating pressure on spray SMD: a) [10]; b) [74].

Consequently, to optimise effervescent atomisation, the ALR should be maximised whilst maintaining internal flow homogeneity. Numerous researchers present correlations for the maximum ALR to maintain a bubbly flow (§A2.4), which is considered to represent the case of optimal effervescent atomisation, beyond which transition to intermittent regimes occurs. Internal flow homogeneity, and hence atomisation performance, can be improved for a given ALR by increasing the number of small bubbles supplying the exit orifice [44, 56, 72, 81, 86]. However a lower limit exists, where bubbles smaller than the exit orifice are reported to play a negligible role in the atomisation process [41] – consequently, numerous investigations have revealed poor atomisation performance at very low ALRs ($\sim < 2\%$) [13, 16, 67, 77, 117, 136]. Numerous optimal bubble size correlations have been cited in the literature (§A2.4).

2.5.2 Effect of Operating Pressure

The “differential pressure” is the difference between the pressure formed in the mixing chamber due to the input of fluids (i.e. “operating pressure”) and the injection atmosphere (i.e. “ambient pressure”). It is unusual for the ambient pressure to be controlled, with the majority of research being performed at atmospheric pressure (i.e. 0 bar_g) – for this reason, the differential pressure and operating pressure are generally equal. The operating pressure is often limited by operational practicalities (e.g. increased weight and cost of system, parasitic losses, sealing difficulties) [11], and therefore the maximum operating pressure is usually known from the outset of atomiser design [28].

The operating pressure is controlled by varying the injection pressure of either fluid and is a common independent variable within effervescent atomiser studies (Figure 2.27). The distribution of investigated operating pressures within the literature (Figure 2.32) demonstrate that effervescent atomisers are typically operated at much lower pressures than alternative techniques – the median value of the reports surveyed is just 5 bar_g, which compares to an arbitrary pressure swirl atomiser for direct gasoline injection at 50 bar [137]. There are, however, some effervescent atomiser studies conducted at comparably high operating pressures, for example Sovani et al. [11] at 365 bar_g and Sovani et al. [106] at 289 bar_g. The effect of increasing the operating pressure has been shown to positively affect both the internal flow and atomisation performance of an effervescent atomiser [29, 74, 130], although some researchers report this effect is minor compared to the ALR [19, 23].

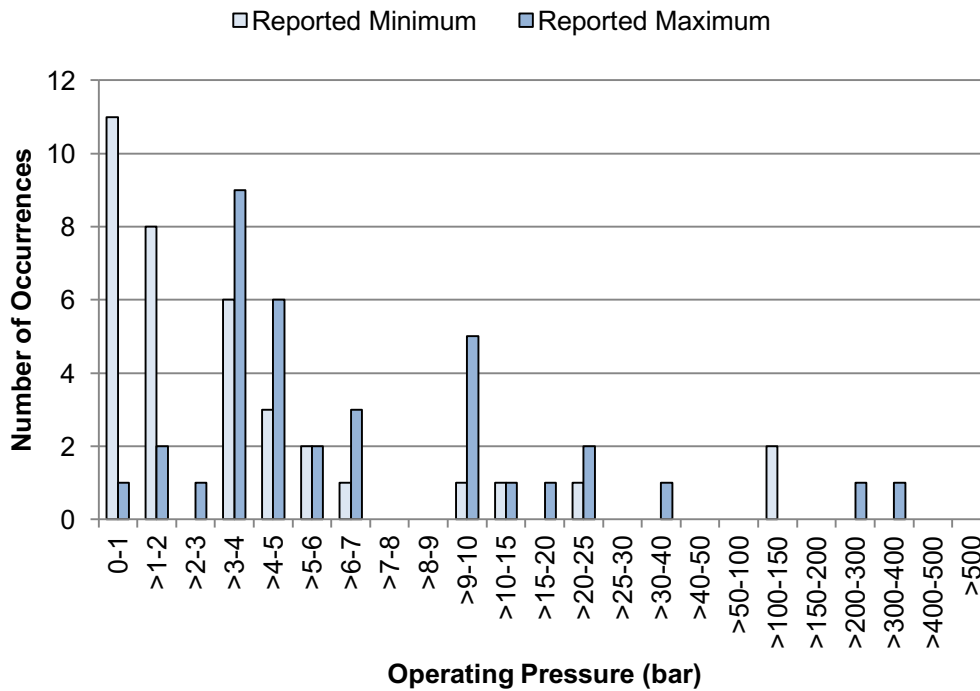


Figure 2.32 Distribution of operating pressure reported in effervescent atomiser literature.

$$(P_{\min} = 0.03 \text{ bar}_g; P_{\max} = 365 \text{ bar}_g; P_{\max, \text{med}} = 5 \text{ bar}_g; P_{\max, \text{mean}} = 25 \text{ bar}_g)$$

Increasing the operating pressure has been shown to have a favourable effect on the internal flow for effervescent atomisation. Firstly, a greater operating pressure acts to increase the liquid mass flow rate through the atomiser (Equation 2.8), which promotes bubbling at the aerator due to an increased liquid cross-flow velocity and turbulent bubble breakup in the mixing chamber [10]. In addition, greater operating pressures compress the gas-phase – this results in a decreased bubble size (Figure 2.33) [56], with a reduced chance of collision and hence suppressed coalescence [30]. Consequently, the range of ALRs over which bubbly flow can be maintained is increased with greater operating pressures [85].

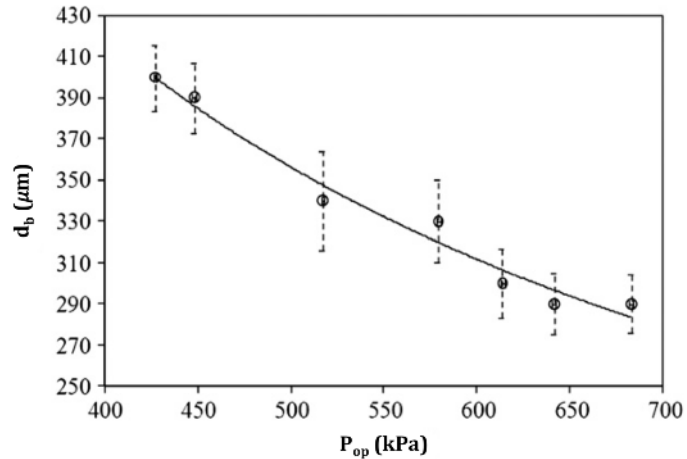


Figure 2.33 Effect of operating pressures on bubble size. [56]

Increasing the operating pressure also promotes improved atomisation due to a greater two-phase atomisation intensity [13] – this is generally reported to result in decreased droplet size [10, 13, 16, 19, 23, 67, 72, 77, 83, 126, 127, 130, 131, 134, 138, 139], increased droplet velocity [114, 116, 133] and increased spray cone angle [11, 90, 127, 134]. However, some researchers report that operating pressure has an insignificant effect [20], particularly for high viscosity liquids [79, 104, 139, 140] and above certain ALRs thought to correspond to the annular flow regime – for example, >20% ALR [13], >15% ALR [141].

The correlations within the literature appear to dispute the effect of operating pressure on the coefficient of discharge. Whilst some researchers report that the coefficient of discharge reduces with operating pressure [10, 19, 77], contradictory evidence reports an increase in coefficient of discharge [28]. This disagreement could be instigated due to the effect of operating pressure on fluid rheology.

2.5.3 Effect of Orientation

The orientation of an effervescent atomiser is heavily dependent on the application – for example, fire suppression atomisers are likely to be operated vertically downwards, whereas floor fired combustion atomisers are operated vertically upwards. However, of the literature surveyed, none investigate orientation as an independent variable (Figure 2.27). The majority of experimental studies investigate effervescent atomiser performance in a vertically downwards orientation (Figure 2.34), which is thought to be preferred due to the increased practicality of spray extraction (i.e. gravity aiding the removal of droplets away from exit orifice). Operation in horizontal orientation forms a minority of studies, with some

researchers investigating other angles of orientation relevant to a specific application. Interestingly, of the literature surveyed, none investigate vertically upwards atomisation.

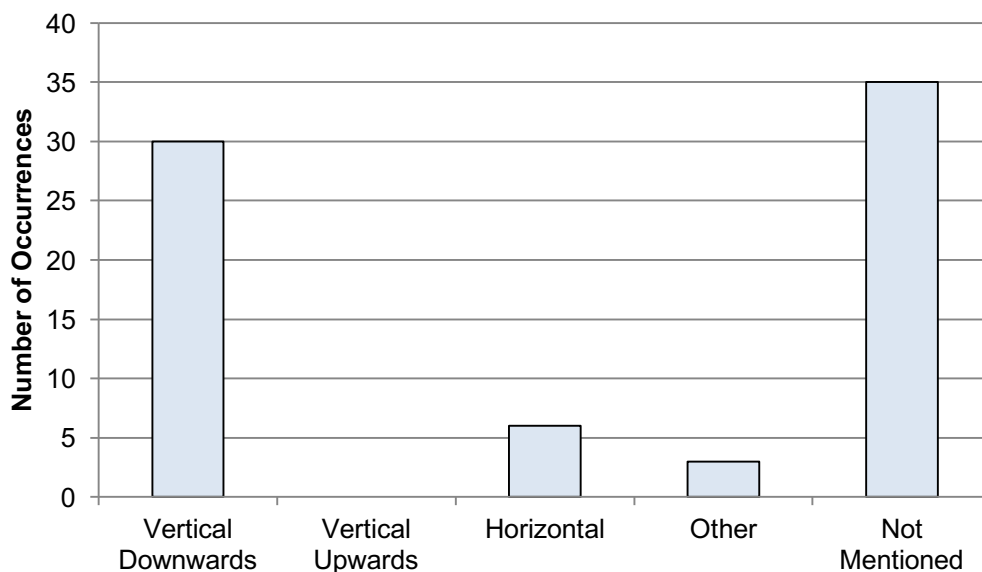


Figure 2.34 Distribution of orientation reported in effervescent atomiser literature.

In the absence of literature to inform on the effect of orientation on effervescent atomisation, assumptions are drawn from alternative research. As previously discussed, orientation is known to affect gas-liquid two-phase flow behaviour, due to the action of buoyancy on gas-phase injection and flow stabilisation processes, and therefore the flow regime for a given atomiser and operating parameters can vary with orientation – for example, formation of stratified flow regimes (i.e. heterogeneous flows) at a critical horizontal angle of orientation. As effervescent atomisation has been shown to vary with the internal flow regime, the atomiser orientation is expected to affect the quality of spray produced, particularly if the superficial flow velocity is not sufficient to prevent phase separation.

2.5.4 Effect of Aerator Design

The purpose of an effervescent atomiser aerator is to inject the gas-phase into the liquid-phase to form dispersed, uniformly sized bubbles and hence generate a homogenous bubbly flow. There are many elements of aerator design (e.g. atomiser configuration, aeration area, orifice diameter) that could affect the internal flow and subsequent atomisation performance and, therefore, there have been many reports considering elements of aerator design as an independent variable (Figure 2.27). Aerator design is considered to have a relatively minor

effect on effervescent atomiser performance in comparison to other parameters (e.g. ALR and operating pressure) [19, 77, 130], however its effects have only been assessed by identifying the flow regimes formed in the mixing chamber and by analysing the spray quality – the effect of aerator design on the gas-injection processes at the aerator itself, and hence the link to the flow regimes, has not been established in the effervescent atomiser literature. This restricts comparability between aerator studies in effervescent atomiser and alternative research fields (e.g. nuclear, waste treatment).

The effervescent atomiser configuration refers to the gas-phase injection scheme, for example those depicted in Figure 2.35. Figure 2.36 shows that the most referenced design within the surveyed literature is an outside-in configuration, whereby the gas-phase is injected from aerator orifices in the periphery of the mixing chamber. This contrasts to an inside-out configuration, whereby the gas-phase is injected through aerator orifices within a central aerator. Other design configurations are rarely cited between studies (e.g. independent injection, swirl chambers) [20, 56, 108, 109, 113], and are therefore thought to be developed to investigate a specific phenomenon. Whilst it is also possible to interchange the injection of the fluids (i.e. inject the liquid-phase through orifices into a gaseous core), this typically causes the liquid to be injected at too high a velocity for the phases to suitably mix and stabilise thus promoting heterogeneous flow regimes [109, 142]. In addition, Petersen et al. [143] recommends that the aeration orifices should be angled perpendicular to the liquid cross-flow, although this appears to be a generally unwritten convention of the designs within the literature.

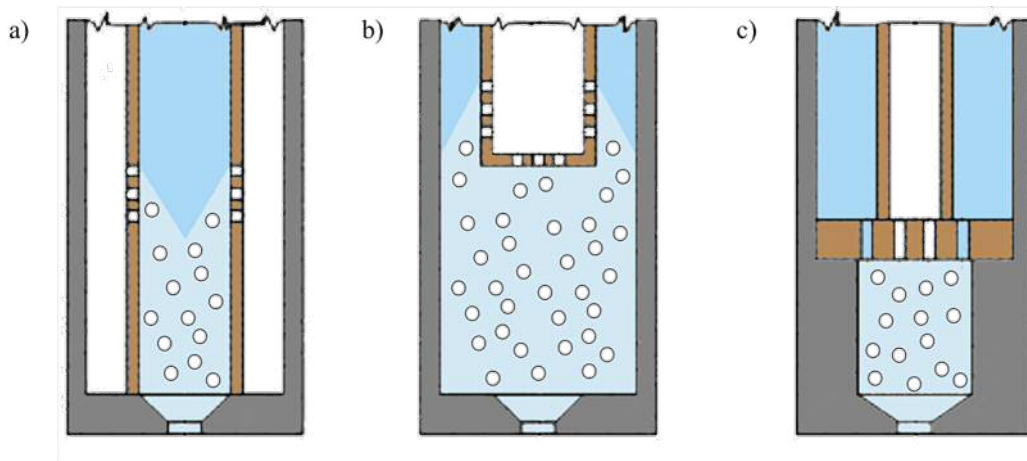


Figure 2.35 Effervescent atomiser design configurations:

a) injection of gas from an outer periphery into an inner liquid core (i.e. outside-in); b) injection of gas through a central aerator into an annular liquid core formed around the aerator (i.e. inside-out); and c) both fluids injected independently into a mixing chamber.

[19]

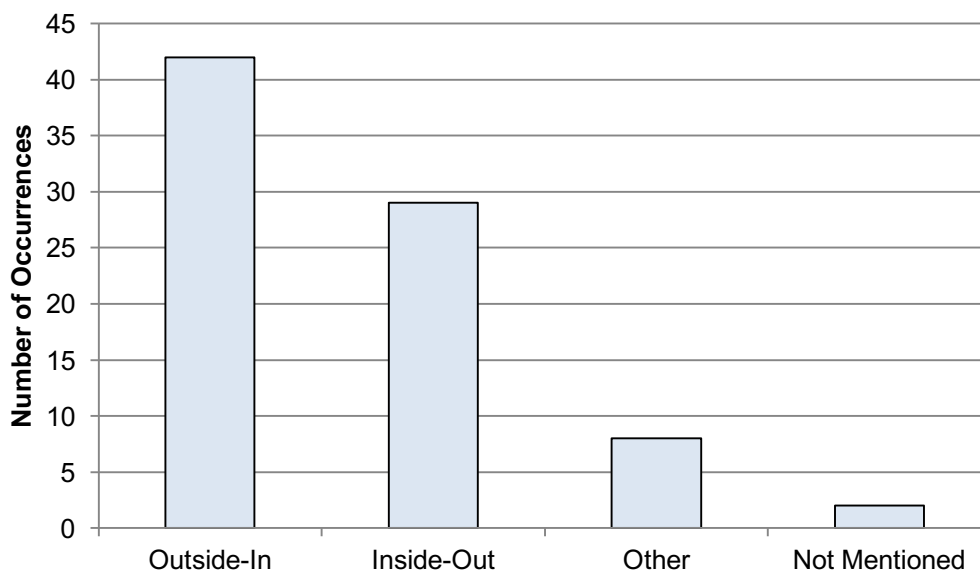


Figure 2.36 Distribution of atomiser configurations reported in effervescent atomiser literature.

The comparative merits between atomiser configurations are rarely studied, however it is reported that, due to having a comparatively large liquid flow area, an outside-in configuration reduced tendency to clog [19] and is therefore preferred for high flow rate applications over the inside-out configuration [74]. A problem thought to exclusively affect inside-out configurations is the bluff body recirculation effects of the aerator body which, as

previously discussed, can result in the formation of a large gas void in the aerator wake [44]. It is thought, however, that bluff body recirculation can be mitigated by streamlining the aerator body to reduce the wake effect and hence improving internal flow performance – this is supported by Jobehdar [44], who reported that gas void formation was prevented with installation of an arbitrary conical aerator tip, which resulted in increased bubbly flow homogeneity and hence improved spray stability.

It has been previously discussed that the gas velocity through the aerator orifice affects the bubbling regime at the aerator, where bubbly flow is encouraged by a low gas injection velocity – for a given gas flow rate, this is achieved by increasing the aeration area. A wide range of aeration areas are referenced within the literature (Figure 2.37), which is thought to reflect the vast array of different fluid flow rates investigated. The result of increasing the aeration area is under-researched within effervescent atomiser literature, with its effect on gas injection and internal flow unreported, and the resulting atomisation quality disputed – some researchers reporting decreased SMD [19, 28], whilst others report an insignificant effect [105, 143]. In a separate study, Jedelsky et al. [114] reported that an increase in aeration area acts to decrease the spray cone angle.

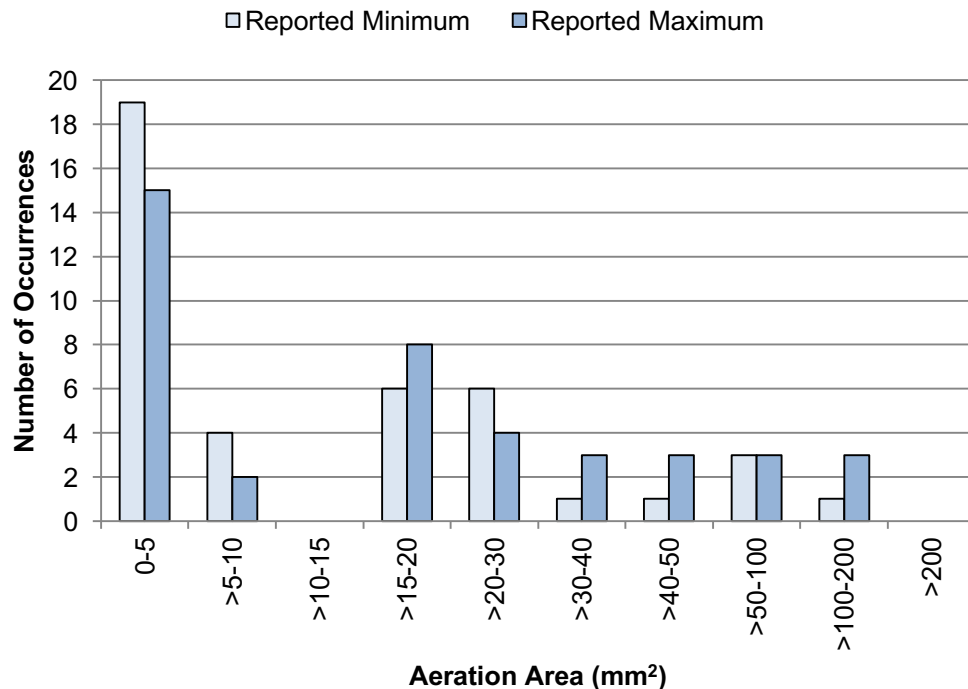


Figure 2.37 Distribution of aeration area reported in effervescent atomiser literature.

$$(A_{\min} = 0.13 \text{ mm}^2; A_{\max} = 190 \text{ mm}^2; A_{\max, \text{med}} = 16 \text{ mm}^2; A_{\max, \text{mean}} = 25 \text{ mm}^2)$$

An additional design parameter reported to affect effervescent atomisation is the ratio of aeration area to exit orifice area (A_a/A_o). This is reported by Chin and Lefebvre [28] to control the pressure drop across the aerator orifices, where a large relative aeration area reduces the gas velocity through the aerator and encourages bubbly flow. Chin and Lefebvre [28] proposed that optimum atomisation is achieved with Equation 2.11; however, Jedelsky et al. [19] disagreed, stating that the optimum relative aeration area is independent of ALR and recommend $A_a/A_o \approx 8 - 12$. Regardless, it follows that the aeration area should always be significantly greater than the exit orifice area.

$$\frac{A_a}{A_o} = 6.3 \cdot \text{ALR} \quad (2.11)$$

A given aeration area can be formed from a single large aerator orifice, or a number of smaller holes in a multi-holed design. It has been previously discussed that the injected bubble size is proportional to the aerator orifice diameter (Equation 2.1) and, therefore, the effect of increasing the number of aerator orifices for a fixed flow area promotes favourable effervescent atomiser internal flow (i.e. high number of small bubbles), increased spray stability [13, 17, 19, 29, 56, 81, 86] and decreased droplet SMD [19]. It is also implied that multi-holed aerators facilitate better mixing, as Jedelsky et al. [19] reported that mixing length had a diminishing effect on droplet SMD with an increased number of aeration holes – this trend was observed to plateau at high orifice numbers, potentially due to the manifestation of passive aerator orifices which occur when minor dissimilarities between multiple aerator orifices result in differing orifice resistances (i.e. the orifices with the least resistance dominate the gas supply, resulting in little growth in the other orifices) [31]. Opposing evidence by Wang et al. [77], Broniarz-Press et al. [105] and Lefebvre [10] reported insignificant changes with aerator orifice diameter.

The extreme of multi-holed aerator design was presented by Ghaemi et al. [81] whereby gas injection through a porous medium was found to increase the number density of small bubbles compared to a geometrically equivalent outside-in multi-holed aerator – this was reported to reduce the droplet SMD, however this is contradicted by Roesler and Lefebvre [67]. A study by Jobehdar [44] at the aerator reported that the interference of a formed or forming gas entity with an aerator orifice can lead to coalescence and hence increased bubble size – therefore, the aerator orifice layout should be considered to ensure adequate spacing of injection holes.

There have been numerous alternative aerator designs reported within literature to further reduce the size of the bubbles. Tesař [31] utilised an oscillating gas supply to generate small bubbles through a fine mesh at low gas injection pressure – despite this investigation being conducted with a flat aerator suitable for wastewater treatment applications, it is envisaged that this technique could be applied to effervescent aerators, although with an assumed negative impact on operational and equipment costs. Loubière et al. [33] investigated the use of a flexible aerator orifice, which was reported to produce a greater number of uniformly sized small bubbles compared to an equivalent fixed diameter aerator orifice.

There is evidence to suggest that bubble formation at the aerator may be not be steady process. The contraction of a bubbles volume through the exit orifice is filled by the liquid phase, causing a sudden acceleration in the flow. This causes slip between the two phases, generating a pressure wave which travels back through the mixing chamber in a process akin to “water-hammer” [14, 41]. In an optical study, Sen et al. [41] reported that this pressure wave acts to disintegrate established bubbles within the mixing chamber and affect the gas injection at the aerator.

2.5.5 Effect of Mixing Chamber Design

The mixing chamber is the region in which the two-phase flow regime is stabilised, with the objective of supplying the exit orifice with the desirable flow conditions. Relatively few researchers have investigated mixing chamber design as an independent variable (Figure 2.27), predominantly thought to be due to the difficulty of varying this aspect of design without significant modifications to the experimental rig. Conventional mixing chambers have cylindrical form, with some researchers utilising rectangular designs to gain beneficial optical properties for internal flow studies [13, 15, 17].

To ensure a suitable flow is supplied to the exit orifice, it is vital that sufficient time (i.e. mixing length) is provided for bubbles to distribute themselves into a uniform and homogenous flow and for air jets to breakup into bubbles [28]. A wide range of mixing lengths are referenced in the literature (Figure 2.38), which is thought to represent the varying degrees of compromise researchers are willing to accept between maximising mixing length to gain sufficient mixing time and minimised mixing length improve practicalities (e.g. size, weight, cost). The mixing length has been widely reported to have a negligible effect on spray quality [16, 19, 114], provided that the two-phase flow is well mixed prior to exit orifice supply [19]. However, Jedelsky et al. [114], Liu et al. [93] and

Jobehdar [44] reported that, when operating in bubbly flow, excessive mixing length can increase bubble coalescence – this has the effect of reducing the homogeneity of the internal flow and, therefore, increases the spray instability. Consequently, there are contrasting accounts of the effect of mixing length on spray quality in the literature, which is thought to represent the differing degrees of mixing achieved across the experimentation – for example, there are researchers who report that increased mixing length decreased the droplet SMD [134, 144], whilst some report increased droplet SMD [93] and others observe insignificant changes [27, 143].

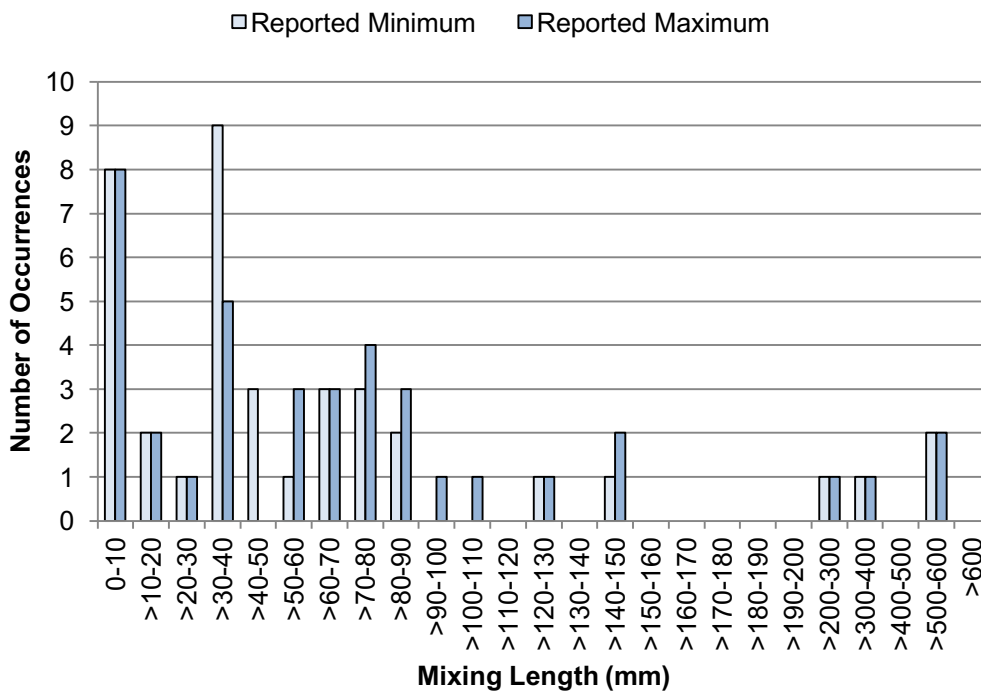


Figure 2.38 Distribution of mixing length reported in effervescent atomiser literature.

$$(l_{m,min} = 0.03 \text{ mm}; l_{m,max} = 559 \text{ mm}; l_{m,max,med} = 60 \text{ mm}; l_{m,max,mean} = 93 \text{ mm})$$

A wide range of mixing chamber diameters are referenced in the literature (Figure 2.39), which are shown to have weak correlation with the intended liquid flow rate (Figure 2.40) – consequently, it is implied that there is little conformity on atomiser size between researchers. However, whilst the superficial fluid velocities within the mixing chamber are controlled by the mixing chamber diameter, it should be noted that for an inside-out effervescent atomiser the liquid cross-flow velocity acting on the injected gas-phase is also a function of the aerator tube diameter. The effect of mixing chamber diameter on the internal flow has not been investigated, however it is reported to have minor influence on the subsequent two-phase atomisation [75], with Petersen et al. [143] reporting it to have an

insignificant effect on droplet SMD. Jedelsky et al. [19], however, reported optimal performance with the mixing chamber diameter designed to be 4 times larger than the exit orifice. Consideration should be given to ensure that it is be suitably small to prevent phase separation or gravitational effects to become dominant over the surface tension (i.e. conditions in which orientation does not affect atomisation) – Kim and Lee [20] reported phase separation can be prevented by diameters less than 10mm, although the majority of effervescent atomiser studies exceed this criterion.

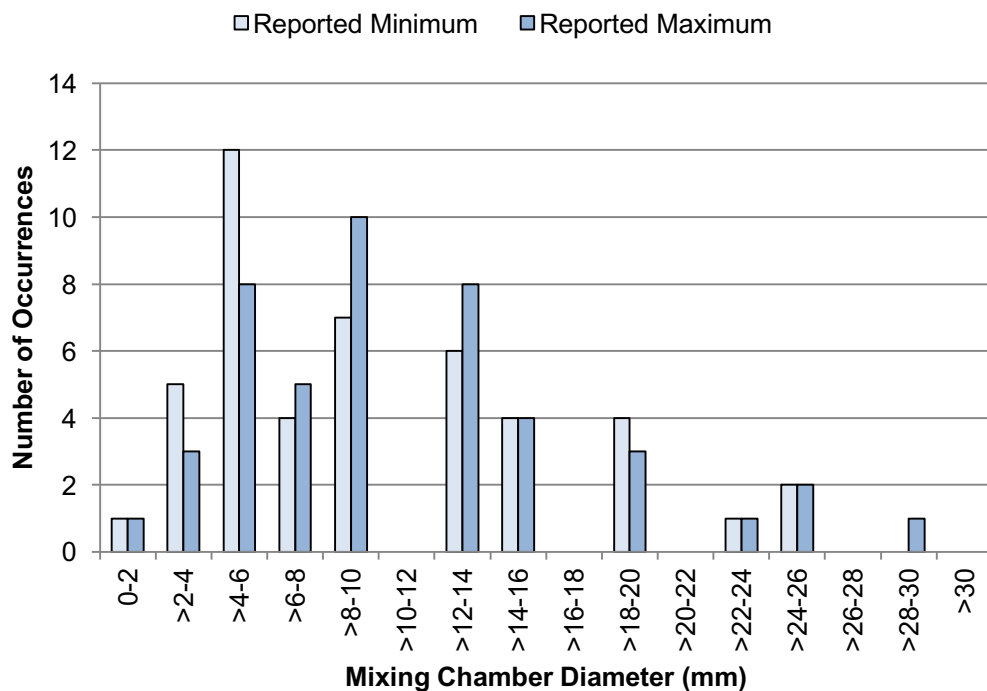


Figure 2.39 Distribution of mixing chamber diameter reported in effervescent atomiser literature.

$$(d_{MC,min} = 2 \text{ mm}; d_{MC,max} = 30 \text{ mm}; d_{MC,max,med} = 10 \text{ mm}; d_{MC,max,mean} = 11.4 \text{ mm})$$

Typically, mixing chambers are a plain design leading from the aerator region into the exit orifice, however some researchers have shown that the addition of design elements can improve the internal flow (i.e. increase the number of small bubbles). For example, the generation of increased turbulence in the mixing chamber has been reported to encourage bubbly flow across a wider range of operating conditions [13]. Jedelsky et al. [19] reported that turbulence can be achieved with static mixers or turbulence generating inserts within the mixing chamber – although it is also plausible for greater turbulence to be generated with increased flow rates. There appears to be turbulent limit though, as Sakai et al. [145] found excessive turbulence can cause areas of low pressure, which encourage bubble coalescence,

and, hence, has a detrimental effect on effervescent atomiser performance and efficiency. The use of mechanical bubble breakers within the mixing chamber (i.e. flow restrictors, such as perforated sheets and wire meshes) have also been demonstrated within the literature as an effective way to breakup large bubbles into smaller more-spherical bubbles [44, 86, 128, 144]. This is due to increased liquid shear at the perforation inlet and greater turbulence through the orifice [44]. Although increasing the likelihood of clogging, decreasing the perforation hole diameter acts to reduce the bubble size [44, 86] and therefore multi-holed bubble breakers generate smaller bubbles than a single-hole design of equivalent flow area. Non-invasive bubble breaker techniques have also been reported. Jagannathan et al. [17] utilised an ultrasonic probe within the mixing chamber to breakup large bubbles just upstream of the exit orifice. Other techniques include using focussed laser light and increasing turbulence to induce shear stresses, although controlling disintegration is complicated and expensive [31].

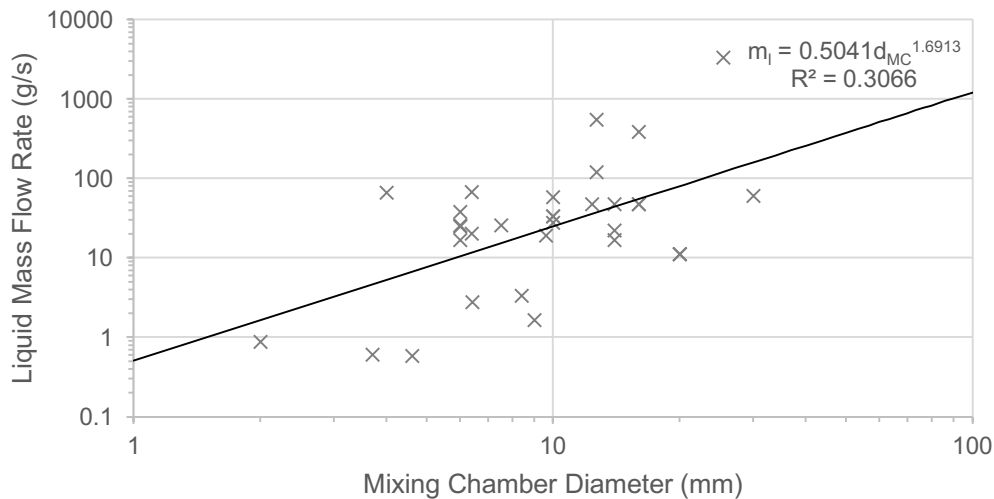


Figure 2.40 Relationship between mixing chamber diameters and liquid mass flow rates reference within effervescent atomisation literature.

2.5.6 Effect of Exit Orifice Design

The function of the exit orifice is to allow specific fluid flow through the atomiser whilst maintaining a pressure drop sufficient to instigate atomisation, where the liquid mass flow rate reduces with exit orifice diameter (Equation 2.8). The exit orifice design is often investigated as an independent variable in effervescent atomiser studies (Figure 2.27), the effect of which is generally reported to be minor [130] or insignificant [15, 74, 76] compared to other independent parameters (e.g. ALR, operating pressure). The vast majority of

effervescent atomiser studies utilise a circular exit orifice, which generates a solid spray cone – although, the use of a rectangular orifice was demonstrated by Catlin and Swithenbank [15] to produce a fan spray and the use of an annular orifice was demonstrated by Whitlow et al. [135] to produce a hollow spray cone.

The exit orifice diameter is inherently linked to the two-phase flow rate through the atomiser and therefore a suitable size must be decided for the intended operating conditions. Consequently, a wide range of exit orifice diameters are referenced in the literature (Figure 2.41), due to the various flow rates investigated. Unlike single-phase atomisers, which generally rely on high liquid velocities through the exit orifice to generate atomisation, the dependence on exit orifice diameter is comparatively low for effervescent atomisers [10, 15, 74, 76, 130], due to the atomisation processes being dominated by forces external to the liquid (i.e. gas-phase disruption and gas-phase expansion). Researchers generally report a decrease in droplet SMD with a decreasing exit orifice diameter [16, 20, 102, 105, 115, 132, 143]. Kim and Lee [20], however, reported that this effect diminishes with increasing ALR, which suggests that the supplied flow regime could be a primary factor affecting the sensitivity of an effervescent atomiser to the exit orifice diameter – this could explain the contradictory reports within the literature [93, 134]. In addition, the literature agrees that an increasing exit orifice diameter acts to decrease the discharge coefficient [10, 77, 99] but has an insignificant effect on the spray cone angle [15, 16].

The two-phase effervescent atomisation breakup mechanisms are thought to be encouraged by an abrupt pressure drop across the exit orifice, therefore a low length-to-diameter ratio (l_o/d_o) improves spray quality [19, 28, 100] – although, this is disputed by Petersen et al. [143] who reported insignificant changes with l_o/d_o . As can be seen from the distribution of literature (Figure 2.42), researchers typically aim for a low l_o/d_o ratio – mechanical factors are thought to increasingly impede the use of lower l_o/d_o ratios, due to manufacturing limitations and increasing probability of material failure due to the stress concentration on the orifice edge.

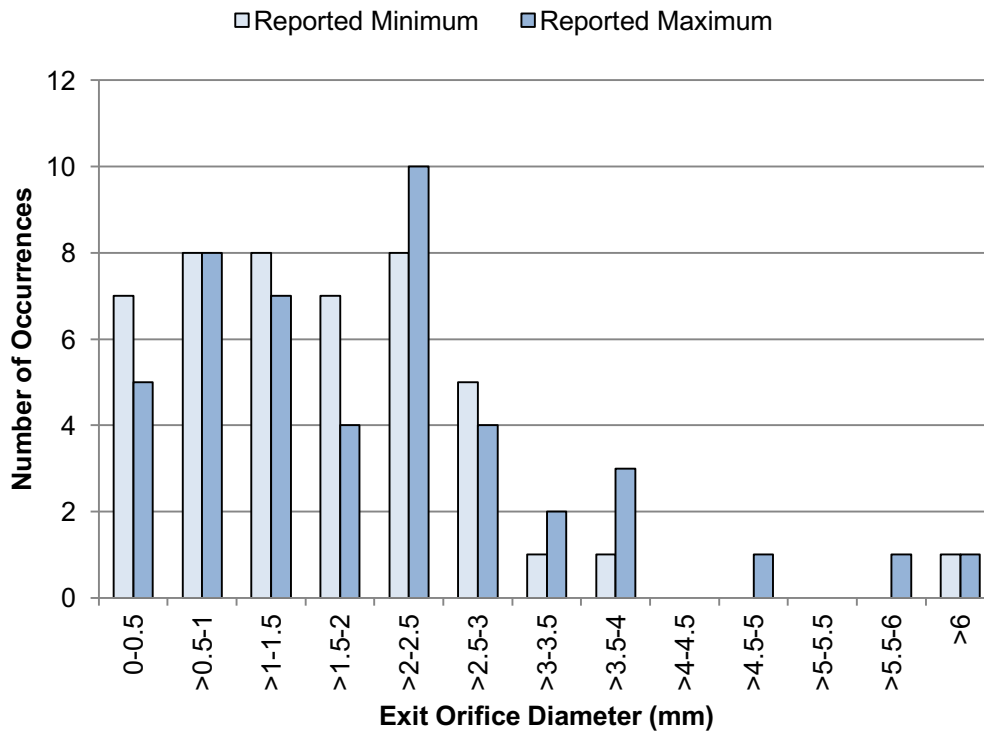


Figure 2.41 Distribution of exit orifice diameter reported in effervescent atomiser literature.
 ($d_{o,min} = 0.25$ mm; $d_{o,max} = 13$ mm; $d_{o,max,med} = 2$ mm; $d_{o,max,mean} = 2$ mm)

Most effervescent atomisers referenced in the literature use a conventional convergent nozzle. The convergence angle has little effect in atomisation performance below a critical limit, reported by Chin and Lefebvre [28] to be $2\beta < 120^\circ$ and Mostafa et al. [144] to be $2\beta < 140^\circ$. Mostafa et al. [144] also reported that spray performance significantly degrades if a plain orifice (i.e. $2\beta = 180^\circ$) is used. The literature recommends $90^\circ < 2\beta < 120^\circ$, such that the nozzle length is minimised whilst maintaining preferable flow characteristics [19, 28]. Favourable atomisation is reportedly achieved with a convergent-divergent exit orifice design (i.e. de Laval nozzle) due to superior choking performance, however these are not commonly used as they require high gas flow rates [28, 146].

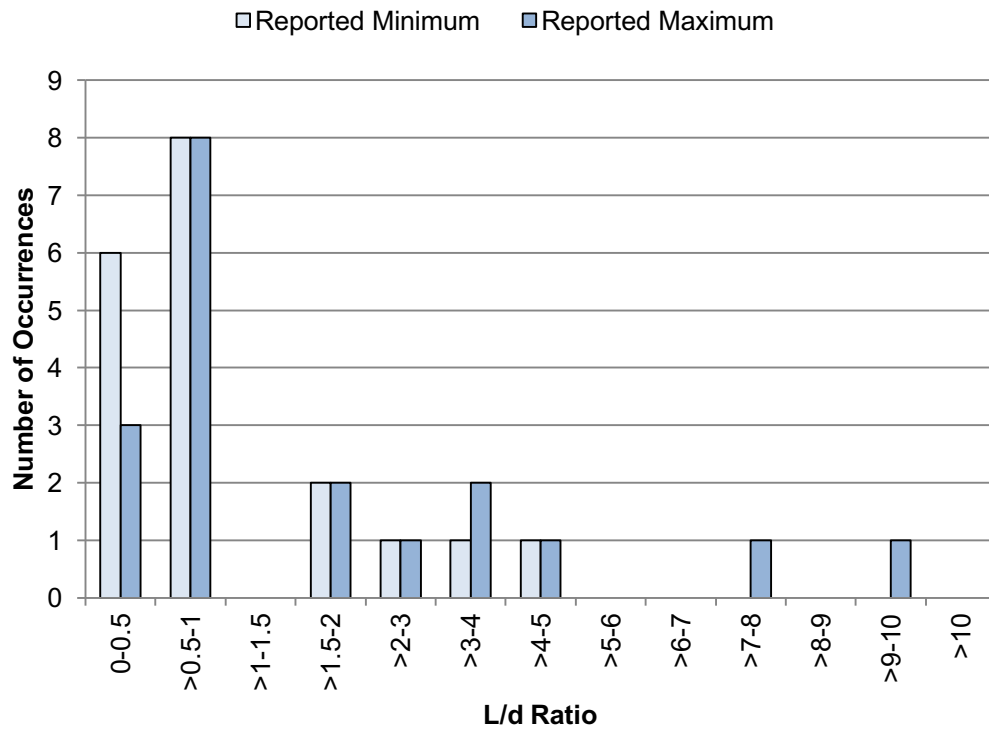


Figure 2.42 Distribution of L/d ratio reported in effervescent atomiser literature.

$$(l_o/d_o \text{ min} = 0.08; l_o/d_o \text{ max} = 10; l_o/d_o \text{ max,med} = 1; l_o/d_o \text{ max,mean} = 2.3)$$

Whilst single hole exit orifice designs are by far the most commonly cited in effervescent atomiser literature, multi-holed exit orifices can be positioned to artificially generate greater spray cone angles [95, 127] – this, therefore, reduces the dependency of other parameters to generate a sufficient spray cone angle. These exit orifices are commonly angled away from the mixing chamber axis to prevent merging of neighbouring sprays and therefore increased droplet coalescence, under which conditions the droplet sizes produced are similar to a single-hole orifice [19, 126, 135, 147]. This implies that multi-holed effervescent atomiser spray performance could be varied specifically for each application by altering the positioning of the exit orifices. This was demonstrated by Jedelsky et al. [24], who exhibited a functioning multi-holed effervescent atomiser with a 60° full angle (i.e. 30° offset from the nozzle axis) that produced a homogenous and symmetrical spray.

2.5.7 Effect of Fluid Properties

As previously mentioned, an effervescent atomiser is typically designed to atomise a specific flow rate of a given liquid, with the primary purpose of gas injection to aid atomisation. It is obvious that, depending on the application, effervescent atomisation will be required to spray

a vast array of different fluid combinations and, therefore, understanding the effect of the input fluids is paramount – potential combinations include, for example, a water/nitrogen mix for fire suppression and diesel/air mix for fuel injection. Many researchers have investigated the effect of liquid properties as independent variables, with a minority investigating atomising gas properties. Generally fluid properties are dependent on each other and, therefore, it is not always possible to isolate a particular property – for example, increasing the liquid temperature tends to affect the viscosity, surface tension and density; therefore liquid properties can vary during operation [16]. As a general rule, the literature reports that fluid properties play a minor [19] or negligible [79, 117, 136] role in the effervescent atomiser process.

Considering the types of liquid investigated in the literature (Figure 2.43), the majority of reports investigate Newtonian liquids (i.e. constant absolute viscosity), with a minority investigating non-Newtonian liquids (i.e. non-linear apparent viscosity depending on, for example, shear rate). Typically water is used for Newtonian studies, thought to be due to its low risk, ready availability and beneficial optical properties. However, there are a multitude of pure and mixed solutions of various other liquids referenced within the literature, which are thought to either replicate an application (e.g. fuel oils, chemicals) or induce specific liquid properties of interest (e.g. non-Newtonian behaviour, viscosity, surface tension) – for example, aqueous solutions of glycerol are frequently referenced to increase liquid viscosity.

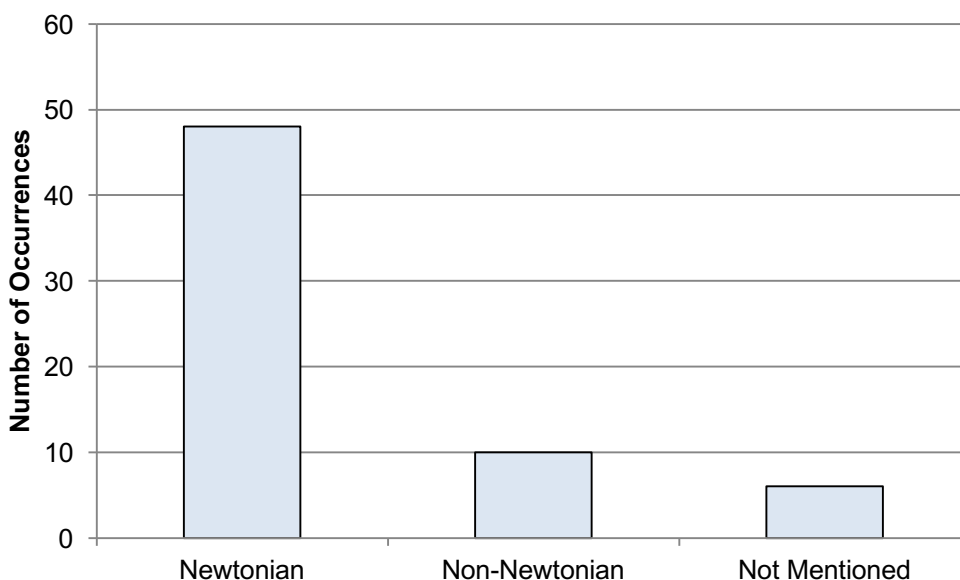


Figure 2.43 Distribution of liquid viscosity type reported in effervescent atomiser literature.

The effect of liquid rheology is reported within the literature to have some effect, even if minor, on the effervescent atomisation process. Whilst an increase in viscosity promotes favourable internal flow by retarding the transition between flow regimes [27, 85] and thus encouraging bubbly flow over a wider range, it is widely reported to have a detrimental effect on the droplet SMD [16, 22, 23, 112, 132, 136, 138, 148-150] – although some researchers report that this effect is insignificant [13, 79, 83, 84, 138]. The effect of increasing liquid density acts to increase the liquid mass flow rate through the atomiser (Equation 2.8), but decrease the droplet SMD [74, 102, 136, 150, 151]. There are conflicting reports as to the effect of surface tension on atomisation with some researchers reporting an increase in droplet SMD with surface tension [74, 102, 151], whilst others report a decrease [136, 150] – Lefebvre [29] explains that this could be attributed to varying flow regimes between studies, where SMD decreases with surface tension in bubbly flow due to a reduction in bubble energy and increases in annular flow where bubble energy has no effect.

By far the most common atomising gas utilised across the literature is air (Figure 2.44), thought to be predominately due to its ready availability and cheap cost, whereas nitrogen is occasionally used to reduce the risk of unintentional combustion. The effect of atomising gas properties on effervescent atomiser performance is typically assessed against its molecular weight as an independent variable, although these studies are relatively rare (Figure 2.27). Rahman et al. [56] and Lund et al. [152] reported a weak dependence of atomising gas molecular weight on internal and external effervescent atomiser performance, which therefore endorses the use of air for experimental trials as an approximation for other gases. However, this contradicts the findings of Lund et al. [152] and Broniarz-Press et al. [105], who reported an increase in droplet SMD with increasing atomising gas molecular weight.

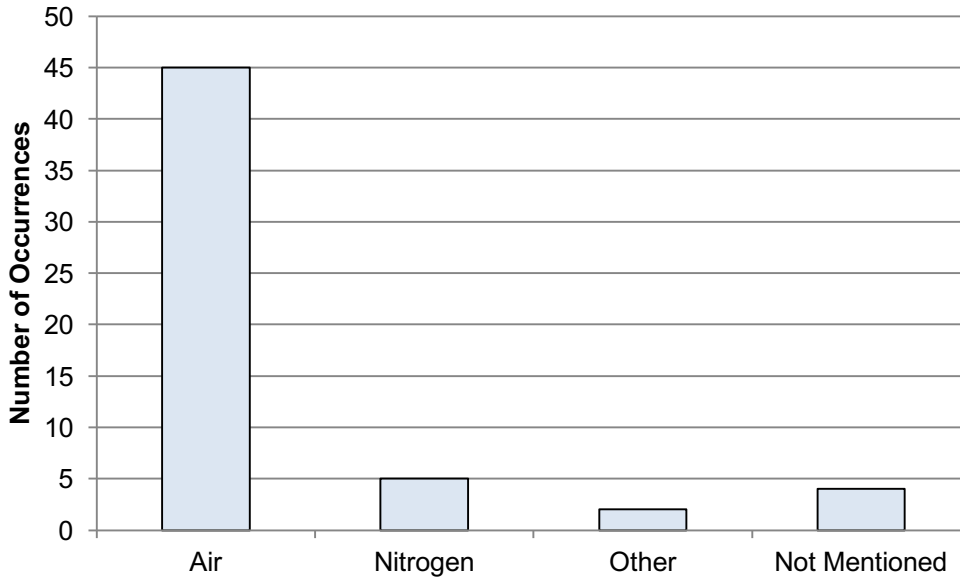


Figure 2.44 Distribution of atomising gases reported in effervescent atomiser literature.

In theory, the presence of suspended solid particles within the liquid (i.e. three-phase gas-liquid-solid flow) has the effect of reducing bubble size due to bubble-particle collisions [30]. If the combined shear force exerted by the flow field and bubble-particle collision are great enough to overcome the restoring forces of the liquid viscosity and surface tension, then a suspended solid will penetrate a bubble potentially leading to bubble breakup [153]. Else, the particle will rebound from the bubble surface. However, Buckner et al. [140] did not observe appreciable differences in the droplet SMD with changes to the size or quantity of solid particulates in three-phase flow.

2.6 Summary

Based on the literature reports, the optimal internal flow for effervescent atomisation would be a number dense, homogenous flow of uniformly sized bubbles, which are larger than the exit orifice. This should correspond with the maximum allowable operating pressure and highest ALR preceding the transition to intermittent regimes. The exit orifice should be sized to allow discharge of the required liquid mass flow rate under these conditions and the mixing chamber should have sufficiently small diameter and sufficiently long mixing length to facilitate complete mixing without phase-separation irrespective of the orientation. An aeration area significantly larger than the exit orifice should be chosen, which should be split up into the maximum number of aerator orifices with diameters suitable to form bubbles larger than the exit orifice and spacing sufficient to prevent coalescence of forming bubbles.

CHAPTER 3. DEVELOPMENT OF FACILITIES

Considering the reported importance of the internal flow on effervescent atomiser spray quality, the number of reports investigating the two-phase flow generated within the mixing chamber are in the minority, with very few also considering the behaviour at the aerator. Hence the aim of the current work is to characterise the complete effervescent atomiser process from gas-injection to spray generation. This work will consider the effects of various independent parameters, with the intention of enabling optimisation of an effervescent atomiser. Therefore, the design and development of a versatile set of experimental apparatus are introduced and described in this chapter. Also discussed are the techniques used to generate data from the effervescent atomiser internal flow and spray rigs and the test matrices developed for the experimentation.

3.1 Optical Effervescent Atomiser (OEA)

The initial aim of the current investigation was to determine the effects of common operating parameters on the internal flow regime and link this to the subsequent atomisation mechanisms.

The vast majority of internal flow studies within effervescent atomiser literature utilised digital imaging, compared to invasive techniques which may interfere with the downstream fluid-flow profiles – examples of these intrusive techniques include capillary suction tubes [154] and wire-mesh sensors [21, 55, 88]. Arguably, the major deterrent of using optical techniques for effervescent atomiser internal flow measurements is that result accuracy is negatively affected by refraction effects along the radial axis of a standard cylindrical mixing chamber [86]. Traditionally, a trade-off has existed between: replicating a standard cylindrical atomiser design and accepting high-levels of refraction, particularly at the boundary wall [27, 72, 81, 86]; or adopting an optically optimised but non-traditional design, such as a rectangular bodied mixing chamber [13, 15, 17]. However, in a recent study, Jobehdar [44] demonstrated that refraction through a cylindrical mixing chamber can be passively minimised by utilising refractive index matching. In this case, the atomiser body

design was a transparent cuboid through which a mixing chamber was bored – as the refractive index of the atomiser body was similar to that of the operating liquid (acrylic glass: 1.50; water: 1.33) and, because the imaging was performed perpendicularly, the refractive indices throughout the atomiser were comparable and hence refraction was minimised.

Using the same method of refraction minimisation, a transparent effervescent atomiser was designed, manufactured and commissioned at Cardiff University to observe the internal flow with minimised refraction. The finalised design, shown in Figure 3.1 with engineering drawings given in §A3.1, is termed the “Optical Effervescent Atomiser”. It consists of a cuboidal acrylic glass block (Perspex[®]), through which an 8.0 mm mixing chamber is bored – this diameter was selected as it:

1. Approximates to the average mixing chamber diameter (i.e. 8.12 mm) for studies of comparable liquid mass flow rates (58.3-66.5 g/s) [16, 20, 115, 121];
2. Is less than 10 mm – recommended by Kim and Lee [20] to prevent phase separation.

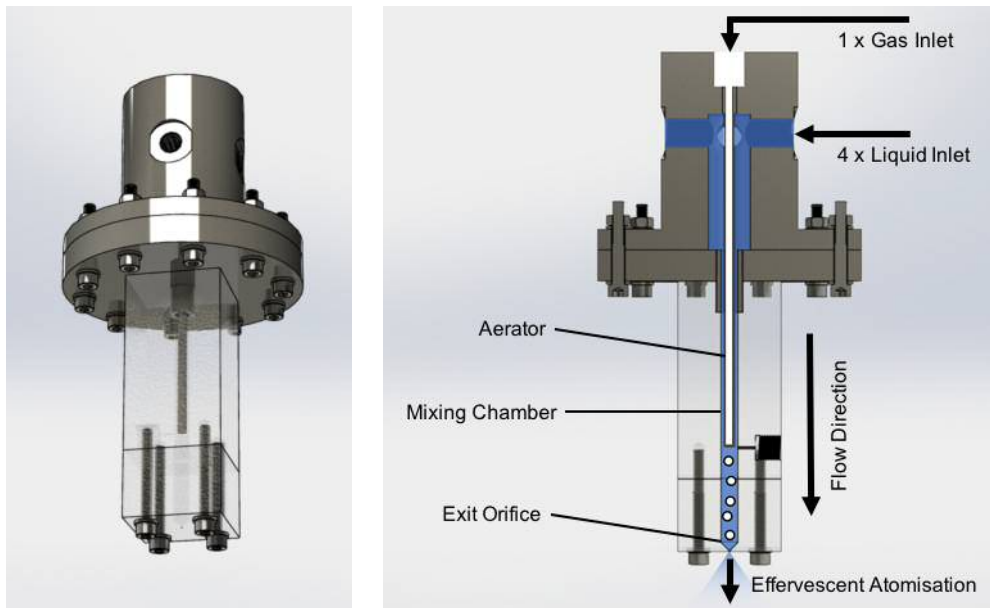


Figure 3.1 Optical Effervescent Atomiser (OEA): a) CAD model; b) operating principle.

Liquid is supplied through four equally sized ports and flows into the mixing chamber around the periphery of a centrally located and customisable aerator, through which gas is injected. The two-phase mixture flows through the mixing chamber with 63 mm mixing length – as the objective of the test was to identify the stabilised flow regimes within the mixing chamber, it was advantageous to use a large mixing length to promote complete

mixing. Optical access to the internal two-phase flow is gained through all four major sides. The flow is then discharged through an interchangeable transparent exit orifice. The generated spray is released into the ambient atmosphere, above a liquid collection tank, which allows for the spray to be quantified.

3.2 Internal Flow Optimisation Rig (IFOR)

The next major aim of the current work was to investigate the effect of various parameters on the internal flow regime of an effervescent atomiser and link it to the gas injection behaviour at the aerator. Using a similar method of refraction minimisation, a novel experimental rig was designed, manufactured and commissioned at Cardiff University to replicate the internal behaviour of a conventional inside-out cylindrical effervescent atomiser across a wide range of design and operating limits.

The finalised design, shown in Figure 3.2 with engineering drawings given in §A3.2, is termed the “Internal Flow Optimisation Rig”. It consists of a transparent cylindrical mixing chamber within a cuboidal tank, with optical access gained through a window on each of the four major sides. Liquid is supplied equally through four ports and flows into the mixing chamber around the periphery of a centrally located aerator, through which gas is injected. The two-phase mixture flows through the length of the mixing chamber, with 325 mm visible length – as with the OEA, the objective of the test was to identify the stabilised flow regimes within the mixing chamber and hence it was advantageous to use a large mixing length to promote complete mixing. Flow is then discharged through a needle valve which allows complete independent control of the fluid flow rates and operating pressure.

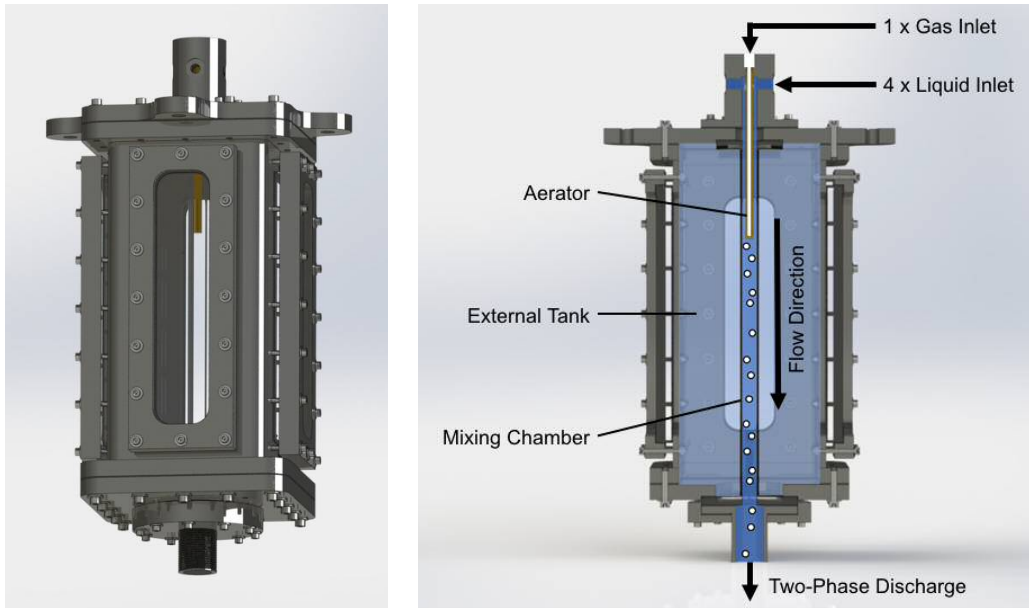


Figure 3.2 Internal Flow Optimisation Rig (IFOR): a) CAD model; b) operating principle.

To minimise refraction, the design exploits the “water tunnel” effect whereby the outer tank is filled with a liquid of similar refractive index to the transparent mixing chamber and windows – in this case, a combination of acrylic glass (i.e. Perspex[®]) and water were selected (acrylic glass: 1.50; water: 1.33). A schematic of this principle is shown in Figure 3.3. The key advantage of adopting this design, as opposed to the solid transparent atomiser body demonstrated by Jobehdar [44], is that it enables the mixing chamber to be interchanged without destructive machining processes on the atomiser body. The consequence of this passive refraction minimisation technique can be compared in Figure 3.4, which shows the same scene of a checkerboard insert within the cylindrical mixing chamber – a noticeable improvement in image distortion is achieved by comparing the results without and with water tunnel – particularly on the mixing chamber boundary.

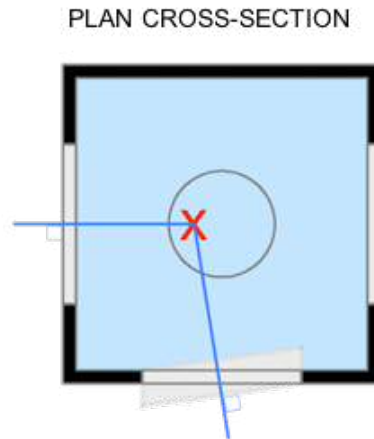


Figure 3.3 Schematic of refractive index matching principle (the blue line is the light path and the red cross is the visual target).

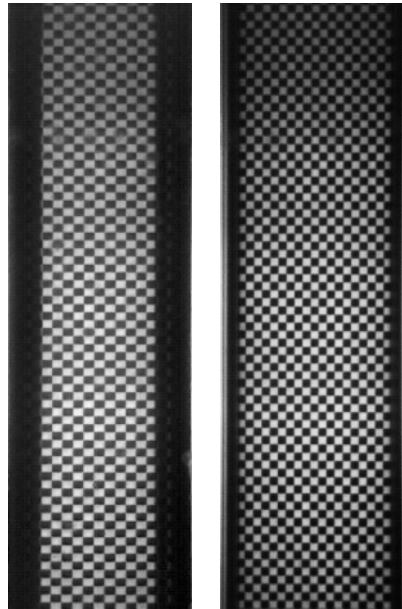


Figure 3.4 Image distortion through a cylindrical mixing chamber:
a) without refraction minimisation; b) with water tunnel.

The current investigation is a continuation of research previously completed at Cardiff University, as presented by Konstantinov [16] – the experimental system within this study represents the extreme maximum scale of effervescent atomiser design within the literature, with mixing chamber diameters varied between 20-30 mm. To allow comparability between these results, the IFOR was designed to a similar scale, allowing investigation of a 14-36 mm mixing chamber diameter range. The aerator tube diameter was also replicated at 10 mm diameter.

3.3 Auxiliary Systems

The auxiliary system consisted of fluid supply, metering and related conduit. A largely common system was used between rigs, as shown in the schematic drawing in Figure 3.5. The four liquid supply lines were connected to the four inlet ports on either the Internal Flow Optimisation Rig (IFOR) or the Optical Effervescent Atomiser (OEA). Liquid supply was provided by a Lowara 3SV29F030T multistage centrifugal pump (LP), which took feed from a 1 m³ unsealed liquid tank (LT). The majority of the pump discharge was re-circulated to the liquid tank, with backpressure controlled by a gate valve (FV-004). The liquid flow to the atomiser was controlled by a needle valve (FV-001) and the liquid mass flow rate, pressure and temperature respectively were measured with an Emerson Micromotion CMF 050 coriolis meter (F-001), a Druck PTX 1400 pressure transmitter (P-001) and Type-K thermocouple (T-001). Air was supplied up to 7 bar_g from the in-house compressed air line (CA) and the gas supply to the rig was controlled with a needle valve (FV-002). The mass flow rate, pressure and temperature along the gas supply line were respectively measured with a Bronkhorst Cori-Tech M14V10I coriolis meter (F-002), a Druck PTX 1400 pressure transmitter (P-002) and Type-K thermocouple (T-002). The operating pressure and temperature within the atomiser were measured with a Druck PTX 1400 pressure transmitter (P-003) and Type-K thermocouple (T-003) respectively. For the Optical Effervescent Atomiser (OEA), the flow through the atomiser was discharged through an exit orifice above the liquid tank. This compares to the Internal Flow Optimisation Rig (IFOR), whereby the fluid discharge into the liquid tank was regulated by a needle valve (FV-003). The uncertainties for all instrumentation over the operating range is shown in Table 3.1.

Table 3.1 Instrumentation uncertainty.

Instrumentation	Tags	Accuracy
Druck PTX 1400 Pressure Transducer	P-001, P-002, P-003	±0.15 %
Emerson CMF 050 Coriolis Flow Meter	F-001	±0.014 %
Bronkhorst M14V10I Coriolis Flow Meter	F-002	±0.5 %
Generic Type K Thermocouple	T-001, T-002, T-003	8.8 %

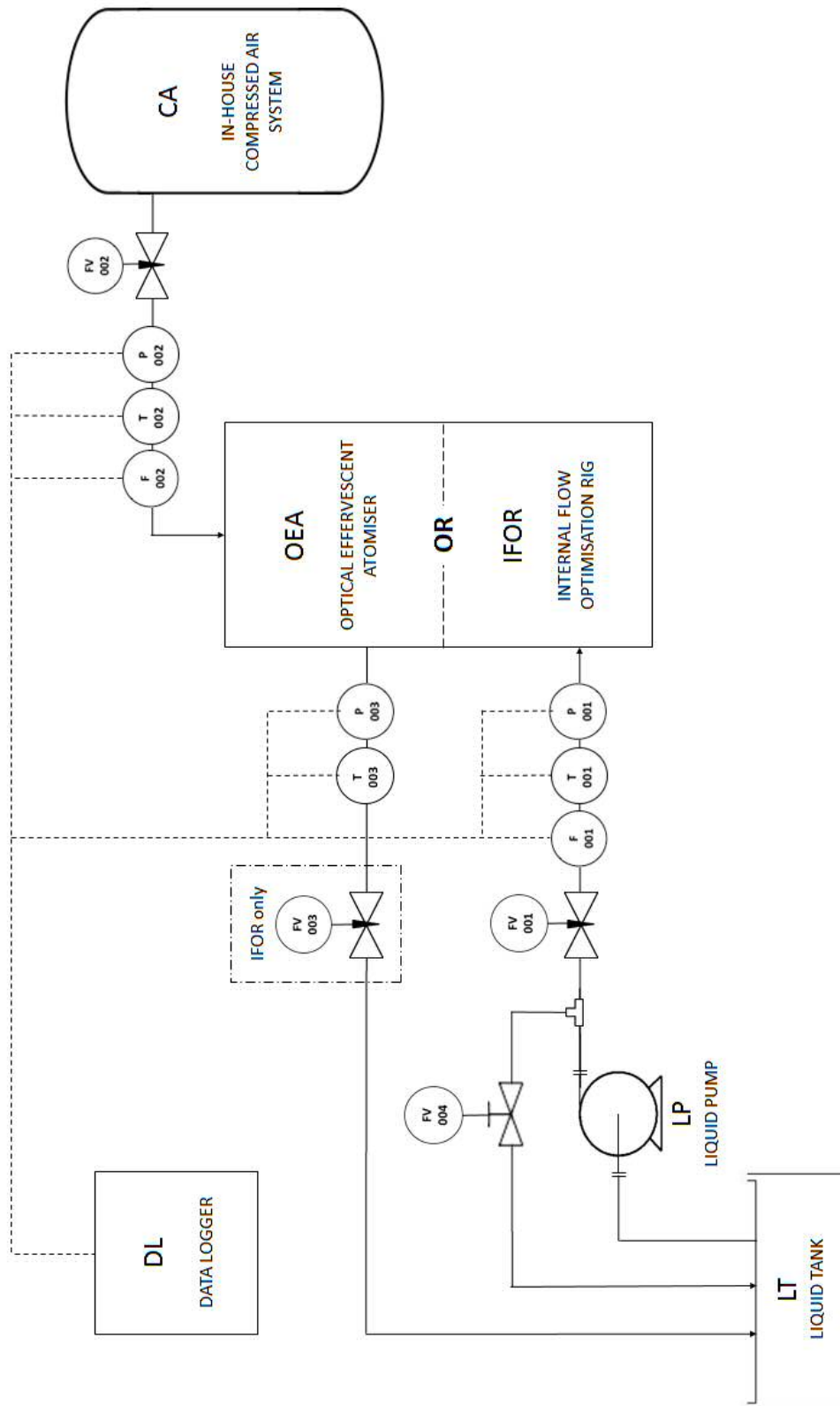


Figure 3.1 Process flow diagram for auxiliary systems.

All instrumentation data was acquired with a National Instruments cDAQ data logger (DL) and transferred to a computer (PC). The signals were processed using National Instruments Signal Express, which also managed presentation and storage at 1 kHz sampling rate – the user was presented with data at 1 Hz frequency, enabling configuration of the experiment system to achieve the desired operating conditions. The sampling duration per test point was not controlled, but was typically in the order of 100 s. The data was post-processed to achieve average results and additional calculations were performed to generate non-measured data – for example, Bakers numbers (Equations 3.1 and 3.2) and fluid velocities. This enabled comparison of experimental test points.

$$(G_l \Psi) = \frac{\dot{m}_l}{A_{MC}} \quad (3.1)$$

$$\left(\frac{G_g}{\lambda}\right) = \frac{\dot{m}_g}{A_{MC}} \quad (3.2)$$

3.4 High-Speed Shadowography

As previously discussed, a common measurement technique within effervescent atomiser literature is digital imaging, which involves capturing images of an illuminated flow in a single or sequence of images through a camera. A key advantage of this technique is the large detection size range of a typical camera lens – for example, Laakkonen et al. [154] reported detection of particles in the range of 0.1-8.0 mm diameter with the digital imaging technique which compared to, for example, Phase Doppler Anemometry (PDA) at 0.005-1.4 mm. Therefore, digital imaging is well suited to measurement of effervescent atomiser internal flows, whereby bubble diameters have been reported to range from 0.27 mm [17] to 10 mm [44], and to detect other useful features within the internal flow, such as flow regimes and surface instabilities. Digital imaging is also effective for imaging near-nozzle spray structures, as the atomisation mechanism can be observed.

The positioning of the lighting to illuminate the measurement scene has a significant effect on the imaged results. When using foreground illumination, the closest particles reflect the most light, with refraction and attenuation reducing the light intensity reflected by deeper particles – this technique is therefore suited to identifying individual particles on the perimeter of a dense flow. Conversely background illumination (termed Shadowography) casts a shadow onto the camera, with the gas-phase periphery shown as a dark outline – this technique is more appropriate for identifying individual particles in a sparse flow and the

silhouette of dense flows. Both techniques have numerous references within effervescent atomiser literature. Shadowography was adopted in the current testing as the detection of gas-injection and flow regimes was a significant aim, which may otherwise be obscured by peripheral bubbles in a forelight scene.

3.4.1 Experimental Set-Up

A Mikrotron MotionBLITZ Cube 2 high-speed camera was used in conjunction with a Navitar 16-160 mm zoom lens to record the flow. Various camera settings and backlighting set-ups were used across the investigation, determined experimentally to minimise image blurring and sufficient illumination – the finalised set-ups are individually described in the Programme of Work (§3.6). The camera was mounted to a computer controlled vertical traverse which allowed for accurate translation of the field of view, depending on the area of interest – for example, between the aerator and mixing chamber for the IFOR and the internal and near nozzle flows for the OEA.

Post-processing was applied to each of the measurement results to enhance the video (Figure 3.6). This was automated for each image within a video sequence using a purpose written MathWorks[®] MATLAB[®] 2016a computer script, the script for which is given in §A4.1.

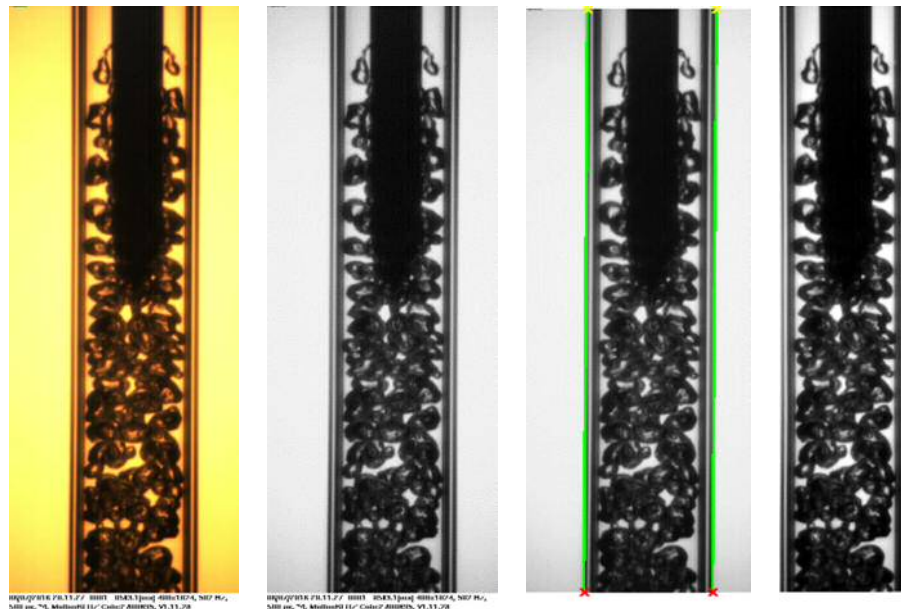


Figure 3.6 Internal flow results image processing example: a) original image; b) converted to grayscale; c) mixing chamber wall automatically detected; d) straightened, cropped and contrast optimised.

3.4.2 Internal Two-Phase Regime Quantification

The internal two-phase regimes (i.e. gas injection regimes, flow regimes) were identified manually for each measurement point using the descriptions reported within the literature (as discussed in §2.1.2 and §2.2.2). Any internal flow observation that did not correspond to the existing regime descriptions were defined as new regimes. Owing to the chaotic nature of the internal two-phase flow, automation of regime identification was not deemed practicable for the current project – there is no evidence of automation of this process within the literature. Due to the size of the final dataset (2484 individual videos), the processing of these results was time-consuming and inherently subjective – particularly as the internal flow does not immediately change, but rather gradually transitions between regimes. Thus, accurately and repeatedly identifying the regime transition is challenging and, consequently, human-error was identified as a potential error mode – for example, it is possible that a regime identification for an identical video may have differing identifications if analysed at the start or end of the process. An analysis method was consequently developed to reduce this identification error:

1. All test points were individually categorised against the literature or newly generated definitions to identify the gas injection and flow regimes;
2. Results were combined into a central database, including averaged parametric data, sample images and a hyperlink to the processed video footage, where results could be filtered and compared based upon a commonality (Figure 3.7) – for example, filtering based upon a specific flow regime, ALR or independent parameter. This allowed for similar results to be directly compared against each other and anomalies;
3. Anomalies were continually re-defined against the literature and newly generated definitions until all results were comparable within each regime category. This process was applied to both gas injection and flow regimes;
4. The identified regimes were further analysed by plotting against their corresponding conditions, to produce regimes maps. Regions of common regimes within these maps can be identified, providing a measure of atomiser performance over the range of examined conditions. A map was produced for each investigated configuration for both gas injection and flow regimes – as will be further discussed in Chapters 4-7.

Hyperlink to Data	Experiment Condition	Bubbling Regime	Upstream Image (-- = vertically downwards)	Flow Regime	Downstream Image (-- = vertically downwards)
0955 A11C 5bar 0.13ALR 202gs	Conical; A5; 20mm MC; Vert Down; 202g/s liq; 0.13% ALR; 5bar.	SB		B	
1055 A11H 5bar 0.25ALR 136gs	Hybrid; A5; 20mm MC; Vert Down; 136g/s liq; 0.25% ALR; 5bar.	SB		B	
1413 A11CA 5bar 0.12ALR 203gs	Circular Arc; A5; 20mm MC; Vert Down; 203g/s liq; 0.12% ALR; 5bar.	SB		B	
1507 A10A 5bar 0.12ALR 252gs	A-DARPA; A4; 20mm MC; Vert Down; 252g/s liq; 0.12% ALR; 5bar.	SB		B	
1440 A11A 5bar 0.12ALR 199gs	A-DARPA; A5; 20mm MC; Vert Down; 200g/s liq; 0.13% ALR; 5bar.	SB		B	
2009 A11A 5bar 0.25ALR 137gs	A-DARPA; A5; 20mm MC; Vert Down; 137g/s liq; 0.24% ALR; 5bar.	SB		B	
2150 A11A 5bar 0.25ALR 92gs	A-DARPA; A5; 20mm MC; Vert Down; 92g/s liq; 0.24% ALR; 5bar.	SB		B	

Figure 3.7 Example section of result database, filtered for bubbly flow cases.

The accuracy of this identification process cannot be quantified, and consequently error-bars cannot be determined, as the regimes definitions in themselves are subjective (i.e. there is no standard datum to assess against). The most repeatable identification is considered to be bubbly flow, as the determination criteria is definite – either discrete uniformly sized bubbles exist or they do not. This is particularly beneficial for the current study concerning effervescent atomisation, considering the reported importance of establishing a bubbly flow. Therefore, the identification of bubbly flow is considered to be sufficiently accurate to enable the desired outcomes in the current investigation.

Similarly, the accuracy of the regime maps cannot be quantified. However, a relatively fine mesh of data points was collected, with a typical map consisting of 63 regime identification points – consequently, the effect of an anomalous or misidentified regime is expected to have a relatively minor effect on the overall identification of regions. Regions are identified by fitting linear trends to the mesh of data points. The aim is to incorporate all relevant identifications into a suitable region, whilst considering the positioning of transition regimes (Table 3.2).

Table 3.2 Regime Map, region allocations

Region	Included Identifications	Transitional Identifications
Gas Injection Regime Maps		
Bubbling	Single Bubbling (§4.1.1) Pulse Bubbling (§4.1.2)	–
Jetting	Elongated Jetting (§4.1.3) Atomised Jetting (§4.1.4)	–
Cavity Forming	Cavity Forming (§4.1.5)	–
Coalesced Jetting	Coalesced Jetting (§4.1.6)	–
Evacuated Chamber	Evacuated Chamber (§4.1.7)	–
Flow Regime Maps		
Bubbly Flow	Bubbly Flow (§4.2.1)	Bubbly-Slug Flow (§4.2.3)
Slug Flow	Slug Flow (§4.2.4)	Bubbly-Slug Flow (§4.2.3)
Churn Flow	Churn Flow (§4.2.5)	–
Annular Flow	Annular Flow (§4.2.8) Annular Flow (liquid droplets) (§4.2.10)	–
Transitional	Disturbed Annular Flow (§4.2.9) Annular Flow (§4.2.8) ^[1] Annular Flow (liquid droplets) (§4.2.10) ^[1]	–
Evacuated Chamber	Annular Flow (§4.2.8) ^[2] Annular Flow (liquid droplets) (§4.2.10) ^[2]	–
Gas Void Formation	Gas Void Disintegration (Bubbly Flow) (§4.2.2) Gas Void Disintegration (Slug Flow) (§4.2.5) Annular Flow (§4.2.8) ^[3]	–

Formed due to: [1] buoyancy effects; [2] evacuated chamber gas injection; [3] aerator bluff body recirculation.

The operating range for a particular regime was determined by calculating the area of the corresponding region within the flow map. This enabled trends to be determined between variables by identifying a line of best fit with closest correlation (i.e. minimum R^2).

3.4.3 Bubble Sizing and Feature Tracking for Internal Flow

All imaging techniques produce inherently qualitative results, with some form of image post-processing required to generate quantitative analysis. Due to the quantity of individual images generated within this high-speed shadowography study (2484 videos, with an average 1500 frames per video), identifying and measuring each bubble by hand would be an extremely time-consuming and tedious process. This section describes the attempt to develop an image processing computer script to automate the bubble sizing process for the experimental images. Whilst this proved successful for sparse bubbly flow, its implementation on dense bubbly flows significantly reduced the measurement accuracy. Consequently, the intention is to advise further researchers on suitable datasets for the current technique, provide a foundation for software development and suggest potential alternative experimental techniques for use in future internal flow studies.

MathWorks[®] MATLAB[®] 2016a was chosen as the coding language for the internal flow image quantification software mostly due to its versatility, established help database and the previous experience of the author – the programming script for this is given in §A4.2. As with all bubble quantification software within the literature, the software relies upon accurate isolation and detection of bubbles within an image. This was achieved for a sparse bubbly flow (Figure 3.8a) in the following process:

1. The original image was converted to a logical array, via a conventional manner reported within internal flow quantification reports [44, 56]. A Gaussian filter was initially applied to the image to isolate the bubbles from the background (Figure 3.8b), before converting to a binary image above an automated threshold and removing bubbles that intersect with the boundary (Figure 3.8c).
2. A “watershed” algorithm is applied to separate clustered bubbles (Figure 3.8d). This process requires bubbles to have a clear edge and, hence, becomes less accurate with an increasing number of bubbles as each bubble has a reduced edge length to identify it. Bubbles with no visible edge (i.e. in the centre of a cluster) cannot be isolated and hence are either not detected or contribute to error in detection of other bubbles.
3. Blob analysis (part of the MathWorks[®] MATLAB[®] 2016a computer vision toolbox) was used to detect and quantify various properties of each separated object (Figure 3.8e) – such as, the area, centroid and shape properties of each bubble.

The software was further developed by adapting MathWorks [155] to perform multiple bubble motion tracking, which allowed for transient properties to be identified (e.g. bubble velocity measurement, shape transformation) – for example, the tracking of a newly inject bubble, as shown in Figure 3.9. This was achieved by comparing sequential images using the Kalman filter and Hungarian assignment algorithm. The Kalman filter is a powerful motion tracking function that uses the previous motion of a detected object to predict its future location. For the succeeding frame, a cost matrix is developed comparing the distance between actual detections and predicted object locations. This cost matrix is solved with the Hungarian assignment algorithm, which uses a predefined cost threshold to match the new detections with pre-existing objects. Applying this theory to bubble detection in a video sequence, in the first frame of the video all objects detected are assigned as bubbles and their positions in the next frame are predicted by the Kalman filter – as there is no evidence of the bubbles previous motion, the prediction of the next location is relatively rough. In the following frame, if any object detected satisfies the Hungarian assignment algorithm, it will be recognised as the same bubble and its predicted location will be updated – as there is now more evidence of the bubbles previous motion, the location predicted by the Kalman filter is more accurate. Any object that is not recognised as a pre-existing bubble is logged as a new bubble.

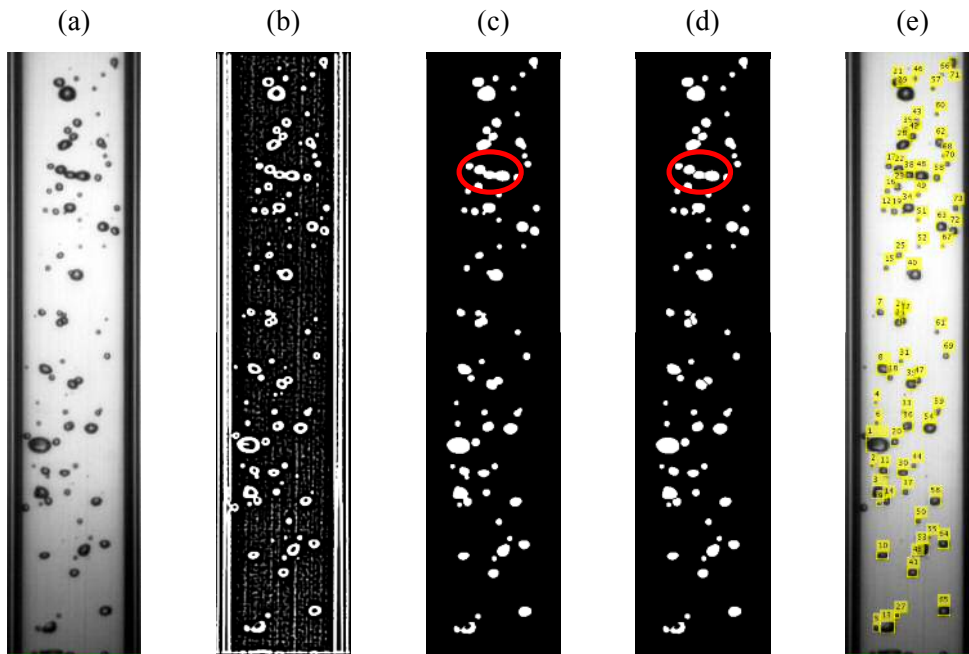


Figure 3.8 Binarisation of a sparse bubbly flow; 0.002% ALR, 233 g/s (§A5.2.1):

- a) original image; b) Gaussian filter applied; c) image binarisation;
 d) watershed algorithm applied; e) bubbles detected and quantified ($n_d=72$, $SMD=1.6$ mm).

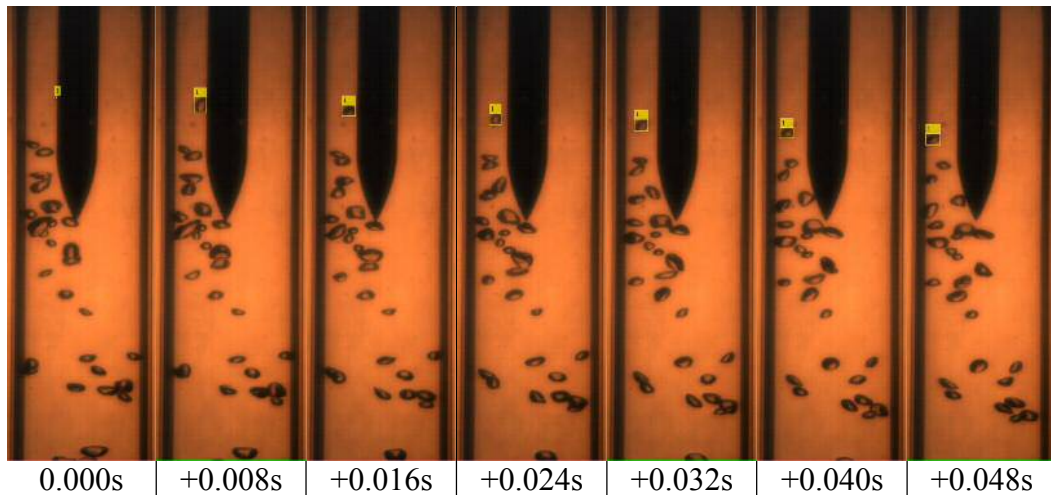


Figure 3.9 Object tracking, bubble injection.

The developed analysis process was found to perform well for datasets featuring dispersed bubbles, where only individual bubbles or small clusters existed. However, the vast majority of experimental images obtained for bubbly flow contained a dense flow, featuring multiple overlapping and/or clustered bubbles (Figure 3.10a) – this was particularly evident in the centreline, where bubbles tend to migrate [65] and due to the increased depth of measurement field. Applying binarisation to these bubbly flow observations was found to result in poor detection accuracy of individual bubbles (Figure 3.10e), due to the absence of defined edges for the majority of bubbles within the images – it can be seen, in this case, that a large proportion of the image is also removed as the cluster of bubbles are identified to intersect the image edge and, hence, are discarded (Figure 3.10b-d). Whilst particularly large features could be filtered out (i.e. analysis conducted on the few isolated, non-clustered bubbles), a subjective size threshold would be required and the sample size would be severely reduced. Furthermore, this analysis would preferentially detect bubbles within the periphery, where the likelihood of overlapping is minimal, and therefore the results may not be representative of the internal flow as a whole. Consequently, the results imply that Shadowography is not an optimal method of bubble quantification with edge detection where a dense bubbly flow may exist.

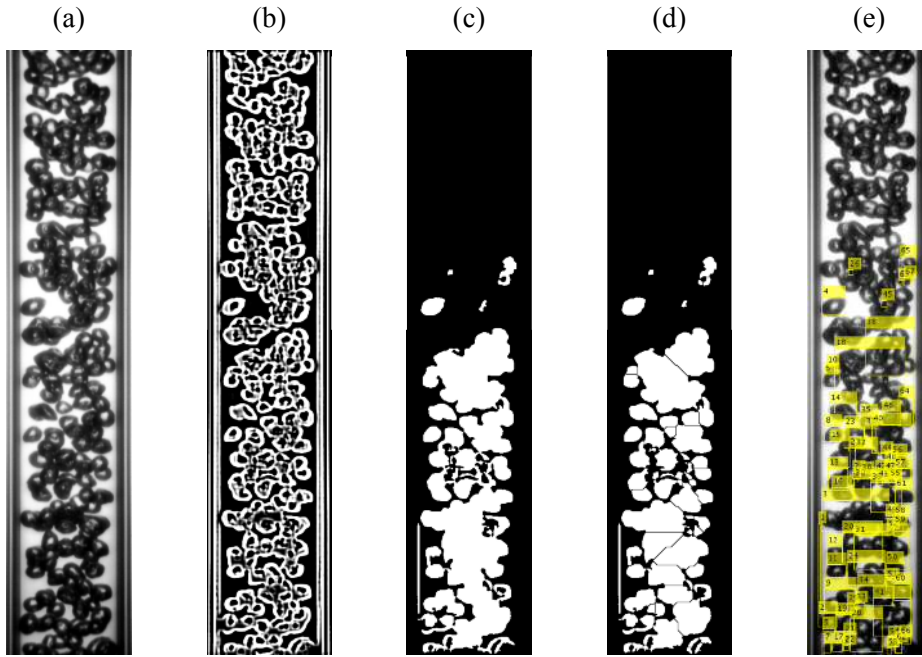


Figure 3.10 Binarisation of a dense bubbly flow; 0.12% ALR, 200 g/s (§A7.1.3)

In an effort to overcome these problems and thus enable bubble quantification, alternative detection techniques were researched. Manual feature detection is the most simplistic resolution, however this must be balanced against use of time resource – in the current investigation, this technique was eliminated due to time restrictions. Alternatively, the orientation of the lighting could be repositioned to the foreground (i.e. forelighting), such that the peripheral bubbles reflect light into the camera – however, this method was not adopted due to concerns that these exterior bubbles could obscure the inner flow regime. Another technique termed “Planar Fluorescence Approach for Bubble Imaging” (PFBI) was reported by Akhmetbekov et al. [156] and Dulin et al. [157] to enable isolation of a single cross-sectional plane within two-phase gas-liquid flow (Figure 3.11). It operates by the addition of a fluorescent dye (e.g. Rhodamine B) into the liquid-phase which, when illuminated with a laser-sheet, emits a different wavelength. All other wavelengths can be eliminated using an optical filter on the camera, which enables individual bubbles intersecting the laser plane to show as rings on the image. Whilst this technique appears promising for internal studies, it was not adopted in the current work due to concerns to human health by spraying the hazardous dye. Owing to these complications, bubble sizing within the current work was not considered practicable and, hence, the scope of the current study was refocussed on defining and optimising the internal flow regime.

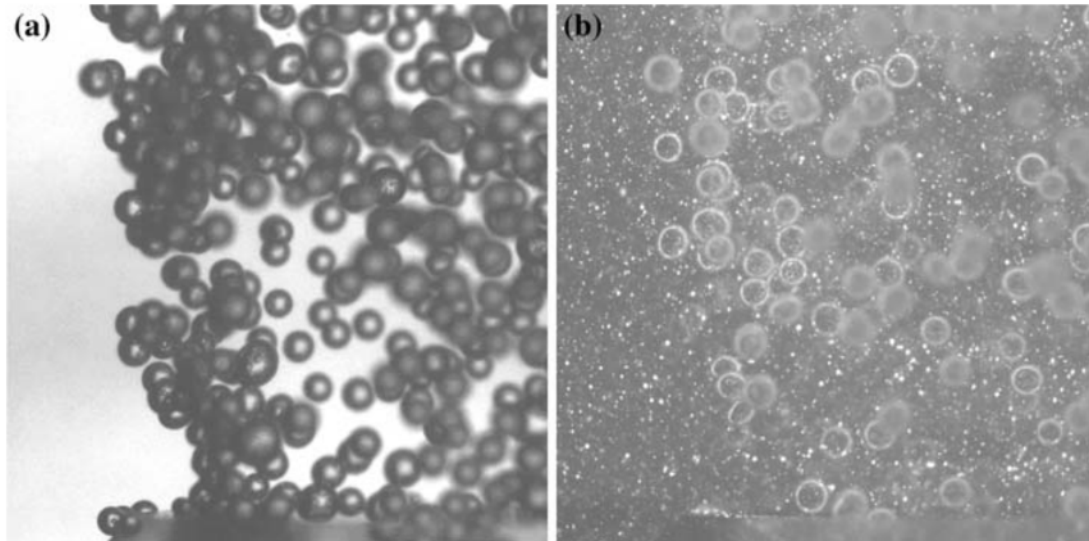


Figure 3.11 Gas-liquid internal two-phase flow imaged with: a) shadowgraphy; b) PFBI.

[157]

3.5 Phase Doppler Anemometry for Spray Characterisation

Phase Doppler Anemometry (PDA) is an alternative optical technique, using light scattering to quantify the number, size and velocity of particles within a flow (e.g. bubbles and droplets). It is a time-averaged point measurement technique, which is suited to detecting small particles in the range of 0.005-1.4 mm diameter [154] – hence, it is a commonly referenced spray characterisation technique within effervescent atomiser studies. A major limitation of PDA is that it is not suitable for dense spray applications, whereby the intensity of measurement light decreases due to attenuation through the spray [86] – experience within Cardiff School of Engineering estimate the capability of PDA to measure a maximum liquid mass flow rate of approximately 60 g/s.

In the interest of a concise discussion, the theory of the PDA working principle is only summarised in the current work – however, it is described in detail within multiple literary sources, such as Konstantinov [16], Kay [92], Dantec Dynamics [158], and shown in Figure 3.12. PDA operates by intersecting multiple laser beams to form a miniscule control volume, consisting of multiple parallel interference fringes of high light intensity. Light is scattered as a particle travels through these fringes which is sensed on a photodetector as a “burst signal”, with the frequency between signal peaks being proportional to the particle velocity. The droplet diameter is calculated by comparing the particle burst signals from three offset photodetectors – the phase difference between these signals is proportional to the particle size. As it is essential to avoid interference from different light scattering modes from

particle burst signals are detected by photomultipliers within the receiving optics, which are transferred and managed by a Dantec[®] 58N10 PDA BSA processing unit before being sent to a computer for further processing, presentation and storage by Dantec Dynamics[®] BSA Flow Software. High quality data was achieved with this set-up using 20% sphericity validation, with data rates in the spray generally over 1 kHz and validation rates over 90%.

Unlike other optical techniques (e.g. digital imaging), PDA is a point measurement technique and so cannot quantify flow across an entire plane in an instance. Therefore, the optics were mounted onto a three-axis traverse, which allowed movement of the control volume within the spray and was automatically controlled via a connected PC with Dantec[®] SIZEWARE software. A suitable traverse mesh should have sufficient measurement locations to provide data representative of the spray profile, however few enough points to minimise computational and time resource. An identical traverse mesh was used across the PDA experimentation (Figure 3.13) and hence the data collection was structured and consistent for all investigations – it was generated with the following considerations:

- As a stable effervescent atomiser spray can be considered axisymmetric [160], a half cross-section of the spray can be assumed to be representative of any spray cross-section and hence is representative of the spray in its entirety – this greatly reduces the complexity and number of measurement points required within the traverse mesh.
- A similar mesh density was used in the current investigation to that utilised by Konstantinov [16] for an effervescent atomiser spray on the same experimental apparatus. In the current investigation, 285 individual measurement locations were examined for each individual investigation, which corresponds to 1 mm radial spacing for 25, 50, 100 and 150 mm axial displacements, and 2 mm radial spacing for 200 and 250 mm axial displacements.
- The spray edge was defined as the radial position at which data rates dropped below 10% of their maximum at that axial location – this method was adopted by Konstantinov [16] and Jedelsky et al. [114]. A preliminary investigation was performed for various atomiser configurations to identify the widest spray cone angle. The radial limit was therefore set in excess of this to minimise measurement points outside of the spray edge – this was found to be effective, as all 10% spray edges for the experimentation were captured within this mesh.

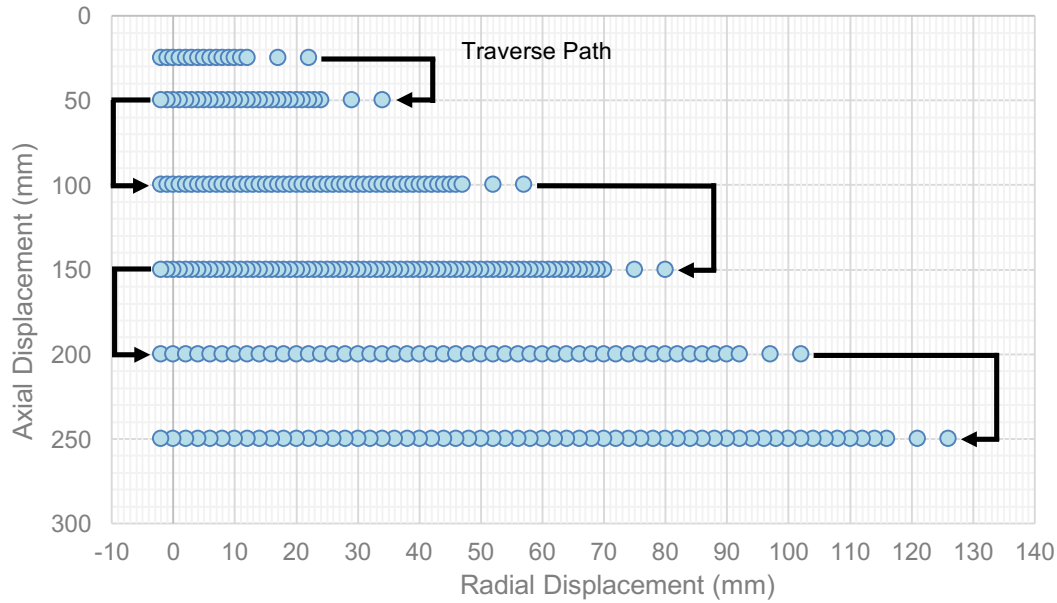


Figure 3.13 Phase Doppler Anemometry, sampling mesh.

A fixed five second sampling duration for each measurement location was adopted – this was reported by Konstantinov [16] to enable droplet size accuracy for effervescent atomiser sprays to within one micrometre of the true value. As a consequence, the resource allocation for a single investigation, consisting of 285 measurement locations, was:

- Time: ~3600 s, comprising of ~1400 s measurement and ~2200 s traverse movement.
- Data Storage: 89-605 MB, depending on the number of droplets detected.

3.5.2 Analysis Techniques

Handling and analysis of all PDA data was performed with MathWorks® MATLAB® 2016a, whereby all measurement locations outside of the 10% spray edge were considered to consist of ambient particles (e.g. airborne particles, recirculated droplets) and neglected from the analysis.

Lefebvre [12] reported that the certainty (i.e. accuracy) of weighted average data (i.e. D32, SMD) decreases with droplet number, due to the addition or absence of dominating large droplets – the percentage accuracy per droplet number was plotted (Figure 3.14) and a trend identified to allow for accuracy estimates for the current investigation.

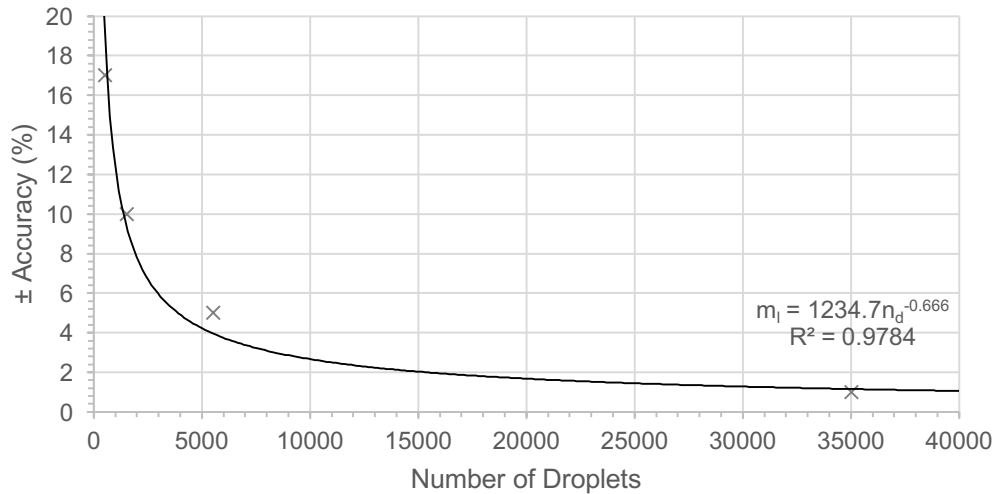


Figure 3.14 Predicted accuracy of weighted droplet diameters statistics. [12]

This relationship was used to quantify the predicted accuracy of the SMD results for cumulative spray data, which was produced by summing all measurement locations within the spray edge (i.e. 1D analysis). The minimum cumulative droplet count for a single investigation in the current work was 483094, whilst the maximum was 3198057 – this corresponds to upper and lower SMD confidence limits of 99.8-99.9% across the current work. This was deemed suitable accuracy, and hence particle size distributions for cumulative spray data were presented in weighted (D32) and unweighted (D10) forms. Cumulative data plots were generated for each investigation with automated computer script developed within MathWorks® MATLAB® 2016a – for example, Figure 4.35.

However, the measurement certainty was seen to dramatically decrease when this data is assessed against its acquisition position within the spray volume (i.e. 2D analysis) – particularly for poorly atomised sprays on the spray edge. In the extreme minimum case, 130 droplets were identified for a single location for the entire sampling duration – this corresponds to an unacceptable 51.9% SMD confidence. To achieve 95% SMD confidence on the spray edge for this case, 5500 droplets would be required. Assuming linear scaling of resource, a single investigation would require:

- Time: ~62500 s, comprising of ~60300 s measurement and ~2200 s traverse movement.
- Storage: 3.8-25.6 GB.

This was deemed an unacceptable allocation of resource, and hence it was not practicable to provide weighted droplet diameters as a function of position. Instead, this data was presented in unweighted form, which enabled comparison between results in the current work and

identification of flow features and spray properties. Positional data plots were generated for each investigation with automated computer scripts developed within MathWorks® MATLAB® 2016a – for example, Figure 4.34.

The gas velocity was determined by assuming that droplets with diameter less than 2 μm act as seeding particles within the gas flow – this technique has been widely used in other research reports [16, 92, 161, 162]. For locations that have no droplets satisfying this criteria, the gas velocity cannot be determined and, hence, is assumed to be zero.

3.6 Programme of Work

The current investigation was conducted over four investigations, which are presented in separate chapters. The experimental methodology for each is provided in this section.

3.6.1 Identification of Optimal Internal Flow to Facilitate Stable Effervescent Atomisation (Chapter 4)

The OEA and auxiliary systems were used within the current study to examine the effect of fluid flow rates on the internal flow behaviour and atomisation mechanisms on effervescent atomisation (Table 3.3). Each test point was conducted at 5 bar_g operating pressure and utilised water and air as the operating fluids. The liquid flow rate was controlled by varying the exit orifice diameter between 1.0-2.0 mm, with gas supply varied in increments up to 5% ALR (i.e. 0.12, 0.25, 0.5, 1.0, 1.5, 2.0, 3.0, 4.0 and 5.0 %). A conventional flat-end and a streamlined aerator body design were investigated (Figure 3.15) – the streamlined aerator utilised a DARPA SUBOFF afterbody [1] design, termed “ADARPA” within this thesis. For both configurations, the aerator had 16 x 0.4 mm aerator orifices (i.e. 2.01 mm²) and an outer tube diameter of 5 mm. The optical mixing chamber was cylindrical and 7 mm in diameter. A worst case operating scenario was adopted, with the OEA orientated vertically downwards and started from unbled conditions (i.e. the mixing chamber evacuated of liquid). The sequence of fluid delivery to the atomiser for each test point was gas supply prior to liquid supply – this is thought to be in accordance with most industrial applications. Various exit orifice diameters were investigated, however each had a common convergence angle of 45° (i.e. $2\beta=90^\circ$).

Table 3.3 Test matrix, Chapter 4.

Section No	§4
Exit Orifice Diameter (mm)	1.0, 1.5, 2.0
ALR (%)	0-5
Aerator Body Design	Flat-End, ADARPA
Aerator Orifice Design	16 x 0.4 mm
Mixing Chamber Diameter (mm)	8
Operating Pressure (bar)	5
Orientation	Vert. Down.

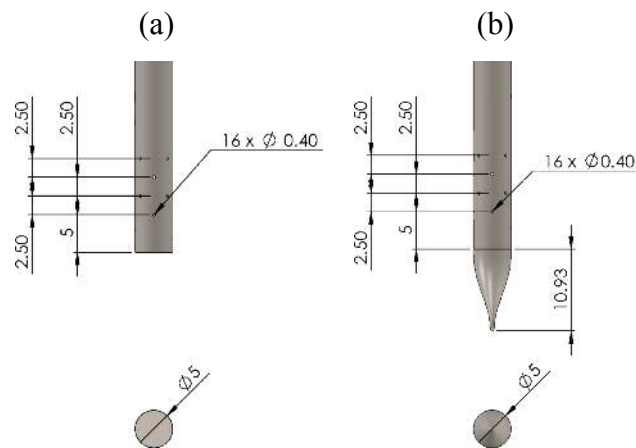


Figure 3.15 Investigated aerator designs (dimensions in mm):
a) conventional flat-end aerator; b) streamlined ADARPA aerator.

High-Speed Shadowgraphy was used to observe the internal flow. The OEA and camera were positioned such that the entire internal flow process (i.e. gas injection to exit orifice supply) was observable within the field of view. Backlighting was provided with two diffused 1000 W halogen light sources – these were positioned such that each light source provided sufficient and even lighting across the scene. Camera settings of 3000 Hz frame rate and 170 μ s shutter time were used across these studies – these were experimentally determined to minimise image blurring, allow sufficient illumination and provide adequate time resolution to track the flow features.

High-Speed Shadowgraphy was also used to observe the near-nozzle atomisation mechanisms (Figure 3.16). The camera was repositioned to allow spray generation to

dominate the field of view. The following camera settings were adapted to optimise the image quality: 1000 Hz frame rate and 30 μ s shutter time.

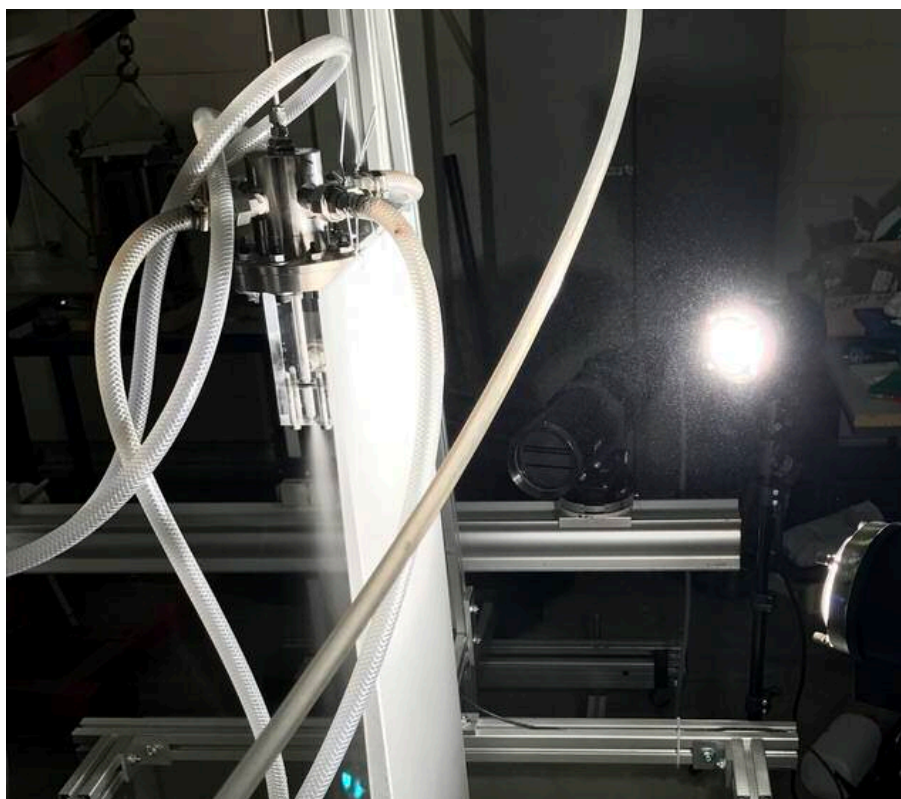


Figure 3.16 OEA, near-nozzle Shadowography study.

Finally, Phase Doppler Anemometry (PDA) was utilised to quantify the spray properties (Figure 3.17). It was previously discussed that the recommended maximum flow rate is approximately 60 g/s – this is based upon the extensive experience held at Cardiff University. Appropriate exit orifice diameters were selected to comply with this limitation – consequently, the maximum liquid flow rate investigated with PDA in this investigation was 63 g/s, corresponding to the 2 mm exit orifice diameter at 5 bar_g operating pressure and 0.12% ALR.



Figure 3.17 OEA, PDA study.

N.B. To aid concise discussion of results, example images of gas-injection and flow regimes identified within the subsequent investigations are also presented within Chapter 4 – the experimental methodology to obtain these results is discussed in the further sections.

3.6.2 Internal Flow Studies of Flat-End Aerators to Optimise Bubbly Flow Operation (Chapter 5)

The IFOR and auxiliary systems were used within the current study to examine the effect of various independent parameters on the internal flow behaviour of conventional flat-end aerator effervescent atomiser designs. Multiple independent variables were varied throughout the investigation and compared to the benchmark configuration, as per Table 3.4. In the benchmark configuration, the aerator design (A5) had 16 x 0.75 mm aerator orifices, an outer tube diameter of 10 mm, fixed aeration area of 7.07 mm² and a conventional flat-end aerator body design. The optical mixing chamber was cylindrical and 20 mm in diameter. Each test point was conducted at 5 bar_g operating pressure and utilised water and air as the operating fluids. A worst case operating scenario was adopted, with the OEA orientated vertically downwards and started from unbled conditions (i.e. the mixing chamber evacuated of liquid). The sequence of fluid delivery to the atomiser for each test point was

gas supply prior to liquid supply – this is thought to be in accordance with most industrial applications. The flow conditions were controlled by varying the discharge nozzle settings and the input fluid flow rates – this simulates two methods of turndown, with the third being operating pressure which is investigated in a further study. Common discharge valve settings were achieved between investigations by adjusting the discharge valve to achieved specific flow rates at 0% ALR (i.e. 30, 60, 90, 120, 180, 240 and 290 g/s at 5 bar_g operating pressure) – each valve setting replicates a different exit orifice diameter and is consequently a method of turndown. The gas supply was varied in increments either up to the maximum achievable flow rate for the given aerator design (7 bar_g maximum supply pressure) or 5% ALR (i.e. 0.12, 0.25, 0.5, 1.0, 1.5, 2.0, 3.0, 4.0 and 5.0 %). Alternative flow conditions were occasional tested, to better define or quantify flow mechanisms within the operating range.

Aerator orifice diameter was investigated as an independent variable for conventional cross-flow aerators within the current investigation – shown as A2-5 in Table 3.7. Each of these aerators had an outer tube diameter of 10 mm, a conventional flat end body and common aeration area of 7.07 mm². To maintain a common aeration area with differing aerator orifice diameters, the aeration orifice configuration (e.g. number of orifices, hole positioning) was required to be varied between the investigated aerators – in general, the intention of the aerator designs was to maximise the orifice spacing within a 15 mm region and 10 mm from the aerator tip.

Unconventional aerator designs were also investigated – shown as A1 and A6 in Table 3.7. The co-flow aerator had a single central 3.0 mm injection orifice located at the base of the aerator – this maintained the common aeration area of 7.07 mm². A porous aerator was also investigated, which injected gas through a sintered stainless steel medium. Both of these aerators had an outer tube diameter of 10 mm and a conventional flat end body.

Table 3.1 Test matrix, Chapter 5.

Independent Variable	Benchmark Configuration	Aerator Orifice Diameter	Unconventional Aerator Designs	Mixing Chamber Diameter	Operating Pressure	Orientation
Section No	§5.2	§5.3	§5.4	§5.5	§5.6	§5.7
Discharge Valve Setting (g/s)	30-290 ^[1]	30-290 ^[1]	30-290 ^[1]	30-290 ^[1]	30-225 ^[2] 30-130 ^[3]	30-290 ^[1]
ALR (%)	0-5	0-5	0-5	0-5	0-5	0-5
Aerator Geometry	A5	A2-A4	A1, A6	A5	A5	A5
Mixing Chamber Diameter (mm)	20	20	20	14	20	20
Operating Pressure (bar)	5	5	5	5	1, 3	5
Orientation	Vert. Down.	Vert. Down.	Vert. Down.	Vert. Down.	Vert. Down.	Vert. Up.

[1] m₃@ 0% ALR, 5 bar: 30, 60, 90, 120, 180, 240, 290 g/s [2] m₃@ 0% ALR, 3 bar: 30, 60, 90, 120, 180, 225 g/s [3] m₃@ 0% ALR, 1 bar: 30, 60, 90, 130 g/s

For each test point, the gas injection regime in the near region of the aerator and the stabilised two-phase flow regime were imaged using High-Speed Shadowography (Figure 3.18). It was advantageous to maximise the observable mixing length, such that the two-phase flow within the mixing chamber has the best chance to stabilise and, hence, the recording was performed at two points in the mixing chamber. Firstly, the camera was positioned to capture the gas injection process from the most upstream aerator orifice (**N.B.** this position varied with respect to the aerator tip), which is considered to represent the start of the internal mixing process. The camera was then accurately moved with a computer controlled traverse in the downstream flow direction, such that the top of the field of view was aligned to the bottom of the initial recording, and the internal flow was recorded. The rig and camera were positioned such that the field of view of the camera enabled measurement of 108 mm flow length, and hence the mixing length assessed for each configuration was 216 mm. Backlighting for Shadowography was provided with a 1000 W diffused halogen light source – this was positioned such that sufficient lighting was provided for upstream and downstream scenes. Camera settings of 500 Hz frame rate and 300 μ s shutter time were used across these studies – these were experimentally determined to minimise image blurring, allow sufficient illumination and provide adequate time resolution to track the flow features.



Figure 3.18 IFOR, Shadowography study.

3.6.3 Internal Flow Studies of Streamlined Aerators to Reduce Wake Effect (Chapter 6)

The IFOR and auxiliary systems were used within the current study to examine the effect of streamlined aerator body designs on the internal flow behaviour of an effervescent atomiser. Four streamlined aerator body designs were investigated and are shown in Figure 3.19 – these were selected from the literature as profiles with minimal coefficient of drag.

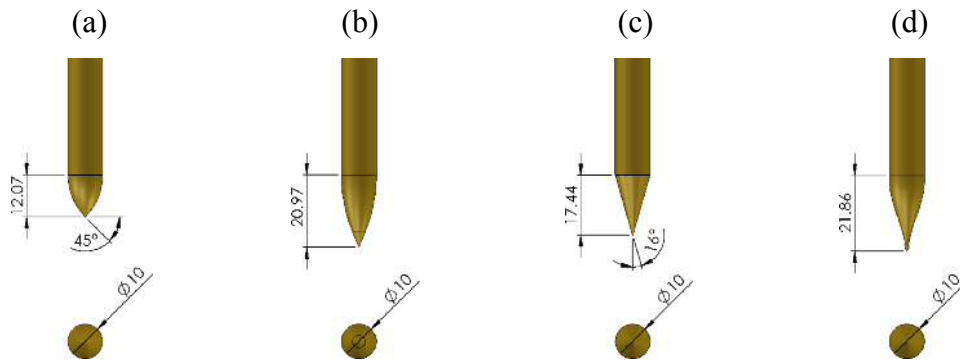


Figure 3.19 Streamlined aerator body designs (dimensions in mm):

- a) CA – 45° “circular arc” [48]; b) H – circular arc/conical “hybrid” [49];
c) C – 16° “conical” [48]; d) A – “ADARPA” [1].

N.B. A streamlined aerator is referenced with the body tag – for example, aerator A5 with an ADARPA body design (body tag “A”) has reference A5A.

The current investigation consisted of two parts. Firstly, the streamlined aerator tips were assessed on their ability to passively bleed the mixing chamber of ambient air upon start-up and detach an established gas void within the aerator wake without gas injection (i.e. 0% ALR) – these tests were developed with respect to the experimental results and so the methodology is described in detail within the results chapter (§6.1).

Finally, the internal flow was quantified for each aerator body design using an identical atomiser configuration and operating procedure from the benchmark configuration in the previous study (§3.6.2) – the relevant test matrix is provided in Table 3.5.

Table 3.5 Test matrix, Chapter 6.

Independent Variable	Benchmark Configuration	Streamlined Aerator Body Design
Section No	§5.2	§6.2
Discharge Valve Setting (g/s)	30-290 ^[1]	30-290 ^[1]
ALR (%)	0-5	0-5
Aerator Geometry	A5	A5CA, A5C, A5H, A5A ^[2]
Mixing Chamber Diameter (mm)	20	20
Operating Pressure (bar)	5	5
Orientation	Vert. Down.	Vert. Down.

[1] m_i @ 0% ALR, 5 bar: 30, 60, 90, 120, 180, 240, 290 g/s

[2] CA = Circular Arc, C = Conical, H = Hybrid, A = ADARPA

An equivalent measurement set-up was used as per the previous study (§3.6.2), in which the gas injection regime in the near region of the aerator and the stabilised two-phase flow regime were imaged using High-Speed Shadowography.

3.6.4 Internal Flow Studies of ADARPA Aerators to Optimise Bubbly Flow Operation (Chapter 7)

The IFOR and auxiliary systems were used within the current study to examine the effect of various independent parameters on the internal flow behaviour of unconventional ADARPA aerator effervescent atomiser designs. Multiple independent variables were varied throughout the investigation and compared to a benchmark configuration, as per Table 3.6 – barring the aerator body design, this was equivalent to the benchmark configuration for the conventional flat-end aerator experiments, discussed in §3.6.2.

Aeration area was also investigated as independent variable for unconventional ADARPA aerators within the current investigation – shown as A5 and A7-9 in Table 3.7. Each of these aerators had an aerator orifice diameter of 0.75 mm, an outer tube diameter of 10 mm and a streamlined ADARPA body.

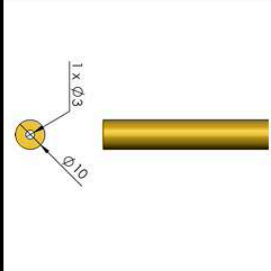
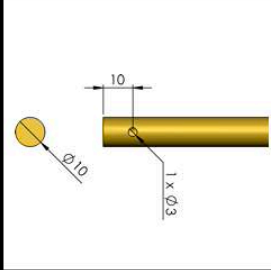
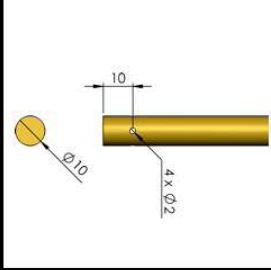
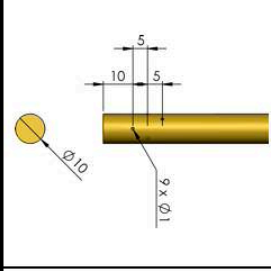
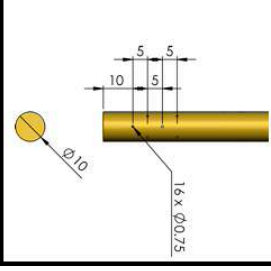
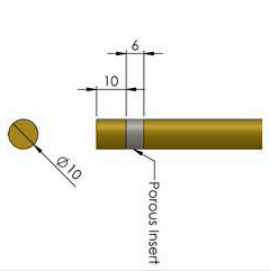
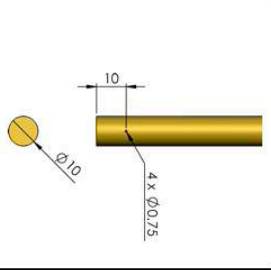
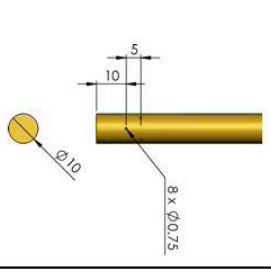
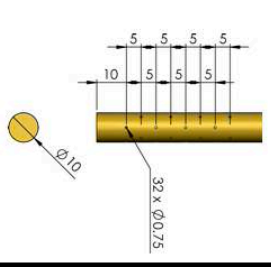
An equivalent measurement set-up was used as per the previous studies (§3.6.2, §3.6.3), in which the gas injection regime in the near region of the aerator and the stabilised two-phase flow regime were imaged using High-Speed Shadowography.

Table 3.2 Test matrix, Chapter 7.

Independent Variable	Benchmark Configuration	Aerator Orifice Diameter	Unconventional Aerator Designs	Aeration Area	Mixing Chamber Diameter	Operating Pressure	Orientation
Section No	§7.2	§7.3	§7.4	§7.5	§7.6	§7.7	§7.8
Discharge Valve Setting (g/s)	30-290 ^[1]	30-290 ^[1]	30-290 ^[1]	30-290 ^[1]	30-290 ^[1]	30-225 ^[2] 30-130 ^[3]	30-290 ^[1]
ALR (%)	0-5	0-5	0-5	0-5	0-5	0-5	0-5
Aerator Geometry	A5A	A2A-A4A	A6A	A7A-A9A	A5A	A5A	A5A
Mixing Chamber Diameter (mm)	20	20	20	20	14, 25	20	20
Operating Pressure (bar)	5	5	5	5	5	1, 3	5
Orientation	Vert. Down.	Vert. Down.	Vert. Down.	Vert. Down.	Vert. Down.	Vert. Down.	Vert. Up.

[1] m₃/@ 0% ALR, 5 bar: 30, 60, 90, 120, 180, 240, 290 g/s [2] m₃/@ 0% ALR, 3 bar: 30, 60, 90, 120, 180, 225 g/s [3] m₃/@ 0% ALR, 1 bar: 30, 60, 90, 130 g/s

Table 3.7 Aerator Designs.

Aerator Tag	A1	A2	A3	A4	A5
Aerator Orifice Diameter	1 x 3.0 mm	1 x 3.0 mm	4 x 2.0 mm	9 x 1.0 mm	16 x 0.75 mm
Aeration Area	7.07 mm ²	7.07 mm ²	7.07 mm ²	7.07 mm ²	7.07 mm ²
Injection Direction	Co-Flow	Cross-Flow	Cross-Flow	Cross-Flow	Cross-Flow
Design					
Aerator Tag	A6	A7	A8	A9	
Aerator Orifice Diameter	Porous	4 x 0.75 mm	8 x 0.75 mm	32 x 0.75 mm	
Aeration Area	7.07 mm ²	1.77 mm ²	3.53 mm ²	14.14 mm ²	
Injection Direction	Cross-Flow	Cross-Flow	Cross-Flow	Cross-Flow	
Design					

CHAPTER 4. IDENTIFICATION OF OPTIMAL INTERNAL FLOW TO FACILITATE STABLE EFFERVESCENT ATOMISATION

This chapter characterises the complete effervescent atomisation process across a wide range of flow conditions and atomiser configurations. The gas injection phenomena at the aerator are identified and quantified and, for the first time, related to the flow regimes generated within the mixing chamber. Finally, the effect of differing internal flows and fluid flow rates on the effervescent atomisation mechanisms are presented.

N.B. This chapter includes internal flow observations of experimentation presented in the further chapters. It is intended to better describe the internal flow and streamline further discussions.

4.1 Observed Gas Injection Regimes

The process of gas injection at the aerator was observed for various inside-out effervescent atomiser configurations and quantified for the first time by categorising each observation into common regimes. This work was performed across various fluid flow rates and independent parameters, which resulted in the identification of seven different gas injection regimes – these are a combination of the standard gas injection regimes defined previously in the literature, and new regimes defined in the current work to better describe the experimental observations.

These were further analysed for each investigated atomiser configuration by plotting each identification against its corresponding operating condition to form a series of gas injection regime maps, which allows for iteration between the tested operating conditions and comparison between the investigated independent parameters – these are presented for all experiments within Appendices 3-5. By analysing these maps, the typical regions for each of the gas injection regimes can be identified and are provided in Figure 4.1. It should be noted

that the formation and positioning of these regions were observed to be heavily dependent on the independent variables – this forms the basis of discussions in the further chapters.

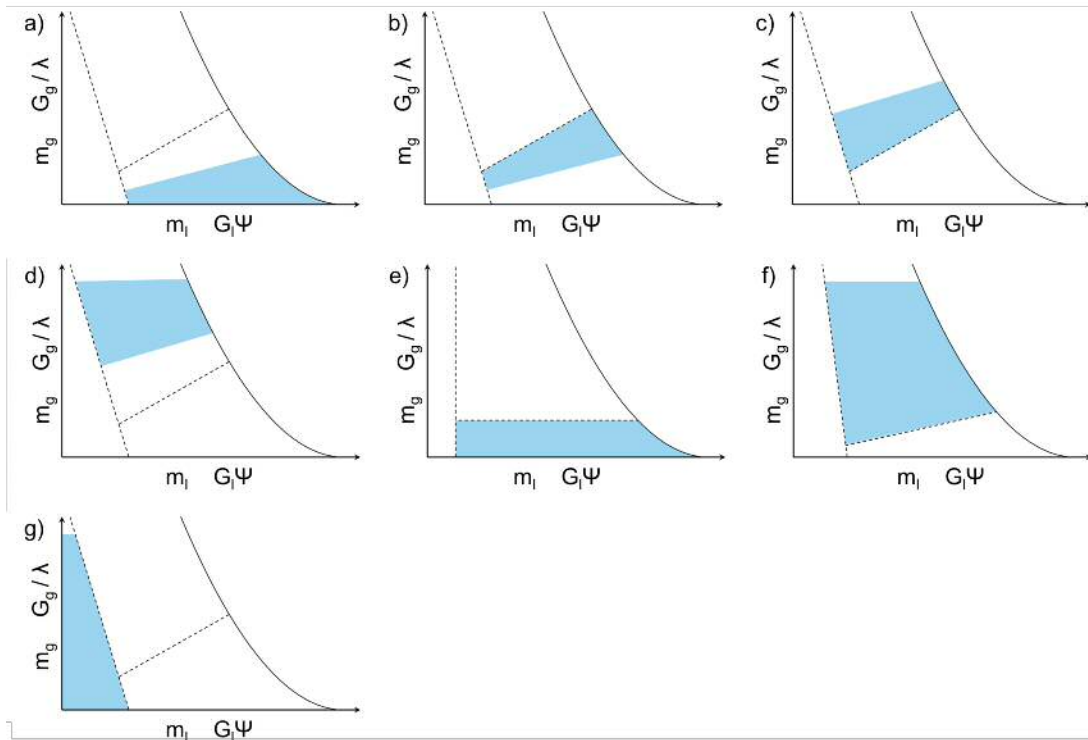


Figure 4.1 Relative positioning of each gas injection regime within a generic map
 a) single bubbling (§4.1.1); b) pulse bubbling (§4.1.2); c) elongated jetting (§4.1.3);
 d) atomised jetting (§4.1.4); e) cavity forming (§4.1.5); f) coalesced jetting (§4.1.6);
 g) evacuated chamber (§4.1.7).

The exit orifice diameter (often simulated with a discharge nozzle in the current investigation) was seen to affect the gas injection regimes throughout the trials, where an increased nozzle restriction acted to reduce the fluid flow rates through the effervescent atomiser at a given operating pressure. This was seen to particularly affect the internal flow when operating in a vertically downwards orientation, where a decreased exit orifice diameter reduced the Bakers numbers (i.e. superficial fluid velocities) – this increased the proportional contribution of gas-phase buoyancy compared to the opposing liquid viscous forces (i.e. drag and inertia). Consequently, at critically low liquid Bakers numbers for all atomiser configurations in a vertically downwards orientation, the liquid shear and momentum upon start-up were insufficient to displace the ambient air within the mixing chamber (i.e. failure to passively bleed mixing chamber) and, therefore, the gas was injected into a pre-existing gas core – these unique observations were characterised into a newly presented gas injection regime, coined evacuated chamber (§4.1.7).

Assuming that the evacuated chamber regime was avoided (e.g. large exit orifice diameter, high operating pressure, vertically upwards orientation), the gas-phase was injected directly into a liquid continuum where, depending on the operating conditions and atomiser configuration, it would either break-up into bubbles within the near-aerator region or form a continuous gas jet. The stability of the emerging gas-phase, and hence its resistance to break-up into bubbles, was seen to decrease with:

1. **High relative detachment forces:** Generated by strong detachment mechanisms, for example viscous forces generated by high liquid cross-flow velocity (e.g. drag, inertia), and weak restoring mechanisms, for example buoyancy. Encouraged by high liquid flow rates (e.g. large exit orifice diameters, increased operating pressure), small mixing chamber diameters and vertically upwards orientation.
2. **High emerging gas-liquid interface area:** Increases the exposed area of the emerging gas-phase over which the detachment mechanisms act. Encouraged by small aerator orifice diameters.
3. **Low injected gas velocity:** Increases the detachment rate of gas within the liquid cross-flow compared to the supply rate – this acts to suppress the generation of long gas necks connecting an otherwise detached bubble to the aerator orifice. Encouraged by low gas flow rates (i.e. low ALRs) and high aeration areas.

Consequently, the effect of increasing the stability of the emerging gas-phase (e.g. increasing the ALR) was seen to increase the size of the gas entities produced at the aerator and, therefore, generally transition the gas-injection regime through the bubbling regimes, from single bubbling (§4.1.1) to pulse bubbling (§4.1.2), and finally to jetting at high ALRs, which featured elongated jetting (§4.1.3) and atomised jetting (§4.1.4) – this is in agreement with the literature reports [32, 39]. However, in exceptional cases and for specific atomiser configurations, alternative gas injection regimes were instead observed which did not follow this trend – for example cavity forming (§4.1.5) and coalesced jetting (§4.1.6).

4.1.1 Single Bubbling

Single bubbling was observed to be the formation of individual uniformly sized bubbles, which were either sheared directly from the emerging gas-phase at the aerator orifice or detached from a short “teardrop” shaped gas neck within the peripheral liquid flow – this is in agreement with the literature descriptions [32, 33, 39]. Single bubbling was observed to be promoted by the injection of a highly unstable gas-phase into a liquid continuum (i.e. highest relative detachment forces, highest emerging gas-liquid interface area and/or lowest injected

gas velocity) and, hence, was promoted by: low ALRs, decreased aerator orifice diameters, increased aeration areas, decreased mixing chamber diameters and increased operating pressures. Example observations of single bubbling across a variety of experiments are shown in Figure 4.2.

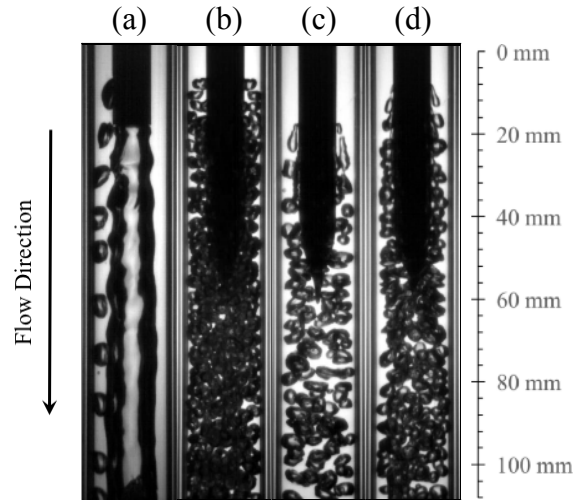


Figure 4.2 Example observations of single bubbling:

- a) 275 g/s, 0.03% ALR (§A5.1.1); b) 92 g/s, 0.24% ALR (§A6.1.3);
 c) 149 g/s, 0.13% ALR (§A7.2.2); d) 194 g/s, 0.12% ALR (§7.2).

Upon injection, the bubbles were drawn away from the aerator with the liquid flow into the mixing chamber. As will be discussed in detail in §5.1, a gas void was observed to be present in the aerator wake region for every instance of single bubbling with a flat-end aerator design and in a vertically downwards orientation (e.g. Figure 4.2a), which indicates that the small bubbles generated through single bubbling do not sufficiently interfere with the gas void to enable its detachment.

4.1.2 Pulse Bubbling

Pulse bubbling was observed for conditions in which the emerging gas-phase had increased stability over single bubbling (e.g. increased ALR, increased aerator orifice diameters, decreased aeration area) and, thus, gas-phase injection generates gas entities of varying size (e.g. bubble and slugs).

In the majority of pulse bubbling cases, a rippling gas neck was observed to be injected into the peripheral liquid flow which resembled a series of interconnected gas entities. Given

sufficient residence time and breakup mechanisms, these instabilities on the gas-liquid interface eventually gain sufficient amplitude to separate the neck into gas entities of varying size. These observations correspond with the definitions provided within the literature [32, 39, 42] and examples are shown in Figure 4.3a-d.

Alternative pulse bubbling modes were observed in isolated cases, in which irregularly sized bubbles were injected into the mixing chamber – these observations do not correspond with existing descriptions within the literature and so are defined within the current work. In some cases, non-uniformly sized gas entities were formed due to break up of a notably elongated gas necks emitting from the aerator (Figure 4.3e-h). In addition, a transient gas injection phenomenon was also observed in some cases, whereby the gas flow rate appears to pulse and form gas entities of varying size (Figure 4.4). This was also defined as pulse bubbling by Balzán et al. [39] and is thought to result from pressure fluctuations within the mixing chamber originating from the discharge of a heterogeneous flow regimes [41] – it was seen to be exaggerated when operating in a vertically upwards orientation due to the additional hydrostatic head of liquid.

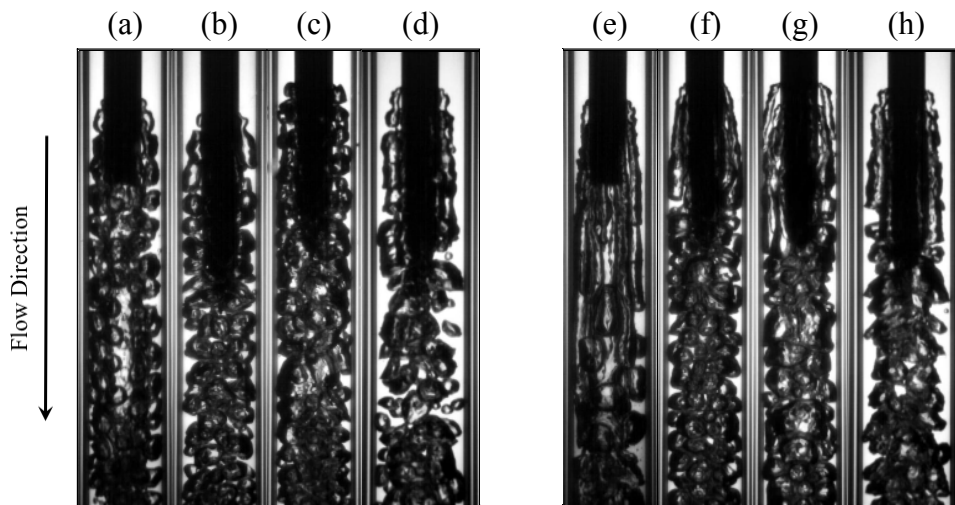


Figure 4.3 Example observations of pulse bubbling:

- a) 221 g/s, 0.38% ALR (§A5.1.3); b) 150 g/s, 0.12% ALR (§A7.1.3);
- c) 234 g/s, 0.25% ALR (§7.2); d) 194 g/s, 0.12% ALR (§A7.5.2);
- e) 221 g/s, 0.40% ALR (§A5.1.3); f) 122 g/s, 0.50% ALR (§A6.1.3);
- g) 122 g/s, 0.50% ALR (§4.1.1); h) 234 g/s, 0.25% ALR (§A7.4.3).

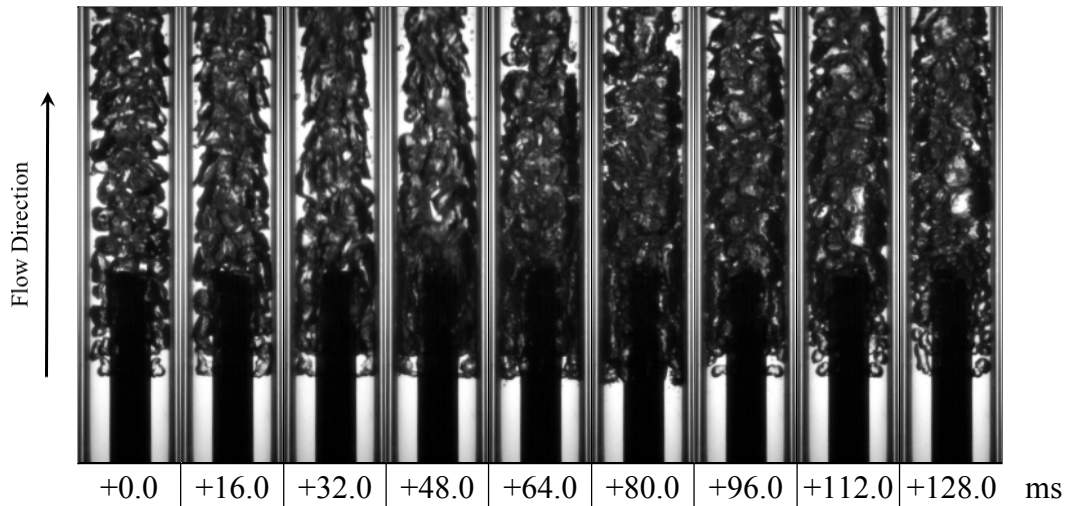


Figure 4.4 Pulse bubbling, transient gas injection. 77 g/s, 0.99% ALR (§A5.5.2).

For flat-end aerator designs in a vertically downwards orientation, pulse bubbling appears to straddle the conditions for which a gas void can be maintained in the aerator wake. Typically, a gas void was present for pulse bubbling at low ALRs, which corresponds to the injection of relatively small gas entities that were forced to flow around the liquid periphery. This void was observed to be displaced at higher ALRs within the pulse bubbling regime, which is thought to be due to the emerging gas generating sufficient interference on the void to overcome its buoyancy within the aerator wake – this was observed to be affected by numerous independent parameters.

4.1.3 Elongated Jetting

The elongated jetting regime was observed with increased stability of the emerging gas-phase (e.g. increased ALR), where a continuous gas jet is injected from the aerator orifice, which can chaotically break up significantly downstream of the aerator – this is in agreement with the description recently proposed by Balzán et al. [39]. Increasing the ALR through the elongated regime causes the gas jet to emerge from the aerator orifice with ever increasing momentum – this can cause it to contact with the mixing chamber, however little churning occurs. Infrequently, a small bubble may be generated due to exposure of the emerging jet to the liquid cross-flow, contact with the mixing chamber wall or shearing of the gas-liquid interface, however this is not considered to constitute as a suitable bubble formation mechanism for effervescent atomisation. Examples of elongated jetting across a variety of experiments are shown in Figure 4.5.

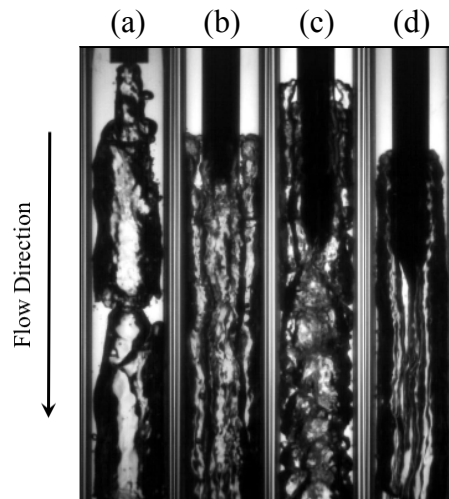


Figure 4.5 Example observations of elongated jetting:

- a) 107 g/s, 0.99% ALR (§A5.2.1); b) 151 g/s, 1.00% ALR (§A5.1.2);
 c) 106 g/s, 0.99% ALR (§A6.1.1); d) 186 g/s, 0.25% ALR (§A7.2.1).

A buoyant gas void within the aerator wake was not observed for any occurrence of elongated jetting within vertically downwards operation with a flat-end aerator, suggesting the emerging gas jet exerts sufficient disruption to prevent its formation but also adequate momentum to counteract the effects of its own buoyancy.

4.1.4 Atomised Jetting

Atomised jetting was promoted by a very stable emerging gas-phase, in which a continuous gas jet was observed to be injected into the mixing chamber. This has visibly more chaos than that associated with elongated jetting and is in agreement with the descriptions recently proposed by Balzán et al. [39]. As the ALR increases within the atomiser jetting regime, the emerging gas jet becomes ever more turbulent and the majority of cases have sufficient momentum to contact the mixing chamber wall, often with significant churning. In addition, a small number of comparatively small bubbles were frequently sheared from the gas jet upon initial exposure of the gas-phase to the liquid cross-flow, contact with the mixing chamber wall or shearing of the gas-liquid interface – this is not considered to constitute as a suitable bubble formation mechanism for effervescent atomisation. Examples of atomised jetting across a variety of experiments are shown in Figure 4.6.

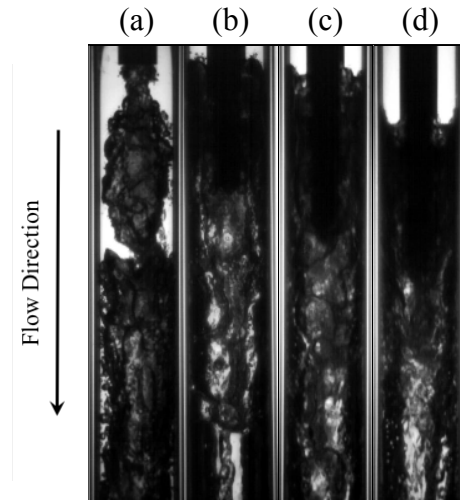


Figure 4.6 Example observations of atomised jetting:

- a) 152 g/s, 2.01% ALR (§A5.2.1); b) 62 g/s, 1.97% ALR (§5.2);
 c) 144 g/s, 2.39% ALR (§A6.4.1); d) 152 g/s, 2.01% ALR (§A7.2.2).

A buoyant gas void within the aerator wake was not observed for any occurrence of atomised jetting within vertically downwards operation, suggesting the emerging gas jet exerts sufficient disruption to prevent its formation, but also adequate momentum to counteract the effects of its own buoyancy.

4.1.5 Cavity Forming

Cavity forming was described in the literature to be the direct supply of gas-phase from the aerator to a pre-existing gas void in the aerator wake [32] which, in the current investigation, was only observed for flat-end aerator body designs in a vertically downwards orientation. This was seen to be encouraged by co-flow aerator design, as the gas-phase is injected directly into the aerator wake to supply a pre-existing gas void (Figure 4.7a) – in this case gas void detachment was only achieved beyond a critical gas flow rate, thought to correspond to conditions of suitably high drag on the gas-liquid interface. For cross-flow aerator designs, the aerator orifices can only be linked to a buoyant gas void in the wake by formation of an interconnecting gas neck (Figure 4.7b) – this requires injection of a sufficiently stable jet to prevent breakup upon exposure to the liquid cross-flow and with low enough gas momentum (i.e. low gas flow rate) for it to remain within the centre of the mixing chamber. For the current investigation, the only suitable conditions corresponded with the largest aerator orifice diameter at low ALRs (§4.6.1). The presence of cavity forming at high ALRs, as reported by Forrester and Rielly [32], was not observed in the

current investigation. Examples of cavity forming across a variety of experiments are shown in Figure 4.7.

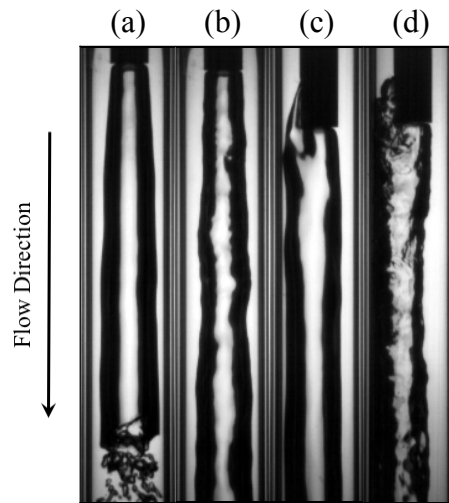


Figure 4.7 Example observations of cavity forming:

- a) 155 g/s, 0.001% ALR (§A5.2.1); b) 230 g/s, 0.31% ALR (§A5.2.1);
 c) 180 g/s, 0.02% ALR (§A5.1.1); d) 238 g/s, 0.24% ALR (§A5.1.1).

N.B. In the current work, a distinction has been made to the cavity forming definition, to avoid cross-over with alternative flow regimes. Cavity forming is only identified if the emerging gas supplies a buoyant gas void within the aerator wake. This compares to a jetting regime, for example, where gas-phase may occupy the aerator wake region but not due to buoyancy effects.

4.1.6 Coalesced Jetting

Coalesced jetting is first presented in the current work to describe gas injection observations whereby the gas-phase emerging from an aerator orifice immediately coalesced with neighbouring orifices to form what visually appears to be the injection of a complete gas core directly from the aerator. This regime was observed to occur when the aeration orifices are in critically close proximity and at sufficient ALRs where the emerging gas phase is not able to fully expand without contacting a neighbouring orifice – this is in keeping with a study by Jobehdar [44], in which it was reported that the interference of a formed or forming gas entity with an aerator orifice can lead to coalescence and hence increased bubble size. The only configurations which satisfied these conditions utilised a porous aerator, in which

coalesced jetting completely replaced the jetting regimes. Examples of coalesced jetting across a variety of experiments are shown in Figure 4.8.

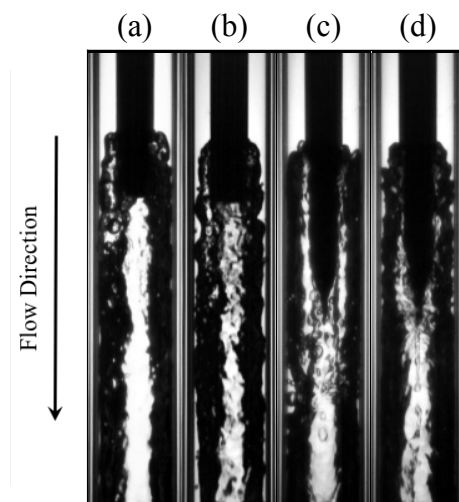


Figure 4.8 Example observations of coalesced jetting:

- a) 75 g/s, 3.02% ALR (§A5.2.2); b) 154 g/s, 2.00% ALR (§A5.2.2);
c) 60 g/s, 2.02% ALR (§A7.3.1); d) 105 g/s, 3.01% ALR (§A7.3.1).

4.1.7 Evacuated Chamber

The evacuated chamber gas injection regime is first presented in the current work to describe a condition in which phase separation is achieved immediately upon liquid injection into the atomiser, resulting in a continuous gaseous core throughout the atomiser into which the gas is directly injected at the aerator. Every observed case of evacuated chamber occurred at critically low liquid flow rates, whereby the liquid drag and momentum upon start-up is insufficient to displace the ambient air within the mixing chamber and hence passive bleeding of the atomiser is not achieved. Examples of evacuated chamber across a variety of experiments are shown in Figure 4.9.

N.B. The term “evacuated” used when describing this regime is not intended to suggest that the mixing chamber is under vacuum, rather that the liquid-phase is evacuated at the point of gas injection.

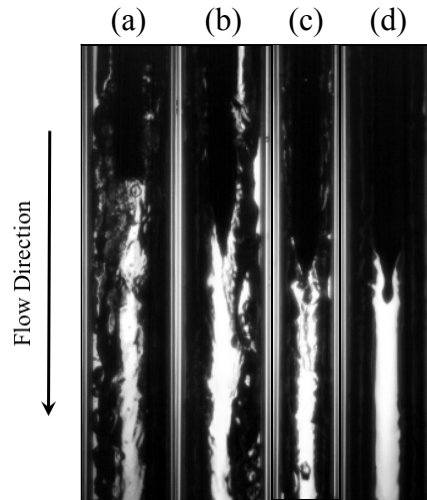


Figure 4.9 Example observations of evacuated chamber:

- a) 47 g/s, 2.97% ALR (§A5.1.3); b) 50 g/s, 1.02% ALR (§A6.1.3);
 c) 11 g/s, 6.84% ALR (§A7.4.1); d) 27 g/s, 0.26% ALR (§A7.5.2).

The formation of evacuated chamber was seen to be well approximated by the liquid Bakers number throughout the experimentation and, in most configurations, tended to be suppressed at high gas flow rates. The transitional limit to evacuated chamber was seen to marginally vary between configurations, which did not appear to follow a trend. Therefore, passive bleeding of the atomiser upon start-up was observed to be dependent on relatively chaotic mechanisms, and hence the generation of evacuated chamber was relatively erratic when operating at low liquid Bakers numbers. All observations of evacuated chamber throughout the current investigation are plotted in Figure 4.10, with a linear relationship applied to encompass all observations (Equation 4.1) – this gives a conservative approximation of minimum liquid Bakers numbers to prevent evacuated chamber based on the current data.

$$(G_l \Psi) = -28.8 \left(\frac{G_g}{\lambda} \right) + 410.6 \quad (4.1)$$

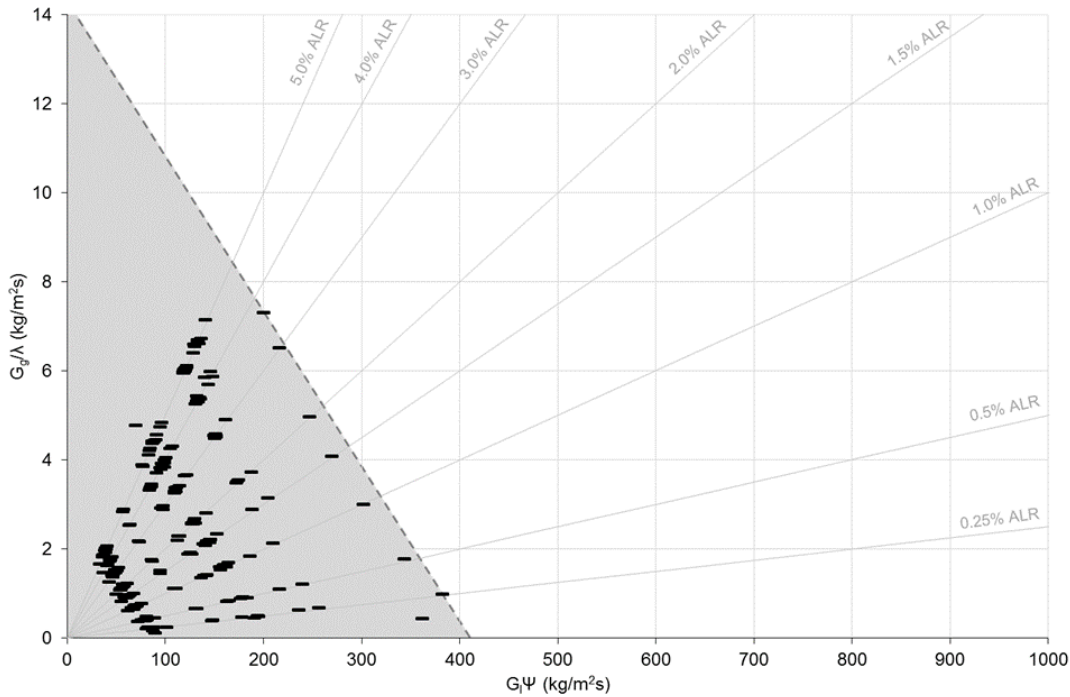


Figure 4.10 Operating conditions of all evacuated chamber observations

4.2 Observed Internal Flow Regimes

Similarly, the internal flow within the mixing chamber was quantified by categorising each observation into common flow regimes. As a result of this work, nine distinct flow regimes were observed across all experiments – these are a combination of standard flow regimes described in the literature and new regimes introduced in the current work to accurately describe the experimental observations. This section aims to discuss the appearance of these flow regimes, provide example observations and, for the first time, explain their formation with respect to the gas injection regimes at the aerator.

As before, the flow regimes for each investigated atomiser configuration were further analysed by plotting each identification against its corresponding operating condition to form a flow regime map – a map was produced for each independent parameter, with all presented within Appendices 3-5. By analysing the flow maps, the general relative operating conditions for each regime can be identified and are provided in Figure 4.11. It should, however, be noted that the formation and positioning of these regions were observed to be heavily dependent on the independent variables, which forms the basis of discussions in the further chapters.

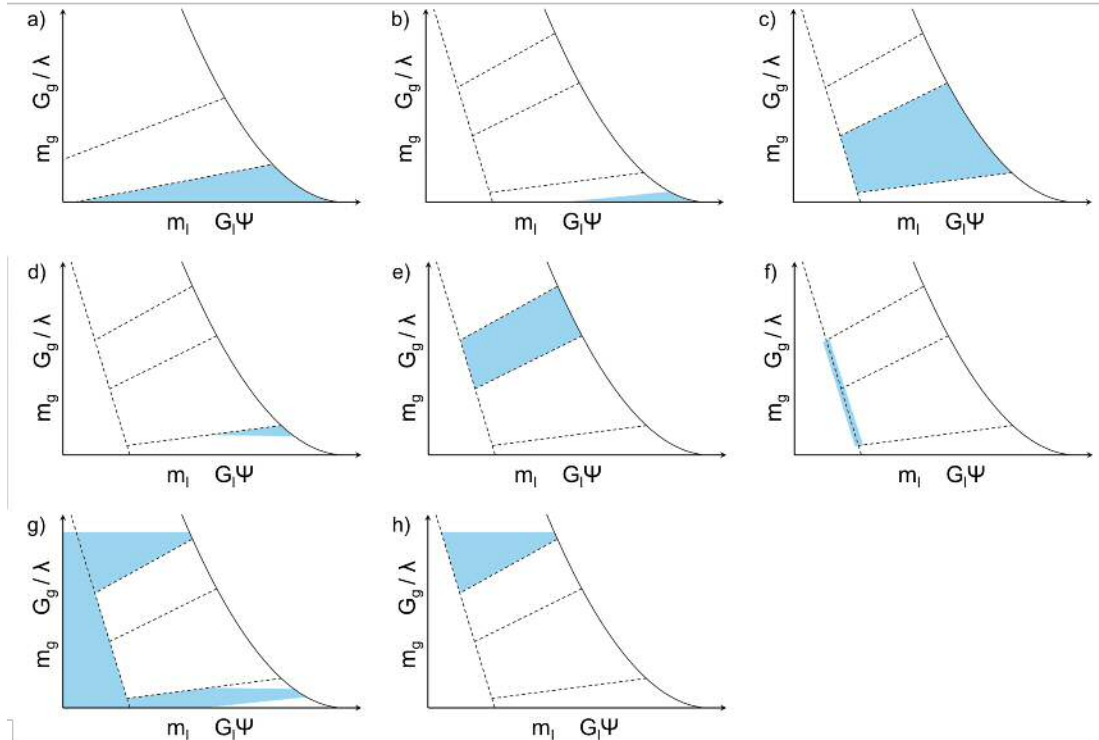


Figure 4.11 Relative positioning of each internal flow regime within a generic map,

- a) bubbly flow (§4.2.1); b) gas void disintegration (bubbly flow) (§4.2.2);
 c) slug flow (§4.2.4); d) gas void disintegration (slug flow) (§4.2.5); e) churn flow (§4.2.6);
 f) disrupted annular flow (§4.2.8); g) annular flow (§4.2.9);
 h) annular flow (liquid droplets) (§4.2.10).

As previously discussed, the general trend with increasing ALR was to transition the gas injection regimes from bubbling to jetting, due to increasing the emerging gas-phase stability. This was seen to also have a significant effect on the flow regime, which was observed to generally transition with increasing ALR: through bubbly flow (§4.2.1); to slug flow (§4.2.4); to churn flow (§4.2.6); before finally achieving an annular flow (§4.2.9, §4.2.10) at high ALRs – these results are in keeping with the literature reports for the effect of increasing ALR [29, 44, 72, 84, 85].

However, there were exceptions to this trend. For example, a gas void was commonly observed to be formed at low ALRs in the aerator wake for conventional flat-end aerator designs – this void was observed to displace bubbles injected at the aerator, either generating an annular flow throughout the mixing chamber or breaking up to form bubbles (§4.2.2) or slugs (§4.2.5).

The relative effect of buoyancy was also observed to have a significant effect on the flow regimes when operating in a vertically downwards orientation – this is inversely proportional to the liquid Bakers number and hence is increased with low liquid flow rates (e.g. small exit orifice diameters, low operating pressures) and large mixing chamber diameters. It has been previously discussed that at critically low liquid Bakers numbers, an evacuated chamber gas injection regime is established – in all cases, this was observed to generate an annular flow regime within the mixing chamber regardless of the ALR or independent parameter. Otherwise, the effect of a greater relative buoyancy was to increase the residence time of the gas-phase within the mixing chamber and hence increase the rate of coalescence – consequently, internal flows at low liquid Bakers numbers tended towards annular flow, with some cases of single bubbling even forming a slug flow or disturbed annular flow (§4.2.8).

4.2.1 Bubbly Flow

A bubbly flow, matching the literature descriptions [44, 63-66], was observed to be a homogenous two-phase flow consisting of uniformly sized bubbles within a liquid continuum, which were produced at the aerator flow and flowed unobstructed into the mixing chamber (Figure 4.12).

However, not all bubbling cases at the aerator were observed to form consistently sized bubbles – for example, pulse bubbling at relatively high ALRs was commonly observed to inject gas entities of variable size (i.e. bubbles and slugs) into the liquid cross-flow. Consequently, bubbly flow was encouraged by the injection of an unstable gas-phase which was prone to rapidly break-up upon exposure to the liquid cross-flow – this was promoted by low ALRs, small aerator orifice diameters, large aeration areas, small mixing chamber diameters and high operating pressures. Therefore, bubbly flow corresponded with the majority of single bubbling cases and low ALR cases of pulse bubbling.

There were however exceptions, which generally occurred under conditions of high relative buoyancy (i.e. low liquid Bakers numbers), in which coalescence of the injected uniformly sized bubbles generated alternative flow regimes (e.g. bubbly-slug flow, slug flow, annular flow). Generation of a bubbly flow was also prevented if the injected bubbles were impeded from flowing into the mixing chamber – throughout the current experimentation, this was seen for a flat-end aerator operating in a vertically downwards orientation in which a buoyant gas void was observed in the aerator wake and displaced the injected bubbles (this is discussed in more detail in §5.1).

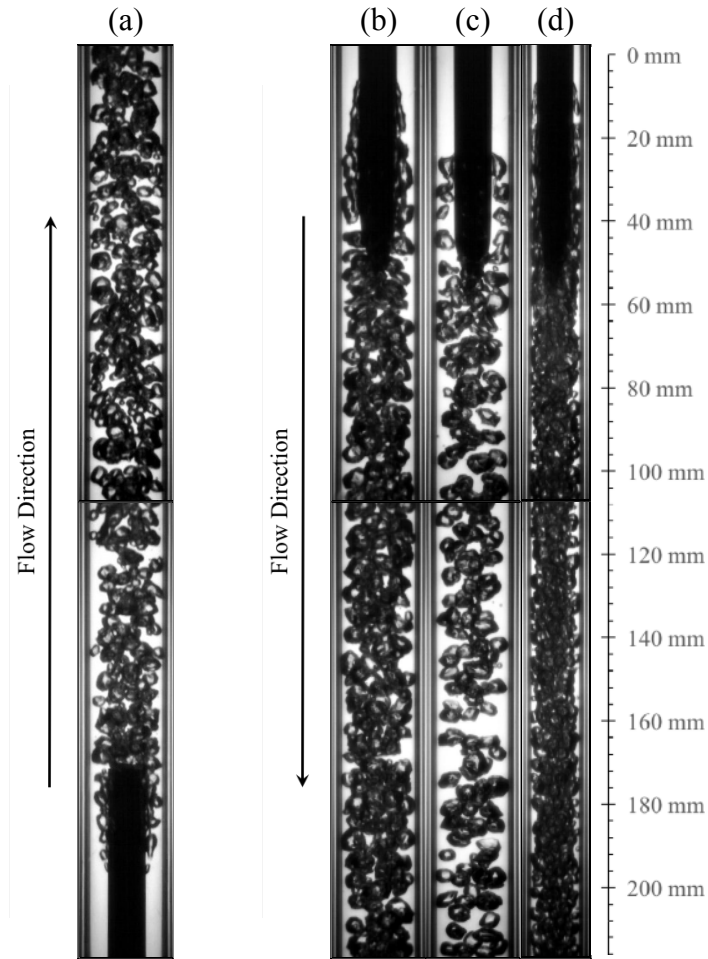


Figure 4.12 Development of bubbly flow:

- a) 181 g/s, 0.25% ALR (§A5.5.2); b) 234 g/s, 0.25% ALR (§A6.1.2);
 c) 148 g/s, 0.12% ALR (§A7.1.2); d) 120 g/s, 0.51% ALR (§A7.4.1).

N.B. Figure constructed of two images per measurement point (separated by central black line), generated by repositioning camera with a traverse.

A number dense bubbly flow is widely cited within the literature to be the optimal flow regime for effervescent atomisation, reportedly producing a stable and efficient spray through single bubble atomisation. This is in agreement with the observations in the current work, in which individual bubbles were seen to expand upon ejection from the nozzle generating an explosion-like event and “bursting” the surrounding liquid phase into droplets and ligaments. An example near-nozzle observation of dense bubbly flow atomisation is shown in Figure 4.13, in which “pulses” of liquid-phase can be identified in the spray – these are thought to correspond with individual bubbles discharging through the exit orifice and rapidly expanding within the ambient atmosphere. As the bubbly flow supplying the nozzle is number dense, the single bubble atomisation events are consistent and regular, producing a relatively stable spray – albeit, in this low ALR case, the atomisation is relatively coarse.

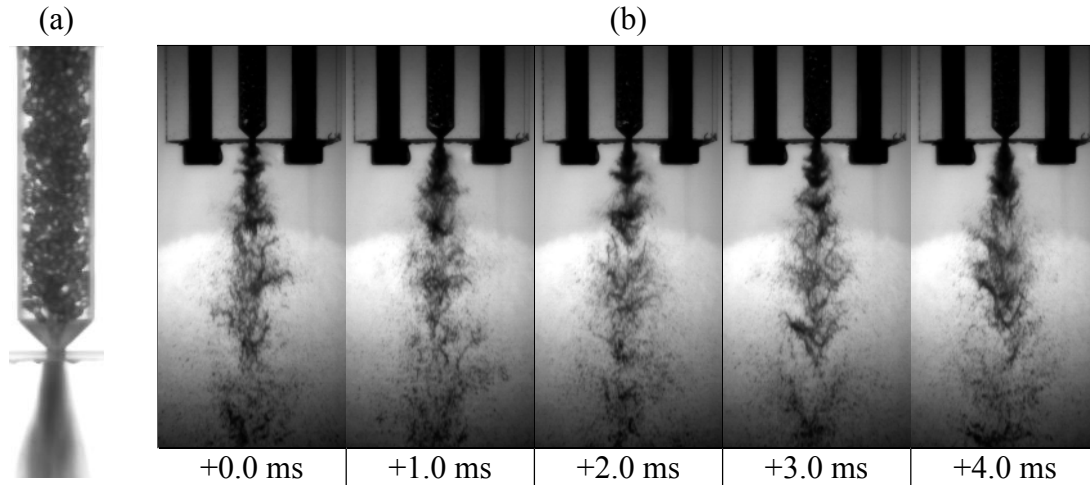


Figure 4.13 Bubbly flow atomisation (58 g/s, 0.26% ALR): a) internal flow, b) near-nozzle.

This contrasts to an alternative experimental observation (Figure 4.14) in which the bubbles supplying the exit orifice were less number dense, and hence the proportion of liquid-phase within the two-phase flow was increased – this corresponds to a decrease in both the bubble number density and the homogeneity of the bubbly flow. As before, the discharge of each bubble was observed to generate a single bubble atomisation event. However, due to the irregularity of bubble supply, there are periods in which a pure liquid continuum is discharged – the primary atomisation mechanisms were observed to be insufficient to break-up this single-phase liquid jet and hence large ligaments were discharged. Consequently, a poorly atomised and inconsistent spray was generated with this reduction in internal flow homogeneity.

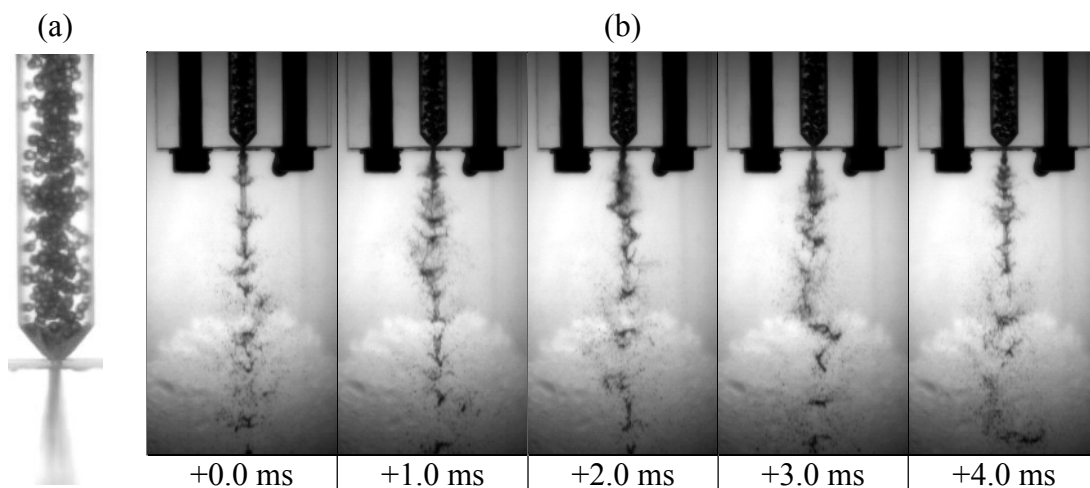


Figure 4.14 Bubbly flow atomisation (20 g/s, 0.12% ALR): a) internal flow, b) near-nozzle.

Figure 4.15 shows the result of an experimental trial in which a visibly larger bubbly flow is generated within the mixing chamber – this represents a decreased bubble number density, due to the increased volume of each bubble. As before, an explosive event is observed as the leading edge of a bubble supplies the exit orifice and rapidly expands into the ambient atmosphere. However, instead of the characteristic rapid explosion of single bubbling, the atomisation process here is prolonged as the large bubble gradually deflates through the exit orifice – this generates a period of atomisation akin to tree-regime atomisation, in which the expanding gas-phase atomises the peripheral liquid phase due to shearing on the gas-liquid interface. Whilst the spray generation is observed to be periodic (i.e. not erratic), each atomisation event is protracted which, based on the literature reports, is expected to reduce the atomiser efficiency compared to rapid single bubble atomisation [13, 73]. As a consequence, the spray has increased transience (i.e. variability) and, hence, decreased stability – where events of relatively coarse atomisation are succeeded by fine atomisations.

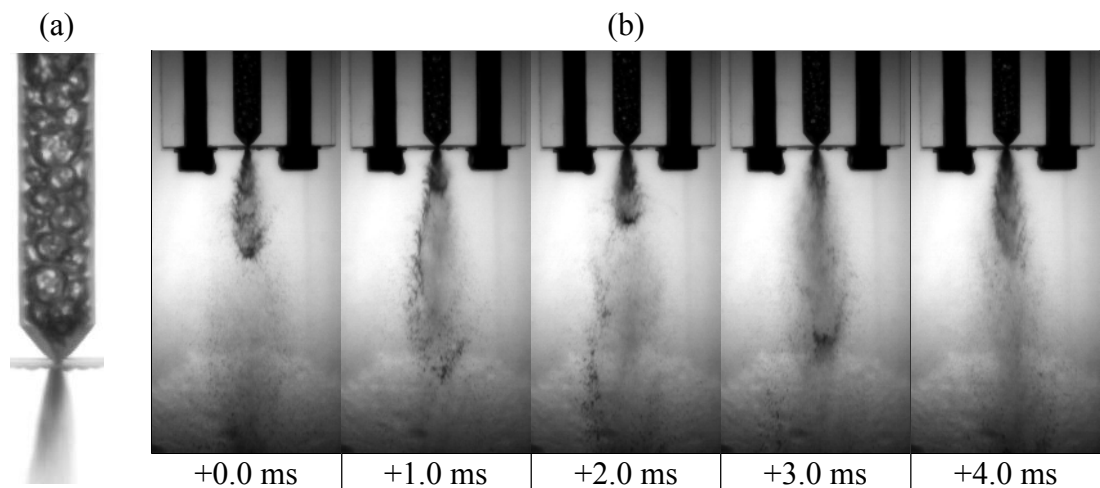


Figure 4.15 Bubbly flow atomisation (12 g/s, 1.53% ALR): a) internal flow, b) near-nozzle.

4.2.2 Gas Void Disintegration (Bubbly Flow)

An alternative bubbly flow mechanism was identified for the first time in the current investigation, in which the leading edge of a gas void disintegrates to form discrete bubbles – this void was typically observed to be formed within the wake of conventional flat-end aerators upon start-up. The process appears to be dominated by the bluff body effect of the gas void, in which high localised areas of reduced pressures are generated on the leading edge of the void (i.e. turbulent eddies) causing the chaotic stripping of bubbles – this gas-phase break-up mechanism is in keeping with literature reports [30, 61]. The bubbles generated in this manner are visibly very small in size (i.e. microbubbles) and, therefore, the

rate of depletion is low. Gas is supplied to the void either directly from the aerator orifice due to cavity forming (Figure 4.16a-b) or by coalescence of surrounding bubbles within the liquid periphery (Figure 4.16c-d). The rate of gas supply and depletion must be balanced within the visible mixing length (i.e. 216 mm) and, therefore, gas void disintegration (bubbly flow) was observed to be very sensitive to the flow conditions, requiring high liquid flow rates and low ALRs.

Anomalous cases of gas void disintegration (bubbly flow) via other means were also observed. One such case was the injection of a constant gas jet with sufficient stability to form a gas void within the mixing chamber, not in the aerator wake – this gradually depleted via the shearing off of bubbles (Figure 4.16e). Another mechanism was the depletion of an established gas void, formed due to evacuated chamber (Figure 4.16f). Both of these cases were isolated and seemingly unpredictable.

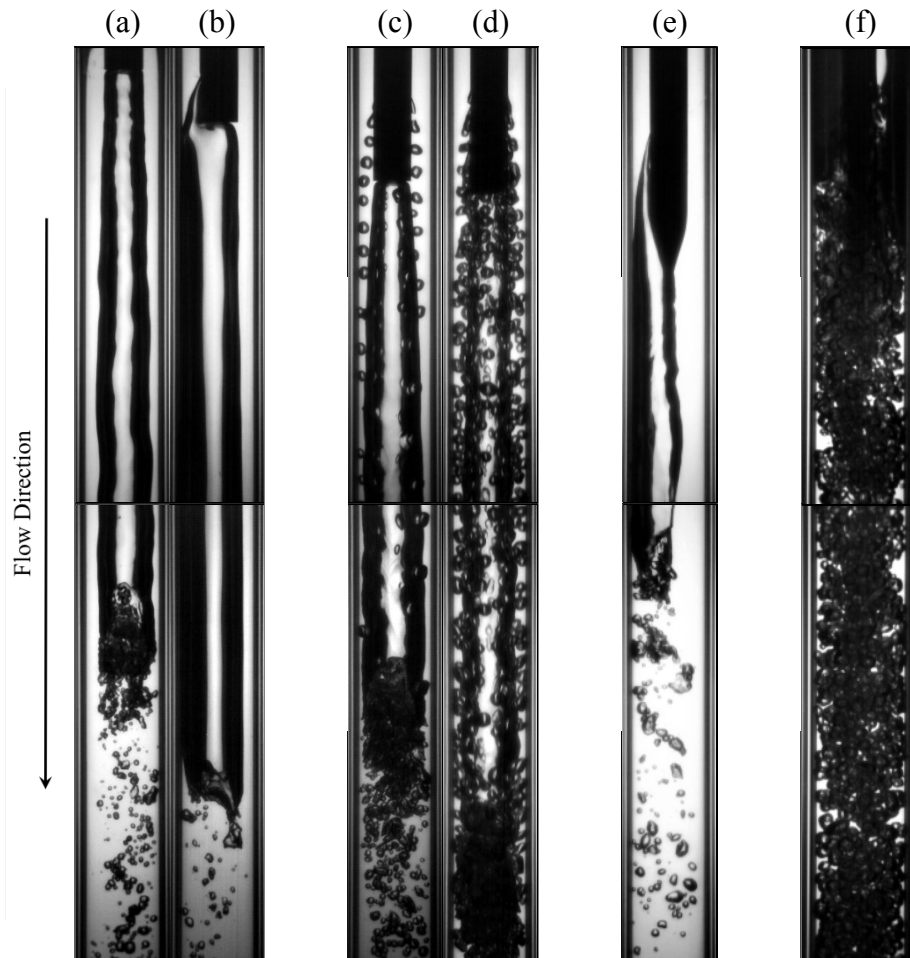


Figure 4.16 Development of gas void disintegration (bubbly flow):
 a) 280 g/s, 0.02% ALR (§A5.2.1); b) 119 g/s, 0.01% ALR (§A5.1.1);
 c) 165 g/s, 0.03% ALR (§A5.1.3); d) 250 g/s, 0.13% ALR (§5.2);
 e) 232 g/s, 0.01% ALR (§A7.1.1); f) 188 g/s, 0.26% ALR (§A7.4.3).

Since gas void disintegration (bubbly flow) has not previously been reported in the literature, its effect on spray performance is unquantified. Figure 4.17 shows a case in which a gas void exists within the mixing chamber, which displaces the injected bubbles to flow around its liquid periphery. However, prior to supply of the exit orifice, the gas void terminates and consequently the primary regime supplying the nozzle is a bubbly flow – the resulting spraying mechanism was observed to be single bubble atomisation, akin to bubbly flow.

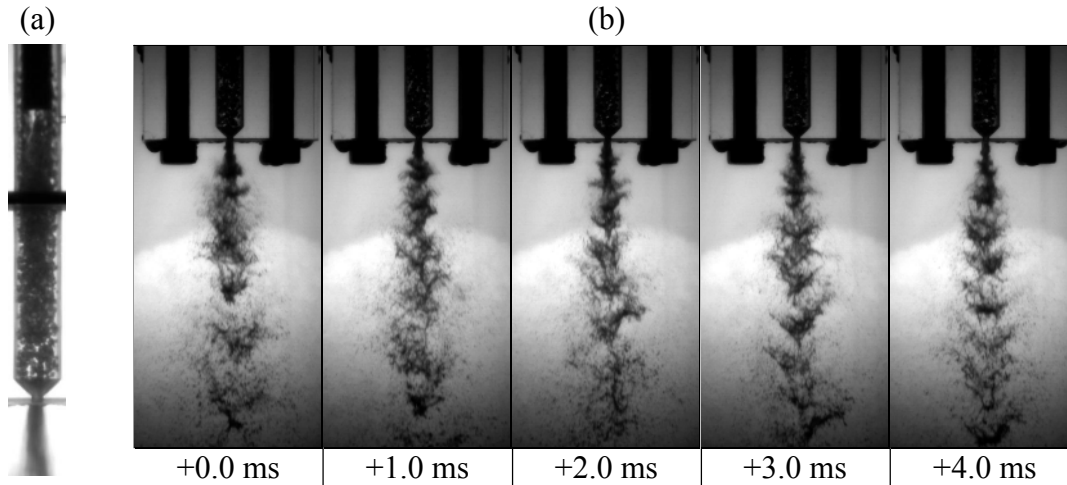


Figure 4.17 Gas void disintegration (bubbly flow) atomisation (63 g/s, 0.12% ALR):
a) internal flow, b) near-nozzle.

However, the length of the gas void was seen to be extremely sensitive to the operating conditions – rapidly growing when gas supply to the void (e.g. cavity forming, coalescence of bubbles) exceeds its depletion rate. It was seen in the spray trials that, if the gas void grows to exceed the length of the mixing chamber, the void itself provides the exit orifice with gas-phase – in this case there are no liquid ligaments to dissect the gas-phase and the spraying mechanism becomes tree-regime atomisation. This supply is, however, temporary as the void rapidly drains of gas-phase, whereby its length reduces and the primary regime continues. An example of this is demonstrated in Figure 4.18, where the primary regime is a sparse bubbly flow, which results in poorly atomised liquid jet via irregular single bubble atomisation. This is seen to dramatically change at +8.0 ms when the gas void has sufficient length to supply the exit orifice, whereby the atomisation mechanism switches to tree regime. Therefore, operation within gas void disintegration (bubbly flow) is not recommended as gas supply to the exit orifice can rapidly switch between the primary regime and gas void supply which, as shown, generates major spray instabilities. The only sourced report which observed similar gas void formation in the aerator wake was an internal flow study by Jobehdar [44] that reported decreased internal flow homogeneity and hence reduced spray stability.

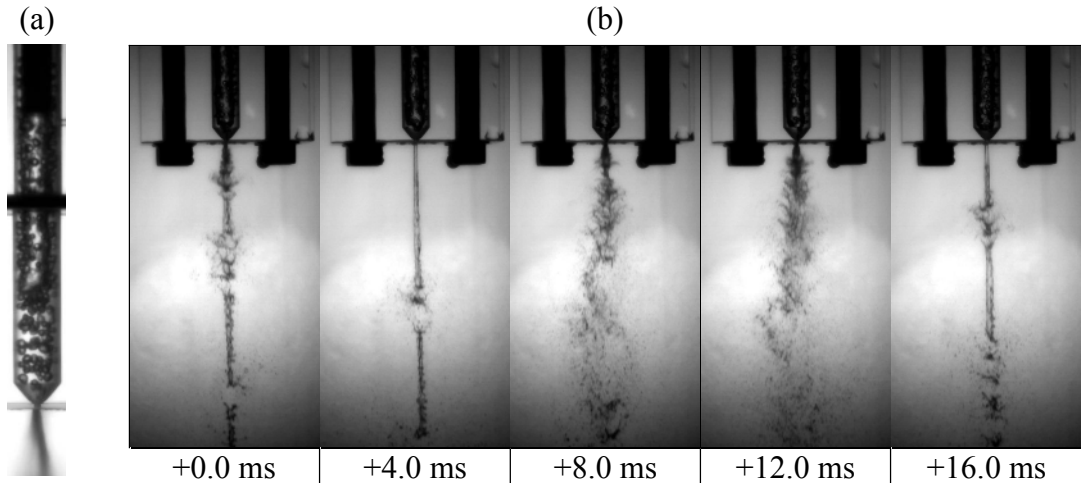


Figure 4.18 Gas void disintegration (bubbly flow) atomisation (20 g/s, 0.12% ALR):
a) internal flow, b) near-nozzle.

4.2.3 Bubbly-Slug Flow

Bubbly-slug flow was presented by Zhou [64] to be an internal flow of inconsistently sized bubbles – the largest bubbles are, however, smaller than the mixing chamber diameter and therefore not classed as gas slugs. This regime was observed in the current work (Figure 4.19) to be initiated by bubbling at the aerator (i.e. single bubbling and pulse bubbling gas injection regimes), due to either the injection of bubbles of varying sizes from the aerator or coalescence of bubbles within the mixing chamber – consequently, it was observed in the transitional ALRs between bubbly flow and slug flow.

The atomisation performance of a bubbly-slug flow was seen to be less structured than a bubbly flow, which coincides with a reduction of internal flow homogeneity supplying the exit orifice. Figure 4.20 shows a case in which relatively small gas slugs are interspersed with bubbles. The resulting spray generation is relatively transient, featuring single bubble atomisation intermixed with erratic tree regime atomisation – this is thought to correspond with individual bubbles being supplied to the exit orifice, with prolonged atomisation akin to tree regime as a large bubble is discharged. Therefore, the spray was observed to have increased instability compared to a homogenous bubbly flow, where the spray can be seen to alternate between coarse and finer atomisation. These findings are in agreement with the literature, which report that the supply of a heterogeneous internal flow to the exit orifice is a prerequisite for significant spray instabilities due to alternating atomisation mechanisms [15, 21, 25, 26, 72, 82, 84, 87-89].

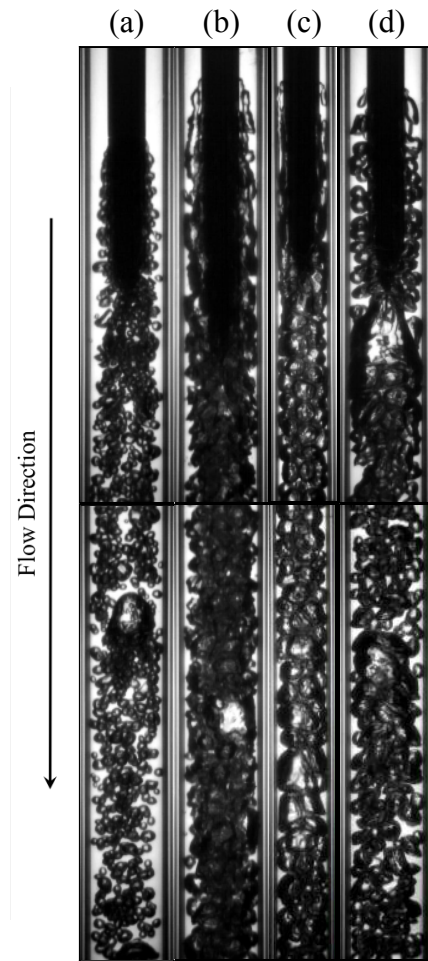


Figure 4.19 Development of bubbly-slug flow:

- a) 252 g/s, 0.12% ALR (§A7.3.1); b) 213 g/s, 0.50% ALR (§A7.2.4);
 c) 47 g/s, 1.00% ALR (§A7.4.1); d) 95 g/s, 0.13% ALR (§A7.5.2).

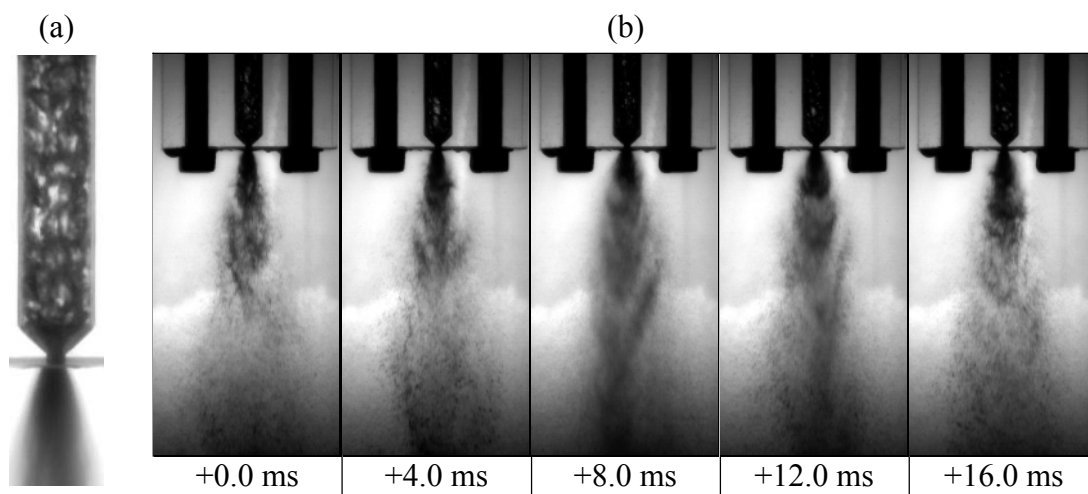


Figure 4.20 Bubbly-slug flow atomisation (36 g/s, 1.50% ALR):

- a) internal flow, b) near-nozzle.

4.2.4 Slug Flow

Slug flow is defined as the intermittent presence of large gas entities within a liquid continuum, which have similar diameter to the mixing chamber – this is a standard flow regime referenced within the literature [44, 63-66]. The formation of a slug flow was identified through multiple mechanisms within the current investigation:

1. Surface instabilities during co-flow gas injection (Figure 4.21a-b). Under high fluid flow conditions in a co-flow gas injection arrangement, surface instabilities are generated on the gas-liquid interface of the injected gas core – at critically high ALRs and high liquid flow rates corresponding to jetting, opposing instabilities have sufficient magnitude to join and separate the void into slugs. This is in-keeping with the literature, in which fluid shearing and surface instabilities are reported as gas-phase break-up mechanisms [30, 61].
2. Coalescence of bubbles within the mixing chamber (Figure 4.21c-d). Coalescence is known to be encouraged by the close proximity of bubbles and high residence time [30, 57-61] – these conditions were achieved at relatively high ALRs and low liquid flow rates, and therefore bubbles within the mixing chamber were commonly observed to coalesce to form gas slugs. This method of slug generation is commonly reported within the literature [63, 64, 66].
3. Direct injection of gas slugs (Figure 4.21e-f). Varying sizes of gas entities are injected into the mixing chamber during pulse bubbling – at relatively high ALRs, this can include the direct injection of gas slugs from the aerator. Occasionally, gas slug injection was observed through a transient “pulsing” of the injected gas, in which the flow rate appears to intermittently increase – this is thought to correspond to pressure variations within the mixing chamber as a pre-existing gas slug is discharged through the exit orifice, which is supported by the observations of Sen et al. [41].
4. Break-up of gas jets into non-uniformly sized bubbles (Figure 4.21g-h). Gas jets injected into the mixing chamber through elongated jetting and atomised jetting were observed to breakup into gas entities of varying sizes, including gas slugs – this matches the description presented by Forrester and Rielly [32]. This mechanism was typically observed at ALRs just above transition to the jetting, where sufficient liquid phase was present to form a continuum.

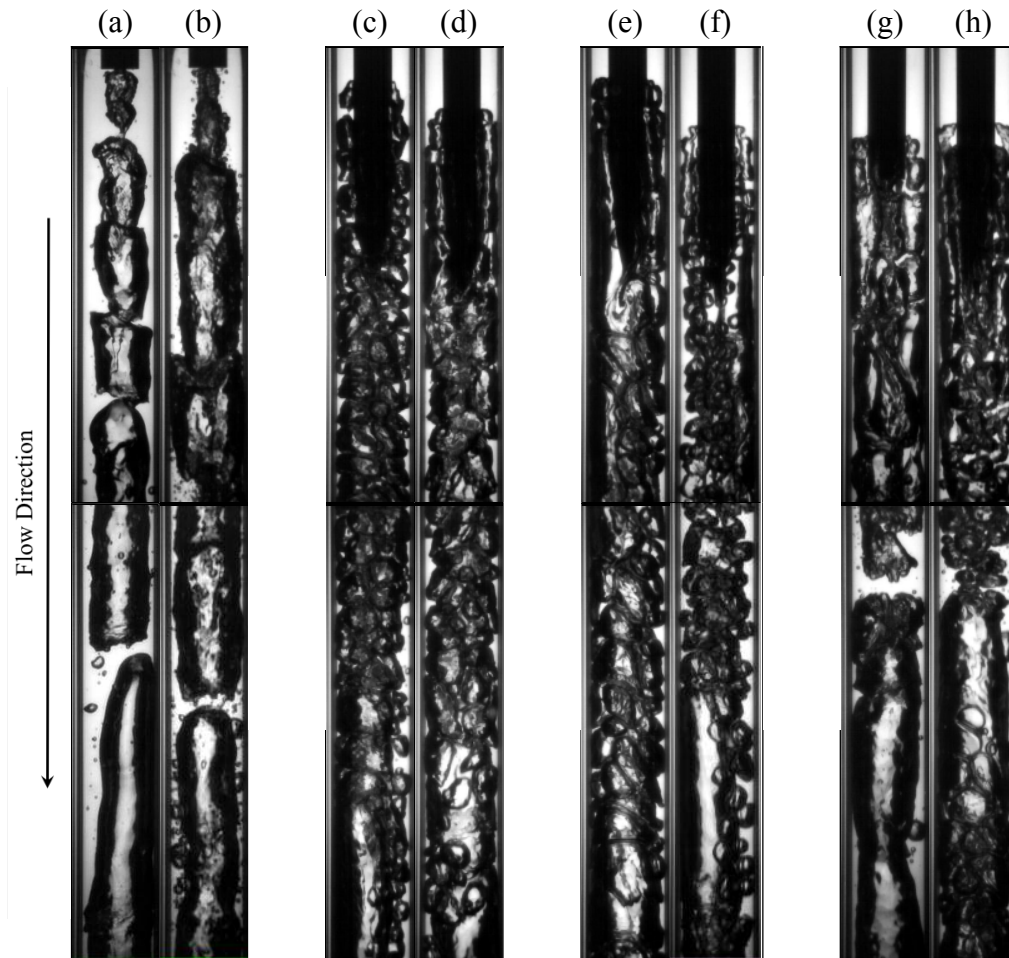


Figure 4.21 Development of slug flow (through gas void shearing):

- a) 214 g/s, 0.49% ALR (§A5.2.1); b) 186 g/s, 0.98% ALR (§A5.2.1);
 c) 84 g/s, 0.49% ALR (§A6.1.2); d) 83 g/s, 0.49% ALR (§A7.1.3);
 e) 64 g/s, 1.00% ALR (§A6.1.2); f) 137 g/s, 0.26% ALR (§A7.2.2);
 g) 169 g/s, 0.50% ALR (§A5.1.2); h) 171 g/s, 0.51% ALR (§A7.2.2).

A relatively transient spray was observed when the exit orifice was supplied with a slug flow. In the example observation shown in Figure 4.22, the dominate spraying mechanism appears to be tree regime atomisation as a gas slug depletes through the exit orifice, which erratically alternates with the generation of coarser liquid pulses due to the intermittent liquid phases.

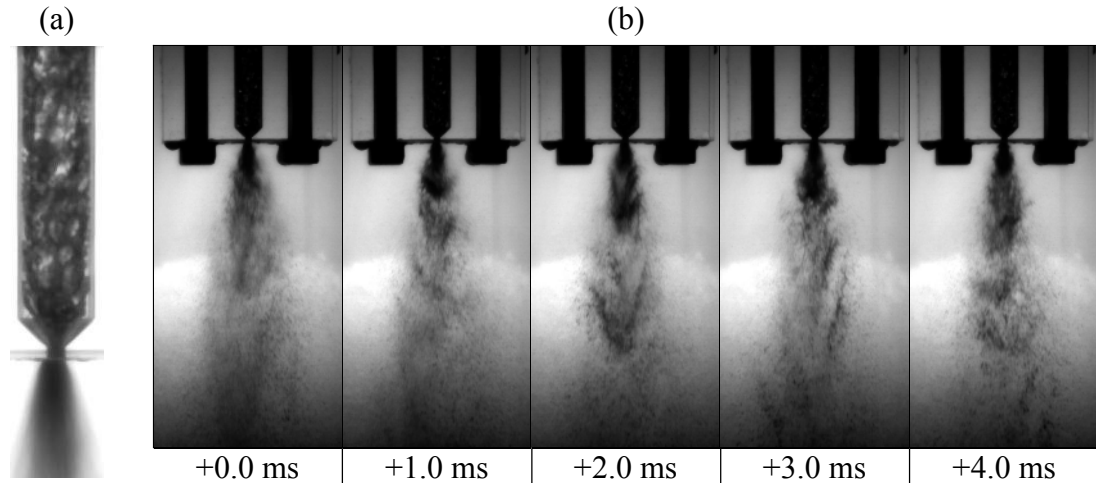


Figure 4.22 Slug flow atomisation (42 g/s, 1.00% ALR): a) internal flow, b) near-nozzle.

4.2.5 Gas Void Disintegration (Slug Flow)

An additional slug flow mechanism was identified to be the disintegration of a gas void into gas slugs. This regime appears to be instigated by the injection of gas entities from the aerator, which generate surface instabilities on the gas-liquid interface as they pass within the liquid peripheral flow (Figure 4.23) – the generation of significant gas-liquid surface instabilities is a gas-phase break-up mechanism reported within the literature [30, 61]. The size of the passing gas entities, and hence the ALR, appears to play a key role – if the bubbles are too small, they pass with minimal interference to the void, whereas too large and they exhibit sufficient disruption to displace the void from the aerator tip.

Since gas void disintegration (slug flow) has not previously been reported in the literature, its effect on spray performance is unquantified. Figure 4.24 shows an experimental case in the current work in which a gas void in the aerator wake breaks up to form gas slugs. These slugs are interspersed with bubbles, which were injected from the aerator and initially forced to flow the liquid periphery of the void. Consequently, the gas entities supplying the exit orifice vary between bubbles and slugs – therefore the spray generation is akin to bubbly-slug flow, in which single bubble atomisation is intermixed with erratic tree regime atomisation. Therefore, the spray was observed to have increased instability compared to bubbly flow. The only sourced report which observed similar gas void formation in the aerator wake was an internal flow study by Jobehdar [44] that reported decreased internal flow homogeneity and hence reduced spray stability.

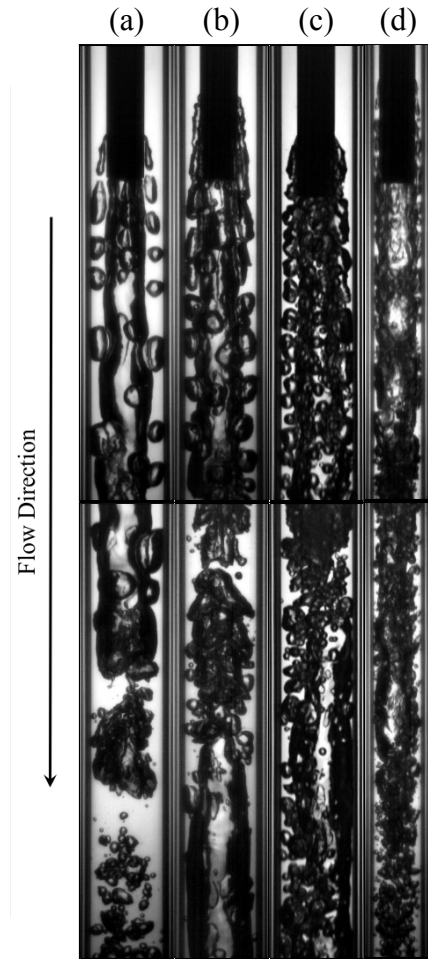


Figure 4.23 Development of slug flow (through gas void shearing):
 a) 254 g/s, 0.13% ALR (§A5.1.2); b) 237 g/s, 0.12% ALR (§A5.1.3);
 c) 237 g/s, 0.24% ALR (§A5.2.2); d) 234 g/s, 0.26% ALR (§A5.3.1).

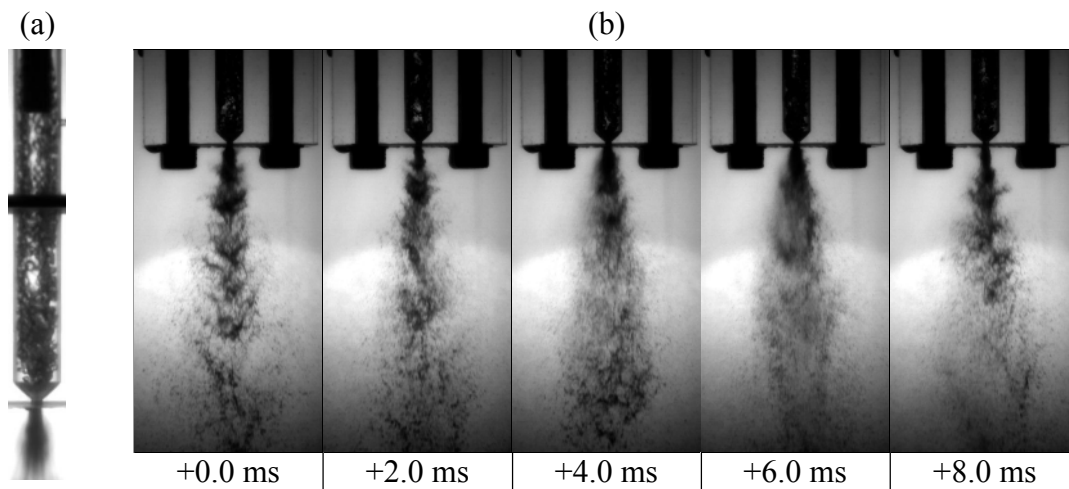


Figure 4.24 Gas void disintegration (slug flow) atomisation (59 g/s, 0.25% ALR):
 a) internal flow, b) near-nozzle.

4.2.6 Churn Flow

Churn flow is a chaotic two-phase flow in which neither phase is continuous [64, 65]. Every instance of churn flow within the current investigation coincided with jetting at the aerator, which mix within the mixing chamber to form a chaotic heterogeneous regime. Example observations of churn flow development are shown in Figure 4.25 for a variety of experiments.

The atomisation of churn flow also displayed transient properties, where spray generation was observed to be dominated by tree regime atomisation with intermittent pulses of coarse spray generation (Figure 4.26) – these variations are thought to correspond with differing proportions of liquid phase supplying the exit orifice, as a result of the heterogeneous nature of the internal flow.

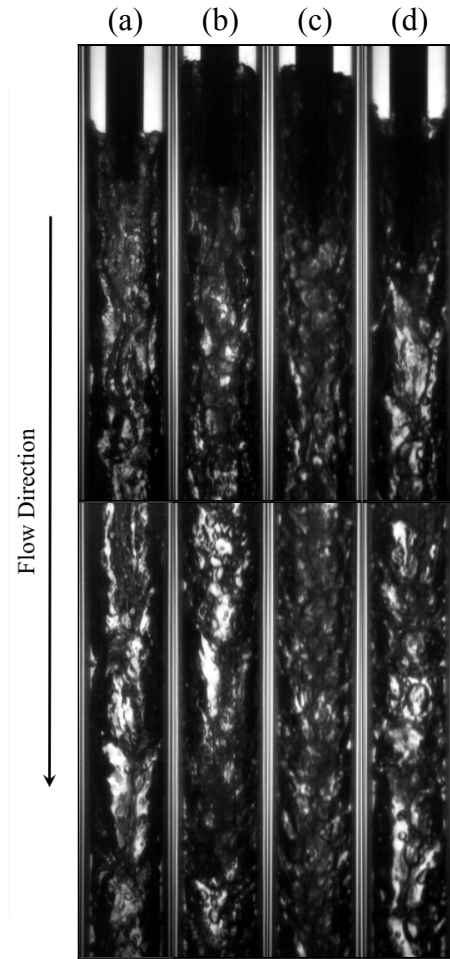


Figure 4.25 Development of churn flow:

- a) 169 g/s, 1.49% ALR (§A5.1.2); b) 104 g/s, 3.19% ALR (§5.2);
- c) 159 g/s, 2.01% ALR (§A6.1.3); d) 123 g/s, 2.00% ALR (§A7.2.2).

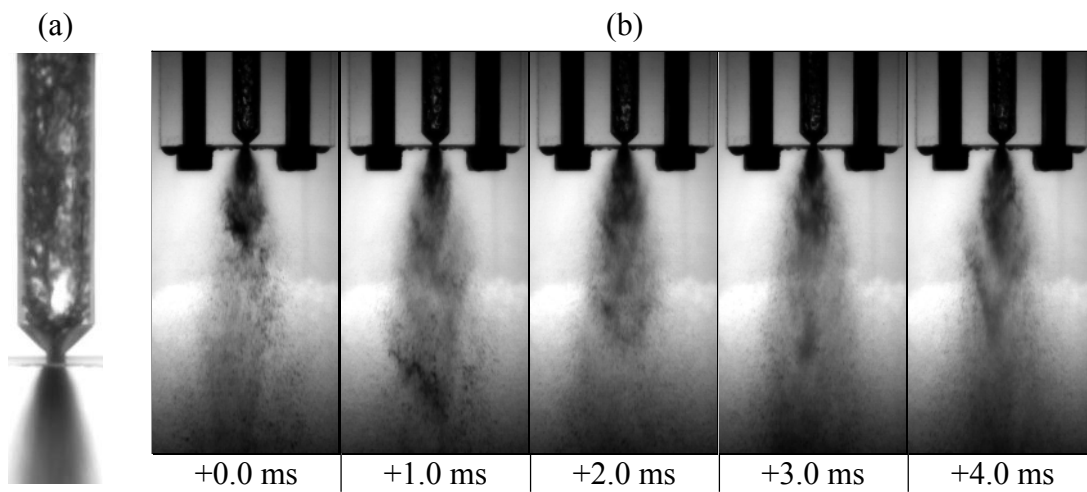


Figure 4.26 Churn flow atomisation (37 g/s, 1.48% ALR): a) internal flow, b) near-nozzle.

4.2.7 Pulsing Flow

Pulsing flow is a unique flow regime identified within the current investigation, defined as a discontinuous internal flow in which gas and liquid continuums alternate within the mixing chamber. These pulsing events, shown in Figure 4.27, appear to coincide with the discharge of a liquid continuum from the exit orifice, which clogs the exit orifice. The injected gas-phase consequently fills the mixing chamber, increasing the pressure within the mixing chamber and resisting supply of the liquid-phase. Once the existing liquid continuum is depleted through the exit orifice, the gas-phase discharges through the exit orifice causing a sudden decrease in operating pressure and an influx of liquid supply, which eventually re-blocks the exit orifice. This cycle was observed to periodically repeat, causing large fluctuations in operating pressure compared to alternative flow regimes (Figure 4.28).

The spray generated through pulsing flow was observed to be extremely transient, alternating between a coarse atomisation when discharging the liquid continuum and a fine spray with the gas continuum (Figure 4.29) – consequently, the atomiser was seen to “splutter”. The liquid continuum was not observed to be well mixed prior to discharge and therefore spray generation was unstructured and chaotic.

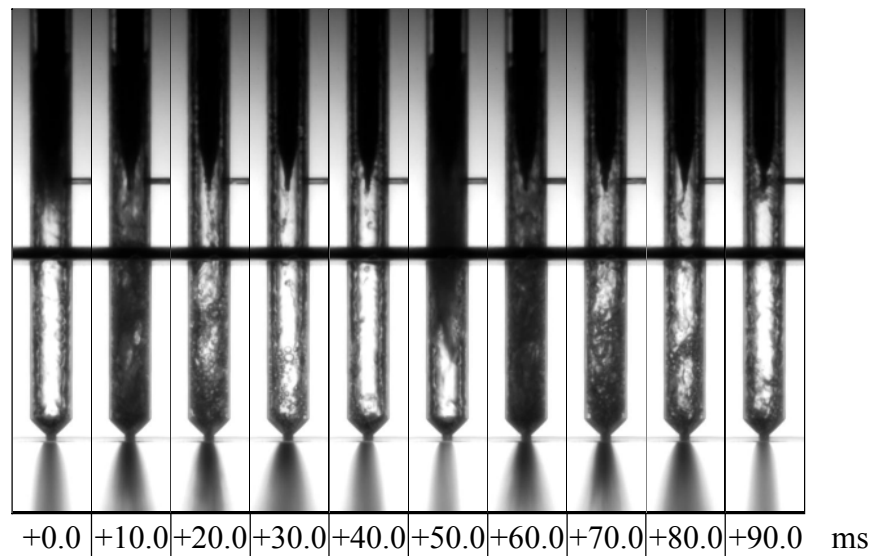


Figure 4.27 Pulsing flow internal flow observations (36 g/s, 2.02% ALR).

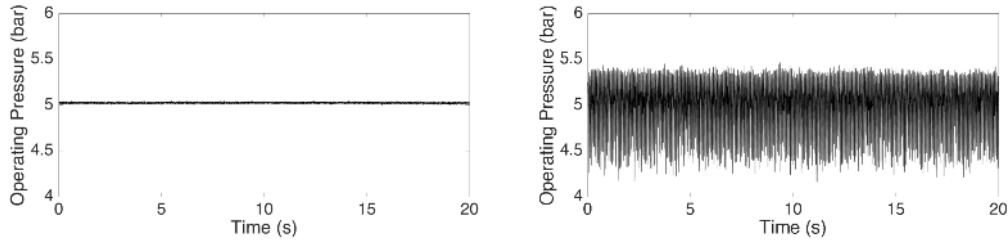


Figure 4.28 Operating pressure variations for an equivalent atomiser configuration when internal flow is: a) bubbly flow – 0.25% ALR, 59 g/s; b) pulsing flow – 5.0% ALR, 26 g/s.

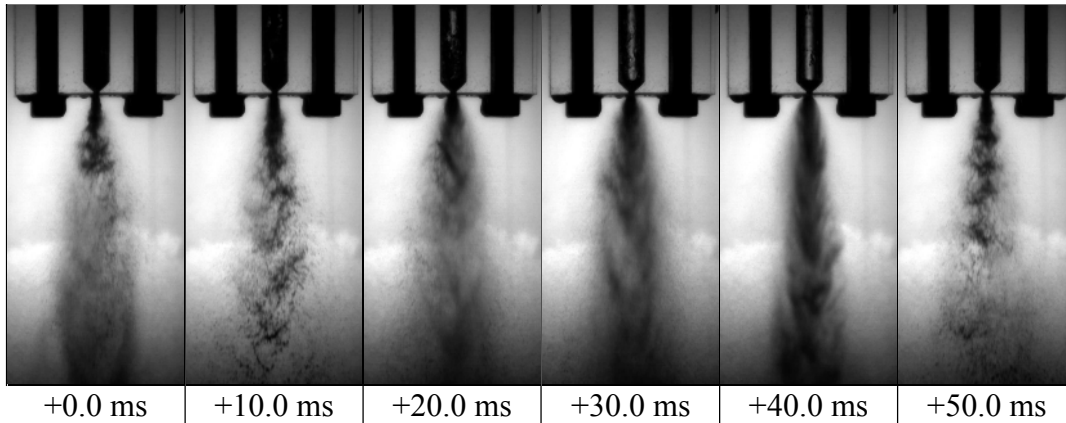


Figure 4.29 Pulsing flow atomisation near-nozzle observations (35 g/s, 1.98% ALR).

4.2.8 Annular Flow

Annular flow is widely cited within the internal flow literature [44, 63-66] to be a continuous gaseous core formed in the centre of the mixing chamber surrounded by a peripheral liquid flow. Any surface instabilities generated on the gas-liquid interface or gas entities within the liquid periphery, are not great enough to generate breakup of the gas core within the length of the mixing chamber. Annular flow was observed to occur across a wide range of conditions and, consequently, for various gas injection regimes. Whilst all observations of annular flow featured a continuous gas core, the appearance of the liquid periphery was seen to vary depending on the development phenomena:

1. Jetting (Figure 4.30a-b): An annular flow was often observed at high ALRs for multi-holed aerators, due to the coalescence of individual jets within the mixing chamber to form a continuous annular core. Alternatively, in the case of a single orifice aerator, a single injected jet can form an annular flow if its integrity is maintained throughout the mixing chamber – this required injection of a sufficiently stable jet.

2. Evacuated chamber (Figure 4.30c-d): The evacuated chamber gas injection regime is formed at low liquid flow rates, which results in the formation an annular flow immediately upon liquid injection. As evacuated chamber occurs at low liquid flow rates, the peripheral liquid film was observed to be thin.
3. Gas void formation (Figure 4.30e-f): A gas void was commonly seen to be formed in the aerator wake of a flat-end aerator. If sufficient breakup mechanisms are not generated on the gas void to cause its breakup, the void extends through the mixing chamber and forms an annular flow. Commonly, the bubbles injected at the aerator can be seen to flow in the liquid periphery surrounding the gas core.

A continuous annular flow was not observed during the spray trials and so its atomisation properties cannot not be identified in the current investigation. However, the literature reports that a highly stable and fine spray is generated through constant tree regime atomisation [72, 82, 84] – this is in agreement with the experimental observations of the intermittent annular flow during pulsing flow. However, when operating in annular flow, an effervescent atomiser behaves akin to an air assist or air blast atomiser and hence adopts its weaknesses [19, 29], including inefficient use of the atomising gas and, therefore, annular flow does not represent effervescent atomisation.

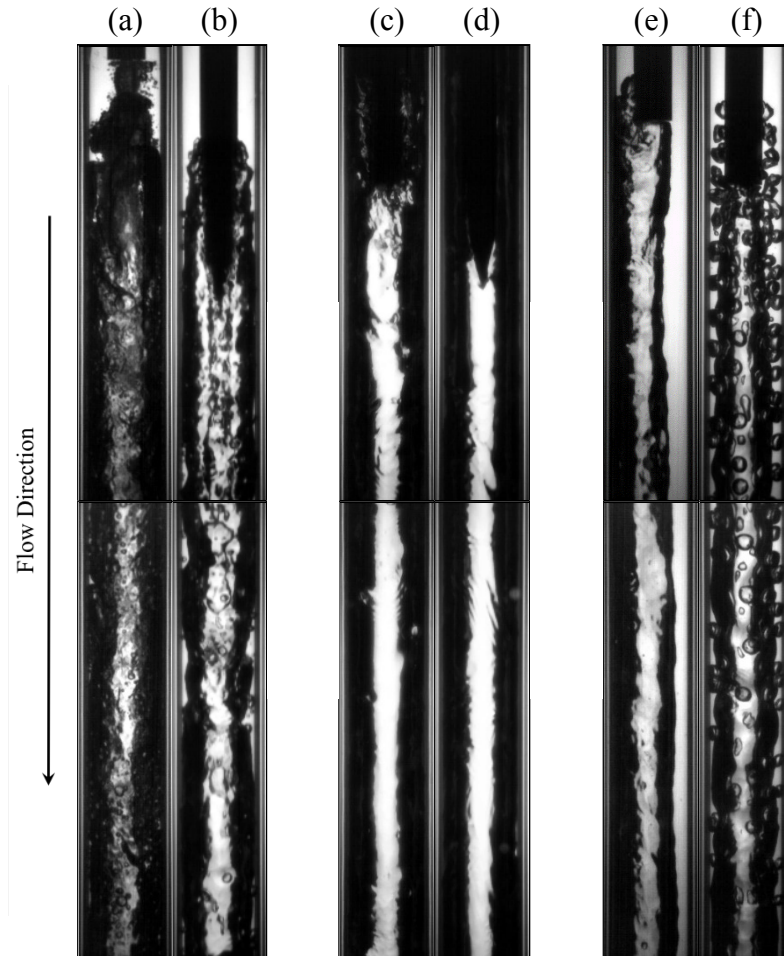


Figure 4.30 Development of annular flow:

- a) 67 g/s, 4.01% ALR (§A5.2.1); b) 149 g/s, 1.00% ALR (§A5.2.2);
 c) 23 g/s, 2.93% ALR (§7.2); d) 21 g/s, 1.00% ALR (§A6.1.2);
 e) 238 g/s, 0.24% ALR (§A7.1.1); f) 149 g/s, 0.14% ALR (§A7.1.3).

4.2.9 Disrupted Annular Flow

Disrupted annular flow is first defined in the current work to describe observations of an otherwise constant gaseous core that is regularly separated by liquid ligaments – therefore, neither fluid phase is completely continuous. It was observed under conditions of high relative buoyancy, due to the incomplete action of either coalescence or breakup:

1. Incomplete coalescence (Figure 4.31a-d): Disrupted annular flow was generally observed at low liquid Bakers numbers, just in excess of evacuated chamber. This corresponds to conditions in which the relative effects of buoyancy are great enough to promote coalescence of the gas-phase and thus prevent the formation of the standard intermittent flow regimes (i.e. slug flow, churn flow), however the

residence time is too low to enable complete coalescence into an annular flow. Consequently, residual liquid ligaments remain across the otherwise constant gas core.

2. Incomplete breakup (Figure 4.31e-h): In unusual cases, liquid ligaments were observed to be generated across a gas core due to the incomplete breakup of the gas-phase – this was observed due to gas-liquid interface surface instabilities and the interference of gas entities within the peripheral liquid flow, without separation being achieved.

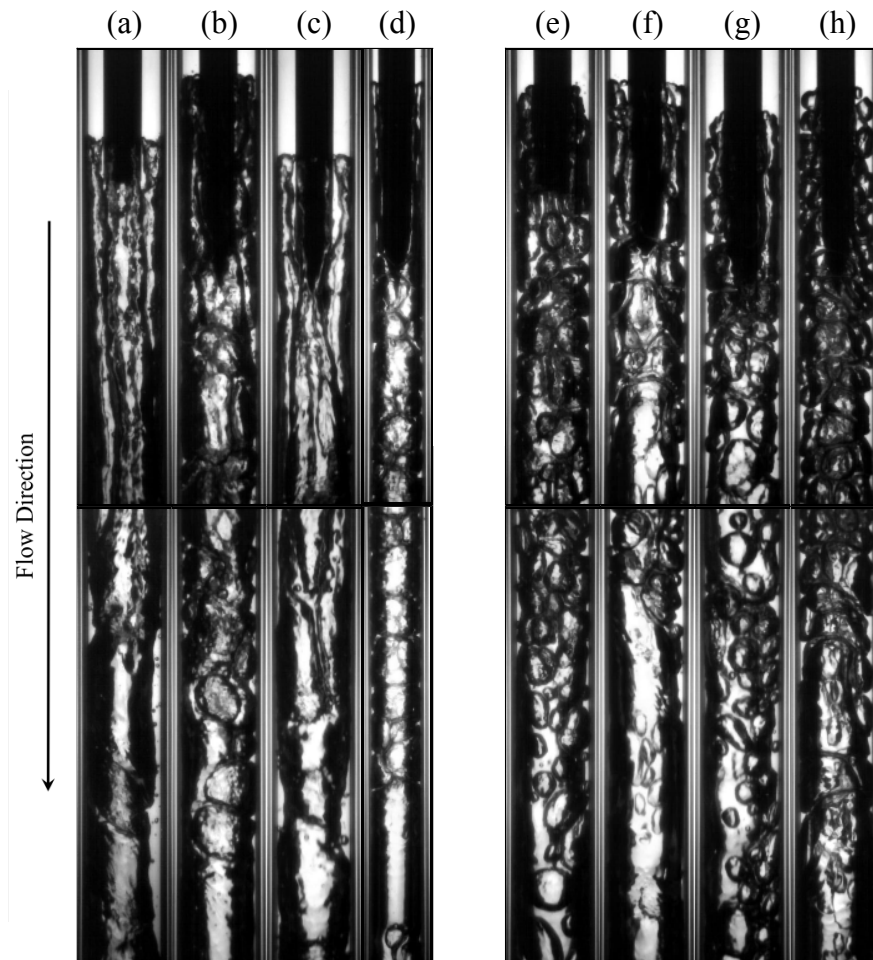


Figure 4.31 Development of disturbed annular flow:

- a) 106 g/s, 1.01% ALR (§A5.1.2); b) 54 g/s, 2.01% ALR (§A6.1.2);
 c) 107 g/s, 0.99% ALR (§A7.1.2); d) 14 g/s, 3.97% ALR (§A7.4.1);
 e) 72 g/s, 0.99% ALR (§5.2); f) 72 g/s, 1.00% ALR (§A6.4.1)
 g) 75 g/s, 0.50% ALR (§A7.1.3); h) 68 g/s, 0.24% ALR (§7.2).

In addition to being a previously unreferenced flow regime, a disturbed annular flow was not observed during the spray trials and so its atomisation properties are unknown. However, as the flow generated has reduced homogeneity compared to annular flow, the findings throughout the current investigation indicate that it would exhibit decreased spray stability.

4.2.10 Annular Flow (Liquid Droplets)

Annular flow (liquid droplets) is a unique flow regime observed in the current experimentation, with its development shown in Figure 4.32. It is defined by a relatively constant annular core, which encloses liquid droplets generated by dripping from the central aerator tube. The liquid droplets are occasionally seen to interfere with the liquid periphery, which can form liquid ligaments spanning the mixing chamber (akin to disrupted annular flow or churn flow). Annular flow (liquid droplets) had a tendency to occur at high liquid flow rates and ALRs, where annular flow would otherwise be expected – although there were some isolated exceptions to this rule. It was not observed during vertically upwards orientated experiments as the liquid droplets are formed under the action of gravity. This flow regime is not thought to apply to outside-in effervescent atomisers, as the central aerator tube from which the liquid drips would not be present.

N.B. Annular flow (liquid droplets) is not equivalent to a “wispy annular flow”, which is occasionally cited in the literature. Wispy annular flow also features liquid droplets within a gaseous core, but these are small droplets are generated due to the inner phase shearing, not large liquid droplets from dripping at the aerator.

Annular flow (liquid droplets) is a previously unreferenced flow regime that was not observed during the current spray trials and, therefore, its atomisation properties are unknown. However, as the flow generated has reduced homogeneity compared to annular flow, the findings throughout the current investigation indicate that it would exhibit decreased spray stability.

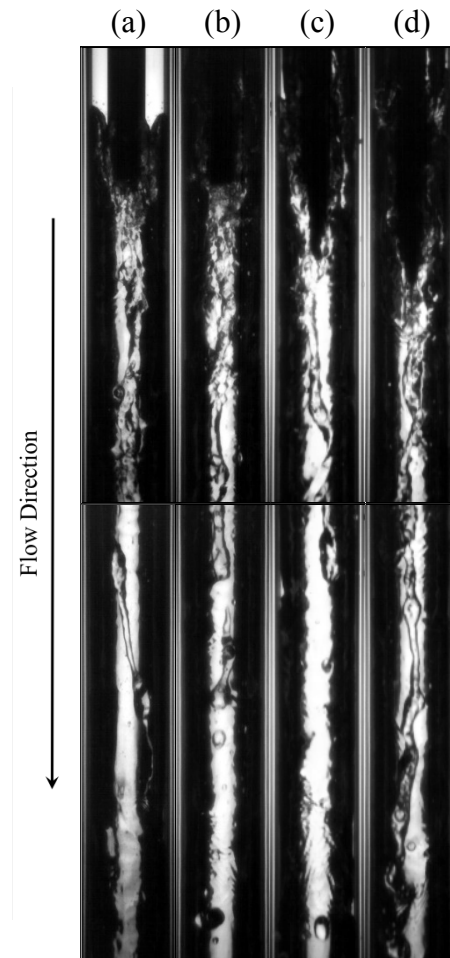


Figure 4.32 Development of annular flow (liquid droplets):
a) 42 g/s, 3.98% ALR (§A5.1.2); b) 27 g/s, 5.02% ALR (§5.2);
c) 31 g/s, 4.02% ALR (§A6.1.3); d) 40 g/s, 4.99% ALR (§A7.2.2).

4.3 Spray Characterisation

A transparent effervescent atomiser was used to characterise the complete effervescent atomiser process at various fluid flow rates. This was achieved using High-Speed Shadowgraphy to identify the internal flow and near-nozzle atomisation mechanisms, and PDA to quantify the spray. It should be noted that PDA data is inherently averaged (i.e. point measurement technique over prolonged period) and, therefore, does not give a measure of transient effects – consequently, near-nozzle imaging and spray data were considered in conjunction when quantifying spray quality.

Figure 4.33 compares the internal flow and near-nozzle observations for a common effervescent atomiser – this featured an 8 mm mixing chamber, 2.0 mm exit orifice diameter and streamlined aerator body profile (i.e. ADARPA design). The internal flow at the lowest ALR (0.12% ALR) was seen to be a bubbly flow, with poor homogeneity due to a low number of small bubbles existing in the liquid continuum – consequently, the single bubble atomisation was relatively irregular and hence the spray quality was poor, with a large quantity of un-atomised liquid ligaments in the spray centreline. The flow regime was varied by raising the ALR, which in turn increased the emerging gas-phase stability. This was initially seen to increase the number density of bubbles within the flow at 0.25% ALR, which resulted in a bubbly flow with greater homogeneity – hence the regularity of the single bubble atomisation was increased, which generated a more consistent and stable spray. However, further increasing the ALR was seen to transition the internal flow to heterogeneous regimes, whereby varying proportions of liquid and gas phases were transiently discharged through the exit orifice – consequently, the atomisation mechanisms were seen to alternate and, hence, the spray stability was observed to decrease. Pulsing flow was identified at the highest ALRs, which featured a highly transient internal flow that would alternate between a liquid continuum and annular flow – consequently, the spray was seen to be very unstable. A continuous annular flow was not observed even at the highest ALRs, which is thought to have been prevented by operating with a sufficiently small mixing chamber diameter – in this case, the surface tension of the liquid is sufficient to prevent phase separation or gravitational effects. The 8 mm mixing chamber diameter in the current investigation is below the limit reported by Kim and Lee [20] (i.e. 10 mm) to enable this phenomenon.

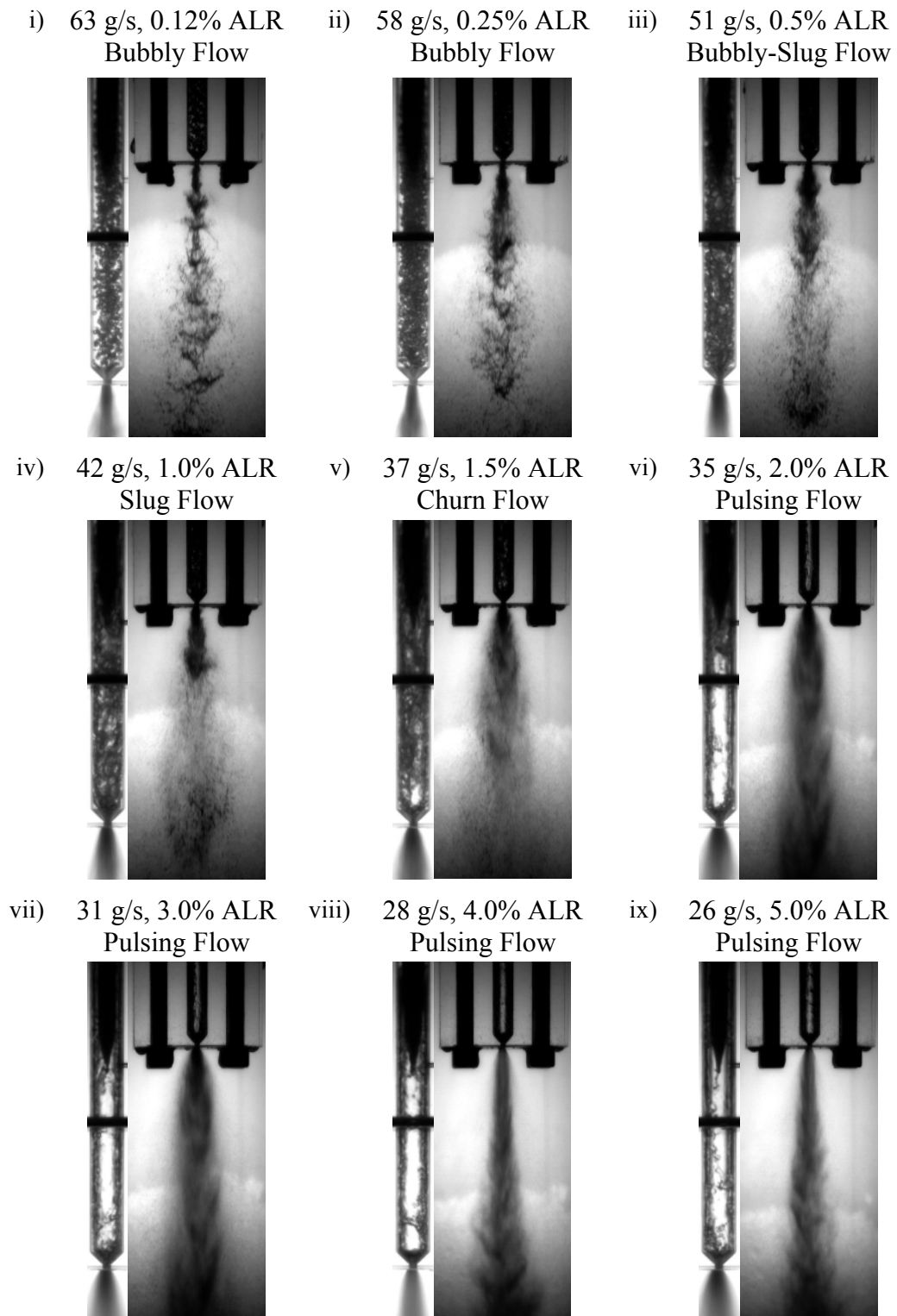


Figure 4.33 Internal flow and near-nozzle atomisation observations.

These observations are mirrored in the droplet size data for the same effervescent atomiser over comparable operating conditions (Figure 4.34). These investigations were not extended to the pulsing flow cases at ALRs in excess of 2.0% as the spray generated was too unstable – this directly contradicts the work of Konstantinov [16], in which stable atomisation was not achieved below 2.0% ALR. The results of this work show that a high number of large droplets exist in the centreline at the lowest ALR (0.12% ALR), which corresponds to the observations of a sparse bubbly flow and hence poorly atomised liquid ligaments. Raising the ALR acts to increase the average gas velocity within the spray (Figure 4.34b), particularly in the near-nozzle region as the gas expands from the exit orifice – consequently, greater destructive mechanisms are exerted on the liquid-phase with increasing ALR and hence finer atomisation is achieved (Figure 4.34a). Furthermore, the largest droplets are seen to migrate to the spray edge as the ALR increases, as the droplet momentum due to the expanding gas carries the larger droplets away from the nozzle axis – this is in keeping with the literature reports [16, 24, 27, 86, 95]. In addition, droplets sizes are seen to decrease with axial distance – thought to be due to the action of secondary atomisation (i.e. action of aerodynamic Weber number), as droplets breakup within the ambient atmosphere.

N.B. The spray width at the greatest axial distances is demonstrated to be significantly wider for low ALRs – this appears to be in conflict with the near nozzle observations. This anomaly can be explained by considering the definition of the spray edge, which is classified as the radial location at which droplet data rates fall below 10% of the maximal value at that axial location – all droplet measurements taken beyond this limit were discarded as ambient. As the number of droplets measured decreased with ALR (e.g. the maximum number of droplet at 250 mm axial displacement was: 9993 at 1.5% ALR; and 2608 at 0.12% ALR), the 10% criterion was more comfortably met at lower ALRs by ambient droplets – consequently, the spray is shown to be wider. As a result, spray cone angle was not calculated from the current results.

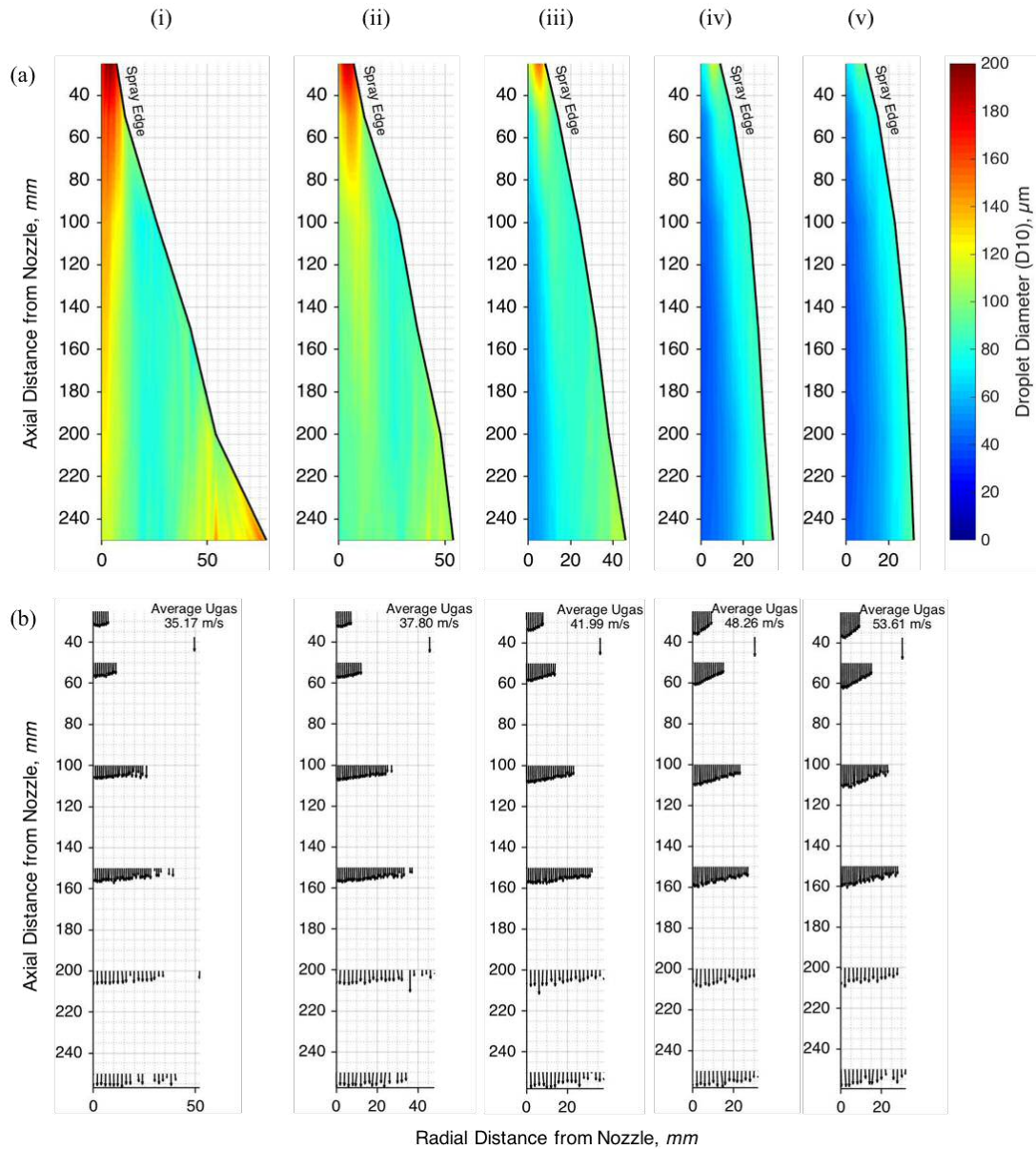


Figure 4.34 a) droplet size spray profiles and b) gas velocity quiver plot for:

i) 63 g/s, 0.12% ALR; ii) 58 g/s, 0.25% ALR; iii) 51 g/s, 0.49% ALR;

iv) 42 g/s 1.00% ALR; v) 36 g/s, 1.51% ALR.

Additional spray characterisation was performed by quantifying the particle distributions within the spray (Figure 4.35). The results show that, by number, the majority of droplets within the measured sprays have diameters below 150 μm , however each feature a small fraction of larger droplets that contribute to a significant proportion of the volume/mass contained within the spray. Nevertheless, this is comparable to conventional atomiser types, which can feature a high droplet diameter ratio of 100:1 [163]. In addition, it can be seen that increasing the ALR acts to increase the proportion of small droplets within the spray and, consequently, the averaged droplet sizes (e.g. D10 and D32) continually decrease.

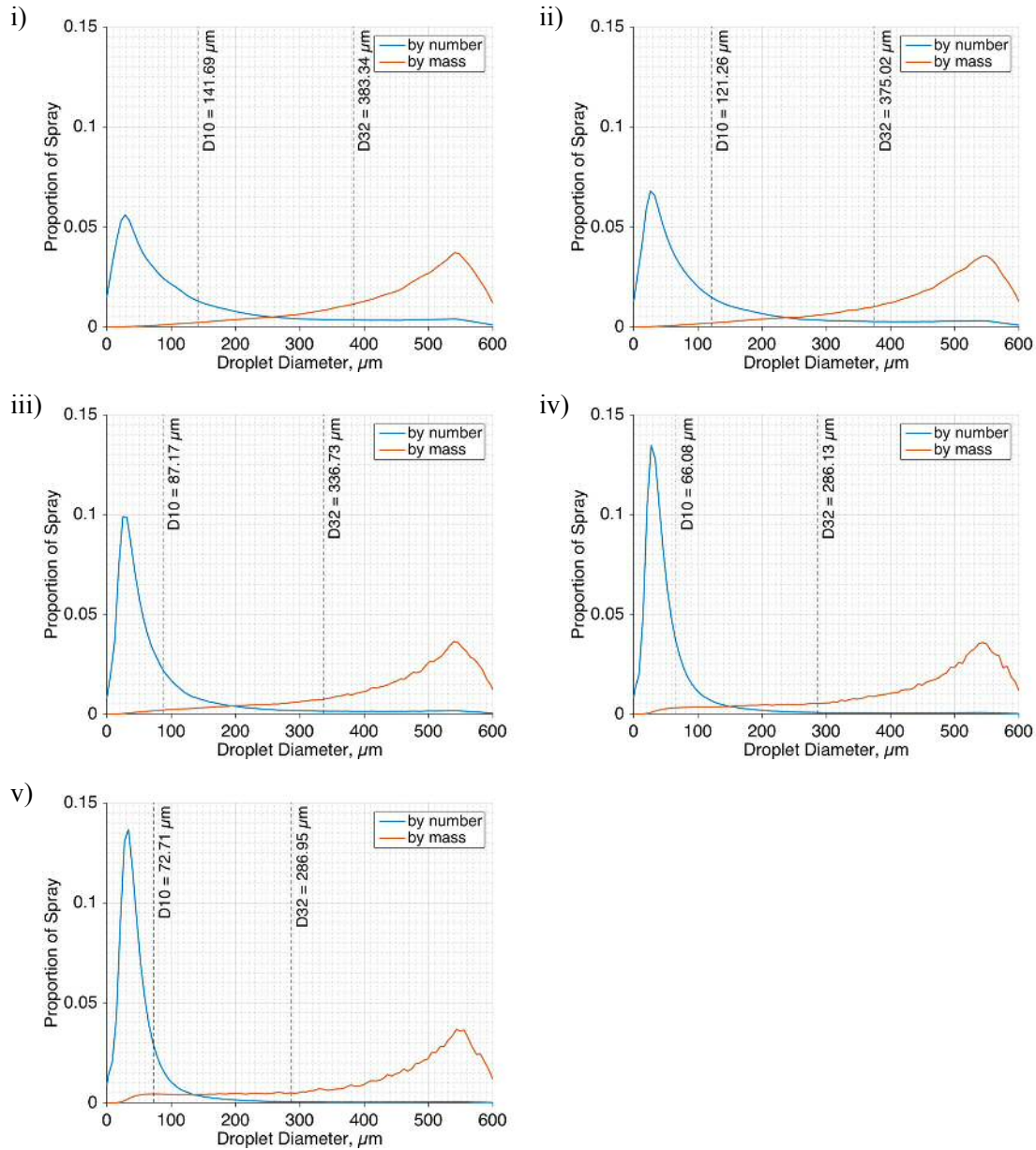


Figure 4.35 Droplet distribution for entire spray:

- i) 63 g/s, 0.12% ALR; ii) 58 g/s, 0.25% ALR; iii) 51 g/s, 0.49% ALR;
 iv) 42 g/s 1.00% ALR; v) 36 g/s, 1.51% ALR.

These characterisation analyses were extended for the effervescent atomiser over multiple exit orifice diameters (i.e. 1.0, 1.5 and 2.0 mm). This allowed for a flow regime map to be generated (Figure 4.36), which shows the effect of varying the fluid flow rates on the flow regimes generated in the mixing chamber at an operating pressure of 5 bar_g. The maximum liquid flow rate of 69 g/s was achieved for the 2 mm exit orifice at 0% ALR which, for the 8 mm mixing chamber, corresponded to a maximum liquid Bakers number of 1363 kg/m²s. The gas supply was varied up to 5% ALR. Analysis of the flow regime map enabled identification of five discrete gas injection regimes, which were categorised into four gas

injection regions. These results demonstrate that bubbly flow was achieved at the lowest ALRs across all exit orifices. This was seen to transition to heterogeneous regimes with sufficient liquid flow rate at increased ALRs.

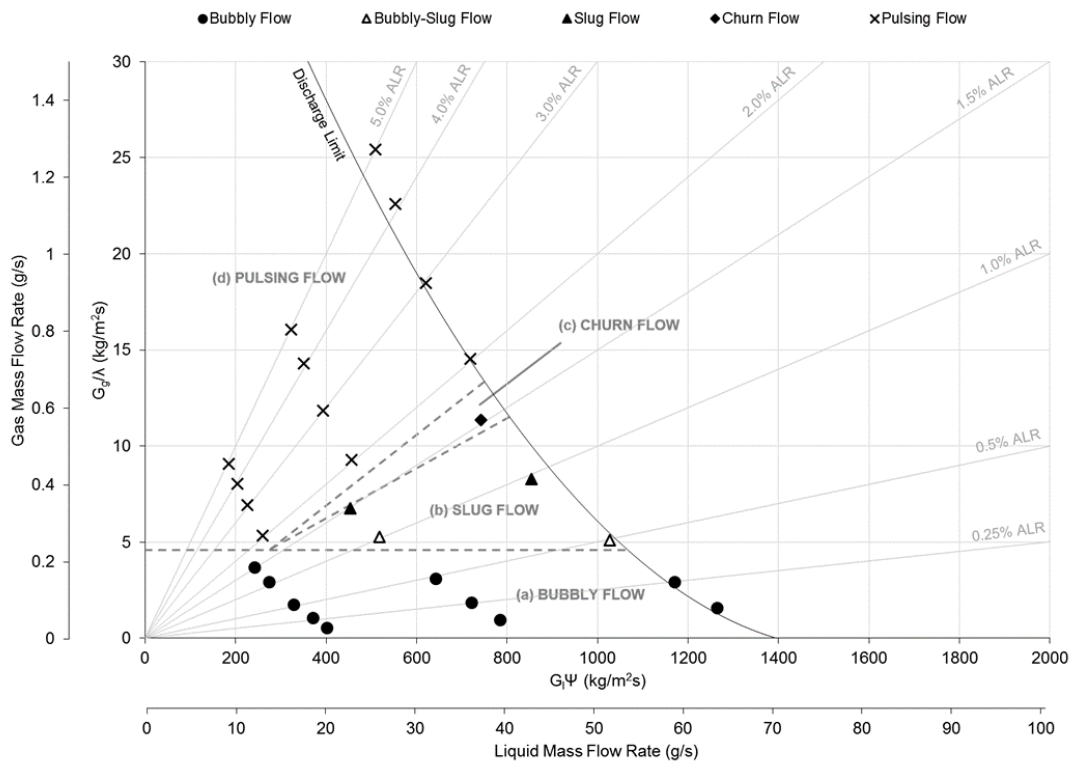


Figure 4.36 Flow regime map for OEA equipped with streamlined ADARPA aerator.

Over the exit orifice diameters investigated, increasing ALR was seen to consistently reduce the droplet size produced through effervescent atomisation (Figure 4.37), although this effect was observed to continually diminish – this is in agreement with the literature findings [10, 19]. In addition, it was seen that reducing the exit orifice diameter resulted in a reduction in the liquid flow rate for comparable ALRs and a corresponding reduction in droplet sizes. This was expected, as reducing the exit orifice diameter essentially acts to scale the atomisation system and therefore the droplet sizes reduce accordingly – this was not seen to be linear, owing to the non-scaled effects of the fluid properties.

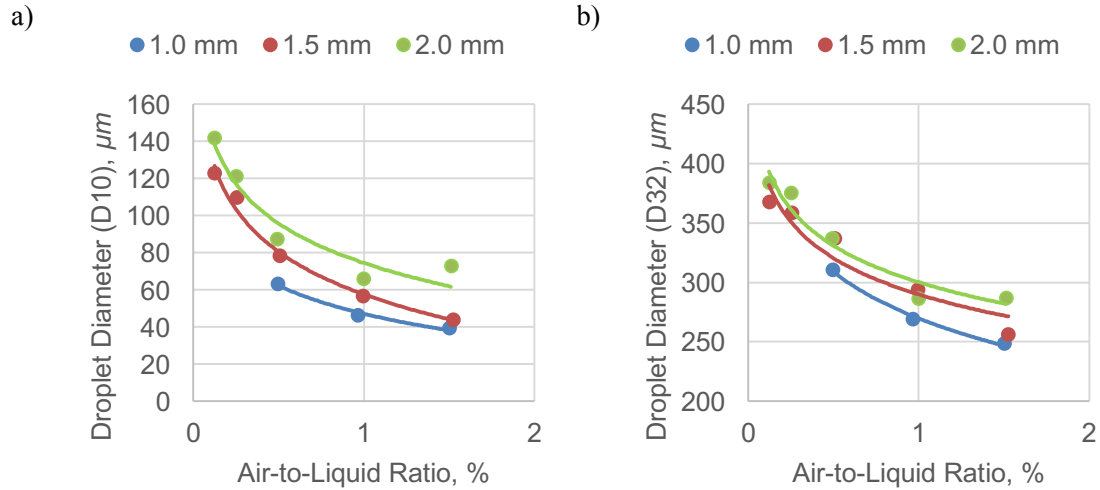


Figure 4.37 Effect of ALR and exit orifice diameter on droplet sizes: a) D10; b) D32.

It has been shown throughout the results that the effect of ALR reduces the size of droplets generated in effervescent atomisation, however it was not previously known whether this is as a result of increased expanding gas-phase velocity or due to differences in the internal flow supplying the exit orifice. Hence to quantify the effect of flow regime on the droplet size produced, the droplet distributions of bubbly flow and gas void disintegration (slug flow) observations were compared in Figure 4.38 – these cases are comparable as both were achieved at equivalent flow rates but were generated with differing aerator tip designs, in which the bubbly flow was generated with a streamlined aerator and gas void disintegration (slug flow) with a convention flat-end aerator. It can be seen that, despite the differing flow regimes supplied to the exit orifice, there is little difference in particle distributions and averaged droplet sizes – the D32 is only 2.2% larger for bubbly flow than for an equivalent gas void disintegration (slug flow). Therefore, it can be concluded that the internal flow regime supplying the exit orifice has a weak effect on the generated droplet size but strong effect on the spray stability.

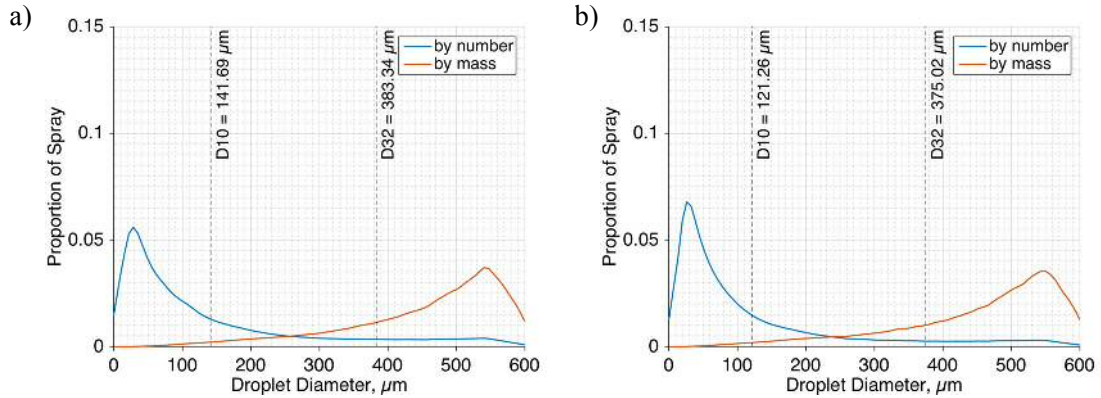


Figure 4.38 Effect of internal flow on droplet distribution at 58 g/s, 0.25% ALR:

a) bubbly flow, ADARPA aerator; b) gas void disintegration (slug flow), flat-end aerator.

It should, however, be noted that the D32 results within the current experimentation are larger than the typical values cited within literature sources – the lowest D32 was measured at 248 μm (Figure 4.39), which compares to similar investigations by Stähle et al. [87] and Ghaemi et al. [81] in which minimum D32s were reported as 25 μm and 10 μm respectively. The D10 result for this case was, however, much more comparable with these literature values at 39 μm , which indicates that the small number of large droplets have a significant effect on the D32 results. The measurement of these large droplets are thought to originate from:

1. The atomiser not being optimised: The intention of the current study was to enable internal flow and spray characterisation of a common effervescent atomiser across various flow rates and, therefore, a high priority was placed on using transparent nozzles. The material used for these nozzles (i.e. acrylic glass) was considerably more fragile than the typical materials used in atomiser manufacture (e.g. brass, stainless steel) and, hence, was more challenging to accurately machine – therefore, safety factors and machining tolerances were suitably increased. Consequently, it is thought that the spray quality could be considerably improved by reducing the L/D ratio of the exit orifices by manufacturing from a high yield strength material at greater accuracy.
2. The sensitivity of experimental technique to large droplets: PDA with a large mask can be more sensitive to larger droplets [16], which have a significantly greater weighting with D32. Comparative techniques include laser diffraction and spray imaging.

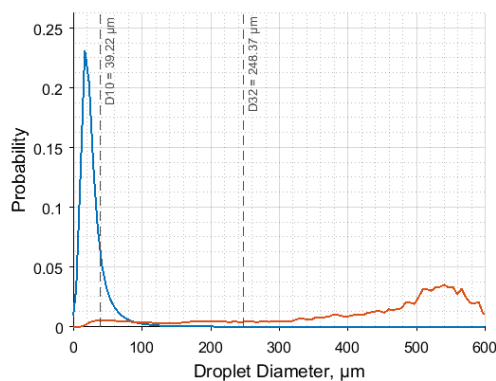


Figure 4.39 Droplet distribution at 30 g/s, 1.50% ALR.

4.4 Summary

In this chapter provided a summary of the internal flow behaviour and spray characteristics of various effervescent atomiser configurations across differing fluid flow rates. In addition to the observation of the commonly referenced gas injection and flow regimes from the literature (e.g. bubbling/jetting gas injection, and bubbly/heterogeneous/annular flow), two new gas injection regimes and five internal flow regimes were identified and presented within the current work – specifically, the coalesced jetting and evacuated chamber gas injection regimes; and the gas void disintegration (bubbly flow), gas void disintegration (slug flow), pulsing flow, disrupted annular flow and annular flow (liquid droplets) flow regimes. It was identified that bubbling at the aerator was linked to bubbly flow generation in the mixing chamber and was encouraged by low emerging gas-phase stability – this was promoted by low ALRs, small aerator orifice diameters, large aeration areas, small mixing chamber diameters and high operating pressures. A number dense bubbly flow was observed to generate regular single bubble atomisation and hence produce a more consistent and stable spray compared to alternative flow regimes – in addition, the single bubbling atomisation mechanism is reported in the literature to be the most efficient spray generation mechanism. Increasing the ALR was shown to decrease the droplet sizes, irrespective of flow regime. Consequently, the optimal effervescent atomiser configuration would enable bubbly flow across the widest range of fluid flow rates and at the highest ALRs – this would correspond to the most stable and efficient spray generation with the lowest droplet sizes.

CHAPTER 5. INTERNAL FLOW STUDIES OF FLAT-END AERATORS TO OPTIMISE BUBBLY FLOW OPERATION

It was determined in the previous chapter that an optimal effervescent atomiser configuration would enable bubbly flow across the widest range of fluid flow rates, corresponding to stable spray generation, and at the highest ALRs, corresponding to fine atomisation. Consequently, this chapter quantifies the fluid flow rates ranges corresponding to bubbling at the aerator and bubbly flow within the mixing chamber for an inside-out effervescent atomiser equipped with various flat-end aerator designs across various independent parameters – these are compared to determine optimal effervescent atomiser design.

N.B. In the interest of a concise discussion, only the findings of significance to effervescent atomisation are presented in the current body of work – the complete gas injection and flow maps for the current study are presented and described in detail within Appendix 5.

5.1 Bluff Body Recirculation of Conventional Flat-End Aerators

A common observation within the current work of major significance for inside-out effervescent atomisation was the formation of a large gas void in the wake of a conventional flat-end aerator (Figure 5.1) – this occurred for all vertically downwards investigations at low ALRs from start-up. The formation of a gas void in this region is particularly problematic for effervescent atomisation, as it was observed to displace the bubbles injected at the aerator and therefore prevent formation of a conventional bubbly flow. The only sourced report which observed similar gas void formation in the aerator wake was an internal flow study by Jobehdar [44], also using a conventional flat-end aerator. The researchers observed that the formation of the gas void lead to decreased internal flow homogeneity, which resulted in reduced spray stability – this agrees with the near-nozzle investigations of the current work, which were reported in the previous chapter (§4). Therefore, the

occurrences of gas void formation in the current internal flow investigation are predicted to yield inferior effervescent atomisation and should be avoided.

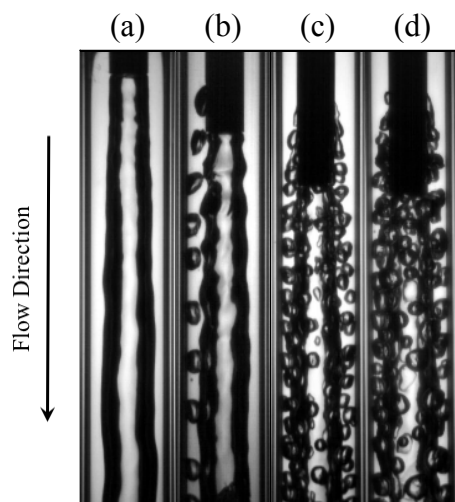


Figure 5.1 Example observations of gas void formation in aerator wake:

- a) 280 g/s, 0.02% ALR (§A5.2.1); b) 275 g/s, 0.03% ALR (§A5.1.1);
 c) 202 g/s, 0.13% ALR (§A5.1.3); d) 136 g/s, 0.25% ALR (§5.2).

It is proposed that this gas void formation can be explained by considering the restoring and detachment mechanisms acting on the gas-phase within the aerator wake region. Firstly, gas void formation was not observed under equivalent vertically upwards conditions and, therefore, it can be inferred that its generation is majorly affected by gas-phase buoyancy. In addition, the positioning of the void directly downstream of the aerator indicates that the axial flow over the flat-end cylinder generates significant bluff body recirculation – this causes a reduced pressure region, within which the liquid viscous forces (e.g. drag, inertia) are reduced. Consequently, the buoyancy of the gas-phase within this region is sufficient to overcome the viscous forces within the aerator wake – however, the high liquid cross-flow velocity around the aerator periphery generates sufficient shear to counteract the buoyancy and, therefore, the gas-phase finds equilibrium satisfied at the aerator tip to form a gas void.

This theory is supported in a supplementary experiment, in which a small quantity of gas was injected into an arbitrary liquid cross-flow (Figure 5.2). The injected gas entities were seen to be “sucked” into the reduced pressure region existing within aerator wake, where all or some of the volume became “trapped”. The trapped gas entities were seen to circulate in close proximity, due to local pressure variations. It is known that prolonged bubble contact promotes coalescence [30, 58-60] and, therefore, with increased gas-phase entrapment (i.e. increased ALR) and sufficient residence time, a gas void would be expected to be formed.

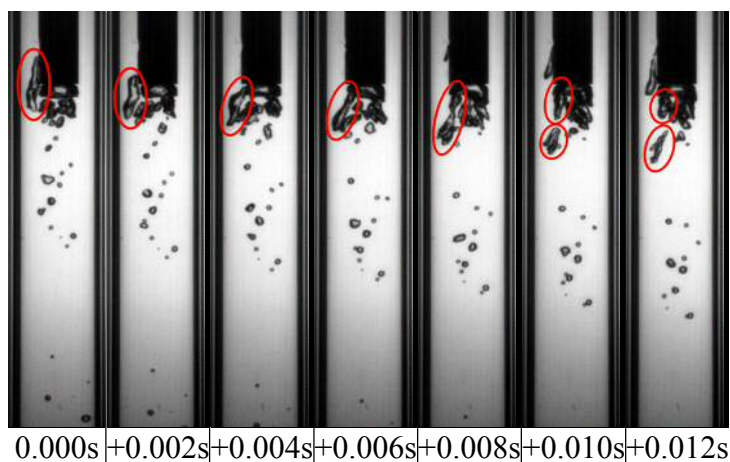


Figure 5.2 Observation of gas entity entrapment in aerator wake from bled start-up:
290 g/s, 0.003% ALR.

However, the process of a gas void slowly growing due to bubble entrapment and coalescence was not observed in the main experimentation, due to a gas void being immediately present upon start-up (Figure 5.3). Unbled start-up conditions were adopted for all investigations in the experimentation, with the atomiser started from atmospheric conditions (i.e. the mixing chamber filled with ambient air) and the gas-phase injected prior to commencement of liquid flow – whilst this represents “worst-case” effervescent atomiser operation, it is expected to best simulate start-up in the majority of applications – whereby the effervescent atomiser would not be bled prior to each use. Therefore, to achieve a liquid continuum, the mixing chamber must be passively bled of ambient air upon start-up under the action of the injected fluids. However, for a flat-end aerator, the bluff-body recirculation effect is too great to allow the mixing chamber to be completely bled upon start-up and, therefore, a gas void containing residual ambient air is formed in the aerator wake.

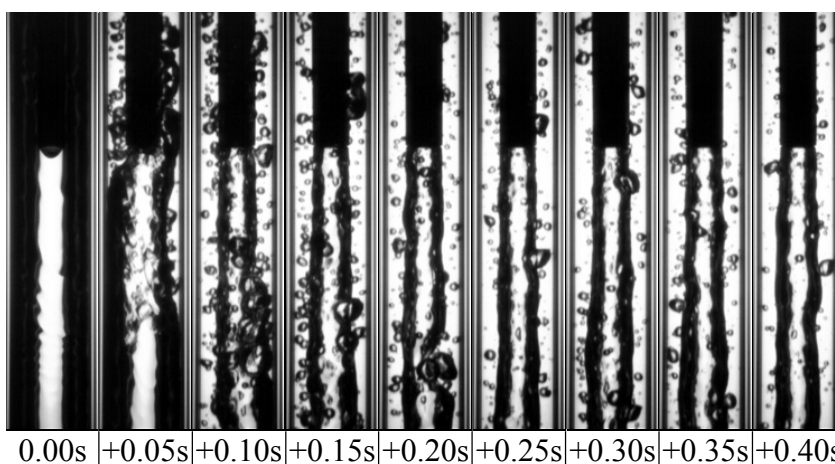


Figure 5.3 Time-lapse of gas void formation from unbled start-up with a flat-end aerator:
289 g/s, 0% ALR, 5 bar_g.

The presence of this gas void was observed to force bubbles injected at the aerator to flow around the liquid periphery, thus preventing formation of a conventional bubbly flow. Furthermore, these bubbles were seen to coalesce with the gas void, due to their close proximity in the liquid periphery, thus supplying it with gas. Another supply mechanism was observed when gas injected from the aerator orifice(s) was linked directly to the void (i.e. the cavity forming gas injection regime, §4.1.7).

Under certain conditions, the gas void was observed to be detached from the aerator tip or break-up to form bubbles or gas slugs. Three discrete mechanisms were observed:

1. Vortex shedding (Figure 5.4a): The gas void itself behaves as a bluff body in the peripheral liquid flow. The liquid flow experiences vortex shedding as it passes the base of the gas void, generating localised areas of reduced pressure. This generates high shear on the gas void and, hence, promotes break-up of the void on the leading edge into bubbles (i.e. gas void disintegration (bubbly flow), §4.2.2). This mechanism was observed to have a very low depletion rate, generating a small number of tiny bubbles that often themselves became trapped in the void wake. Hence, increasing the gas flow rate (i.e. increasing the supply rate to the void) was seen to dramatically elongate the gas void. At critical conditions, the length of the gas void exceeded the measurement mixing length and the flow regime is classified as annular flow (§4.2.7).
2. Fluid shearing (Figure 5.4b): Surface instabilities were observed to be generated on the gas-liquid interface of the void, due to the combined shearing action of the injected gas (internal to void) and peripheral liquid (external to void). At critical conditions, this can generate sufficient drag to detach the void from the aerator tip. This was observed to be promoted by increased ALR.
3. Gas entity interference (Figure 5.4c): Passing gas entities injected from the aerator were observed to interfere with the void generating surface instabilities on the gas-liquid interface. This was seen to be encouraged by the presence of large bubbles or jets in the liquid periphery. Under critical conditions, this was seen to either completely detach the gas void from the aerator tip or strip volumes of gas from the void within the mixing chamber – the flow regime resulting from this process has been previously defined as gas void disintegration (slug flow) within §4.2.3.

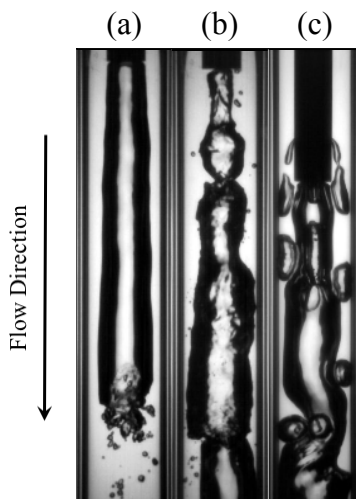


Figure 5.4 Examples of gas void shearing: a) 233 g/s, 0.002% ALR (§A5.2.1);
b) 190 g/s, 0.41% ALR (§A5.2.1); c) 147 g/s, 0.14% ALR (§A5.1.2).

Gas void formation was seen to be prevented at high ALRs, which is thought to correspond with conditions where the emerging gas-phase exerts a significant disruptive effect on the gas void. However, all observations corresponding to single bubbling at the aerator were not sufficient to detach the gas void and so, in every vertically downwards investigation, bubbly flow was prevented. Some cases of pulse bubbling at relatively high ALRs were able to detach the gas void, but the gas entities generated were sufficiently large to form a slug flow in the mixing chamber. Alternatively, the gas void was observed to be removed by orientating the atomiser vertically upwards, implying that a critical angle exists beyond which gas void formation is prevented – whilst this solution did allow generation of a bubbly flow due to bubble injection at the aerator, it would limit the use of inside-out effervescent atomisation to orientations in excess of a critical angle and, hence, majorly restrict the suitable applications. A potential solution was reported in the literature by Jobehdar [44] whereby gas void formation was prevented by streamlining the aerator body with an arbitrary conical tip, thus reducing the bluff body recirculation effect – therefore, streamlined aerator body design is investigated as an independent variable in subsequent chapters of the current work. Alternatively, the effervescent atomiser design could be restricted to outside-in configurations, which removes the aerator body and, hence, bluff body effect – there have been no observations of gas void formation within outside-in effervescent atomiser literature.

5.2 Effect of Fluid Flow Rates, including Air-to-Liquid Ratio

As discussed in the previous chapter, the effect of fluid flow rates (i.e. ALR and exit orifice diameter) were seen to have a significant effect on the internal flow performance of an effervescent atomiser, which in turn was proven to have a significant effect on the stability of the spray. In the present study, the effervescent atomiser was configured in its benchmark configuration for the conventional flat-end aerator design (i.e. the default cases for each independent variable were used; Table 3.4) – hence, the results are comparable with all other flat-end aerator investigations presented within this thesis.

Figure 5.5 shows the effect of varying ALR for a common effervescent atomiser, equipped with a conventional flat-end aerator tip and with a fully open discharge nozzle setting. The emerging gas-phase has low stability at the lowest ALR, due to having a low injected gas velocity. Consequently, small bubbles are observed to be formed almost immediately upon exposure to the liquid cross-flow (i.e. single bubbling), which flow in the liquid periphery around an established gas void in the aerator wake. However, as the injected gas velocity increases, so does the emerging gas-phase stability – in addition, the liquid cross-flow decreases as the gas increasingly blocks the exit orifice, which in turn reduces the detachment mechanisms acting on the emerging bubble. Consequently, increasing the ALR was observed to increase the length of gas neck from which bubbles are formed (i.e. pulse bubbling) and, hence, visibly increase their size – by 0.51% ALR gas entities are large enough to exert sufficient disruption to detach the gas void from the aerator wake, leading to the formation of a slug flow. Further raising the ALR transitions the gas injection to jetting, which features increasingly chaotic flow patterns within the mixing chamber – at the highest gas flow rates the jet was observed to have sufficient momentum to emerge perpendicular to the liquid flow and contact the mixing chamber wall, generating a churn flow in the mixing chamber.

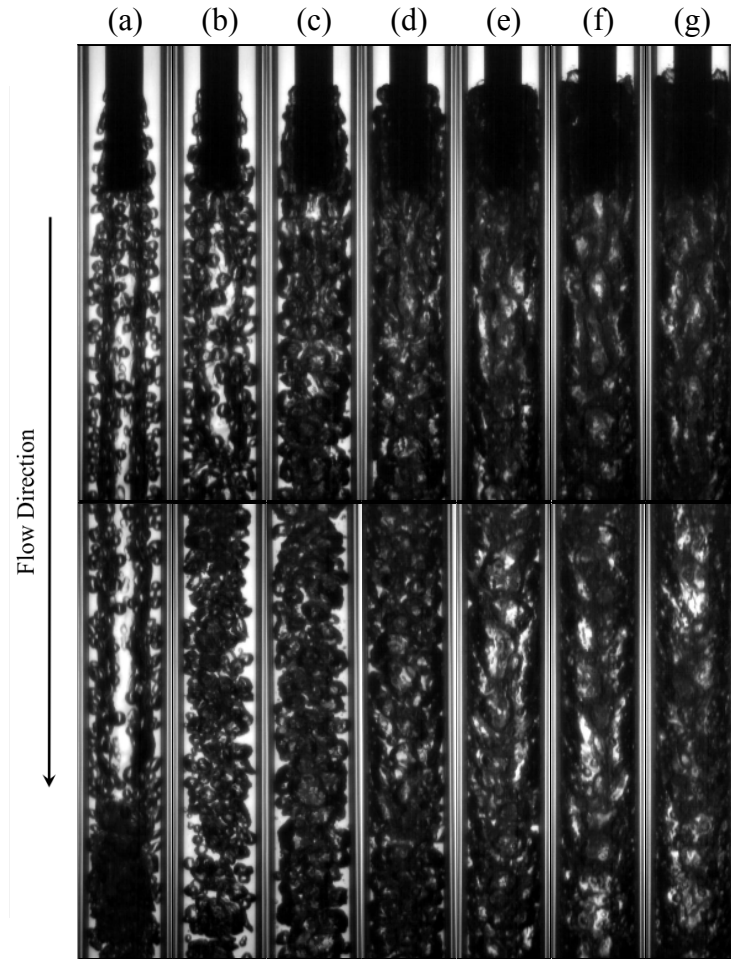


Figure 5.5 Comparable observations with varying ALR:

- a) 250 g/s, 0.13% ALR; b) 234 g/s, 0.25% ALR; c) 212 g/s, 0.51% ALR;
 d) 185 g/s, 1.00% ALR; e) 167 g/s, 1.49% ALR; f) 153 g/s, 2.01% ALR;
 g) 148 g/s, 2.26% ALR.

Figure 5.6 shows the effect of varying the discharge nozzle setting (i.e. the exit orifice diameter) for a common atomiser configuration and ALR. Decreasing the exit orifice diameter reduces the liquid cross-flow past the aerator (Equation 2.8), thus lessening the relative detachment forces acting on the emerging gas-phase – however, by maintaining a constant ALR proportionally reduces the injected gas velocity and, hence, a similar gas injection process was observed. However, the relative effect of buoyancy is increased and, consequently at a critically low liquid flow rate (in this case 60 g/s), the peripheral liquid flow is insufficient to displace the ambient gas from the mixing chamber upon start-up and hence an evacuated chamber regime is established within the mixing chamber.

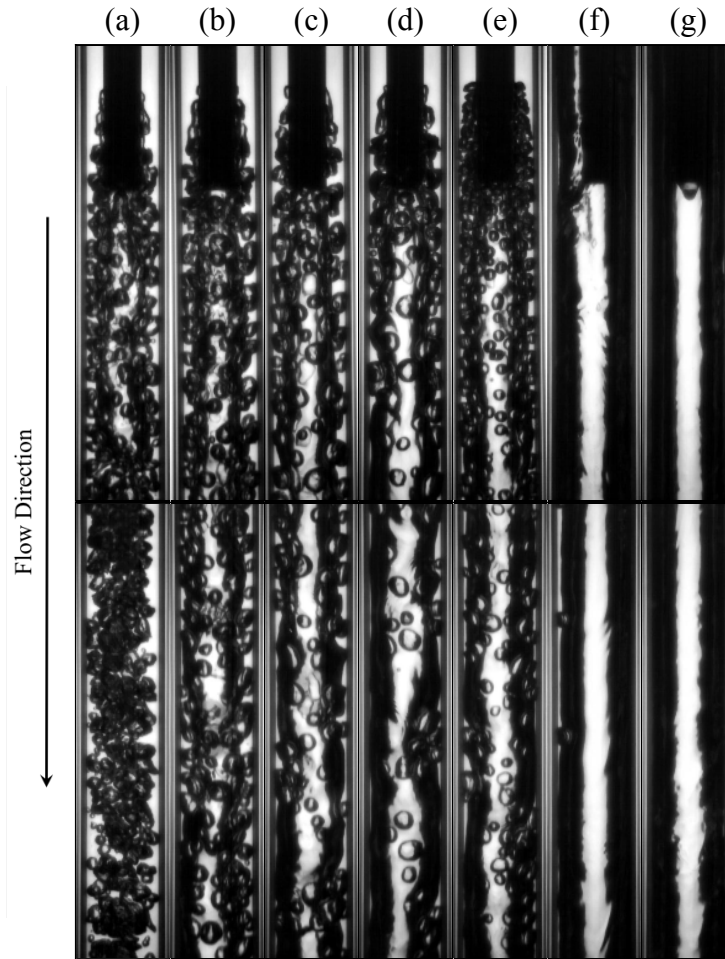


Figure 5.6 Comparable observations with varying discharge nozzle settings:

- a) 234 g/s, 0.25% ALR; b) 188 g/s, 0.25% ALR; c) 136 g/s, 0.25% ALR;
- d) 92 g/s, 0.24% ALR; e) 81 g/s, 0.26% ALR; f) 60 g/s, 0.24% ALR;
- g) 27 g/s, 0.27% ALR.

These analyses were extended across various ALRs and discharge nozzle settings. Figure 5.7 is the resulting gas injection regime map for the benchmark atomiser configuration, which shows the effect of varying the fluid flow rates on the gas injection processes at the aerator. Analysis of this map enabled identification of five discrete gas injection regimes, which were categorised into three gas injection regions.

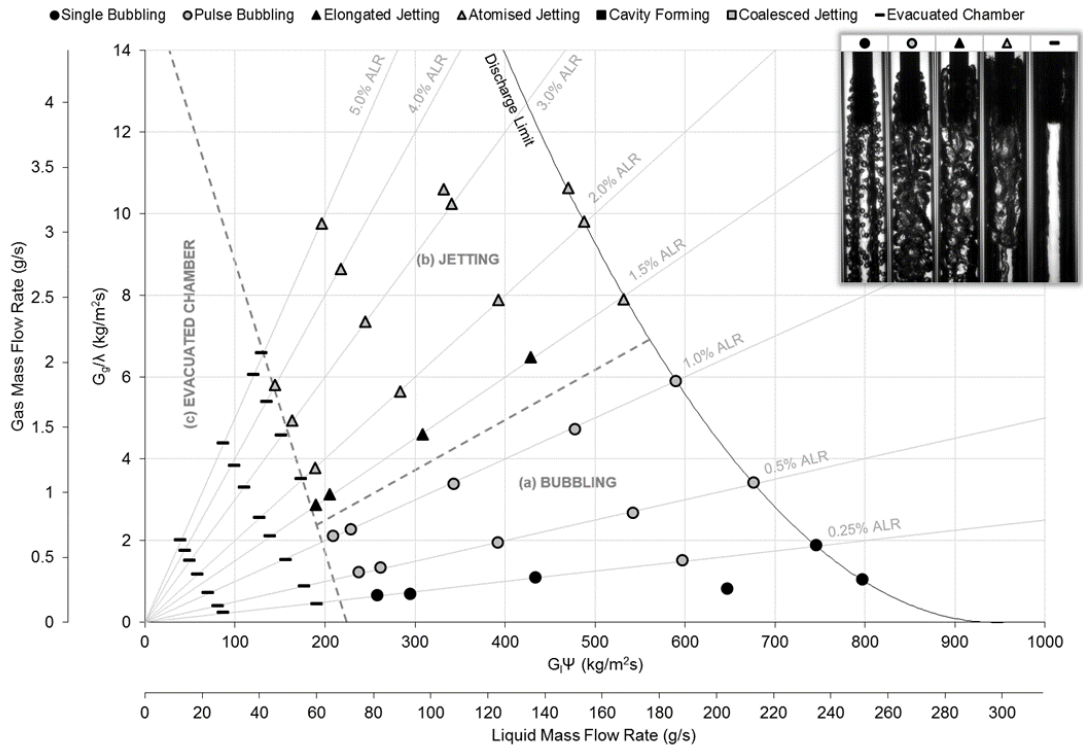


Figure 5.7 Gas injection regime map for the benchmark configuration (aerator A5 with flat-end body design, 20 mm mixing chamber diameter, 5 bar_g operating pressure, vertically downwards orientation).

A region of evacuated chamber was identified in the near aerator region at relatively low liquid flow rates (Figure 5.7c), where buoyancy has a significant relative effect and hence phase separation occurred prior to fluid injection. Whilst operating in this region, the effect of ALR did not have a significant effect on the internal flow and consequently evacuated chamber was consistently observed regardless of gas flow rate. Formation of evacuated chamber in this case appeared to be marginally suppressed with high gas flow rates.

The ALR was observed to have a considerably more pronounced effect at liquid flow rates exceeding evacuated chamber. At low ALRs, a large region of bubbling (Figure 5.7a) was identified in which individual bubbles were observed to be formed at, or near to, the aerator across a range of operating conditions – instances of single bubbling were observed at the lowest ALRs (typically at or below 0.25% ALR) and pulse bubbling up to 1.0% ALR. Further increasing the ALR instigates transition of the gas injection process to jetting (Figure 5.7b), which initially features a small number of elongated jetting observations with atomised jetting at the highest ALRs.

In order to identify the effects of fluid flow rates on the flow regimes and establish trends between the gas injection behaviour and the formation of internal flow regimes, the same mapping process was applied to the mixing chamber observations. The resulting flow regime map for the benchmark configuration, shown in Figure 5.8, identified seven discrete flow regimes across the various fluid flow rates which were grouped into six regions.

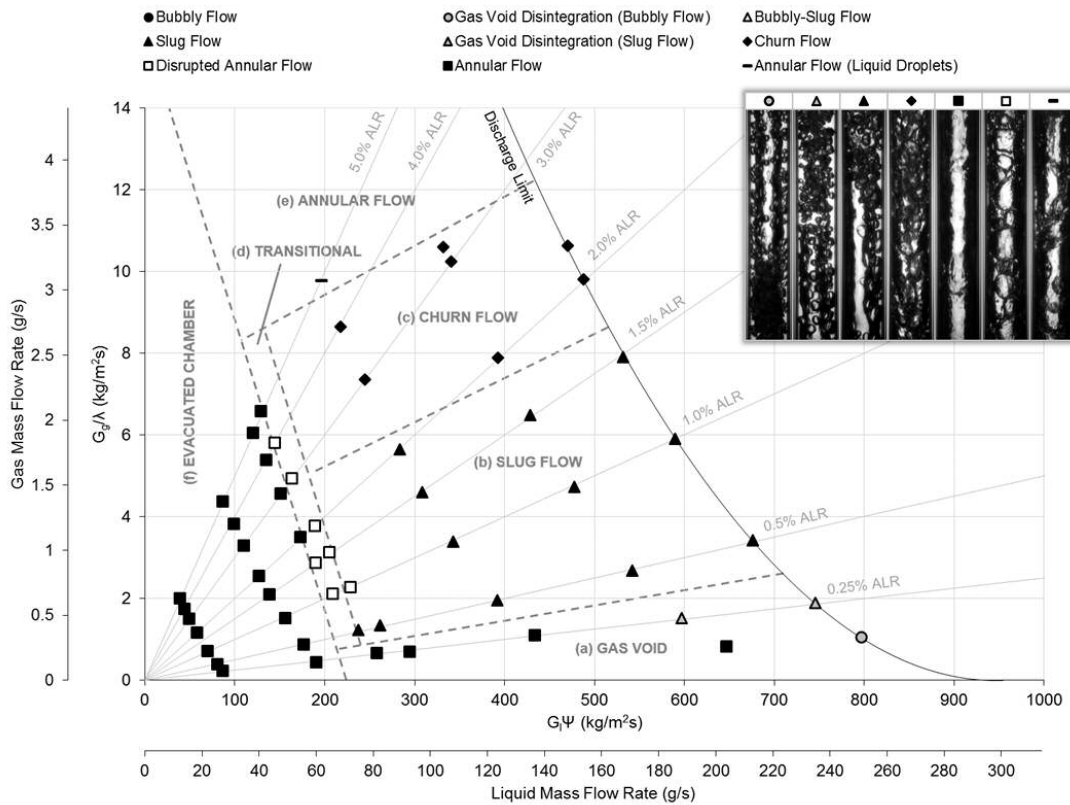


Figure 5.8 Flow regime map for the benchmark configuration

(aerator A5 with flat-end body design, 20 mm mixing chamber diameter, 5 bar_g operating pressure, vertically downwards orientation).

It is immediately noticeable that, despite bubbling at the aerator, a conventional bubbly flow was not formed within the mixing chamber throughout the range of flow rates tested and, therefore, this atomiser configuration is not considered optimal for effervescent atomisation. At conditions expected to encourage bubbly flow (i.e. high liquid flow rates and low ALRs), instead a gas void was formed within the aerator wake (Figure 5.8a) which displaced the injected bubbles into the liquid periphery and, thus, prevented a bubbly flow. This void was only observed to breakup under specific conditions, forming an unconventional bubbly flow at the highest liquid flow rate and lowest ALR, and an unconventional slug flow at higher ALRs – for all other cases in which a gas void was formed, the destructive mechanisms were insufficient to generate breakup within the mixing length and hence an annular flow was

established. The formation of a gas void within the aerator wake was observed to coincide with all instances of single bubbling and some low ALR cases of pulse bubbling, in which the injected bubbles do not generate sufficient disruption on the gas void to displace it from the wake.

Consequently, the gas void was only observed to be detached at high ALRs when sufficient disruption was generated by the injected gas-phase – but in these cases, the gas flow rate was too great to enable uniformly sized bubbles to be produced. Therefore, a region of intermittent flow regimes were established at ALRs in excess of gas void formation, which were observed to transition from slug flow (Figure 5.8b) to churn flow (Figure 5.8c) with increasing ALR. A single instance of annular flow was identified at the highest ALR, due to the complete coalescence of the injected gas jets – in this case, liquid droplets were present within the core.

A thin annular flow was identified for all conditions corresponding to the evacuated chamber gas injection regime (Figure 5.8f), occurring at the lowest liquid flow rates. A transitional region (Figure 5.8d) was observed at liquid flow rates just in excess of the evacuated chamber regime, which featured a heavy proportion of disturbed annular flow cases – this was caused by the incomplete action of either coalescence or breakup due to high relative buoyancy.

This same mapping process for the gas injection and flow regimes was completed for each independent parameter using a conventional flat-end aerator, which enabled comparison between studies and, for the first time, quantification of the internal flow performance of an effervescent atomiser in various configurations. In the interest of a concise discussion, only the findings of significance to effervescent atomisation are presented in the current body of work (i.e. the bubbling region within the gas injection regime maps and the bubbly flow region within the flow regime maps) – however, the complete gas injection and flow maps for these studies are presented and described in detail within Appendix 5.

5.3 Effect of Aerator Orifice Diameter

The effect of aerator orifice diameter on effervescent atomiser internal flow was investigated between 0.75-3.0 mm for a common aeration area of 7.07 mm² and with a conventional flat-end aerator body design (i.e. aerators A2-A5). As the injected bubble size is known to be proportional to the aerator orifice diameter (Equation 2.2), a reduction in aerator orifice

diameter was expected to reduce the bubble size for a given ALR and, hence, increase the internal flow homogeneity.

Figure 5.9 shows the effect for all aerator orifice diameters under comparable flow conditions – specifically, a flat-end aerator body design, 0.13% ALR and fully open discharge nozzle setting. Decreasing the aerator orifice diameter can be visibly seen to decrease the size and, hence, increase the number of bubbles produced. This is thought to be because decreasing the aerator orifice diameter increases the emerging gas-liquid interface area and, hence, decreases the stability of the injected gas phase. At the largest aerator orifice diameter investigated (i.e. 3.0 mm), the emerging gas jet is sufficiently stable upon injection to resist break-up and, thus, coalesces with the gas void in the aerator wake, forming a cavity forming regime. In all of these vertically downwards cases at low ALRs, a gas void can be observed to have formed in the aerator wake which is observed to interfere with the gas injection, either due to coalescence with the emerging gas jets (i.e. cavity forming) or displacing any injected bubbles.

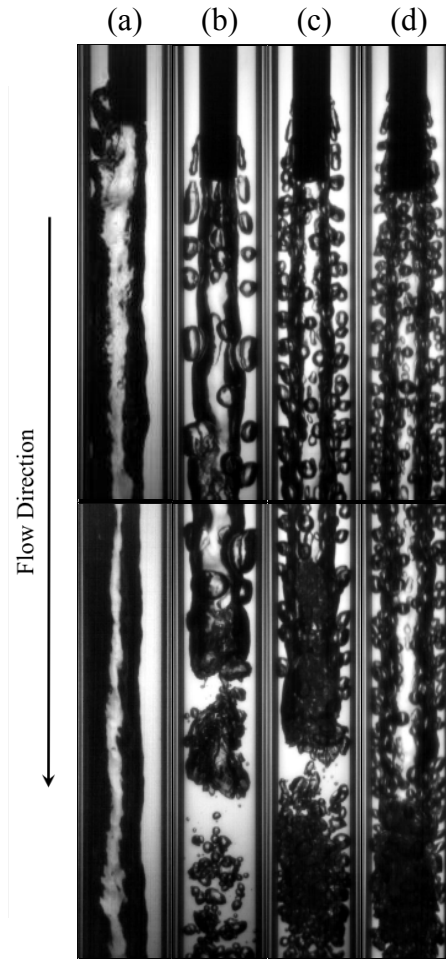


Figure 5.9 Comparable observations with varying aerator orifice diameter:

- a) Aerator A2 – 1 x 3.0 mm, 252 g/s, 0.13% ALR;
- b) Aerator A3 – 4 x 2.0 mm, 254 g/s, 0.13% ALR;
- c) Aerator A4 – 9 x 1.0 mm, 249 g/s, 0.13% ALR;
- d) Aerator A5 – 16 x 0.75 mm, 250 g/s, 0.13% ALR [benchmark].

The investigation was extended by analysing the gas injection regime maps for each atomiser configuration in which aerator orifice diameter was investigated as an independent parameter. The purpose of an effervescent atomiser aerator is to inject the gas-phase into the liquid-phase to form uniformly sized bubbles and, hence, generate a homogenous bubbly flow. Consequently, bubbling at the aerator is considered the most relevant gas injection regimes for effervescent atomisation – these regions are compared in Figure 5.10 for the aerator orifice diameter studies. For all of these cases, the bubbling region was restricted at:

- High ALRs, by the transition to jetting regimes. Decreasing the aerator orifice diameter increases the ALR at which bubbling transitions to jetting, which indicates

a less stable emerging gas-phase – this is thought to be caused by the increased emerging gas-liquid interface area over which the detachment mechanisms act.

- Low liquid flow rates, by the generation of evacuated chamber. Whilst this limit was observed to vary between aerator orifice diameters, the trend was not predictable – it is thought that the differences are due to the chaotic mechanisms affecting passive bleeding of the atomiser upon start-up and not the effect of aerator orifice diameter.
- High liquid flow rates, by the flow limit of the discharge valve. Increasing the ALR acts to further restrict the valve and hence the liquid flow rate continually decreases. The effect of aerator orifice diameter was not seen to have a significant effect on the discharge limit.

The operating range for each configuration was determined by calculating the area of the flow map corresponding to bubbling and a trend was determined by identifying a line of best fit with closest correlation (i.e. minimum R^2). The results of this work are shown in Figure 5.10, in which it can be determined that the range of fluid flow rates corresponding to bubbling is increased with a decrease in aerator orifice diameter. Consequently, bubbling was observed to be encouraged with multi-holed aerator design, which is in agreement with the literature reports [13, 17, 19, 29, 56, 81, 86].

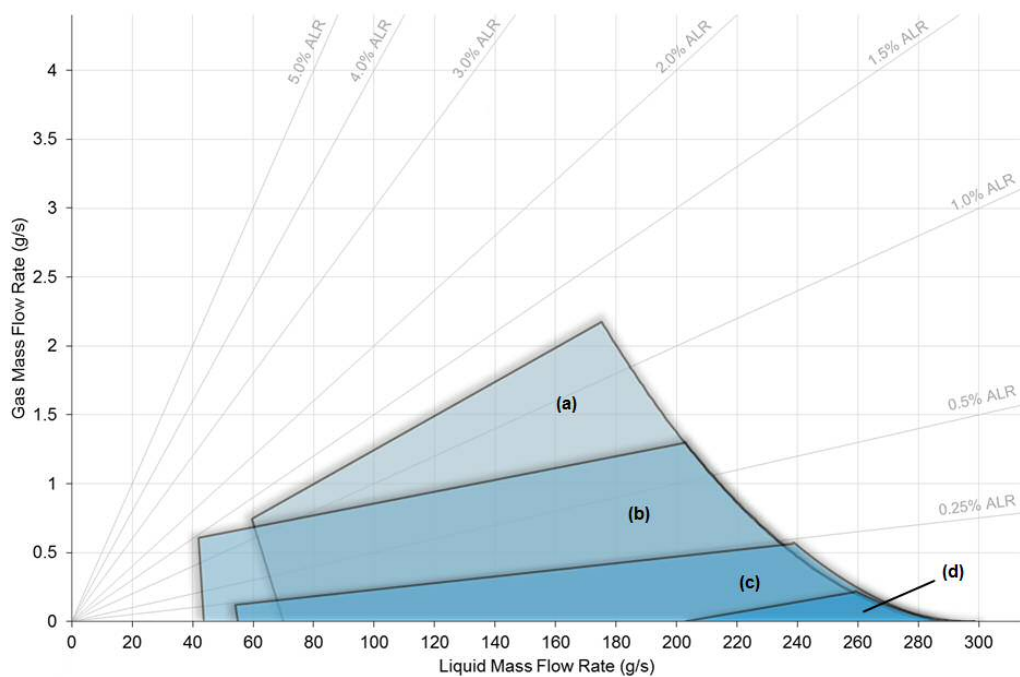


Figure 5.10 Effect of aerator orifice diameter on bubbling operating range:

- a) aerator A5, 16 x 0.75 mm (§5.2) [benchmark]; b) aerator A4, 9 x 1.0 mm (§A5.1.3);
 c) aerator A3, 4 x 2.0 mm (§A5.1.2); d) aerator A2, 1 x 3.0 mm (§A5.1.1).

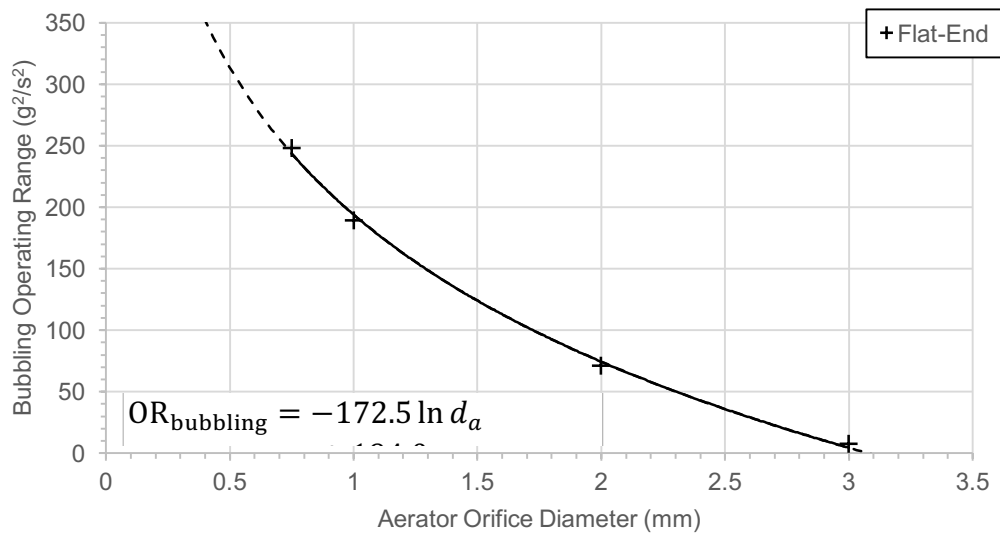


Figure 5.11 Effect of aerator orifice diameter on bubbling operating range.

However, throughout all investigations and irrespective of aerator orifice diameter, there were no observations of a conventional bubbly flow being formed in the mixing chamber and, therefore, none of the investigated atomiser configurations are considered suitable for effervescent atomisation. This was due to the formation of a gas void in the aerator wake at

low ALRs, which was observed to displace any injected bubbles. Decreasing the aerator orifice diameter was visibly seen to decrease the size of the injected bubbles and, hence, reduce interference on the gas void – consequently, the range of fluid flow rates for which a gas void was formed was marginally increased with decreasing aerator orifice diameter. The gas void was observed to be detached with increased ALRs (typically within the pulse bubbling region), however this corresponded with conditions in which intermittent regimes (e.g. slug flow and churn flow) were formed.

5.4 Effect of Unconventional Aerator Designs

Two unconventional aerator designs were tested to investigate the extreme cases referenced within the literature.

A co-flow aerator (i.e. gas injection through the base of the aerator body, parallel to the liquid flow) was stated by Stähle et al. [87] to encourage formation of an annular flow – this atomiser configuration was coined an “air-core-liquid-ring” (ACLR) design. These findings were validated in the current investigation, whereby a co-flow aerator design (i.e. aerator A1) was observed to promote annular flow due to cavity forming, even at the very lowest ALRs (Figure 5.12a) – this was due to gas being injected directly into the aerator wake, where conditions are suited to gas void formation. Consequently, bubbling at the aerator was not observed for any condition and therefore a conventional bubbly flow was prevented – consequently, co-flow aerators are not thought to be suitable for effervescent atomisation.

A porous aerator was reported by Ghaemi et al. [81] to have excellent potential for effervescent atomisation, due to increasing the number density of bubbles, compared to a geometrically equivalent outside-in multi-holed aerator – this was, however, disputed by Roesler and Lefebvre [67]. In the current work, a porous aerator (i.e. aerator A6) was observed to generate bubbling at low ALRs (Figure 5.12b), with the formed bubbles forced to flow within a liquid periphery around a gas void. The size of the bubbles generated were seen to be smaller than the conventional multi-holed aerator, which is thought to relate to the reduced size of the aeration orifices (i.e. pore size).

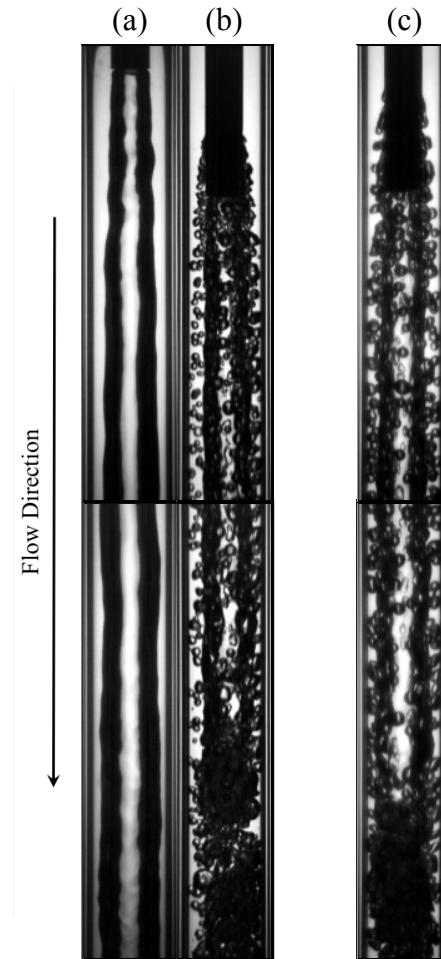


Figure 5.12 Example observations of unconventional aerator designs:

a) Aerator A1 – single hole co-flow, 247 g/s, 0.17% ALR;

b) Aerator A6 – porous cross-flow, 253 g/s, 0.12% ALR.

Both at comparable ALRs and discharge nozzle setting to a conventional aerator design:

c) Aerator A5 – multi-hole cross flow, 250 g/s, 0.13% ALR [benchmark].

The bubbling region for a porous aerator was compared to a conventional multi-holed aerator in Figure 5.13 – it was seen to be restricted at:

- High ALRs, due to transition to coalesced jetting. This was caused by the close proximity of aeration pores, where bubbles were not able to fully expand before coalescing with a neighbouring pore – consequently, the bubbling region was seen to be decreased compared to a conventional multi-holed aerator, which transitions to jetting at greater ALRs.
- Low liquid flow rates, by the generation of evacuated chamber. Whilst this limit was observed to vary between the conventional multi-holed and porous aerator designs, it

is thought to be caused by the chaotic mechanisms affecting passive bleeding of the atomiser upon start-up and not the effect of the aerator design.

- High liquid flow rates, by the flow limit of the discharge valve. Increasing the ALR acts to further restrict the valve and, hence, the liquid flow rate continually decreases. The effect of aerator design was not seen to have a significant effect on the discharge limit.

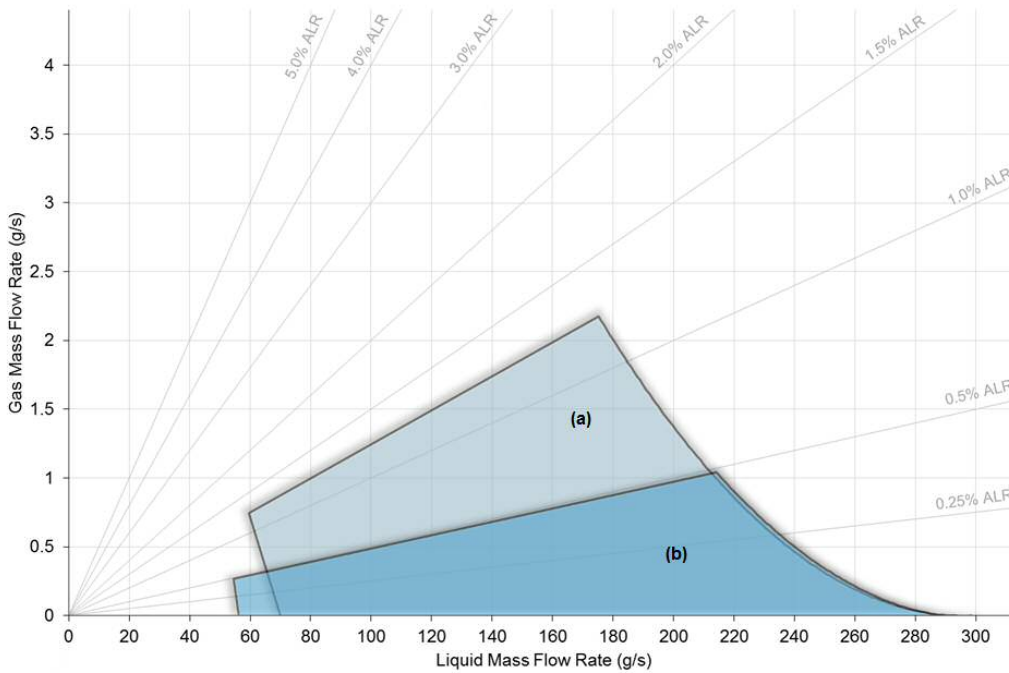


Figure 5.13 Effect of unconventional aerator design on bubbling operating range:
 a) aerator A5, 16 x 0.75 mm (§5.2) [benchmark]; b) aerator A6, porous (§A5.2.2).

Since coalesced jetting occurred prior to complete expansion of the emerging bubbles, the bubbling region of the porous aerator was seen to be reduced compared to a conventional multi-holed aerator (Figure 5.14).

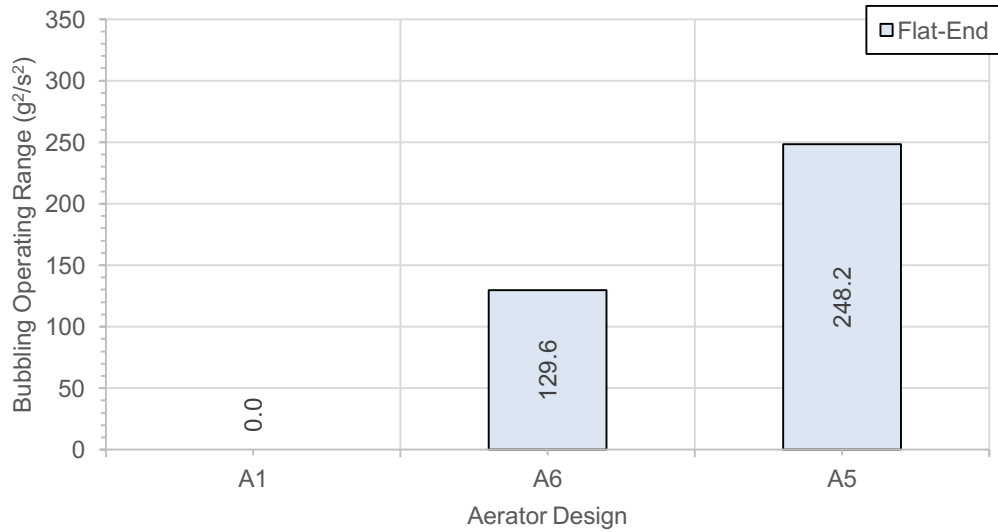


Figure 5.14 Effect of aerator design on bubbling operating range.

However, despite many observations of bubbling for the porous aerator, there were no observations of a conventional bubbly flow being formed in the mixing chamber. This was due to the formation of a gas void in the aerator wake at low ALRs, which was observed to displace any injected bubbles. The gas void was observed to be detached with increased ALRs, corresponding to pulse bubbling, however the gas entities injected generated a slug flow. However, a benefit of a porous aerator was that the formation of coalesced jetting promoted annular flow and, thus, restricted intermittent flow regimes. Therefore, it is thought that the optimum pore spacing for effervescent atomisation would sit within a limited range: where the emerging gas-phase is able to fully expand to form bubbles (i.e. maximise the bubbling range), but coalesce prior to jetting to form an annular flow – this would minimise the range of conditions corresponding to heterogeneous regimes and, therefore, optimise spray stability.

5.5 Effect of Mixing Chamber Diameter

The effect of mixing chamber on effervescent atomiser internal flow was investigated for the first time by comparing a 14 mm diameter mixing chamber to the 20 mm benchmark configuration. It is known that, to maintain continuity, decreasing the mixing chamber diameter for given input fluid flow rates acts to increase the superficial fluid velocities and, hence, the Bakers numbers throughout the atomiser – this includes increasing the liquid cross-flow velocity around the aerator periphery. The influence of increasing the liquid

cross-flow velocity is reported to encourage the detachment of forming bubbles, typically before fully expanded [39].

Figure 5.15 shows the effect of mixing chamber diameter on the internal flow of an effervescent atomiser at a comparable ALR and exit orifice diameter (i.e. discharge nozzle set to fully open). Bubbles were seen to prematurely detach with a reduced mixing chamber diameter, generating a visibly greater number of small bubbles – this can be attributed to greater viscous detachment mechanisms acting on the emerging gas-phase at the aerator, due to the increased liquid cross-flow velocity. A gas void in the aerator wake was observed for both configurations, however the void length appears significantly shorter in the smaller mixing chamber diameter case, due to the greater effect of shearing on the gas void with the increased peripheral liquid flow.

The investigation was extended by analysing the gas injection regime maps for the 14 mm and 20 mm mixing chamber diameters. Figure 5.16 shows the bubbling regions for both cases, which were limited at:

- High ALRs, by the transition to jetting regimes. The transition from bubbling to jetting was seen to occur at a marginally higher ALR for the larger mixing chamber diameter – this is contradictory to expectations, as the greater liquid cross-flow velocity was expected to encourage gas-phase break-up and, hence, bubbling at high ALRs. This anomaly was thought to occur due to the relatively close proximity of the mixing chamber wall with the smallest diameter, which encouraged churning at lower ALRs and, hence, identification of jetting. However, a greater proportion of the bubbling region comprised of single bubbling cases for the reduced mixing chamber diameter, with some cases observed at 0.50% ALR for the 14 mm diameter case compared to the maximum 0.25% ALR for the 20 mm benchmark configuration – this is thought to be evidence the increased detachment mechanisms with the greater liquid cross-flow velocity.
- Low liquid flow rates, by the generation of evacuated chamber. As previously discussed, the formation of the evacuated chamber regime is well approximated by the liquid Bakers number. As the liquid Bakers number for a given mass flow rate dramatically increases with a reduction in the mixing chamber diameter, the evacuated chamber regime was suppressed and bubbling promoted with a reduction in mixing chamber diameter – for example, the liquid Bakers numbers at the maximum liquid mass flow rate of 289 g/s were 1880 kg/m²s for the 14 mm diameter and 923 kg/m²s for the 20 mm diameter benchmark configuration.

- High liquid flow rates, by the flow limit of the discharge valve. Increasing the ALR acts to further restrict the valve and hence the liquid flow rate continually decreases. The effect of mixing chamber diameter was not seen to have a significant effect on the discharge limit.

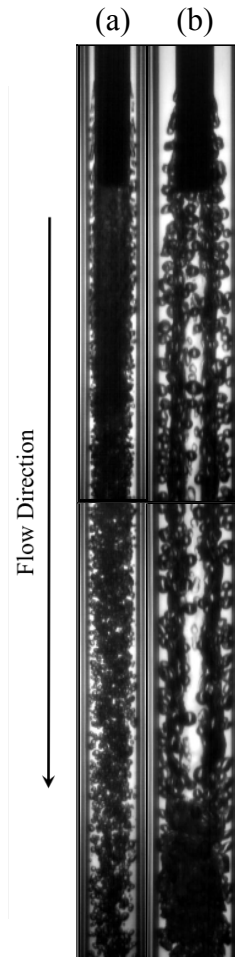


Figure 5.15 Example observations of the effect of mixing chamber diameter at comparable ALRs and fully open discharge nozzle setting (i.e. equivalent exit orifice diameter):

- a) 14 mm diameter, 252 g/s, 0.12% ALR;
- b) 20 mm diameter, 250 g/s, 0.13% ALR [benchmark].

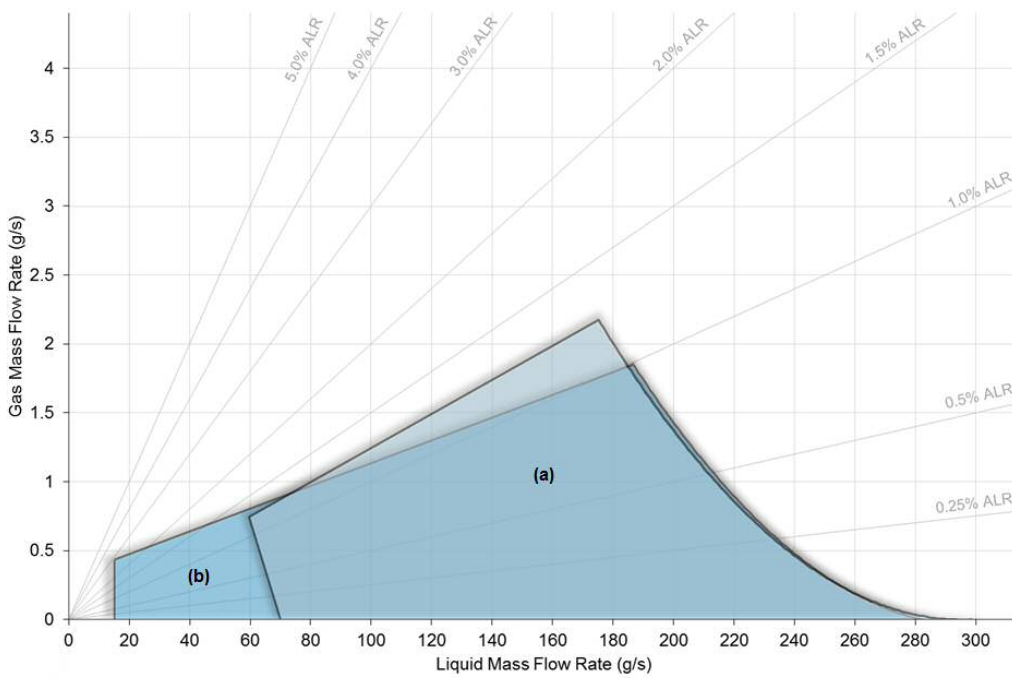


Figure 5.16 Effect of mixing chamber diameter on bubbling operating range, with respect to the fluid mass flow rates: a) 20 mm diameter (§5.2) [benchmark]; b) 14 mm diameter (§A5.3.1).

Consequently, the operating range corresponding to bubbling was seen to be marginally increased with a reduction in mixing chamber diameter (Figure 5.17).

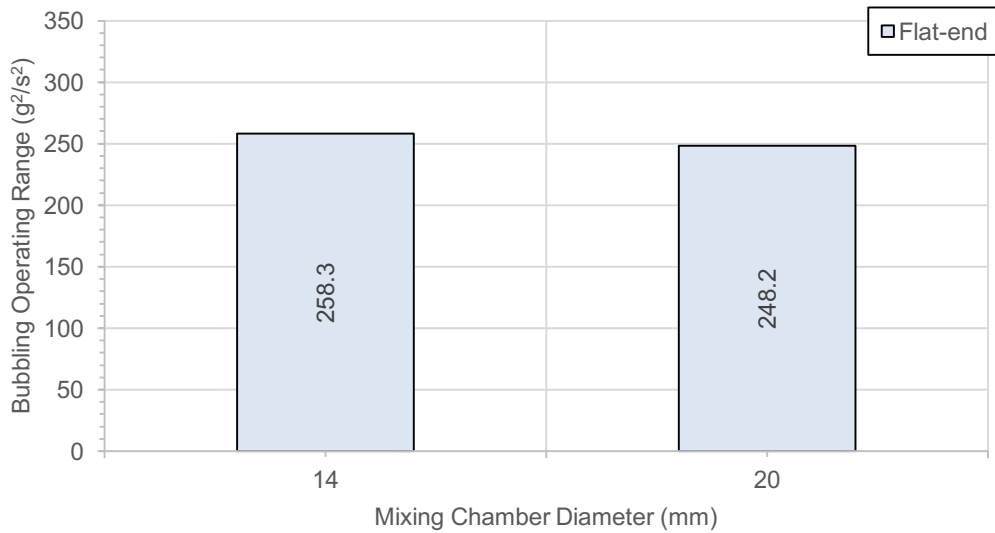


Figure 5.17 Effect of mixing chamber diameter on bubbling operating range.

However, throughout all investigations and irrespective of mixing chamber diameter, there were no observations of a conventional bubbly flow being formed. The effect of increased superficial liquid velocity, due to a decreased mixing chamber diameter, was observed to promote break-up of the gas void. However, the greater rate of depletion was not observed to be sufficient to remove the gas void, even at the lowest ALRs. In fact, gas void formation was observed across a greater number of flow rates with a decreased mixing chamber, which implies that the increased superficial velocities result in a disproportionate increase in aerator bluff body effect. The gas void was observed to be detached with increased ALRs (typically within the pulse bubbling region), however this corresponded with conditions in which intermittent regimes (i.e. slug flow and churn flow) were formed.

5.6 Effect of Operating Pressure

The effect of operating pressure on effervescent atomiser internal flow was investigated for 1, 3 and 5 bar_g. A greater operating pressure increases the achievable fluid flow rates through the atomiser, as described by Equation 2.8 – this relates to increased superficial fluid velocities and Bakers numbers throughout the atomiser and is, therefore, expected to encourage premature detachment of the forming bubbles [39]. In addition, an increased operating pressure acts to compress the gas-phase.

Figure 5.18 shows the effect of operating pressure for a comparable atomiser configuration – specifically at 0.25% ALR with the discharge nozzle setting fully open (i.e. equivalent exit orifice diameter) in which, as expected, the liquid mass flow rate was measured to increase with greater operating pressures. The bubbles produced from the aerator were observed to visibly decrease in size with increasing operating pressure, which is thought to result from a combination of factors. Firstly, the increased liquid cross-flow velocities generated greater breakup mechanisms (e.g. increased viscous drag and inertia), which acted to prematurely detach the emerging gas phase – consequently, in the given cases, the effect of increasing operating pressure is seen to transition the gas injection regimes from pulse bubbling to single bubbling. In addition, an increased operating pressure compressed the gas-phase (i.e. decrease the void fraction) and, hence, as the operating pressure increases, the bubbles are compressed to a smaller size and a greater proportion of liquid-phase can be observed within the mixing chamber despite an equivalent ALR being maintained – this is in agreement with the literature [56]. For the 1 bar_g case, a gas void was prevented in the aerator wake – this further supports the theory that the injection of larger gas entities exerts greater interference on the gas void and promotes gas void detachment.

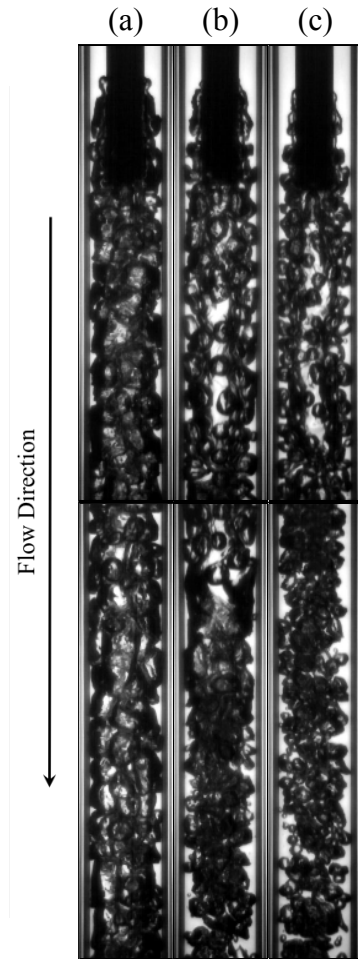


Figure 5.18 Example observations of the effect of operating pressure at comparable ALRs and fully open discharge nozzle setting (i.e. equivalent exit orifice diameter):

- a) 1 bar_g, 103 g/s, 0.25% ALR; b) 3 bar_g, 180 g/s, 0.25% ALR;
 c) 5 bar_g, 234 g/s, 0.25% ALR [benchmark].

The investigation was extended by analysing the gas injection regime maps for each operating pressure. Figure 5.19 shows the bubbling regions for all cases, which were limited at:

- High ALRs, by the transition to jetting regimes. Whilst this limit was observed to occur at an increased ALR for the highest operating pressure, this was not reflected at lower operating pressures and hence a trend cannot be established from the current results.
- Low liquid flow rates, by the generation of evacuated chamber. Whilst this limit was observed to marginally vary between the investigated operating pressures, it is thought to be caused by the chaotic mechanisms affecting passive bleeding of the atomiser upon start-up and not the effect of operating pressure.

- High liquid flow rates, by the discharge limit of the exit nozzle. Increasing the operating pressure was seen to dramatically increase the discharge limit (i.e. increase the maximum liquid flow rates across all ALRs) – where the maximum liquid mass flow rates (and equivalent liquid Baker numbers) for 1 bar_g, 3 bar_g and 5 bar_g cases at 0% ALR were 130 g/s (413 kg/m²s), 225 g/s (717 kg/m²s) and 290 g/s (921 kg/m²s) respectively.

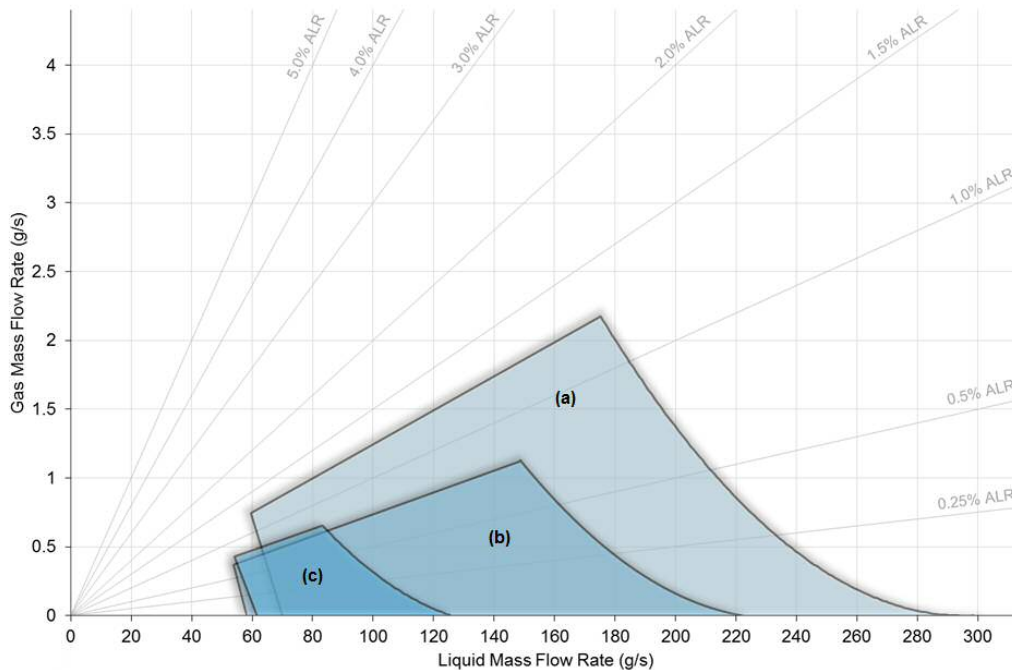


Figure 5.19 Effect of operating pressure on bubbling operating range:
 a) 5 bar_g (§5.2) [benchmark]; b) 3 bar_g (§A5.4.2); c) 1 bar_g (§A5.4.3).

Consequently, the operating range corresponding to bubbling was seen to be increased with a reduction in mixing chamber diameter (Figure 5.20).

However, irrespective of bubbling at the aerator, a conventional bubbly flow was not identified for any of the operating pressures tested due to the formation of a gas void in the aerator wake at low ALRs – this was observed to correspond with all single bubbling cases and some low ALR pulse bubbling cases. As with previous independent parameters, the gas void was observed to be displaced at sufficiently high ALRs within the pulse bubbling region when the injected gas entities are considered large enough to exert a suitably high disruptive effect. A region of intermittent flow regimes were established at ALRs in excess

of the gas void region. The effect of increasing the operating pressure was seen to increase the transitional limits between these flow regimes.

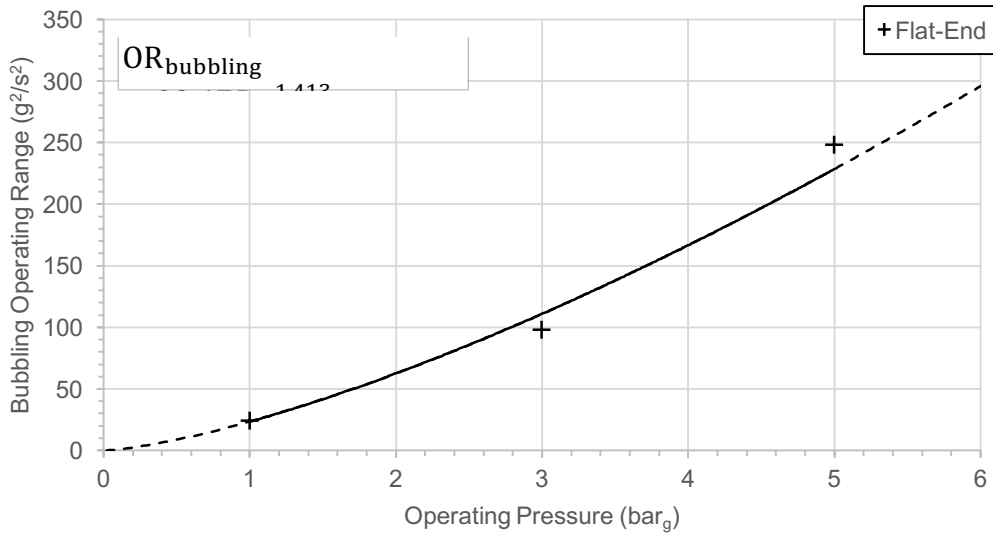


Figure 5.20 Effect of operating pressure on bubbling operating range.

5.7 Effect of Orientation

For the first time, the effect of atomiser orientation on the internal flow has been investigated. The effect of changing the orientation between vertically downwards and upwards reverses the direction of buoyancy relative to the fluid flow. This is expected to aid detachment of the emerging gas-phase for the vertically upwards orientation.

Figure 5.21 shows the effect of atomiser orientation at comparable ALRs and with the discharge nozzle set to fully open (i.e. equivalent exit orifice diameter). Whilst both orientations produce approximately equivalent sized bubbles through single bubbling, the most obvious observation is the prevention of gas void formation in the wake of the aerator when the atomiser was operated in a vertically upwards orientation and, hence, the enablement of a bubbly flow within the mixing chamber – this confirms the previous assumption that the formation of a gas void in vertically downwards orientation is, at least in part, aided by buoyancy. The effect of bluff body recirculation can, however, be visualised by observing the flow path of injected bubbles, which appear to be “sucked” into the aerator wake upon passing the aerator tip and, therefore, migrate towards to the centre of the mixing chamber – in fact, a small pocket of gas can be observed at the aerator tip, which demonstrates that the wake effect is sufficiently high in this region to resist the considerable action of buoyancy.

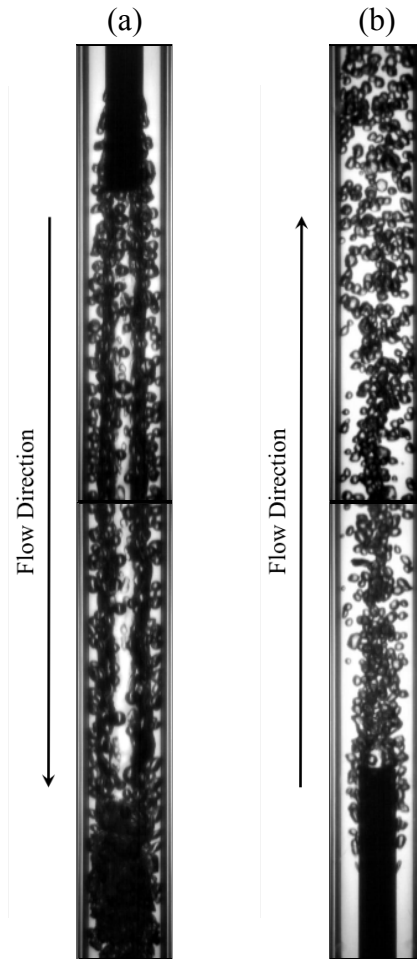


Figure 5.21 Example observations of the effect of orientation at comparable ALRs and fully open discharge nozzle setting (i.e. equivalent exit orifice diameter):

- a) Vertically downwards, 250 g/s, 0.13% ALR [benchmark];
- b) Vertically upwards, 252 g/s, 0.12% ALR.

The investigation was extended by analysing the gas injection regime maps for both orientations (Figure 5.22), within which the bubbling regions were limited at:

- High ALRs, by the transition to jetting regimes. It was expected that the direction of buoyancy for vertically upwards orientation would aid bubble detachment and, hence, the transition to jetting would occur at greater ALRs compared to vertically downwards. Whilst this was the case at low liquid flow rates, the trend was reversed at high liquid flow rates. The reason for this is unknown, but could be due to the significantly greater pressure variations within the mixing chamber when operating in a vertically upwards orientation upon discharge of heterogeneous flow regimes formed at high ALRs within the bubbling region – this is exaggerated when

operating in a vertically upwards orientation due to the additional hydrostatic head of liquid.

- Low liquid flow rates for the vertically downwards orientations, by the generation of evacuated chamber. However, for the vertically upwards case, the mixing chamber was passively bled upon start-up regardless of the liquid flow rate and hence evacuated chamber was prevented for all cases – this was due to buoyancy acting in a common direction to the liquid momentum to displace the ambient gas within the mixing chamber upon start-up. Hence, bubbling in a vertically upwards configuration was seen to extend into lower liquid flow rates than the vertically downwards case.
- High liquid flow rates, by the discharge limit of the exit nozzle. Increasing the ALR acts to further restrict the valve and hence the liquid flow rate continually decreases. The effect of orientation was not seen to have a significant effect on the discharge limit.

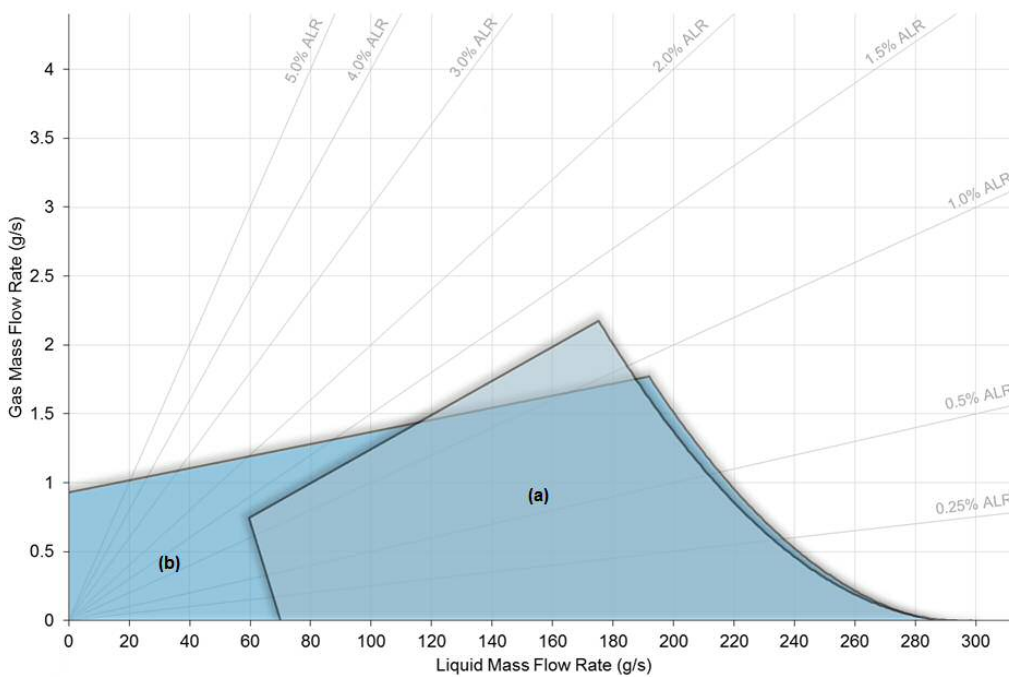


Figure 5.22 Effect of orientation on bubbling operating range:

a) vertically downwards (§5.2) [benchmark]; b) vertically upwards (§A5.5.2).

Consequently, the operating range corresponding to bubbling was seen to be increased for vertically upwards orientation, compared to vertically downwards (Figure 5.23).

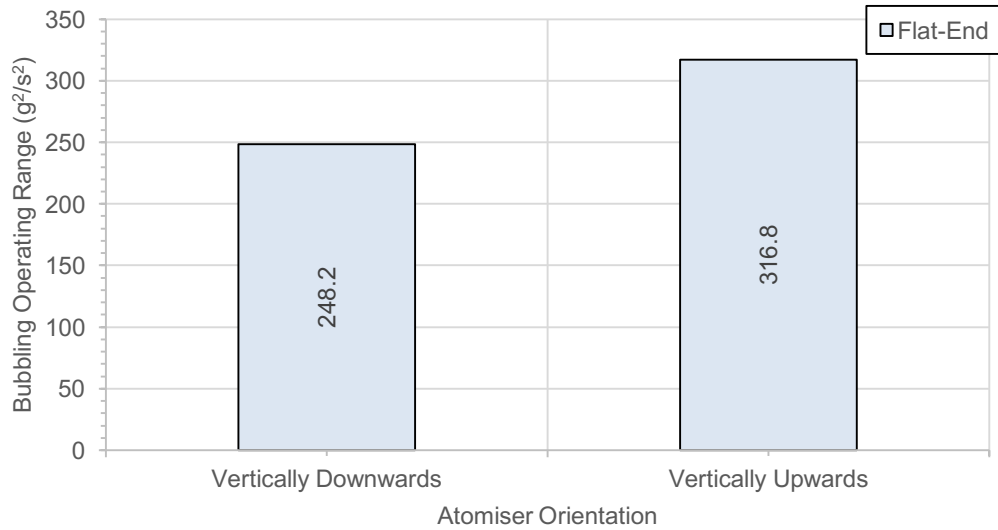


Figure 5.23 Effect of atomiser orientation on bubbling operating range.

A gas void was not formed in the aerator wake for any vertically upward flow condition, as the effect of buoyancy aids detachment from the aerator tip – this contrasts with the vertically downwards benchmark case, where buoyancy is an obstruction to gas void detachment. Consequently, injected bubbles were no longer displaced within the mixing chamber and hence a bubbly flow region was enabled (Figure 5.24). The bubbly flow region was restricted at high ALRs by slug flow generation, due to the injection of irregularly sized bubbles from the aerator and coalescence of bubbles within the mixing chamber. Consequently, not all observations of bubbling at the aerator generated a bubbly flow in the mixing chamber – in this case, every instance occurred at or under 0.25% ALR and coincided with single bubbling at the aerator. Bubbly flow was also restricted at the highest liquid flow rates due to the discharge limit of the exit nozzle. The bubbly flow operating region was measured to be 105.5 g²/s².

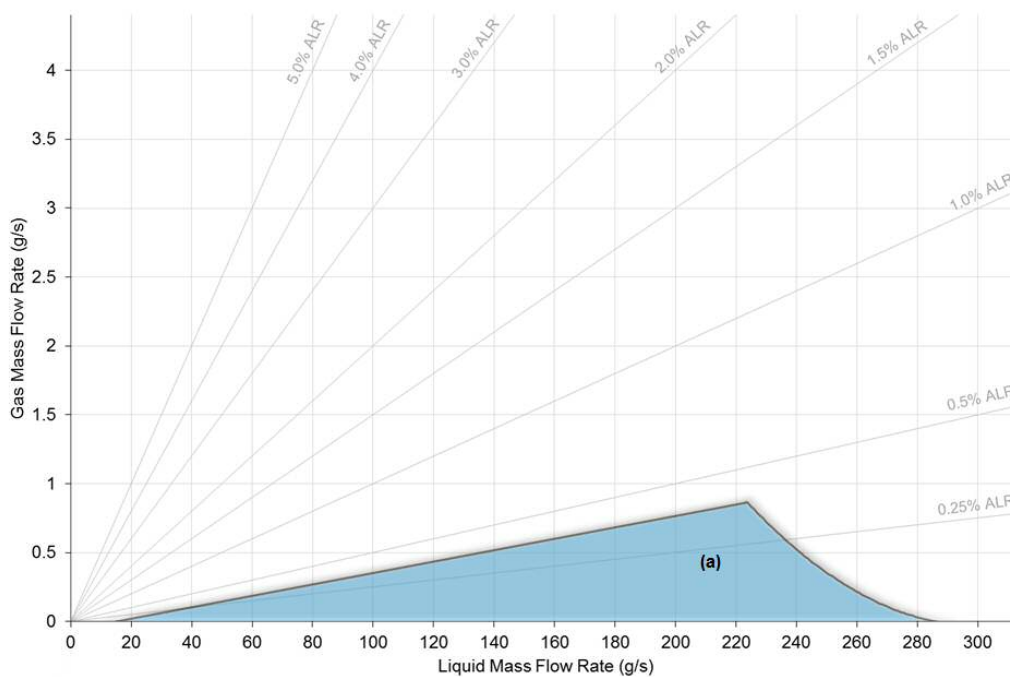


Figure 5.24 Effect of orientation on bubbly flow range:

a) vertically upwards (§A5.5.2)

5.8 Summary

In this chapter, an inside-out effervescent atomiser with a conventional flat-end aerator was investigated over various fluid flow rates and independent parameters, which enabled a series of gas injection and flow regimes maps to be generated – these are presented in Appendix 5. The investigated variables were seen to have a significant effect on the regime regions within the generated maps. Therefore, it is implied that generic flow maps may not accurately represent effervescent atomiser internal flow behaviour unless they were generated at comparable operating and design conditions – consequently, researchers should be cautious when relying upon generic flow maps to predict internal flows (e.g. in non-transparent atomisers).

Bubbling at the aerator was found to be encouraged by:

- Decreased ALR – aids bubble detachment by decreasing injected gas velocity and increasing liquid cross-flow velocity;
- Increased exit orifice diameter – at critically low liquid flow rates (i.e. small exit orifice diameters) for vertically downwards operation, an evacuated chamber regime was generated which prevented bubbling;

- Decreased aerator orifice diameter – the bubbling operating range increased from 7.7 g^2/s^2 to 248.2 g^2/s^2 , for 3 mm to 0.75 mm aerator orifices respectively;
- Decreased mixing chamber diameter – the bubbling operating range increased from 248.2 g^2/s^2 to 258.2 g^2/s^2 , for 20 mm and 14 mm mixing chamber diameters respectively;
- Increased operating pressure – the bubbling operating range increased from 24.4 g^2/s^2 to 248.2 g^2/s^2 , for 1 bar_g to 5 bar_g operating pressures respectively;

Despite bubbling having been achieved across a wide range of parameters, a bubbly flow was not observed for a vertically downwards orientation. This was due to the formation of a buoyant gas void in the aerator wake for all experiments at low ALR, which displaced bubbles injected at the aerator and prevented formation of bubbly flow regardless of the various independent parameters investigated. Consequently, a bubbly flow was only observed when operating in a vertically upwards orientation, due to removing the obstructive effect of buoyancy. As the study was conducted at comparable conditions to Konstantinov [16], it can be concluded that bubbly flow was not achieved in this preceding study and hence effervescent atomisation was not achieved – this phenomena could also have effected other non-transparent inside-out effervescent atomiser studies, for example Ochowiak et al. [99], Broniarz-Press et al. [105], Gadgil et al. [107], and Sutherland et al. [128].

CHAPTER 6. INTERNAL FLOW STUDIES OF STREAMLINED AERATORS TO REDUCE WAKE EFFECT

In the previous research chapter (§5), a gas void was observed to be formed in the wake of a conventional flat-end aerator for all vertically downwards investigations. This was caused by the buoyancy of the gas-phase overcoming the liquid shear within the aerator wake, due to the bluff body recirculation effect of the axial flow across the aerator body. The formation of a void in this region was observed to be particularly problematic for effervescent atomisation, as it was seen to displace any injected bubbles and, therefore, prevent a bubbly flow. The effects of increased liquid flow rate (up to 290 g/s), decreased mixing chamber diameter (from 14 mm diameter, corresponding to a maximum liquid Bakkers number of 1880 kg/m²s) or increased operating pressure (up to 5 bar_g) were unable to displace the gas void. The gas void was seen to be prevented by orientating the atomiser vertically upwards as, in this case, buoyancy aids void detachment.

An alternative solution to detach the void is to reduce the bluff body recirculation effect of the aerator body, for example with streamlined tips – this was reported to be an effective solution by Jobehdar [44], who studied the effect of an arbitrary conical end tip. This chapter aims to investigate the effect of applying various streamlined profiles to the aerator, to investigate their effect on gas void detachment.

N.B. In the interest of a concise discussion, only the findings of significance to effervescent atomisation are presented in the current body of work – the complete gas injection and flow maps for the current study are presented and described in detail within Appendix 6.

6.1 Bluff Body Recirculation of Streamlined Aerator Designs

The four streamlined aerator body designs were investigated for their ability to passively bleed the mixing chamber of ambient air upon start-up, in which the effervescent atomiser

was initially under atmospheric conditions (i.e. the mixing chamber evacuated of liquid and occupied with ambient air). Liquid was then suddenly supplied to the atomiser at the liquid discharge limit of 289 g/s (corresponding to liquid Bakers number 923 kg/m²), without any gas injection (i.e. 0% ALR), and the response in the near aerator region was studied. The results of this investigation for each streamlined aerator design are shown in Figure 6.1, which can be compared to a conventional flat-end aerator in Figure 5.3. These demonstrate that all of the investigated streamlined aerator designs succeeded in passively bleeding the mixing chamber of ambient air from start-up at the discharge limit – this is due to having sufficiently low bluff body recirculation, and the clearing ambient air has sufficiently high momentum, to prevent gas-phase from becoming entrapped within the aerator wake and forming a gas void. This contrasts to the conventional flat-end aerator, which features a gas void in the aerator wake upon identical start up conditions.

This investigation was extended for various liquid flow rates, ranging from 30-289 g/s (corresponding to liquid Bakers numbers 95.5-923 kg/m²), with the discharge valve setting controlled to maintain 5 bar_g operating pressure. Each test was repeated three times to determine repeatability. All streamlined aerator tips were consistently able to passively bleed the mixing chamber from start-up for liquid flow rates above 99 g/s (corresponding to a liquid Bakers number of 315 kg/m²s), whereas the conventional flat-end aerator was unable to prevent gas void formation under any of the tested conditions. An evacuated chamber regime was consistently observed for all designs below a liquid flow rate of 75 g/s (corresponding to a liquid Bakers number of 239 kg/m²s), which is thought to occur when the liquid shear around the aerator periphery is insufficient to overcome the buoyancy of the ambient air and displace it from above the aerator. Low repeatability was achieved between these limits, with results tending towards successful passive bleeding at high liquid flow rates and evacuated chamber at low flow rates – indicating that the process enabling passive bleeding are relatively chaotic. Therefore, fair comparison of the aerator body designs was not possible.

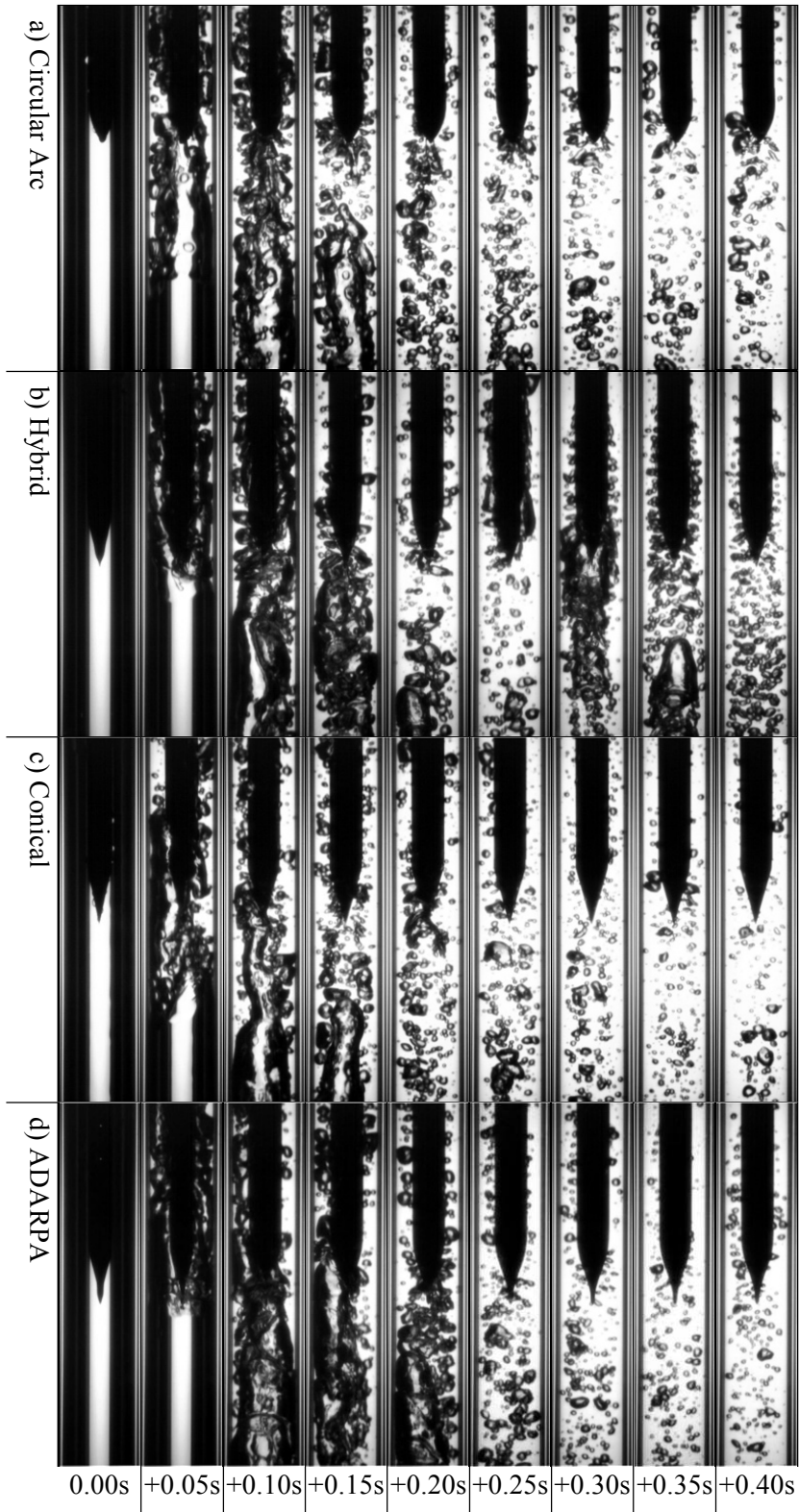


Figure 6.1 Ability of aerator tip to passively bleed mixing chamber of ambient gas:
 289 g/s, 0% ALR, 5 bar_g.

For the cases in which passive bleeding was achieved, the clearing ambient air has momentum as it passes the aerator tip, which aids the prevention of gas void formation in the aerator wake region. Therefore, the ability of the aerator body designs to remove an established gas void was investigated. Unlike the previous test, the discharge valve was kept fully open and, therefore, the operating pressure was not controlled. A gas void was successfully and repeatedly established in the wake region of each aerator by overcoming the evacuated chamber regime at an arbitrarily high liquid flow rate. Upon achieving a liquid continuum about the aerator periphery, the liquid flow rate was reduced to 50 g/s such that the gas-phase found equilibrium at the aerator tip to form a gas void. The liquid flow rate was gradually increased by approximately 1 g/s increments in 10 second intervals until either the gas void was detached from the aerator tip or the maximum 5 bar_g operating pressure was reached (corresponding to a maximum liquid mass flow rate of 289 g/s and liquid Bakkers number of 923 kg/m²). An example image sequence of gas void detachment from an aerator wake is shown in Figure 6.2.

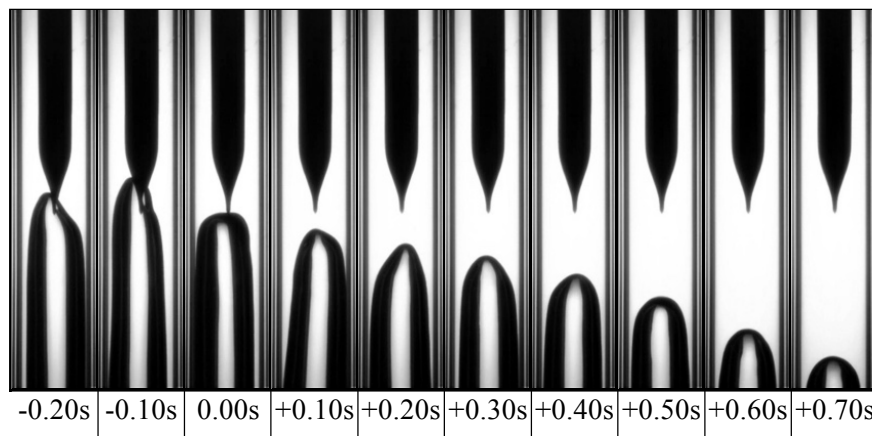
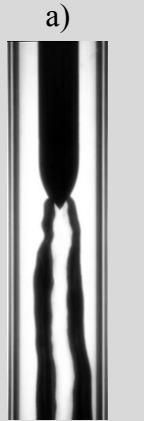
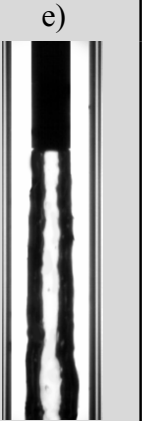


Figure 6.2 Time sequence showing the displacement of an established gas void from the wake of an of ADARPA aerator: 76 g/s, 0% ALR, 0.3 bar_g.

The results of this study, shown in Table 6.1, proved that the ADARPA aerator tip required the lowest liquid flow rate of all the investigated aerator body designs to detach an established gas void from the aerator wake region and is, therefore, considered to have the lowest wake effect for use as an aerator body design in inside-out effervescent atomiser. Both the flat-end and circular arc designs were shown to prevent gas void detachment across all conditions tested, including at the highest investigated liquid flow rate – however, the circular arc design was previously shown to passively bleed the atomiser at flow rates far below this. This demonstrates that, in addition to the aerator wake effect, the momentum of the clearing ambient air past the aerator tip has a key role in preventing gas void formation

upon start-up. Therefore, inside-out effervescent atomisers should be designed to allow suitably high liquid Bakers numbers around the periphery of the aerator to ensure passive bleeding as, if not achieved, the flow rate required to detach an established gas void can be significantly greater – across the investigations, successful passive bleeding was shown to correlate with Equation 4.1.

Table 6.1 Displacement conditions of a gas void from wake of streamlined aerators

	 a)	 b)	 c)	 d)	 e)
	Circular Arc	Hybrid	Conical	ADARPA	Flat-end
Gas void:	Not cleared	Cleared	Cleared	Cleared	Not cleared
Conditions:	$G_1\Psi = 923 \text{ kg/m}^2$ $m_1 = 289 \text{ g/s}$ $P = 5.0 \text{ barg}$	$G_1\Psi = 277 \text{ kg/m}^2$ $m_1 = 87 \text{ g/s}$ $P = 0.4 \text{ barg}$	$G_1\Psi = 271 \text{ kg/m}^2$ $m_1 = 85 \text{ g/s}$ $P = 0.4 \text{ barg}$	$G_1\Psi = 242 \text{ kg/m}^2$ $m_1 = 76 \text{ g/s}$ $P = 0.3 \text{ barg}$	$G_1\Psi = 923 \text{ kg/m}^2$ $m_1 = 289 \text{ g/s}$ $P = 5.0 \text{ barg}$

6.2 Effect of Aerator Body Design

The investigation of streamlined aerators was furthered by examining each design with the addition of gas-injection – this better simulates their use within an effervescent atomiser. Figure 6.3 shows the effect of varying the aerator body designs as an independent parameter at comparable flow conditions – specifically, ~0.12% ALR and fully open discharge nozzle setting, which corresponds to ~251 g/s. For every previous investigation using a flat-end aerator in a vertically downwards orientation, the presence of a gas void in the aerator wake was observed to displace bubbles injected at the aerator into the liquid periphery and, thus, prevent a bubbly flow – this same phenomenon was observed for the flat-end case in the current investigation (Figure 6.3e). This contrasts to the performance of the streamlined aerator tips (Figure 6.3a-d), which can be seen to prevent formation of this void – consequently, all of the streamlined aerators can be seen to enable a bubbly flow to be generated in the mixing chamber for the investigated condition.

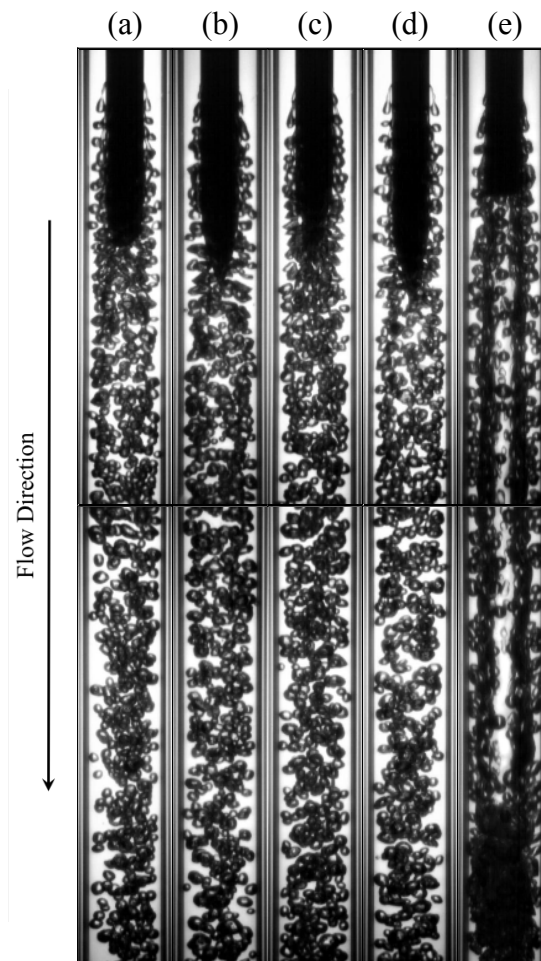


Figure 6.3 Comparable observations with varying aerator body design:
 a) Circular arc, 252 g/s, 0.12% ALR; b) Hybrid, 252 g/s, 0.12% ALR;
 c) Conical, 251 g/s, 0.13% ALR; d) ADARPA, 251 g/s, 0.12% ALR;
 e) Flat-end, 250 g/s, 0.13% ALR [benchmark].

The investigation was extended by analysing the gas injection regime maps for each atomiser configuration in which aerator body design was investigated as an independent parameter. To promote a concise and focussed discussion, only the sections of these maps most relevant to effervescent atomisation are presented in the current report – the complete maps are presented for the circular arc, hybrid and conical aerator body designs in Appendix 6, whereas the maps for the flat-end and ADARPA designs are presented in §5.2 and §7.2 respectively. As previously discussed, the purpose of an effervescent atomiser aerator is to inject the gas-phase into the liquid-phase to form uniformly sized bubbles and, hence, generate a homogenous bubbly flow. Consequently, bubbling at the aerator is considered the most relevant gas injection regimes for effervescent atomisation – these regions are

compared for the aerator body designs in Figure 6.4. For all of these cases, the bubbling region was restricted at:

- High ALRs, by the transition to jetting regimes. Slight variations were observed between aerator body designs, although these were relatively minor and corresponded to only a couple of differing identifications – these could be caused by identification error or could be anomalous results. Regardless, the effect of aerator body design has a relatively marginal effect on transition to jetting.
- Low liquid flow rates, by the generation of evacuated chamber. Whilst this limit was observed to marginally vary between aerator body designs, the trend was not predictable – it is thought that the differences are due to the chaotic mechanisms affecting passive bleeding of the atomiser upon start-up and not the effect of aerator body design.
- High liquid flow rates, by the flow limit of the discharge valve. Increasing the ALR acts to further restrict the valve and hence the liquid flow rate continually decreases. The effect of aerator body design was not seen to have a significant effect on the discharge limit.

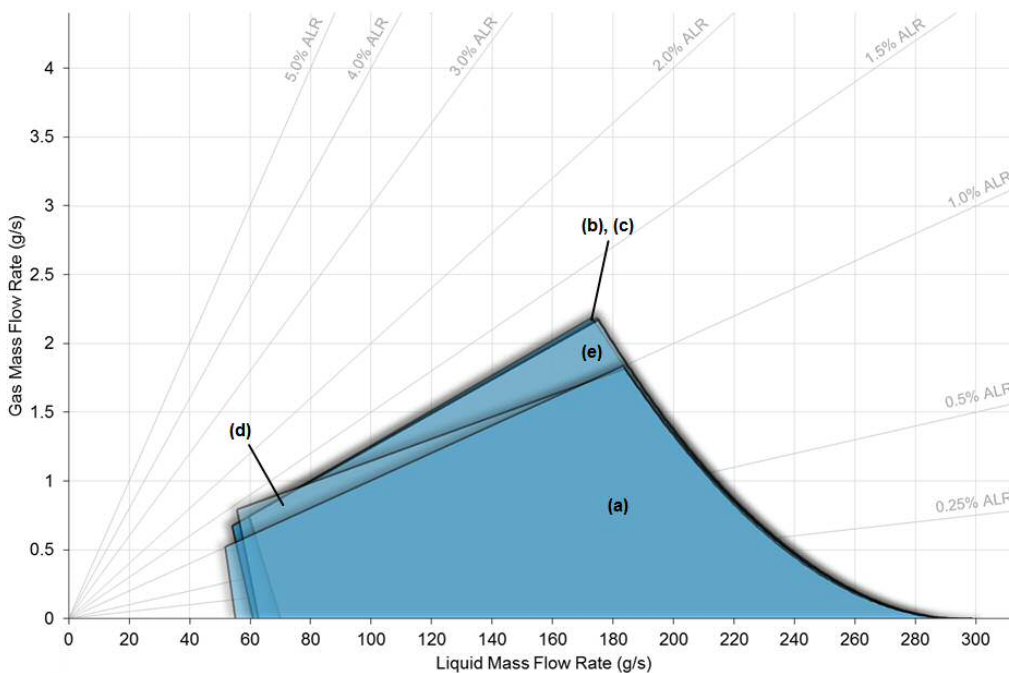


Figure 6.4 Effect of aerator body design on bubbling operating range:

a) circular arc; b) hybrid; c) conical; d) ADARPA; e) flat-end.

Consequently, it can be concluded that the bubbling process at the aerator is not significantly affected by the aerator body design (Figure 6.5). In all of these cases, transition from bubbling to jetting occurs with excessive ALR and to evacuated chamber at insufficient liquid flow rates.

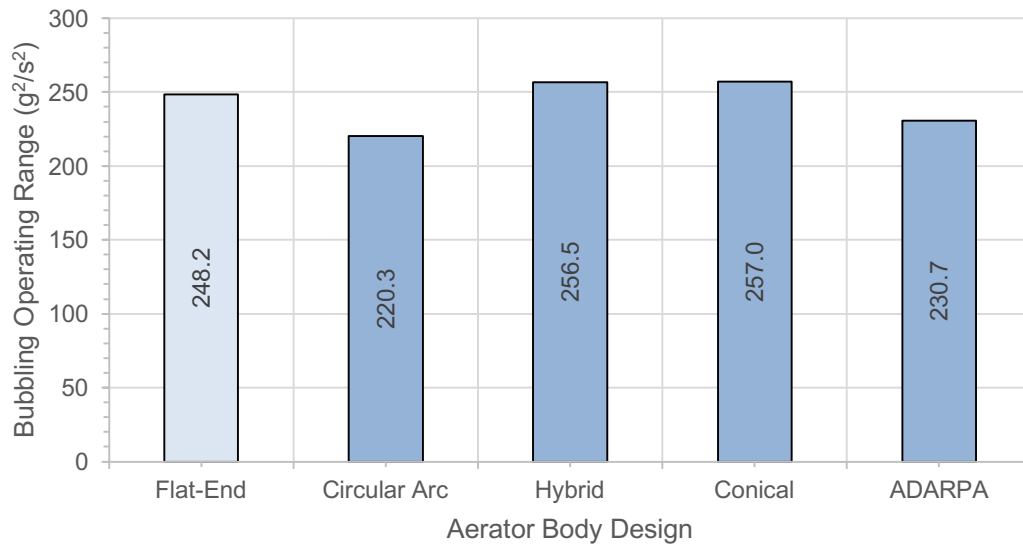


Figure 6.5 Effect of aerator body design on bubbling operating range.

For all the previous vertically downwards studies utilising a flat-end aerator, the presence of a gas void in the aerator wake prevented formation of bubbly flow – therefore, irrespective of the operating range corresponding to bubbling at the aerator, none of the atomiser configurations were considered suitable for effervescent atomisation. However, it has already been shown that streamlined aerator body designs can enable bubbly flow in vertically downwards orientation, as a result of enabling passive bleeding of the atomiser upon start-up and preventing subsequent coalescence of injected gas-phase in the aerator wake – this is due to a reduction in the bluff body recirculation effects. Figure 6.6 compares the operating ranges over which bubbly flow is achieved for these designs – **N.B.** as the flat-end aerator design does not achieve a bubbly flow under any condition, it does not feature in this figure. For all of these cases, the bubbly flow region was restricted at:

- High ALRs, due to formation of slug flow. Gas slugs were observed to be directly injected as a result of pulse bubbling at the aerator, or formed due to coalescence of bubbles within the mixing chamber – consequently, not all bubbling cases were observed to form a bubbly flow. The ADARPA aerator was determined to have a marginally larger bubbly flow region, due to a greater number of transitional bubbly-slug observations at high ALRs.

- Low liquid flow rates, due to the high relative effects of buoyancy compared to viscous forces. Under these conditions, the gas-phase has greater residence time in the mixing chamber, which increases the gas-phase coalescence. Consequently, injected bubbles and jets were observed to coalesce within the mixing chamber to form disturbed annular and annular flows.
- High liquid flow rates, by the flow limit of the discharge valve. As discussed, the effect of aerator body design was not seen to have a significant effect on the discharge limit.

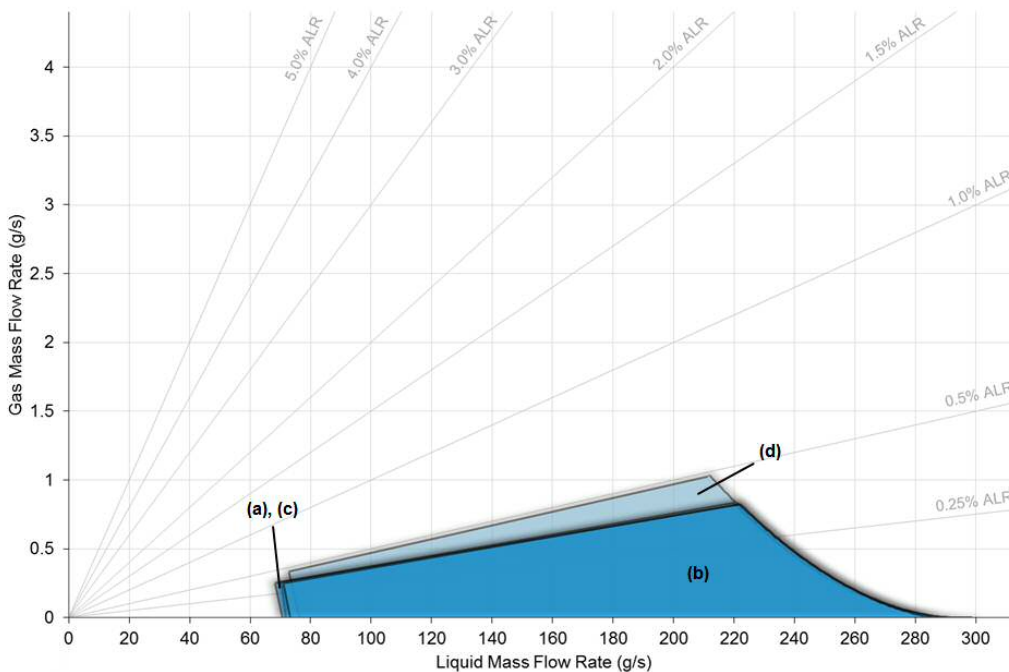


Figure 6.6 Effect of aerator body design on bubbly flow operating range:
 a) circular arc; b) hybrid; c) conical; d) ADARPA.

Consequently, the streamlined aerator body design was observed to have an insignificant effect on the bubbly flow operating range (Figure 6.7) – with bubbly flow consistently observed at low ALRs for all streamlined aerators, with transition to slug flow, churn flow and finally annular flow with increasing ALR. All streamlined designs represent a significant improvement over a conventional flat-end aerator design for effervescent atomisation by enabling a bubbly flow to be produced.

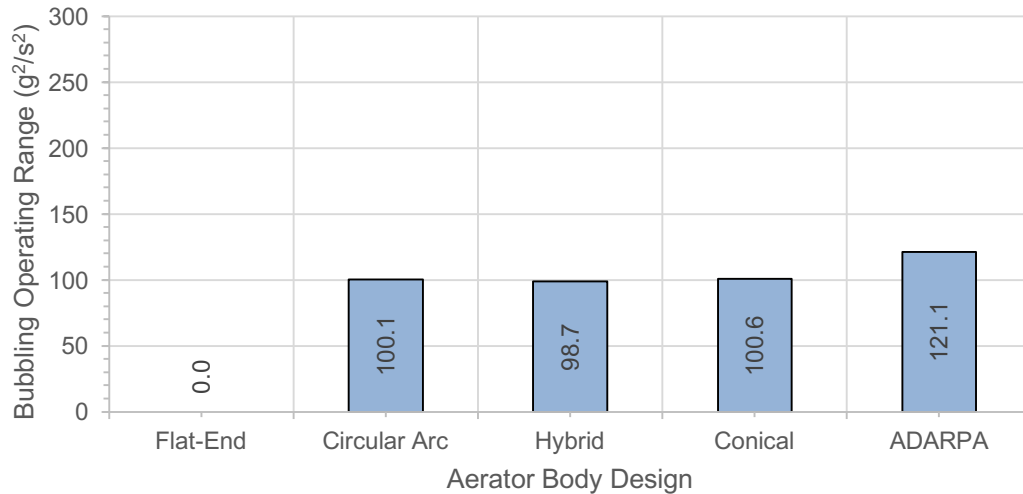


Figure 6.7 Effect of aerator body design on bubbly flow operating range.

6.3 Summary

It has been established that an optimal effervescent atomiser configuration would feature bubbly flow across a wide range of operating conditions and at maximum ALR – conditions which have been proven previously in the current research and are reported within the literature to encourage formation of a stable and fine spray. Consequently, all of the investigated streamlined aerator body designs are considered suitable for inside-out effervescent atomisation, as they all succeeded in preventing a gas void and therefore enabled generation of bubbly flow across a wide range of conditions. This compares to a conventional flat-end aerator, which was unable to generate a bubbly flow across equivalent conditions. The ADARPA aerator tip is considered the optimal aerator tip design of the investigated selection, due to having been determined to have the weakest wake effect.

CHAPTER 7. INTERNAL FLOW STUDIES OF ADARPA AERATORS TO OPTIMISE BUBBLY FLOW OPERATION

In the initial study of the present work (§5), the unsuitability of the conventional flat-end aerator body design for inside-out effervescent atomiser was demonstrated when operating in a vertically downwards orientation. This was due to the formation of a buoyant gas void within the aerator wake, which was seen to displace the injected bubbles and prevent a bubbly flow for all experiments regardless of atomiser design. However, in a further study (§6), bubbly flow was proven to be enabled in a vertically downwards orientation by streamlining the aerator body. Whilst all of the streamlined aerator tips investigated in this work were observed to successfully prevent formation of a gas void and, therefore, enable effervescent atomisation, the ADARPA profile was proven to be optimal due to exhibiting the weakest drag effect. Consequently, in the current chapter, an ADARPA profile was adopted as the aerator body design and the effect of various independent parameters were tested.

N.B. In the interest of a concise discussion, only the findings of significance to effervescent atomisation are presented in the current body of work – the complete gas injection and flow maps for the current study are presented and described in detail within Appendix 7.

7.1 Bluff Body Recirculation of Streamlined ADARPA Aerators

It was previously identified that the utilisation of an ADARPA streamlined profile for the aerator body design prevented formation of a gas void in the aerator wake upon start up and across all operating flows for the default atomiser set up. This analysis was extended in the current study to include investigation of an ADARPA aerator design across various independent parameters.

Example comparisons between the conventional flat-end and ADARPA aerator body designs are provided for equivalent operating conditions in Figure 7.1. The effects of the reduced bluff body recirculation effect for the streamlined case is evident when operating in a vertically downwards orientation, where a gas void is no longer formed in the aerator wake – in fact, a gas void failed to establish in the aerator wake for any condition throughout the current investigation.

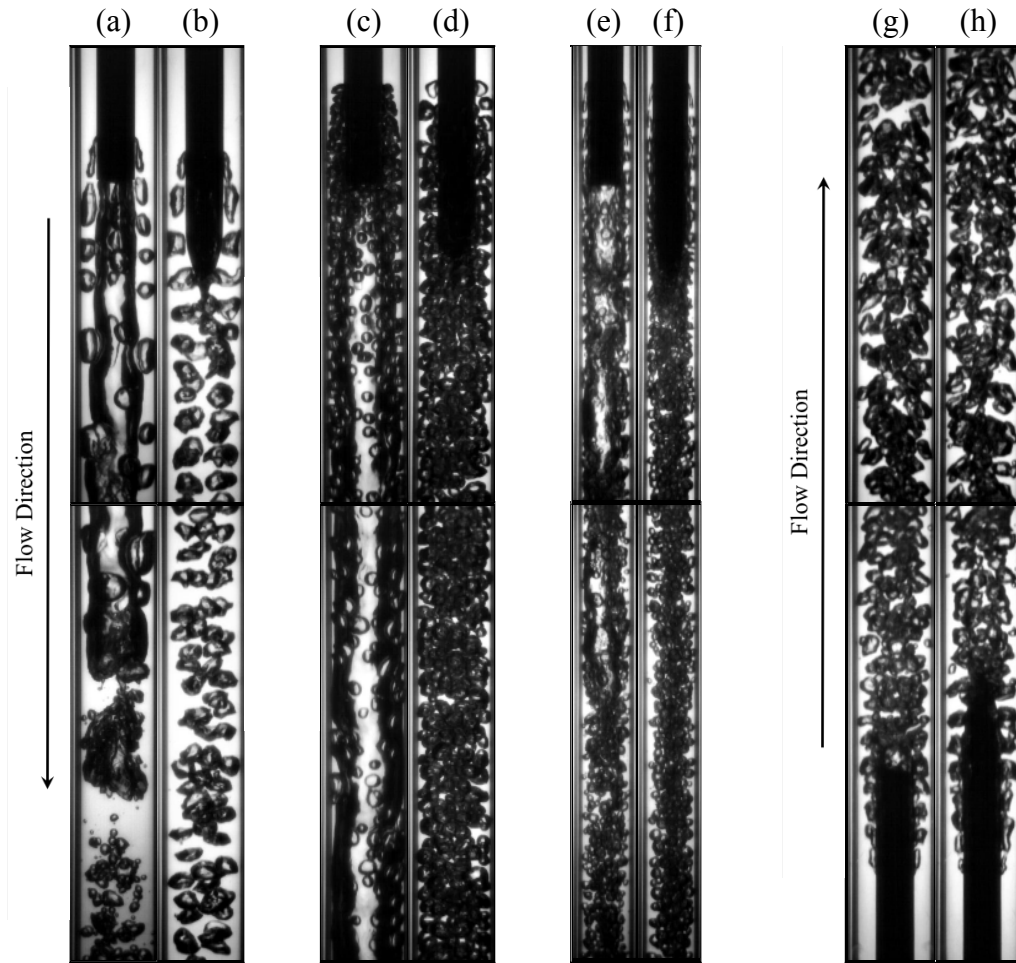


Figure 7.1 Comparison of flat-end and ADARPA aerator body designs for equivalent operating conditions:

- a) Flat-end: 254 g/s, 0.13% ALR (§A5.1.2); b) ADARPA: 252 g/s, 0.12% ALR (§A7.1.2);
- c) Flat-end: 81 g/s, 0.26% ALR (§5.2); d) ADARPA: 82 g/s, 0.25% ALR (§7.2);
- e) Flat-end: 136 g/s, 0.25% ALR (§A5.3.1); f) ADARPA: 136 g/s, 0.26% ALR (§A7.4.1);
- g) Flat-end: 234 g/s, 0.25% ALR (§A5.5.1); h) ADARPA: 235 g/s, 0.25% ALR (§A7.6.2).

Whilst the ADARPA aerator tip was observed to prevent gas void formation due to bluff body recirculation effects, a gas void was occasionally observed to be formed under

conditions of high relative buoyancy. For these cases, typically at liquid flow rates just in excess of evacuated chamber generations, a buoyant gas void was observed to establish within the mixing chamber and find equilibrium just below the aerator orifices (Figure 7.2) – this is thought to occur when the combined action of liquid shear around the aerator periphery and the drag exerted by the emerging gas phase is sufficient to balance the buoyancy of the gas void. Therefore, some instance of bubbling at the aerator were observed to form an annular flow. This was often a transient process, where the gas void was periodically cleared and reformed.

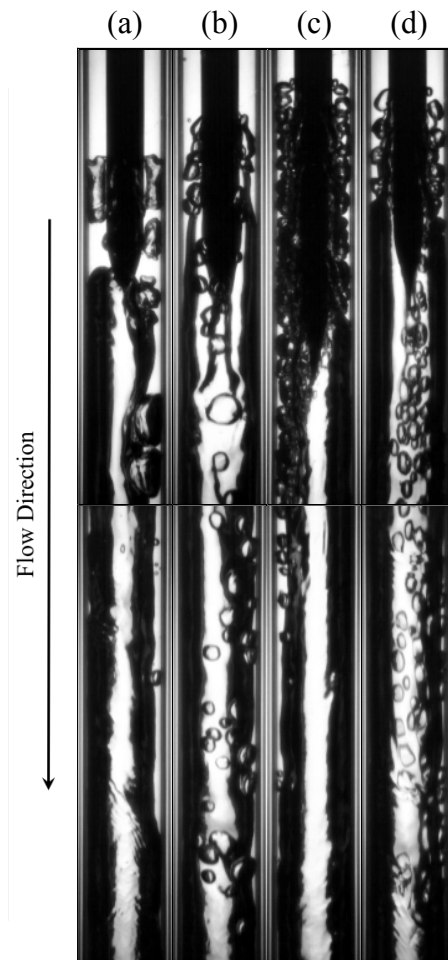


Figure 7.2 Example observations of buoyant gas void with ADARPA aerator tip:

- a) 62 g/s, 0.25% ALR (§A7.1.2); b) 61 g/s, 0.26% ALR (§A7.1.3);
- c) 56 g/s, 0.50% ALR (§A7.2.4); d) 71 g/s, 0.24% ALR. (§A7.5.2).

Whilst the bluff body recirculation effect of the ADARPA profile was proven to be significantly reduced compared to the flat-end design, aerator wake effects were still observed to prevent bubbling at the aerator from forming a bubbly flow under extremely isolated conditions in the current investigation. One of these instances occurred with reduced

operating pressure (3 bar_g) at low liquid flow rates (just in excess of evacuated chamber), where large gas bubbles were observed to nucleate within the aerator wake and periodically detach – thus, forming a bubbly-slug flow (Figure 7.3a). Another set of conditions, affecting only two conditions, occurred with reduced mixing chamber diameter (14 mm) and high liquid flow rates, in which bubbles appear to be encouraged to collide in the aerator wake region and hence coalesce into gas slugs (Figure 7.3b).

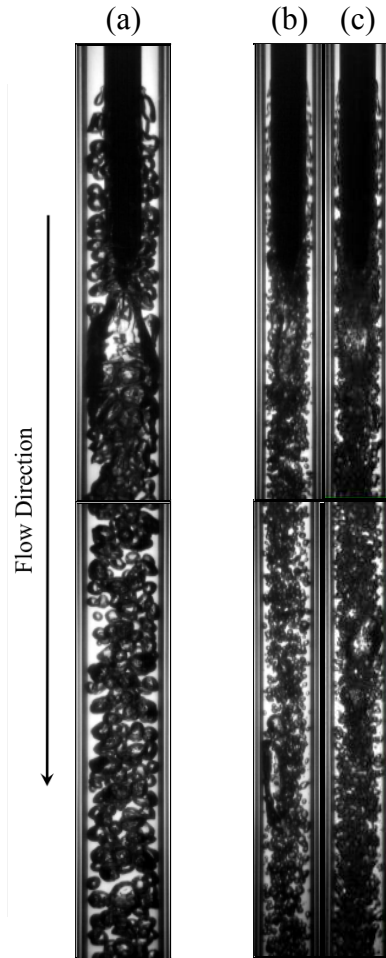


Figure 7.3 Observations of ADARPA aerator bluff body recirculation flow disruption:

- a) 95 g/s, 0.13% ALR (§A7.5.2); b) 253 g/s, 0.12% ALR (§A7.4.1);
c) 235 g/s, 0.26% ALR (§A7.4.1).

7.2 Effect of Fluid Flow Rates, including Air-to-Liquid Ratio

As discussed in the previous chapters, the effect of fluid flow rates (i.e. ALR and exit orifice diameter) were seen to have a significant effect on the internal flow performance of an effervescent atomiser, which in turn was proven to have a significant effect on the stability

of the spray. In the present study, the effervescent atomiser was configured in its benchmark configuration for the ADARPA aerator design (i.e. the default cases for each independent variable were used; Table 3.6) – hence, the results are comparable with all other ADARPA aerator investigations presented within this thesis.

Figure 7.4 shows the effect of varying ALR for a common effervescent atomiser, equipped with an ADARPA streamlined aerator tip and with a fully open discharge nozzle setting – this configuration is directly comparable with the results presented in Figure 5.5 for the flat-end aerator. The emerging gas-phase has low stability at the lowest ALR, due to having a low injected gas velocity, and consequently small bubbles are observed to be formed almost immediately upon exposure to the liquid cross-flow (i.e. single bubbling). However, unlike the conventional flat-end aerator body, the formation of a gas void in the aerator wake is avoided and, hence, the bubbles are able to flow unimpeded into the mixing chamber to form a bubbly flow. As the injected gas velocity increases, so does the emerging gas-phase stability – in addition, the liquid cross-flow decreases as the gas increasingly blocks the exit orifice, which in turn reduces the detachment mechanisms acting on the emerging bubble. Consequently, increasing the ALR was observed to increase the length of gas neck from which bubbles are formed (i.e. pulse bubbling) and hence visibly increase their size – by 0.50% ALR gas entities are large enough to form a bubbly-slug flow. Further raising the ALR transitions the gas injection to jetting, which features increasingly chaotic flow patterns within the mixing chamber – at the highest gas flow rates the jet was observed to have sufficient momentum to emerge perpendicular to the liquid flow and contact the mixing chamber wall, generating a churn flow in the mixing chamber.

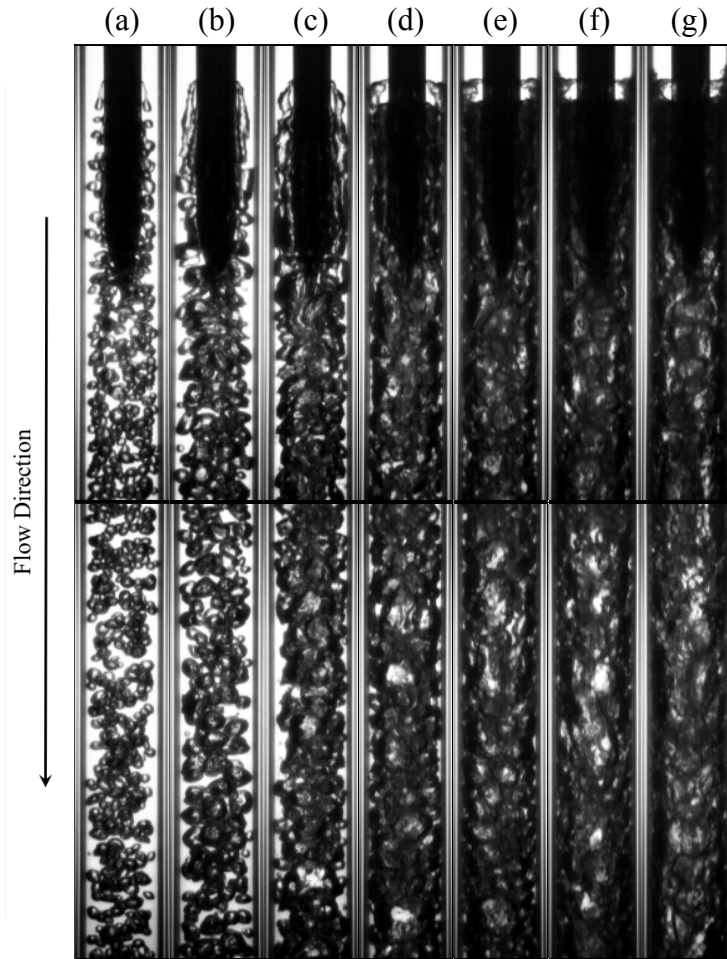


Figure 7.4 Comparable observations with varying ALR:

- a) 251 g/s, 0.12% ALR; b) 234 g/s, 0.25% ALR; c) 213 g/s, 0.50% ALR;
 d) 184 g/s, 1.00% ALR; e) 165 g/s, 1.50% ALR; f) 151 g/s, 1.99% ALR;
 g) 143 g/s, 2.38% ALR.

Figure 7.5 shows the effect of varying the discharge nozzle setting (i.e. exit orifice diameter) for a common ALR and atomiser configuration, equipped with an ADARPA streamlined aerator tip – this is directly comparable to the equivalent flat-end aerator case shown in Figure 5.6. As previously discussed, decreasing the exit orifice diameter reduces the liquid cross-flow past the aerator (Equation 2.8), thus lessening the relative detachment forces acting on the emerging gas-phase – however, maintaining a constant ALR proportionally reduces the injected gas velocity and, hence, a similar gas injection process was observed. Consequently, the relative effect of buoyancy is increased and hence at a critically low liquid flow rate, in this case 61 g/s, the peripheral liquid flow is insufficient to displace the ambient gas from the mixing chamber upon start-up and, hence, an evacuated chamber regime is

established in the mixing chamber. This compares well with the conventional flat-end aerator observations.

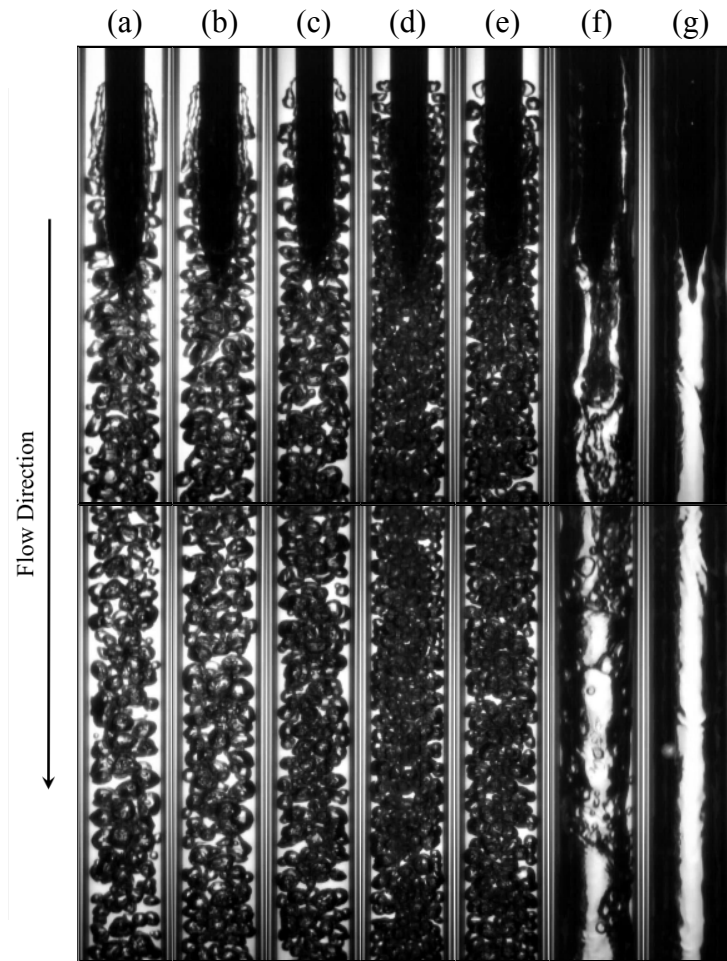


Figure 7.5 Comparable observations with varying discharge nozzle settings:
 a) 234 g/s, 0.25% ALR; b) 185 g/s, 0.25% ALR; c) 137 g/s, 0.24% ALR;
 d) 92 g/s, 0.25% ALR; e) 82 g/s, 0.25% ALR; f) 61 g/s, 0.24% ALR;
 g) 26 g/s, 0.28% ALR.

These analyses were extended across various ALRs and discharge nozzle settings. Figure 7.6 is the resulting gas injection regime map for the benchmark atomiser configuration, which shows the effect of varying the fluid flow rates on the gas injection processes at the aerator. Analysis of this map enabled identification of five discrete gas injection regimes, which were categorised into three gas injection regions.

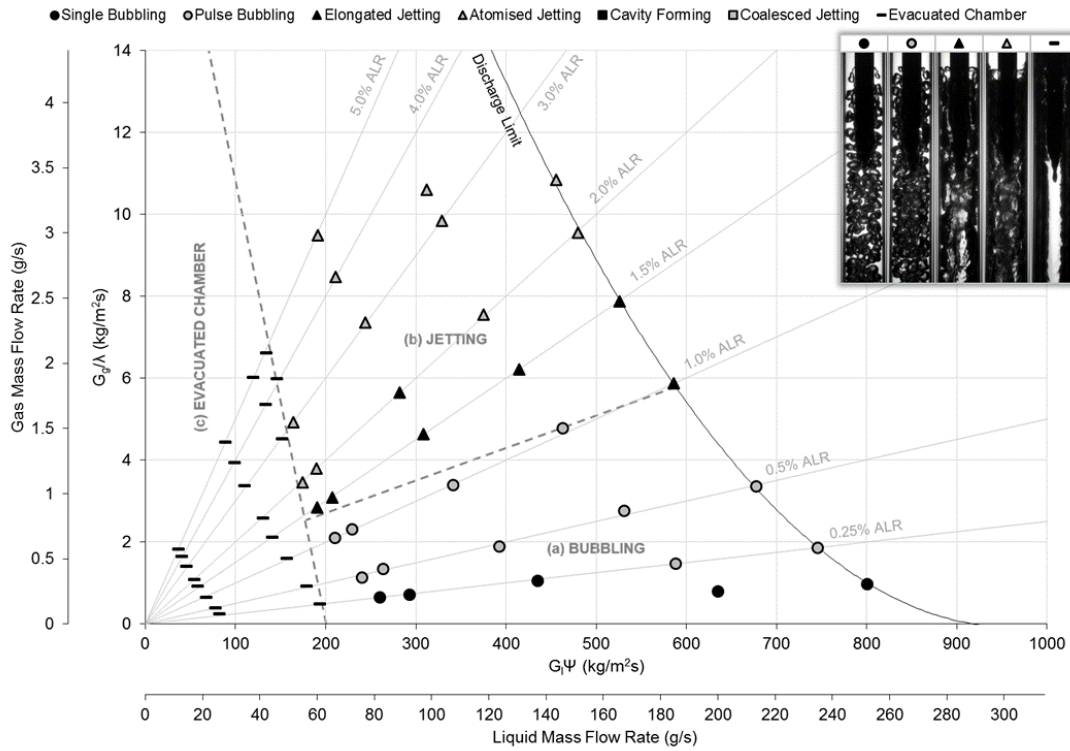


Figure 7.6 Gas injection regime map for the benchmark configuration (aerator A5 with ADARPA body design, 20 mm mixing chamber diameter, 5 bar_g operating pressure, vertically downwards orientation).

As previously discussed, the effect of aerator body design does not have a significant effect on the gas injection behaviour at the aerator and, consequently, the gas injection regime map for the current ADARPA test is very similar to the comparable flat-end aerator configuration (Figure 5.7).

A region of evacuated chamber was identified at relatively low liquid flow rates (Figure 7.6c) where phase separation occurs prior to fluid injection. Whilst operating in this region, the effect of ALR did not have a significant effect on the internal flow and, consequently, evacuated chamber was consistently observed regardless of the gas flow rate. Formation of an evacuated chamber regime in the case appeared to be marginally suppressed with high gas flow rates. It was observed to be formed in a similar region to the previous investigations.

The ALR was observed to have a considerably more pronounced effect at liquid flow rates exceeding evacuated chamber regime. At low ALRs, a large region of bubbling (Figure 7.6a) was identified in which individual bubbles were observed to be formed at, or near to, the aerator across a range of operating conditions – instances of single bubbling were observed at the lowest ALRs (typically at or below 0.25% ALR) and pulse bubbling up to 1.0% ALR.

Further increasing the ALR instigates transition of the gas injection process to jetting (Figure 7.6b), which featured a small number of elongated jetting observations with atomised jetting at the highest ALRs.

In order to identify the effects of fluid flow rates on the flow regimes and establish trends between the gas injection behaviour and the formation of internal flow regimes, the same mapping process was applied to the mixing chamber observations. The resulting flow regime map for the benchmark configuration, shown in Figure 7.7, identified seven discrete flow regimes across the various fluid flow rates which were grouped into six regions.

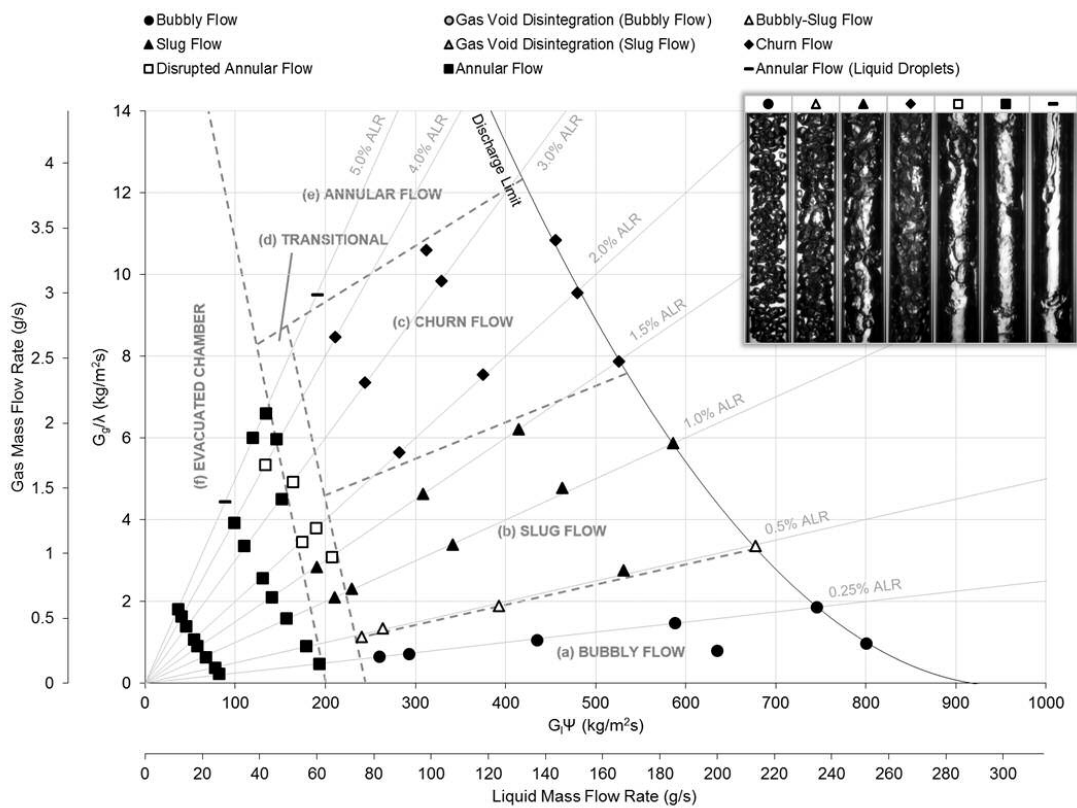


Figure 7.7 Flow regime map for the benchmark configuration (aerator A5 with ADARPA body design, 20 mm mixing chamber diameter, 5 bar_g operating pressure, vertically downwards orientation).

Unlike all vertically downwards investigations using a conventional flat-end aerator, including the equivalent set up shown in Figure 5.8, a bubbly flow region (Figure 7.7a) was enabled when the aerator body had a streamlined ADARPA profile – this was observed to occur at low ALRs and at comparable operating conditions to those which formed a gas void in the comparable flat-end case. The majority of bubbly flow cases coincided with single bubbling at the aerator, although some pulse bubbling cases at low ALR was also observed

to form a bubbly flow. There were a number of bubbly-slug cases identified upon transition from bubbly flow to slug flow, due to either the injection of bubbles of varying sizes from the aerator or coalescence of bubbles in the mixing chamber.

The internal flow performance in all other parts of the flow regime map were observed to be comparable with the flat-end case. Regions of intermittent flow regimes were observed, in which bubbly flow transitions to slug flow (Figure 7.7b) and churn flow (Figure 7.7c) with increasing ALR – this is due to the injected having increasing stability, which resists break-up into uniformly sized bubbles. A single observation of annular flow was identified at the highest ALR (Figure 7.7e) – in this isolated case, liquid droplets were identified to run off the aerator and fall within the gas core to form an annular flow (liquid droplets) regime.

A thin annular flow was identified for all conditions corresponding to the evacuated chamber gas injection regime (Figure 7.7f) at the lowest liquid flow rates. A transitional region (Figure 7.7d) was observed at liquid flow rates just in excess of the evacuated chamber regime, which featured a heavy proportion of disturbed annular flow cases – this was caused by incomplete action of either coalescence or breakup due to high relative buoyancy.

7.3 Effect of Aerator Orifice Diameter

In a comparable study to the previously investigated flat-end aerator study (§5.3), the effect of aerator orifice diameter on effervescent atomiser internal flow was investigated between 0.75-3.0 mm for a common aeration area of 7.07 mm² and with a streamlined ADARPA aerator body design (i.e. aerators A2A-A5A). As previously discussed, the injected bubble size is known to be proportional to the aerator orifice diameter (Equation 2.2) and, therefore, a reduction in aerator orifice diameter was expected to reduce the bubble size for a given ALR and, hence, increase flow homogeneity.

Figure 7.8 shows the effect of varying the aerator orifice diameter at 0.12% ALR and with a fully open discharge nozzle setting – this configuration is directly comparable with the results presented in Figure 5.9 for a conventional flat-end aerator. The key difference compared to the flat-end aerator is the prevention of a gas void in the aerator wake for all investigated cases and, therefore, all gas entities produced at the aerator are unimpeded into the mixing chamber. As with the flat-end aerator, reducing the aerator orifice diameter is observed to reduce to stability of the emerging gas-phase and, therefore, promote the detachment of bubbles. For the largest aerator orifice diameter investigated (Figure 7.8a), the emerging gas-phase is relatively stable and, therefore, a gas jet is formed, which irregularly

detaches from the orifice to form a very large gas slugs. This compares to the reduced aerator diameters (Figure 7.8b-d), in which the gas-phase was observed to break-up into bubbles upon exposure to the liquid cross-flow and form a bubbly flow in the mixing chamber. Due to the increasingly premature detachment of the gas-phase, the bubble size is visibly observed to reduce with decreasing aerator orifice diameter.

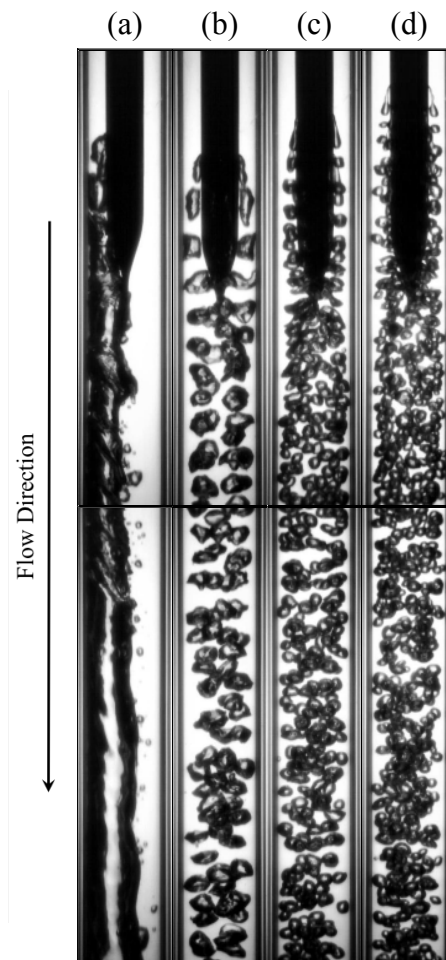


Figure 7.8 Comparable observations with varying aerator orifice diameter:

- a) Aerator A2A – 1 x 3.0 mm, 253 g/s, 0.12% ALR;
- b) Aerator A3A – 4 x 2.0 mm, 252 g/s, 0.12% ALR;
- c) Aerator A4A – 9 x 1.0 mm, 252 g/s, 0.12% ALR;
- d) Aerator A5A – 16 x 0.75 mm, 251 g/s, 0.12% ALR [benchmark].

The investigation was extended by analysing the gas injection regime maps for each atomiser configuration in which aerator orifice diameter was investigated as an independent parameter. As previously discussed, the purpose of an effervescent atomiser aerator is to inject the gas-phase into the liquid-phase to form uniformly sized bubbles and, hence,

generate a homogenous bubbly flow. Consequently, bubbling at the aerator is considered the most relevant gas injection regimes for effervescent atomisation – these regions are compared for the aerator orifice diameter studies in Figure 7.9. For all of these cases, the bubbling region was restricted at:

- High ALRs, by the transition to jetting regimes. Decreasing the aerator orifice diameter increases the ALR at which bubbling transitions to jetting, as a result of a less stable emerging gas-phase – this is thought to be caused by an increased emerging gas-liquid interface area over which the detachment mechanisms act.
- Low liquid flow rates, by the generation of evacuated chamber. Whilst this limit was observed to marginally vary between aerator orifice diameters, the trend was not predictable – it is thought that the differences are due to the chaotic mechanisms affecting passive bleeding of the atomiser upon start-up and not the effect of aerator orifice diameter.
- High liquid flow rates, by the flow limit of the discharge valve. Increasing the ALR acts to further restrict the valve and, hence, the liquid flow rate continually decreases. The effect of aerator orifice diameter was not seen to have a significant effect on the discharge limit.

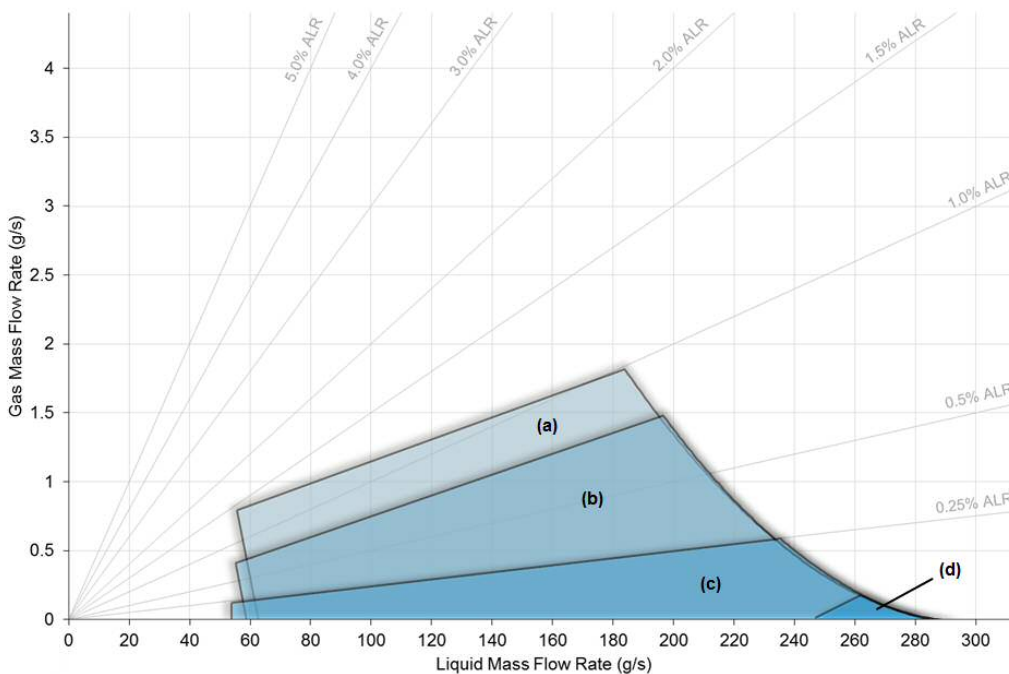


Figure 7.9 Effect of aerator orifice diameter on bubbling operating range:

- a) aerator A5, 16 x 0.75 mm (§7.2) [benchmark]; b) aerator A4, 9 x 1.0 mm (§A7.1.3);
 c) aerator A3, 4 x 2.0 mm (§A7.1.2); d) aerator A2, 1 x 3.0 mm (§A7.1.1).

Therefore, the results further evidence that the range of fluid flow rates corresponding to bubbling is increased with a decrease in aerator orifice diameter (Figure 7.10) and hence bubbling is encouraged with multi-holed aerator design – this is, again, in agreement with the literature reports [13, 17, 19, 29, 56, 81, 86]. In addition, the streamlined aerator body design was seen to have an insignificant effect on the bubbling operating ranges compared to the flat-end case, with relatively minor differences between the identified bubbling regions.

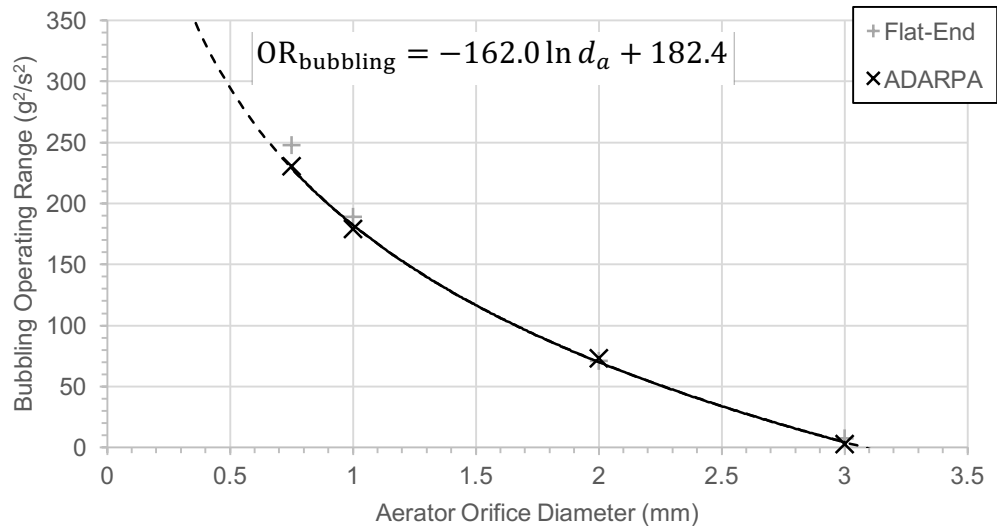


Figure 7.10 Effect of aerator orifice diameter on bubbling operating range.

Considering the downstream internal flow behaviour for the various aerator orifice diameters, the streamlined aerator profile was seen to have a significant improvement over the conventional flat-end aerator design, due to preventing formation of a gas void in the aerator wake for all investigated conditions – this enabled a bubbly flow to be formed. Figure 7.11 compares the operating ranges over which bubbly flow is achieved for all aerator orifice diameter investigations – **N.B.** as Aerator A2 does not achieve a bubbly flow under any condition (§A7.1.1), it does not feature in this figure. For all of these cases, the bubbly flow region was restricted at:

- High ALRs, due to formation of slug flow. Gas slugs were observed to be directly injected as a result of pulse bubbling at the aerator, or formed due to coalescence of bubbles within the mixing chamber – consequently, not all bubbling cases were observed to form a bubbly flow. Decreasing the aerator orifice diameter promotes detachment of bubbles at the aerator, increasing the proportion of small uniformly sized bubbles in the mixing chamber and, hence, delaying transition from bubbly flow to slug flow.

- Low liquid flow rates, due to the high relative effect of buoyancy compared to viscous forces. Under these conditions, the gas-phase has greater residence time in the mixing chamber, which increases the gas-phase coalescence. Consequently, injected bubbles and jets were observed to coalesce within the mixing chamber to form disturbed annular and annular flows.
- High liquid flow rates, by the flow limit of the discharge valve. As previously observed, the effect of aerator orifice diameter was not seen to have a significant effect on the discharge limit.

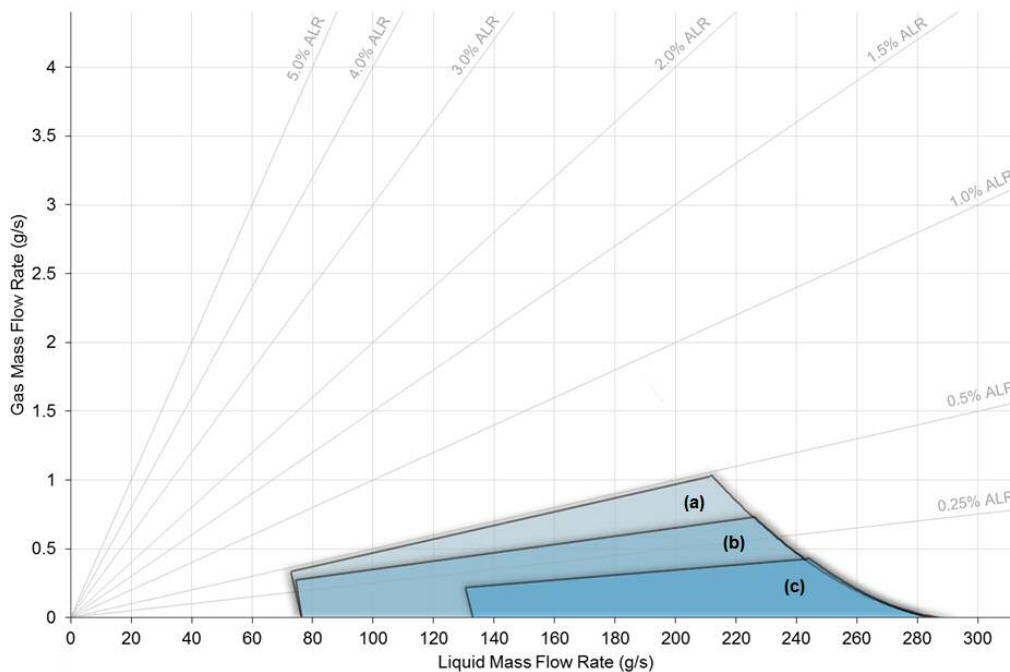


Figure 7.11 Effect of aerator orifice diameter on bubbly flow range:

- a) aerator A5, 16 x 0.75 mm (§7.2) [benchmark]; b) aerator A4, 9 x 1.0 mm (§A7.1.3);
 c) aerator A3, 4 x 2.0 mm (§A7.1.2).

Consequently, the effect of decreasing the aerator orifice diameter with a streamlined aerator body was seen to increase the range of operating conditions corresponding to bubbly flow (Figure 7.12) and, hence, a minimal aerator orifice diameter is thought to be preferred for effervescent atomisation. This must be balanced against machining limitations and sufficient spacing between orifices should be ensured to prevent premature coalesced jetting. In addition, designs featuring a large number of holes may suffer from “passive aerator orifices”, which occurs when minor dissimilarities between multiple aerator orifices result in differing orifice resistances – the orifices with the least resistance dominate the gas supply,

resulting in little or no growth from the other orifices [31]. Regardless, considering the application of effervescent atomisation, a significant improvement was observed compared the conventional flat-end aerator cases, where a bubbly flow was enabled for equivalent conditions.

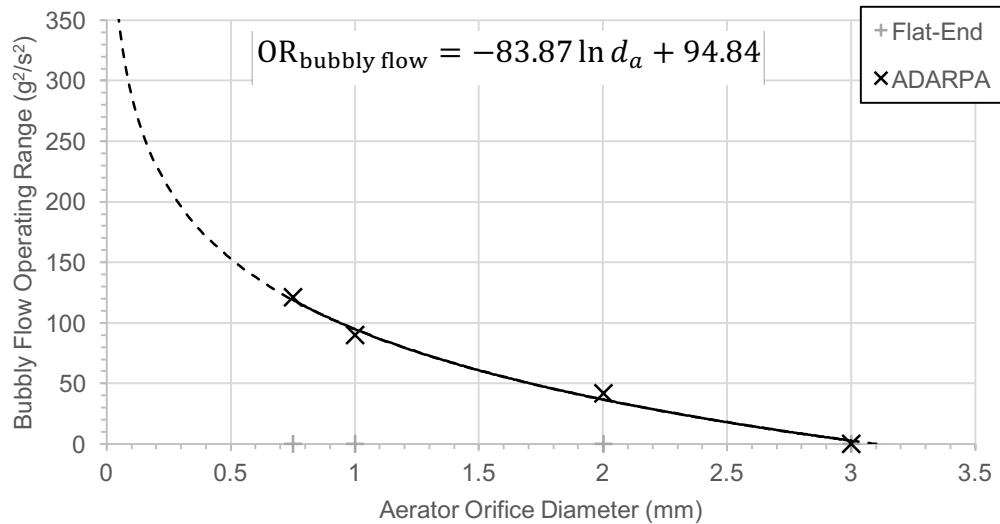


Figure 7.12 Effect of aerator orifice diameter on bubbly flow operating range.

7.4 Effect of Aeration Area

The effect of aerator aeration area on effervescent atomiser internal flow was investigated between 1.77-14.14 mm² with an ADARPA aerator body design (i.e. aerators A5 and A7-A9). In order to maintain continuity, increasing the aeration area acts to decrease the injected gas velocity – this is reported in the literature to favour bubbling [32]. In the current investigation, the aeration area was varied for the same aerator orifice diameter by increasing the number of holes.

Figure 7.13 shows the effect of aeration area on the internal flow of an effervescent atomiser at a comparable ALR and exit orifice diameter (i.e. discharge nozzle set to fully open). At the lowest aeration area, the injected gas velocity was highest and, hence, the rate of gas supply to the emerging gas-phase was high compared to the detachment rate within the liquid cross-flow – this promoted formation of gas jets from the orifices, which intermittently detach from the orifice in a pulse bubbling regime to form a slug flow. However, the effect of increasing the aeration area decreases the injected gas velocity and, hence, was seen to reduce the length of the gas neck from which bubbles are formed –

therefore, the rate of detachment increases and single bubbling and bubbly flow are promoted.

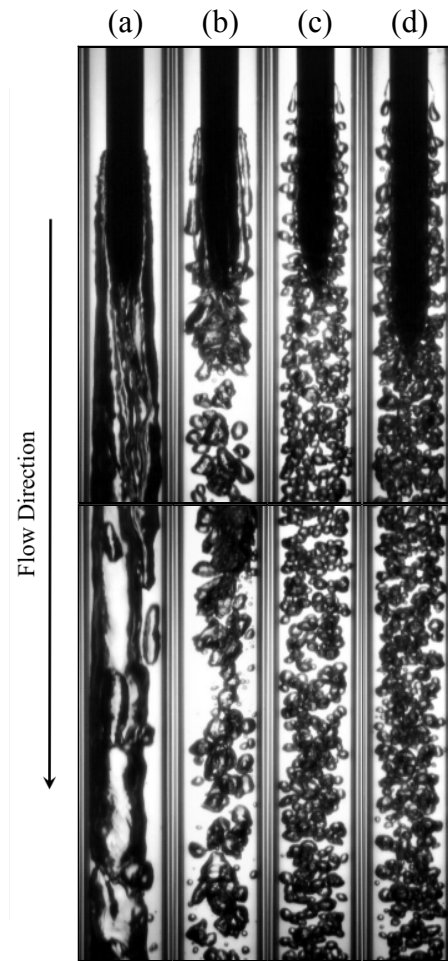


Figure 7.13 Comparable observations of varying aeration area:

- a) Aerator A7A – 1.77 mm^2 , 253 g/s, 0.12% ALR;
- b) Aerator A8A – 3.53 mm^2 , 253 g/s, 0.12% ALR;
- c) Aerator A5A – 7.07 mm^2 , 251 g/s, 0.12% ALR [benchmark];
- d) Aerator A9A – 14.14 mm^2 , 252 g/s, 0.12% ALR.

The investigation was extended by analysing the gas injection regime maps for the various aeration areas. Figure 7.14 shows the bubbling regions for all cases, which were limited at:

- High ALRs, by the transition to jetting regimes. Increasing the aeration area increased the ALR at which bubbling transitions to jetting, which indicates a less stable emerging gas-phase – this is thought to be caused by a reduced injected gas velocity, which increases the detachment rate of gas compared to the supply rate.

- Low liquid flow rates, by the generation of evacuated chamber. Whilst this limit was observed to vary between the investigated aerator areas, the trend was not predictable – it is thought that the differences are due to the chaotic mechanisms affecting passive bleeding of the atomiser upon start-up and not the effect of aerator area.
- High liquid flow rates, by the flow limit of the discharge valve. Increasing the ALR acts to further restrict the valve and, hence, the liquid flow rate continually decreases. The effect of aeration area was not seen to have a significant effect on the discharge limit.

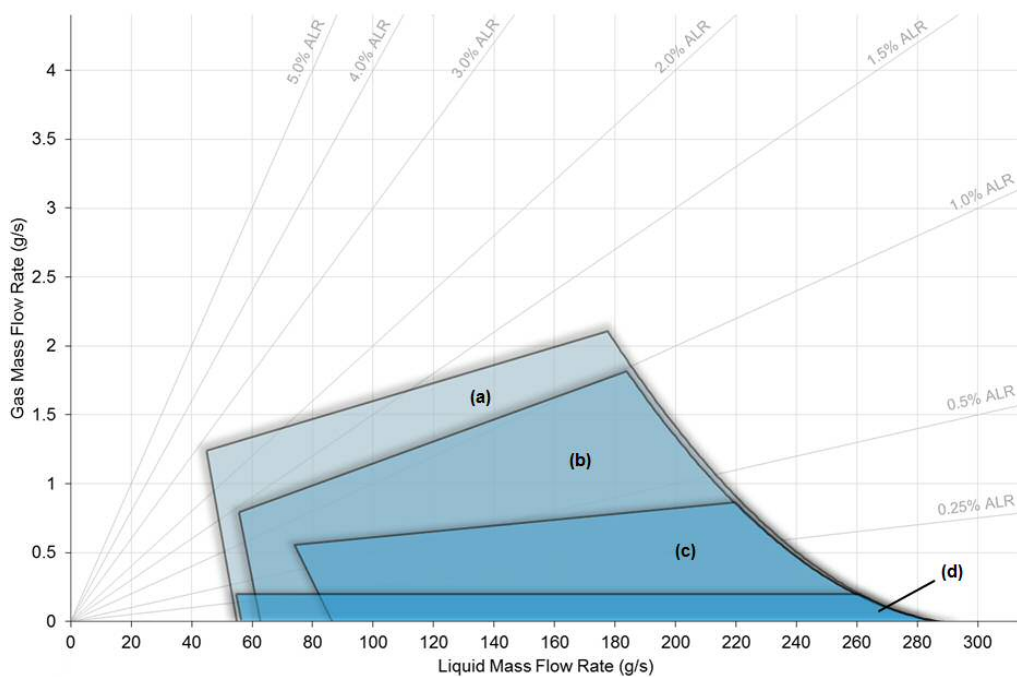


Figure 7.14 Effect of aeration area on bubbling operating range:

- a) aerator A9, 14.14 mm² (§A7.2.4); b) aerator A5, 7.07 mm² (§7.2) [benchmark];
 c) aerator A8, 3.53 mm² (§A7.2.2); d) aerator A7, 1.77 mm² (§A7.2.1).

Consequently, the operating range corresponding to bubbling was seen to be increased with greater aeration areas (Figure 7.15).

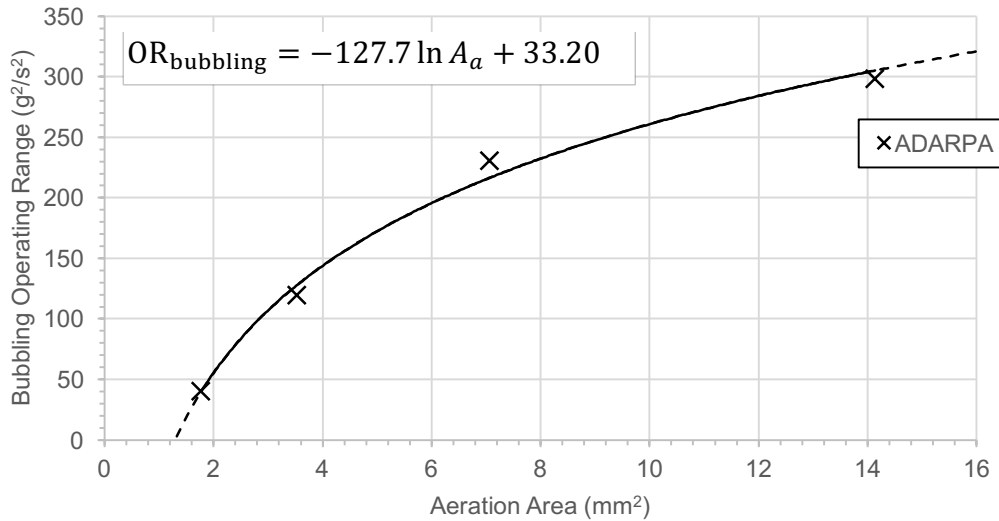


Figure 7.15 Effect of aeration area on bubbling operating range.

Figure 7.16 compares the operating ranges over which bubbly flow is achieved for all aeration area investigations – **N.B.** as Aerator A7 does not achieve a bubbly flow under any condition (§A7.3.1), it does not feature in this figure. For all of these cases, the bubbly flow region was restricted at:

- High ALRs, due to formation of slug flow. Gas slugs were observed to be directly injected as a result of pulse bubbling at the aerator, or formed due to coalescence of bubbles within the mixing chamber – consequently, not all bubbling cases were observed to form a bubbly flow. Increasing the aeration area, promotes detachment of bubbles at the aerator and, hence, slug is suppressed – hence, the transition from bubbly flow to slug flow is delayed. This effect was observed to plateau at the highest aeration areas, suggesting a limit exists beyond which aeration area has an insignificant effect – potentially due to formation of passive aerator orifices.
- Low liquid flow rates, due to the high relative effects of buoyancy compared to viscous forces. At the highest aeration areas (i.e. 7.07 mm² and 14.14 mm²), the buoyancy is sufficient to encourage coalescence and, hence, injected bubbles and jets were coalesce to form disturbed annular and annular flows. However, at 3.53 mm² and critically low liquid flow rates, a transitional region was not identified – with the evacuated chamber gas injection regime generated under comparable flow conditions and an annular flow formed. Regardless, neither eventuality is conducive to preferred effervescent atomisation and, hence, the aeration area was not seen to have a significant effect on bubbly flow at low liquid flow rates.

- High liquid flow rates, by the flow limit of the discharge valve. The effect of aeration area was not seen to have a significant effect on the discharge limit.

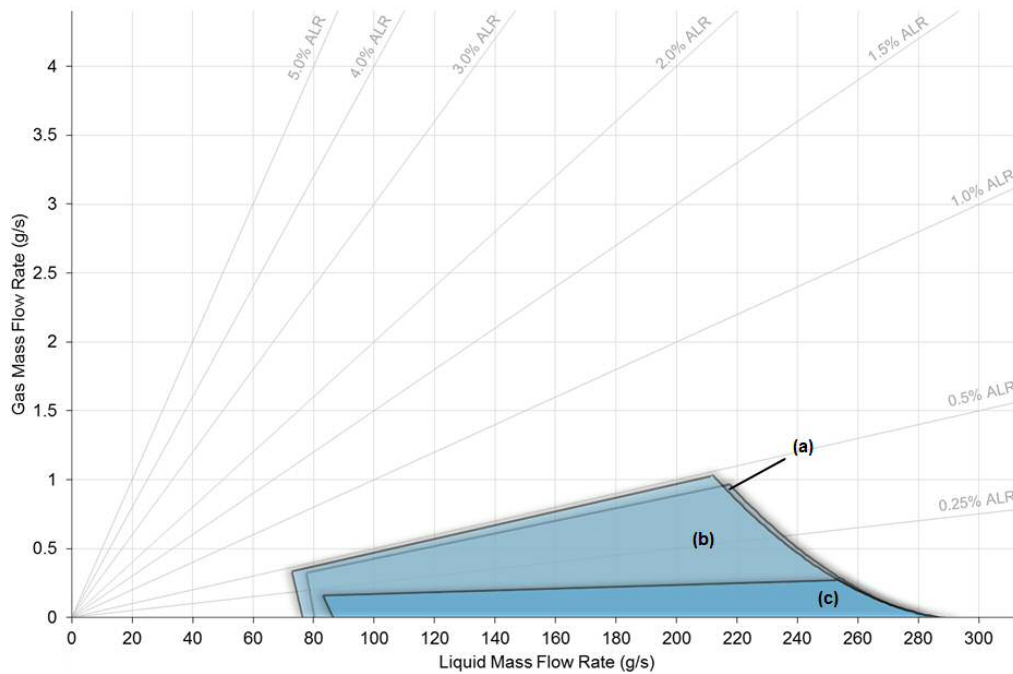


Figure 7.16 Effect of aeration area on bubbly flow operating range:

- a) aerator A9, 14.14 mm^2 (§A7.2.4); b) aerator A5, 7.07 mm^2 (§7.2) [benchmark];
 c) aerator A8, 3.53 mm^2 (§A7.2.2).

Consequently, comparing the extremes of the investigated designs, the effect of aeration area with a streamlined aerator tip was seen to increase the range of operating conditions corresponding to bubbly flow (Figure 7.17) and, hence, a high aeration area is preferred for effervescent atomisation. However, a limit is thought to exist where passive aerator orifices could occur at high orifice numbers – this is thought to have occurred between 7.07 mm^2 and 14.14 mm^2 for the current investigation.

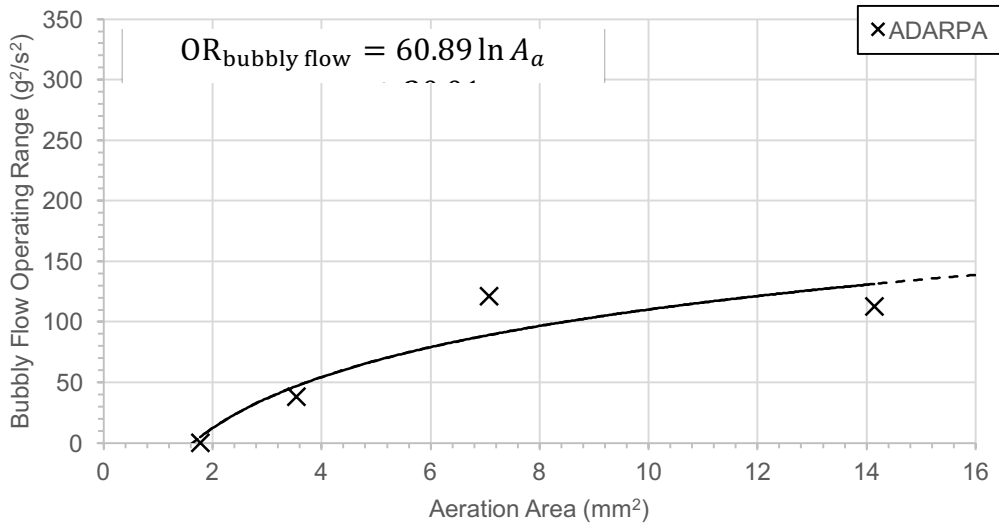


Figure 7.17 Effect of aeration area on bubbly flow operating range.

7.5 Effect of Unconventional Aerator Designs

The same unconventional porous aerator investigated in the flat-end aerator trial (§5.4), was tested with a streamlined ADARPA aerator body in the current experimentation (i.e. aerator A6) – **N.B.** due to the profile of the aerator tip, a co-flow aerator was not able to be tested. Consequently, the effect of only the porous aerator is compared to a conventional multi-holed design at comparable operating conditions within Figure 7.18. As with the previous observations, a gas void was not observed in the wake of the aerator, which enabled injected bubbles to be transferred unimpeded into the mixing chamber. However, bubble formation for the porous aerator was observed to be less structured than the conventional multi-holed alternative and, hence, very dense regions of bubbles were produced, where bubbles appear to flow in very close locality. Consequently, bubbles were observed to coalesce to form relatively small gas slugs and prompt a bubbly-slug flow within the mixing chamber – this contrasts to the bubbly flow formed by a multi-holed aerator under comparable conditions.

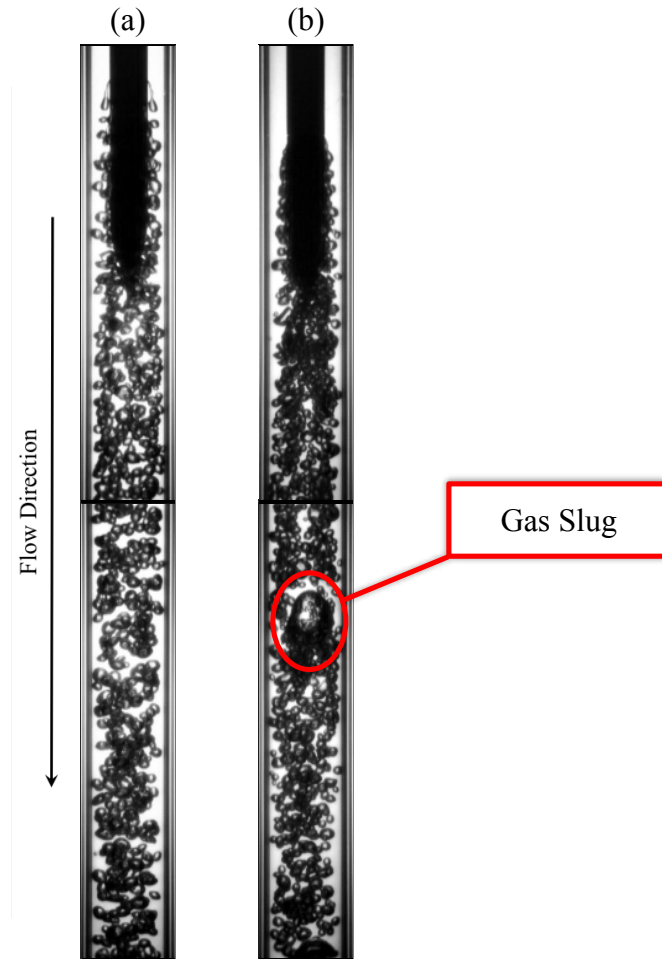


Figure 7.18 Example observations of conventional and unconventional aerator designs:

- a) Aerator A5A – 16 x 0.75 mm, 251 g/s, 0.12% ALR [benchmark];
- b) Aerator A6A – porous, 252 g/s, 0.12% ALR.

The bubbling region for a porous aerator was compared to a conventional multi-holed aerator in Figure 7.19 – it was seen to be restricted at:

- High ALRs, due to transition to coalesced jetting. This was caused by the close proximity of aeration pores, where bubbles were not able to fully expand before coalescing with a neighbouring pore – consequently, the bubbling region was seen to be decreased compared to a conventional multi-holed aerator, which transitions to jetting at greater ALRs.
- Low liquid flow rates, by the generation of evacuated chamber. Whilst this limit was observed to marginally vary between the investigated aerator designs, it is thought to be caused by the chaotic mechanisms affecting passive bleeding of the atomiser upon start-up and not the effect of aerator design.

- High liquid flow rates, by the flow limit of the discharge valve. Increasing the ALR acts to further restrict the valve and hence the liquid flow rate continually decreases. The effect of aerator design was not seen to have a significant effect on the discharge limit.

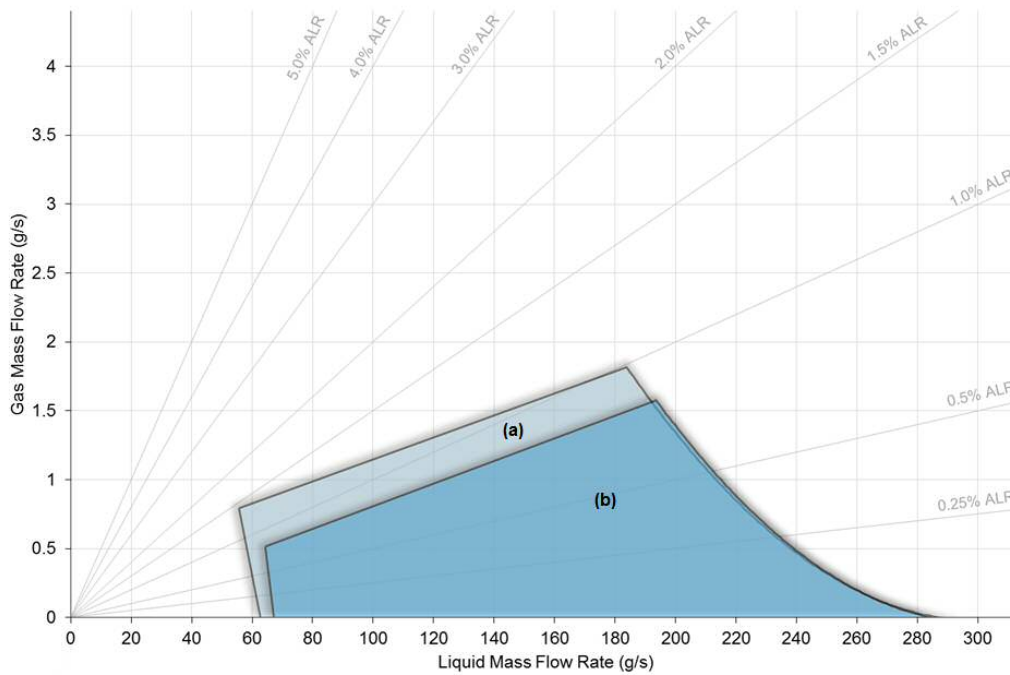


Figure 7.19 Effect of unconventional aerator design on bubbling operating range:
 a) aerator A5, 16 x 0.75 mm (§7.2) [benchmark]; b) aerator A6, porous (§A7.3.1).

Consequently, the bubbling region of the porous aerator was seen to be reduced compared to a conventional multi-holed aerator (Figure 7.20). A relatively significant difference was identified between the flat-end and ADARPA aerator body designs for the porous aerator, suggesting that aerator body design influences bubbling at the aerator – this contradicts the previous results and, thus, indicates that the current finding is anomalous. An example of differing identifications between the two aerator body designs for comparable operating conditions is shown in Figure 7.21. The differing identifications between the two designs could potentially be caused by:

1. The interference of the gas void in the aerator wake (i.e. present in the flat-end case, but not for the ADARPA design), which could aid coalescence of emerging gas jets.
2. The unstructured nature of the porous medium and, therefore, the rotation of the aerator within the mixing chamber could generate visibly different results – aerator rotation was not controlled in this investigation.

3. Marginal differences in operating conditions – although these small discrepancies were also present in other investigations.

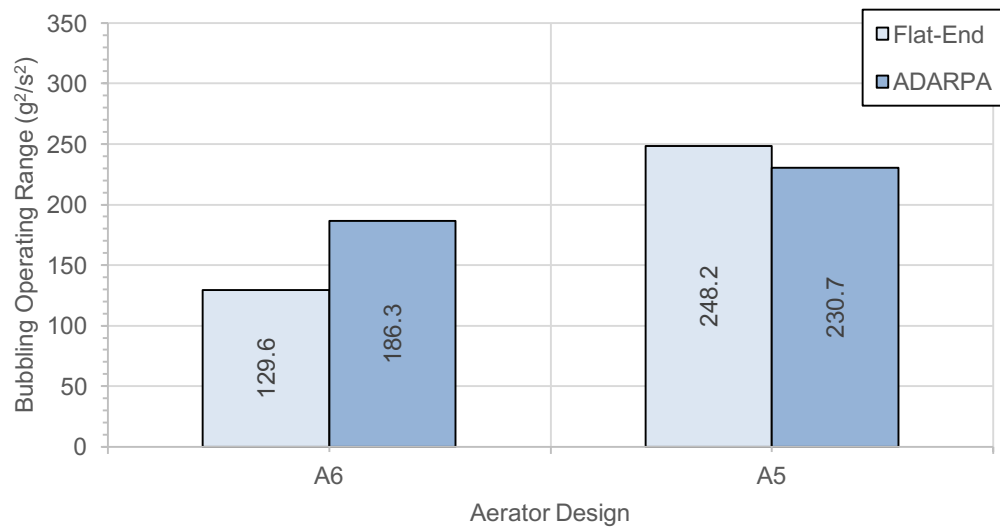


Figure 7.20 Effect of aerator design on bubbling operating range.

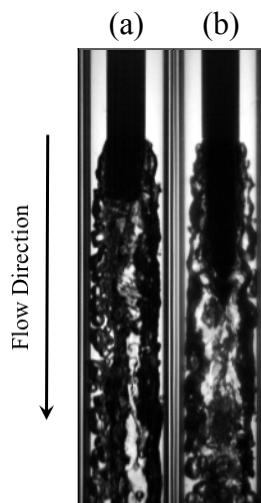


Figure 7.21 Gas injection regime identification differences between aerator body designs:

- a) Coalesced jetting, flat-end, 215 g/s, 0.50% ALR (§A5.2.2);
- b) Pulse bubbling, ADARPA, 213 g/s, 0.49% ALR (§A7.3.1).

Considering the downstream internal flow behaviour, the streamlined aerator profile was seen to have a significantly improvement over the conventional flat-end aerator design due to preventing formation of a gas void in the aerator wake for all investigated conditions – this enabled a bubbly flow to be formed. Figure 7.22 compares the operating ranges over which

bubbly flow is achieved for the porous and multi-holed aerator, in which the bubbly flow region was restricted at:

- High ALRs, due to formation of slug flow. Due to the non-uniformity of the porous medium, gas slugs were observed to be directly injected into the mixing chamber as a result of pulse bubbling at lower ALRs compared to the multi-holed aerator. Hence, the porous aerator had a reduced transitional ALR compared to the conventional multi-holed aerator.
- Low liquid flow rates, due to the high relative effects of buoyancy compared to viscous forces. Under these conditions, the gas-phase has greater residence time in the mixing chamber, which increases the gas-phase coalescence. Consequently, injected bubbles and jets were observed to coalesce within the mixing chamber to form disturbed annular and annular flows. The porous aerator was seen to encourage coalescence due to the unstructured gas injection and, hence, premature transition was observed compared to a conventional multi-holed design.
- High liquid flow rates, by the flow limit of the discharge valve. As previously observed, the effect of porous aeration was not seen to have a significant effect on the discharge limit. However, a number of bubbly-slug cases were identified at high liquid flow rates, as a result of unstructured bubble formation.

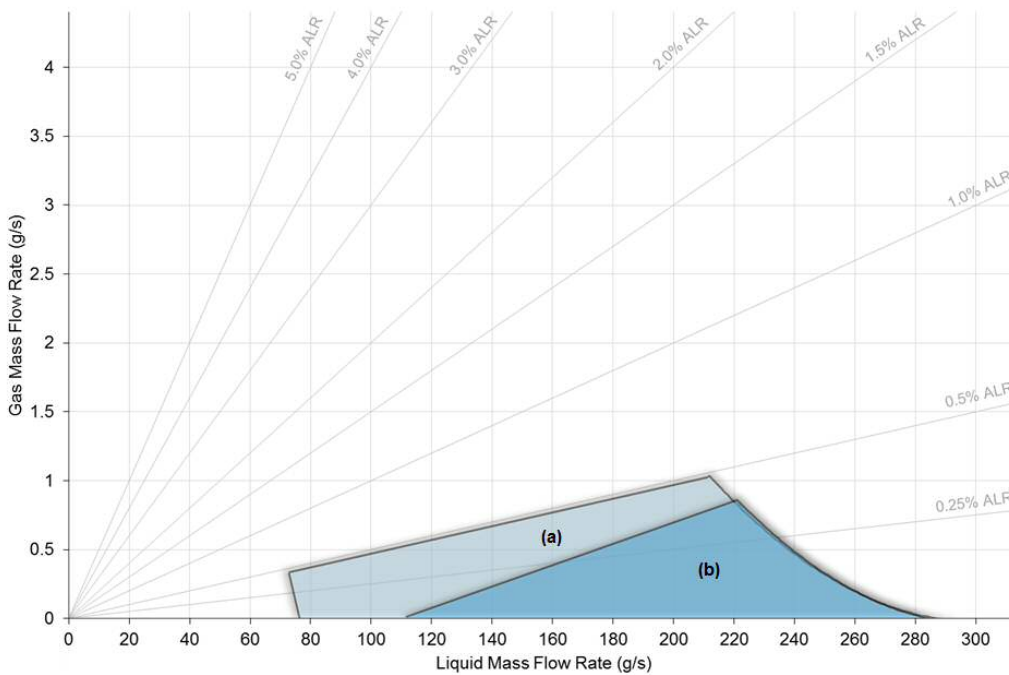


Figure 7.22 Effect of unconventional aerator design on bubbly flow operating range:
 a) aerator A5, 16 x 0.75 mm (§7.2) [benchmark]; b) aerator A6, porous (§A7.3.1).

Consequently, porous aeration with a streamlined aerator tip was seen to decrease the range of operating conditions corresponding to bubbly flow (Figure 7.23). However, it is thought that performance could be improved by selecting a porous medium with sufficient spacing and uniform pore size, whereby bubbles are able to fully expand and bubbles formation is more structured. This could be further optimised by utilising a design in which neighbouring jets coalesce prior to generating heterogeneous regimes. Regardless, considering the application of effervescent atomisation, a significant improvement was observed compared the conventional flat-end aerator cases, where a bubbly flow was enabled for equivalent conditions.

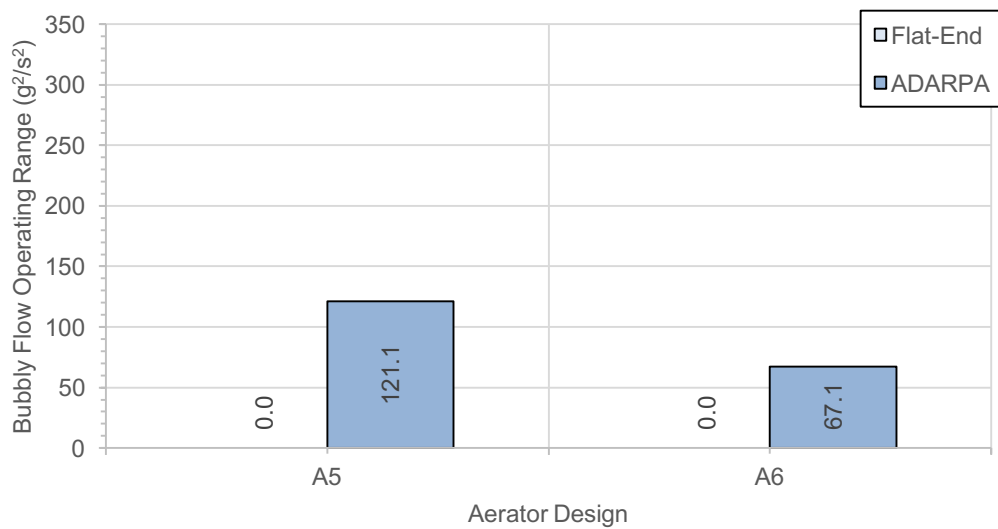


Figure 7.23 Effect of aerator design on bubbly flow operating range.

7.6 Effect of Mixing Chamber Diameter

The effect of mixing chamber diameter on effervescent atomiser internal flow was investigated for 14, 20 and 25 mm diameters. As previously discussed, decreasing the mixing chamber diameter for given input fluid flow rates acts to increase the superficial fluid velocities and Bakers numbers throughout the atomiser, including increasing the liquid cross-flow velocity around the aerator periphery. The influence of increasing the liquid cross-flow velocity encourages detachment of the forming bubbles, typically before fully expanded [39].

Figure 7.24 shows the effect of mixing chamber diameter on the internal flow of an effervescent atomiser at a comparable ALR and exit orifice diameter (i.e. discharge nozzle

set to fully open). The bubbles produced are visibly seen to decrease in size with reducing mixing chamber diameter. Compared to the equivalent operating conditions tested for a flat-end aerator (Figure 5.15), a gas void was not established in the aerator wake whilst using the ADARPA aerator body and, therefore, bubbling at the aerator enabled formation of a bubbly flow. For the largest mixing chambers (i.e. 20 mm and 25 mm), single bubbling was observed to form a bubbly flow within the mixing chamber. However, at the lowest mixing chamber diameter (i.e. 14 mm), the liquid cross-flow velocity was observed to be sufficient to induce bluff-body recirculation effects and, hence, bubbles were observed to coalesce in the wake region to form a small void, which sporadically detaches to generate a slug flow. Therefore, despite the reduced bluff body effect of an ADARPA aerator body design, high superficial Baker numbers were observed to generate unwanted wake effects.

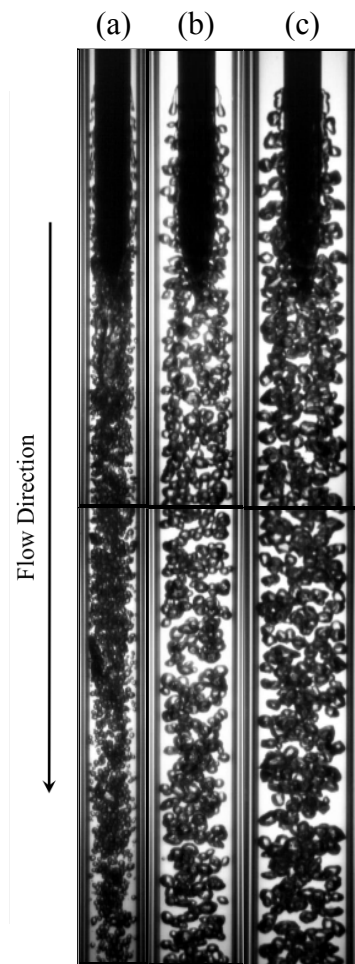


Figure 7.24 Comparable observations of varying mixing chamber diameter:

- a) 14 mm diameter, 253 g/s, 0.12% ALR;
- b) 20 mm diameter, 251 g/s, 0.12% ALR [benchmark];
- c) 25 mm diameter, 251 g/s, 0.12% ALR.

The investigation was extended by analysing the gas injection regime maps for the various mixing chamber diameters. Figure 7.25 shows the bubbling regions for each case, which were limited at:

- High ALRs, by the transition to jetting regimes. Comparing the investigated extremes (i.e. 14 mm and 25 mm), the mixing chamber diameter is seen to increase the ALR at which transition from bubbling to jetting occurs – this is thought to be due to the increase in liquid cross-flow velocity encouraging detachment of the emerging gas-phase. However, the trend was observed to plateau at the smallest mixing chamber diameters (i.e. 14 mm and 20 mm), where transition occurred at comparable ALRs ($\sim 1.0\%$). Despite this, a greater proportion of the bubbling region comprised of single bubbling cases with a reduced mixing chamber diameter, with some cases observed at 0.50% ALR for the 14 mm diameter case compared to 0.25% ALR for the 20 mm benchmark configuration for comparable liquid flow rates – this is thought to be caused by increased detachment mechanisms promoting premature bubble detachment.
- Low liquid flow rates, by the generation of evacuated chamber. As previously discussed, the formation of the evacuated chamber regime is well approximated by the liquid Bakers number. As the liquid Bakers number for a given mass flow rate dramatically increases with a reduction in the mixing chamber diameter, the evacuated chamber regime was suppressed and bubbling promoted with a reduction in mixing chamber diameter – for example, the liquid Bakers numbers at the maximum liquid mass flow rate of 289 g/s were 1890 kg/m²s for the 14 mm diameter and 589 kg/m²s for the 25 mm diameter benchmark configuration.
- High liquid flow rates, by the flow limit of the discharge valve. Increasing the ALR acts to further restrict the valve and hence the liquid flow rate continually decreases. The effect of mixing chamber diameter was not seen to have a significant effect on the discharge limit.

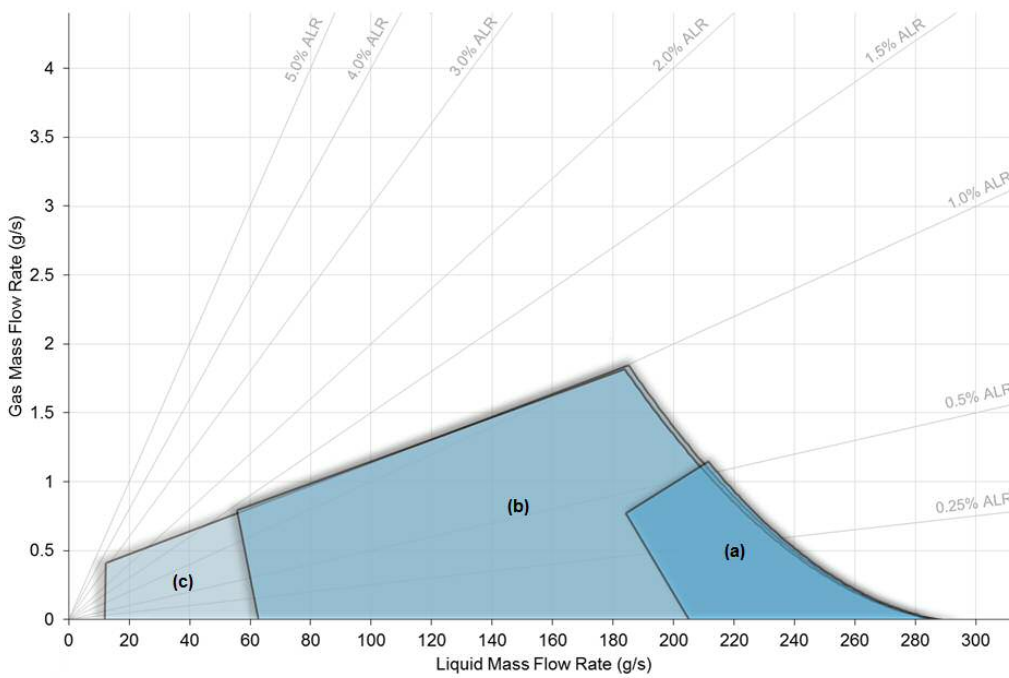


Figure 7.25 Effect of mixing chamber diameter on bubbling operating range, with respect to the fluid mass flow rates: a) 25 mm diameter (§A7.4.3);
 b) 20 mm diameter (§7.2) [benchmark]; c) 14 mm diameter (§A7.4.1).

Consequently, the operating range corresponding to bubbling was seen to be increased with a reduction in mixing chamber diameter (Figure 7.26). The effect of aerator body design was seen to have an insignificant effect on the bubbling operating range.

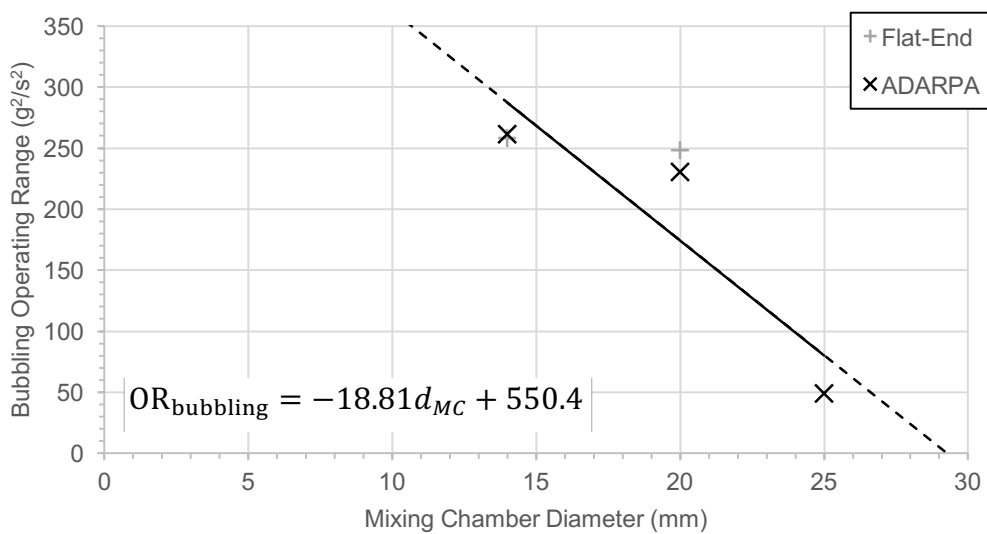


Figure 7.26 Effect of mixing chamber design on bubbling operating range.

Considering the downstream internal flow behaviour for the various mixing chamber diameters, the streamlined aerator profile was seen to have a significantly improvement over the conventional flat-end aerator design, due to preventing formation of a gas void in the aerator wake for all investigated conditions – this enabled a bubbly flow to be formed. Figure 7.27 compares the operating ranges over which bubbly flow is achieved for all mixing chamber diameter investigations. The bubbly flow region was restricted at:

- High ALRs, due to formation of slug flow. Gas slugs were observed to be directly injected as a result of pulse bubbling at the aerator, or formed due to coalescence of bubbles within the mixing chamber – consequently, not all bubbling cases were observed to form a bubbly flow. Decreasing the mixing chamber diameter increases the liquid cross-flow velocity, promoting detachment of bubbles at the aerator and, hence, delaying transition from bubbly flow to slug flow.
- Low liquid flow rates, due to the high relative effects of buoyancy compared to viscous forces. It has been previously discussed that high relative buoyancy promotes annular flow regimes (i.e. annular flow and disturbed annular flow), with the process being well approximated by the liquid Bakers number. Hence, reducing the mixing chamber diameter (i.e. increasing the liquid Bakers number) was seen to dramatically decrease the transitional liquid flow rate for which buoyancy has sufficient disruptive effect to prevent bubbling.
- High liquid flow rates. For the largest mixing chamber diameters (20 mm and 25 mm), bubbly flow is restricted by the flow limit of the discharge valve. However, sufficient bluff-body recirculation effects for the ADARPA streamlined aerator body are generated at critically high axial fluid velocities, in which irregular voids nucleate and detach from the aerator wake to generate a slug flow. Therefore, even for the optimal streamlined aerator tip investigated within the current work, there is an upper flow limit beyond which bubbly flow is prevented due to bluff-body recirculation effects – for the current ADARPA design, this is approximated by Equation 7.1. This indicates an inherent weakness of the inside-out atomiser configuration and, consequently, bluff-body recirculation effects should be considered when selecting a suitable mixing chamber diameter and aerator body design for inside-out effervescent atomisation.

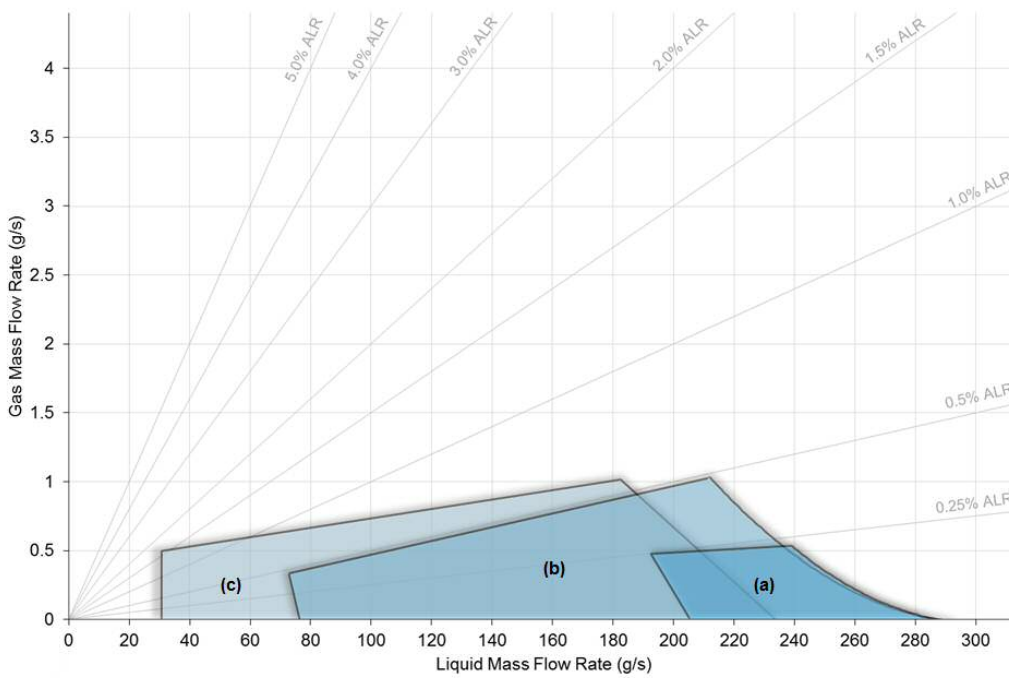


Figure 7.27 Effect of mixing chamber diameter on bubbly flow operating range, with respect to the fluid mass flow rates: a) 25 mm diameter (§A7.4.3);
 b) 20 mm diameter (§7.2) [benchmark]; c) 14 mm diameter (§A7.4.1).

$$(G_l \Psi) = -0.0196 \left(\frac{G_g}{\lambda} \right) + 30.08 \tag{7.1}$$

The effect of decreasing the mixing chamber diameter with a streamlined aerator tip was seen to increase the range of operating conditions corresponding to bubbly flow (Figure 7.28). Hence a minimal mixing chamber diameter is preferred for effervescent atomisation, so long as the conditions relating to disruptive bluff-body recirculation effects are avoided. Regardless, considering the application of effervescent atomisation, a significant improvement was observed compared the conventional flat-end aerator cases, where a bubbly flow was enabled for equivalent conditions.

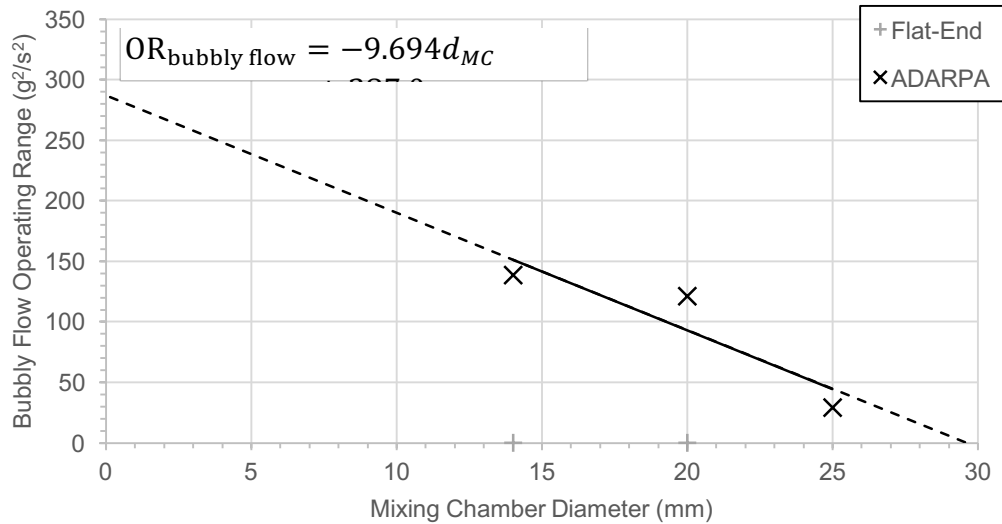


Figure 7.28 Effect of mixing chamber design on bubbly flow operating range.

7.7 Effect of Operating Pressure

The effect of operating pressure on effervescent atomiser internal flow was investigated for 1, 3 and 5 bar_g. A greater operating pressure increases the achievable fluid flow rate through the atomiser, as described by Equation 2.8 – this relates to increased superficial fluid velocities and Bakers numbers throughout the atomiser and is, therefore, expected to encourage premature detachment of the forming bubbles [39]. In addition, an increased operating pressure acts to compress the gas-phase.

Figure 7.29 shows this effect at 0.12% ALR with the discharge nozzle setting fully open (i.e. equivalent exit orifice diameter) in which, as expected, the liquid mass flow rate was measured to increase with greater operating pressures. Unlike the flat-end aerator body design, a gas void was prevented in the aerator wake when using the ADARPA streamlined profile – this enabled bubbling at the aerator to generate a bubbly flow. The bubbles produced from the aerator were visibly seen to decrease in size with increasing operating pressure which, as previously discussed, is thought to result from a combination of factors – specifically, increased greater detachment mechanisms (i.e. increased viscous drag and inertia) and increased gas-phase compression. Consequently, in the given cases, the effect of increasing operating pressure is seen to transition the gas injection regimes from pulse bubbling to single bubbling.

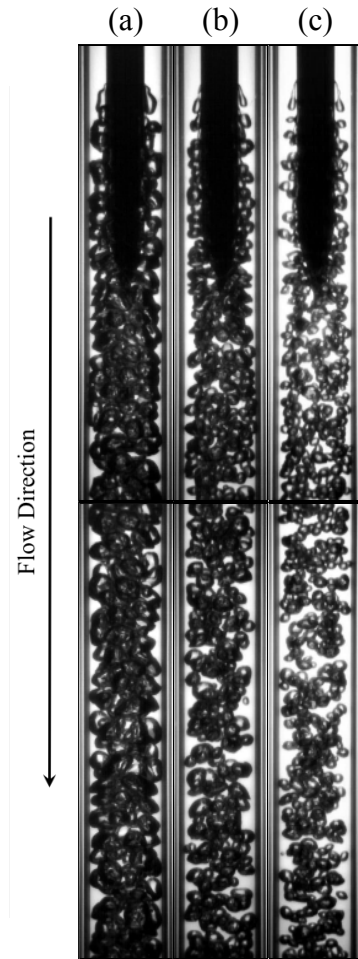


Figure 7.29 Comparable observations of varying operating pressure:

- a) 1 bar_g, 110 g/s, 0.12% ALR; b) 3 bar_g, 194 g/s, 0.12% ALR;
- c) 5 bar_g, 251 g/s, 0.12% ALR [benchmark].

The investigation was extended by analysing the gas injection regime maps for each operating pressure. Figure 7.30 shows the bubbling regions for both cases, which were limited at:

- High ALRs, by the transition to jetting regimes. Whilst this limit was observed to occur at an increased ALR for the highest operating pressure, this was not reflected at lower operating pressures and hence a trend cannot be established from the current results. This is similar to the results observed when using the flat-end aerator.
- Low liquid flow rates, by the generation of evacuated chamber. This limit was observed to marginally vary between the investigated operating pressures, which is thought to be caused by the chaotic mechanisms affecting passive bleeding of the atomiser upon start-up and not the effect of operating pressure.

- High liquid flow rates, by the discharge limit of the exit nozzle. Increasing the operating pressure was seen to dramatically increase the discharge limit (i.e. increase the maximum liquid flow rates across all ALRs), where the maximum liquid mass flow rates (and equivalent liquid Baker numbers) for 1 bar_g, 3 bar_g and 5 bar_g cases at 0% ALR were 130 g/s (413 kg/m²s), 225 g/s (717 kg/m²s) and 289 g/s (923 kg/m²s) respectively. This was expected, as stipulated by Equation 2.8.

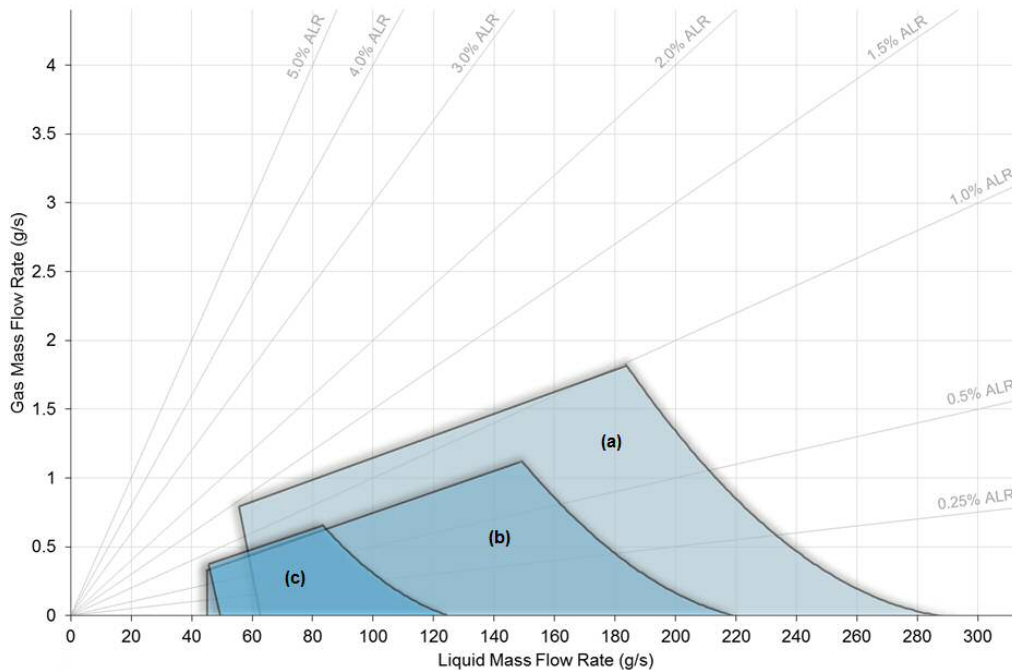


Figure 7.30 Effect of operating pressure on bubbling operating range:
 a) 5 bar_g (§7.2) [benchmark]; b) 3 bar_g (§A7.5.2); c) 1 bar_g (§A7.5.3).

Consequently, the operating range corresponding to bubbling was seen to increase with operating pressure (Figure 7.31). Once again, the aerator body design was seen to have an insignificant effect on the gas injection performance at the aerator.

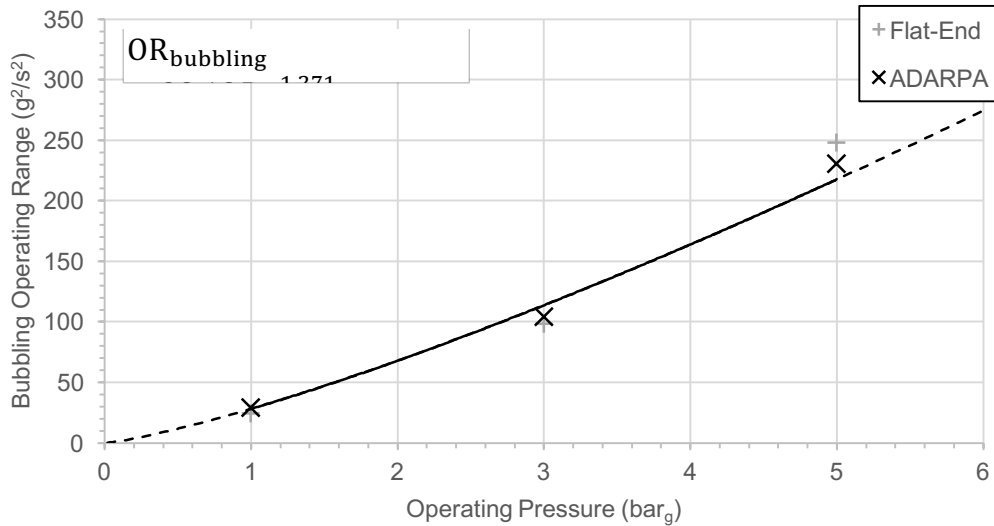


Figure 7.31 Effect of operating pressure on bubbling operating range.

Unlike the flat-end case, a bubbly flow was enabled for all investigated operating pressures using an ADARPA streamlined aerator body. Figure 7.32 compares the operating ranges over which bubbly flow is achieved for these cases, which was restricted at:

- High ALRs, due to formation of slug flow. Gas slugs were observed to be directly injected as a result of pulse bubbling at the aerator, or formed due to coalescence of bubbles within the mixing chamber – consequently, not all bubbling cases were observed to form a bubbly flow. Increasing the operating pressure was seen to increase the transitional ALR to slug flow – this is due to enabling a greater liquid flow rate and, thus, promoting detachment of bubbles at the aerator.
- Low liquid flow rates, due to the high relative effects of buoyancy compared to viscous forces. Under these conditions, the gas-phase has greater residence time in the mixing chamber, which increases the gas-phase coalescence. Consequently, injected bubbles and jets were observed to coalesce within the mixing chamber to form disturbed annular and annular flows. The operating pressure was not observed to have a predictable effect on these transitional regimes.
- High liquid flow rates, due to the discharge limit of the exit nozzle. As previously discussed, an increased operating pressure dramatically increases the discharge limit which enabled bubbly flow to be achieved at considerably greater liquid flow rates.

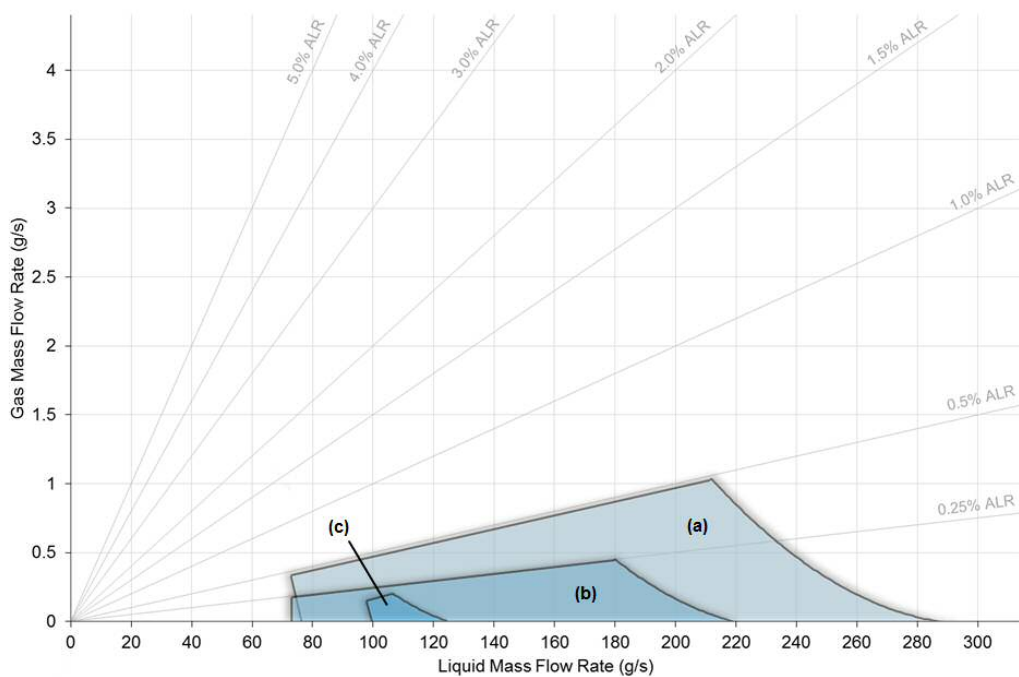


Figure 7.32 Effect of operating pressure on bubbly flow operating range:

a) 5 bar_g (§7.2) [benchmark]; b) 3 bar_g (§A7.5.2); c) 1 bar_g (§A7.5.3).

Consequently, the effect of increasing the operating pressure with a streamlined aerator tip was seen to increase the range of operating conditions corresponding to bubbly flow (Figure 7.33) – this is in agreement with Chin and Lefebvre [85]. Hence a maximal operating pressure is preferred for effervescent atomisation, however this must be considered against the disadvantages of operating at high pressures (e.g. inefficiencies, the atomiser and supply system size and cost). Regardless, considering the application of effervescent atomisation, a significant improvement was observed compared the conventional flat-end aerator cases, where a bubbly flow was enabled for equivalent conditions.

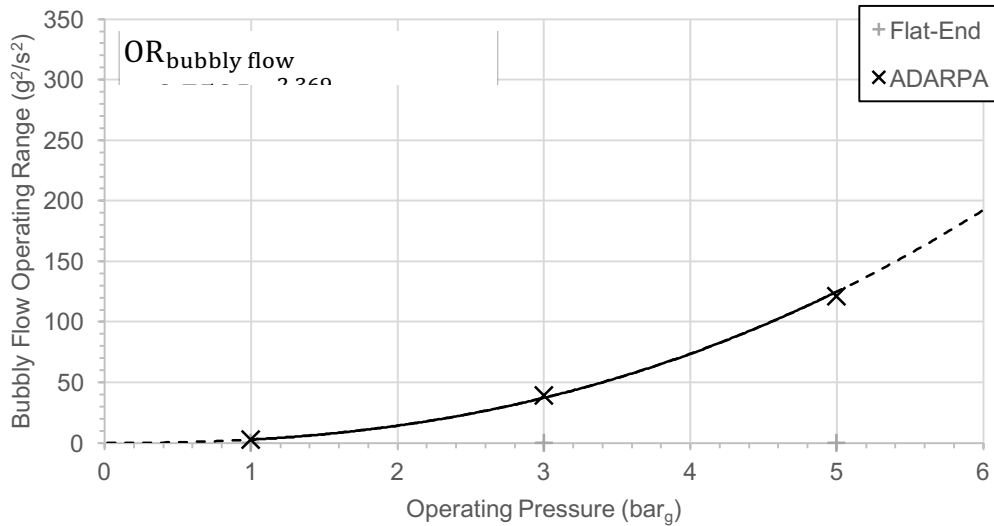


Figure 7.33 Effect of operating pressure on bubbly flow operating range.

7.8 Effect of Orientation

The extremes of atomiser orientation on effervescent atomiser internal flow were investigated for an ADARPA aerator body, where the effect of changing the orientation between vertically downwards and upwards reverses the direction of buoyancy relative to the fluid flow. Figure 7.34 shows this effect for a common effervescent atomiser, equipped with an ADARPA streamlined aerator and with a fully open discharge nozzle setting – this configuration is directly comparable with the results presented in Figure 5.21 for a conventional flat-end aerator. Unlike these equivalent flat-end aerator tests, a gas void was not formed in the aerator wake for either investigated orientation – therefore the criticality of atomiser orientation on effervescent atomisation is removed for with a streamlined aerator.

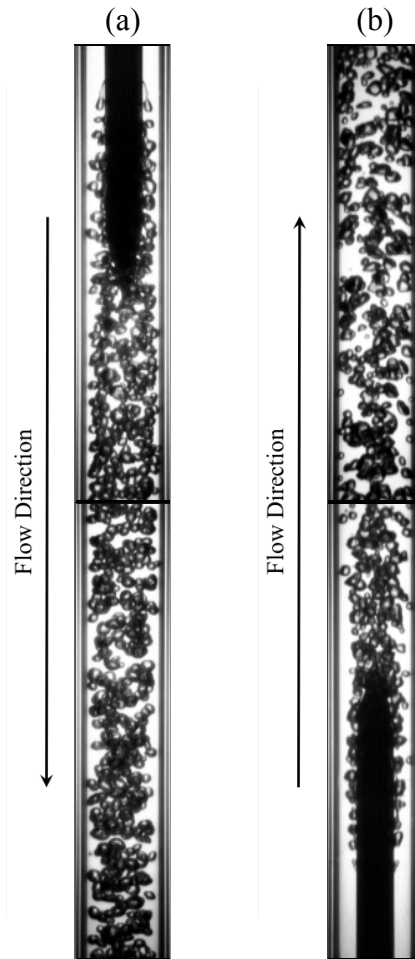


Figure 7.34 Comparable observations of varying orientation:
 a) Vertically downwards, 251 g/s, 0.12% ALR [benchmark];
 b) Vertically upwards, 251 g/s, 0.12% ALR.

The investigation was extended by analysing the gas injection regime maps for both orientations (Figure 7.35), within which the bubbling regions were limited at:

- High ALRs, by the transition to jetting regimes. The transitional ALR was seen to be slightly higher for the vertically upward orientation, particularly at low liquid flow rates – this is thought to be due to buoyancy aiding bubble detachment.
- Low liquid flow rates for the vertically downwards orientations, by the generation of evacuated chamber. However, for the vertically upwards case, the mixing chamber was passively bled upon start-up regardless of the liquid flow rate and, hence, evacuated chamber was prevented for all cases – this was due to buoyancy acting in a common direction to the liquid momentum to displace the ambient gas within the mixing chamber upon start-up. Hence, bubbling in a vertically upwards

configuration was seen to extend into lower liquid flow rates than the vertically downwards case.

- High liquid flow rates, by the discharge limit of the exit nozzle. Increasing the ALR acts to further restrict the valve and hence the liquid flow rate continually decreases. The effect of orientation was not seen to have a significant effect on the discharge limit.

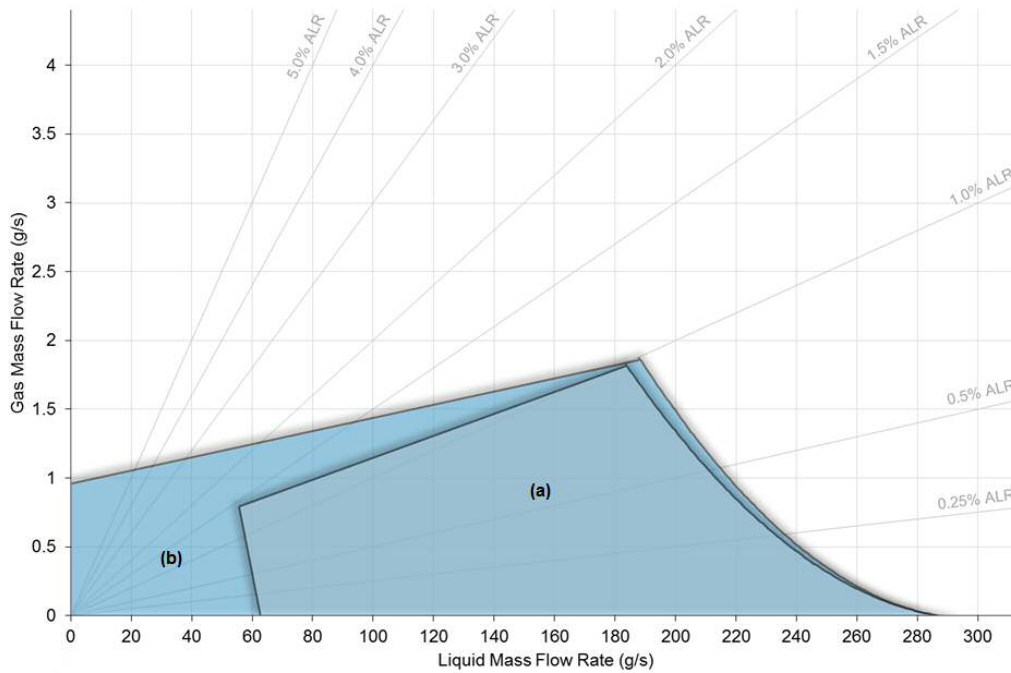


Figure 7.35 Effect of orientation on bubbling operating range:

a) vertically downwards (§7.2) [benchmark]; b) vertically upwards (§A7.6.2).

Consequently, the operating range corresponding to bubbling was seen to be increased for vertically upwards orientation, compared to vertically downwards (Figure 7.34). The bubbling performance of both aerator body designs were seen to be comparable and, hence, the effect was proven to be negligible.

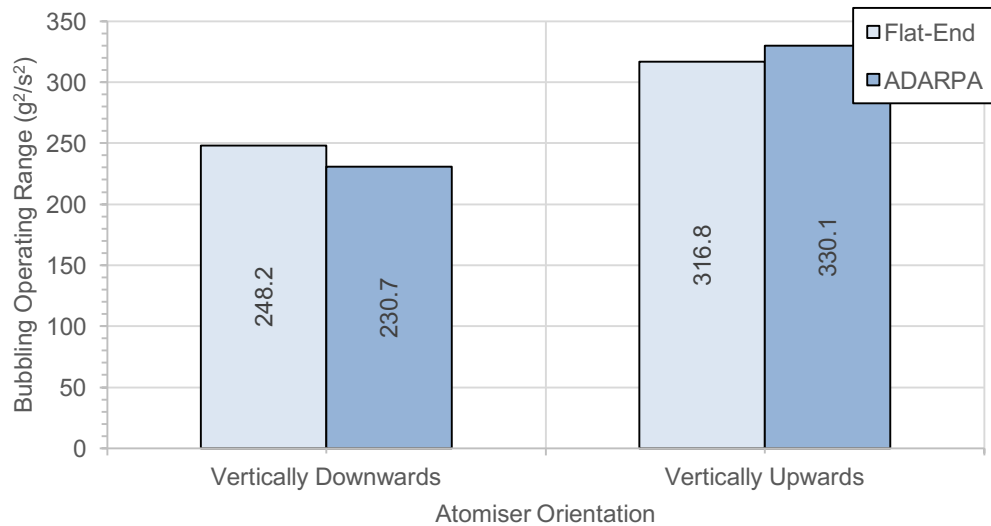


Figure 7.36 Effect of atomiser orientation on bubbling operating range.

Unlike the flat-end aerator body, a bubbly flow was enabled in a vertically downwards orientation when using an ADARPA streamlined aerator body. Figure 7.37 compares the operating ranges over which bubbly flow is achieved for these cases, which was restricted at:

- High ALRs, due to formation of slug flow. Gas slugs were observed to be directly injected as a result of pulse bubbling at the aerator, or formed due to coalescence of bubbles within the mixing chamber – consequently, not all bubbling cases were observed to form a bubbly flow. The effect of atomiser orientation was observed to have an insignificant effect on slug flow generation, with transition occurring in both cases at $\sim 0.5\%$ ALR.
- Low liquid flow rates for the vertically downwards orientated atomiser, due to the high relative effects of buoyancy compared to viscous forces. Under these conditions, the gas-phase has greater residence time in the mixing chamber, which increases the gas-phase coalescence. Consequently, injected bubbles and jets were observed to coalesce within the mixing chamber to form disturbed annular and annular flows. This compares to the vertically upwards orientated case, where the buoyancy aided discharge of the gas-phase and, hence, bubbly flow was not obstructed by low liquid flow rates.
- High liquid flow rates, due to the discharge limit of the exit nozzle. Increasing the ALR acts to further restrict the valve and hence the liquid flow rate continually decreases. The effect of orientation was not seen to have a significant effect on the discharge limit.

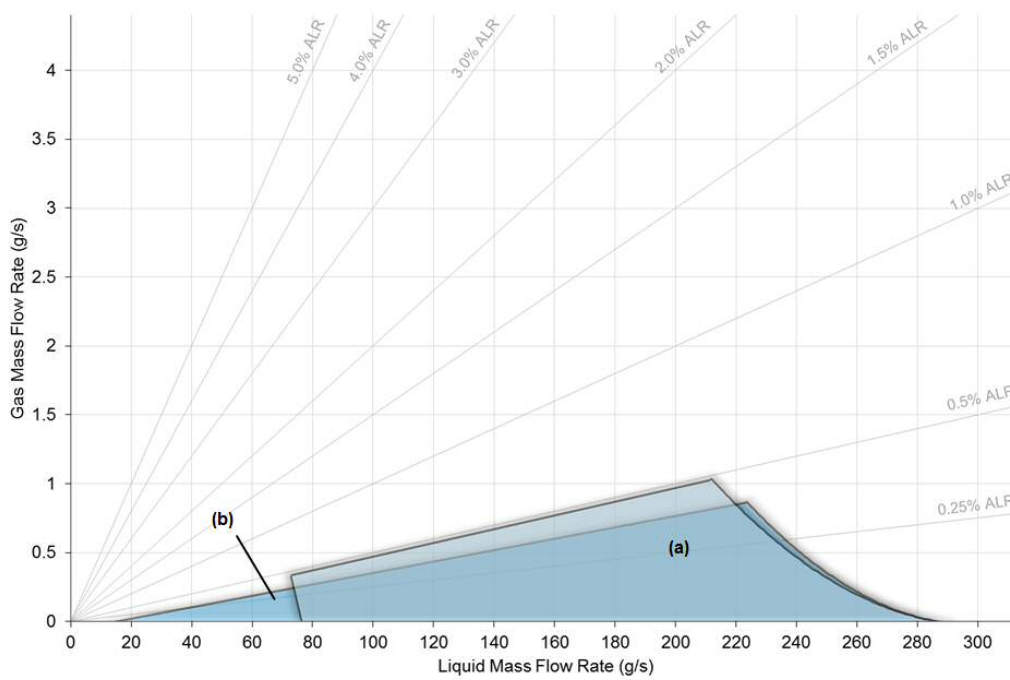


Figure 7.37 Effect of orientation on bubbly flow operating range:

a) vertically downwards (§7.2) [benchmark]; b) vertically upwards (§A7.6.2).

The effect of orientation on the bubbly flow operating range was seen to have a significantly diminished effect for the streamlined ADARPA aerator design compared to the conventional flat-end case (Figure 7.38), where a bubbly flow was enabled in a vertically downwards orientation. Consequently, the use of a streamlined aerator body design was proven to reduce the criticality of orientation on effervescent atomisation and, thus, significantly expands the potential suitable applications.

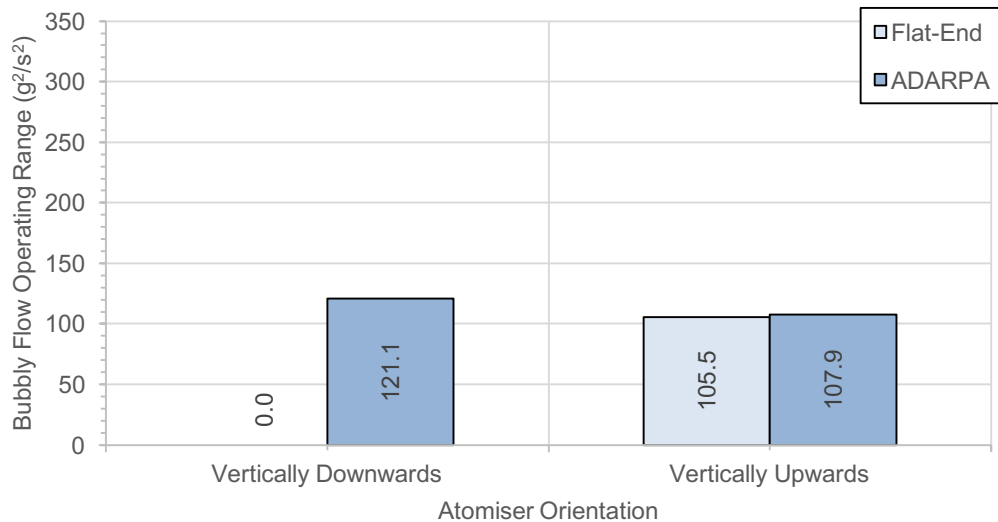


Figure 7.38 Effect of atomiser orientation on bubbly flow operating range.

7.9 Summary

In this chapter, an inside-out effervescent atomiser with a streamlined “ADARPA” aerator body design was investigated over various fluid flow rates and independent parameters, which enabled a series of gas injection and flow regimes maps to be generated – these are presented in Appendix 7.

The streamlined aerator body was found to have an insignificant on bubbling at the aerator compared to the conventional flat-end aerator investigated in a previous research chapter. Consequently, as for the flat-end aerator studies, bubbling was seen to be encouraged by: decreased ALR; decreased aerator orifice diameter; increased aeration area; decreased mixing chamber diameter and increased operating pressure. Similarly, bubbling was completely prevented at critically low liquid flow rates due to formation of an evacuated chamber regime.

However, unlike the flat-end aerator, a gas void was not formed in the aerator wake when operating in a vertically downwards orientation – this indicates that the reduced bluff body recirculation effect of the streamlined design is sufficient to prevent gas void formation across the investigated conditions. Consequently, bubbles injected at the aerator were not displaced and a bubbly flow was enabled.

Bubbling at the aerator was found to encourage the formation of a bubbly flow within the aerator and, therefore, the investigated parameters were seen to also have a significant effect on the internal flow regimes. Bubbly flow was found to be promoted by:

- Decreased ALR;
- Increased exit orifice diameter;
- Decreased aerator orifice diameter – the bubbly flow operating range increased from $0 \text{ g}^2/\text{s}^2$ to $121.1 \text{ g}^2/\text{s}^2$, for 3 mm to 0.75 mm aerator orifices respectively;
- Increased aeration area – the bubbly flow operating range increased from $0 \text{ g}^2/\text{s}^2$ to $121.1 \text{ g}^2/\text{s}^2$, for 1.77 mm^2 to 7.07 mm^2 aeration areas respectively;
- Decreased mixing chamber diameter – the bubbly flow operating range increased from $29.4 \text{ g}^2/\text{s}^2$ to $138.6 \text{ g}^2/\text{s}^2$, for 24 mm to 14 mm mixing chamber diameters respectively;
- Increasing operating pressure – the bubbly flow operating range increased from $2.7 \text{ g}^2/\text{s}^2$ to $121.1 \text{ g}^2/\text{s}^2$, for 1 bar_g to 5 bar_g operating pressures respectively.

Based on these results, a universal bubbly flow operating range correlation would be expected to take the form of Equation 7.1.

$$\text{OR}_{\text{bubbly flow}} = f([\ln d_a + C_1][\ln A_a + C_2][d_{MC} + C_3][P_{op}^{2.369}]) \quad (7.1)$$

CHAPTER 8. CONCLUSIONS AND FUTURE WORK

8.1 Conclusions of the Experimental Findings

- By number, the majority of droplets within the measured sprays had diameters below 150 μm , however each featured a small fraction of larger droplets that contributed to a significant proportion of the volume/mass contained within the spray. The droplet size was seen to decrease with decreasing exit orifice diameter and increasing ALR in a smooth, decaying manner. Larger droplets were seen to reposition from the spray centreline to the spray edge with increasing ALR, due to an increase in the expanding gas-phase velocity and hence greater momentum transfer to the largest droplets. Droplet sizes were seen to decrease with axial displacement, due to secondary atomisation.
- The internal flow regime was shown to have a weak effect on the generated droplet size, but strong effect on the spray stability. Bubbly flow was observed to produce a consistent and regular spray through a continuous single bubble atomisation mode. Optimal stability was achieved with a regular supply of bubbles to the exit orifice and, therefore, a homogenous bubbly flow at the highest ALR is preferred for effervescent atomisation. Alternative heterogeneous flow regimes (e.g. slug flow, churn flow) were observed to have alternating atomisation modes, which caused spray instability. In the extreme case, a pulsing internal flow was identified at a critically low mixing chamber diameter (i.e. 8.0 mm diameter) when operating in excess of 2.0% ALR and in a vertically downwards operation – this generated significant spray instabilities.
- The transitional limits within the gas injection and flow regime maps were seen to vary with operating conditions and atomiser design. Therefore, only regime maps closely matching the operational set-up should be used to predict the internal flow within an effervescent atomiser.
- Bubble generation from the aerator is encouraged with the injection of an “unstable” gas-phase from the aerator into a liquid cross-flow – this is caused by high relative detachment forces, high emerging gas-liquid interface area and low injected gas

velocity. Consequently, bubble injection at the aerator is promoted by low ALR, high liquid flow rate (e.g. large exit orifice diameter, high operating pressure), small aerator orifice diameter, high aeration area and small mixing chamber diameter. As the aerator body design does not influence the emerging gas-phase stability, it was shown to have a negligible effect on bubbling at the aerator.

- A conventional flat-end aerator was found to be unsuitable for inside-out effervescent atomisation in a vertically downwards orientation, due to the formation of a gas void in the aerator wake – this was shown to induce spray instability upon supply to the exit orifice. The formation of the gas void was caused by the significant bluff body recirculation effect of the aerator tube in the axial two-phase flow, which caused a reduced pressure region in the aerator wake and allowed the ambient gas to find equilibrium at the aerator tip upon unbled start-up. The formation of a void in this region was observed to be particularly problematic for effervescent atomisation as it was seen to displace any injected bubbles and, therefore, prevent a bubbly flow. The effects of increased liquid flow rate (up to 290 g/s), decreased mixing chamber diameter (from 14 mm diameter, corresponding to a maximum liquid Bakers number of 1880 kg/m²s) and increased operating pressure (up to 5 bar_g) were unable to displace the gas void. The gas void was seen to be prevented by orientating the atomiser vertically upwards as, in this case, buoyancy aids void detachment – however, this is limiting for industrial applications.
- A series of streamlined aerator body designs were investigated, each with reported low bluff body recirculation effect. All designs succeeded in preventing a gas void in the aerator wake upon start-up and further operation with gas injection – this enabled generation of bubbly flow across a wide range of conditions. The DARPA SUBOFF afterbody [1] (“ADARPA”) design was found to be the optimal of the investigated selection, due to having the weakest wake effect and therefore enabling bubbly flow across the widest range of flow conditions.
- Bubbly flow was seen to be encouraged by bubbling at the aerator and, therefore, was promoted by low ALR, high liquid flow rate (e.g. large exit orifice diameter, high operating pressure), small aerator orifice diameter, high aeration area and small mixing chamber diameter. The following proportionalities were identified for the bubbly flow operating range for the investigated parameters:

- For aerator orifice diameters ranging 0.75-3.0 mm:

$$OR_{\text{bubbly flow}} \propto \ln d_a + C_1$$

- For aeration area ranging 1.77-14.14 mm²:

$$OR_{\text{bubbly flow}} \propto \ln A_a + C_2$$

- For mixing chamber diameter ranging 14-25 mm:

$$OR_{\text{bubbly flow}} \propto d_{MC} + C_3$$

- For operating pressure ranging 1-5 bar_g:

$$OR_{\text{bubbly flow}} \propto P_{op}^{2.369}$$

Consequently, a universal bubbly flow operating range correlation would take the form:

$$OR_{\text{bubbly flow}} = f([\ln d_a + C_1][\ln A_a + C_2][d_{MC} + C_3][P_{op}^{2.369}])$$

- However, not all instances of bubbling at the aerator were observed to form a bubbly flow. At high ALRs, non-uniformly sized bubbles or gas slugs were injected into the mixing chamber due to pulse bubbling. At low liquid flow rates, buoyancy had a proportionally greater contribution over the viscous forces, which increased the residence time of gas-phase in the mixing chamber and, thus, encouraged coalescence. In addition, at critically high liquid Bakers numbers, the bluff body recirculation effect of the ADARPA streamlined aerator body design was seen to be sufficient to allow bubbles to nucleate and coalesce to form gas slugs.
- In addition, at critically low liquid Bakers numbers, the buoyancy of the gas-phase was observed to overcome the viscous forces around the aerator and form an “evacuated chamber” regime, whereby the gas-phase find equilibrium above the aerator tip – this was seen prevent development of a liquid continuum and, hence, prevented a bubbly flow.
- Consequently, to increase the bubbly flow operating range, the following is recommended for inside-out effervescent atomisers:
 - The aerator body should be streamlined, particularly if operating outside of vertically upwards – the optimal body design investigated in the current work is the ADARPA streamlined profile.
 - The aerator should have minimal aerator orifice diameter and maximal aeration area.
 - The operating pressure should be as high as reasonably practicable.
 - The mixing chamber diameter and operating pressure should be selected to ensure that the liquid Bakers number is sufficient to prevent evacuated chamber formation, but not too high to generate bluff body recirculation effects. For the ADARPA streamlined profile, this corresponded to:

$$-28.8 \left(\frac{G_g}{\lambda} \right) + 410.6 < (G_l \Psi) < -0.0196 \left(\frac{G_g}{\lambda} \right) + 30.08$$

8.2 Novelty of the Current Investigation

The following contributions of the current work are considered novel within the research community for inside-out effervescent atomisation:

- The identification and quantification of the gas injection regimes at the aerator.
- The association of the gas injection and flow regimes.
- The internal flow investigation of mixing chamber diameter as an independent variable.
- The internal flow investigation of orientation as an independent variable.
- The internal flow investigation of aeration area as an independent variable.
- The internal flow investigation of streamlined aerator tips as an independent variable.
- The internal flow investigation of an effervescent atomiser from unbled start up conditions – thought to be applicable to most industrial applications.

The following accomplishments are considered to further the scientific community:

- Presentation of regime maps specific to inside-out effervescent atomisers from unbled start up across a range of common parameters.
- Observation and explanation of gas void formation in aerator wake and potential solutions.

8.3 Recommendations for Future Work

- Internal flow experimentation to identify bubbly flow operating range of the atomiser configuration utilising the optimal case of each independent parameter (i.e. ADARPA streamlined aerator body design, 0.75 mm aerator orifice diameter, 14.14 mm² aeration area, 14 mm mixing chamber diameter, 5 bar_g operating pressure).
- Optimisation of the Optical Effervescent Atomiser (OEA) exit orifice, to investigate if comparative spray quality can be achieved to alternative effervescent atomiser studies.
- Extend experimentation of independent parameters to include atomisation quantification. This could be achieved using the OEA, in which a streamlined aerator tip should be used.
- Extend the range of independent parameters to identify limitations and further refine the bubbly flow operating range correlations.

- Perform an in-depth study of streamlined profiles for cylinders in an axial flow, to identify if the ADARPA design has an optimally low bluff body recirculation effect – a decreased recirculation effect would be expected to increase the bubbly flow range at high liquid flow rates.
- Investigate the effect of alternative parameters on effervescent atomiser internal flow (e.g. fluid properties and mixing chamber length). In particular, it would be beneficial to compare the internal flow performance of an inside-out effervescent atomiser to an equivalent outside-in configuration – it is expected that gas void formation would not interfere with the transfer of bubbles into the mixing chamber without the interference of aerator tube and, therefore, could improve the bubbly flow operating range. This could be performed with the current Internal Flow Optimisation Rig (IFOR) by orientating the system in a vertically downwards orientation and machining aerator holes into the top of the mixing chamber – the external tank could then be part filled and pressurised with air to enable gas injection into the mixing chamber.
- Perform a quantitative internal flow study to identify if an optimal bubble size exists for effervescent atomisation and, therefore, if there is a limit to the homogeneity of the internal flow for a given ALR – for example, Sen et al. [41] reports that bubbles smaller than the exit orifice have a negligible effect on effervescent atomisation. Shadowography was shown in the current work to be an ineffective method for bubble sizing in dense flows, due the difficulties of isolating overlapping and clustered bubbles within an image. An alternative technique termed “Planar Fluorescence Approach for Bubble Imaging” (PFIB) is reported by Akhmetbekov et al. [156] and Dulin et al. [157] to enable isolation of a single plane within two-phase gas-liquid flow and, therefore, could be better suited to internal flow quantification.

REFERENCES

1. Groves, N. C. et al., *Geometric Characteristics of DARPA (Defense Advanced Research Projects Agency) SUBOFF Models (DTRC Model Numbers 5470 and 5471)*. 1989, DTIC Document.
2. Harker, J. H. and Backhurst, J. R., *Fuel and Energy*. 1981, London: Academic Press Inc. (London) LTD.
3. Cheng, J., *Biomass to Renewable Energy Processes*. 2010, Boca Raton: CRC Press, Taylor and Francis Group.
4. Department of Energy & Climate Change. *Increasing the use of low-carbon technologies*. 2014 [21 January 2014]; Department of Energy & Climate Change policy]. Available from:
<https://www.gov.uk/government/policies/increasing-the-use-of-low-carbon-technologies>.
5. Department of Energy & Climate Change. *Reducing the UK's greenhouse gas emissions by 80% by 2050*. 2014 [21 January 2014]; Department of Energy & Climate Change policy]. Available from:
<https://www.gov.uk/government/policies/reducing-the-uk-s-greenhouse-gas-emissions-by-80-by-2050>.
6. Department of Energy & Climate Change. *Supporting international action on climate change*. 2014 [21 January 2014]; Department of Energy & Climate Change policy]. Available from:
<https://www.gov.uk/government/policies/taking-international-action-to-mitigate-climate-change>.
7. Aleiferis, P. G. et al., *Effect of fuel temperature on in-nozzle cavitation and spray formation of liquid hydrocarbons and alcohols from a real-size optical injector for direct-injection spark-ignition engines*. International Journal of Heat and Mass Transfer, 2010. **53**(21-22): p. 4588-4606.
8. Aleiferis, P. G. and Van Romunde, Z. R., *An analysis of spray development with iso-octane, n-pentane, gasoline, ethanol and n-butanol from a multi-hole injector under hot fuel conditions*. Fuel, 2013. **105**: p. 143-168.

9. Department of Energy & Climate Change, *Energy Consumption in the UK (2013) – Chapter 1 Overall energy consumption*. 2013.
10. Lefebvre, A. H., *A novel method of atomization with potential gas turbine applications*. Defence Science Journal, 1988. **38**(4): p. 353-361.
11. Sovani, S. D. et al., *High pressure effervescent atomization: Effect of ambient pressure on spray cone angle*. Fuel, 2001. **80**(3): p. 427-435.
12. Lefebvre, A. H., *Atomization and sprays*. 1989: London: Taylor & Francis.
13. Sojka, P. E. and Lefebvre, A. H., *A Novel Method of Atomizing Coal-Water Slurry Fuels*. 1990, Purdue University: Indiana, United States of America.
14. Bar-Kohany, T. and Sher, E., *Effervescent atomization under sub-sonic and choked conditions - A theoretical approach*. Chemical Engineering Science, 2004. **59**(24): p. 5987-5995.
15. Catlin, C. A. and Swithenbank, J., *Physical processes influencing effervescent atomizer performance in the slug and annular flow regimes*. Atomization and Sprays, 2001. **11**(5): p. 575-595.
16. Konstantinov, D. D., *Effervescent Atomisation for Complex Fuels including Bio-Fuels*, in *School of Engineering*. 2012, University of Wales Cardiff. p. 273.
17. Jagannathan, T. K. et al., *Effect of ultrasound on bubble breakup within the mixing chamber of an effervescent atomizer*. Chemical Engineering and Processing: Process Intensification, 2011. **50**(3): p. 305-315.
18. Gosselin, P. G. et al., *Consumer product package incorporating a spray device utilizing large diameter bubbles*, U.S. Patent, Editor. 1994, The Procter Gamble Company: United States. p. 28.
19. Jedelsky, J. et al., *Development of an effervescent atomizer for industrial burners*. Energy and Fuels, 2009. **23**(12): p. 6121-6130.
20. Kim, J. Y. and Lee, S. Y., *Dependence of spraying performance on the internal flow pattern in effervescent atomizers*. Atomization and Sprays, 2001. **11**(6): p. 735-756.
21. Lörcher, M. et al., *Effervescent atomization of liquids*. Atomization and Sprays, 2005. **15**(2): p. 145-168.
22. Flachs Nielsen, A. et al., *Investigation and comparison of performance of effervescent and standard pneumatic atomizer intended for soluble aqueous*

-
- coating*. *Pharmaceutical Development and Technology*, 2006. **11**(2): p. 243-253.
23. Petersen, F. J. et al., *Effervescent atomization of aqueous polymer solutions and dispersions*. *Pharmaceutical Development and Technology*, 2001. **6**(2): p. 201-210.
24. Jedelsky, J. et al., *Characterization of spray generated by multihole effervescent atomizer and comparison with standard Y-jet atomizer*, in *Proceedings of the Ninth International Conference on Liquid Atomization and Spray Systems (ICLASS-2003)*. 2003: Sorrento, Italy.
25. Jicha, M. and Jedelsky, J., *Unsteadiness in effervescent sprays: A new evaluation method and the influence of operational conditions*. *Atomization and Sprays*, 2008. **18**(1): p. 49-83.
26. Luong, J. T. K. and Sojka, P. E., *Unsteadiness in effervescent sprays*. *Atomization and Sprays*, 1999. **9**(1): p. 87-109.
27. Liu, M. et al., *Evaluation of unsteadiness in effervescent sprays by analysis of droplet arrival statistics - The influence of fluids properties and atomizer internal design*. *Experimental Thermal and Fluid Science*, 2011. **35**(1): p. 190-198.
28. Chin, J. S. and Lefebvre, A. H., *A design procedure for effervescent atomizers*. *Journal of Engineering for Gas Turbines and Power*, 1995. **117**(2): p. 266-271.
29. Lefebvre, A. H., *Some recent developments in twin-fluid atomization*. *Particle and Particle Systems Characterization*, 1996. **13**(3): p. 205-216.
30. Yang, G. Q. et al., *Bubble formation and dynamics in gas-liquid-solid fluidization- A review*. *Chemical Engineering Science*, 2007. **62**(1-2): p. 2-27.
31. Tesař, V. *MICROBUBBLE GENERATION BY FLUIDICS. PART II: BUBBLE FORMATION MECHANISM*. in *Colloquium FLUID DYNAMICS 2012*. 2012. Prague: Institute of Thermomechanics.
32. Forrester, S. E. and Rielly, C. D., *Bubble formation from cylindrical, flat and concave sections exposed to a strong liquid cross-flow*. *Chemical Engineering Science*, 1998. **53**(8): p. 1517-1527.

33. Loubière, K. et al., *Bubble formation at a flexible orifice with liquid cross-flow*. Chemical Engineering and Processing: Process Intensification, 2004. **43**(6): p. 717-725.
34. Shuyi, X., *Bubble Formation at Multiple Orifices*, in *Department of Chemical and Environmental Engineering*. 2003, National University of Singapore.
35. Liu, C. et al., *Effects of orifice orientation and gas-liquid flow pattern on initial bubble size*. Chinese Journal of Chemical Engineering, 2013. **21**(11): p. 1206-1215.
36. Nahra, H. K. and Kamotani, Y., *Bubble formation from wall orifice in liquid cross-flow under low gravity*. Chemical Engineering Science, 2000. **55**(20): p. 4653-4665.
37. McCann, D. J. and Prince, R. G. H., *Regimes of bubbling at a submerged orifice*. Chemical Engineering Science, 1971. **26**(10): p. 1505-1512.
38. Marshall, S. H., *Air bubble formation from an orifice with liquid cross-flow*, in *Faculty of Engineering*. 1990, University of Sydney.
39. Balzán, M. A. et al., *Bubble formation regimes during gas injection into a liquid cross flow in a conduit*. The Canadian Journal of Chemical Engineering, 2017. **95**(2): p. 372-385.
40. Johnson, B. D. et al., *THEORETICAL MODEL FOR BUBBLE FORMATION AT A FRIT SURFACE IN A SHEAR FIELD*. SEP SCI TECHNOL, 1982. **V** **17**(N 8): p. 1027-1039.
41. Sen, D. et al., *Bubble formation and flow instability in an effervescent atomizer*. Journal of Visualization, 2014. **17**(2): p. 113-122.
42. Rigby, G. D. et al., *Modelling of gas flow from a submerged orifice in liquid cross-flow*. Chemical Engineering Research and Design, 1995. **73**(A3): p. 234-240.
43. Raleigh, L., *On the stability of cylindrical surfaces*. Philosophical Magazine, 1892. **34**: p. 177-180.
44. Jobehdar, M. H., *Experimental Study of Two-Phase Flow in a Liquid Cross-Flow and an Effervescent Atomizer*, in *Mechanical and Materials Engineering*. 2014, University of Western Ontario.
45. Van Dyke, M., *An album of fluid motion*. 1982: The Parabolic Press.

-
46. Saeidinezhad, A. and Dehghan, A. A., *Nose shape effect on the visualized flow field around an axisymmetric body of revolution at incidence*. Journal of Visualization, 2015. **18**(1): p. 83-93.
 47. Buresti, G. et al., *Proceedings of the 3rd International Colloquium on Bluff Body Aerodynamics and Applications Influence of afterbody rounding on the pressure drag of an axisymmetrical bluff body*. Journal of Wind Engineering and Industrial Aerodynamics, 1997. **69**: p. 179-188.
 48. Silhan, F. V. and Cabbage, J. M., *Drag of Conical and Circular-Arc Boattail Afterbodies at Mach Numbers From 0.6 to 1.3*. 1957: National Advisory Committee for Aeronautics.
 49. Mair, W., *Reduction of base drag by boat-tailed afterbodies in low-speed flow (Drag reduction on blunt-based body of revolution with boat-tailed afterbodies in low speed flow)*. Aeronautical Quarterly, 1969. **20**: p. 307-320.
 50. Buresti, G. et al., *METHODS FOR THE DRAG REDUCTION OF BLUFF BODIES AND THEIR APPLICATION TO HEAVY ROAD-VEHICLES*. 2007.
 51. Peterson, R. L., *Drag Reduction Obtained by the Addition of a Boattail to a Box Shaped Vehicle*. NASA CR-163113, Aug, 1981.
 52. Gross, A. et al. *Simulation of flow over SUBOFF bare hull model*. in *49th AIAA aerospace sciences meeting*. 2011.
 53. Gross, A. et al., *Numerical and experimental investigation of unsteady three-dimensional separation on axisymmetric bodies*. International Journal of Heat and Fluid Flow, 2013. **44**: p. 53-70.
 54. Viswanath, P., *Flow management techniques for base and afterbody drag reduction*. Progress in Aerospace Sciences, 1996. **32**(2): p. 79-129.
 55. Hampel, U. et al., *Miniature conductivity wire-mesh sensor for gas-liquid two-phase flow measurement*. Flow Measurement and Instrumentation, 2009. **20**(1): p. 15-21.
 56. Rahman, M. A. et al., *Effects of the gas phase molecular weight and bubble size on effervescent atomization*. International Journal of Multiphase Flow, 2012. **38**(1): p. 35-52.
 57. Liao, Y. and Lucas, D., *A literature review on mechanisms and models for the coalescence process of fluid particles*. Chemical Engineering Science, 2010. **65**(10): p. 2851-2864.

58. Tse, K. et al., *Visualisation of bubble coalescence in a coalescence cell, a stirred tank and a bubble column*. Chemical Engineering Science, 1998. **53**(23): p. 4031-4036.
59. Laakkonen, M. et al., *Validation of bubble breakage, coalescence and mass transfer models for gas-liquid dispersion in agitated vessel*. Chemical Engineering Science, 2006. **61**(1): p. 218-228.
60. Shinnar, R. and Church, J. M., *Statistical Theories of Turbulence in Predicting Particle Size in Agitated Dispersions*. Industrial & Engineering Chemistry, 1960. **52**(3): p. 253-256.
61. Cheung, S. C. P. et al., *Classification of bubbles in vertical gas-liquid flow: Part 2 - A model evaluation*. International Journal of Multiphase Flow, 2012. **39**: p. 135-147.
62. Weisman, J., *Two-phase flow patterns*. Handbook of fluids in motion, 1983: p. 409-425.
63. Furukawa, T. and Fukano, T., *Effects of liquid viscosity on flow patterns in vertical upward gas-liquid two-phase flow*. International Journal of Multiphase Flow, 2001. **27**(6): p. 1109-1126.
64. Zhou, J., *Flow patterns in vertical air/water flow with and without surfactant*. 2013, University of Dayton.
65. Usui, K. and Sato, K., *Vertically downward two-phase flow,(I) Void distribution and average void fraction*. Journal of Nuclear Science and Technology, 1989. **26**(7): p. 670-680.
66. Bhagwat, S. M., *STUDY OF FLOW PATTERNS AND VOID FRACTION IN VERTICAL DOWNWARD TWO PHASE FLOW*, in *Mechanical and Aerospace Engineering Department*. 2011, Oklahoma State University.
67. Roesler, T. C. and Lefebvre, A. H. *STUDIES ON AERATED-LIQUID ATOMIZATION*. 1987. Boston, MA, USA: ASME, USA, 8p.
68. Khirani, S. et al., *Microbubble generation through porous membrane under aqueous or organic liquid shear flow*. Industrial and Engineering Chemistry Research, 2012. **51**(4): p. 1997-2009.
69. Brennen, C. E., *Fundamentals of multiphase flow*. 2005: Cambridge university press.

-
70. Coleman, J. W. and Garimella, S., *Characterization of two-phase flow patterns in small diameter round and rectangular tubes*. International Journal of Heat and Mass Transfer, 1999. **42**(15): p. 2869-2881.
 71. Kataoka, I. and Serizawa, A. *BUBBLE FLOW*. 2010 7 September 2010 [cited 2015 22/05/2015]; Available from:
<http://www.thermopedia.com/content/8/?tid=104&sn=>.
 72. Huang, X. et al., *Visualization of two phase flow inside an effervescent atomizer*. Journal of Visualization, 2008. **11**(4): p. 299-308.
 73. Jedelsky, J. and Jicha, M., *Energy conversion during effervescent atomization*. Fuel, 2013. **111**: p. 836-844.
 74. Sovani, S. D. et al., *Effervescent atomization*. Progress in Energy and Combustion Science, 2001. **27**(4): p. 483-521.
 75. Jardine, K. J., *Effervescent atomization on non-Newtonian fluids at high flow rates*. 1991.
 76. Chawla, J. M. *ATOMISATION OF LIQUIDS EMPLOYING THE LOW SONIC VELOCITY IN LIQUID/GAS MIXTURES*. in *ICLASS - 85: 3rd International Conference on Liquid Atomisation and Spray Systems*. 1985. London, Engl: Inst of Energy.
 77. Wang, X. F. et al. *Influence of Gas-Injector Geometry on Atomization Performance of Aerated-Liquid Nozzles*. 1987. Pittsburgh, PA, USA: ASME.
 78. Santangelo, P. J. and Sojka, P. E., *A HOLOGRAPHIC INVESTIGATION OF THE NEAR-NOZZLE STRUCTURE OF AN EFFERVESCENT ATOMIZER-PRODUCED SPRAY*. Atomization and Sprays, 1995. **5**(2): p. 137-155.
 79. Buckner, H. N. and Sojka, P. E., *EFFERVESCENT ATOMIZATION OF HIGH-VISCOSITY FLUIDS: PART I. NEWTONIAN LIQUIDS*. 1991. **1**(3): p. 239-252.
 80. Roesler, T. and Lefebvre, A. *Photographic studies on aerated-liquid atomization, combustion fundamentals and applications*. in *Proceedings of the Meeting of the Central States Section of the Combustion Institute (Indianapolis, Indiana), Paper*. 1988.
 81. Ghaemi, S. et al., *Effect of bubble generation characteristics on effervescent atomization at low gas-liquid ratio operation*. Atomization and Sprays, 2010. **20**(3): p. 211-225.

82. Sun, C. et al., *Time-frequency analysis of acoustic and unsteadiness evaluation in effervescent sprays*. Chemical Engineering Science, 2015. **127**: p. 115-125.
83. Schröder, J. et al., *Characterization of gelatinized corn starch suspensions and resulting drop size distributions after effervescent atomization*. Journal of Food Engineering, 2011. **105**(4): p. 656-662.
84. Stähle, P. et al., *Investigation on the Applicability of the Effervescent Atomizer in Spray Drying of Foods: Influence of Liquid Viscosity on Nozzle Internal Two-Phase Flow and Spray Characteristics*. Journal of Food Process Engineering, 2015. **38**(5): p. 474-487.
85. Chin, J. and Lefebvre, A., *Flow regimes in effervescent atomization*. Atomization Sprays, 1993. **3**(3): p. 463-475.
86. Gomez, J., *Influence of bubble size on an effervescent atomization*. 2010, University of Alberta.
87. Stähle, P. et al., *Comparison of an Effervescent Nozzle and a Proposed Air-Core-Liquid-Ring (ACLR) Nozzle for Atomization of Viscous Food Liquids at Low Air Consumption*. Journal of Food Process Engineering, 2015.
88. Lörcher, M. and Mewes, D., *Atomization of liquids by two-phase gas-liquid flow through a plain-orifice nozzle: Flow regimes inside the nozzle*. Chemical Engineering & Technology, 2001. **24**(2): p. 167-172.
89. Jedelsky, J. and Jicha, M. *Effervescent atomizer - Temporal and spatial variation of spray structure*. 2006. Kyoto.
90. Chen, S. K. and Lefebvre, A. H., *Spray cone angles of effervescent atomizers*. Atomization and Sprays, 1994. **4**(3).
91. Lefebvre, A. H. and Chen, S. K., *SPRAY CONE ANGLES OF EFFERVESCENT ATOMIZERS*. 1994. **4**(3): p. 291-301.
92. Kay, P. J., *Characterising Thermofluid Spray Dynamics For Energy-Efficient Automotive Engines*, in *School of Engineering*. 2006, University of Wales Cardiff. p. 414.
93. Liu, M. et al., *Evaluation of effervescent atomizer internal design on the spray unsteadiness using a phase/Doppler particle analyzer*. Experimental Thermal and Fluid Science, 2010. **34**(6): p. 657-665.

-
94. Hong, M. et al., *Unsteadiness of the internal flow in an effervescent atomizer nozzle*. Experiments in Fluids, 2014. **55**(12): p. 1-15.
 95. Jedelský, J. and Jícha, M., *Spray characteristics and liquid distribution of multi-hole effervescent atomisers for industrial burners*. Applied Thermal Engineering, 2016. **96**: p. 286-296.
 96. Schröder, J. et al., *Viscosity ratio: A key factor for control of oil drop size distribution in effervescent atomization of oil-in-water emulsions*. Journal of Food Engineering, 2012. **111**(2): p. 265-271.
 97. McNeil, D. A. and Stuart, A. D., *The effects of a highly viscous liquid phase on vertically upward two-phase flow in a pipe*. International Journal of Multiphase Flow, 2003. **29**(9): p. 1523-1549.
 98. McNeil, D. A. and Stuart, A. D., *Vertically upward two-phase flow with a highly viscous liquid-phase in a nozzle and orifice plate*. International Journal of Heat and Fluid Flow, 2004. **25**(1): p. 58-73.
 99. Ochowiak, M. et al., *The discharge coefficient of effervescent atomizers*. Experimental Thermal and Fluid Science, 2010. **34**(8): p. 1316-1323.
 100. Lefebvre, A. H. and Chen, S. K., *Discharge Coefficients for Plain-Orifice Effervescent Atomizers*. 1994. **4**(3): p. 275-290.
 101. Ramamurthi, K. et al., *Performance characteristics of effervescent atomizer in different flow regimes*. Atomization and Sprays, 2009. **19**(1): p. 41-56.
 102. Lefebvre, A. H. *Twin-fluid atomization. Factors influencing mean drop size*. 1991. Gaithersburg, MD, USA: Publ by Natl Inst of Standards & Technology.
 103. Jedelsky, J. et al., *Discharge coefficient and operational flow characteristics of multihole effervescent atomizer*, in *Proceedings of the Ninth International Conference on Liquid Atomization and Spray Systems (ICLASS-2003)*. 2003: Sorrento, Italy.
 104. Geckler, S. C. and Sojka, P. E., *Effervescent atomization of viscoelastic liquids: Experiment and modeling*. Journal of Fluids Engineering, Transactions of the ASME, 2008. **130**(6).
 105. Broniarz-Press, L. et al., *Atomization of PEO aqueous solutions in effervescent atomizers*. International Journal of Heat and Fluid Flow, 2010. **31**(4): p. 651-658.

106. Sovani, S. D. et al., *Structure and steady-state spray performance of an effervescent diesel injector*. Fuel, 2005. **84**(12-13): p. 1503-1514.
107. Gadgil, H. et al., *Mass distribution studies in effervescent sprays*. Atomization and Sprays, 2011. **21**(5): p. 375-390.
108. Kourmatzis, A. et al., *Combined effervescent and airblast atomization of a liquid jet*. Experimental Thermal and Fluid Science, 2016. **75**: p. 66-76.
109. Mlkvik, M. et al., *Twin-fluid atomization of viscous liquids: The effect of atomizer construction on breakup process, spray stability and droplet size*. International Journal of Multiphase Flow, 2015. **77**: p. 19-31.
110. Stähle, P. et al., *Influence of feed viscosity on the two-phase flow inside the exit orifice of an effervescent atomizer and on resulting spray characteristics*. Food Research International, 2015. **77**: p. 55-62.
111. Hájek, J. et al., *Analysis of effervescent spray quality for oil-fired furnace application*. Clean Technologies and Environmental Policy, 2015. **17**(5): p. 1195-1205.
112. Ochowiak, M. et al., *The effect of extensional viscosity on the effervescent atomization of polyacrylamide solutions*. Journal of Industrial and Engineering Chemistry, 2012. **18**(6): p. 2028-2035.
113. Ochowiak, M. et al., *Characteristics of spray angle for effervescent-swirl atomizers*. Chemical Engineering and Processing: Process Intensification, 2015. **98**: p. 52-59.
114. Jedelsky, J. et al., *Effervescent Atomizer: Influence of the Operation Conditions and Internal Geometry on Spray Structure; Study Using PIV-PLIF*. Proc. ILASS, 2008.
115. Ma, X. et al., *Atomization of petroleum-coke sludge slurry using effervescent atomizer*. Experimental Thermal and Fluid Science, 2013. **46**: p. 131-138.
116. Panchagnula, M. V. and Sojka, P. E., *Spatial droplet velocity and size profiles in effervescent atomizer-produced sprays*. Fuel, 1999. **78**(6): p. 729-741.
117. Sutherland, J. J. et al., *Ligament-controlled effervescent atomization*. Atomization and Sprays, 1997. **7**(4): p. 383-406.
118. Lund, M. and Sojka, P. *Effervescent atomization at low mass flow-rates. Part 2: the structure of the spray*. in *Proceedings of the Fifth Annual Conference on Liquid Atomization and Spray Systems, San Ramon, CA*. 1992.

-
119. Broukal, J. and Hájek, J., *Validation of an effervescent spray model with secondary atomization and its application to modeling of a large-scale furnace*. Applied Thermal Engineering, 2011. **31**(13): p. 2153-2164.
 120. Lubarsky, E. and Levy, Y., *Experimental investigation of flame-holding system for the suppression of ramjet rumble*. Symposium (International) on Combustion, 1998. **2**: p. 2033-2037.
 121. Yu, G. et al. *An experimental study of kerosene combustion in a supersonic model combustor using effervescent atomization*. 2005. Chicago, IL.
 122. Kermes, V. and Bělohradský, P., *Biodiesel (EN 14213) heating oil substitution potential for petroleum based light heating oil in a 1 MW stationary combustion facility*. Biomass and Bioenergy, 2013. **49**: p. 10-21.
 123. Ferreira, M. and Teixeira, J. C., *Application of variance analysis to the combustion of residual oils*, in *12th International Conference on Computational Science and Its Applications, ICCSA 2012*. 2012: Salvador de Bahia. p. 174-186.
 124. Chen, S. K. et al., *Factors influencing the circumferential liquid distribution form pressure-swirl atomizers*. Journal of Engineering for Gas Turbines and Power, 1993. **115**(3): p. 447-452.
 125. Lefebvre, A. H., *Role of fuel preparation in low-emission combustion*. Journal of Engineering for Gas Turbines and Power, 1995. **117**(4): p. 617-654.
 126. Li, J. et al. *Effervescent atomizers for small gas turbines*. 1994. Hague, Neth: Publ by ASME.
 127. Whitlow, J. D. and Lefebvre, A. H., *EFFERVESCENT ATOMIZER OPERATION AND SPRAY CHARACTERISTICS*. 1993. **3**(2): p. 137-155.
 128. Sutherland, J. J. et al., *Entrainment by ligament-controlled effervescent atomizer-produced sprays*. International Journal of Multiphase Flow, 1997. **23**(5): p. 865-884.
 129. Bush, S. G. et al., *Momentum rate probe for use with two-phase flows*. Review of Scientific Instruments, 1996. **67**(5): p. 1878-1885.
 130. Lefebvre, A. H. et al., *Spray characteristics of aerated-liquid pressure atomizers*. Journal of Propulsion and Power, 1988. **4**(4): p. 293-298.

131. Huang, X. et al. *Characterization of an effervescent atomization water mist nozzle and its fire suppression tests*. 2011.
132. Ochowiak, M., *The effervescent atomization of oil-in-water emulsions*. Chemical Engineering and Processing: Process Intensification, 2012. **52**: p. 92-101.
133. Sankar, S. V. et al. *Swirl effervescent atomizer for spray combustion*. 1995. San Francisco, CA, USA: ASME.
134. Wade, R. A. et al., *Effervescent atomization at injection pressures in the MPa range*. Atomization and Sprays, 1999. **9**(6): p. 651-667.
135. Whitlow, J. et al. *Experimental studies on effervescent atomizers with wide spray angles*. in *In AGARD, Fuels and Combustion Technology for Advanced Aircraft Engines 11 p (SEE N94-29246 08-25)*. 1993.
136. Lund, M. T. et al., *EFFERVESCENT ATOMIZATION AT LOW MASS FLOW RATES. PART I: THE INFLUENCE OF SURFACE TENSION*. 1993. **3**(1): p. 77-89.
137. Vanderwege, B. A. and Hochgreb, S., *The effect of fuel volatility on sprays from high-pressure swirl injectors*. Symposium (International) on Combustion, 1998. **27**(2): p. 1865-1871.
138. Chen, S. K. et al., *Influence of ambient air pressure on effervescent atomization*. Journal of Propulsion and Power, 1993. **9**(1): p. 10-15.
139. Geckler, S. C. and Sojka, P. E. *High mass flow rate effervescent atomization of viscoelastic fluids*. 1993. New Orleans, LA, USA: Publ by ASME.
140. Buckner, H. N. et al. *Effervescent atomization of coal-water slurries*. 1990. New Orleans, LA, USA: Publ by ASME.
141. Sojka, P. E. and Buckner, H. N., *EFFERVESCENT ATOMIZATION OF HIGH-VISCOSITY FLUIDS: PART II. NON-NEWTONIAN LIQUIDS*. 1993. **3**(2): p. 157-170.
142. Kufferath, A. et al., *Influence of liquid flow conditions on spray characteristics of internal-mixing twin-fluid atomizers*. Proceedings of the 1998 14th International Conference on Liquid Atomization and Spray Systems, 1999. **20**(5): p. 513-519.

-
143. Petersen, F. J. et al., *Design and Atomization Properties for an Inside-Out Type Effervescent Atomizer*. Drug Development and Industrial Pharmacy, 2004. **30**(3): p. 319-326.
 144. Mostafa, A. et al. *Measurements of spray characteristics produced by effervescent atomizers*. in *40th AIAA/ASME/SAE/ASEE Joint Propulsion Conference and Exhibit*. 2004. Fort Lauderdale, FL.
 145. Sakai, T. et al. *Characteristics of internal mixing twin-fluid atomizer*. in *Proceedings of the 1st International Conference on Liquid Atomization and Sprays, Tokyo*. 1978.
 146. Bates, C. J. et al., *Influence of exit orifice characteristics on transition between effervescent atomization flow regimes*, in *Proceedings of the Eighth International Conference on Liquid Atomization and Spray Systems (ICLASS-2000)*. 2000: Pasadena, California.
 147. Dutta, P. et al., *Global properties of high liquid loading turbulent crude oil+ methane/air spray flames*. Combustion and flame, 1994. **97**(3-4): p. 251-260.
 148. Ochowiak, M., *The experimental study on the viscosity effect on the discharge coefficient for effervescent atomizers*. Experimental Thermal and Fluid Science, 2013. **50**: p. 187-192.
 149. Satapathy, M. et al. *The effect of ambient density on the performance of an effervescent atomizer operating in the MPa injection pressure range*. in *Proceedings of the Technical Meeting of the Central States Section of the Combustion Institute*. 1998. The Combustion Institute Pittsburgh, PA.
 150. Weber, C., *Disintegration of liquid jets*. Z. Angew. Math. Mech, 1931. **11**(2): p. 136-159.
 151. Lefebvre, A. H., *Energy considerations in twin-fluid atomization*. Journal of Engineering for Gas Turbines and Power, 1992. **114**(1): p. 89-96.
 152. Lund, M. T. et al., *The Influence of Atomizing Gas Molecular Weight on Low Mass Flowrate Effervescent Atomizer Performance*. Journal of Fluids Engineering, Transactions of the ASME, 1998. **120**(4): p. 750-754.
 153. Clift, R. et al., *Bubbles, Drops and Particles*. 1978, New York: Academic Press.

154. Laakkonen, M. et al., *Local bubble size distributions in agitated vessel - Comparison of three experimental techniques*. Chemical Engineering Research & Design, 2005. **83**(A1): p. 50-58.
155. MathWorks. *MATLAB Documentation: Motion-Based Multiple Object Tracking*. 2015 [cited 2015 20 September 2015]; Available from: <http://uk.mathworks.com/help/vision/examples/motion-based-multiple-object-tracking.html>.
156. Akhmetbekov, Y. K. et al., *Planar fluorescence for round bubble imaging and its application for the study of an axisymmetric two-phase jet*. Experiments in fluids, 2010. **48**(4): p. 615-629.
157. Dulin, V. M. et al., *A Technique for Round Bubbles Imaging via Planar Fluorescence*, in *17th International Symposium on Applications of Laser Techniques to Fluid Mechanics*. 2014: Lisbon, Portugal.
158. Dantec Dynamics, *BSA Flow Software, Installation and User's Guide*. 4.10 ed. 2006.
159. Dantec Dynamics. *Measurement Principles of PDA*. 2017 [21/03/2017]; Available from: <https://www.dantecdynamics.com/measurement-principles-of-pda>.
160. Konstantinov, D. et al., *Effervescent atomization for industrial energy-technology review*. Atomization and Sprays, 2010. **20**(6): p. 525-552.
161. Lee, C. H. and Lee, C. S., *Analysis of size-classified spray structure and atomization mechanism for a gasoline direct injector*. Atomization and Sprays, 2004. **14**(6).
162. Mundo, C. et al., *Numerical and experimental investigation of spray characteristics in the vicinity of a rigid wall*. Experimental thermal and fluid science, 1997. **15**(3): p. 228-237.
163. Nasr, G. G. et al., *Next generation of consumer aerosol valve design using inert gases*. Proceedings of the Institution of Mechanical Engineers, Part C: Journal of Mechanical Engineering Science, 2015. **229**(16): p. 2952-2976.
164. Bush, S. G. and Sojka, P. E. *Entrainment by effervescent sprays at low mass flow rates*. 1993. New Orleans, LA, USA: Publ by ASME.
165. Chen, S. K. and Lefebvre, A. H., *Discharge coefficients for plain-orifice effervescent atomizers*. Atomization and Sprays, 1994. **4**(3).

APPENDIX 1: PUBLISHED OUTCOMES

A Refraction Reduced Optical Study of Effervescent Atomiser Internal Flow

A. Niland*, R. Marsh, P. J. Bowen

Cardiff School of Engineering, Cardiff University, Wales

*Corresponding author: nilanda@cardiff.ac.uk

Abstract

A novel transparent “inside-out” effervescent atomiser was designed and commissioned at Cardiff School of Engineering. Refraction through the atomiser was shown to be minimised by utilising the “water tunnel” effect, enabling accurate optical measurement of the internal two-phase gas-liquid flow. A qualitative shadowography investigation was performed to identify the bubbling and flow regimes of the effervescent atomiser under various operating conditions and aerator designs. The flow regime within the mixing chamber was observed to vary with differing input gas and liquid mass flow rates and also aerator design. Formation of discrete bubbles was only observed from aerators injecting into a liquid cross-flow, suggesting that bubble formation at the aerator orifice is encouraged by exposure to high liquid shear. A multi-holed aerator design was demonstrated to produce bubbles under the widest range of flow conditions. An annular gas void was commonly formed in the wake of the aerators, thus preventing bubble formation at the aerator from generating a bubbly flow. It is therefore recommended that further research be completed to investigate the effect of reducing the aerator wake on inside-out effervescent atomiser performance.

1. Introduction

Effervescent atomisation is a twin-fluid spray generation technique, that utilises the injection of a small quantity of gas through an aerator into the flow of an atomising liquid, prior to ejection through a nozzle. The injection of the gas-phase can be grouped into characteristic bubbling regimes as presented in Figure 1. The two-phase gas-liquid flow develops within the main body of the atomiser (i.e. the mixing chamber) and can be similarly characterised into flow regimes – these are well reported within the literature and shown in Figure 2 for a vertically orientated mixing chamber.

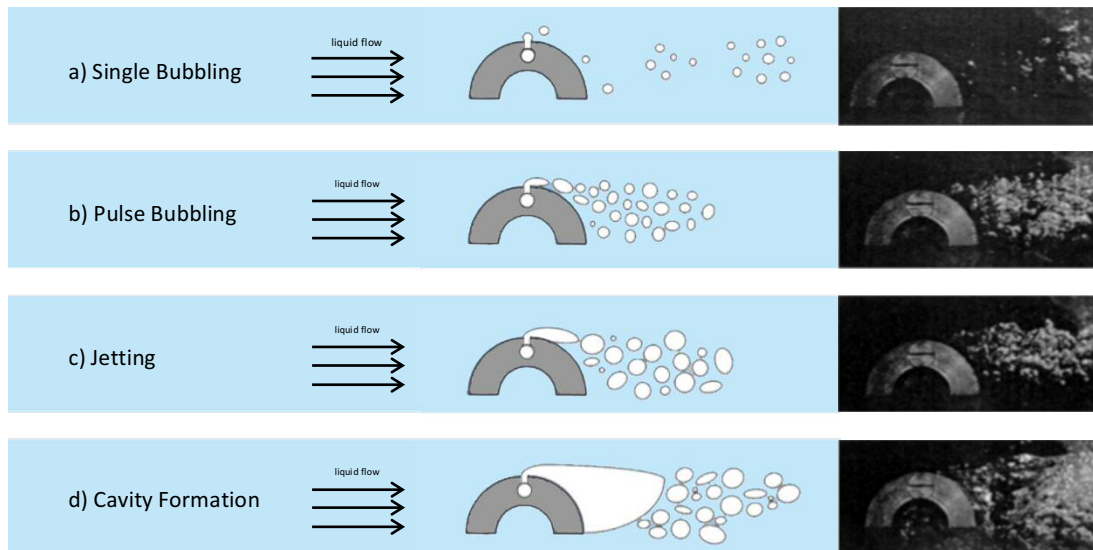


Figure 1. Bubbling regimes in a liquid cross-flow for a concave blade section [1]:
 a) Single Bubbling - discrete bubbles formed from aerator orifice;
 b) Pulse Bubbling - bubble formation from an elongated gas neck;
 c) Jetting - no longer produces bubbles but takes the appearance of a gas jet;
 d) Cavity Formation - a separation bubble forms in the wake of the aerator.

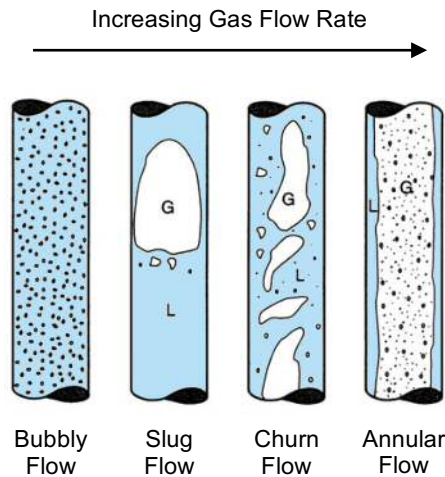


Figure 2. Vertical two-phase flow regimes, in order of increasing gas flow rate [2]:
 a) Bubbly Flow - regularly sized bubbles in a liquid continuum;
 b) Slug Flow - irregularly sized bubbles in a liquid continuum;
 c) Churn Flow - irregularly sized bubbles where neither phase is continuous;
 d) Annular Flow - a continuous gas core with liquid flow around mixing chamber periphery.

It is widely reported in effervescent atomiser literature that the flow regime produced within the mixing chamber has a considerable effect on the quality of the spray produced. Therefore, understanding and quantifying the effect that the operating and geometric variables have on the internal flow is paramount to describing the effervescent atomisation process as a whole. Generally, the aim is to operate an effervescent atomiser within the Bubbly Flow regime, where a solid spray cone is produced and the most efficient use is made of the atomising gas energy [3,4,5]. Consequently, the role of an effervescent atomiser aerator is to produce bubbles within the mixing chamber for the intended operating conditions.

There is consensus amongst previous researchers that the fluid flow rates supplied are the primary variables affecting the effervescent atomisation process [6,7,8] – generally, these are presented relative to one another, termed the air-to-liquid ratio (ALR). Conversely, the role of aerator design within effervescent atomiser literature is unclear, with many researchers reporting it to have a relatively minor influence on the atomisation performance compared to other factors [7,9,10,11]. This paper aims to investigate qualitatively the effect of aerator design on effervescent atomiser internal flow at varying input fluid flow rates.

2. Facilities and Methodology

Optical imaging techniques are increasingly being used within the scientific community to determine effervescent atomiser internal flow. However, there exists a trade off between: modelling a standard cylindrical atomiser design [8,12,13,14], with high-levels of refraction and hence image distortion, particularly at the boundary wall; or adopting an optically optimised but non-traditional design, such as rectangular bodied mixing chamber [6,15,16].

To examine this further, a novel rig was designed and commissioned at Cardiff School of Engineering to allow optical investigation within a cylindrical bodied effervescent atomiser, whilst minimising refraction (Figure 3). The optical effervescent atomiser is a transparent replica of a cylindrical bodied inside-out effervescent atomiser, which is capable of investigating the extreme limits of current effervescent atomiser design and is suitable for optical internal flow measurements. Refraction through the Perspex mixing chamber is minimised passively by exploiting the “water tunnel” effect, in which the atomiser body is submerged in a cubic body of water. As a result, all non-perpendicular faces have common refractive indices and refraction through the cylindrical mixing chamber is minimised – the consequence of which can be compared visually in Figure 4.

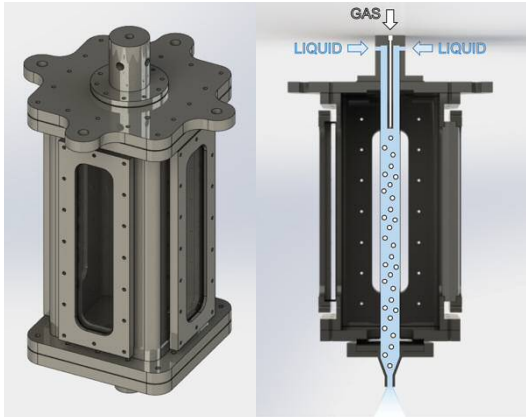


Figure 3. Optical effervescent atomiser rig concept: a) CAD model, isometric view; b) operation diagram

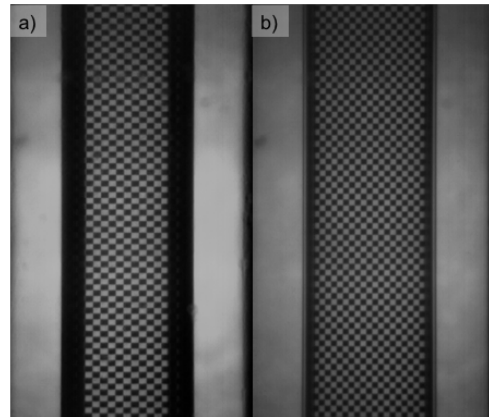


Figure 4. The same transparent checkerboard was submerged centrally in the cylindrical mixing chamber and imaged using a) standard techniques; b) passive refraction elimination.

A schematic drawing of the optical effervescent atomiser system is given in Figure 5. Liquid supply to the optical effervescent atomiser (OEA) was supplied by a Lowara 3SV29F030T multistage centrifugal pump (LP), which took feed from a 1 m³ unsealed liquid tank (LT). The majority of the pump discharge was re-circulated to the liquid tank, with backpressure controlled by a gate valve (FV-004). The liquid flow to the atomiser was controlled by a needle valve (FV-001) and the liquid mass flow rate, pressure and temperature respectively were measured with an Emerson Micromotion CMF 050 coriolis meter (F-001), a Druck PTX 1400 pressure transmitter (P-001) and Type-K thermocouple (T-001). Air was supplied from the in-house compressed air line (CA) and the gas supply to the rig was controlled with a needle valve (FV-002). The mass flow rate, pressure and temperature along the gas supply line respectively were measured with a Bronkhorst Cori-Tech M14V10I coriolis meter (F-002), a Druck PTX 1400 pressure transmitter (P-002) and Type-K thermocouple (T-002). The operating pressure within the atomiser was measured with a Druck PTX 1400 pressure transmitter (P-003) and regulated by a needle valve (FV-003), which discharged the operating fluids above the liquid tank. All instrumentation data was sampled at 1 Hz with a National Instruments cDAQ data logger (DL).

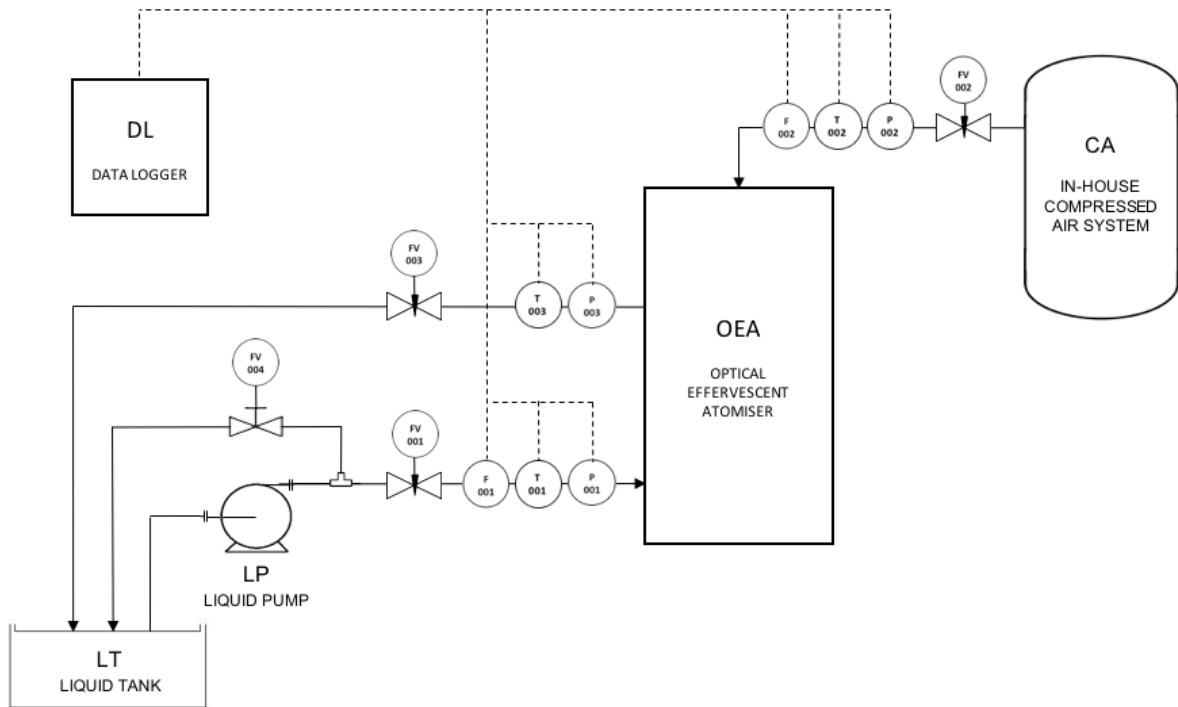


Figure 5. Effervescent atomiser rig schematic

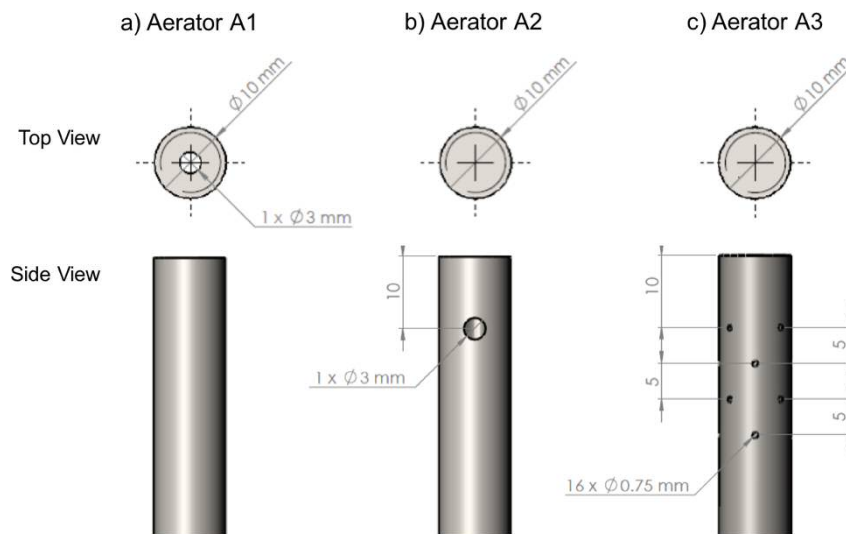


Figure 6. Aerator hole layout:

a) Aerator A1, single hole co-flow; b) Aerator A2, single hole cross-flow; c) Aerator A3, multi-holed cross-flow.

In the present study, three distinct aerator designs were investigated at various fluid flow rates. The inside-out optical effervescent atomiser had a 20 mm diameter mixing chamber and was orientated vertically downwards. Each aerator design had outer diameter of 10 mm, fixed aeration area of 7.07 mm² and flat tip – the hole layout was varied as shown in Figure 6. The experimentation utilised water and air as the operating liquids and maintained 5 bar_g operating pressure. The supply liquid flow rate ranged between 12-290 g/s (corresponding to superficial liquid velocities: 0.042-1.146 m/s around the aerator; and 0.032-0.859 m/s in the mixing chamber), with ALRs of up to 5%. The sequence of fluid delivery to the atomiser for each test point was gas supply prior to liquid supply – this was thought to be in accordance with most potential industrial applications.

For each test point, the bubbling regime in the near region of the aerator and the two-phase flow regime 108 mm downstream of the aerator were imaged using Shadowgraphy. A Mikrotron MotionBLITZ Cube high speed camera was used to record the flow, with backlighting provided by a 1000 W diffused light source. The camera frame rate was set to 500 Hz and shutter speed to 400 μs – these settings were determined empirically to: minimise image blurring; allow sufficient illumination; and provide adequate time resolution to track the flow features. Due to the chaotic nature of the two-phase flow, automating the identification of either regime via image analysis was not deemed feasible and therefore each was determined by human eye with reference to the regime descriptions provided in the Introduction. Plotting each regime occurrence against their corresponding operating conditions (i.e. gas against liquid mass flow rate) generated flow maps, which provide a measure of aerator performance. Each flow map was assessed to identify regions where specific regimes can be expected to occur.

3. Results

3.1 Single Hole Co-Flow Aerator [Aerator A1]

The gas-phase was injected through a single 3 mm diameter hole at the base of the aerator, into a liquid co-flow. Three distinct bubbling regimes were observed across all operating conditions for this aerator. Plotting these occurrences against their corresponding operating conditions produced the bubbling regime map shown in Figure 7, with the bubbling regime regions marked and labelled.

Cavity Forming (Figure 7a): The injected gas supply directly feeds a large gas void. The upward buoyancy of the gas is sufficient to overcome the bubble detachment mechanisms (e.g. the drag of the liquid flow and the injected gas momentum), thus preventing separation from the orifice as bubbles or slugs. However, the buoyancy is not great enough to overcome the liquid flow around the periphery of the aerator, thus preventing the gas void from rising above the aerator. The equilibrium position is at the tip of the aerator, where a large gas void is formed.

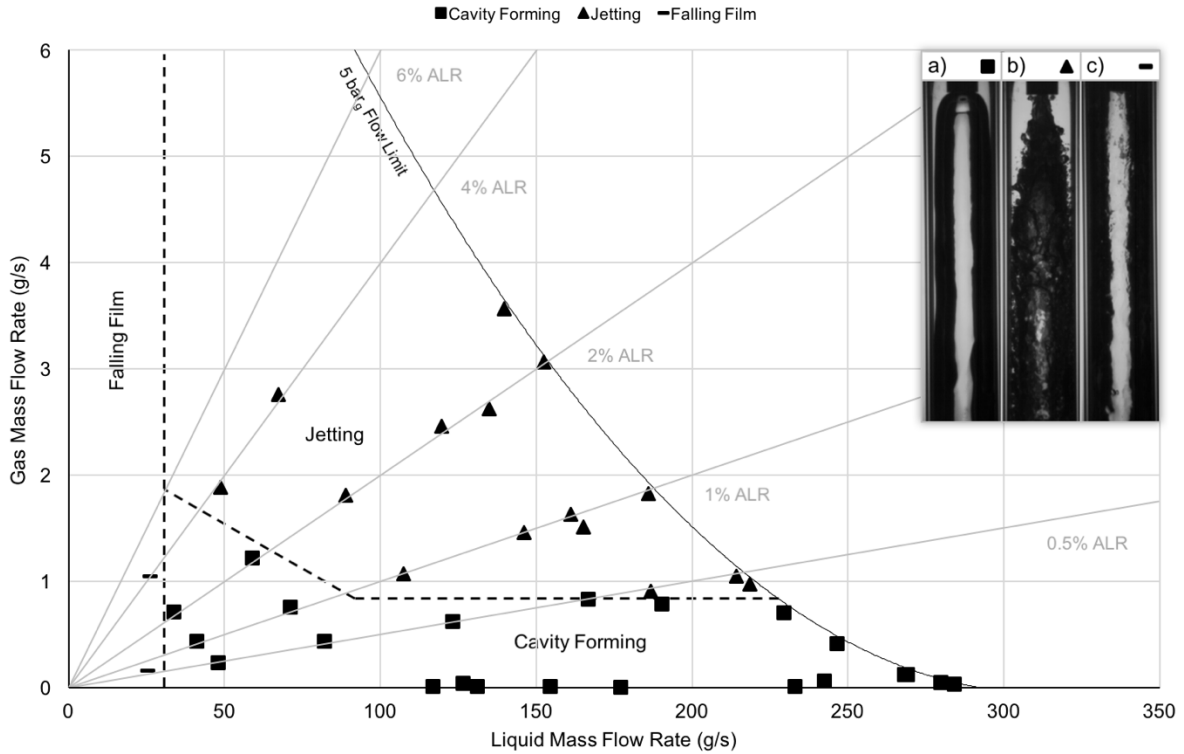


Figure 7. Bubbling regime map for the single hole co-flow aerator (A1). Regions of interest marked and labelled. a) Cavity Forming; b) Jetting; c) Falling Film.

Jetting (Figure 7b): The bubble detachment mechanisms are great enough to overcome the upward buoyancy of the injected gas, however, the gas velocity is too high to form discrete bubbles and therefore a gas jet emits from the aerator orifice.

Falling Film (Figure 7c): The upward buoyancy of the injected gas is great enough to overcome both the bubble detachment mechanisms and also the drag of the liquid flow around the periphery of the aerator. The equilibrium position of the gas void is above the aerator and therefore the liquid flows around the mixing chamber periphery prior to the aerator. The injected gas is supplied directly into the gas void.

The two-phase flow regimes were measured 108 mm downstream of the aerator orifice. Four distinct flow regimes were identified across all operating conditions. Plotting these occurrences against their corresponding operating conditions produced the flow regime map shown in Figure 8, with the flow regime regions marked and labelled.

Bubbly Flow (through annular shearing) (Figure 8a): A large gas void is formed at the aerator, which continues into the mixing chamber. Both the internal gas flow and external liquid flow generate shear on the gas-liquid interface causing surface instabilities. Given sufficient mixing length, these surface instabilities become great enough to overcome the restoring action of the surface tension and bubbles are stripped from the gas void. Liquid shear is thought to dominate this process, as the gas flow rate is low. Increasing the gas flow rate forms a longer gas void, allowing greater surface instabilities to be generated and leading to increased bubble generation – this greater depletion rate is balanced by the increased gas supply, and hence the mixing length is stabilised at point further downstream.

Annular Flow (Figure 8b): A continuous gaseous core is formed in the centre of the mixing chamber, with a film of liquid flowing around the periphery. This regime was identified at higher gas flow rates in both Cavity Forming and Jetting bubbling regimes. Any surface instabilities generated on the gas-liquid interface, either due to liquid or gas shearing, are not great enough to generate break up of the gas void within the length of the mixing chamber.

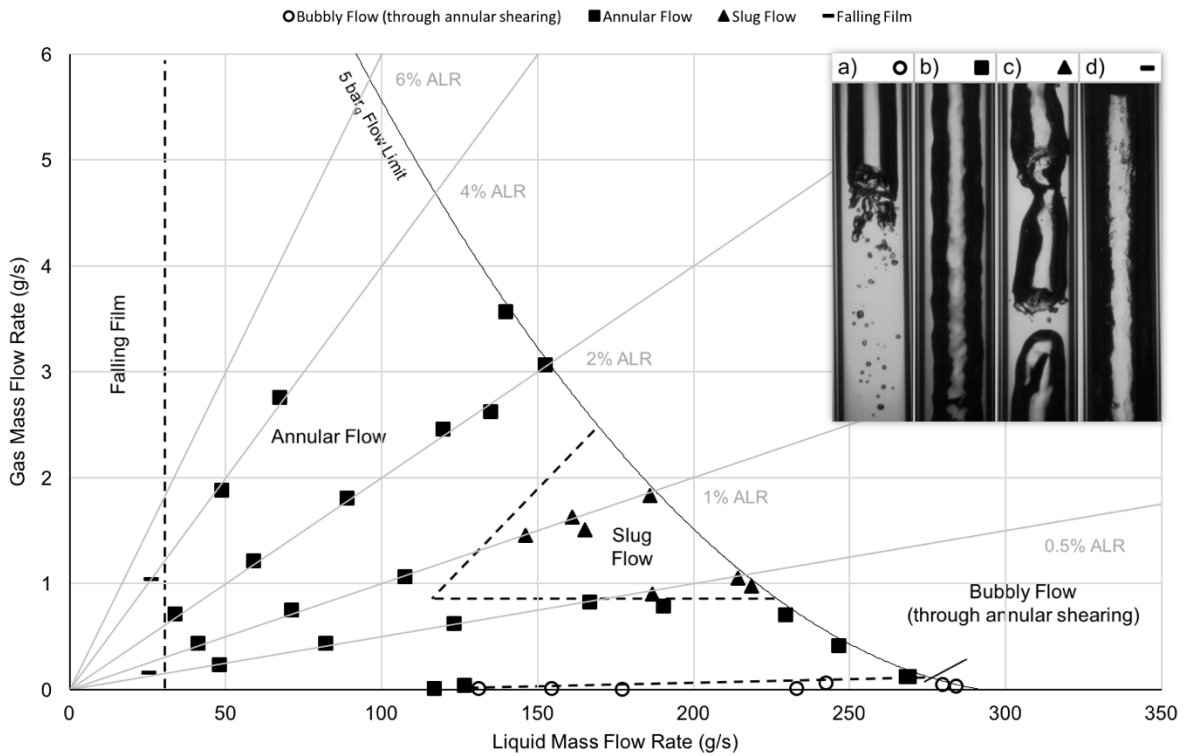


Figure 8. Flow regime map for the single hole co-flow aerator (A1). Regions of interest marked and labelled.
 a) Bubbly Flow (through annular shearing); b) Annular Flow; c) Slug Flow; d) Falling Film.

Slug Flow (Figure 8c): Observed only under specific conditions within the Jetting bubbling regime, this flow regime leads to the formation of large, irregularly sized bubbles in the liquid continuum. Similar to annular flow, an initial gaseous core is formed in the centre of the mixing chamber, with a film of liquid flowing around the periphery. However, it appears that the gas flow rate is sufficiently high to generate suitably large surface instabilities on the gas-liquid interface to form liquid ligaments across the void. This separates the annular core into large slugs of gas which travel downstream with the liquid.

Falling Film (Figure 8d): A continuation of the Falling Film bubbling regime. A large central gas core exists, with liquid flowing in a thin film around the mixing chamber periphery.

3.2 Single Hole Cross-Flow Aerator [Aerator A2]

The gas-phase was injected through a single 3 mm diameter hole in the side of the aerator, into a liquid cross-flow. Five distinct bubbling regimes were observed across all operating conditions for this aerator. Plotting these occurrences against their corresponding operating conditions produced the bubbling regime map shown in Figure 9, with the bubbling regime regions marked and labelled.

Single Bubbling (Figure 9a): Discrete bubbles are formed from the aerator orifice and are drawn away with the liquid flow into the mixing chamber. A central gas void is present within the wake of the aerator, which forces the bubbles to flow in the liquid periphery. Regular coalescence of the bubbles and gas void was observed, preventing its depletion.

Pulse Bubbling (Figure 9b): Bubbles are formed from a neck of gas downstream of the aerator orifice. The neck and/or bubbles flow around a central gas void within the wake of the aerator. Regular coalescence of the injected gas and the gas void was observed, preventing its depletion.

Cavity Forming (Figure 9c): A gas neck forms from the aerator orifice and, before bubble formation can occur, coalesces with the gas void in the aerator wake. The gas supply then directly feeds the gas void, which prevents its depletion.

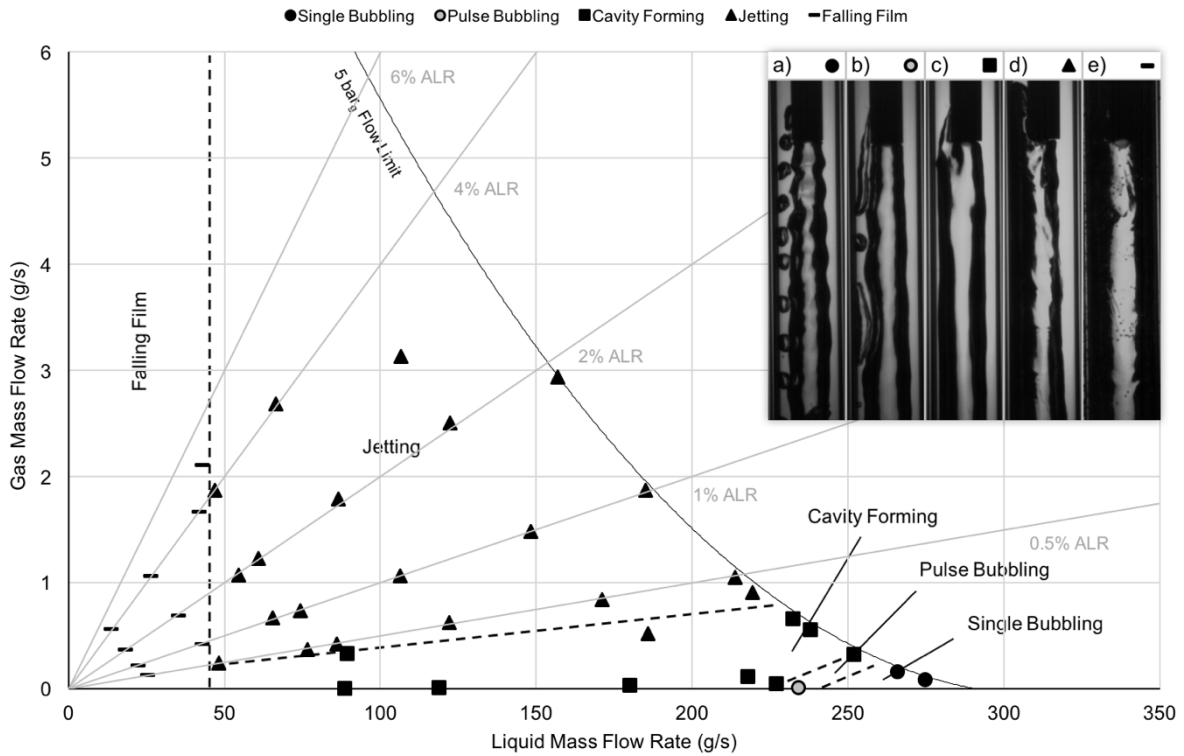


Figure 9. Bubbling regime map for the single hole cross-flow aerator (A2). Regions of interest marked and labelled. a) Single Bubbling; b) Pulse Bubbling; c) Cavity Forming; d) Jetting; e) Falling Film.

Jetting (Figure 9d): The injected gas-phase has sufficient momentum to be emitted as a jet, which hits the mixing chamber wall. The gas jet coalesces with the gas void in the aerator wake, preventing its depletion.

Falling Film (Figure 9e): As observed with aerator A1, the upward buoyancy of the injected gas causes a gas void to rise above the aerator. The injected gas is supplied directly into the gas void and the liquid flows around the mixing chamber periphery.

The two-phase flow regimes were measured 108 mm downstream of the aerator orifice. Four distinct flow regimes were identified across all operating conditions. Plotting these occurrences against their corresponding operating conditions produced the flow regime map shown in Figure 10, with the flow regime regions marked and labelled.

Bubbly Flow (through annular shearing) (Figure 10a): As observed with aerator A1, bubbles are formed far downstream of the aerator via shearing of the annular gas core. In this case, bubbles formed at the aerator flow around the core, regularly coalescing with it.

Slug Flow (through annular shearing) (Figure 10b): A process akin to Bubbly Flow (through annular shearing), however irregularly sized bubbles (i.e. slugs) are sheared from the annular core far downstream of the aerator. Bubbles formed at the aerator flow around the core, regularly coalescing with it.

Annular Flow (Figure 10c): As observed with aerator A1, a continuous gaseous core is formed in the mixing chamber, with a film of liquid flowing around the periphery. In this case, the annular core is often non-centralised due to the asymmetry of the aerator. Bubbles may also be present in the liquid periphery if formed at the aerator orifice and regularly coalesce with the core.

Falling Film (Figure 10d): A continuation of the Falling Film bubbling regime. A large central gas core exists with liquid flowing in a thin film around the mixing chamber periphery.

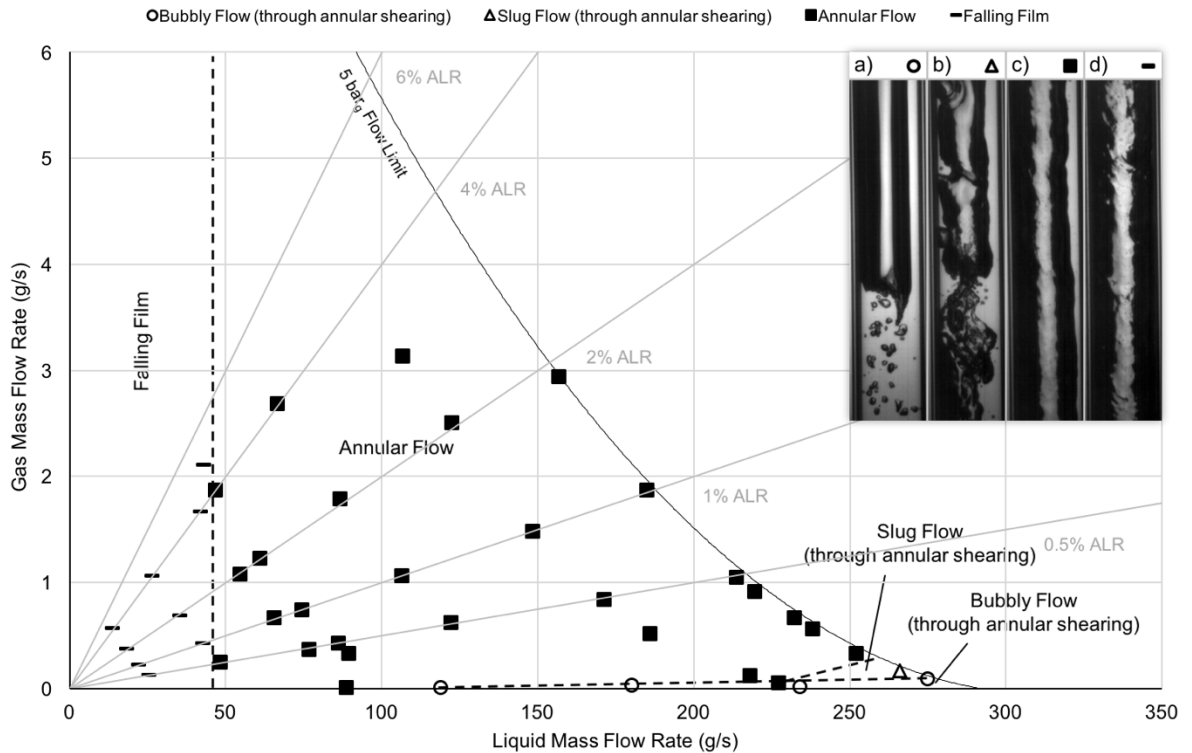


Figure 10. Flow regime map for the single hole cross-flow aerator (A2). Regions of interest marked and labelled. a) Bubbly Flow (through annular shearing); b) Slug Flow (through annular shearing); c) Annular Flow; d) Falling Film.

3.3 Multi-Holed Cross-Flow Aerator [Aerator A3]

The gas-phase was injected through sixteen 0.75 mm diameter holes in the side wall of the aerator, into a liquid co-flow. Four distinct bubbling regimes were observed across all operating conditions for this aerator. Plotting these occurrences against their corresponding operating conditions produced the bubbling regime map shown in Figure 11, with the bubbling regime regions marked and labelled.

Single Bubbling (Figure 11a): As observed with aerator A2, discrete bubbles are formed at the aerator and flow around an established gas void present in the aerator wake.

Pulse Bubbling (Figure 11b): The gas-phase is emitted for the aerator orifice as a rippling neck of gas. Large, irregularly sized bubbles are formed at the aerator tip in a chaotic manner. Unlike the Pulse Bubbling regime observed with aerator A2, there does not appear to be a gas void generated in the aerator wake.

Jetting (Figure 11c): The injected gas-phase has sufficient momentum to hit the mixing chamber. Large, irregularly sized slugs are formed at the aerator tip. Unlike the Jetting bubbling regime reported for aerator A2, there does not appear to be a gas void generated in the aerator wake.

Falling Film (Figure 11d): As observed with aerators A1 and A2, the upward buoyancy of the injected gas causes a gas void to rise above the aerator. The injected gas is supplied directly into the gas void and the liquid flows around the mixing chamber periphery.

The two-phase flow regimes were measured 108 mm downstream of the aerator orifice. Six distinct flow regimes were identified across all operating conditions. Plotting these occurrences against their corresponding operating conditions produced the flow regime map shown in Figure 12, with the flow regime regions marked and labelled.

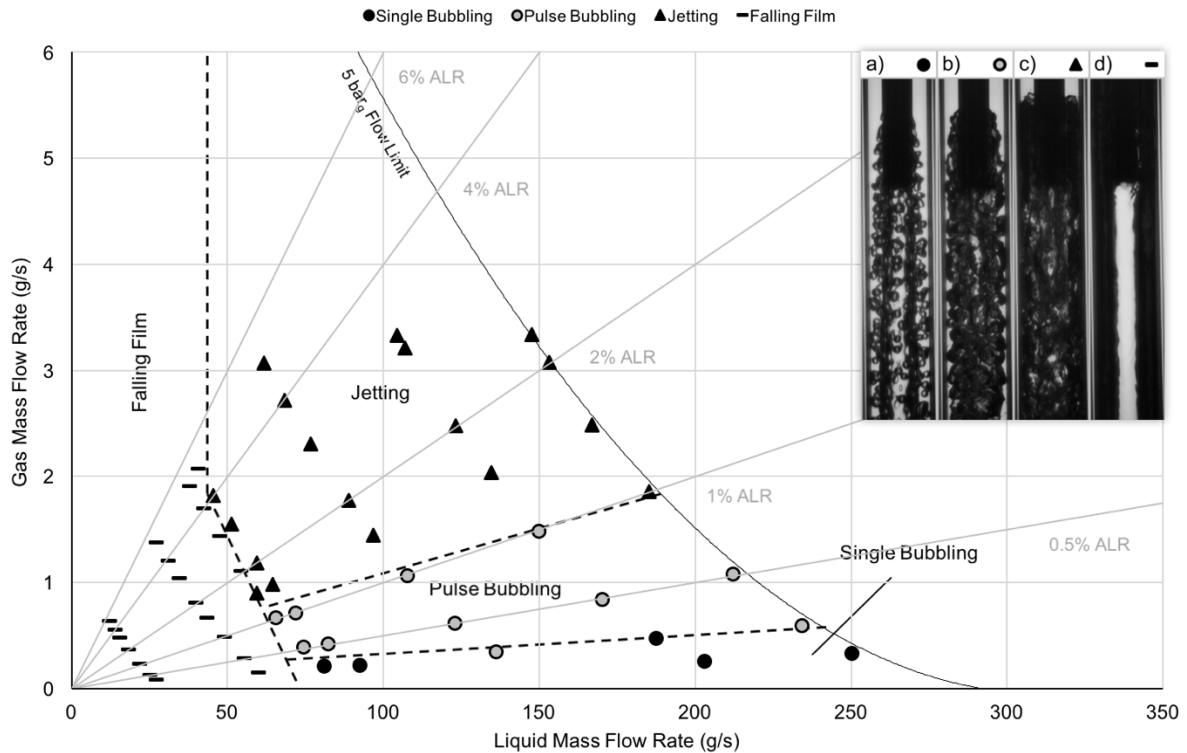


Figure 11. Bubbling regime map for the multi-holed cross-flow aerator (A3). Regions of interest marked and labelled.

a) Single Bubbling; b) Pulse Bubbling; c) Jetting; d) Falling Film.

Bubbly Flow (through annular shearing) (Figure 12a): As observed with aerators A1 and A2, bubbles are formed far downstream of the aerator via shearing of the annular gas core. In this case, bubbles formed at the aerator flow around the core, regularly coalescing with it.

Annular Flow (Figure 12b): As observed with aerators A1 and A2, a continuous gaseous core is formed in the mixing chamber, with a film of liquid flowing around the periphery. Bubbles may also be present in the liquid periphery if formed at the aerator orifice and regularly coalesce with the core.

Slug Flow (through annular shearing) (Figure 12c): As observed with aerator A2, irregularly sized bubbles are sheared from the annular core far downstream of the aerator. Bubbles formed at the aerator flow around the aerator core. Some coalesce with the gas void.

Slug Flow (Figure 12d): Irregularly sized bubbles are formed at the aerator. The gas flow rate is sufficient low for the bubbles to exist within a liquid continuum. Some bubbles coalesce to form large slugs.

Churn Flow (Figure 12e): Irregularly sized bubbles are formed at the aerator. Neither phase is continuous. Some bubbles coalesce to form large slugs.

Falling Film (Figure 12f): A continuation of the Falling Film bubbling regime. A large central gas core exists with liquid flowing in a thin film around the mixing chamber periphery.

4. Discussion

As discussed in the Introduction, Bubbly Flow is generally the preferred flow regime for an effervescent atomiser and, therefore, the role of an aerator is to produce discrete bubbles to supply the mixing chamber. The results demonstrated that, contrary to expectations, the configuration of aerator geometry has a significant effect on bubble formation phenomena and hence the observed flow regime. This is predicted to affect significantly the atomisation performance of an inside-out effervescent atomiser.

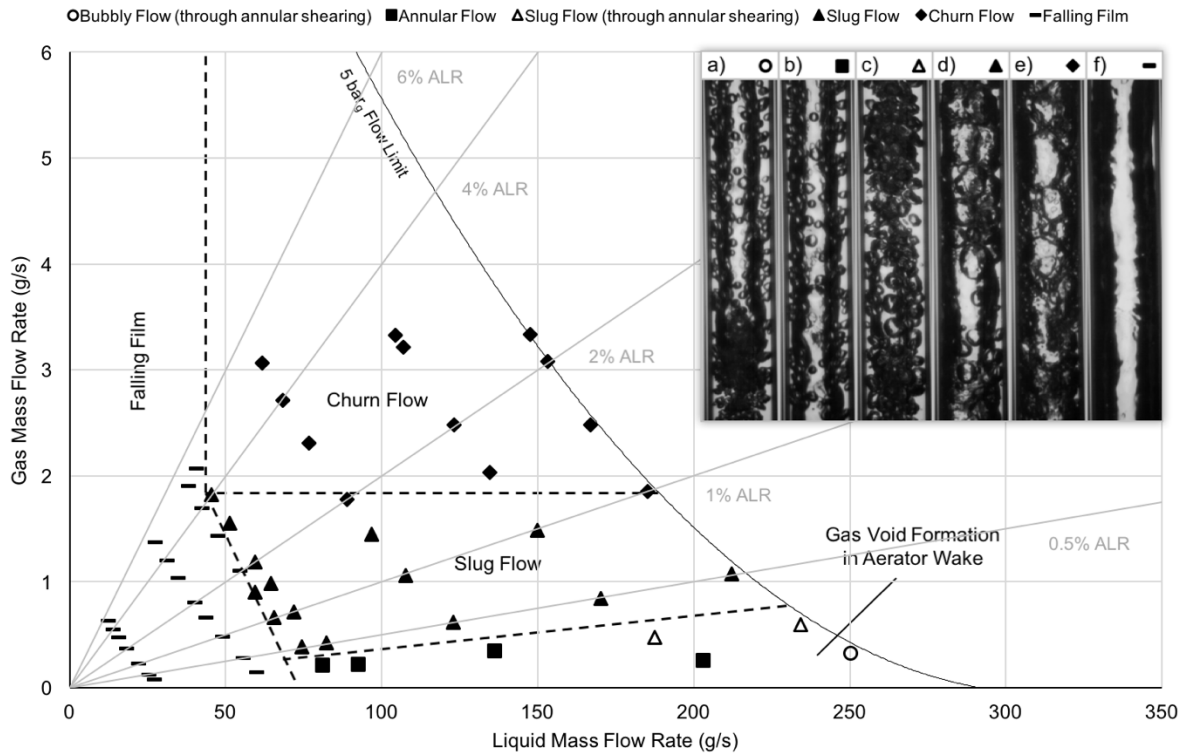


Figure 12. Flow regime map for the multi-holed cross-flow aerator (A3). Regions of interest marked and labelled.
a) Bubbly Flow (through annular shearing); b) Annular Flow; c) Slug Flow (through annular shearing);
d) Slug Flow; e) Churn Flow; f) Falling Film.

The aeration orifice orientation was found to be important, where bubble formation was only observed for cross-flow aerators. The results indicate that high liquid shear is critical to enabling bubble detachment, as bubble formation was seen to be encouraged by injection into the liquid flow around the aerator (i.e. where the superficial liquid velocity is highest) and increasing liquid flow rates. It can therefore be inferred that reducing the mixing chamber diameter would increase bubble formation at the aerator, although further research would be required to confirm this hypothesis.

As expected, the flow regime was observed to vary with differing input gas and liquid mass flow rates, however, bubbly flow was only observed through an annular shearing mechanism. Bubble formation in this manner was seen to be highly sensitive to operating conditions, requiring high liquid flow rate and very low gas flow rate – it is therefore not thought to be suitable for effervescent atomisation.

Each test condition was achieved by activating the gas supply prior to liquid, and therefore the atomiser is not initially bled of gas – this start-up procedure is considered applicable to the majority of potential industrial applications. Consequently, a gas void was commonly observed to form in the aerator wake where the detachment mechanisms (e.g. the drag of the liquid flow and the injected gas momentum) were not sufficient to separate it. Therefore, the generation of a bubbly flow through bubbling at the aerator was prevented, as the gas void was seen to displace the bubbles from the centre of the mixing chamber and force them to flow around a thin liquid periphery. Furthermore, the close exposure of the bubbles to this wake encourages coalescence and hence the gas void is not seen to deplete over time. It is predicted that an aerator with a wake reducing tip could prevent the attachment of this gas void and hence enable the bubbles formed at the aerator orifice to form a bubbly flow.

None of the atomiser configurations tested are therefore deemed suitable for inside-out effervescent atomisation due to their inability to generate a stable bubbly flow. The current results demonstrate that multi-holed cross-flow aerators produce bubbles under the widest range of flow conditions, however further research should be completed to investigate prevention of a gas void forming in wake of the aerator.

5. Conclusions

- A qualitative shadowgraphy investigation of three aerator designs was performed on a transparent inside-out effervescent atomiser.

- Refraction through a transparent cylindrical mixing chamber was shown to be minimised by utilising the “water tunnel” effect, enabling accurate optical measurement of internal two-phase gas-liquid flow.
- Bubbling was only observed from aerators injecting into a liquid cross flow, suggesting that bubble formation at the aerator orifice is encouraged by exposure to high liquid shear.
- A multi-holed aerator design produced bubbles under the widest range of flow conditions.
- The flow regime was observed to vary with differing input gas and liquid mass flow rates, however, Bubbly Flow was only observed through an annular shearing mechanism. Bubble formation in this manner was highly sensitive to operating conditions and is not considered suitable for effervescent atomisation.
- An annular gas void was commonly formed in the wake of the aerator, which prevented bubbling at the aerator from generating Bubbly Flow within the mixing chamber. It is recommended that further research be completed to investigate the effect of reducing the aerator wake.

Nomenclature

ALR Air-to-liquid ratio

References

- [1] Forrester, S. E. and Rielly, C. D. 1998. *Bubble formation from cylindrical, flat and concave sections exposed to a strong liquid cross-flow*. Chemical Engineering Science 53(8), pp. 1517-1527.
- [2] Brennen, CE. 2005. *Fundamentals of Multiphase Flow*. Cambridge University Press, pp 170.
- [3] Sojka, P. E. and Lefebvre, A. H. 1990. *A Novel Method of Atomizing Coal-Water Slurry Fuels*. Indiana, United States of America: Purdue University.
- [4] Lefebvre, A. H. and Chen, S. K. 1994. *Discharge Coefficients for Plain-Orifice Effervescent Atomizers*. 4(3), pp. 275-290.
- [5] Gomez, J. 2010. *Influence of bubble size on an effervescent atomization*. University of Alberta.
- [6] Kim, J. Y. and Lee, S. Y. 2001. *Dependence of spraying performance on the internal flow pattern in effervescent atomizers*. Atomization and Sprays 11(6), pp. 735-756.
- [7] Jedelsky, J. et al. 2009. Development of an effervescent atomizer for industrial burners. Energy and Fuels 23(12), pp. 6121-6130.
- [8] Rahman, M. A. et al. 2012. *Effects of the gas phase molecular weight and bubble size on effervescent atomization*. International Journal of Multiphase Flow 38(1), pp. 35-52.
- [9] Wang, X. F. et al. eds. 1987. *Influence of Gas-Injector Geometry on Atomization Performance of Aerated-Liquid Nozzles*. Pittsburgh, PA, USA. ASME.
- [10] Lefebvre, A. H. 1988. *Novel method of atomization with potential gas turbine applications*. Defence Science Journal 38(4), pp. 353-361.
- [11] Konstantinov, D. et al. 2012. *The Influence of Atomizer Geometry on Effervescent Atomization*. In: 12th Triennial International Conference on Liquid Atomization and Spray Systems. Heidelberg, Germany.
- [12] Ghaemi, S. et al. 2010. *Effect of bubble generation characteristics on effervescent atomization at low gas-liquid ratio operation*. Atomization and Sprays 20(3), pp. 211-225.
- [13] Huang, X. et al. 2008. *Visualization of two phase flow inside an effervescent atomizer*. Journal of Visualization 11(4), pp. 299-308.
- [14] Liu, M. et al. 2011. *Evaluation of unsteadiness in effervescent sprays by analysis of droplet arrival statistics - The influence of fluids properties and atomizer internal design*. Experimental Thermal and Fluid Science 35(1), pp. 190-198.
- [15] Catlin, C. A. and Swithenbank, J. 2001. *Physical processes influencing effervescent atomizer performance in the slug and annular flow regimes*. Atomization and Sprays 11(5), pp. 575-595.
- [16] Jagannathan, T. K. et al. 2011. *Effect of ultrasound on bubble breakup within the mixing chamber of an effervescent atomizer*. Chemical Engineering and Processing: Process Intensification 50(3), pp. 305-315.

APPENDIX 2: LITERATURE REVIEW

A2.1 Experiment Details

PAPER DETAILS				EXPERIMENT DETAILS		
Author	Title	Year	Source	Independent Parameters Investigated	Dependent Parameters Investigated	Experimental Techniques
Broniarz-Press, L. et al.	Atomization of PEO aqueous solutions in effervescent atomizers	2010	Original publication	1. ALR 2. Fluid properties 3. Aerator design 4. Exit orifice design	1. Droplet size 2. Near nozzle spray structure	1. Spray imaging
Broukal, J. and Hájek, J.	Validation of an effervescent spray model with secondary atomization and its application to modeling of a large-scale furnace	2011	Original publication	None	1. Droplet size 2. Validation of theoretical Droplet size model 3. Combustion simulation	1. PDA
Buckner, H. N. and Sojka, P. E.	Effervescent atomization of high-viscosity fluids: part I. Newtonian liquids	1991	Sovani, S. D. et al. 2001.	-	1. Droplet size	-
Buckner, H. N. et al.	Effervescent atomization of coal-water slurries	1990	Sovani, S. D. et al. 2001.	-	1. Droplet size	-
Bush, S. G. and Sojka, P. E.	Entrainment by effervescent sprays at low mass flow rates	1993	Sovani, S. D. et al. 2001.	-	1. Entrainment	-
Bush, S. G. et al.	Momentum rate probe for use with two-phase flows	1996	Sovani, S. D. et al. 2001.	-	1. A probe for measurement of effervescent spray momentum rate	-
Catlin, C. A. and Swithenbank, J.	Physical processes influencing effervescent atomizer performance in the slug and annular flow regimes	2001	Original publication	1. ALR 2. Operating pressure 3. Exit orifice design	1. Droplet size 2. Internal flow visualisation 3. Near nozzle spray structure 4. Spray instability 5. Discharge coefficient	1. Internal flow imaging 2. Spray imaging 3. Laser diffraction
Chen, S. K. et al.	Influence of ambient air pressure on effervescent atomization	1993	Sovani, S. D. et al. 2001.	-	1. Droplet size	-
Ferreira, M. and Teixeira, J. C.	Application of variance analysis to the combustion of residual oils	2012	Original publication	1. ALR 2. Operating pressure 3. Swirl 4. Excess air	1. Combustion testing	-
Flachs Nielsen, A. et al.	Investigation and comparison of performance of effervescent and standard pneumatic atomizer intended for soluble aqueous coating	2006	Original publication	1. Comparison with air-blast 2. ALR 3. Liquid mass flow rate 4. Fluid properties	1. Droplet sizing	1. Laser diffraction
Gadgil, H. et al.	Mass distribution studies in effervescent sprays	2011	Original publication	1. ALR	1. Near nozzle spray structure 2. Patternation 3. Spray instability	1. Spray imaging (planar)
Geckler, S. C. and Sojka, P. E.	Effervescent atomization of viscoelastic liquids: Experiment and modeling	2008	Original publication	1. ALR 2. Fluid properties	1. Droplet size 2. Near nozzle spray structure	1. Laser diffraction 2. Spray imaging
Geckler, S. C. and Sojka, P. E.	High mass flow rate effervescent atomization of viscoelastic fluids	1993	Sovani, S. D. et al. 2001.	-	1. Droplet size 2. Near nozzle spray structure	-
Ghaemi, S. et al.	Effect of bubble generation characteristics on effervescent atomization at low gas-liquid ratio operation	2010	Original publication	1. Aerator design	1. Droplet size 2. Near nozzle spray structure 3. Internal flow visualisation	1. Internal flow imaging 2. Spray imaging
Gomez, J.	Influence of bubble size on an effervescent atomization	2010	Original publication	1. ALR 2. Liquid mass flow rate 3. Bubble breaker design	1. Droplet size 2. Droplet velocity 3. Internal flow quantification	1. Internal flow imaging 2. Spray imaging
Hájek, J. et al.	Analysis of effervescent spray quality for oil-fired furnace application	2015	Original publication	1. ALR 2. Operating pressure	1. Droplet size 2. Droplet velocity 3. Spray instability 4. Near nozzle spray structure 5. Gas entrainment	1. Spray imaging 2. PDA
Hampel, U. et al.	Miniature conductivity wire-mesh sensor for gas-liquid two-phase flow measurement	2009	Original publication	1. ALR 2. Operating pressure	1. Internal flow visualisation	1. Wire mesh sensor
Hong, M. et al.	Unsteadiness of the internal flow in an effervescent atomizer nozzle	2014	Original publication	1. ALR 2. Liquid mass flow rate	1. Internal flow visualisation 2. Near nozzle spray structure 3. Pressure analysis	1. Internal flow imaging 2. Spray imaging
Huang, X. et al.	Characterization of an effervescent atomization water mist nozzle and its fire suppression tests	2011	Original publication	1. ALR 2. Operating pressure	1. Droplet size 2. Droplet velocity	1. PDA
Huang, X. et al.	Visualization of two phase flow inside an effervescent atomizer	2008	Original publication	1. ALR 2. Operating pressure 3. Liquid mass flow rate	1. Internal flow visualisation 2. Droplet size 3. Droplet velocity	1. Internal flow imaging 2. PDA
Jagannathan, T. K. et al.	Effect of ultrasound on bubble breakup within the mixing chamber of an effervescent atomizer	2011	Original publication	1. Bubble breaker design 2. ALR	1. Internal flow quantification 2. Spray cone angle 3. Near nozzle spray structure	1. Internal flow imaging 2. Spray imaging
Jedelský, J. and Jicha, M.	Energy conversion during effervescent atomization	2013	Original publication	1. ALR 2. Operating pressure	1. Droplet size 2. Near nozzle spray structure 3. Spray efficiency	1. Spray imaging 2. Infrared thermography
Jedelský, J. and Jicha, M.	Spray characteristics and liquid distribution of multi-hole effervescent atomizers for industrial burners	2016	Original publication	1. ALR 2. Operating pressure	1. Droplet size distribution 2. Droplet velocity distribution 3. Spray cone angle 4. Spray instability	1. Spray imaging 2. PDA
Jedelský, J. et al.	Development of an effervescent atomizer for industrial burners	2009	Original publication	1. ALR 2. Operating pressure 3. Mixing chamber design 4. Mixing length 5. Aerator design	1. Droplet size	1. PDA
Jedelský, J. et al.	Characterization of spray generated by multihole effervescent atomizer and comparison with standard Y-jet atomizer	2003	Original publication	1. ALR 2. Operating pressure	1. Droplet size 2. Spray mass flux	1. PDA 2. PLIF
Jedelský, J. et al.	Discharge coefficient and operational flow characteristics of multihole effervescent atomizer	2003	Original publication	1. ALR 2. Operating pressure 3. Mixing chamber design 4. Aerator design	1. Discharge coefficient	-

PAPER DETAILS				EXPERIMENT DETAILS		
Author	Title	Year	Source	Independent Parameters Investigated	Dependent Parameters Investigated	Experimental Techniques
Jedelský, J. et al.	Effervescent Atomizer: Influence of the Operation Conditions and Internal Geometry on Spray Structure Study Using PIV-PIV	2008	Original publication	1. ALR 2. Operating pressure 3. Mixing chamber design 4. Aerator design 5. Exit orifice design	1. Droplet velocity 2. Spray mass flux 3. Spray cone angle	1. PIV 2. PIV
Jobehtar, M. H.	Experimental Study of Two-Phase Flow in a Liquid Cross-Flow and an Effervescent Atomizer	2014	Original publication	1. ALR 2. Aerator design 3. Bubble breaker design	1. Internal flow quantification (refraction minimised) 2. Droplet size 3. Droplet velocity	1. Internal flow imaging 2. Spray imaging
Kermes, V. and Štěpánek, P.	Biodiesel (FN 14213) heating oil substitution potential for petroleum based light heating oil in a 1 MW stationary combustion facility	2013	Original publication	1. ALR 2. Fluid properties	1. Combustion testing	-
Kim, J. Y. and Lee, S. Y.	Dependence of spraying performance on the internal flow pattern in effervescent atomizers	2001	Original publication	1. ALR 2. Operating pressure 3. Exit orifice design	1. Internal flow visualisation 2. Droplet size 3. Near nozzle spray structure	1. Internal flow imaging 2. Spray imaging
Konstantinov, D. D.	Effervescent Atomisation for Complex Fuels including Bio-Fuels	2012	Original publication	1. ALR 2. Operating pressure 3. Exit orifice design 4. Mixing chamber design 5. Atomiser design 6. Fluid properties	1. Droplet size 2. Droplet velocity 3. Intrainment	1. PDA
Kourmatzis, A. et al.	Combined effervescent and airblast atomization of a liquid jet	2016	Original publication	1. ALR 2. Air-blast velocity	1. Near nozzle spray structure 2. Droplet velocity 3. Spray instability	1. Spray imaging 2. LDA
Lee, W. Y. and Sojka, P. E.	Influence of fluid viscoelasticity on low mass flow rate effervescent atomization	1993	Sovani, S. D. et al. 2001.	-	1. Droplet size	-
Lefebvre, A. H.	Novel method of atomization with potential gas turbine applications	1988	Original publication	1. ALR 2. Operating pressure 3. Exit orifice design 4. Aerator design	1. Droplet size 2. Discharge coefficient	-
Lefebvre, A. H. et al.	Spray characteristics of aerated-liquid pressure atomizers	1988	Sovani, S. D. et al. 2001.	-	1. Droplet size	-
Li, J. et al.	Effervescent atomizers for small gas turbines	1994	Sovani, S. D. et al. 2001.	-	1. Droplet size 2. Patternation	-
Liu, M. et al.	Evaluation of effervescent atomizer internal design on the spray unsteadiness using a phase/Doppler particle analyzer	2010	Original publication	1. ALR 2. Operating pressure	1. Internal flow visualisation 2. Near nozzle spray structure 3. Droplet size 4. Droplet velocity 5. Spray instability	1. Internal flow imaging 2. Spray imaging 3. PDA
Liu, M. et al.	Evaluation of unsteadiness in effervescent sprays by analysis of droplet arrival statistics - The influence of fluids properties and atomizer internal design	2011	Original publication	1. ALR 2. Fluid properties	1. Internal flow visualisation 2. Droplet size 3. Spray instability	1. Internal flow imaging 2. PDA
Lörcher, M. and Mewes, D.	Atomization of liquids by two-phase gas-liquid flow through a plain-orifice nozzle: Flow regimes inside the nozzle	2001	Original publication	1. Operating pressure 2. Atomiser configuration	1. Wire mesh sensor parameters 2. Internal flow visualisation 3. Near nozzle spray structure	1. Internal flow imaging 2. Spray imaging 3. Wire mesh sensor
Lörcher, M. et al.	Effervescent atomization of liquids	2005	Original publication	1. Void fraction (~ALR) 2. Operating pressure 3. Atomiser configuration	1. Internal flow visualisation 2. Void fraction measurement 3. Validation of theoretical critical mass model	1. Internal flow imaging 2. Wire mesh sensor
Lubarsky, E. and Levy, Y.	Experimental investigation of flame-holding system for the suppression of ramjet rumble	1998	Original publication	None	1. Droplet velocity 2. Combustion testing	1. PDA 2. PIV
Lund, M. T. et al.	The influence of Atomizing Gas Molecular Weight on Low Mass Flowrate Effervescent Atomizer Performance	1998	Original publication	1. ALR 2. Operating pressure 3. Fluid properties	1. Droplet size 2. Droplet velocity	1. Laser diffraction 2. PDA
Lund, M. T. et al.	Effervescent atomization at low mass flow rates. Part I: the influence of surface tension	1993	Sovani, S. D. et al. 2001.	-	1. Droplet size	-
Luong, J. T. K. and Sojka, P. E.	Unsteadiness in effervescent sprays	1999	Sovani, S. D. et al. 2001.	-	1. Droplet size	-
Ma, X. et al.	Atomization of petroleum-coke sludge slurry using effervescent atomizer	2013	Original publication	1. ALR 2. Operating pressure 3. Fluid properties	1. Droplet size	1. Laser diffraction
Mikvik, M. et al.	Twin-fluid atomization of viscous liquids: The effect of atomizer construction on breakup process, spray stability and droplet size	2015	Original publication	1. Atomiser configuration 2. ALR 3. Operating pressure	1. Droplet size 2. Near Nozzle Spray Structure 3. Spray instability	1. Laser diffraction 2. Spray imaging
Ochowiak, M.	The experimental study on the viscosity effect on the discharge coefficient for effervescent atomizers	2013	Original publication	1. ALR 2. Fluid properties	1. Discharge Coefficient	-
Ochowiak, M.	The effervescent atomization of oil-in-water emulsions	2012	Original publication	1. ALR 2. Fluid properties 3. Exit orifice design	1. Droplet size	1. Spray imaging
Ochowiak, M. et al.	The discharge coefficient of effervescent atomizers	2010	Original publication	1. ALR 2. Exit orifice design	1. Discharge coefficient	-

PAPER DETAILS				EXPERIMENT DETAILS		
Author	Title	Year	Source	Independent Parameters Investigated	Dependent Parameters Investigated	Experimental Techniques
Ochowiak, M. et al.	Characteristics of spray angle for effervescent-swirl atomizers	2015	Original publication	1. AIR 2. Fluid properties 3. Exit orifice design	1. Spray cone angle	1. Spray imaging
Ochowiak, M. et al.	The effect of extensional viscosity on the effervescent atomization of polyacrylamide solutions	2012	Original publication	1. AIR 2. Fluid properties	1. Droplet size 2. Near nozzle spray structure	1. Spray imaging
Panchagnula, M. V. and Sojka, P. E.	Spatial droplet velocity and size profiles in effervescent atomizer-produced sprays	1999	Original publication	1. AIR 2. Liquid mass flow rate	1. Droplet size 2. Droplet velocity	1. PDA
Petersen, F. J. et al.	Effervescent atomization of aqueous polymer solutions and dispersions	2001	Original publication	1. AIR 2. Operating pressure 3. Fluid properties	1. Droplet size	1. Laser diffraction
Petersen, F. J. et al.	Design and Atomization Properties for an Inside-Out Type Effervescent Atomizer	2004	Original publication	1. AIR 2. Exit orifice design 3. Aerator design	1. Droplet size	1. Laser diffraction
Rahman, M. A. et al.	Effects of the gas phase molecular weight and bubble size on effervescent atomization	2012	Original publication	1. AIR 2. Fluid properties	1. Internal flow quantification 2. Validation of multiple internal flow models 3. Near nozzle spray structure 4. Droplet size	1. Internal flow imaging 2. Spray imaging 3. PDA
Roesler, T. C. and Lefebvre, A. H.	Studies on aerated-liquid atomization	1987	Sovani, S. D. et al. 2001.	–	1. Droplet size	–
Sankar, S. V. et al.	Swirl effervescent atomizer for spray combustion	1995	Sovani, S. D. et al. 2001.	–	1. Droplet size	–
Santangelo, P. J. and Sojka, P. E.	A holographic investigation of the near-nozzle structure of an effervescent atomizer-produced spray	1995	Sovani, S. D. et al. 2001.	–	1. Near nozzle spray structure	–
Schröder, J. et al.	Characterization of gelatinized corn starch suspensions and resulting drop size distributions after effervescent atomization	2011	Original publication	1. AIR 2. Operating pressure 3. Mixing chamber design 4. Exit orifice design 5. Fluid properties	1. Droplet size	1. Laser diffraction
Schröder, J. et al.	Viscosity ratio: A key factor for control of oil drop size distribution in effervescent atomization of oil-in-water emulsions	2012	Original publication	1. AIR 2. Fluid properties	1. Droplet size	1. Laser diffraction
Sen, D. et al.	Bubble formation and flow instability in an effervescent atomizer	2014	Original publication	1. AIR	1. Internal flow visualisation	1. Internal flow imaging
Sojka, P. E. and Lefebvre, A. H.	A novel method of atomizing coal-water slurry fuels	1990	Original publication	1. AIR 2. Fluid properties	1. Droplet size 2. Nozzle efficiency	1. Internal flow imaging 2. Spray imaging 3. PDA 4. Laser diffraction
Sovani, S. D. et al.	High pressure effervescent atomization: Effect of ambient pressure on spray cone angle	2001	Original publication	1. AIR 2. Operating pressure	1. Spray cone angle 2. Validation of theoretical spray cone angle model 3. Near nozzle spray structure	1. Spray imaging
Sovani, S. D. et al.	Structure and steady-state spray performance of an effervescent diesel injector	2005	Original publication	1. AIR 2. Operating pressure 3. Aerator design 4. Exit orifice design 5. Needle lift	1. Droplet size 2. Spray cone angle 3. Near nozzle spray structure	1. Spray imaging 2. Laser diffraction
Stähle, P. et al.	Influence of feed viscosity on the two-phase flow inside the exit orifice of an effervescent atomizer and on resulting spray characteristics	2015	Original publication	1. Liquid mass flow rate 2. Fluid properties	1. Droplet size 2. Near nozzle spray structure 3. Gas-phase distribution	1. Internal optical sensor 2. Spray imaging
Stähle, P. et al.	Comparison of an Effervescent Nozzle and a Proposed Air-Core-Liquid-Ring (ACLRL) Nozzle for Atomization of Viscous Food Liquids at Low Air Consumption	2015	Original publication	1. Atomiser configuration 2. Fluid properties	1. Internal flow visualisation 2. Droplet size 3. Spray unsteadiness	1. Internal flow imaging 2. Laser diffraction
Stähle, P. et al.	Investigation on the Applicability of the Effervescent Atomizer in Spray Drying of Foods: Influence of Liquid Viscosity on Nozzle Internal Two-Phase Flow and Spray Characteristics	2015	Original publication	1. Liquid mass flow rate 2. Fluid properties	1. Internal flow visualisation 2. Droplet size 3. Spray unsteadiness	1. Internal flow imaging 2. Laser diffraction
Sun, C. et al.	Time-frequency analysis of acoustic and unsteadiness evaluation in effervescent sprays	2015	Original publication	1. AIR 2. Liquid mass flow rate	1. Acoustic emission 2. Spray instability	1. Acoustic emission 2. Spray imaging
Sutherland, J. J. et al.	Entrainment by ligament-controlled effervescent atomizer-produced sprays	1997	Original publication	1. AIR 2. Liquid mass flow rate 3. Fluid properties	1. Droplet size 2. Droplet velocity 3. Entrainment	1. Entrainment device 2. PDA
Sutherland, J. J. et al.	Ligament-controlled effervescent atomization	1997	Sovani, S. D. et al. 2001.	–	1. Droplet size	–
Wade, R. A. et al.	Effervescent atomization at injection pressures in the MPa range	1999	Sovani, S. D. et al. 2001.	–	1. Droplet size 2. Spray cone angles	–
Wang, X. F. et al.	Influence of gas-injector geometry on atomization performance of aerated-liquid nozzles	1987	Sovani, S. D. et al. 2001.	–	1. Droplet size	1. Laser diffraction
Whitlow, J. D. and Lefebvre, A. H.	Effervescent atomizer operation and spray characteristics	1993	Sovani, S. D. et al. 2001.	–	1. Patternation	–
Yu, G. et al.	An experimental study of kerosene combustion in a supersonic model combustor using effervescent atomization	2005	Original publication	1. AIR 2. Operating pressure	1. Combustion testing	1. Flame imaging 2. Schlieren imaging 3. PLIF

A2.2 Fluid Properties and Operating Conditions

PAPER DETAILS				FLUID PROPERTIES					OPERATING CONDITIONS			
Author	Title	Year	Source	Liquid Name	Liquid Type	Density (kg/m ³)	Viscosity Range (kg/m ² s)	Surface Tension (N/m)	Mixing Gas	Air-to-Liquid Ratio (%)	Operating Pressure (bar)	Liquid Mass Flow Rate (g/s)
Bouvier-Peyre, L. et al.	Atomization of PED aqueous solutions in effervescent atomizers	2010	Original publication	[1] Water; [2] Various PED polymers	Single component; [1] Newtonian; [2] non-Newtonian	998.2	[1] 0.004-12; 0.289-0.95; 0.002-0.001	0.072	Air	2.8-6.3%	Not mentioned	1.4-1.1
Boudal, J. and Wojcik, I.	Validation of an effervescent spray model with secondary atomization and its application to modeling of a large-scale furnace	2011	Original publication	Fine-light fuel-oil	Single component; Newtonian	870.7	0.0185	0.0297	Air	10%	3	21.6
Budner, H. N. and Sotka, P. E.	Effervescent atomization of high-viscosity fluids: part I: Newtonian fluids	1991	Soven, S. D. et al. 2021.	Glycerine-water mixture	Two-component; non-Newtonian	~1225	0.4-0.968	-	Air	5-62%	8.8-20	-
Budner, H. N. et al.	Effervescent atomization of cool-water slurries	1990	Soven, S. D. et al. 2021.	Cool water slurry	Two-component; non-Newtonian	~1000	-	-	Air	4-10%	2.5-10.5	-
Burn, S. G. and Sotka, P. E.	Entrainment by effervescent sprays at low mass flow rates	1993	Soven, S. D. et al. 2021.	Water and hydrocarbon oils	Single component; Newtonian	Not mentioned	0.004-0.021	-	Air	2-10%	Not mentioned	-
Burn, S. G. et al.	Numerical rate price for use with Newtonian flows	1996	Soven, S. D. et al. 2021.	-	-	-	-	-	Air	5-10%	-	-
Collin, C. A. and Switzer-Bayes, J.	Physical processes influencing effervescent atomizer performance in the high and annular flow regimes	2001	Original publication	Water	Single component; Newtonian	1000	0.001	0.072	Air	8.7-15.2%	1.4-4.8	6.7-20
Chen, S. K. et al.	Influence of ambient air pressure on effervescent atomization	1993	Soven, S. D. et al. 2021.	Water	Single component; Newtonian	1000	0.001	0.072	Air	1.8%	1.4-1.8	-
Ferreira, M. and Tegner, J. C.	Application of welfare analysis to the contribution of radial jets	2012	Original publication	Recycled oil	Single component	898	0.046	Not mentioned	Air	25-62%	4.5-5.5	2.75
Hecht-Nielsen, A. et al.	Investigation and comparison of performance of effervescent and standard pneumatic atomizer increase for soluble aqueous coating	2006	Original publication	Mixture of water with [1] Acromalcolac; or [2] Pavecone 8900	Two components; [1] Newtonian; [2] non-Newtonian	Not mentioned	[1] 0.004-0.086; [2] 0.004-0.025; 1.03-1.025; 0.011-2.674	[1] 0.045-0.072; [2] 0.045	Air	8.5-16.6%	Not mentioned	0.16-0.583
Gadgil, V. et al.	Mass distribution studies in effervescent sprays	2011	Original publication	Water	Single component; Newtonian	1000	0.001	0.072	Air	0.1-3.1%	1-4	Not mentioned
Gaskler, S. C. and Sotka, P. E.	Effervescent atomization of viscoelastic liquids: Experiment and modeling	2008	Original publication	Water-glycerin and PED mixture	Three-component; non-Newtonian	1200	0.010-0.018	0.0626-0.0678	Air	2-10%	Not mentioned	Not mentioned
Gaskler, S. C. and Sotka, P. E.	High mass flow rate effervescent atomization of viscoelastic fluids	1993	Soven, S. D. et al. 2021.	Glycerine water polymer mixtures	Three-component; non-Newtonian	~1225	-	-	Air	2-10%	Not mentioned	-
Ghaheri, S. et al.	Effect of bubble generation character on effervescent atomization at low gas-liquid ratio	2010	Original publication	Water	Single component; Newtonian	1000	0.001	0.072	Air	1.48-2.67%	4.1	3.33
Comet, J.	Influence of bubble size on an effervescent atomizer	2010	Original publication	Water	Single component; Newtonian	1000	0.001	0.072	Air	1.4%	6.9-20.7	833-3333
Hight, J. et al.	Analysis of effervescent spray quality for oil-fired furnace application	2015	Original publication	Water	Single component; Newtonian	1000	0.001	0.072	Air	5-15%	0.3-4	8.5-16.7
Hampel, U. et al.	Miniature conductivity wire mesh sensor for gas-liquid two-phase flow measurement	2009	Original publication	Water	Single component; Newtonian	1000	0.001	0.072	Air	0.01-25%	1-5	Not mentioned
Hong, M. et al.	Unsteadiness of the internal flow in an effervescent atomizer nozzle	2014	Original publication	Water	Single component; Newtonian	1200	0.001	0.072	Air	0.001-0.2%	Not mentioned	180-550
Huang, X. et al.	Characterization of an effervescent atomization water mist nozzle and its fire suppression tests	2011	Original publication	Water	Single component; Newtonian	1000	0.001	0.072	Nitrogen	~0.05-20%	2-4	~11.1-31.5
Huang, X. et al.	Visualization of two-phase flow inside an effervescent atomizer	2008	Original publication	Water	Single component; Newtonian	1000	0.001	0.072	Nitrogen	~0.05-20%	1-4	~2.79-16.7

PAPER DETAILS			FLUID PROPERTIES					OPERATING CONDITIONS				
Author	Title	Year	Source	Liquid Name	Liquid Type	Density (kg/m ³)	Viscosity Range (kg/m ² s)	Surface Tension (N/m)	Atomising Gas	Air-to-Liquid Ratio (x)	Operating Pressure (bar)	Liquid Mass Flow Rate (g/s)
Jaganathan, T. K. et al.	Effect of ultrasound on bubble breaking within the mixing chamber of an ultrasonic atomizer	2011	Original publication	Water	Single component, Newtonian	1000	0.001	0.072	Air	0.033-0.063%	1	Not mentioned
Jedlický, J. and Jirka, M.	Energy conversion during effervescent atomization	2013	Original publication	Light heating oil	Single component, Newtonian	874	0.0185	0.0267	Air	3-10%	3-5	Not mentioned
Jedlický, J. and Jirka, M.	Spray characteristics and liquid distribution of multi-hole-effervescent atomizers for industrial burners	2016	Original publication	Light heating oil	Single component, Newtonian	Not mentioned	Not mentioned	Not mentioned	Air	3-10%	2-10	45-182
Jedlický, J. et al.	Development of an effervescent atomizer for industrial burners	2019	Original publication	Light heating oil	Single component, Newtonian	874	0.0185	0.0267	Air	0.6-10%	1-5	16.0-47.1
Jedlický, J. et al.	Characterization of spray generated by multiple effervescent atomizers and comparison with standard V-jet identifier	2020	Original publication	Light heating oil	Single component	Not mentioned	Not mentioned	Not mentioned	Air	3-10%	3-10	7-9-47.5
Jedlický, J. et al.	Drop size coefficient and operational flow characteristics of multiple effervescent atomizer	2020	Original publication	Light heating oil	Single component	Not mentioned	Not mentioned	Not mentioned	Air	3-10%	2-10	7-9-47.5
Jedlický, J. et al.	Effervescent Atomizer: Influence of the Operating Conditions on the Spray Quality Using Froude/Fr	2020	Original publication	Light heating oil	Single component, Newtonian	874	0.0185	0.0267	Air	2-10%	3-10	Not mentioned
Jochims, M. K.	Experimental Study of Two-Phase Flow in a Liquid Cross-Flow and an Effervescent Atomizer	2024	Unpublished	Water	Single component, Newtonian	1000	0.001	0.072	Air	0.53-9.53%	Not mentioned	12.67-24.91
Kern, V. and Eldredsky, P.	Backflow (BFL) heating oil substitution potential for petroleum based heating oil in industrial applications: Operational and field study	2023	Original publication	[1] Motor oil [2] Water [3] Water [4] Water	Single component, Newtonian	[1] 825-882 [2] 1000 [3] 1000 [4] 1000	[1] 0.0015-0.0018 [2] 0.0018 [3] 0.0018 [4] 0.0018	Not mentioned	Not mentioned	10-20%	10	31
Kim, I. Y. and Lee, S. Y.	Dependence of spraying performance on the internal flow pattern in effervescent atomizers	2001	Original publication	Water	Single component, Newtonian	1000	0.001	0.072	Air	0.06-13%	2-4	6.5-66.5

PAPER DETAILS				FLUID PROPERTIES					OPERATING CONDITIONS			
Author	Title	Year	Source	Liquid Name	Liquid Type	Density (kg/m ³)	Viscosity Range (kg/m ³)	Surface Tension (N/m)	Aerosol Gas	Air-to-Liquid Ratio (%)	Operating Pressure (bar)	Liquid Mass Flow Rate (kg/s)
Konstantinov, D. D.	Efficient Atomization for Complex Parts Including also Fuels	2012	Original publication	[1] Water, [2] Water/glycerol solution	[1] Single component, Newtonian; [2] Two-component, Newtonian	[1] 1000; [2] mentioned	[1] 0.001; [2] 0.002-0.01	[1] 0.072; [2] mentioned	Air	0.8-12.2%	~7	10-60
Kourmatzis, A. et al.	Combined effervescent and air-atomized atomization of a liquid jet	2016	Original publication	Water	Single component, Newtonian	1000	0.001	0.072	Air	0-3.8%	1.8	0.87
Lee, W. Y. and Sakai, P. E.	Influence of fluid viscosity on low pressure air effervescent atomization	1993	Sween, S. D., et al. 2021.	Glycerine-water-polymer mixtures	Three-component, non-Newtonian	Not mentioned	-	-	Air	3-12%	3.37-6.53	-
LeFebvre, A. H.	New method of atomization with potential gas turbine applications	1988	Original publication	Water	Single component, Newtonian	1000	0.001	0.072	Nitrogen	Not mentioned	0.35-6.9	Not mentioned
Lefebvre, A. H. et al.	Spray characteristics of atomized liquid pressure atomizers for small gas turbines	1988	Sween, S. D., et al. 2021.	Water	Single component, Newtonian	1000	0.001	0.072	Nitrogen	2.22%	0.0346-6.9	-
Li, J. et al.	Effervescent atomizers for small gas turbines	1994	Sween, S. D., et al. 2021.	Water	Single component, Newtonian	1000	0.001	0.072	Air	15.85%	9.3	-
Lu, M. et al.	Evaluation of effervescent atomizer internal design on the spray characteristics using a phase Doppler particle analyzer	2010	Original publication	Water	Single component, Newtonian	1000	0.001	0.072	Air	0.59-10%	2.4	Not mentioned
Lu, M. et al.	Evaluation of unsteadiness in effervescent sprays by analysis of droplet arrival statistics. The influence of flow properties and atomizer internal design	2011	Original publication	[1] Water, [2] Glycerol/water solution; [3] Various glycerol/water/glycol solutions	[1] Single component, Newtonian; [2] Two-component, Newtonian; [3] Three-component, non-Newtonian	[1] 998; [2] 1200; [3] 1100-1130	[1] 0.001; [2] 0.19; [3] 0.871-0.877	[1] 0.072; [2] 0.064; [3] 0.05-0.068	Air	3-20%	4	10-33
Luchter, M. and Mewes, D.	Atomization of liquids by two-phase gas-liquid flow through a plain-orifice nozzle. Flow regimes inside the nozzle	2001	Original publication	Not mentioned	Not mentioned	Not mentioned	Not mentioned	Not mentioned	Not mentioned	Not mentioned	3-10	Not mentioned
Luchter, M. et al.	Effervescent atomization of liquids	2003	Original publication	Water	Single component, Newtonian	1000	0.001	0.072	Air	0.3-100%	3-15	0.46-27.7
Lubarsky, E. and Levy, Y.	Experimental investigation of flame-holding system for the suppression of pre-ignition	1998	Original publication	Not mentioned	Not mentioned	Not mentioned	Not mentioned	Not mentioned	Not mentioned	Not mentioned	Not mentioned	Not mentioned
Lund, M. T. et al.	The Influence of Atomizing Gas Pressure on the Spray Characteristics of a Two-Phase Effervescent Atomizer	1988	Original publication	Alberts sweet crude oil	Single component, Newtonian	916	0.005	0.03	Helium and carbon dioxide mixture	5-50%	Not mentioned	0.3
Lund, M. T. et al.	Effervescent atomization at low mass flow rates. Part I: The influence of surface tension	1993	Sween, S. D., et al. 2021.	Glycerine-water mixture and SMO oil	Single and two-component, Newtonian	~980	0.001-0.008	-	Air	3-7%	2.39-5.15	-
Luong, J. T. K. and Soliz, P. L.	Unsteadiness in effervescent sprays	1999	Sween, S. D., et al. 2021.	glycerine-water mixture	Two-component, Newtonian	Not mentioned	0.02	-	Air	2%	Not mentioned	-
Mu, X. et al.	Atomization of petroleum coker sludge slurry using effervescent atomizer	2013	Original publication	Petroleum coker sludge slurry (PCS), with varying proportions of sewage sludge	Single component, non-Newtonian	Not mentioned	0.15-0.52%	Not mentioned	Air	2-14%	~6	25-58.3

PAPER DETAILS				FLUID PROPERTIES				OPERATING CONDITIONS				
Author	Title	Year	Source	Liquid Name	Liquid Type	Density (kg/m ³)	Viscosity Range (kg/m.s)	Surface Tension (N/m)	Atomising Gas	Air-to-liquid Ratio (%)	Operating Pressure (bar)	Liquid Mass Flow Rate (g/s)
Milak, M. et al.	Two-fluid atomization of viscous liquids: The effect of atomizer geometry on breakup process, spray stability and droplet size	2015	Original publication	Various water/methanol/free solutions	Two-component, Newtonian	1180-1282	0.06-0.308	0.0782-0.077928	Air	2.5-20%	1.6-3.4	0.25-1.65
Chowdhury, M.	The experimental study on the viscosity effect on the discharge coefficient for effervescent atomizers	2013	Original publication	[1] Water; [2] Various water/glycerol solutions	[1] Single component, Newtonian; [2] Two-component, Newtonian	[1] 1000; [2] 1150-1190	[1] 0.001; [2] 0.015-0.102	0.0715	Air	1.4-5%	Neg mentioned	1.4-1.1
Chowdhury, M.	The effervescent atomization of ethin-water emulsions	2012	Original publication	[1] Water; [2] Various water/mineral oil emulsions	[1] Single component, Newtonian; [2] Two-component, non-Newtonian	[1] 1000; [2] n: 0.78-0.97	[1] 0.001; [2] 0.015	[1] 0.072; [2]	Air	1.6-5%	Neg mentioned	1.4-1.1
Chowdhury, M. et al.	The effect of nozzle geometry on the effect of atomization efficiency on polyethylene solidifiers	2010	Original publication	Water	Single component, Newtonian	1000	0.001	0.072	Air	1.6-6%	Neg mentioned	1.4-1.1
Chowdhury, M. et al.	Characteristics of spray angle for effervescent swirl atomizers	2015	Original publication	[1] Water; [2] Acoustic solutions of glycerol (Various concentrations); [3] Acoustic solutions of isopropyl alcohol; [4] Various solutions of alcohol and Ethanol (Various concentrations)	[1] Single component, Newtonian; [2] Two-component, non-Newtonian; [3] Two-component, non-Newtonian; [4] Two-component, non-Newtonian	[1] 998; [2] 1058-1152; [3] 998; [4] 713-1142	[1] 0.001; [2] 0.002; [3] 0.012; [4] 0.012-0.0716	[1] 0.0716; [2] 0.0716; [3] 0.0716; [4] 0.0716-0.0716	Air	0.2-2%	Neg mentioned	2-11
Chowdhury, M. et al.	The effect of atomization efficiency on the effervescent atomization of polyethylene solidifiers	2012	Original publication	[1] Water/glycerol solution; [2] Various glycerol solutions with various concentrations of glycerol	[1] Two-component, Newtonian; [2] Multi-component, non-Newtonian	Neg mentioned	[1] 0.001; [2] n: 0.385-0.718	0.0715	Neg mentioned	1.6-5%	Neg mentioned	1.4-1.1
Parthasarathy, M. V. and Sollich, P. E.	Signal energy velocity and size prediction of effervescent atomizer produced spray	2009	Original publication	Carbonyl	Single component, Newtonian	1200	0.9	0.07	Air	1.0%	Neg mentioned	20-120
Freeman, F. J. et al.	Effervescent atomization of aqueous polymer solutions and dispersions	2001	Original publication	[1] Water; [2] Aqueous solutions of various polymers	[1] Single component, Newtonian; [2] Two-component	[1] 1000; [2] Neg	[1] 0.001; [2] 0.001-0.228	[1] 0.072; [2] 0.04-0.068	Air	10-80%	3.5-3.9	Neg mentioned
Freeman, F. J. et al.	Scaling and Atomization Properties for an Inlet-Out Type Effervescent Atomizer	2004	Original publication	[1] Water; [2] Water and 10% K-10 solution; [3] Water and 10% phosphaat 019	[1] Single component, Newtonian; [2] Two-component; [3] Two-component	[1] 1000; [2] Neg; [3] Neg	[1] 0.001; [2] 0.005; [3] 0.046	[1] 0.071; [2] 0.06; [3] 0.044	Air	10-50%	11.72	Neg mentioned
Palumbo, M. A. et al.	Effects of the RB phase molecular weight and molecular weight on the spray characteristics of effervescent atomization	2012	Original publication	Water	Single component, Newtonian	1000	0.001	0.072	Air	1-6%	4.3-6.8	40-110
Rochow, T. C. and Lufkin, A. H.	Studies of air-aid liquid atomization	1987	Smart, S. B. et al. 2001.	Water	Single component, Newtonian	1000	0.002	0.073	Air	0.1-5%	1.78-6.9	-
Sankar, S. V. et al.	Smart effervescent atomizer for spray combustion	1995	Smart, S. B. et al. 2001.	Water	Single component, Newtonian	1000	0.001	0.072	Air	5-35%	1.38-4.14	-
Sankar, S. V. et al.	A topographic investigation of the microstructure of spray	1995	Smart, S. B. et al. 2001.	Water-con (various mixture and SMC III)	Single and two component, Newtonian	1068-1235	0.1-0.82	-	Nitrogen	1-10%	1.02-30.88	-
Schroeder, J. et al.	Characterization of gas-liquid atomization experiments using acoustic phase detection	2011	Original publication	Various water/glycerol (CS)	Two-component	Neg mentioned	0.01-0.1	0.072	Air	5-20%	0.2-4.2	Neg mentioned

PAPER DETAILS				FLUID PROPERTIES				OPERATING CONDITIONS				
Author	Title	Year	Source	Liquid Name	Liquid Type	Density (kg/m ³)	Viscosity Range (kg/m.s)	Surface Tension (N/m)	Atomizing Gas	Air-Liquid Ratio (%)	Operating Pressure (bar)	Liquid Mass Flow Rate (g/s)
Schroeder, J. et al.	Viscosity ratio: A key factor for control of spray atomization of oil-water emulsions	2012	Original publication	Oil-in-water emulsions: demulsified water emulsions (various concentrations), water, vegetable oil	Multi-component; [1] Newtonian (<40% maltodextrin); [2] non-Newtonian (>50% maltodextrin)	994-1023	0.0024-0.7289	0.0444-0.0483	Air	10-50%	Not mentioned	Not mentioned
Sen, D. et al.	Bubble formation and flow instability in an effervescent atomizer	2014	Original publication	Water	Single component, Newtonian	1000	0.001	0.072	Air	0.0031-0.02654	1.81	259
Sajko, P. E. and LeFebvre, A. H.	A novel method of atomizing coal-water slurry fuels	1990	Original publication	[1] Glycol/water solutions; [2] Coal-water slurry	[1] Single component Newtonian; [2] Single component non-Newtonian; Two component non-Newtonian	[1] 1240; [2] 1130-1230; [3] 1202	[1] 0.4-0.8; [2] 0.1-0.3; [3] 0.05-0.08; [4] 0.078-1.03; [5] 0.131-1.364	[1] 0.004; [2] 0.005-0.008; [3] 0.024-0.078	Air	4.3-340%	6-21	Not mentioned
Sovell, S. D. et al.	High pressure effervescent atomization: Effect of ambient pressure on spray cone angle	2001	Original publication	Non-combustible Diesel fuel substitute	Two-component, Newtonian	1015	0.00275	0.027	Nitrogen	0.8-13.6%	126-365	Not mentioned
Sevens, S. D. et al.	Structure and steady state spray performance of an effervescent diesel injector	2005	Original publication	Diesel Substitute: Rock Valley Oil and Chemical Co.'s "Diesel 1188/AMV2 SAE J867"	Single component, Newtonian	795	0.0028	0.028	Nitrogen	1-8%	122-288	Not mentioned
Stable, P. et al.	Influence of feed viscosity on the two-phase flow inside the exit orifice of an effervescent atomizer and on resulting spray characteristics	2015	Original publication	[1] Water; [2] Various aqueous solutions of maltodextrin	[1] Single component, Newtonian; [2] Two-component, Newtonian	[1] 1000; [2] 1131-1241	[1] 0.001; [2] 0.214-0.308	[1] 0.072; [2] 0.074-0.076	Air	1-51%	4	2.7-24.6
Stable, P. et al.	Comparison of an Effervescent Nozzle with a Non-Effervescent Injecting (ACI) Nozzle for Atomization of Various Fuel Fluids at Low Air Consumption	2015	Original publication	[1] Water; [2] Various aqueous solutions of maltodextrin	[1] Single component, Newtonian; [2] Two-component, Newtonian	[1] 1000; [2] 1183-1241	[1] 0.001; [2] 0.080-0.308	[1] 0.072; [2] 0.074-0.076	Air	1.5-41.8%	4	2.7-25.3
Stable, P. et al.	Investigation on the Applicability of the Effervescent Atomizer in Spray Drying of Foods: Influence of Liquid Viscosity and Spray Characteristics	2015	Original publication	[1] Water; [2] Various aqueous solutions of maltodextrin	[1] Single component, Newtonian; [2] Two-component, Newtonian	[1] 1000; [2] 1131-1241	[1] 0.001; [2] 0.214-0.308	[1] 0.072; [2] 0.074-0.076	Air	1-51%	4	2.7-25.3
Sun, C. et al.	Time-frequency analysis of acoustic and ultrasonic evaluation in effervescent sprays	2015	Original publication	Water	Single component, Newtonian	1000	0.001	0.072	Air	0.1-35%	1-5	0.3-46.7
Sutherland, J. J. et al.	Comparison by laminar controlled effervescent atomizer produced sprays	1997	Original publication	[1] Water; [2] Various glycol/water mixtures; [3] Various 5003 mixtures	[1] Single component, Newtonian; [2] Two-component, Newtonian	[1] 998; [2] 1170-1217; [3] 804-807	[1] 0.001; [2] 0.02-0.08; [3] 0.02-0.04	[1] 0.072; [2] 0.074-0.076	Air	0.75-3.75%	Not mentioned	0.5 & 6.8
Sutherland, J. J. et al.	Laminar controlled effervescent atomization	1997	Sovell, S. D. et al., 2001	Water, glycol/water mixtures	Single and two-component, Newtonian	~858-1225	0.001-0.308	-	Air	0.5-4%	2.9-7.8	-
Wade, R. A. et al.	Effervescent atomization at injection pressures in the MPa range	1989	Sovell, S. D. et al., 2001	A diesel fuel substitute	Single component, Newtonian	~1275	0.0027	-	Nitrogen	5-50%	110-530	-
Wang, X. F. et al.	Influence of gas injector geometry on atomization performance of aerated effervescent sprays	1987	Sovell, S. D. et al., 2001	Water	Single component, Newtonian	1000	0.001	0.072	Nitrogen	2-23%	0.34-5.9	-
Whitby, J. D. and LeFebvre, A. H.	The atomization operation and spray characteristics	1993	Sovell, S. D. et al., 2002	Water	Single component, Newtonian	1000	0.001	0.072	Air	0-67%	0.09-6.89	-
Yu, G. et al.	An experimental study of two-phase combustion in a supersonic micro combustor using effervescent atomization	2005	Original publication	Kerosene	Single component, Newtonian	Not mentioned	~0.0014	Not mentioned	Air	0.2-2%	23.95	68

A2.3 Atomiser Design

PAPER DETAILS				ATOMISER DESIGN						
Author	Title	Year	Source	Atomiser Configuration	Orientation	Aerator Design	Mixing Chamber Design	Mixing Length (mm)	Bubble Breaker Design	Exit Orifice Design
Bromberg, L. et al.	Atomisation of FFD equinox sulfolins in effervescent sprays	2010	Original publication	Inlet-Out	Vertically downwards	Multiple inlets: 3rd orifice, 1.2-8 mm orifice dia, 19 mm tube dia.	Not mentioned	Not mentioned	No	Single orifice, 1.5 mm dia.
Reichel, J. and Heik, J.	Validation of an effervescent spray model with secondary atomisation and its application to modeling of a spray scale turbine	2011	Original publication	Outlets-in	Vertically downwards	80 orifices, 1 mm orifice dia.	14 mm dia., cylindrical	35	No	Single orifice, 0.2-2.5 mm dia.
Shahmorad, H. N. and Sohrab, F. E.	Effervescent atomization of high-boiling liquids: Part I: Newtonian liquids	1991	Sovani, S. D. et al. 2003.	Outlets-in	-	-	-	-	-	Single orifice, 0.2-2.5 mm dia.
Shahmorad, H. N. et al.	Effervescent atomization of non-water slurries	1990	Sovani, S. D. et al. 2003.	Outlets-in	-	-	-	-	-	Single orifice, 0.2-2.1 mm dia.
Bah, S. G. and Sohrab, F. E.	Entrainment by effervescent sprays at low mass flow rates	1983	Sovani, S. D. et al. 2003.	Inlet-Out	-	-	-	-	-	Single orifice, 0.34 mm dia.
Bah, S. G. et al.	Non-perturbative probe for use with the present spray	1995	Sovani, S. D. et al. 2003.	Inlet-Out	-	-	-	-	-	Single orifice, 0.38-0.51 mm dia.
Chellu, C. A. and Swireerath, J.	Physical processes influencing effervescent atomizer performance in the slug and annular flow regimes	2001	Original publication	Outlets-in	Not mentioned	12 orifices, 0.8 mm orifice dia.	8x8 mm, rectangular cross section	Not mentioned	No	Multiple orifices: Single main orifice, 4 mm length, [1] 1.5 mm dia., circular, [2] 0.5-0.864 mm, rectangular
Chen, S. K. et al.	Influence of ambient air pressure on effervescent atomization	1993	Sovani, S. D. et al. 2003.	Outlets-in	-	-	-	-	-	Single orifice, 1.3-2.4 mm dia.
Veronesi, M. and Pasqua, L. C.	Application of variance analysis to the atomization of reactive dyes	2012	Original publication	Outlets-in	Not mentioned	36 orifices, 0.2 mm orifice dia.	6.3 mm dia., cylindrical	30	No	Main holes: 3 orifices, 1 mm dia.
Hecht-Nielsen, A. et al.	Investigation and comparison of performance of effervescent and standard pneumatic atomizer rendered for stable aqueous coating	2005	Original publication	Inlet-Out	Not mentioned	1 orifice, 0.4 mm orifice dia.	4.4 mm dia., cylindrical	3.4	No	Single main orifice, 0.5 mm dia.
Gaillard, H. et al.	Mass-driven atomizer studies in effervescent sprays	2011	Original publication	Inlet-Out	Vertically downwards	2 orifices, 0.3 mm orifice dia.	30 mm dia., cylindrical	27	No	Single convergent orifice, 2 mm dia.
Geddes, S. C. and Sohrab, F. E.	Effervescent atomization of microfluidic liquids: Experiment and modeling	2008	Original publication	Outlets-in	Not mentioned	Not mentioned	Not mentioned	Not mentioned	No	Single orifice, 1 mm dia., 90° convergent
Geddes, S. C. and Sohrab, F. E.	High mass flow rate effervescent atomization of microfluidic liquids	1993	Sovani, S. D. et al. 2003.	Outlets-in	-	-	-	-	-	Single orifice, 1.5 mm dia.
Chen, S. et al.	Effect of bubble generation characteristics on effervescent atomization at low gas-liquid ratio operation	2010	Original publication	Inlet-Out	Vertically downwards	6.4 mm tube dia., 11.77 orifice, 0.5 mm orifice dia., [2] porous separator, 0.5 mm orifice dia.	8.4 mm dia., cylindrical	2.8	No	Single orifice, 0.8 mm dia., 45° convergent
Gomez, J.	Influence of bubble size on an effervescent atomization	2010	Original publication	Not mentioned	Horizontal	Not mentioned	25.4 mm dia., cylindrical	Not mentioned	-	Patent US 6062799: Convergent divergent nozzle, 13 mm exit orifice dia.
Heik, J. et al.	Analysis of effervescent spray quality for oil field furnace application	2015	Original publication	Outlets-in	Vertically downwards	80 orifices, 1.0 mm dia.	14 mm dia., cylindrical	35	No	Single orifice, 2.5 mm dia., 0.7 mm length, 50° convergent.
Harper, U. et al.	Miniature conductivity wire mesh sensor for gas-liquid two-phase flow measurement	2009	Original publication	Inlet-Out	Not mentioned	Not mentioned	8 mm dia., cylindrical	85	Yes	Not mentioned
Hoog, M. et al.	Understanding of the internal flow in an effervescent atomizer nozzle	2014	Original publication	Outlets-in	Horizontal	1.588 mm (61th) tube	12.7 mm dia., cylindrical	558.8	No	Single orifice, 1.7x2.15 mm, rectangular cross section
Huang, X. et al.	Characterization of an effervescent atomization water mist nozzle and its fire suppression tests	2011	Original publication	Outlets-in	Vertically downwards	24 orifices, 0.3 mm orifice dia.	5 mm dia., cylindrical	80	No	Multiple orifices, orifice (1) central orifice with a vertical passage, 1.8 mm dia.
Huang, X. et al.	Modeling of two-phase flow inside an effervescent atomizer	2008	Original publication	Outlets-in	Vertically downwards	24 orifices, 0.3 mm orifice dia.	5 mm dia., cylindrical	80	No	Single convergent orifice, 1.3 mm dia.

PAPER DETAILS				ATOMISER DESIGN						
Author	Title	Year	Source	Atomiser Configuration	Orientation	Aerosol Design	Mixing Chamber Design	Mixing Length (mm)	Bubble Breaker Design	Exit Orifice Design
Papayannathan, T. K. et al.	Effect of ultrasonic on bubble breakup within the mixing chamber of an effervescent atomiser	2011	Original publication	Inside-Out	Horizontal	1 orifice, 0.5 mm dia., 20 mm sub-orb. dia.	20x20 mm, rectangular cross section	50-95	Yes, 20 kHz ultrasonic probe	Single convergent orifice, 4 mm dia., 7 mm length
Jeridehly, J. and Aiche, M.	Energy conversion during effervescent atomization	2013	Original publication	Outside-In	Vertically downwards	24 orifices, 1 mm dia.	14 mm dia., cylindrical	35	No	Single orifice, 3.5 mm dia., 0.7 mm length, 60° convergence
Jeridehly, J. and Aiche, M.	Spray characteristics and liquid distribution of multi-hole effervescent atomisers for industrial burners	2016	Original publication	Outside-In	Horizontal	Multiple designs: 4-188 orifices, 1.2 mm orifice dia.	16 mm dia., cylindrical, various inserts (e.g. conical, radial)	31-70	No	Multi-hole, 6 orifices, 2.7 mm dia., 2.0 mm length
Jeridehly, J. et al.	Development of an effervescent atomiser for industrial burners	2009	Original publication	Outside-In	Vertically downwards	Multiple designs: 850 orifices, 0.7x1.5 mm orifice dia.	Multiple designs: 5.5-14.0 mm dia., cylindrical	35-99	No	Single orifice, 2.5 mm dia., 0.7 mm length, 60° convergence
Jeridehly, J. et al.	Characterization of spray generated by multi-hole effervescent atomiser with standard jet atomiser	2003	Original publication	Outside-In	30° from vertical, vertical downwards spray	188 orifices, 1.2 mm orifice dia.	Increasing from 1.5x0.9 mm dia., cylindrical	Not mentioned	No	Multi-hole, 6 orifices, 2.2 mm dia.
Jeridehly, J. et al.	Discharge coefficient and operational flow characteristics of multi-hole effervescent atomiser	2003	Original publication	Outside-In	30° from vertical, vertical downwards spray	Multiple designs: [1] 7 orifices, 1.2 mm orifice dia.; [2] 148 orifices, 1.2 mm orifice dia.	Multiple designs: 16.0 mm dia.; diverging from 1-15.0 mm dia., conical	76	No	Multi-hole, 6 orifices, 2.2 mm dia.
Jeridehly, J. et al.	Effervescent Atomiser: Influence of the Operation Conditions and Internal Geometry on Spray Structure Study Using PIV-PIV	2008	Original publication	Outside-In	Vertically downwards	Multiple designs: 32-40 orifices, 0.6-1.5 mm orifice dia.	Multiple designs: 6.0-10.0 mm dia., cylindrical	33-105	No	Multiple designs: Single orifice, 2.5 mm dia., 0.2-0.9 mm length, 60° convergence
Jabeesh, M. H.	Experimental Study of Two-Phase Flow in a Liquid Cross-Flow and an Effervescent Atomiser	2024	Original publication	Inside-Out	Vertically downwards	18 orifices, 0.32 mm orifice dia., 6.3 mm tube dia. Varying end tube designs.	9.6 mm dia., cylindrical	32-75	20 mm length; [1] Single orifice, 2.5 mm orifice dia.; [2] Multi-hole, 1.42-3.18 mm orifice dia., constant flow area	Single convergent orifice, 2.5 mm dia., 6.3 mm length
Ismael, V. and Akhbari, P.	Biocatalytic (BA14213) heating oil substitution potential for petroleum based light heating oil in a 1 MW effervescent atomiser	2023	Original publication	Outside-In	Horizontal	40 orifices, 1 mm orifice dia.	100 mm dia., cylindrical	5	No	Multi-hole, 6 orifices, 1 mm dia.
Kim, J. Y. and Lee, S. Y.	Dependence of spray performance on the internal flow pattern in effervescent atomisers	2001	Original publication	Independent injection	Vertically downwards	Porous sinter, 20 µm average pore size	248 mm, rectangular cross section	55	No	Multiple designs: Single orifice, 1.2-2.0 mm dia., 1.0-20.0 mm length, 60° convergence

PAPER DETAILS				ATOMISER DESIGN						
Author	Title	Year	Source	Atomiser Configuration	Orientation	Avatar Design	Mixing Chamber Design	Mixing Length (mm)	Bubble Breaker Design	Exit Orifice Design
Komandarov, D. B.	Ethervocent Atomization for Complex Tasks Including Bio-Tasks	2012	Original publication	Inside-O-A	Vertically downwards	Multiple designs: 15-10 orifice, 2-2.5 mm orifice dia., 10 mm tube dia.	Multiple designs: 200-500 mm dia., cylindrical	64-140	No	Multiple designs: single orifice, 2-4 mm dia., 0.5-2 mm length
Komandarov, A. et al.	Combined ethervocent and orificent atomization of a liquid jet	2016	Original publication	Outside-in, with combined air-ethit	vertically downwards	16 orifice, 0.75 mm dia.	2 mm dia, cylindrical	Not mentioned	No	Single orifice, 0.5 mm dia.
Lee, W. Y. and Sojka, P. E.	Influence of fluid viscosity on low pressure ethervocent atomization	1993	Sojka, S. D. et al 2001	Inside-O-A	-	-	-	-	-	Single orifice dia. Not mentioned
Lefebvre, A. H.	Novel method of atomization with potential gas turbine applications	1988	Original publication	Inside-O-A	Not mentioned	6.3 mm tube dia., [1] orifice, 0.8 mm orifice dia., [2] 20 orifice, 0.5 mm orifice dia.	25.4 mm dia., cylindrical	250	No	Single orifice, 0.3, 1.8 & 2.2 mm dia.
Lefebvre, A. H. et al.	Spray characteristics of aerosol-liquid pressure atomizers for small gas turbines	1988	Sojka, S. D. et al 2001	Inside-O-A	-	-	-	-	-	Single orifice, 0.8-2.4 mm dia.
Li, J. et al.	Ethervocent atomizers for small gas turbines	1994	Sojka, S. D. et al 2001	Outside in	-	-	-	-	-	Multi orifice, 1.8-2 mm dia.
Liu, M. et al.	Evaluation of ethervocent atomizer internal design on the spray characteristics using shadow/Doppler particle analyzer	2010	Original publication	Outside-in	Vertically downwards	Multiple designs: 28 orifice, 1.0-1.5 mm orifice dia.	10 mm dia., cylindrical	42-55	No	Multiple designs: single convergent-divergent orifice, 2.0 mm diameter and 2.5 mm length, or 50 convergent and divergent orifices, 45° convergence and divergence
Liu, M. et al.	Evaluation of unsteadyness in ethervocent spray by analysis of optical probe statistics - the influence of jet geometry and diameter	2011	Original publication	Outside-in	Vertically downwards	Multiple designs: 28 orifice, 1.0-1.5 mm orifice dia.	10 mm dia., cylindrical	42-53	No	Single convergent-divergent orifice, 2.0 mm diameter and 2.5 mm length, or 50 convergent and divergent orifices, 45° convergence and divergence
Lubben, M. and Mowen, D.	Atomization of liquids by two-phase gas-liquid flow through a plan orifice nozzle: flow regimes inside the nozzle	2001	Original publication	[1] Inside-O-A, [2] Outside-In, [3] Inside-O-A, dependent configuration	Not mentioned	24 orifice, 1.5 mm orifice dia.	5 mm dia, 10 mm dia., cylindrical	Not mentioned	No	Multiple designs: single convergent orifice, 0.5-2 mm dia., 1-20 mm length, 60° convergence
Lubben, M. et al.	Ethervocent atomization of liquids	2005	Original publication	[1] Outside-In, [2] Inside-O-A, alternate configuration	vertically downwards	[1] 24 orifice, 0.5 mm orifice dia., [2,3] Not mentioned	[1] Multiple designs: 5-10 mm dia., cylindrical, [2,3] 15 mm dia., cylindrical	Not mentioned	No	Multiple designs: single convergent orifice, 0.5-2 mm dia., 1-20 mm length, 60° convergence
Lubben, E. and Levy, Y.	Experimental investigation of flame-holding system for the suspension of engine combustor	1998	Original publication	Outside in	Not mentioned	28 orifice, 1.0 mm orifice dia.	4 mm dia, cylindrical	Not mentioned	No	single convergent orifice, 2.0 mm dia.
Lund, M. T. et al.	The influence of atomizer design on the performance of ethervocent atomizers	1998	Original publication	Inside-O-A	Not mentioned	Not mentioned	Not mentioned	Not mentioned	No	Single convergent orifice dia. Not mentioned
Lund, M. T. et al.	Ethervocent atomization at low mass flow rates: Part I - the influence of surface tension	1993	Sojka, S. D. et al 2001	Inside-O-A	-	-	-	-	-	Single orifice, dia. Not mentioned
Lung, J. T. K. and Sojka, P. E.	Unsteadyness in ethervocent sprays	1999	Sojka, S. D. et al 2001	Inside-O-A	-	-	-	-	-	Single orifice, dia. Not mentioned
Ma, X. et al.	Atomization of petroleum coke sludge slurry using ethervocent atomizer	2013	Original publication	Outside-in	Not mentioned	28 orifice, 1.0 mm orifice dia.	10 mm dia., cylindrical	55	No	Multiple designs: single convergent-divergent orifice, 3.0-3.5 mm diameter and 10 mm length, or 10 mm diameter and 10 mm length, 40° convergence and divergence

PAPER DETAILS				ATOMISER DESIGN						
Author	Title	Year	Source	Atomiser Configuration	Orientation	Aerator Design	Mixing Chamber Design	Wiring Length (mm)	Bubble Breaker Design	Exit Orifice Design
Mishra, M. et al.	Two fluid atomization of viscous liquids: The effect of atomizer construction on breakup process, spray stability and droplet size	2015	Original publication	[1] Outside-in [2] Outside-in alternate configuration (i.e. liquid injection gas continuous) [3] Swirl Chamber	Vertically downwards	20 orifices, 1.0 mm orifice dia., used for (1) gas injection; (2) liquid injection. (3) No aerator, 2 mm gap injection port, 40 mm inner diameter liquid injection port.	9 mm dia., cylindrical	Not mentioned	No	Single orifice, 0.7 mm dia.
Orłowski, M.	The experimental study on the viscosity effect on the discharge coefficient for effervescent atomizers	2013	Original publication	Inside-out	Vertically downwards	40 orifices, 0.8 mm orifice dia.	20 mm dia., cylindrical	67	No	Single plain orifice, 2.7 mm dia.
Orłowski, M.	The effervescent atomization of oil-in-water emulsions	2012	Original publication	Inside-Out	Vertically downwards	9 orifices, 1.5 mm orifice dia., 15 mm tube dia.	Not mentioned	8	No	Multiple designs: Single plain orifice, 2.6 mm dia.
Orłowski, M. et al.	The discharge coefficient of effervescent atomizers	2010	Original publication	Inside-Out	Vertically downwards	20 orifices, 1 mm orifice dia., 15 mm tube dia.	20 mm dia., cylindrical	8	No	Multiple designs: Single plain orifice, 1.7-4.9 mm dia., 1.5 mm length
Orłowski, M. et al.	Characteristics of spray angle for effervescent swirl atomizers	2015	Original publication	Swirl Chamber	Vertically downwards	Multiple designs: (1) 40 orifices, 0.8 mm orifice dia. (2) No aerator, 2.5 mm gap injection part	Not mentioned	20	No	Multiple designs: Various orifice diameters, 0.8 plain, converging, diverging, radial, 2.5 mm dia., 2.5-10 mm length
Orłowski, M. et al.	The effect of orifice geometry on the effervescent atomization of polyacrylamide solutions	2012	Original publication	Inside-Out	Vertically downwards	Unmentioned number of orifices, 2 mm orifice dia., 15 mm tube dia.	20 mm dia., cylindrical	130	No	Single plain orifice, 2.7 mm dia.
Panchagnab, M. V. and Saha, P. E.	Spatial droplet velocity and size profiles in effervescent atomizer produced spray	1999	Original publication	Outside-in	Vertically downwards	Not mentioned	12.7 mm dia., cylindrical	~150	No	Single convergent orifice, 3.0 & 4.0 mm dia.
Rezzani, F. J. et al.	Effervescent atomization of aqueous polymer solutions and dispersions	2001	Original publication	Inside-Out	Not mentioned	2 orifices, 0.4 mm and 0.35 mm orifice dia.	Not mentioned	Not mentioned	No	Single orifice, 0.8 mm
Rezzani, F. J. et al.	Design and Atomization Properties for an Inside-Out Type Effervescent Atomizer	2004	Original publication	Inside-Out	Not mentioned	Multiple designs: 1-2 orifices, 0.3-0.5 mm orifice dia.	Multiple designs: 3.0, 3.5 & 4.6 mm dia., cylindrical	1.5-9.5	No	Multiple designs: Single orifice, 0.5-0.7 mm, 1.0 mm dia., 0.25, 1.88 & 3.75 mm length
Rahman, M. A. et al.	Effects of the gas-phase molecular weight and bubble size on effervescent atomization	2012	Original publication	Independent Injection	Not mentioned	Not mentioned	Conical diverging design	358	No	Single convergent orifice, 3.1 mm dia.
Reauster, T. C. and Lefebvre, A. H.	Studies on aerosol-liquid atomization	1987	Sovani, S. D. et al. 2000	Outside-in	-	-	-	-	-	Single orifice, 0.5-2.5 mm dia.
Reauster, S. V. et al.	Swirl effervescent atomizer for spray combustion	1995	Sovani, S. D. et al. 2001	Inside-Out	-	-	-	-	-	Single annular orifice, 5 mm dia.
Santangelo, P. J. and Solaja, P. E.	A holographic investigation of the near-nozzle structure of an effervescent atomizer produced spray	1995	Sovani, S. D. et al. 2001	Outside-in	-	-	-	-	-	Single orifice, 1.3 mm dia.
Scandola, J. et al.	Characterization of jet-breaker combustion suspensions and resulting drop size distributions after effervescent atomization	2011	Original publication	Outside-in	Not mentioned	9 orifices, 0.5 mm dia.	Multiple designs: 6 & 10 mm dia., cylindrical	Not mentioned	No	Multiple designs: Single orifice, 1.3-2.0 mm dia.

PAPER DETAILS				ATOMISER DESIGN						
Author	Title	Year	Source	Atomiser Configuration	Orientation	Aerator Design	Mixing Chamber Design	Mixing Length (mm)	Bubble Breaker Design	Exit Orifice Design
Schroeder, J. et al.	Velocity ratios & key design parameters of all drop size distribution in effervescent atomization of high-viscosity emulsions	2012	Original publication	Outside-In	Not mentioned	Not mentioned	6 mm dia, cylindrical	Not mentioned	No	Multiple designs: Single orifice: 1.5 mm dia, 1.5-15 mm length
San, D. et al.	Bubble formation and flow instability in an effervescent atomizer	2014	Original publication	Outside-In	Horizontal	1 orifice, 0.21 mm orifice dia.	Rectangular, 12.7 mm hydraulic diameter	540	No	Single orifice, 0.8 mm dia.
Saha, P. E. and Leffew, A. H.	A novel method of atomizing coal-water slurry fuels	1990	Original publication	Outside-In	Not mentioned	Porous tube	5 mm dia, cylindrical	82	No	Single orifice, 1.8 & 2.5 mm dia.
Stevens, S. D. et al.	High pressure effervescent atomization: Effect of ambient pressure on spray cone angle	2001	Original publication	Outside-In	Vertically downwards	Not mentioned	Not mentioned	Not mentioned	No	Single orifice, 0.24 mm dia, 0.8 mm length, 45° cone angle
Sorensen, S. D. et al.	Structure and steady-state spray performance of an effervescent atomizer	2005	Original publication	Outside-In	72.5° from vertically downwards, spray vertically downwards	Multiple designs: Porous sinter, 1.5 μm & 8 μm pore size	Not mentioned	0.025-0.218	No	Multiple designs: 1 plain orifice 0.25 & 0.33 mm dia, 1 mm length
Shah, P. et al.	Influence of fluid viscosity on the two-phase flow inside the exit orifice of an effervescent atomizer and on resulting spray characteristics	2015	Original publication	Outside-In	Vertically downwards	24 orifices, 1 mm orifice dia.	6 mm dia, cylindrical	32	No	Single orifice, 1.5 mm dia, 1.5 mm length, 50° cone angle
Shah, P. et al.	Investigation on the spray spray characteristics of effervescent atomizer: A Proposed Air-Cone-Scaling (ACCS) Model for Atomization of Viscous Fluids at Low Air Consumption	2015	Original publication	[1] Outside-In, [2] Inside-Out	Vertically downwards	[1] 24 orifices, 1 mm orifice dia, [2] 1 orifice, 1.5 mm orifice dia, 4.5 mm tube dia.	[1] 6 mm dia, cylindrical [2] 7.5 mm dia, cylindrical	30.5	No	Single orifice, 1.5 mm dia, 1.5 mm length, 50° cone angle
Shah, P. et al.	Investigation on the spray characteristics of effervescent atomizer: A Proposed Air-Cone-Scaling (ACCS) Model for Atomization of Viscous Fluids at Low Air Consumption	2015	Original publication	Outside-In	Vertically downwards	24 orifices, 1 mm orifice dia.	6 mm dia, cylindrical	30.5	No	Single orifice, 1.5 mm dia, 1.5 mm length, 50° cone angle
Shin, C. et al.	The frequency analysis of acoustic and water stress evaluation in effervescent spray	2015	Original publication	Outside-In	Vertically downwards	20 orifices, 0.2 mm orifice dia.	12x10 mm, rectangular cross section	65	No	Single orifice, 1 mm dia, 1.5 mm length
Schroeder, J. J. et al.	Enhancement by ligament-controlled effervescent atomizer produced sprays	1997	Original publication	Inside-Out	Vertically downwards	2 orifices, 0.2 mm tube dia.	3.7 mm dia, cylindrical	Not mentioned	Yes, porous sinter, 20 μm pore size	Single orifice, 0.38 mm dia, 0.75 mm length
Schroeder, J. J. et al.	Ligament-controlled effervescent atomization in the WPA range	1998	Sevens, S. D. et al. 2001	Inside-Out	-	-	-	-	-	Single orifice, 0.38 mm dia.
Wang, B. et al.	Effervescent atomization at injection pressures in the WPA range	1998	Sevens, S. D. et al. 2001	Outside-In	-	-	-	-	-	Single orifice, 0.28-0.84 mm dia.
Wang, B. et al.	Influence of gas injector geometry on atomization performance of air-water effervescent atomizer	1997	Sevens, S. D. et al. 2001	Inside-Out	-	-	-	-	-	Single orifice, 0.8 & 0.5 mm
Whitlow, J. D. and Leffew, A. H.	Effervescent atomizer operation and spray characteristics	1993	Sevens, S. D. et al. 2001	Outside-In	-	-	-	-	-	Single orifice, dia not mentioned
Yu, G. et al.	An experimental study of kerosene combustion in a supersonic model combustor using effervescent atomization	2005	Original publication	Inside-out alternate configuration (i.e. Inlet Inlet and Gas Outflow)	Not mentioned	1.3 mm dia, used for liquid injection	4 mm dia, cylindrical	15	No	Single orifice, 0.18 & 0.8 mm dia.

A2.4 Correlations

Bubble Expansion Energy Correlations		Source
$e_b = (\gamma - 1)^{-1} P_{op} \left(\frac{\pi}{6} \right) d_b^3 \left(1 - \left(\frac{P_{amb}}{P_{op}} \right)^{\gamma-1/\gamma} \right)$ <p>where: $\gamma = 1.4$ for isentropic expansion</p>	(A2.4.1)	[29]
$e_b = RT \left(\frac{m_g}{m_l} \right) \ln \left(\frac{P_g}{P_l} \right)$ <p>where: P_g is the gas injection pressure; P_l is the liquid injection pressure</p>	(A2.4.2)	[102]
Optimal Bubble Size Correlations		Source
$d_b = \frac{8\sigma_l d_a}{C_d \rho_l U_l^2}$ <p>where: $C_d = 0.5$ for spherical bubbles at $Re=10^3-10^5$</p>	(A2.4.3)	[29]
$d_b = 2.4 \sqrt{\frac{Q_g}{U_l}}$	(A2.4.4)	[29]
$d_b = 34445 ALR^{-0.736}$	(A2.4.5)	[20]
Discharge Coefficient Correlations		Source
$C_d = c \left(1 - \frac{Q_G}{Q_G + Q_L} \right)^{-0.3} \left(1 + \frac{1}{ALR} \right)^{0.15}$ <p>where: c is a constant ($c_{water} = 0.385$)</p>	(A2.4.6)	[100]
$C_d = 0.30 - 0.0002(ALR \cdot \sqrt{Re})$	(A2.4.7)	[101]
$C_d = 0.0088 \left(ALR \cdot \frac{d_o}{d_{MC}} \right)^{-0.75}$	(A2.4.8)	[99]
$C_d = \frac{U_M}{\sqrt{2P_{op}\rho_l}} (\mu'^{0.04} \sigma'^{0.02}) \left(\frac{1}{1 + ALR} \right) \left(0.062 \left(\frac{l_o}{d_o} \right) \sqrt{\sin 2\beta} \right)^{-0.11}$ <p>where: μ' is the liquid/water viscosity ratio; σ' is the liquid/water surface tension ratio; and U_M is the total mass velocity (calculated)</p>	(A2.4.9)	[19]
$C_d = (\mu'^{0.04} \sigma'^{0.02}) \left(a \left[\left(\frac{l_o}{d_o} \right) \sqrt{\sin 2\alpha} \right]^{-0.1} \left[\left(1 + \frac{1}{ALR} \right)^{0.25} - 1 \right] \left[\frac{P_{op}}{239} \right]^{0.05} - b \right)$ <p>where: a & b are functions of atomiser geometry</p>	(A2.4.10)	[28]
$C_d = \frac{m_l}{\frac{\pi}{4} d_o^2 \sqrt{2\rho_l P_{op}}}$	(A2.4.11)	[10, 77]

$C_d = \left(1 + ALR \left(\frac{\rho_l}{\rho_g} \right) \right)^{-1}$	(A2.4.12)	[102]
--	-----------	-------

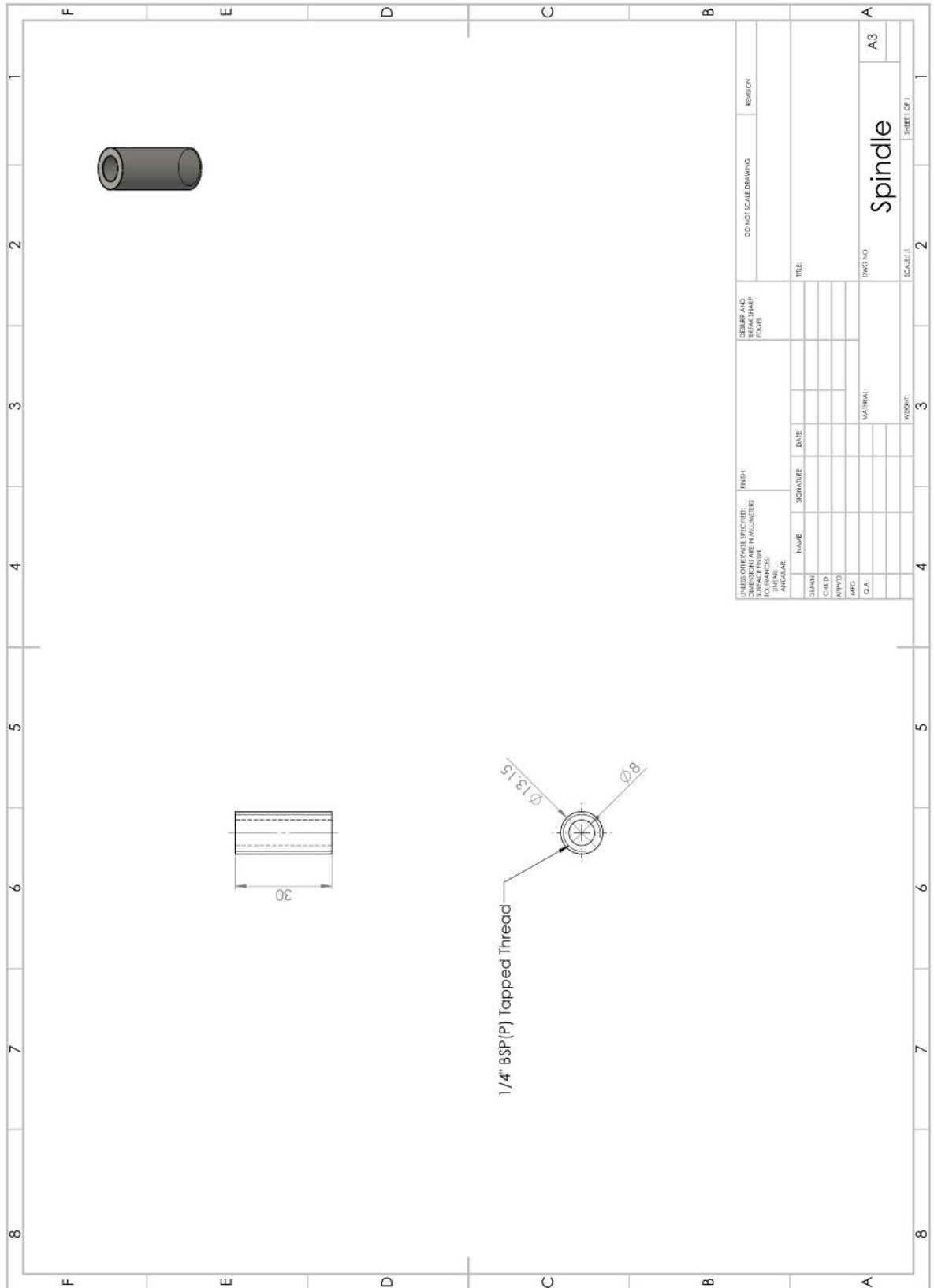
Spray Cone Angle Correlations	Source
$\frac{\alpha}{2} = (0.0451P_{amb}^4 - 0.6211P_{amb}^3 + 2.7551P_{amb}^2 - 3.62P_{amb}) + 0.15ALR + 0.39P_{op} + 7$	(A2.4.13) [11]

SMD Correlations	Source
$SMD = 1.21^{-2} d_o M_W^{0.25} ALR^{-0.23}$	(A2.4.14) [105]
$SMD = \frac{12\sigma}{\rho \left(U_l^2 + \epsilon ALR U_g^2 - \frac{U_l + \epsilon ALR U_g}{1 + \epsilon ALR} \right)}$ <p style="text-align: center; margin-top: 5px;">where: ϵ is a model coefficient determined from experimental data</p>	(A2.4.15) [74]
$SMD = \sqrt[3]{\frac{3}{2} \sqrt{2} \pi d_{lig}^3 \sqrt{1 + \frac{3\mu_l}{\sqrt{\rho_l \sigma_l d_{lig}}}}}$ <p style="text-align: center; margin-top: 5px;">where: d_{lig} is the ligament diameter</p>	(A2.4.16) [136]
$SMD = \sqrt[3]{1.52 \sqrt{2} \pi d_{lig}^3 \sqrt{1 + \frac{3\mu_l}{\rho_l \sigma_l d_{lig}}}}$	(A2.4.17) [150]
$SMD = 3 \left[\frac{1}{t} + \frac{0.007 \rho_l U_g^2}{4 \sigma_l (1 + ALR^{-1})} \right]^{-1}$ <p style="text-align: center; margin-top: 5px;">where: t is the initial sheet thickness</p>	(A2.4.18) [151]
$SMD = 1.5 d_o \left[1 + \frac{C \rho_l T_g \left(\frac{P_{op}}{P_{amb}} \right)}{\sigma_l (1 + ALR^{-1})} \right]^{-1}$ <p style="text-align: center; margin-top: 5px;">where: C is the process efficiency</p>	(A2.4.19) [102]
$SMD = \sqrt[3]{\frac{3\pi d_{lig}^3}{\zeta_{opt}}}$ <p style="text-align: center; margin-top: 5px;">where: ζ_{opt} is the relative gas-liquid velocity</p>	(A2.4.20) [117]
$SMD = 55 d_o^{-0.93} P_{op}^{-0.9} ALR^{0.005}$	(A2.4.21) [134]

Entrainment Correlations	Source
$\frac{\dot{m}_e}{\dot{m}_l} = E \sqrt{\frac{4}{\pi}} \left(\frac{Y}{d_o}\right) \sqrt{\frac{\rho_e(ALR\rho_l + SR\rho_g)}{\rho_l\rho_g}} \left(\frac{1}{SR} + ALR\right) \quad (\text{A2.4.22})$ <p>where: E is the entrainment number; $\frac{\dot{m}_e}{\dot{m}_l}$ is the normalised entrainment mass flow rate; ρ_e is the entrained gas density; SR is the slip ratio</p>	[164]
Maximum ALR for Bubbly Flow Correlations	Source
$ALR_{max} = \left(\frac{\rho_g}{\rho_l}\right) \left(\frac{1}{\alpha_{max} - 1}\right)^{-1} \quad (\text{A2.4.23})$ <p>where: α_{max} is the maximum void fraction for bubbly flow, which is fairly constant at 0.82 for water air</p> <p>$\therefore ALR_{max} \approx 4.6 \left(\frac{\rho_g}{\rho_l}\right)$ for water/air</p>	[127]
$ALR_{max} = 91 - 127 \left(1 - \frac{d_o}{d_{MC}}\right)^2 \left(\frac{\rho_g}{\rho_l}\right) \quad (\text{A2.4.24})$	[165]
$ALR_{max} \approx 4.8 \left(\frac{\rho_g}{\rho_l}\right) \quad (\text{A2.4.25})$	[102]

APPENDIX 3: ENGINEERING DRAWINGS OF TEST RIGS

A3.1 Optical Effervescent Atomiser (OEA)



UNLESS OTHERWISE SPECIFIED: DIMENSIONS ARE IN MILLIMETERS SURFACE FINISH TOLERANCES: ANGULAR		FINISH:	DEBURR AND REMOVE SHARP EDGES		DO NOT SCALE DRAWING	REVISION
DRW	NAME	SIGNATURE	DATE	TITLE:		
CHKD						
APP'D						
MFG						
D.A.						
				MATERIAL:		
				DWG NO:	A3	
				SCALE: 1:1	SHEET 1 OF 1	
				QUANTITY:	2	

Spindle

A3

SHEET 1 OF 1

SCALE: 1:1

QUANTITY:

2

A3

SHEET 1 OF 1

SCALE: 1:1

QUANTITY:

2

A3

SHEET 1 OF 1

SCALE: 1:1

QUANTITY:

2

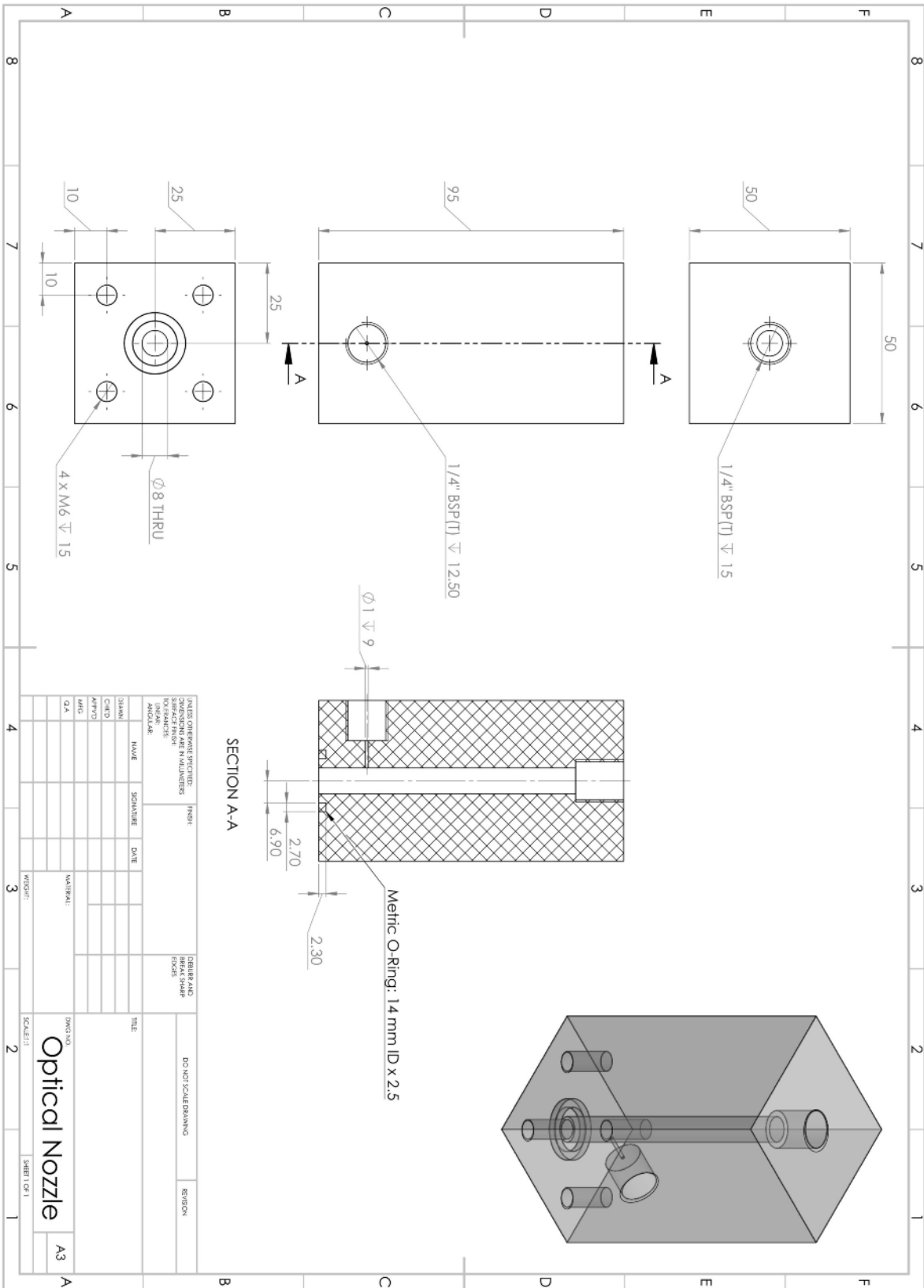
A3

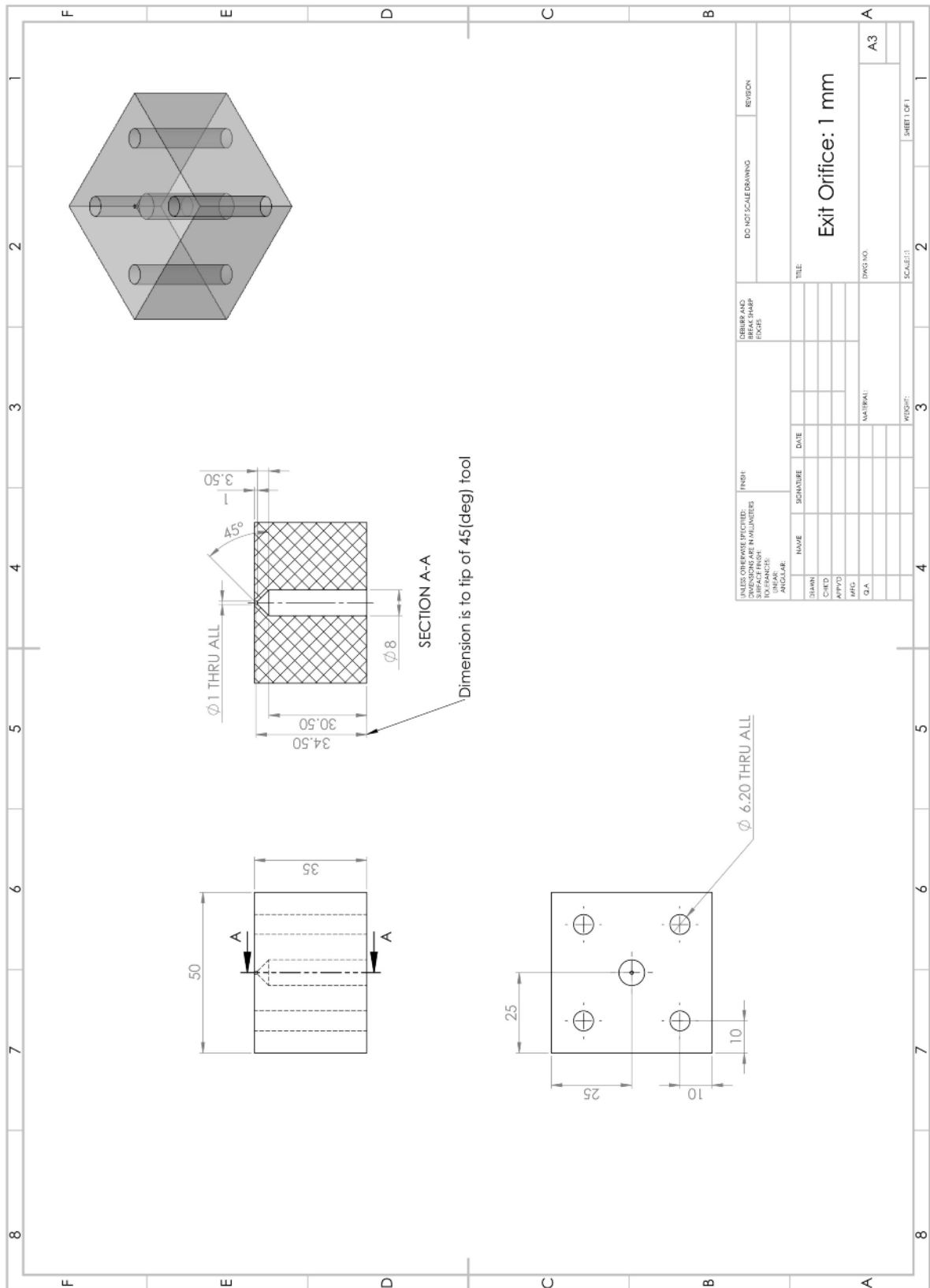
SHEET 1 OF 1

SCALE: 1:1

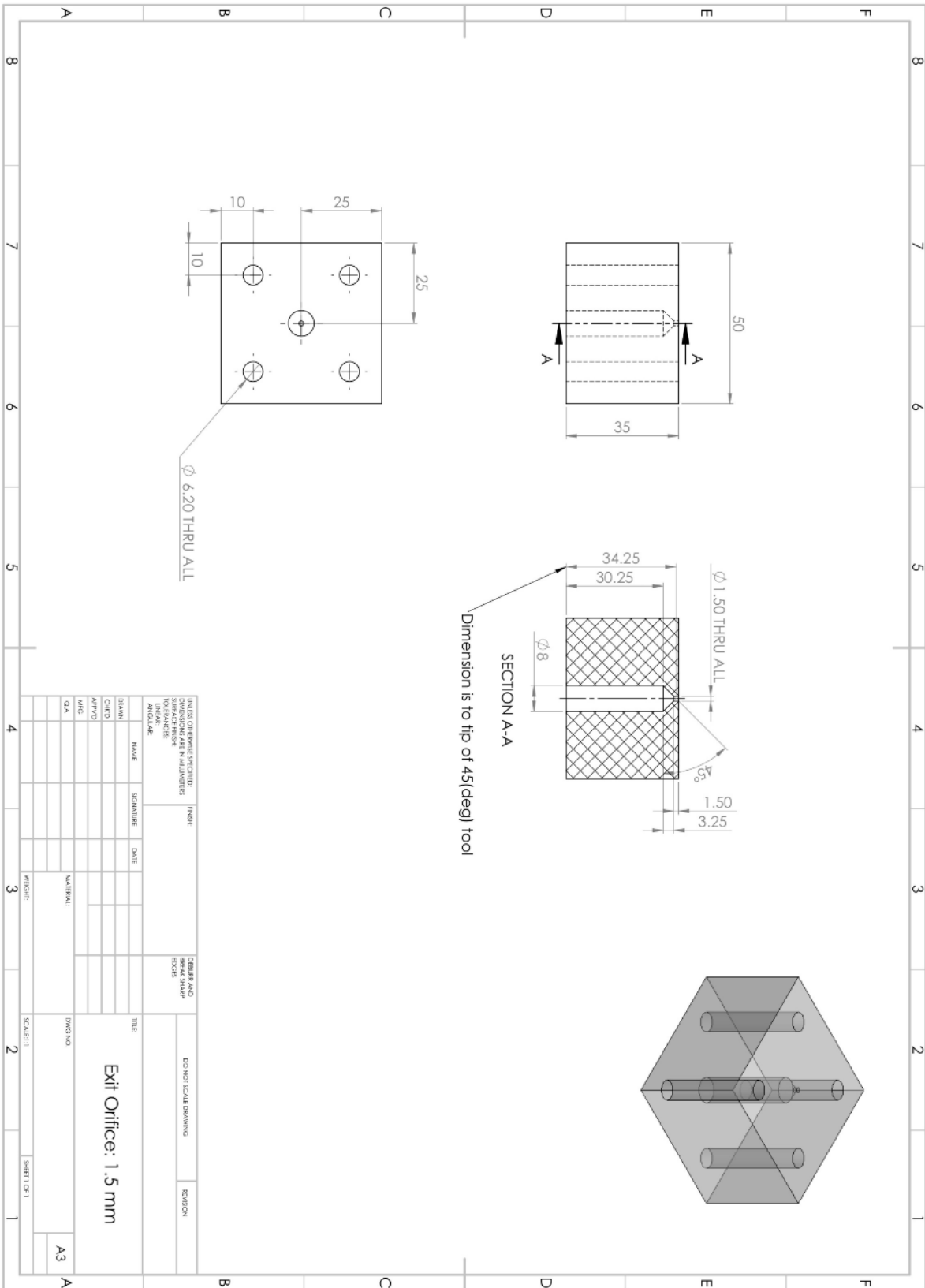
QUANTITY:

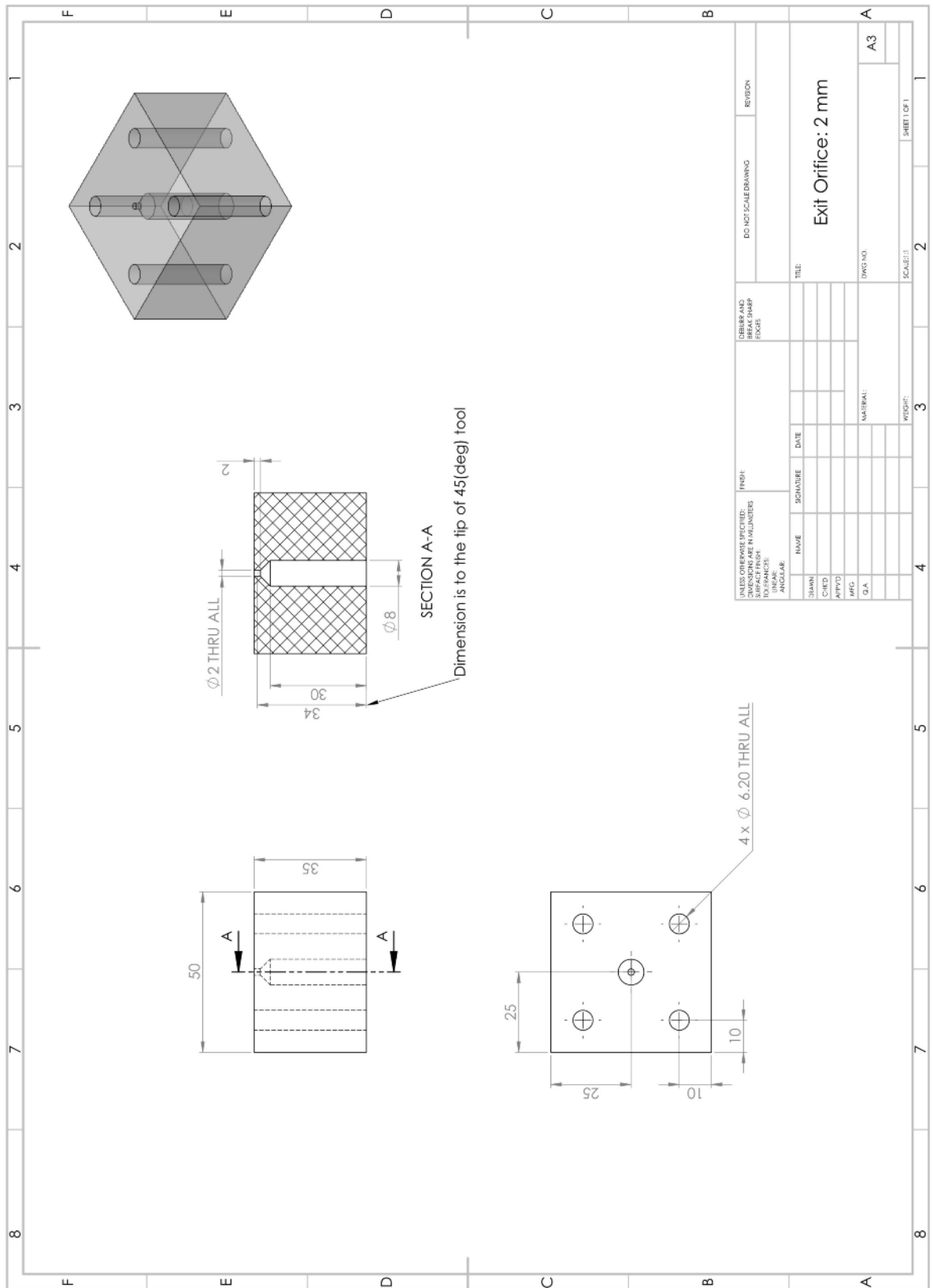
2





UNLESS OTHERWISE SPECIFIED: DIMENSIONS ARE IN MILLIMETERS DIMENSIONS IN PARENTHESES ARE DIMENSIONS IN INCHES		FINISH: SURFACE FINISH: INTERNAL ANGLE:		DEBURR AND REMOVE SHARP EDGES		DO NOT SCALE DRAWING		REVISION	
NAME	SIGNATURE	DATE							
DRW									
CHKD									
APP'D									
MFG									
Q.A.									
TITLE: Exit Orifice: 1 mm		DWG NO: A3		SHEET NO: 1		SCALE: 1:1		SHEET OF 1	

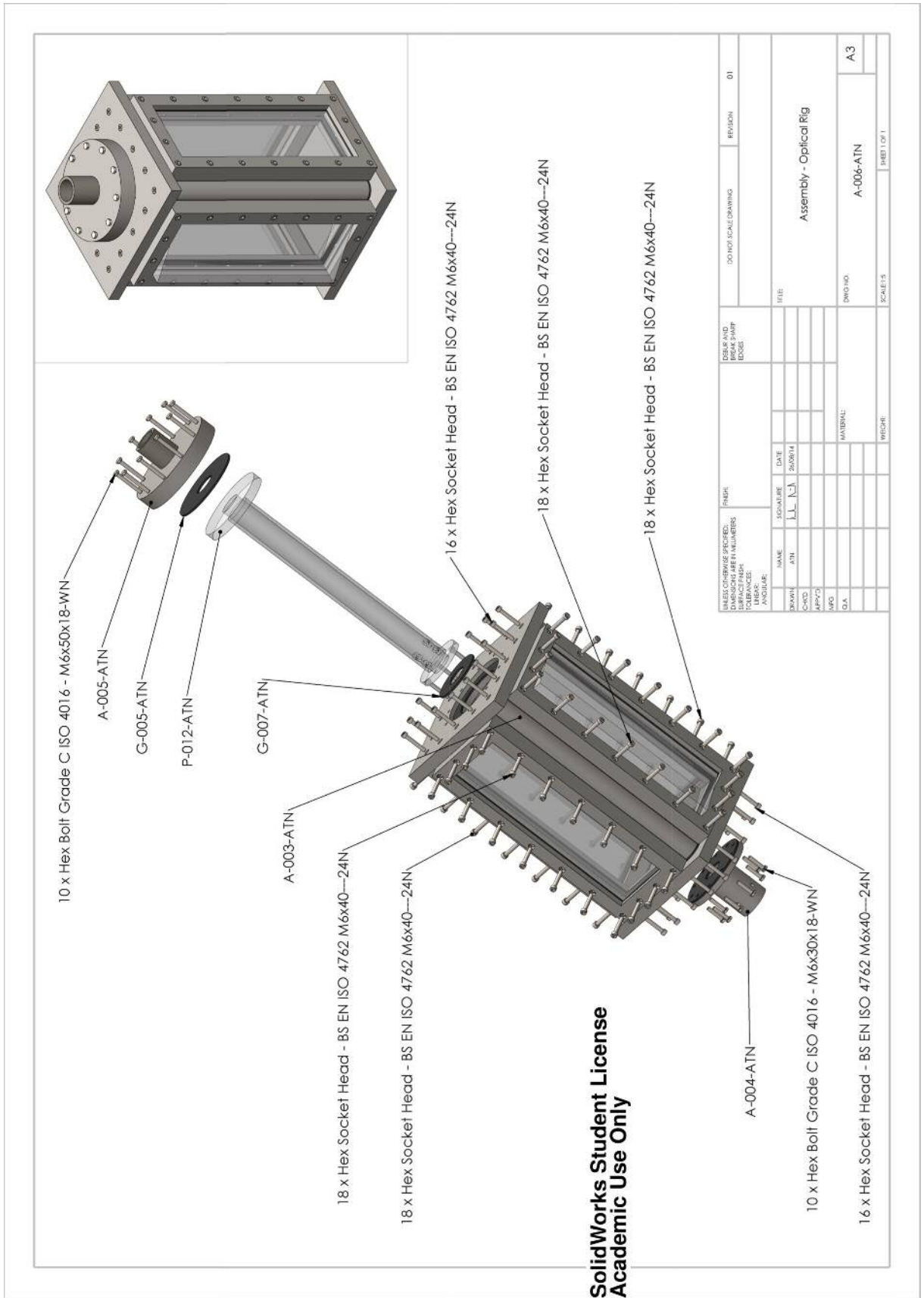




UNLESS OTHERWISE SPECIFIED: DIMENSIONS ARE IN MILLIMETERS SURFACE FINISH: TOLERANCES: ANGULAR:		FINISH:		DEBURR AND REMOVE SHARP EDGES		DO NOT SCALE DRAWING		REVISION	
NAME	SIGNATURE	DATE	TITLE						
DRAWN									
CHECKED									
APPROVED									
MFG									
Q.A.									
MATERIAL:			DWG NO:			SCALE: 1:1			
			A3			SHEET 1 OF 1			
WEIGHT:			2			3			

Exit Orifice: 2 mm

A3.2 Internal Flow Optimisation Rig (IFOR)

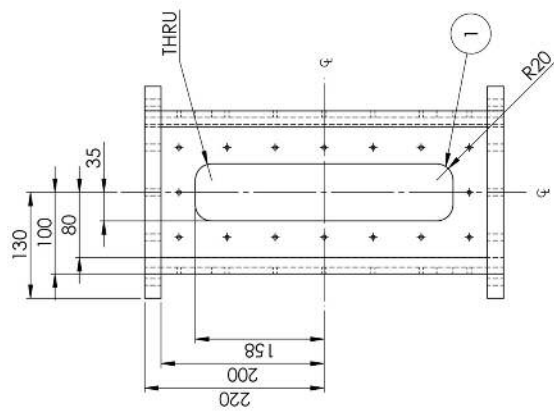


UNLESS OTHERWISE SPECIFIED: DIMENSIONS ARE IN MILLIMETERS TOLERANCES: FRACTIONS DECIMALS ANGLES		DATE 20/08/14		SCALE		DO NOT SCALE DRAWING		REVISION		01	
DESIGN AND DRAWING CHECKED	DATE	SCALE		TITLE		DWG NO.		SCALE 1:5		SHEET 1 OF 1	
NAME JIN	DATE 20/08/14	SCALE		TITLE Assembly - Optical Rig		DWG NO. A-006-ATN		SCALE 1:5		SHEET 1 OF 1	
APP'D											
MFG											
DIA.											
MATERIAL											
WEIGHT											

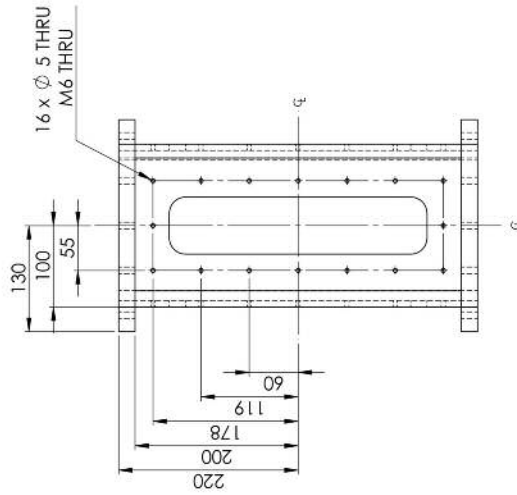
UNLESS OTHERWISE SPECIFIED: DIMENSIONS ARE IN MILLIMETERS		NAME		DATE	DRAWING NO.		REVISION	
SKETCH	ATN	DATE	2008/14	A-007-ATN		01		
CHKD								
APP'D								
MFG								
D/A								
				MATERIAL:		SCALE: 1 OF 2		
				WEIGHT:		SHEET 1 OF 2		
				TITLE:		A3		
				SQUARE BOX SECTION ASSEMBLY				

**SolidWorks Student License
Academic Use Only**

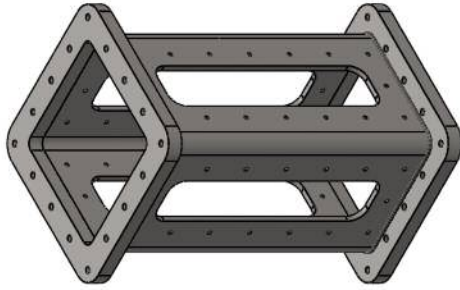
N.B. This drawing describes the machining template for a single face. It applies to all four equally sized faces of the Square Box Section Assembly.



WINDOW
TOLERANCE IS ±0.2 mm



TAPPED HOLES
TOLERANCE IS ±0.1 mm



Notes
1 All four window radii are equal

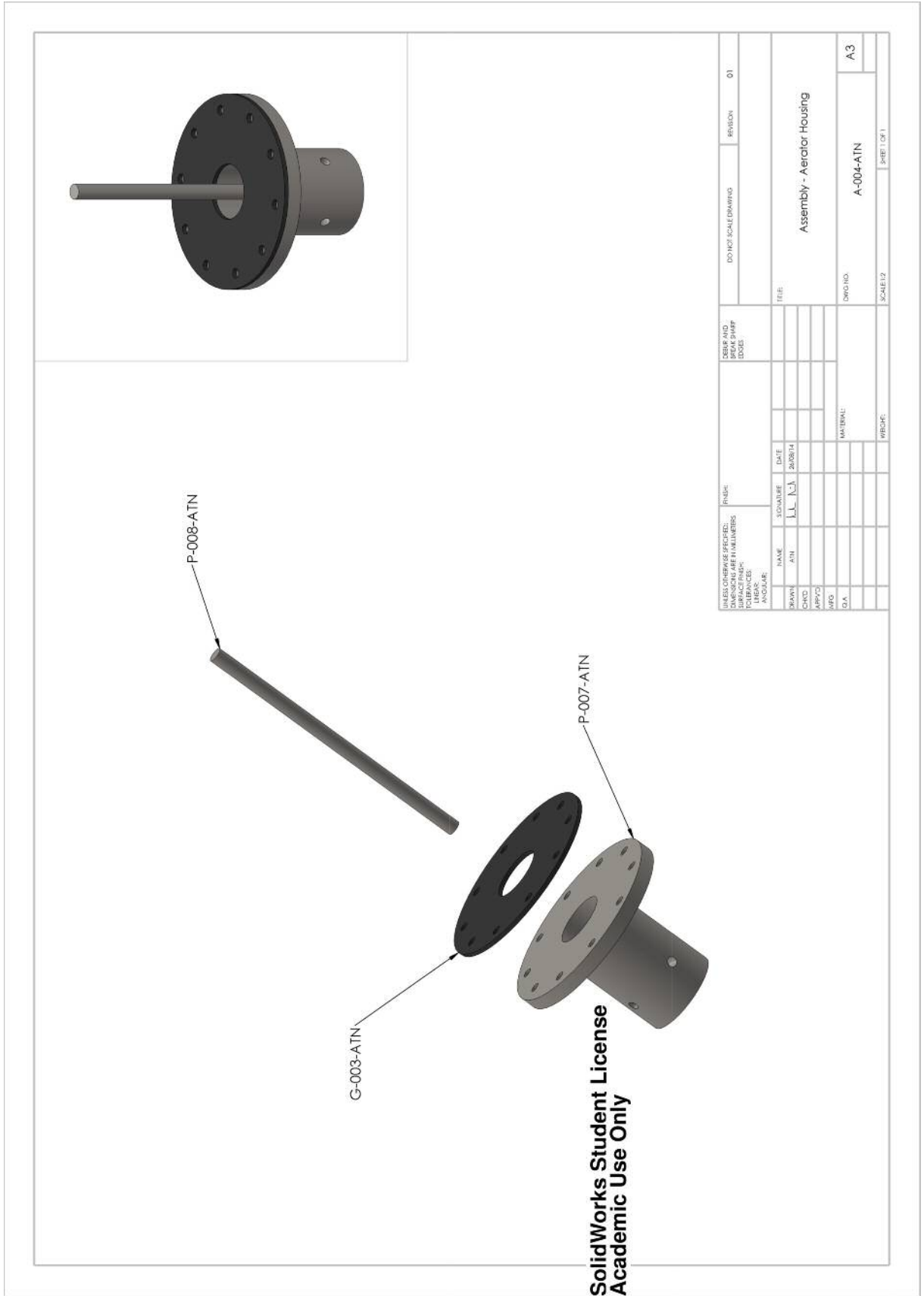
UNLESS OTHERWISE SPECIFIED: DIMENSIONS ARE IN MILLIMETRES TOLERANCE IS ±0.2 mm		DEBAR AND FINISH: SHARP FINISH:		DO NOT SCALE DRAWING	REVISION	DT
SWORN	NAME	SCALE	DATE	TITLE:		
CHKD	ANN	1:1	11/02/14	Square Box Section Assembly - Machining Template		
APP'D				DWG NO		
D.A.				A-007-ATN		
				MATERIAL: Stainless Steel Grade 304		
				WEIGHT:		
				SCALE IS		
				SHEET 1 OF 1		

**SolidWorks Student Edition.
For Academic Use Only.**

Exploded view of a window assembly. The assembly consists of several parts: a top frame (G-002-ATN), a middle panel (P-004-ATN), a bottom frame (G-002-ATN), and a base frame (P-006-ATN). The parts are shown in a disassembled state to illustrate their relative positions and how they fit together. An inset drawing shows the assembled window frame from a perspective view.

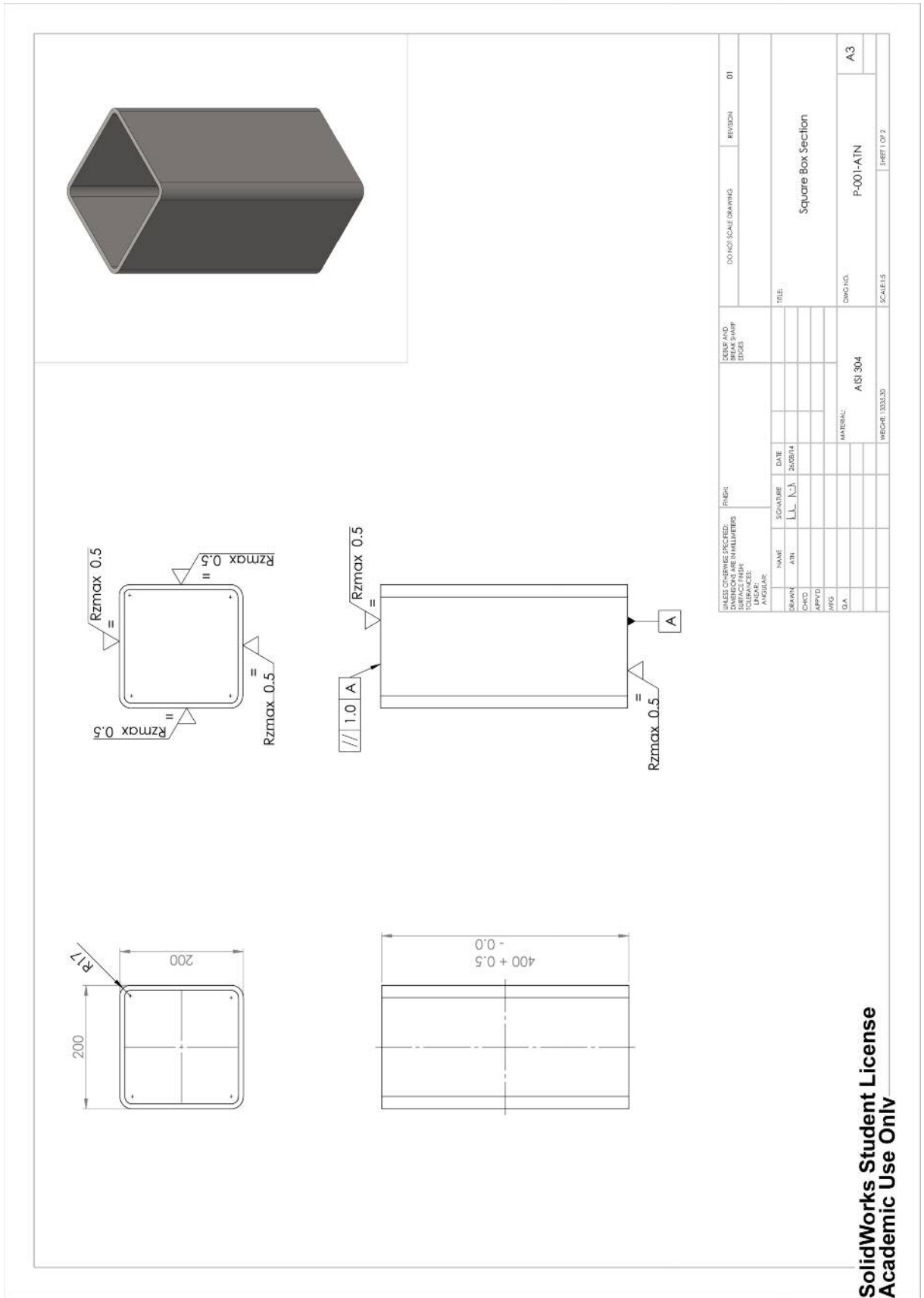
UNLESS OTHERWISE SPECIFIED:				FINISH		DIMENSIONS AND DIMENSIONS		DIMENSIONS AND DIMENSIONS	
SURFACE FINISH				TOLERANCES		TOLERANCES		TOLERANCES	
ANGULAR				ANGULAR		ANGULAR		ANGULAR	
DRAWN	DATE	SCALE	DATE	DATE	DATE	DATE	DATE	DATE	DATE
CHKD	DATE	SCALE	DATE	DATE	DATE	DATE	DATE	DATE	DATE
APP'D	DATE	SCALE	DATE	DATE	DATE	DATE	DATE	DATE	DATE
QA	DATE	SCALE	DATE	DATE	DATE	DATE	DATE	DATE	DATE
MATERIAL				MATERIAL		MATERIAL		MATERIAL	
WEIGHT				WEIGHT		WEIGHT		WEIGHT	
SCALE: 1:2				SCALE: 1:2		SCALE: 1:2		SCALE: 1:2	
TITLE				TITLE		TITLE		TITLE	
Assembly - Window, Non Angled				Assembly - Window, Non Angled		Assembly - Window, Non Angled		Assembly - Window, Non Angled	
DWG NO. A-001-ATN				DWG NO. A-001-ATN		DWG NO. A-001-ATN		DWG NO. A-001-ATN	
SHEET 01				SHEET 01		SHEET 01		SHEET 01	
A3				A3		A3		A3	

SolidWorks Student License
Academic Use Only

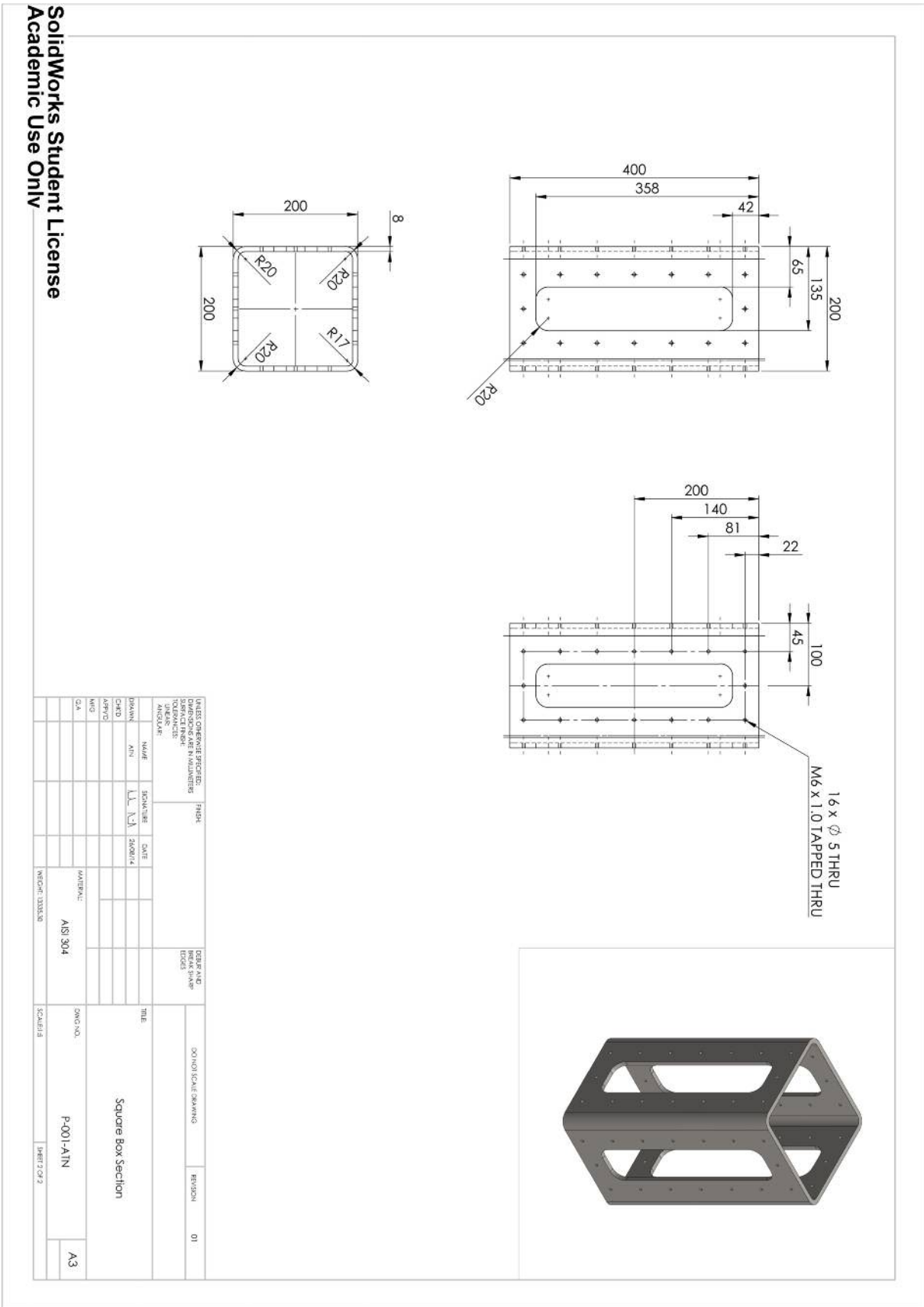


SolidWorks Student License
Academic Use Only

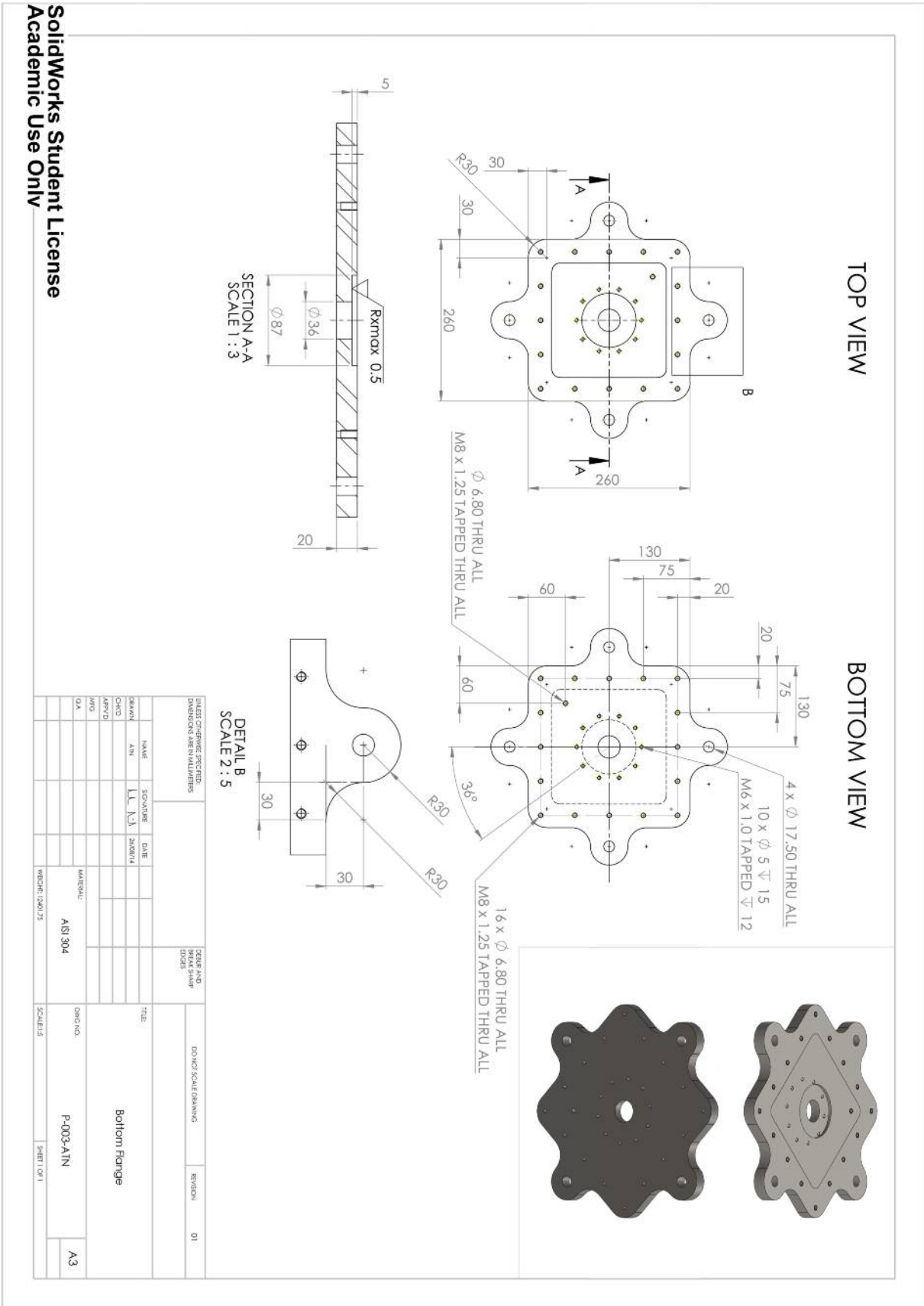
UNLESS OTHERWISE SPECIFIED: DIMENSIONS ARE IN MILLIMETERS TOLERANCES: FRACTIONS DECIMALS ANGLES		FINISH:	DATE:	20/08/14	DESIGN AND DRAWING SHEET NO.	REVISED	01
NAME:	NUMBER:	DATE:	20/08/14	TITLE:	Assembly - Aerator Housing		
SKETCH:	3/11	1/1	1/1				
CHKD:							
APP'D:							
MFG:							
DIA:							
					MATERIAL:		
					WEIGHT:		
					DWG NO.:	A-004-ATN	A3
					SCALE: 1:2		SHEET 1 OF 1

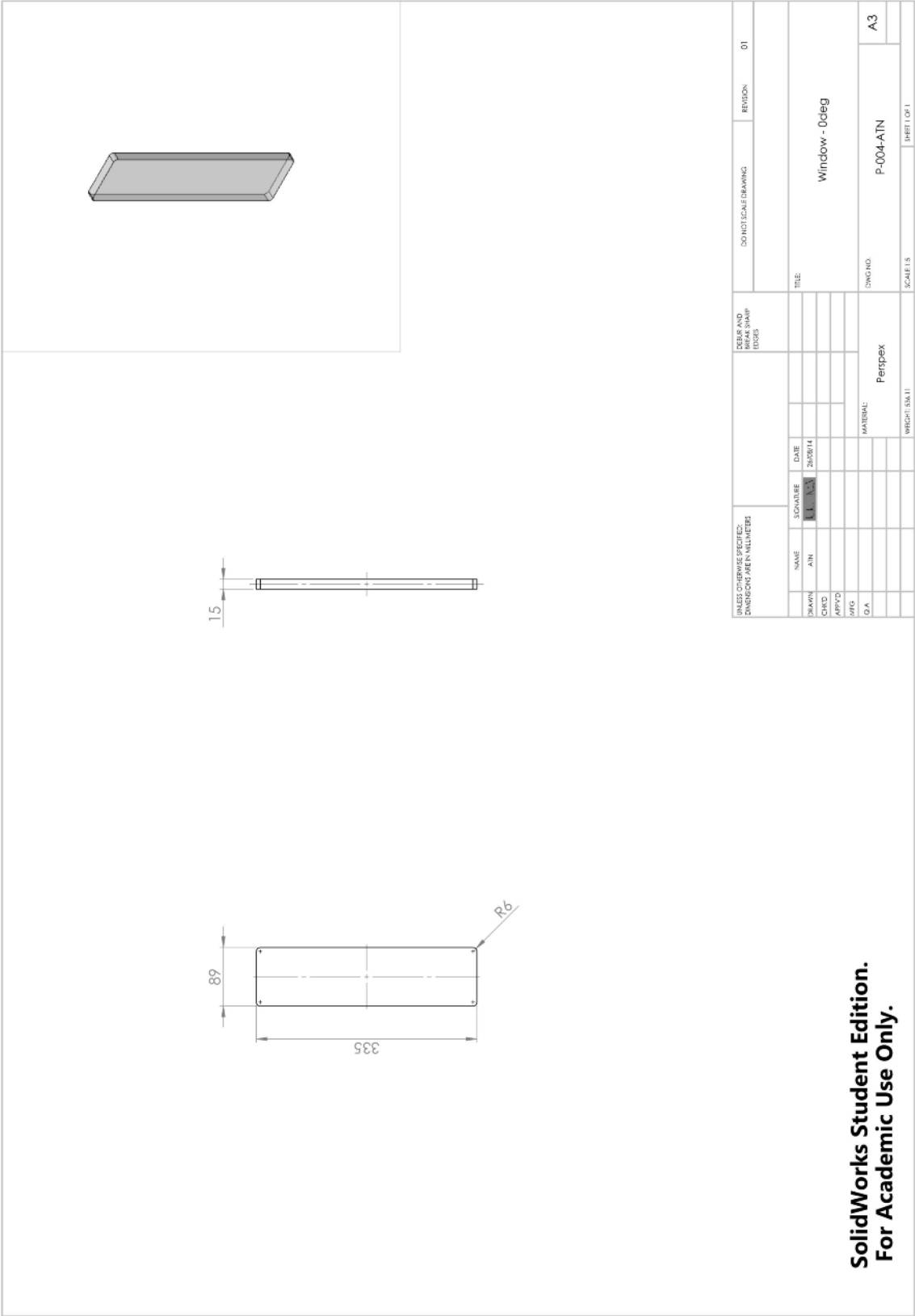


SolidWorks Student License
Academic Use Only



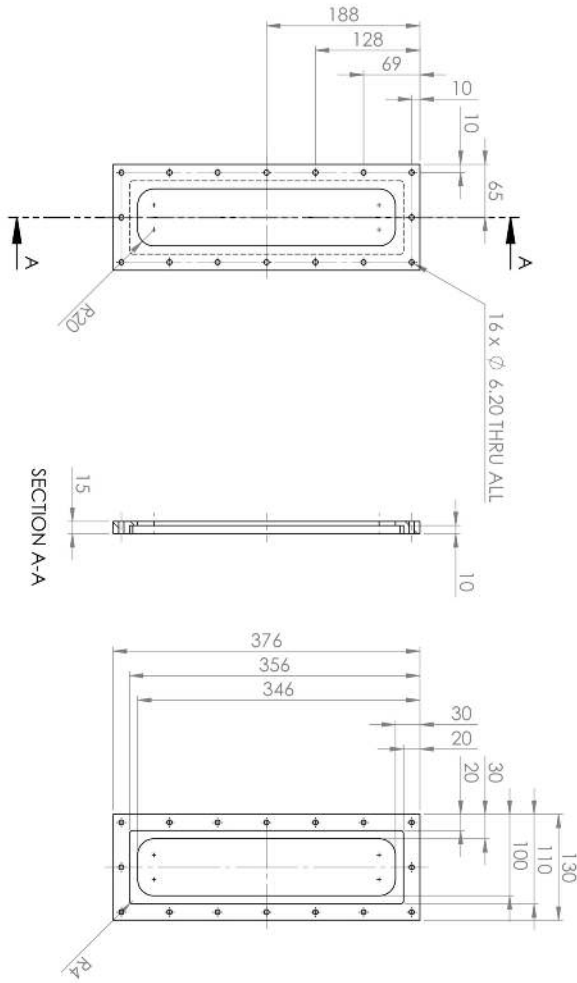
SolidWorks Student License
Academic Use Only





**SolidWorks Student Edition.
For Academic Use Only.**

SolidWorks Student Edition.
For Academic Use Only.



DATE OF CHANGE SPECIFIED				REVISION		SCALE		SHEET NO.	
NO.	DESCRIPTION	DATE	BY	NO.	DESCRIPTION	SCALE	NO.	DESCRIPTION	NO.
1	ISSUE			1		1:1	1		1

DESIGNER	NAME	DATE	TITLE
ENGINEER	AN	2023/11/14	Window Cassette
DRAWN			
CHECKED			
APPROVED			
QA			

DATE OF CHANGE SPECIFIED	REVISION	SCALE	SHEET NO.
1	1	1:1	1

DESIGNER	NAME	DATE	TITLE
ENGINEER	AN	2023/11/14	Window Cassette
DRAWN			
CHECKED			
APPROVED			
QA			

DESIGNER	NAME	DATE	TITLE
ENGINEER	AN	2023/11/14	Window Cassette
DRAWN			
CHECKED			
APPROVED			
QA			

DESIGNER	NAME	DATE	TITLE
ENGINEER	AN	2023/11/14	Window Cassette
DRAWN			
CHECKED			
APPROVED			
QA			

DESIGNER	NAME	DATE	TITLE
ENGINEER	AN	2023/11/14	Window Cassette
DRAWN			
CHECKED			
APPROVED			
QA			

DESIGNER	NAME	DATE	TITLE
ENGINEER	AN	2023/11/14	Window Cassette
DRAWN			
CHECKED			
APPROVED			
QA			

DESIGNER	NAME	DATE	TITLE
ENGINEER	AN	2023/11/14	Window Cassette
DRAWN			
CHECKED			
APPROVED			
QA			

DESIGNER	NAME	DATE	TITLE
ENGINEER	AN	2023/11/14	Window Cassette
DRAWN			
CHECKED			
APPROVED			
QA			

DESIGNER	NAME	DATE	TITLE
ENGINEER	AN	2023/11/14	Window Cassette
DRAWN			
CHECKED			
APPROVED			
QA			

DESIGNER	NAME	DATE	TITLE
ENGINEER	AN	2023/11/14	Window Cassette
DRAWN			
CHECKED			
APPROVED			
QA			

DESIGNER	NAME	DATE	TITLE
ENGINEER	AN	2023/11/14	Window Cassette
DRAWN			
CHECKED			
APPROVED			
QA			

DESIGNER	NAME	DATE	TITLE
ENGINEER	AN	2023/11/14	Window Cassette
DRAWN			
CHECKED			
APPROVED			
QA			

DESIGNER	NAME	DATE	TITLE
ENGINEER	AN	2023/11/14	Window Cassette
DRAWN			
CHECKED			
APPROVED			
QA			

DESIGNER	NAME	DATE	TITLE
ENGINEER	AN	2023/11/14	Window Cassette
DRAWN			
CHECKED			
APPROVED			
QA			

DESIGNER	NAME	DATE	TITLE
ENGINEER	AN	2023/11/14	Window Cassette
DRAWN			
CHECKED			
APPROVED			
QA			

DESIGNER	NAME	DATE	TITLE
ENGINEER	AN	2023/11/14	Window Cassette
DRAWN			
CHECKED			
APPROVED			
QA			

DESIGNER	NAME	DATE	TITLE
ENGINEER	AN	2023/11/14	Window Cassette
DRAWN			
CHECKED			
APPROVED			
QA			

DESIGNER	NAME	DATE	TITLE
ENGINEER	AN	2023/11/14	Window Cassette
DRAWN			
CHECKED			
APPROVED			
QA			

DESIGNER	NAME	DATE	TITLE
ENGINEER	AN	2023/11/14	Window Cassette
DRAWN			
CHECKED			
APPROVED			
QA			

DESIGNER	NAME	DATE	TITLE
ENGINEER	AN	2023/11/14	Window Cassette
DRAWN			
CHECKED			
APPROVED			
QA			

DESIGNER	NAME	DATE	TITLE
ENGINEER	AN	2023/11/14	Window Cassette
DRAWN			
CHECKED			
APPROVED			
QA			

DESIGNER	NAME	DATE	TITLE
ENGINEER	AN	2023/11/14	Window Cassette
DRAWN			
CHECKED			
APPROVED			
QA			

DESIGNER	NAME	DATE	TITLE
ENGINEER	AN	2023/11/14	Window Cassette
DRAWN			
CHECKED			
APPROVED			
QA			

DESIGNER	NAME	DATE	TITLE
ENGINEER	AN	2023/11/14	Window Cassette
DRAWN			
CHECKED			
APPROVED			
QA			

DESIGNER	NAME	DATE	TITLE
ENGINEER	AN	2023/11/14	Window Cassette
DRAWN			
CHECKED			
APPROVED			
QA			

DESIGNER	NAME	DATE	TITLE
ENGINEER	AN	2023/11/14	Window Cassette
DRAWN			
CHECKED			
APPROVED			
QA			

DESIGNER	NAME	DATE	TITLE
ENGINEER	AN	2023/11/14	Window Cassette
DRAWN			
CHECKED			
APPROVED			
QA			

DESIGNER	NAME	DATE	TITLE
ENGINEER	AN	2023/11/14	Window Cassette
DRAWN			
CHECKED			
APPROVED			
QA			

DESIGNER	NAME	DATE	TITLE
ENGINEER	AN	2023/11/14	Window Cassette
DRAWN			
CHECKED			
APPROVED			
QA			

DESIGNER	NAME	DATE	TITLE
ENGINEER	AN	2023/11/14	Window Cassette
DRAWN			
CHECKED			
APPROVED			
QA			

DESIGNER	NAME	DATE	TITLE
ENGINEER	AN	2023/11/14	Window Cassette
DRAWN			
CHECKED			
APPROVED			
QA			

DESIGNER	NAME	DATE	TITLE
ENGINEER	AN	2023/11/14	Window Cassette
DRAWN			
CHECKED			
APPROVED			
QA			

DESIGNER	NAME	DATE	TITLE
ENGINEER	AN	2023/11/14	Window Cassette
DRAWN			
CHECKED			
APPROVED			
QA			

DESIGNER	NAME	DATE	TITLE
ENGINEER	AN	2023/11/14	Window Cassette
DRAWN			
CHECKED			
APPROVED			
QA			

DESIGNER	NAME	DATE	TITLE
ENGINEER	AN	2023/11/14	Window Cassette
DRAWN			
CHECKED			
APPROVED			
QA			

DESIGNER	NAME	DATE	TITLE
ENGINEER	AN	2023/11/14	Window Cassette
DRAWN			
CHECKED			
APPROVED			
QA			

DESIGNER	NAME	DATE	TITLE
ENGINEER	AN	2023/11/14	Window Cassette
DRAWN			
CHECKED			
APPROVED			
QA			

DESIGNER	NAME	DATE	TITLE
ENGINEER	AN	2023/11/14	Window Cassette
DRAWN			
CHECKED			
APPROVED			
QA			

DESIGNER	NAME	DATE	TITLE
ENGINEER	AN	2023/11/14	Window Cassette
DRAWN			
CHECKED			
APPROVED			
QA			

DESIGNER	NAME	DATE	TITLE
ENGINEER	AN	2023/11/14	Window Cassette
DRAWN			
CHECKED			
APPROVED			
QA			

DESIGNER	NAME	DATE	TITLE
ENGINEER	AN	2023/11/14	Window Cassette
DRAWN			
CHECKED			
APPROVED			
QA			

DESIGNER	NAME	DATE	TITLE
ENGINEER	AN	2023/11/14	Window Cassette
DRAWN			
CHECKED			
APPROVED			
QA			

DESIGNER	NAME	DATE	TITLE
ENGINEER	AN	2023/11/14	Window Cassette
DRAWN			
CHECKED			
APPROVED			
QA			

DESIGNER	NAME	DATE	TITLE
ENGINEER	AN	2023/11/14	Window Cassette
DRAWN			
CHECKED			
APPROVED			
QA			

DESIGNER	NAME	DATE	TITLE
ENGINEER	AN	2023/11/14	Window Cassette
DRAWN			
CHECKED			
APPROVED			
QA			

DESIGNER	NAME	DATE	TITLE
ENGINEER	AN	2023/11/14	Window Cassette
DRAWN			
CHECKED			
APPROVED			
QA			

DESIGNER	NAME	DATE	TITLE
ENGINEER	AN	2023/11/14	Window Cassette
DRAWN			
CHECKED			
APPROVED			
QA			

DESIGNER	NAME	DATE	TITLE
ENGINEER	AN	2023/11/14	Window Cassette
DRAWN			
CHECKED			
APPROVED			
QA			

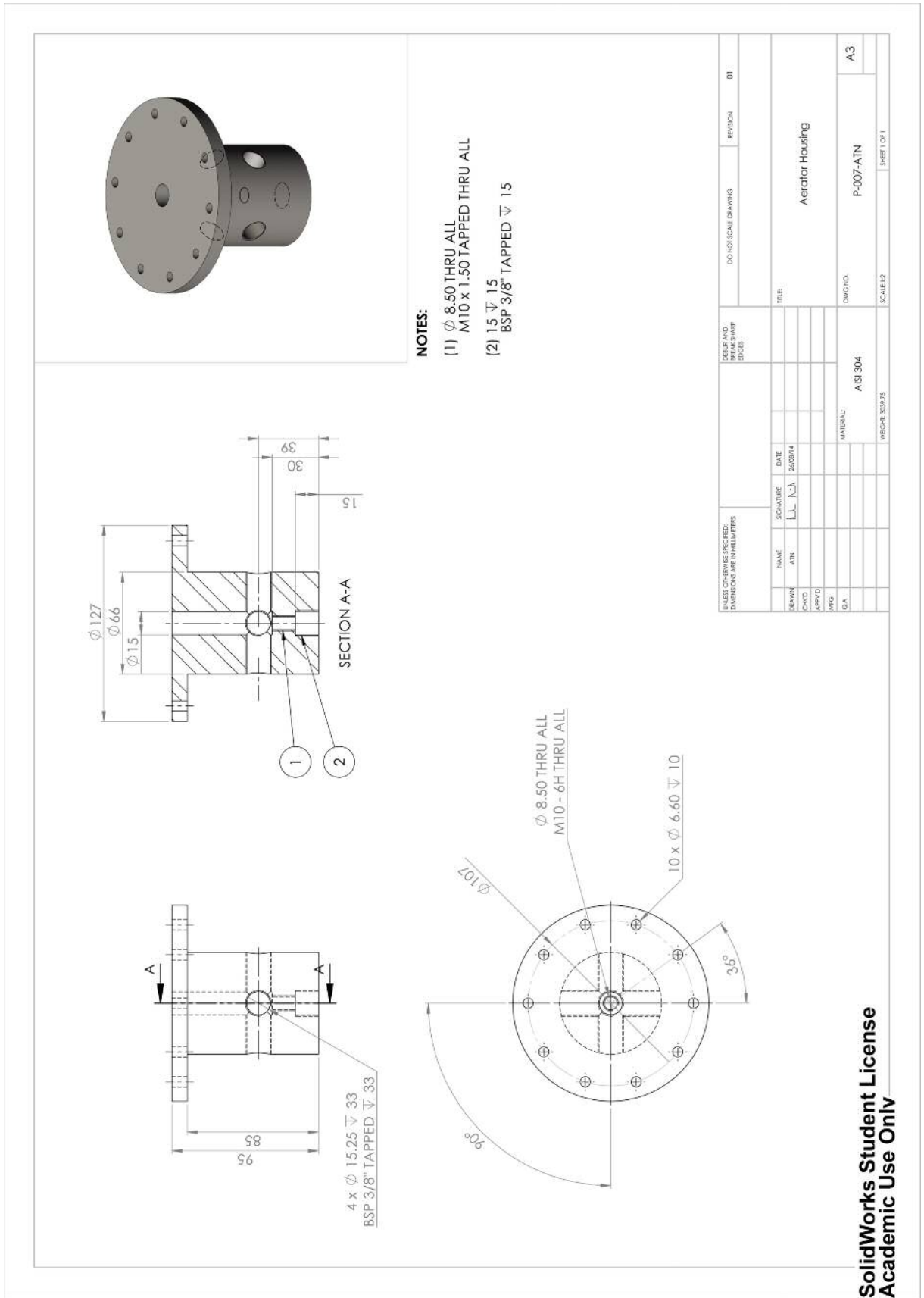
DESIGNER	NAME	DATE	TITLE
ENGINEER	AN	2023/11/14	Window Cassette
DRAWN			
CHECKED			
APPROVED			
QA			

DESIGNER	NAME	DATE	TITLE
ENGINEER	AN	2023/11/14	Window Cassette
DRAWN			
CHECKED			
APPROVED			
QA			

DESIGNER	NAME	DATE	TITLE
ENGINEER	AN	2023/11/14	Window Cassette
DRAWN			
CHECKED			
APPROVED			
QA			

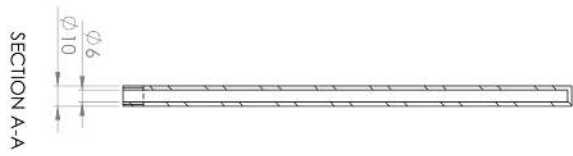
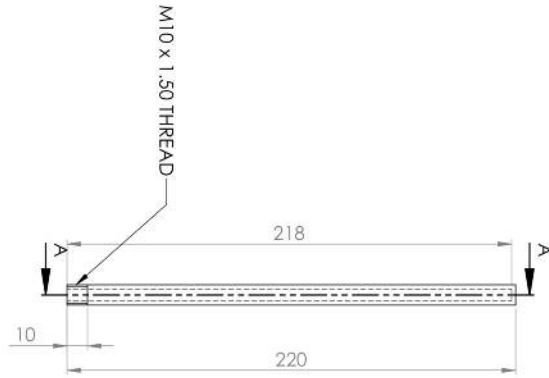
DESIGNER	NAME	DATE	TITLE
ENGINEER	AN	2023/11/14	Window Cassette
DRAWN			
CHECKED			
APPROVED			
QA			

DESIGNER	NAME	DATE	TITLE
ENGINEER	AN	2023/11/14	Window Cassette
DRAWN			



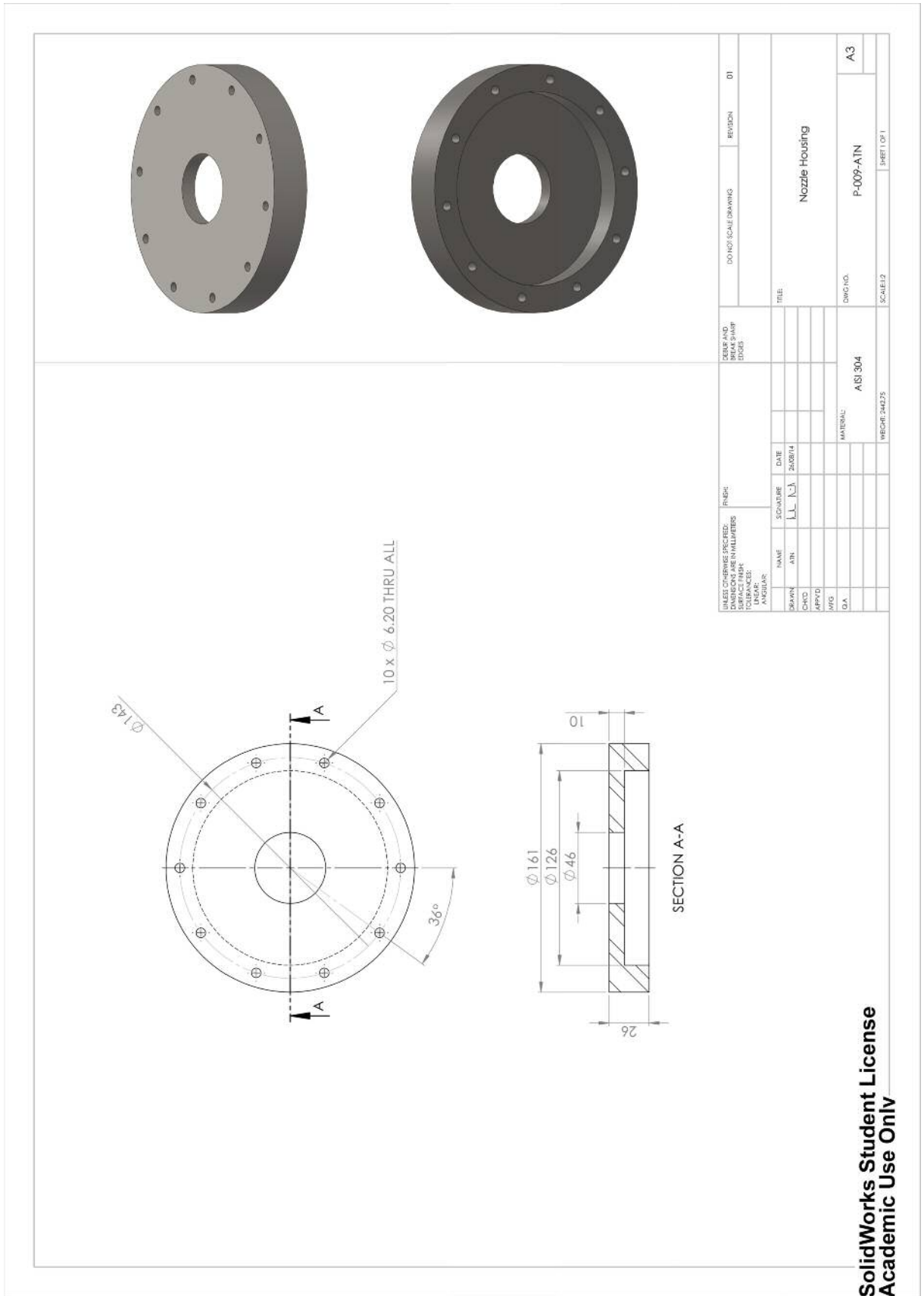
SolidWorks Student License
Academic Use Only

SOLIDWORKS Student Edition.
For Academic Use Only.



DESIGN CHANGES SPECIFIC TO THIS DRAWING				DATE AND REVISION		SHEET NUMBER	
NO.	DESCRIPTION	DATE	BY	NO.	DATE	OF	TOTAL
1	ISSUED FOR MANUFACTURE			1		1	1

DESIGNER	NAME	DATE	TITLE
CHKD	AIN		Aerolox Blank, 220 mm
APP'D			
Q/A			
MATERIAL		SCALE	
AISI 304		1:2	
WEIGHT REF		PART 1 OF 1	
PROJECT NO. P-008-2-A1N			
SHEET NO. A.3			

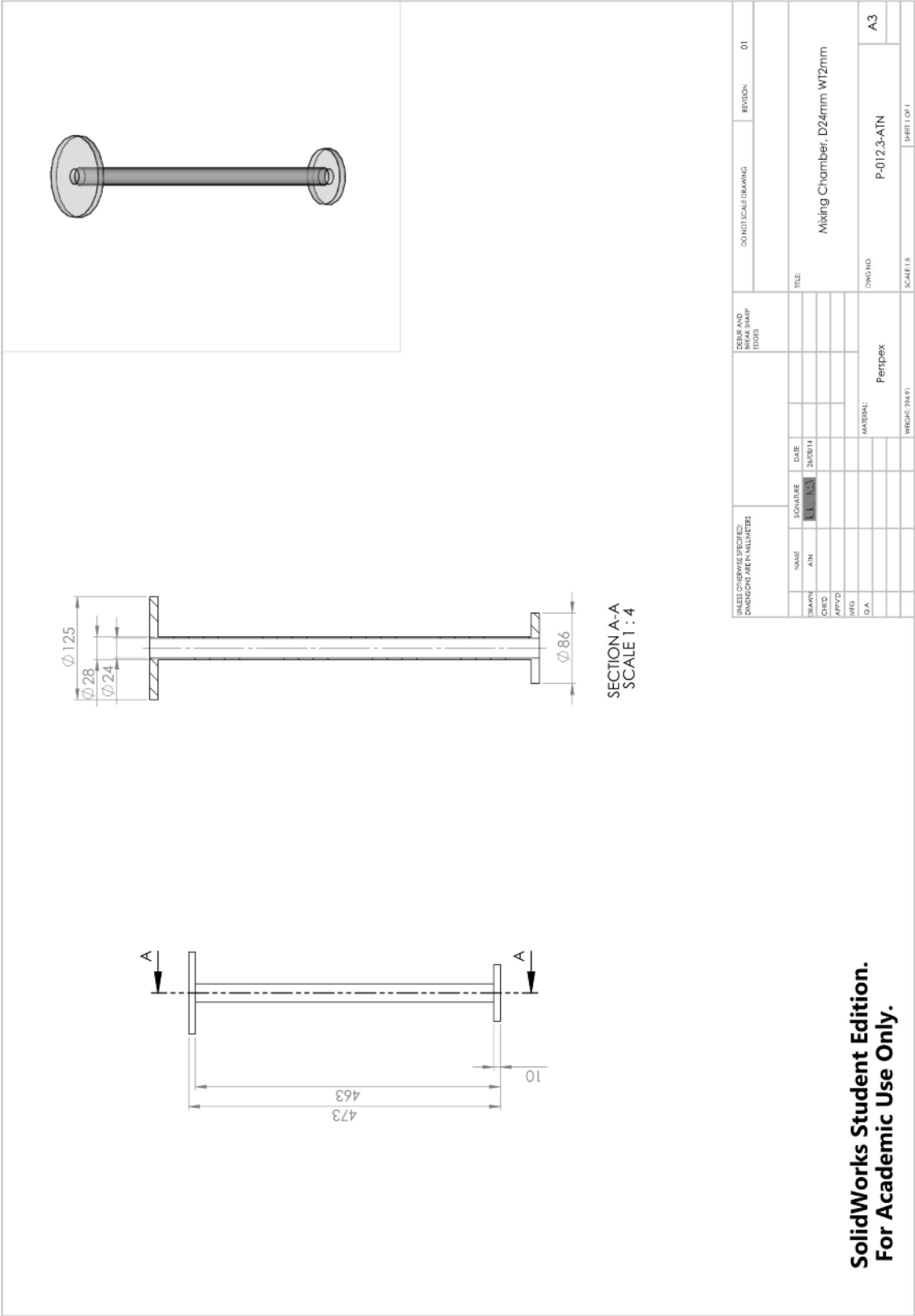


UNLESS OTHERWISE SPECIFIED: DIMENSIONS ARE IN MILLIMETERS TOLERANCES: FRACTIONS DECIMALS ANGLES:		FINISH: SURFACE TEXTURE		DEBUR AND REMOVE SHARP EDGES		DO NOT SCALE DRAWING		REVISION		DTI	
NAME	DATE	SCALE	DATE	TITLE		NOZZLE HOUSING					
SKETCH	DATE	SCALE	DATE								
CHKD	DATE	SCALE	DATE								
APP'D	DATE	SCALE	DATE								
MFG	DATE	SCALE	DATE								
DIA	DATE	SCALE	DATE								
				MATERIAL: AISI 304		DWG NO: P-009-A1N		SCALE: 1:1		SHEET 1 OF 1	
				WEIGHT: 248.25							

SolidWorks Student License
Academic Use Only

UNITS: DIMENSIONS SPECIFIED:		FRISH		DATE AND		REVISION	
DIMENSIONS		SIGNATURE		TIME		NO.	
DRWNR	ATV	[Signature]	[Signature]				
CHKD							
APP'D							
CLA							
MATERIAL: ALSI 304				SCALE: 1:1		REVISION: 01	
TITLE: Nozzle (Basic Discharge)				DRAWING NO.: P-010.1-ATN		SHEET NO.: A3	
PROJECT: MECH-120124				SCALE: 1:1		SHEET: 01	

SolidWorks Student License
Academic Use Only



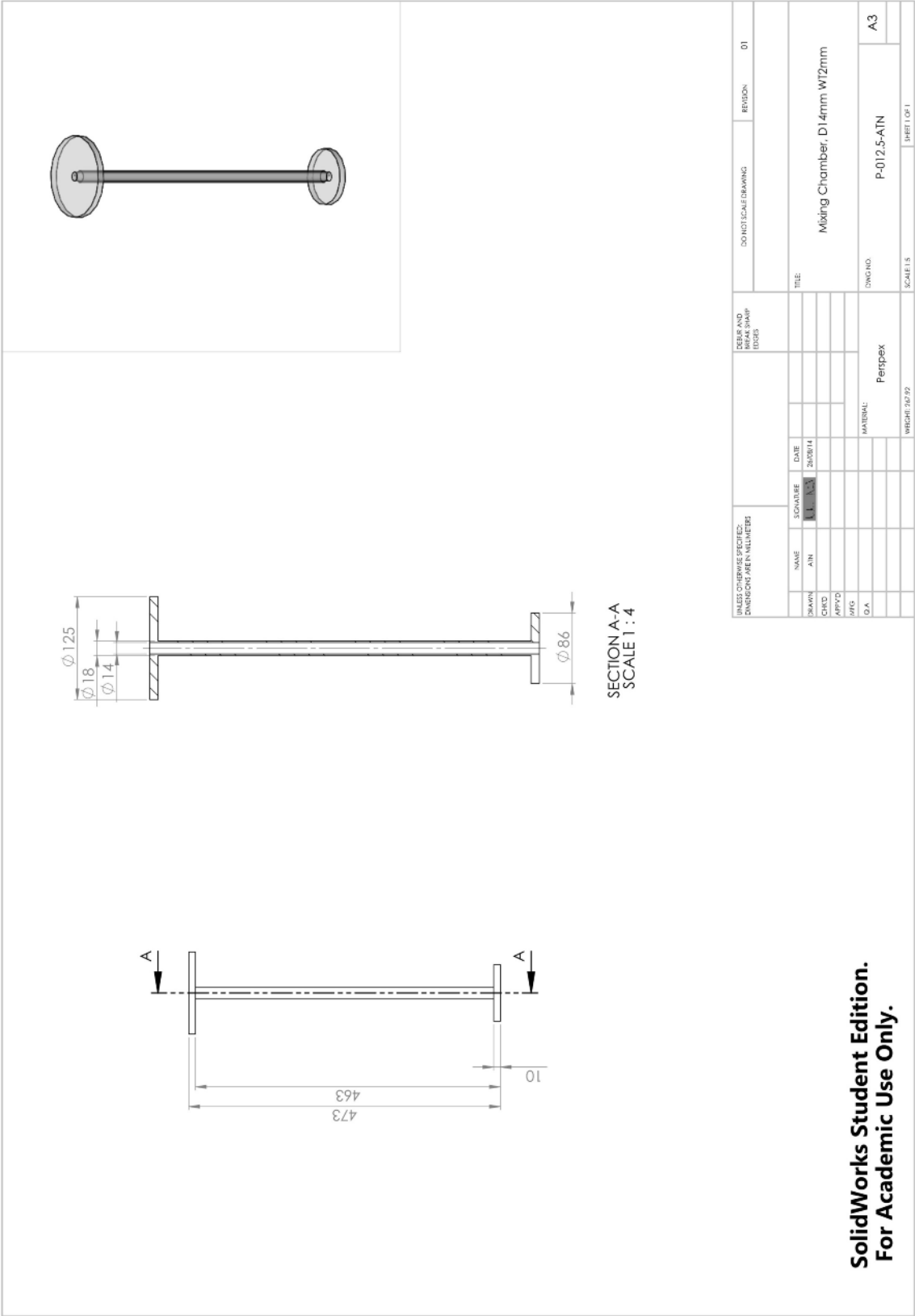
**SolidWorks Student Edition.
For Academic Use Only.**

UNLESS OTHERWISE SPECIFIED: DIMENSIONS ARE IN MILLIMETERS		DRAWING NO.		DO NOT SCALE DRAWING		REVISION		D1	
NAME	AN	SCALE	1:4	DATE	20/08/14	TITLE			
SHAPE						Mixing Chamber, D24mm WT2mm			
CHKD						DWG NO.			
APP'D						P-012.3-ATN			
MFG						SCALE			
D/A						A3			
MATERIAL						Perspex			
WEIGHT						24.91			
SHEET						1 OF 1			

SECTION A-A
SCALE 1 : 4

UNITS GIVEN IN PARENTHESES DIMENSIONS ARE IN MILLIMETERS		DATE AND DRAWN BY		DRAWN BY		SCALE		REVISION	
DATE	SIGNATURE	DATE	SCALE	BY	BY	BY	BY	NO.	DESCRIPTION
MATERIAL		TITLE		DWG NO.		SHEET NO.		SHEET TOTAL	
Permpex		Mixing Chamber, D20mm W12mm		P-0124-A1N		A3			

SolidWorks Student License
Academic Use Only

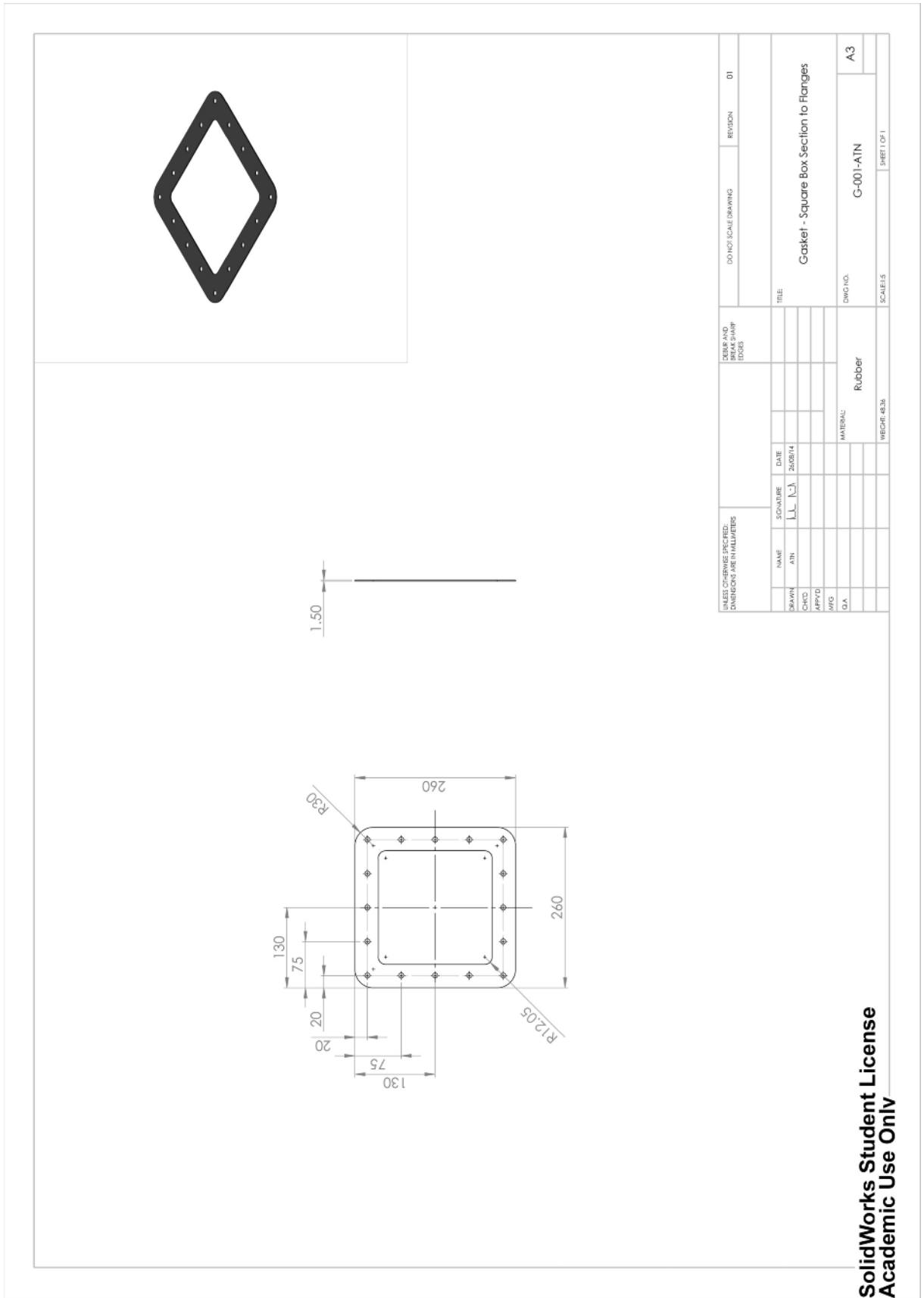


**SolidWorks Student Edition.
For Academic Use Only.**

UNLESS OTHERWISE SPECIFIED: DIMENSIONS ARE IN MILLIMETERS		NAME		DATE	DESK AND PLOT NUMBER		DO NOT SCALE DRAWING		REVISION	DWG NO.	SHEET 1 OF 1
SWORN	AIN	SCALE	DATE	20/08/14			MIXING CHAMBER, DI 14mm WT2mm				
CHKD											
APP'D											
MFG											
D/A											
					MATERIAL		PERSPEX		P-012.5-ATN		A3
					WEIGHT		260.99		SCALE		1:5

SolidWorks Student License
Academic Use Only

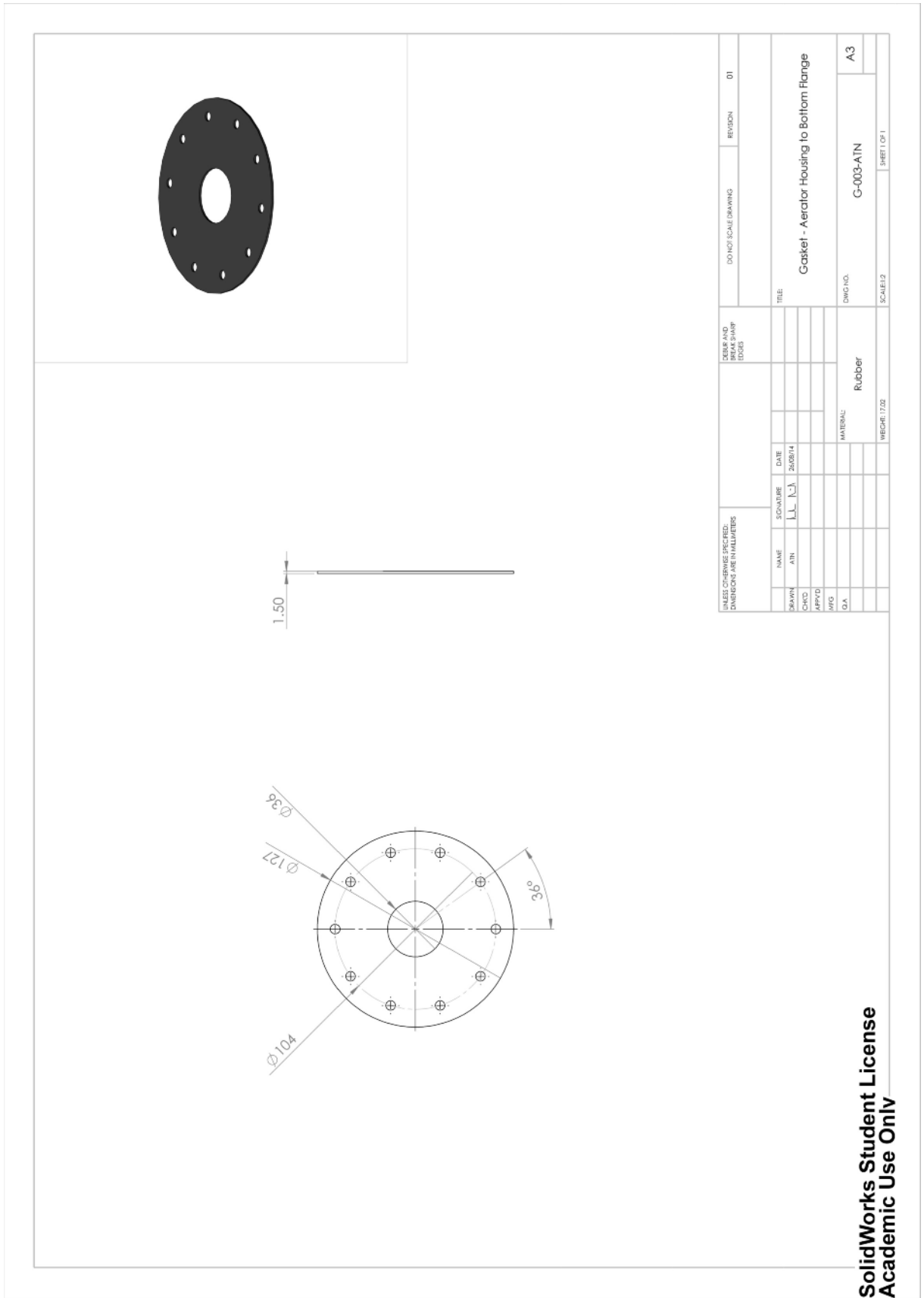
UNITS: DIMENSIONS: MILLIMETERS				FINISH		DATE AND TIME		SCALE	
TOLERANCES: ANGULAR				DATE		SCALE		REVISION	
DESIGN	DATE	SCALE	DATE	MATERIAL		DRAWING NO.		SHEET NO.	
APP'D	DATE	SCALE	DATE	MATERIAL		P-013-AN		A3	
CHK'D	DATE	SCALE	DATE	MATERIAL		P-013-AN		A3	
ENG	DATE	SCALE	DATE	MATERIAL		P-013-AN		A3	
CL	DATE	SCALE	DATE	MATERIAL		P-013-AN		A3	
INFORM. SYSTEMS				SCALE		SHEET NO.		SHEET TOTAL	



UNLESS OTHERWISE SPECIFIED: DIMENSIONS ARE IN MILLIMETERS				DATE AND DRAWN BY		DRAWN SCALE		REVISION	
NAME	SIGNATURE	DATE							
ATV	<i>[Signature]</i>								
DRAWN									
CHECKED									
APPROVED									
MFG									
C/A									
				MATERIAL		DRAWING NO.		SHEET NO.	
				Rubber		G-002-ANN		A3	
				WEIGHT: 13.2A		SCALE: 1:1		SHEET 1 OF 1	

DO NOT SCALE DRAWING	REVISION	01
TITLE		
Gasket - Window to Cassette		

SolidWorks Student License
Academic Use Only

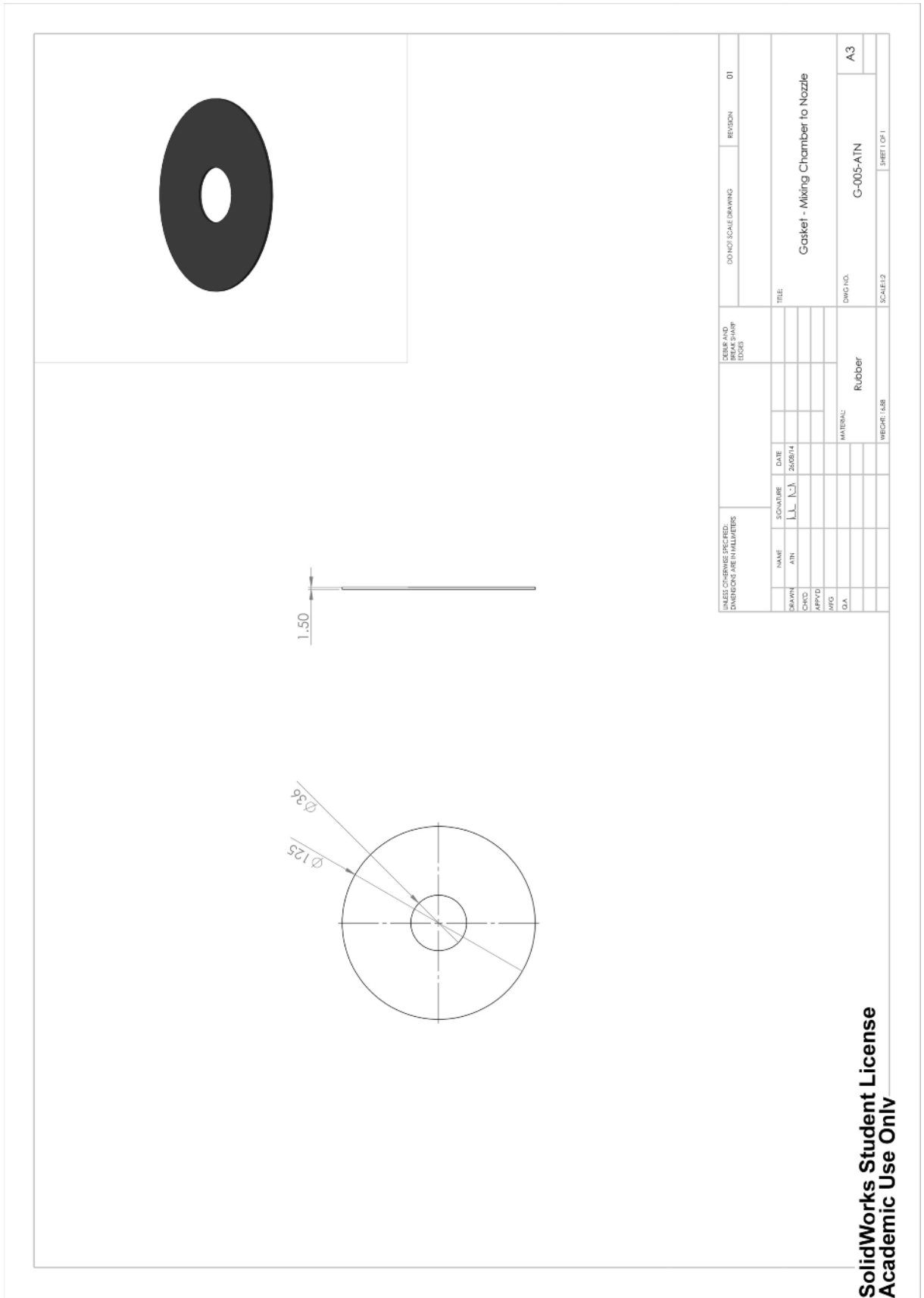


SolidWorks Student License
Academic Use Only

$\varnothing 125$
 $\varnothing 46$
 1.50

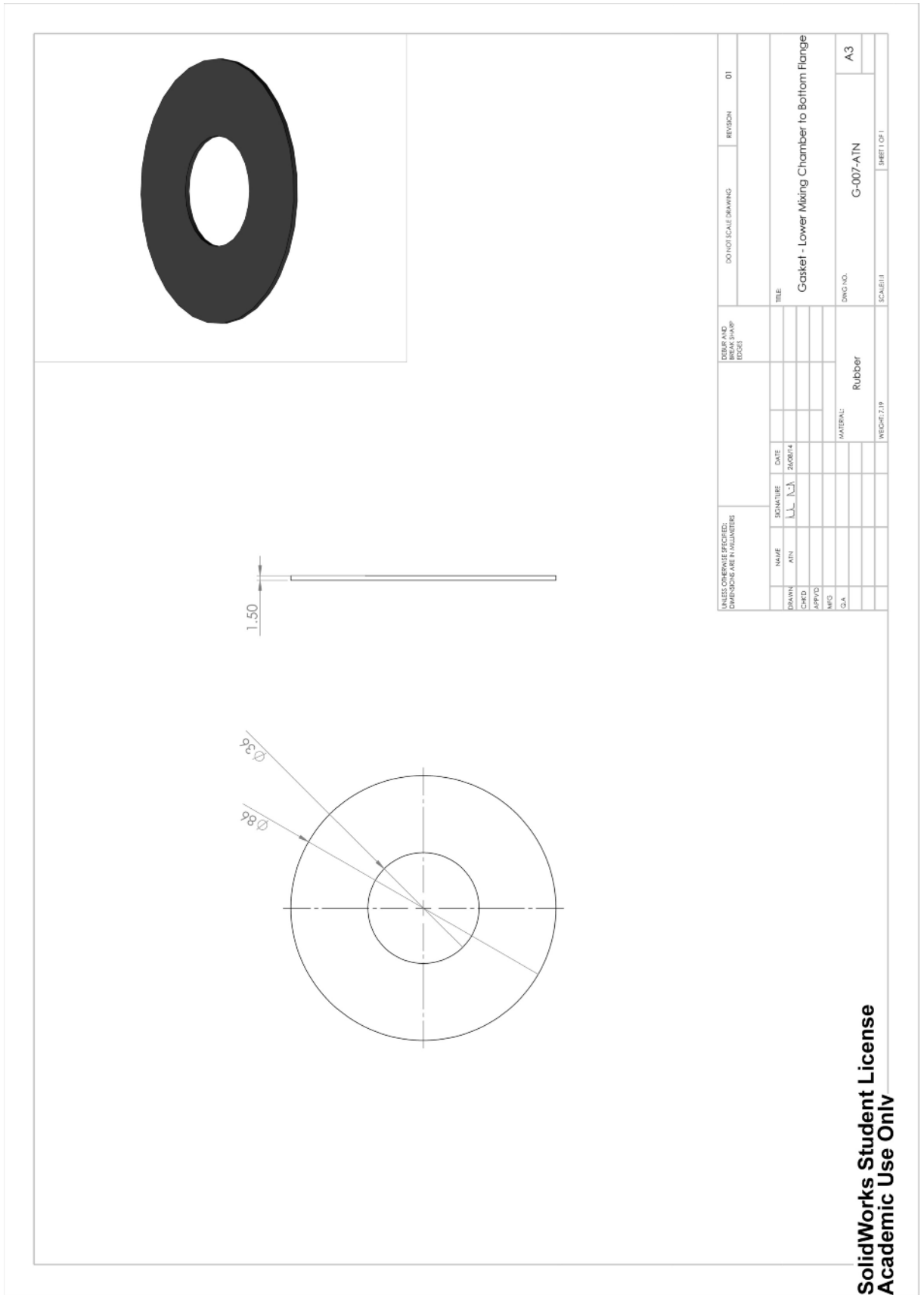
UNLESS OTHERWISE SPECIFIED: DIMENSIONS ARE IN MILLIMETERS				DATE AND DRAWN BY		DO NOT SCALE DRAWING		REVISION	
DRAWN	NAME	SIGNATURE	DATE						
CHKD	ATV	<i>[Signature]</i>							
APP'D									
MFG									
C/A									
				MATERIAL		SCALE		SHEET	
				Rubber		G-004-ANN		A3	
				WEIGHT (kg)		GASKET - Nozzle Housing to Nozzle		01	
				DRAWING NO.		G-004-ANN		01	
				SCALE		1:1		01	

SolidWorks Student License
Academic Use Only



UNLESS OTHERWISE SPECIFIED: DIMENSIONS ARE IN MILLIMETERS		DRAWING SCALE DRAWING		REVISION		D1	
DEBUR AND FILLS SHARP EDGES		TITLE		Gasket - Mixing Chamber to Nozzle		A3	
NAME	SKETCHER	DATE	MATERIAL		DWG NO.		SCALE
JIN	L. L.	26/08/14	Rubber		G-005-A1N		SHEET 1 OF 1
CHKD			WEIGHT: 1.488				
APP'D							
MFG							
D.A.							

SolidWorks Student License
Academic Use Only



SolidWorks Student License
Academic Use Only

APPENDIX 4: MATHWORKS[®] MATLAB[®] SCRIPTS

A4.1 Optimisation of High-Speed Internal Flow Imagery

PROCESS RAW RESULTS VIDEO

Straightens and crops raw video files to the mixing chamber dimensions

Contents

- [Run Function](#)
- [Initialise](#)
- [Define Directories](#)
- [Process Video Files](#)

Run Function

```
function CreateResultsVideoFromAVIData
```

Initialise

```
clear; clc; close all;
path(path,genpath('/Users/Andrew_Niland/Documents/MATLAB/Additional
Functions/uipickfiles'));
path(path,genpath('/Users/Andrew_Niland/Documents/MATLAB/Additional
Functions/mmread'));
path(path,genpath('/Users/Andrew_Niland/Documents/MATLAB/Additional
Functions/export_fig'));
path(path,genpath('/Users/Andrew_Niland/Documents/MATLAB/Additional
Functions')); %Specify additional function directories
```

Define Directories

```
Home=cd; %Specify root directory

Dir_RawResults='/Volumes/AN PhD Data/Study 1 - Aerator Characterisation/Raw
Data'; %Specify directory of original video
Dir_NewResults='/Volumes/AN PhD Data/Study 1 - Aerator
Characterisation/Processed Data'; %Specify target directory for processed
video

UserFolderSelection=uipickfiles('FilterSpec',Dir_RawResults,'Output','struct
'); %REF: http://uk.mathworks.com/matlabcentral/fileexchange/10867-
uipickfiles--uigetfile-on-steroids

ListofContents_ORGFolders=[]; %Initiate List of Contents for Target Folder

for x=1:length(UserFolderSelection) %Process List of Contents in Target
Folder

    Temp=subdir(UserFolderSelection(x).name); %REF:
http://uk.mathworks.com/matlabcentral/fileexchange/1492-subdir--new-

    ListofContents_ORGFolders=[ListofContents_ORGFolders;UserFolderSelection(x).
name;Temp'];

end

fprintf('Starting Video Processing\n');

[Temp,~]=size(ListofContents_ORGFolders); %Calculate number of files in
Target Folder
```

Starting Video Processing

Process Video Files

```

for y=1:Temp %For each file

    fprintf('%d\n',y)

    ListofContents_avi=dir(char(strcat(ListofContents_ORGFolders(y,:), '/*.avi'))
); %Find only .AVI video files

    n=0; %Remove .AVI files less than 10MB
    while n<length(ListofContents_avi)
        n=n+1;
        if ListofContents_avi(n).bytes<10000
            ListofContents_avi(n)=[];
            n=n-1;
        end
    end

    for n=1:length(ListofContents_avi) %For .AVI files > 10MB

        fprintf('%d.%d\n',y,n)

        %Specify Naming and Directories
        fileName=ListofContents_avi(n).name;
        Dir_OLDFolder=ListofContents_ORGFolders(y,:);
        Dir_OLDFolder=Dir_OLDFolder{1};
        Dir_NEWFolder=strrep(Dir_OLDFolder,Dir_RawResults,Dir_NewResults);

        cd(Home);
        ConvertVideo(fileName,Dir_OLDFolder,Dir_NEWFolder); %Convert Video
with function "Convert Video"

        close all;

    end

end

```

1

2

2.1

3

end

Published with MATLAB® R2015b

STRAIGHTEN AND CROP RAW VIDEO FILES

Perform the process of straightening and cropping the raw video files to the mixing chamber dimensions

Contents

- [Run Function](#)
- [Initialise](#)
- [Process Single Image](#)
- [Process Video](#)

Run Function

```
% function
[ConvertedVideoName]=ConvertVideo(fileName,Dir_OLDFolder,Dir_NEWFolder)
```

Initialise

```
cd(Dir_OLDFolder) %Go to Original Video location

Dir_File=[Dir_OLDFolder,'/',fileName]; %Specify video directory
VideoInfo=mmfileinfo(Dir_File); %Read video details
Name={VideoInfo.Filename(1:(end-4))}; %Specify video file name
Name=Name{1,1};
ConvertedVideoName=[Dir_NEWFolder,'/',Name,' Converted Video.avi'];
%Specify processed video file directory
```

Process Single Image

```
%Take first image of original video (process depends on video format)
switch VideoInfo.Video.Format
case 'None'
    obj = VideoReader(Dir_File); %Read original video
    frames = obj.NumberOfFrames; %Calculate number of frames
    Pic = read(obj,1); %Take first image
    Pic=rgb2gray(Pic); %Convert image to grayscale
    [length,width]=size(Pic); %Calculate resolution of image/video
    widthdiff=(width-390)/2; %Specifies crop window
    Pic=imcrop(Pic,[round(widthdiff),0,(width-
(2*round(widthdiff))),1024]); %Crop image to window
    case 'RGB 24'
        obj = VideoReader(Dir_File);
        frames = obj.NumberOfFrames;
        Pic = read(obj,1);
        Pic=rgb2gray(Pic);
        [length,width]=size(Pic);
        widthdiff=(width-390)/2;
        Pic=imcrop(Pic,[round(widthdiff),0,(width-
(2*round(widthdiff))),1024]);
    case 'Xvid'
        vid=mmread(Dir_File);
        [~,frames]=size(vid.frames);
        Pic=rgb2gray(vid.frames(1).cdata);
        [length,width]=size(Pic);
        widthdiff=(width-390)/2;
        Pic=imcrop(Pic,[round(widthdiff),0,(width-
(2*round(widthdiff))),1024]);
    case 'XVID'
        vid=mmread(Dir_File);
        [~,frames]=size(vid.frames);
        Pic=rgb2gray(vid.frames(1).cdata);
        [length,width]=size(Pic);
```

```

        widthdiff=(width-390)/2;
        Pic=imcrop(Pic,[round(widthdiff),0,(width-
(2*round(widthdiff))),1024]);
        case 'Motion JPEG'
            obj = VideoReader(Dir_File);
            frames = obj.NumberOfFrames;
            Pic = read(obj,1);
            Pic=rgb2gray(Pic);
            [length,width]=size(Pic);
            widthdiff=(width-390)/2;
            Pic=imcrop(Pic,[round(widthdiff),0,(width-
(2*round(widthdiff))),1024]);
        end

PicBW = edge(Pic,'prewitt'); %Convert image to logical array based on edges
se = strel('disk',5); %Specify discontinuity threshold
PicBW = imclose(PicBW,se); %Merge discontinuities
[l,w]=size(PicBW); %Calculate image size
PicBW=[ones(1,w);PicBW;ones(1,w)]; %Close image with rows of 1 on top and
bottom
for x=1:floor(l/100)
    y=100*x;
    PicBW=[PicBW(1:y,:);ones(1,w);PicBW(y+1:end,:)];
end
PicBW=imfill(PicBW,'holes'); %Close holes (i.e. fill mixing chamber as 1)
PicBW(1,:)=[]; PicBW(end,:)=[]; %Delete rows of 1 on top and bottom
for x=1:floor(l/100)
    y=100*x;
    a=x-1;
    PicBW(y-a,:)=[];
end
PicBW = edge(PicBW,'prewitt'); %Calculate logical array for edge of mixing
chamber

%Find Mixing Chamber Edge in Image

[H, theta, rho] = hough(PicBW,'Theta',-45:0.01:45);
P = houghpeaks(H,2,'threshold',ceil(0.3*max(H(:)))));
lines = houghlines(Pic,theta,rho,P,'FillGap',5,'MinLength',7);

%Determine Co-ordinates of mixing chamber edge image
linestart=[];
lineend=[];
[~,Temp]=size(lines);
for k = 1:Temp
    linestart(k,:)=lines(k).point1;
    lineend(k,:)=lines(k).point2;
end
for k = 1:Temp
    linestart(k,3)=lines(k).theta;
    lineend(k,3)=lines(k).theta;
end

linestart=sortrows(linestart);
lineend=sortrows(lineend);
linestart2=linestart;
lineend2=lineend;

val = 195; %value to find
tmp = abs(linestart-val);

[ida]=find(linestart(:,1)>195);
linestart2(ida,:)=[];
tmp = abs(linestart2-val);
[idb idb] = min(tmp(:,1)); %index of closest value
x1 = linestart2(idb,1); %closest value

```

```

y1 = linestart2(idb,2); %closest value
thetal = linestart2(idb,3);

[ida]=find(linestart(:,1)<195);
lineend2(ida,:)=[];
tmp = abs(lineend2-val);
[idb idb] = min(tmp(:,1)); %index of closest value
x2 = lineend2(idb,1); %closest value
y2 = lineend2(idb,2); %closest value
theta2 = lineend2(idb,3); %closest value

theta=(thetal+theta2)/2;

%Perform Straighten and Crop Image

s=size(Pic);
marker=zeros(s);
marker(y1,x1)=1;
marker_rot = imrotate(marker,theta,'bilinear');
[~,location] = max(marker_rot(:));
[y1n,x1n]=ind2sub(size(marker_rot),location);

s=size(Pic);
marker=zeros(s);
marker(y2,x2)=1;
marker_rot = imrotate(marker,theta,'bilinear');
[~,location] = max(marker_rot(:));
[y2n,x2n]=ind2sub(size(marker_rot),location);

cropect=[x1n,y1n,x2n-x1n,y2n-y1n];

s=size(Pic);
sample=ones(s);
sampleRot=imrotate(sample,theta,'bilinear');
sampleRot=imcrop(sampleRot,cropect);
rows_to_remove = any(sampleRot<1, 2); sampleRot(rows_to_remove,:) = [];
columns_to_remove = any(sampleRot<1, 1); sampleRot(columns_to_remove,:) =
[];

```

Process Video

```

writerObj=VideoWriter(ConvertedVideoName); %PRIMES THE VideoWriter FUNCTION,
WHERE EACH EXPERIMENTAL IS ADDED INDIVIDUALLY THROUGHOUT ANALYSIS TO FORM A
VIDEO SEQUENCE
writerObj.FrameRate=20; %THE FRAME RATE OF THE PROCESSED VIDEO MATCHES THE
ORIGINAL VIDEO
open(writerObj); %STARTS THE VideoWriter FUNCTION

for x = 1 : frames %For all video frames
    switch VideoInfo.Video.Format %Take image of original video (process
depends on video format) and apply crop and straightening determined above
        case 'None'
            Pic = read(obj,x);
            Pic=rgb2gray(Pic);
            Pic=imcrop(Pic,[round(widthdiff),0,(width-
(2*round(widthdiff))),length]);
            PicRot=imrotate(Pic,theta,'bilinear');
            PicRot=imcrop(PicRot,cropect);
            PicRot(rows_to_remove,:) = []; PicRot(columns_to_remove,:) = [];
            PicRot=imadjust(imsharpen(PicRot));
            PicRot=wiener2(PicRot);
            writeVideo(writerObj,PicRot); %WRITE FRAME TO VIDEO
        case 'RGB 24'
            Pic = read(obj,x);
            Pic=rgb2gray(Pic);

```

```

        Pic=imcrop(Pic,[round(widthdiff),0,(width-
(2*round(widthdiff))),length]);
        PicRot=imrotate(Pic,theta,'bilinear');
        PicRot=imcrop(PicRot,cropect);
        PicRot(rows_to_remove,:) = []; PicRot(columns_to_remove,:) = [];
        PicRot=imadjust(imsharpen(PicRot));
        PicRot=wiener2(PicRot);
        writeVideo(writerObj,PicRot); %WRITE FRAME TO VIDEO
    case 'Xvid'
        Pic=rgb2gray(vid.frames(x).cdata);
        Pic=imcrop(Pic,[round(widthdiff),0,(width-
(2*round(widthdiff))),length]);
        PicRot=imrotate(Pic,theta,'bilinear');
        PicRot=imcrop(PicRot,cropect);
        PicRot(rows_to_remove,:) = []; PicRot(columns_to_remove,:) = [];
        PicRot=imadjust(imsharpen(PicRot));
        PicRot=wiener2(PicRot);
        writeVideo(writerObj,PicRot); %WRITE FRAME TO VIDEO
    case 'XVID'
        Pic=rgb2gray(vid.frames(x).cdata);
        Pic=imcrop(Pic,[round(widthdiff),0,(width-
(2*round(widthdiff))),length]);
        PicRot=imrotate(Pic,theta,'bilinear');
        PicRot=imcrop(PicRot,cropect);
        PicRot(rows_to_remove,:) = []; PicRot(columns_to_remove,:) = [];
        PicRot=imadjust(imsharpen(PicRot));
        PicRot=wiener2(PicRot);
        writeVideo(writerObj,PicRot); %WRITE FRAME TO VIDEO
    case 'Motion JPEG'
        Pic = read(obj,x);
        Pic=rgb2gray(Pic);
        Pic=imcrop(Pic,[round(widthdiff),0,(width-
(2*round(widthdiff))),length]);
        PicRot=imrotate(Pic,theta,'bilinear');
        PicRot=imcrop(PicRot,cropect);
        PicRot(rows_to_remove,:) = []; PicRot(columns_to_remove,:) = [];
        PicRot=imadjust(imsharpen(PicRot));
        PicRot=wiener2(PicRot);
        writeVideo(writerObj,PicRot); %WRITE FRAME TO VIDEO
    end
end
close(writerObj); %STOP RECORDING VIDEO

%end

```

Published with MATLAB® R2015b

A4.2 Bubble Sizing and Feature Tracking for Internal Flow

BUBBLE IMAGE ANALYSIS SOFTWARE

The BUBBLE IMAGE ANALYSIS SOFTWARE quantifies discrete bubbles within images and outputs results to a user defined directory.

Contents

- INITIALISE
- DETERMINE DIRECTORIES
- IMAGE SCALE
- SAMPLE IMAGE OPTIMISATION
- IMAGE ANALYSIS
- FINALISE

INITIALISE

```
clear all; clc; close; %CLEAR WORKSPACE AND COMMAND WINDOW

%SOFTWARE INTRODUCTION MENU - USER COMMUNICATION USES fprintf FOR SIMPLE
DISPLAY (\n = new line, \t = tab, <a href=""> </a> = hyperlink) OR
str2double(cell2mat(inputdlg()) FOR USER str2double(cell2mat(inputdlg
fprintf(2, '\n\t\t\t<strong>                BUBBLE IMAGE ANALYSIS SOFTWARE
</strong>\n
_____ ') %#ok<PRTCAL>

fprintf('\n\nThe BUBBLE IMAGE ANALYSIS SOFTWARE quantifies discrete bubbles
within images and outputs results \nto a user defined directory.\n\n')
fprintf('This software was compiled by Andrew Niland, with reference to:')
fprintf('\n\t1. <a
href="http://uk.mathworks.com/help/matlab/?refresh=true">MATLAB
Documentation</a>')
fprintf('\n\t2. <a
href="http://uk.mathworks.com/help/vision/examples/motion-based-multiple-
object-tracking.html">Matlab Documentation: Motion-Based Multiple Object
Tracking</a>')
fprintf('\n\t3. <a href="http://uk.mathworks.com/videos/image-processing-
made-easy-81718.html">Matlab Webinar: Image Processing</a>')
fprintf('\n\t4. <a
href="http://www.mathworks.com/matlabcentral/fileexchange/10959-sort-nat--
natural-order-sort">Function: Sort_Nat (Douglas M. Schwarz)</a>')
fprintf('\n\t5. <a href="http://blogs.mathworks.com/pick/2010/09/17/sorting-
structure-arrays-based-on-fields/">Function: Sort_Struct (Jiro Doke)</a>')
fprintf('\n\t6. <a
href="http://www.mathworks.com/matlabcentral/fileexchange/10564-convert-
struct-to-cell-array-with-column-headers">Function:
StructToCellArrayWithHeaders (Andrew Blackburn)</a>')
fprintf('\n\t7. <a
href="http://uk.mathworks.com/matlabcentral/newsreader/view_thread/28286">Fu
nction: UI Control, Slider Bar (Lars Gregersen)</a>')
fprintf('\n\t8. <a
href="http://uk.mathworks.com/matlabcentral/answers/56236-how-to-constantly-
update-a-plot-off-of-a-slider-being-pulled">Function: UI Control, Slider Bar
Callback (Teja Muppirala, edited by John Kelly)</a>\n\n')

_____ <strong>                BUBBLE IMAGE ANALYSIS SOFTWARE
_____

</strong>
```

The BUBBLE IMAGE ANALYSIS SOFTWARE quantifies discrete bubbles within images and outputs results

to a user defined directory.

This software was compiled by Andrew Niland, with reference to:

1. [MATLAB Documentation](http://uk.mathworks.com/help/matlab/?refresh=true)
2. [Matlab Documentation: Motion-Based Multiple Object Tracking](http://uk.mathworks.com/help/vision/examples/motion-based-multiple-object-tracking.html)
3. [Matlab Webinar: Image Processing](http://uk.mathworks.com/videos/image-processing-made-easy-81718.html)
4. [Function: Sort_Nat \(Douglas M. Schwarz\)](http://www.mathworks.com/matlabcentral/fileexchange/10959-sort-nat--natural-order-sort)
5. [Function: Sort_Struct \(Jiro Doke\)](http://blogs.mathworks.com/pick/2010/09/17/sorting-structure-arrays-based-on-fields/)
6. [Function: StructToCellArrayWithHeaders \(Andrew Blackburn\)](http://www.mathworks.com/matlabcentral/fileexchange/10564-convert-struct-to-cell-array-with-column-headers)
7. [Function: UI Control, Slider Bar \(Lars Gregersen\)](http://uk.mathworks.com/matlabcentral/newsreader/view_thread/28286)
8. [Function: UI Control, Slider Bar Callback \(Teja Muppirala, edited by John Kelly\)](http://uk.mathworks.com/matlabcentral/answers/56236-how-to-constantly-update-a-plot-off-of-a-slider-being-pulled)

DETERMINE DIRECTORIES

```
fprintf('
_____
\n\n<strong>DETERMINE
DIRECTORIES</strong>\nDetermine directories allows the user to select the
file locations critical to program operation.\n')

while 2==2 %ARBITRARY TRUE CONDITION USED TO START INFINITE WHILE LOOP

    fprintf('\n\t1 of 3: Please locate the Bubble Analysis Program Files\n')
    Dir_Home=uigetdir('/Users/Andrew_Niland/Dropbox/Documents/CARDIFF
UNIVERSITY/2013-2016 PhD','Locate the Bubble Analysis Program Files');
    %PROMPTS USER TO SELECT THE PROGRAM'S MATLAB SCRIPT FOLDER
    fprintf('\t2 of 3: Please locate the directory in which the Experimental
Images are held\n\t\tN.B. If not already, the image showing the calibration
scale should be \n\t\t\trepositioned in the selected directory\n')
    Dir_Images=uigetdir('/Users/Andrew_Niland/Dropbox/Documents/CARDIFF
UNIVERSITY/2013-2016 PhD','Locate the Experimental Images'); %PROMPTS USER
TO SELECT IMAGE FOLDER
```

```

    fprintf('\t3 of 3: Please locate the directory into which the Results
    can be outputted\n\t\tN.B. A new folder can be created from the selection
    window\n')
    Dir_AllResults=uigetdir('/Users/Andrew_Niland/Dropbox/Documents/CARDIFF
    UNIVERSITY/2013-2016 PhD','Select a Directory for Results'); %PROMPTS USER
    TO SELECT SAVE LOCATION

    if all(Dir_Home)==true && all(Dir_Images)==true &&
    all(Dir_AllResults)==true %IF DIRECTORIES ARE COMPLETE, PROGRAM WILL
    CONTINUE TO IMAGE SCALE
        fprintf('
        ----- \n\nDETERMINE DIRECTORIES COMPLETE\n')
        break
    end
    fprintf('\n\nDETERMINE DIRECTORIES INCOMPLETE\n') %IF DIRECTORIES ARE
    INCOMPLETE, THE USER HAS THE OPTION TO EXIT OR REDO THE PROCESS
    UserSelection=str2double(cell2mat(inputdlg('Do you want to continue
    (1=Yes/2=No): ')));
    switch UserSelection
        case 2
            error('***BUBBLE IMAGE ANALYSIS SOFTWARE - TERMINATED BY
    USER***')
        otherwise
            continue
    end
end

save([Dir_AllResults,'/Directories.mat'],'Dir_Home','Dir_Images','Dir_AllRes
ults') %SAVE DIRECTORIES VARIABLES

```

DETERMINE DIRECTORIES

Determine directories allows the user to select the file locations critical to program operation.

1 of 3: Please locate the Bubble Analysis Program Files

2 of 3: Please locate the directory in which the Experimental Images are held

N.B. If not already, the image showing the calibration scale should be

repositioned in the selected directory

3 of 3: Please locate the directory into which the Results can be outputted

N.B. A new folder can be created from the selection window

DETERMINE DIRECTORIES COMPLETE

IMAGE SCALE

```

diary([Dir_AllResults, '/Bubble Analysis Log']); %START PROGRAM LOG
cd(Dir_Images) %CHANGE PROGRAM LOCATION TO IMAGE DIRECTORY
fprintf('
-----\n\n<strong>IMAGE SCALING</strong>\nImage
scaling allows the program to convert between image pixels and physical
space.\n\n\t1 of 3: Please locate the calibration scale image\n\t\tN.B. If
not already, the calibration scale image should be repositioned in the
\n\t\t\tExperimental Image directory\n')

Raw_ScaleIMG=imread(uigetfile([Dir_Images, '/*.jpg'], 'Select the Calibration
Scale Image', Dir_Images)); %PROMPT USER TO SELECT CALIBRATION IMAGE AND
ASSIGN IT TO Raw_ScaleIMG
fprintf('\t2 of 3: Using the loaded image, please position the line
inbetween scaleable points\n')
imshow(Raw_ScaleIMG, 'InitialMagnification', 65) %DISPLAY Raw_ScaleIMG IN
FIGURE WINDOW
Line=imdistline; %DISPLAY MOVEABLE LINE IN FIGURE. USER SHOULD POSITION
BETWEEN SCALEABLE POINTS
set(gcf, 'units', 'normalized', 'outerposition', [0 0 1 1]); %SET FIGURE
SETTINGS

while 2==2 %ARBITRARY TRUE CONDITION USED TO START INFINITE WHILE LOOP

    fprintf('\t\t\t');
    UserSelection=str2double(cell2mat(inputdlg('Are you satisfied with the
line positioning? (1=Yes/2=Exit): ')));
    switch UserSelection %ANY str2double(cell2mat(inputdlg WILL CONTINUE
ANALYSIS, 2 WILL TERMINATE
        case 2
            error('***BUBBLE IMAGE ANALYSIS SOFTWARE - TERMINATED BY
USER***')
        otherwise
            Pixels=round(getDistance(Line));
            close all
            break
        end
    end

end

fprintf('\t3 of 3: ')
Scale=str2double(cell2mat(inputdlg('What is the scale grid spacing in mm?:
'))); %PROMPT USER TO INSERT PHYSICAL DISTANCE (mm) ASSOCIATED WITH THE
FIGURE LINE
PixPerMm=Pixels/Scale; %CALCULATE NUMBER OF PIXELS PER mm

fprintf('
-----\n\nIMAGE SCALING COMPLETE\n')
close all; %CLOSE ALL FIGURES
save([Dir_AllResults, '/ImageScale.mat'], 'PixPerMm') %SAVE IMAGE SCALE
VARIABLES

```

IMAGE SCALING

optimal settings for image analysis. These settings are saved to the results folder and can be

loaded for future use.

N.B. Image Optimisation should be redone for each new dataset.

```
Warning: Image is too big to fit on screen; displaying at
67%
```

```
1 of 4: Image Binarisation
```

```
2 of 4: Inverting image
```

```
3 of 4: Fill Bubbles
```

```
4 of 4: Remove Noise
```

```
-----
IMAGE OPTIMISATION COMPLETE
```

```
Results saved to <a
href="/Users/Andrew_Niland/Desktop/PUBLISH/Optimised Image.jpg">Optimised
Image.jpg</a>.
```

IMAGE ANALYSIS

```
fprintf('_____
_____ \n\n<strong>IMAGE ANALYSIS</strong>\nImage
analysis will automatically optimise all experimental images within the pre-
specified \nlocation and output the following results:\n')
fprintf('\tBubble Results:\n\t\t1. Image of Bubble\n\t\t2. Pathline\n\t\t3.
Active Frames\n\t\t4. Average Velocity\n\t\t5. Area\n\t\t6. Growth
Rate\n\t\t7. Eccentricity\n')
fprintf('\tFrame Results:\n\t\t1. Number of Bubbles\n\t\t2. Bubble SMD\n')
fprintf('\tComplete Dataset:\n\t\t1. Number of Bubbles\n\t\t2. Bubble
SMD\n')
fprintf('N.B. Only discrete bubbles will be analysed (i.e. bubbles
intersecting the image boundaries will \nbe neglected from the
analysis).\n\n\t')

while 2==2 %ARBITRARY TRUE CONDITION USED TO START INFINITE WHILE LOOP

    UserSelection=str2double(cell2mat(inputdlg('Is analysis for a single
image (1) or multiple images forming a video (2): '))); %PROMPT USER TO
ANALYSE EITHER SINGLE IMAGE OR VIDEO SEQUENCE
    fprintf('\t')
    switch UserSelection

        case 1 %SINGLE IMAGE

            fprintf('Please select the image for analysis.\n');
            cd(Dir_Images) %CHANGE PROGRAM LOCATION TO IMAGE DIRECTORY
```

```

        Raw_IMG=imread(uigetfile([Dir_Images, '/*.jpg'], 'Please Select
the Image for Analysis')); %PROMPT USER TO IDENTIFY SINGLE IMAGE FOR
ANALYSIS

        cd(Dir_Home) %CHANGE PROGRAM LOCATION TO PROGRAM DIRECTORY
        fprintf('
-----
\n\nIMAGE ANALYSIS IN PROGRESS
('ctrl+C' to abort)\n')

[Bubble_Results, Image_NumberofBubbles, Image_BubbleSMD]=ImageAnalysis(Dir_Hom
e, Dir_AllResults, Raw_IMG, BWThresh, Complement, Limit_Join, Limit_Rem, PixPerMm,
UserSelection_BackgroundIMG, Gray_BackgroundIMG, UserSelection_Crop, CropRect);
%RUN FUNCTION ImageAnalysis TO ANALYSE OBJECTS IN A SINGLE IMAGE

fprintf('%c%c%c%c%c%c%c%c%c%c%c%c%c%c%c%c%c\n', 8, 8, 8, 8, 8, 8, 8, 8, 8, 8, 8,
, 8, 8, 8, 8, 8, 8, 8) %DELETE PREVIOUS IMAGE ANALYSIS IN PROGRESS DISPLAY
        fprintf('
-----
\n\nIMAGE ANALYSIS
COMPLETE\n\tResults saved to the <a href="%s">Results
Folder</a>.', Dir_AllResults) %DISPLAY RESULTS LOCATION
        fprintf('\n\tNumber of Bubbles = %g', Image_NumberofBubbles)
%DISPLAY NUMBER OF BUBBLES DETECTED
        fprintf('\n\tBubble SMD = %g\n\n', Image_BubbleSMD) %DISPLAY
BUBBLE SMD

        break

    case 2 %VIDEO SEQUENCE

[Frame_Results, Bubble_Results, Dataset_NumberofBubbles, Dataset_BubbleSMD]=Vid
eoAnalysis(Dir_Home, Dir_Images, Dir_AllResults,
BWThresh, Complement, Limit_Join, Limit_Rem, PixPerMm,
UserSelection_BackgroundIMG, Gray_BackgroundIMG, UserSelection_Crop, CropRect);
%RUN FUNCTION VideoAnalysis TO ANALYSE OBJECTS IN A SERIES OF IMAGES

        fprintf('
-----
\n\nIMAGE ANALYSIS
COMPLETE\n\tResults saved to the <a href="%s">Results
Folder</a>', Dir_AllResults) %DISPLAY RESULTS LOCATION
        fprintf('\n\tNumber of Bubbles = %g', Dataset_NumberofBubbles)
%DISPLAY NUMBER OF BUBBLES DETECTED
        fprintf('\n\tBubble SMD = %g\n\n', Dataset_BubbleSMD) %DISPLAY
BUBBLE SMD

        break

    otherwise
        fprintf('\n\n\tEntry not recognised. ')
    end
end
end

```

IMAGE ANALYSIS

Image analysis will automatically optimise all experimental images within the pre-specified

location and output the following results:

Bubble Results:

1. Image of Bubble
2. Pathline
3. Active Frames
4. Average Velocity
5. Area
6. Growth Rate
7. Eccentricity

Frame Results:

1. Number of Bubbles
2. Bubble SMD

Complete Dataset:

1. Number of Bubbles
2. Bubble SMD

N.B. Only discrete bubbles will be analysed (i.e. bubbles intersecting the image boundaries will

be neglected from the analysis).

1 of 2: Naming Format

For all files in a location to be identified, the naming format must be established.

Wildcards are denoted by *. The following images have naming format "*Image*":

1ImageA.jpg

2ImageB.jpg

3ImageC.jpg

...

130 images were identified in the pre-specified location.

```
-----  
-----  
  
IMAGE ANALYSIS IN PROGRESS ('ctrl+C' to abort)
```

```
-----  
-----  
  
IMAGE ANALYSIS COMPLETE
```

```
      Results saved to the <a  
href="/Users/Andrew_Niland/Desktop/PUBLISH">Results Folder</a>
```

```
      Number of Bubbles = 38
```

```
      Bubble SMD = 55.7799
```

FINALISE

```
diary off; %STOP PROGRAM LOG  
clear java; close all %CLEAR ALL
```

Published with MATLAB® R2014a

IMAGE OPTIMISATION

RUN FUNCTION ImageOptimisation TO DETERMINE THE IMAGE OPTIMISATION PROPERTIES

Contents

- LAUNCH FUNCTION
- LOAD SAMPLE IMAGE
- DETERMINE IMAGE OPTIMISATION CRITERIA
- SAVE IMAGE OPTIMISATION RESULTS

LAUNCH FUNCTION

```
% function
[BWThresh,Complement,Limit_Join,Limit_Rem,UserSelection_BackgroundIMG,Gray_BackgroundIMG,UserSelection_Crop,CropRect]=ImageOptimisation(Dir_Home,Dir_Images,Dir_AllResults, PixPerMm)
```

LOAD SAMPLE IMAGE

```
%LOAD SAMPLE IMAGE
cd(Dir_Images) %CHANGE PROGRAM LOCATION TO IMAGE DIRECTORY
Raw_SampleIMG=imread(uigetfile('*.jpg','Select Any Bubble Image From Dataset',Dir_Images)); %PROMPT USER TO SELECT SAMPLE IMAGE AND ASSIGN IT TO Raw_SampleIMG
if size(Raw_SampleIMG,3)==3 %DETERMINE SAMPLE IMAGE TYPE (RGB OR GRAYSCALE).
size(Raw_SampleIMG,x): x=1 is the X dimension; x=2 is the Y dimension; x=3 is the # of image layers (RGB has 3 layers).
    Gray_SampleIMG=rgb2gray(Raw_SampleIMG); %CONVERT RGB IMAGE (TRUECOLOUR) TO GRAYSCALE IMAGE (INTENSITY) AND ASSIGN AS Gray_SampleIMG
else
    Gray_SampleIMG=Raw_SampleIMG;
end

%REMOVE BACKGROUND IMAGE
while 2==2 %ARBITRARY TRUE CONDITION USED TO START INFINITE WHILE LOOP
    fprintf('\t')
    UserSelection_BackgroundIMG=str2double(cell2mat(inputdlg('Would you like to remove a background image? (1=Yes/2=No): '))); %GIVE USER OPTION OF REMOVING BACKGROUND IMAGE. BOTH IMAGES MUST BE GRAYSCALE.
    switch UserSelection_BackgroundIMG
        case 1
            Raw_BackgroundIMG=imread(uigetfile('*.jpg','Select The Background Image From Dataset',Dir_Images)); %PROMPT USER TO SELECT BACKGROUND IMAGE AND ASSIGN IT TO Raw_BackgroundIMG
            if size(Raw_BackgroundIMG,3)==3 %DETERMINE BACKGROUND IMAGE TYPE AND CONVERT TO GRAYSCALE
                Gray_BackgroundIMG=rgb2gray(Raw_BackgroundIMG);
            else
                Gray_BackgroundIMG=Raw_BackgroundIMG;
            end
            Gray_SampleIMG=imsubtract(Gray_BackgroundIMG,Gray_SampleIMG);
        %SUBTRACT BACKGROUND IMAGE FROM GRAYSCALE SAMPLE IMAGE
            break
        case 2
            Gray_BackgroundIMG=0; %ARBITRARY VALUE ASSIGNED AS BACKGROUND IMAGE IF NONE TO BE REMOVED
            break
        otherwise
            fprintf('\n\n\tEntry not recognised. ')
    end
end
```

```

%CROP IMAGE
while 2==2 %ARBITRARY TRUE CONDITION USED TO START INFINITE WHILE LOOP
    imshow(Raw_SampleIMG) %DISPLAY THE RAW SAMPLE IMAGE
    fprintf('\t')
    UserSelection_Crop=str2double(cell2mat(inputdlg('Would you like to crop
the image? (1=Yes/2=No): '))); %GIVE USER OPTION OF CROPPING THE IMAGE
    switch UserSelection_Crop
        case 1
            [~,~,Raw_SampleIMG,CropRect]=imcrop(Raw_SampleIMG); %LOAD FIGURE
WITH CROP TOOL. THE CROP RECTANGLE IS ASSIGNED TO CropRect AND THE RAW
SAMPLE IMAGE IS CROPPED.
            Gray_SampleIMG=imcrop(Gray_SampleIMG,CropRect); %CROP THE
GRAYSCALE SAMPLE IMAGE
            break
        case 2
            CropRect=0; %ARBITRARY VALUE ASSIGNED AS TO THE CROP RECTANGLE
IF NOT CROPPED
            break
        otherwise
            fprintf('\n\n\tEntry not recognised. ')
    end
end
end

close all %CLOSE ALL FIGURES
cd(Dir_Home)

```

Warning: Image is too big to fit on screen; displaying at 67%

DETERMINE IMAGE OPTIMISATION CRITERIA

```

fprintf('\t1 of 4: Image Binarisation')

%BINARISE IMAGE
while 2==2 %ARBITRARY TRUE CONDITION USED TO START INFINITE WHILE LOOP
    fprintf('\n\t\t')
    BWThresh=BW_Optimisation(Gray_SampleIMG); %CONVERT TO BINARY IMAGE (RUN
FUNCTION BW_Optimisation). DETERMINES THE OPTIMUM SHADE THRESHOLD ABOVE
WHICH THE PIXEL IS CONVERTED TO BLACK (0) AND BELOW WHICH THE PIXEL IS
CONVERTED TO WHITE (1).
    BW_SampleIMG=im2bw(Gray_SampleIMG,BWThresh); %APPLY RESULTS. CONVERT THE
GRAYSCALE SAMPLE IMAGE TO A BINARY IMAGE AND ASSIGN AS BW_SampleIMG.
    UserSelection=str2double(cell2mat(inputdlg('Determine the threshold for
the darkest discrete bubbles? (1=Continue,2=Exit): '))); %PAUSES THE PROGRAM
UNTIL USER IS SATISFIED WITH THE THRESHOLD
    close all; %CLOSE ALL FIGURES
    switch UserSelection
        case 1
            break
        otherwise
            error('***BUBBLE IMAGE ANALYSIS SOFTWARE - TERMINATED BY
USER***')
    end
end
end

[BW_SampleIMG,Complement]=BW_Complement(BW_SampleIMG); %INVERT BINARY IMAGE
(RUN FUNCTION BW_Complement). OBJECTS IN THE IMAGE MUST BE WHITE (1) SO IT
ALLOWS USER TO SELECT IF IMAGE NEEDS TO BE INVERTED (COMPLIMENTED).

BW_SampleIMG=RemoveObjectsOnBoundary(BW_SampleIMG); %REMOVE OBJECTS
INTERSECTING BOUNDARY (RUN FUNCTION RemoveObjectsOnBoundary). OBJECTS
OBSCURED BY THE BOUNDARY DO NOT ACCURATELY REPRESENT THEIR TRUE SHAPE.

%FILL HOLES IN IMAGE

```

```

fprintf('\t3 of 4: Fill Bubbles\t')
while 2==2 %ARBITRARY TRUE CONDITION USED TO START INFINITE WHILE LOOP
    fprintf('\n\t\t')
    Limit_Join=JoinBrokenLines_Optimisation(Gray_SampleIMG,BW_SampleIMG);
    %JOIN GAPS AND FILL (RUN FUNCTION JoinBrokenLines). ALLOWS THE USER TO
    DETERMINE THE THRESHOLD FOR JOINING TOGETHER NEAR PIXELS.
    BW_SampleIMG=imclose(BW_SampleIMG,(strel('disk',Limit_Join))); %APPLY
    RESULTS. JOIN TOGETHER NEAR PIXELS BASED ON THE DETERMINED THRESHOLD.
    Filled_BW_SampleIMG=imfill(BW_SampleIMG,'holes'); %FILL ENCLOSED SHAPES
    UserSelection=str2double(cell2mat(inputdlg('Determine the fill threshold
    for the discrete bubbles? (1=Continue,2=Exit): '))); %PAUSES THE PROGRAM
    UNTIL USER IS SATISFIED WITH THE THRESHOLD
    close all; %CLOSE ALL FIGURES
    switch UserSelection
        case 1
            break
        otherwise
            error('***BUBBLE IMAGE ANALYSIS SOFTWARE - TERMINATED BY
    USER***')
    end
end

[Filled_BW_SampleIMG,Limit_Rem]=RemoveNoise(Filled_BW_SampleIMG,PixPerMm);
%REMOVE NOISE (RUN FUNCTION RemoveNoise). DELETES ALL OBJECTS BELOW THE
MINIMUM DETECTION THRESHOLD.

```

1 of 4: Image Binarisation

2 of 4: Inverting image

3 of 4: Fill Bubbles

4 of 4: Remove Noise

SAVE IMAGE OPTIMISATION RESULTS

```

cd(Dir_AllResults) %CHANGE PROGRAM LOCATION TO RESULTS DIRECTORY

Results_OptimisedIMG=figure('name','Results of Image Optimisation'); %SAVE
COMPARATIVE FIGURE OF RAW IMAGE AND FINAL OPTIMISED IMAGE
subplot(1,2,1)
imshow(Raw_SampleIMG)
subplot(1,2,2)
imshow(Filled_BW_SampleIMG)
set(gcf,'visible','off')
saveas(Results_OptimisedIMG,[Dir_AllResults,'/Sample Converted
Image'],'jpeg')

save ImageOptimisationProperties.mat BWThresh Complement Limit_Join
Limit_Rem UserSelection_BackgroundIMG Gray_BackgroundIMG UserSelection_Crop
CropRect %SAVE IMAGE OPTIMISATION PROPERTIES

cd(Dir_Home) %CHANGE PROGRAM LOCATION TO PROGRAM DIRECTORY

% end

```

IMAGE ANALYSIS

RUN FUNCTION ImageAnalysis TO ANALYSE OBJECTS IN A SINGLE IMAGE

Contents

- LAUNCH FUNCTION
- APPLY IMAGE OPTIMISATION PROPERTIES TO IMAGE
- ANALYSIS OF IMAGE
- SAVE RESULTS DATA

LAUNCH FUNCTION

```
% function
[Bubble_Results,Image_NumberofBubbles,Image_BubbleSMD]=ImageAnalysis(Dir_Home,Dir_AllResults,
Raw_IMG,BWThresh,Complement,Limit_Join,Limit_Rem,PixPerMm,UserSelection_BackgroundIMG,Gray_BackgroundIMG,UserSelection_Crop,CropRect)
```

APPLY IMAGE OPTIMISATION PROPERTIES TO IMAGE

```
if size(Raw_IMG,3)==3
    Gray_IMG=rgb2gray(Raw_IMG);
else
    Gray_IMG=Raw_IMG;
end

if UserSelection_BackgroundIMG==1
    Gray_IMG=imsubtract(Gray_BackgroundIMG,Gray_IMG);
end

if UserSelection_Crop==1
    Raw_IMG=imcrop(Raw_IMG,CropRect);
    Gray_IMG=imcrop(Gray_IMG,CropRect);
end

BW_IMG=im2bw(Gray_IMG,BWThresh);
if Complement==1
    BW_IMG=imcomplement(BW_IMG);
end
BW_IMG=RemoveObjectsOnBoundary(BW_IMG);
BW_IMG=imclose(BW_IMG,(strel('disk',Limit_Join)));
Filled_BW_IMG=imfill(BW_IMG,'holes');
Filled_BW_IMG=imopen(Filled_BW_IMG,(strel('disk',Limit_Rem)));
```

ANALYSIS OF IMAGE

```
%INITIALISE RESULTS STRUCTURE Bubble_Results
Bubble_Results = struct(...
    'BubbleNumber', {}, ...
    'Image', {}, ...
    'Area', {}, ...
    'EquivalentDiameter', {}, ...
    'Centroid', {}, ...
    'Circularity', {});

Filled_BW_IMG=logical(Filled_BW_IMG); %CONVERT BINARY IMAGE TO LOGICAL IMAGE
H=vision.BlobAnalysis('PerimeterOutputPort',true,'MaximumCount',1000000);
%INITIALISE BLOB ANALYSIS
[areas,centroids,bboxes,perimeters]=step(H,Filled_BW_IMG); %DETECT OBJECTS
IN LOGICAL IMAGE

di2=0;
```

```

di3=0;

for n=1:length(areas)

    %RUN OBJECT PROPERTY CALCULATIONS
    area=double(areas(n,:))*(1/PixPerMm)^2;
    bbox=bboxes(n,:);
    centroid=centroids(n,:);
    perimeter=double(perimeters(n,:))*(1/PixPerMm);
    circularity=(4*pi()*area)/(perimeter^2);
    EquivalentDiameter=sqrt((4*area)/pi());
    di2=di2+(EquivalentDiameter)^2;
    di3=di3+(EquivalentDiameter)^3;

    %INITIALISE RESULTS STRUCTURE Bubble_Results
    Bubble_Results(n).BubbleNumber=n;
    Bubble_Results(n).Image=imcrop(Raw_IMG,bbox);
    Bubble_Results(n).Area=area;
    Bubble_Results(n).EquivalentDiameter=EquivalentDiameter;
    Bubble_Results(n).Centroid=centroid;
    Bubble_Results(n).Circularity=circularity;

    Raw_IMG = insertObjectAnnotation(Raw_IMG, 'rectangle', bbox, n); %UPDATE
RAW IMAGE TO IDENTIFY OBJECTS

end

Image_NumberofBubbles=length(Bubble_Results);
Image_BubbleSMD=di3/di2;

```

SAVE RESULTS DATA

```

cd(Dir_AllResults)

save('ImageAnalysisResults.mat','Bubble_Results','Image_NumberofBubbles','Image_BubbleSMD')
imwrite(Raw_IMG,'ImageAnalysisResults.jpg')
cd(Dir_Home)

% end

```

VIDEO ANALYSIS

RUN FUNCTION VideoAnalysis TO ANALYSE OBJECTS IN A SERIES OF IMAGES

Contents

- LAUNCH FUNCTION
- DEFINE VIDEO PROPERTIES
- PREPARE FOR OBJECT DETECTION
- BEGIN OBJECT DETECTION
- READ IN FRAME IMAGE
- APPLY IMAGE OPTIMISATION PROPERTIES TO IMAGE
- OBJECT DETECTION (BLOB ANALYSIS etc.)
- WRITE FRAME RESULTS
- DETERMINE THE PREDICTED NEXT LOCATION FOR ALL DETECTIONS
- KALMAN FILTER - OBJECT MOTION TRACKING
- UPDATE ALL OBJECTS FOUND IN CURRENT FRAME (i.e. assignments)
- UPDATE ALL OBJECTS UNDETECTED IN CURRENT FRAME (i.e. unassignedTracks)
- CREATE ALL NEW OBJECTS FOUND IN CURRENT FRAME
- PRODUCE VISUAL RESULTS
- SAVE VISUAL RESULTS

LAUNCH FUNCTION

```
%function
[Frame_Results,Bubble_Results,Dataset_NumberofBubbles,Dataset_BubbleSMD]=Vid
eoAnalysis(Dir_Home,Dir_Images,Dir_AllResults,
BWThresh,Complement,Limit_Join,Limit_Rem,PixPerMm,
UserSelection_BackgroundIMG,Gray_BackgroundIMG,UserSelection_Crop,CropRect)
%RUN FUNCTION VideoAnalysis TO ANALYSE OBJECTS IN A SERIES OF IMAGES
```

DEFINE VIDEO PROPERTIES

```
fprintf('1 of 2: Naming Format')
fprintf('\n\t\tFor all files in a location to be identified, the naming
format must established.\n\t\tWildcards are denoted by *. The following
images have naming format
"*Image*":\n\t\t\t1ImageA.jpg\n\t\t\t2ImageB.jpg\n\t\t\t3ImageC.jpg\n\t\t\t.
..\n')
while 2==2
    fprintf('\t\t')
    NamingFormat = cell2mat(inputdlg('Please enter the naming format for the
experimental images: ','s')); %PROMPT USER TO ENTER NAMING FORMAT OF IMAGES
(WHERE * IS THE WILDCARD ENTRY), SUCH THAT ONLY THE INTENDED IMAGES ARE
ANALYSED

    ListofContents_Dir_Images=dir([Dir_Images,'/',NamingFormat,'*.jpg']);
%CURRENTLY SET FOR .JPG FILES - CAN BE CHANGED TO MATCH OTHER FILE TYPES
    ListofContents_Dir_Images=Sort_Struct(ListofContents_Dir_Images); %(REF)
RUN FUNCTION Sort_Struct - PERFORMS A 'SORT ROWS' FUNCTION TO STRUCTURE
ARRAY
    [NumberOfImages,~]=size(ListofContents_Dir_Images); %DETERMINES NUMBER
OF IMAGES MATCHING SELECTION
    fprintf('\t\t%g images were identified in the pre-specified
location.\n\t\t',NumberOfImages'); %PROMPT USER TO CONFIRM VALIDITY OF
SELECTION
    UserSelection=str2double(cell2mat(inputdlg('Is this correct?
(1=Yes/2=No/3=Exit): ')));
    switch UserSelection
        case 1
            break
        case 2
            continue
```

```

        case 3
            error('***BUBBLE IMAGE ANALYSIS SOFTWARE - TERMINATED BY
USER***')
        end
    end
end

fprintf('\t')
fps=str2double(cell2mat(inputdlg('2 of 2: What frame rate was used in the
image recording?: '))); %PROMPTS USER FOR FRAME RATE USED IN RECORDING

fprintf('
-----
          \n\nIMAGE ANALYSIS IN PROGRESS ('ctrl+C' to
abort): ');
writerObj=VideoWriter([Dir_AllResults,'/Bubble Animation']); %PRIMES THE
VideoWriter FUNCTION, WHERE EACH EXPERIMENTAL IS ADDED INDIVIDUALLY
THROUGHOUT ANALYSIS TO FORM A VIDEO SEQUENCE
writerObj.FrameRate=fps; %THE FRAME RATE OF THE PROCESSED VIDEO MATCHES THE
ORIGINAL VIDEO
open(writerObj); %STARTS THE VideoWriter FUNCTION

mkdir(Dir_AllResults,'Frames'); %CREATES DIRECTORY TO SAVE THE PROCESSED
FRAMES
Dir_Result=[Dir_AllResults,'/Frames']; %SETS THE PROCESSED FRAME DIRECTORY
IN MEMORY

```

1 of 2: Naming Format

For all files in a location to be identified, the naming format must be established.

Wildcards are denoted by *. The following images have naming format "*Image*":

1ImageA.jpg

2ImageB.jpg

3ImageC.jpg

...

130 images were identified in the pre-specified location.

IMAGE ANALYSIS IN PROGRESS ('ctrl+C' to abort): Warning: Directory already exists.

PREPARE FOR OBJECT DETECTION

%AS AN OBJECT IS DETECTED, ITS PROPERTIES ARE STORED WITHIN A STRUCTURE ARRAY NAMED tracks. THIS SCRIPT PREPARES AN EMPTY STRUCTURE ARRAY FOR POPULATION.

```

tracks = struct(...
    'id', {}, ...
    'image', {}, ...

```

```

'pathline', {}, ...
'bbox', {}, ...
'initialcentroid', {}, ...
'latestcentroid', {}, ...
'initialframe', {}, ...
'latestframe', {}, ...
'initialarea', {}, ...
'latestarea', {}, ...
'circularity', {}, ...
'kalmanFilter', {}, ...
'age', {}, ...
'totalVisibleCount', {}, ...
'consecutiveInvisibleCount', {});

%EACH VIDEO FRAME IS ANALYSED AND RESULTS ARE STORED WITHIN A STRUCTURE
ARRAY NAMED Frame_Results. THIS SCRIPT PREPARES AN EMPTY STRUCTURE ARRAY FOR
POPULATION.
Frame_Results = struct(...
    'Frame', nan, ...
    'NumberofBubbles', nan, ...
    'BubbleSMD', nan);

nextId=1; %SETS THE INITIAL UNIQUE OBJECT ID

```

BEGIN OBJECT DETECTION

```

%MOTION-BASED MULTIPLE OBJECT TRACKING PROGRAM (REF:
http://uk.mathworks.com/help/vision/examples/motion-based-multiple-object-tracking.html).
%PREPARES IMAGES AND DETECTS OBJECTS IN THE SAME WAY AS PREVIOUS. "THE
ASSOCIATION OF DETECTIONS TO THE SAME OBJECT IS BASED SOLELY ON MOTION. THE
MOTION OF EACH TRACK IS ESTIMATED BY A KALMAN FILTER.
%THE FILTER IS USED TO PREDICT THE TRACK'S LOCATION IN EACH FRAME, AND
DETERMINE THE LIKELIHOOD OF EACH DETECTION BEING ASSIGNED TO EACH TRACK. IN
ANY GIVEN FRAME, SOME DETECTIONS MAY BE ASSIGNED TO TRACKS,
%WHILE OTHER DETECTIONS AND TRACKS MAY REMAIN UNASSIGNED. THE ASSIGNED
TRACKS ARE UPDATED USING THE CORRESPONDING DETECTIONS. THE UNASSIGNED TRACKS
ARE MARKED INVISIBLE. AN UNASSIGNED DETECTION BEGINS A NEW TRACK."

for frame=1:NumberofImages %ANALYSES EACH FRAME FRAME INDIVIDUALLY
%    Percent_Complete=round(100*frame/NumberofImages); %PERCENTAGE COMPLETE
READ-OUT
%    fprintf('%03d%%',Percent_Complete)

```

READ IN FRAME IMAGE

```

ResultName=['Frame ', num2str(frame)];
cd(Dir_Images)
Dir_IMG=[Dir_Images, '/', ListofContents_Dir_Images(frame).name];
Raw_IMG=imread(Dir_IMG);

```

APPLY IMAGE OPTIMISATION PROPERTIES TO IMAGE

```

cd(Dir_Home)

if size(Raw_IMG,3)==3
    Gray_IMG=rgb2gray(Raw_IMG);
else
    Gray_IMG=Raw_IMG;
end

if UserSelection_BackgroundIMG==1

```

```

    Gray_IMG=imsubtract(Gray_BackgroundIMG,Gray_IMG);
end

if UserSelection_Crop==1
    Raw_IMG=imcrop(Raw_IMG,CropRect);
    Gray_IMG=imcrop(Gray_IMG,CropRect);
end

BW_IMG=im2bw(Gray_IMG,BWThresh);
if Complement==1
    BW_IMG=imcomplement(BW_IMG);
end
BW_IMG=RemoveObjectsOnBoundary(BW_IMG);
BW_IMG=imclose(BW_IMG,(strel('disk',Limit_Join)));
Filled_BW_IMG=imfill(BW_IMG,'holes');
Filled_BW_IMG=imopen(Filled_BW_IMG,(strel('disk',Limit_Rem)));

```

OBJECT DETECTION (BLOB ANALYSIS etc.)

```

    Filled_BW_IMG=logical(Filled_BW_IMG); %CONVERT BINARY IMAGE TO LOGICAL
    IMAGE

H=vision.BlobAnalysis('PerimeterOutputPort',true,'MaximumCount',1000000);
%INITIALISE BLOB ANALYSIS
[areas,centroids,bboxes,perimeters]=step(H,Filled_BW_IMG); %DETECT
OBJECTS IN LOGICAL IMAGE

```

WRITE FRAME RESULTS

```

    Frame_Results(frame).Frame=frame; %WRITE FRAME NUMBER
    Frame_Results(frame).NumberofBubbles=length(areas); %DETERMINE NUMBER OF
    BUBBLES IN FRAME

%DETERMINE BUBBLE SMD IN FRAME
di2=0;di3=0;
for n=1:length(areas)
    area=double(areas(n,:))*(1/PixPerMm)^2;
    di=sqrt((4*area)/pi());
    di2=di2+di^2;
    di3=di3+di^3;
end
    Frame_Results(frame).BubbleSMD=di3/di2;

```

DETERMINE THE PREDICTED NEXT LOCATION FOR ALL DETECTIONS

N.B. FRAME 1 IS SKIPPED AS tracks HAS NO LENGTH

```

    for i = 1:length(tracks) %FOR ALL OBJECTS
        bbox = tracks(i).bbox; %DETERMINE THE LAST ASSIGNED BOUNDING BOX
        predictedCentroid = predict(tracks(i).kalmanFilter); % USING THE
        KALMAN FILTER, PREDICT THE CURRENT LOCATION OF THE OBJECT
        predictedCentroid = int32(predictedCentroid) - (bbox(3:4)/2); %
        SHIFT THE BOUNDING BOX SO THAT ITS CENTRE IS AT THE PREDICTED LOCATION
        tracks(i).bbox = [predictedCentroid, bbox(3:4)]; %UPDATE THE OBJECTS
        LOCATION INFORMATION
    end

```

KALMAN FILTER - OBJECT MOTION TRACKING

```

%ASSIGN THE DETECTIONS IN THE CURRENT FRAME TO OBJECTS PREVIOUSLY
DETECTED

nTracks = length(tracks); %DETERMINE NUMBER OF PREVIOUS DETECTIONS
nDetections = size(centroids,1); %DETERMINE NUMBER OF CURRENT OBJECTS
cost = zeros(nTracks, nDetections); %PREPARE AN EMPTY COST MATRIX

%COMPUTE THE 'COST' OF ASSIGNING EACH NEW DETECTION TO AN EXISTING
OBJECT
for i = 1:nTracks
    cost(i, :) = distance(tracks(i).kalmanFilter, centroids);
end

%SOLVE THE ASSIGNMENT PROBLEM
costOfNonAssignment = 10; %VARIABLE: DETERMINE THE 'COST' OF ASSIGNING A
NEW DETECTION TO AN EXISTING OBJECT.
[assignments, unassignedTracks, unassignedDetections] =
assignDetectionsToTracks(cost, costOfNonAssignment); %CREATE MATRICIES OF
[1] NEW DETECTIONS ASSIGNED TO AN EXISTING OBJECT, [2] LOST OBJECTS AND [3]
UNASSIGNED DETECTIONS

```

UPDATE ALL OBJECTS FOUND IN CURRENT FRAME (i.e. assignments)

N.B. FRAME 1 IS SKIPPED AS tracks HAS NO LENGTH

```

for i = 1:size(assignments, 1) %UPDATE EACH DETECTED OBJECT INDIVIDUALLY

    trackIdx = assignments(i, 1); %DETERMINE OBJECT ID
    detectionIdx = assignments(i, 2); %DETERMINE DETECTION ID

    %UPDATE OBJECT PROPERTIES
    tracks(trackIdx).latestframe = frame; %UPDATE LATEST FRAME
    tracks(trackIdx).latestarea = double(areas(detectionIdx,
:))*(1/PixPerMm)^2; %UPDATE CROSS-SECTIONAL AREA
    tracks(trackIdx).latestcentroid = centroids(detectionIdx, :);
%UPDATE CENTROID
    tracks(trackIdx).pathline((frame+1)-tracks(trackIdx).initialframe,:)
= tracks(trackIdx).latestcentroid; %UPDATE PATHLINE
    tracks(trackIdx).bbox = bboxes(detectionIdx, :); %REPLACE THE
PREDICTED BOUNDING BOX WITH THE DETECTED BOUNDING BOX

    %UPDATE VISIBILITY TRACKERS
    tracks(trackIdx).age = tracks(trackIdx).age + 1; %UPDATE AGE
    tracks(trackIdx).totalVisibleCount =
tracks(trackIdx).totalVisibleCount + 1; %UPDATE TOTAL FRAMES VISIBLE
    tracks(trackIdx).consecutiveInvisibleCount = 0; %RESET CONSECUTIVE
FRAMES UNDETECTED

    %UPDATE KALMAN FILTER
    correct(tracks(trackIdx).kalmanFilter,
tracks(trackIdx).latestcentroid); %CORRECT THE ESTIMATE OF THE OBJECT
LOCATION USING THE NEW DETECTION

end

```

UPDATE ALL OBJECTS UNDETECTED IN CURRENT FRAME (i.e. unassignedTracks)

N.B. FRAME 1 IS SKIPPED AS tracks HAS NO LENGTH

```

for i = 1:length(unassignedTracks) %UPDATE EACH UNDETECTED OBJECT
INDIVIDUALLY

    ind = unassignedTracks(i); %DETERMINE UNDETECTED OBJECT ID

    %UPDATE VISIBILITY TRACKERS
    tracks(ind).age = tracks(ind).age + 1; %UPDATE AGE
    tracks(ind).consecutiveInvisibleCount =
tracks(ind).consecutiveInvisibleCount + 1; %UPDATE UNDETECTED COUNT

end

```

CREATE ALL NEW OBJECTS FOUND IN CURRENT FRAME

```

%DETERMINE OBJECT PROPERTIES FOR ALL NEW OBJECTS
areas = areas(unassignedDetections, :);
centroids = centroids(unassignedDetections, :);
bboxes = bboxes(unassignedDetections, :);
perimeters = perimeters(unassignedDetections, :);

for i = 1:size(centroids, 1) %CREATE A NEW OBJECT INDIVIDUALLY

    %DETERMINE THE OBJECT PROPERTIES FOR THIS NEW OBJECT
    area = double(areas(i,:));
    centroid = centroids(i,:);
    bbox = bboxes(i,:);
    perimeter = perimeters(i,:);

    kalmanFilter = configureKalmanFilter('ConstantVelocity', centroid,
[200, 50], [100, 25], 100); %CREATE A NEW KALMAN FILTER OBJECT

    %ADD THE NEW OBJECT TO THE LIST OF DETECTED OBJECTS
    tracks(end + 1) = struct(...
        'id', nextId, ...
        'image', imcrop(Raw_IMG,bbox), ...
        'pathline', centroid, ...
        'bbox', bbox, ...
        'initialcentroid', centroid, ...
        'latestcentroid', nan, ...
        'initialframe', frame, ...
        'latestframe', nan, ...
        'initialarea', area*(1/PixPerMm)^2, ...
        'latestarea', nan, ...
        'circularity', (4*pi()*area)/(perimeter^2), ...
        'kalmanFilter', kalmanFilter, ...
        'age', 1, ...
        'totalVisibleCount', 1, ...
        'consecutiveInvisibleCount', 0);

    nextId = nextId + 1; %UPDATE UNIQUE OBJECT ID

end

```

PRODUCE VISUAL RESULTS

```

Raw_IMG = im2uint8(Raw_IMG); % CONVERT THE RAW IMAGE (Raw_IMG) INTO
uint8 RGB.

```

```

    minVisibleCount = 0; %VARIABLE: ONLY DISPLAY TRACKS THAT HAVE BEEN
    VISIBLE FOR MORE THAN A MINIMUM NUMBER OF FRAMES, TO REMOVE NOISY DETECTIONS
    TEND

    if ~isempty(tracks) %ADDS OBJECT ANNOTATION IN IMAGE, SO LONG AS OBJECTS
    HAVE BEEN DETECTED

        reliableTrackInds = [tracks(:).totalVisibleCount] > minVisibleCount;
        reliableTracks = tracks(reliableTrackInds); %LISTS OBJECTS WHICH
    ABIDE WITHIN THE PREDEFINED NOISE VARIABLE

        %OVERLAY OBJECT LABELS ON RAW IMAGE
        if ~isempty(reliableTracks)

            %CREATE LABELS FOR DETECTED OBJECTS
            bboxes = cat(1, reliableTracks.bbox); % IMPORT THE BOUNDING
    BOXES

            ids = int32([reliableTracks(:).id]); %IMPORT IDS
            labels = cellstr(int2str(ids));

            %CREATE LABELS FOR PREDICTED OBJECTS
            predictedTrackInds =
    [reliableTracks(:).consecutiveInvisibleCount] > 0;
            isPredicted = cell(size(labels));
            isPredicted(predictedTrackInds) = {' predicted'};
            labels = strcat(labels, isPredicted);

            %OVERLAY LABELS ON THE RAW IMAGE
            Raw_IMG = insertObjectAnnotation(Raw_IMG, 'rectangle', bboxes,
    labels);

            end

        end
    end
end

```

SAVE VISUAL RESULTS

```

    cd(Dir_Result)

    imwrite(Raw_IMG, [ResultName, '.jpg']) %WRITE INDIVIDUAL FRAME RESULTS
    cd(Dir_Home)

    writeVideo(writerObj, imread([Dir_Result, '/', ResultName, '.jpg'])); %WRITE
    FRAME TO VIDEO

    close all

    %    fprintf('%c%c%c%c', 8,8,8,8) %DELETE 4 CHARACTERS (REMOVES THE CURRENT
    PERCENTAGE)

```

WDEavRCxr17Z286

```

end

close(writerObj); %STOP RECORDING VIDEO

%INITIALISE Bubble_Results STRUCTURE ARRAY
Bubble_Results = struct(...
    'BubbleNumber', {tracks.id}, ...
    'Image', {tracks.image}, ...
    'Pathline', {tracks.pathline}, ...
    'InitialFrame', {tracks.initialframe}, ...
    'FinalFrame', {tracks.latestframe}, ...
    'AvgVel_Vert', nan, ...

```

```

    'AvgVel_Hori', nan, ...
    'AvgVel_Magn', nan, ...
    'AvgVel_Angle', nan, ...
    'Area', {tracks.initialarea}, ...
    'GrowthRate', nan, ...
    'Circularity', {tracks.circularity});

%POPULATE Bubble_Results
for n=1:length(tracks)

    displacement = double(tracks(n).latestcentroid -
tracks(n).initialcentroid)*(1/PixPerMm);
    activeframes = tracks(n).latestframe - tracks(n).initialframe;
    activetime = activeframes*(1/fps);
    average_velocity_components = displacement / activetime;
    growth = tracks(n).latestarea - tracks(n).initialarea;
    Bubble_Results(n).AvgVel_Hori = average_velocity_components(1,1);
    Bubble_Results(n).AvgVel_Vert = -average_velocity_components(1,2);
    Bubble_Results(n).AvgVel_Magn = sqrt(Bubble_Results(n).AvgVel_Hori^2 +
Bubble_Results(n).AvgVel_Vert^2);
    Bubble_Results(n).AvgVel_Angle =
radians(atan(Bubble_Results(n).AvgVel_Hori/Bubble_Results(n).AvgVel_Vert^2)
);
    Bubble_Results(n).GrowthRate = growth / activetime;

end

%AVERAGED RESULTS
Dataset_NumberofBubbles=length(Bubble_Results);
Dataset_BubbleSMD=mean([Frame_Results.BubbleSMD]);

fprintf('%c%c\n',8,8)

cd(Dir_AllResults)
save('VideoAnalysisResults.mat','Frame_Results','Bubble_Results','Dataset_Nu
mberofBubbles','Dataset_BubbleSMD') %SAVE RESULTS
cd(Dir_Home)
%end

```

Published with MATLAB® R2014a

APPENDIX 5: REGIME MAPS FOR CONVENTIONAL FLAT-END AERATOR DESIGNS

A5.1 Effect of Aerator Orifice Diameter

A5.1.1 1 x 3.0 mm (Aerator A2)

Figure A5.1 is the gas injection regime map of Aerator A2 (i.e. 1 x 3.0 mm aerator orifice in a liquid cross-flow). This shows the effect of varying the supply liquid mass flow rate up to 290 g/s, which corresponds to the discharge limit at 0% ALR with the discharge valve fully open and 5 bar_g operating pressure, and relates to a maximum liquid Bakkers number of 923 kg/m²s in the 20 mm mixing chamber. The gas supply was varied up to the maximum achievable flow rate for the given aerator design (7 bar_g maximum gas supply pressure) or, if possible, 5% ALR. Analysis of the gas injection map enabled identification of six discrete gas injection regimes, which were categorised into four gas injection regions.

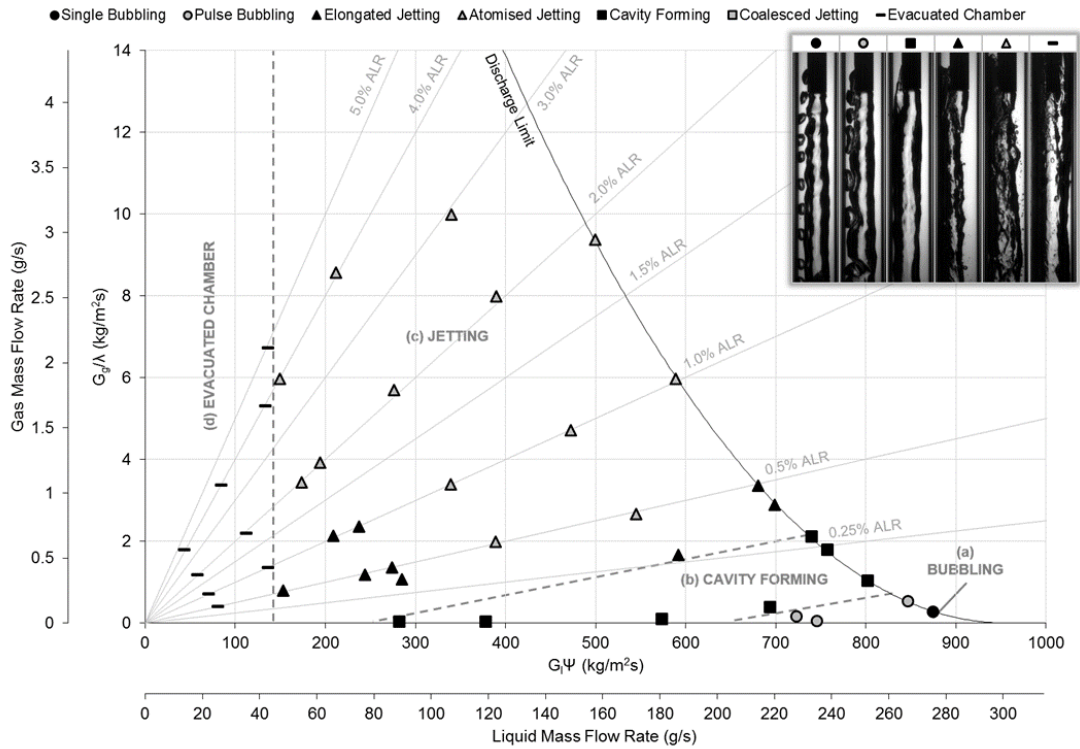


Figure A5.1 Gas injection regime map for aerator A2, with conventional flat-end body.

A significantly reduced bubbling region (Figure A5.1a) was identified compared to the benchmark case (Figure 5.7), which suggests that increasing the aerator orifice diameter acts to suppress bubbling. As with the benchmark configuration, increasing the ALR transitions single bubbling to pulse bubbling, however, this occurs at a significantly higher liquid flow rate and lower ALR – therefore, the formation of single bubbling is suppressed compared to the benchmark configuration. A solitary occurrence of single bubbling was identified at 275 g/s liquid mass and 0.03% ALR flow rate, which visibly produced comparatively large bubbles.

Unlike the benchmark case, a region of cavity forming was observed to separate the bubbling and jetting regions (Figure A5.1b). This is thought to correspond to conditions in which the gas flow is sufficiently high to generate a weak gas jet, but sufficiently low that the emerging gas does not dislodge the gas void – consequently, the gas jet coalesces with the gas void. The gas injection map was seen to be dominated by the jetting region (Figure A5.1c), with a general trend of elongated jetting transitioning to atomised jetting with increasing ALR. An evacuated chamber region (Figure A5.1d) was identified at low liquid flow rates, which corresponded to a liquid Bakers number of $140 \text{ kg/m}^2\text{s}$ – this is in a comparable region to the benchmark case, however, appears to be independent of the gas flow rate.

Figure A5.2 is the flow injection regime map of Aerator A2, which shows the effect of varying fluid flow rates on the flow regimes with areas of common regimes identified and marked. The three discrete flow regimes identified were grouped into three regions.

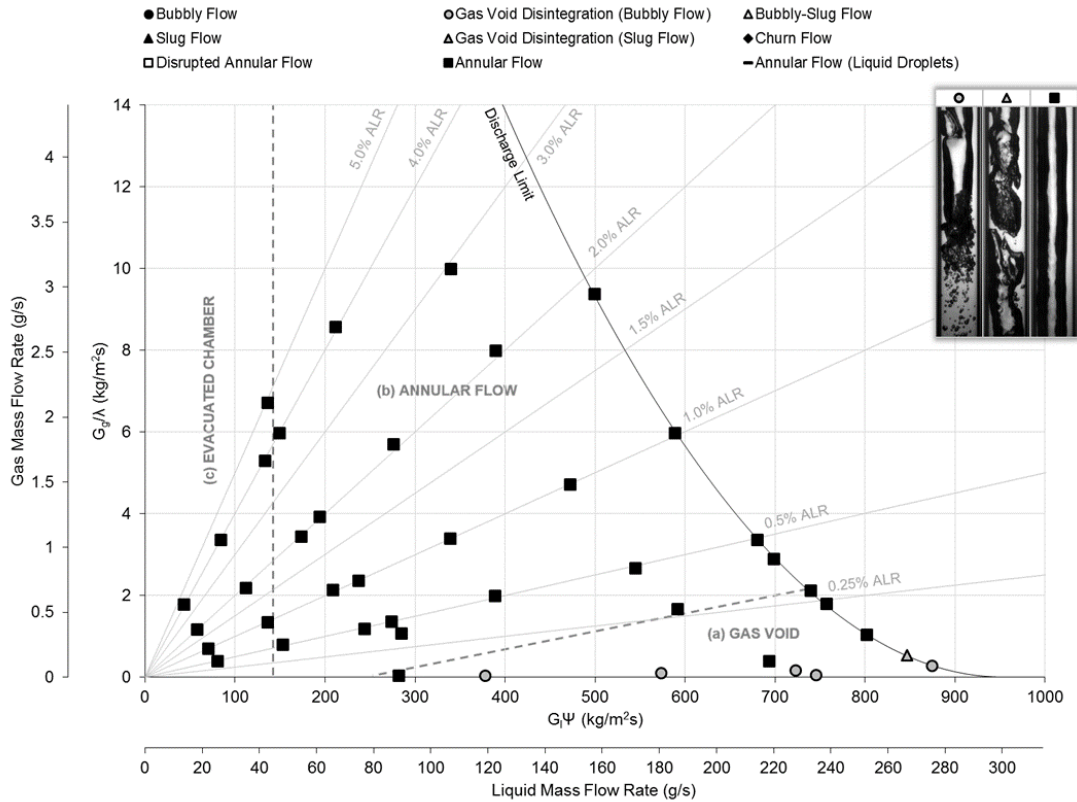


Figure A5.2 Flow regime map for aerator A2, with conventional flat-end body.

A conventional bubbly flow was not identified for any of the conditions tested due to the formation of a gas void in the aerator wake at low ALRs (Figure A5.2a) which displaced any injected bubbles. The range of operating conditions for gas void formation was comparable with the benchmark configuration (Figure 5.8) and coincided with all instances of single bubbling and cavity forming regimes.

Similarly, the gas void was seen to breakup under a limited range of conditions, forming gas void disintegration (bubbly flow) at very low ALRs and gas void disintegration (slug flow) in an isolated case at a higher ALR. Under all other flow conditions, the gas void was observed to form an annular flow.

Otherwise, annular flow was observed to dominate the flow regime map with no evidence of intermittent regimes. This correlated with every instance of jetting (in which an asymmetric gas core was formed that favoured the injection side of the aerator orifice) (Figure A5.2b)

and evacuated chamber (in which a thin film of peripheral liquid was generated) (Figure A5.2c).

A5.1.2 4 x 2.0 mm (Aerator A3)

Figure A5.3 is the gas injection regime map of Aerator A3 (i.e. 4 x 2.0 mm aerator orifices in a liquid cross-flow). This shows the effect of varying the supply liquid mass flow rate up to 290 g/s, which corresponds to the discharge limit at 0% ALR with the discharge valve fully open and 5 bar_g operating pressure, and relates to a maximum liquid Bakkers number of 923 kg/m²s in the 20 mm mixing chamber. The gas supply was varied up to the maximum achievable flow rate for the given aerator design (7 bar_g maximum gas supply pressure) or, if possible, 5% ALR. Analysis of the gas injection map enabled identification of five discrete gas injection regimes, which were categorised into three gas injection regions.

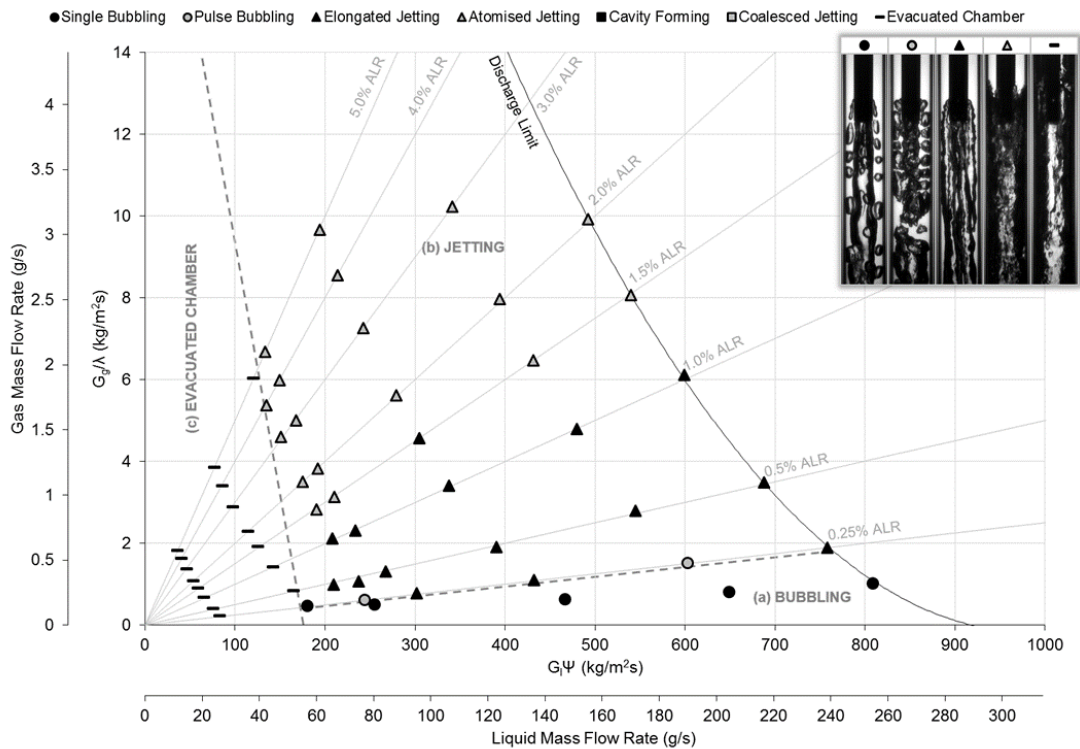


Figure A5.3 Gas injection regime map for aerator A3, with conventional flat-end body.

The bubbling region (Figure A5.3a) was observed to be substantially smaller than the benchmark case (Figure 5.7), but larger than aerator A2 (Figure A5.1). Single bubbling was observed at the lowest ALRs, with transition to pulse bubbling occurring at higher ALRs than aerator A2, but lower ALRs than the benchmark. This further evidences that reducing

aerator orifice diameter has the effect of increasing the operating conditions in which bubbling, including single bubbling, can be generated.

The transition from bubbling to jetting regions was observed at lower ALRs across all valve settings compared to the benchmark. Consequently, the gas injection map was seen to be dominated by the jetting region (Figure A5.3b). The general trend of elongated jetting transitioning to atomised jetting with increasing ALR was maintained. An evacuated chamber region was identified at low liquid velocities (Figure A5.3c), which was observed to be at a comparable level to the benchmark case and was also suppressed with increasing ALR. A cavity forming region was not identified in the current results, with the comparable conditions to cavity forming in Aerator A2 observed to break up into single bubbling and pulse bubbling in the current study. These results demonstrate that cavity forming regime requires a critically stable jet – hence, it was only achievable for large aerator orifices in excess of 2.0 mm for the current test conditions.

Figure A5.4 is the flow injection regime map of Aerator A3, which shows the effect of varying fluid flow rates on the flow regimes with areas of common regimes identified and marked. The six discrete flow regimes identified were grouped into six regions.

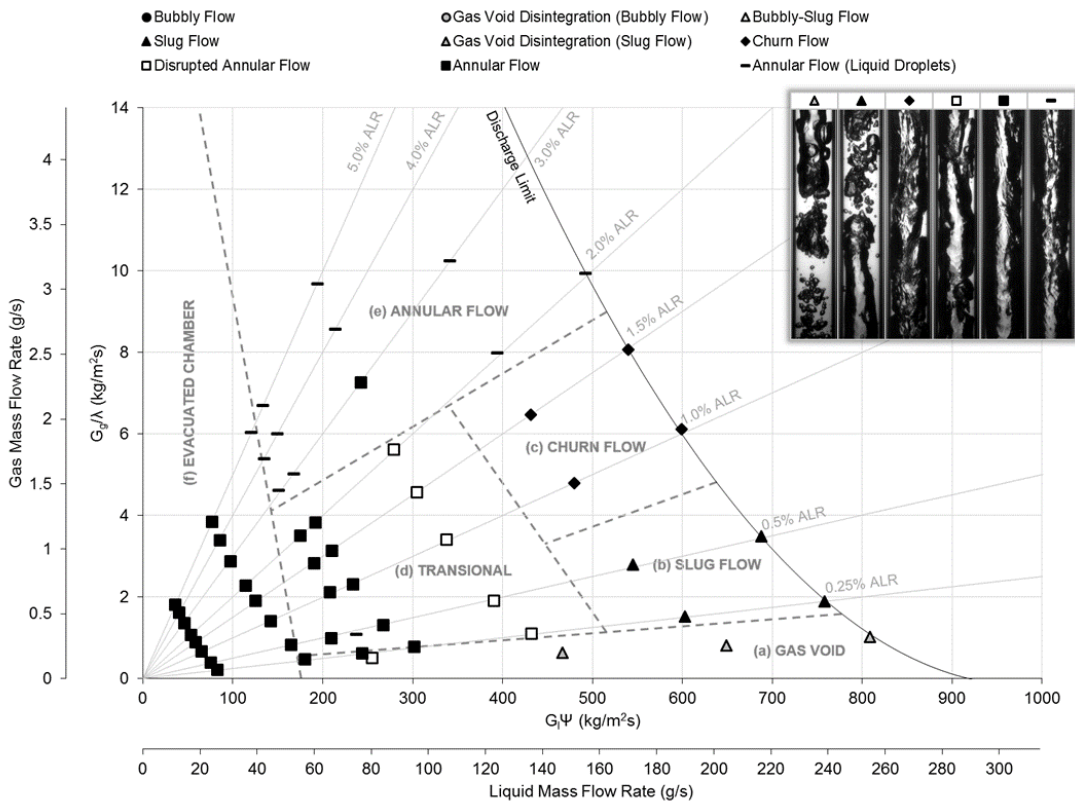


Figure A5.4 Flow regime map for aerator A3, with conventional flat-end body.

A conventional bubbly flow was not identified for any of the conditions tested due to the formation of a gas void in the aerator wake at low ALRs (Figure A5.4a). This coincided with all instances of single bubbling, which was observed to displace any injected bubbles. The range of operating conditions for gas void formation was seen to marginally increase compared to the Aerator A2, but was smaller than the benchmark case.

At relatively high liquid flow rates, the gas void was seen to break up to form gas void disintegration (slug flow), with all other flow conditions forming an annular flow. Gas void disintegration (bubbly flow) was not observed, however this would be expected if additional tests has been completed at lower ALRs and high liquid flow rates.

Unlike the larger aerator orifice diameter case (Figure A5.2), a region of intermittent flow regimes were established beyond the gas void region – like the benchmark case, these were observed to transition from slug flow (Figure A5.4b) to churn flow (Figure A5.4c) with increasing ALR. Compared to the benchmark configuration, the transition between the intermittent regimes occurred at lower ALRs and with a greater dependency on high liquid flow rates. Like the benchmark case, churn flow was observed to transition to annular flow at high ALRs (Figure A5.4e) – in every one of these cases, liquid droplets were identified to run off the aerator and fall within the gas core to form the annular flow (liquid droplets) regime. A thin annular flow was also identified for all conditions corresponding to the evacuated chamber gas injection regime (Figure A5.4f). Like the benchmark configuration, a transition region (Figure A5.4d) was identified between the evacuated chamber and intermittent flow regions, which notably featured disturbed annular flow on the border of the intermittent regimes – this region was observed to be substantially larger than the benchmark case.

A5.1.3 9 x 1.0 mm (Aerator A4)

Figure A5.5 is the gas injection regime map of Aerator A4 (i.e. 9 x 1.0 mm aerator orifice in a liquid cross-flow). This shows the effect of varying the supply liquid mass flow rate up to 290 g/s, which corresponds to the discharge limit at 0% ALR with the discharge valve fully open and 5 bar_g operating pressure, and relates to a maximum liquid Bakkers number of 923 kg/m²s in the 20 mm mixing chamber. The gas supply was varied up to the maximum achievable flow rate for the given aerator design (7 bar_g maximum gas supply pressure) or, if possible, 5% ALR. Analysis of results enabled identification of five discrete gas injection regimes, which were categorised into three gas injection regions.

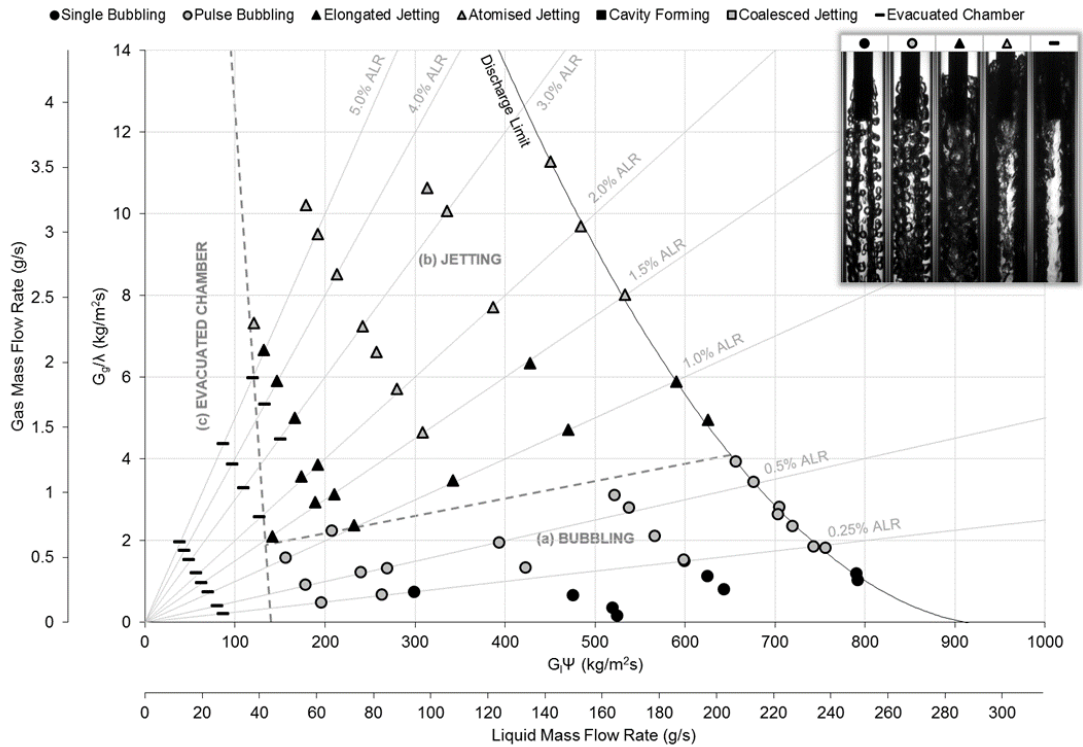


Figure A5.5 Gas injection regime map for aerator A4, with conventional flat-end body.

The bubbling region (Figure A5.5a) was observed to be marginally smaller than the benchmark case (Figure 5.7), but larger than aerators A2 and A3 (Figures A5.1 and A5.3). Single bubbling was observed at the lowest investigated ALRs, with transition to pulse bubbling occurring at higher ALRs than aerator A2 and A3, but lower ALRs than the benchmark. This further evidences that reducing aerator orifice diameter has the effect of increasing the operating conditions in which bubbling, including single bubbling, can be generated.

As with all previous cases, a jetting region (Figure A5.5b) was observed at ALRs in excess of the bubbling region. This maintained the general trend of elongated jetting transitioning to atomised jetting with increasing ALR. An evacuated chamber region was identified at low liquid velocities (Figure A5.5c), which was at comparable levels to the previous cases. In a few specific cases, evacuated chamber was identified within the jetting regime, but in close proximity of the evacuated chamber region – these results are thought to be anomalous.

Figure A5.6 is the flow injection regime map of Aerator A4, which shows the effect of varying fluid flow rates on the flow regimes with areas of common regimes identified and marked. The seven discrete flow regimes identified were grouped into six regions.

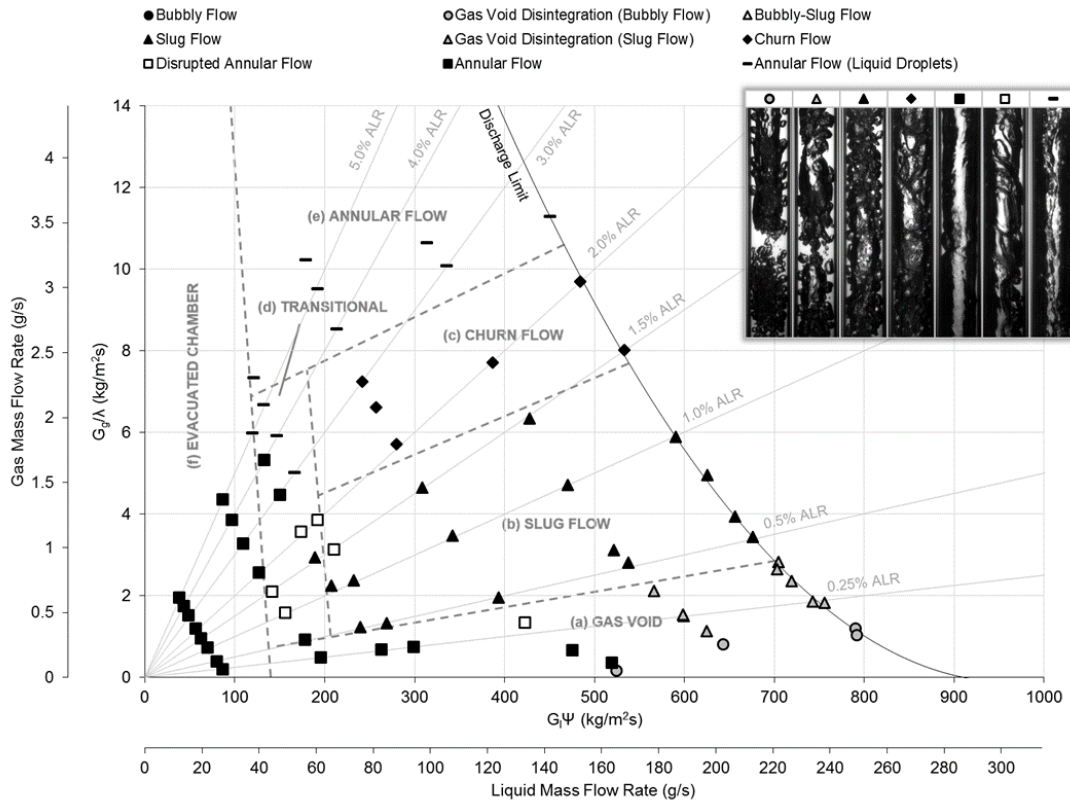


Figure A5.6 Flow regime map for aerator A4, with conventional flat-end body.

A conventional bubbly flow was not identified for any of the conditions tested due to the formation of a gas void in the aerator wake at low ALRs (Figure A5.6a). This coincided with all instances of single bubbling and low ALR pulse bubbling cases, and was observed to displace any injected bubbles. The range of operating conditions for gas void formation was seen to marginally increase compared to the Aerator A3, but was marginally smaller than the benchmark case.

Gas void disintegration (bubbly flow) was promoted by the lowest gas and highest liquid velocities, with further gas void break up observed at higher ALRs and high liquid flow velocities due to gas void disintegration (slug flow). In all other cases, the destructive mechanisms were insufficient to generate breakup within the mixing length and hence an annular flow was established.

A region of intermittent flow regimes were established beyond the gas void region, in which flow was observed to transition from slug flow (Figure A5.6b) to churn flow (Figure A5.6c) with increasing ALR. The transition between the intermittent regimes occurred at marginally lower ALRs than the benchmark case, but greater ALRs than aerator A3. Churn flow was observed to transition to annular flow at high ALRs (Figure A5.6e) – in every one of these

cases, liquid droplets were identified to run off the aerator and fall within the gas core to form the annular flow (liquid droplets) regime. This region was observed to occur at a greater ALRs than aerator A3, but at reduced ALRs compared to the benchmark. A thin annular flow was also identified for all conditions corresponding to the evacuated chamber gas injection regime (Figure A5.6f). A transition region (Figure A5.6d) was identified between the evacuated chamber and intermittent flow regions – which was seen to correspond well with the benchmark case.

A5.1.4 16 x 0.75 mm (Aerator A5)

This configuration is the benchmark case for the flat-end aerator body investigations for the flat-end aerator body investigations. The gas injection and flow regime maps are presented in §5.2.

A5.2 Effect of Unconventional Aerator Designs

A5.2.1 Co-Flow Aerator (Aerator A1)

Figure A5.7 is the gas injection regime map of Aerator A1 (i.e. 1 x 3.0 mm aerator orifice in a liquid co-flow). This shows the effect of varying the supply liquid mass flow rate up to 290 g/s, which corresponds to the discharge limit at 0% ALR with the discharge valve fully open and 5 bar_g operating pressure, and relates to a maximum liquid Bakers number of 923 kg/m²s in the 20 mm mixing chamber. The gas supply was varied up to the maximum achievable flow rate for the given aerator design (7 bar_g maximum gas supply pressure) or, if possible, 5% ALR. Analysis of the results enabled identification of four discrete gas injection regimes, which were categorised into three gas injection regions.

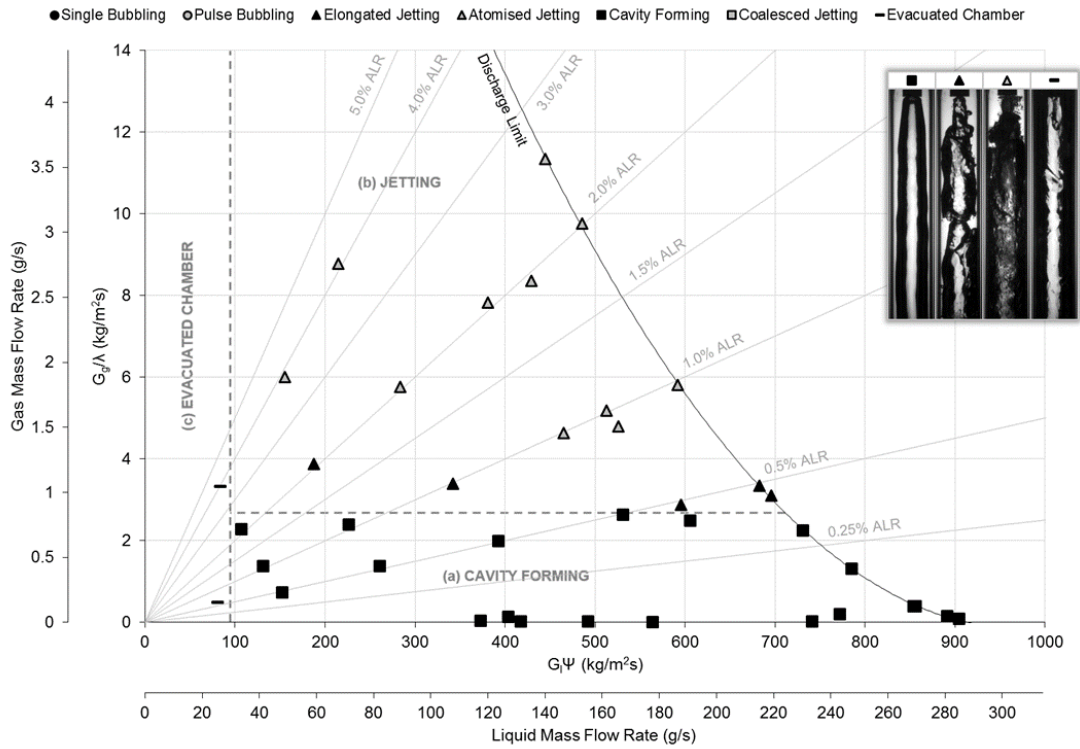


Figure A5.7 Gas injection regime map for aerator A1, with conventional flat-end body.

No instances of bubbling were identified for this configuration across the conditions tested. Instead, a large region of cavity forming was identified at relatively low gas injection velocities (Figure A5.7a), where gas was seen to be injected directly from the aerator orifice into a buoyant gas void in the aerator wake.

The gas void was seen to be displaced from the aerator tip at critically high gas injection velocities, thought to be when the combined shearing action of the gas (internal to void) and liquid (external to void) are sufficient to overcome the buoyancy of the gas void. This enables the generation of a large jetting region (Figure A5.7b), which is dominated by atomised jetting at high ALRs. The evacuated chamber regime was observed to be suppressed compared to the benchmark case (Figure A5.7c), where transition observed to occur at 93 kg/m²s. Therefore evacuated chamber occurs at a lower liquid flow rate than the benchmark, which is thought to be due to the effect of gas momentum counteracting the action of buoyancy when injected vertically downwards.

Figure A5.8 is the flow injection regime map of Aerator A1, which shows the effect of varying fluid flow rates on the flow regimes with areas of common regimes identified and marked. The three discrete flow regimes identified were grouped into four regions.

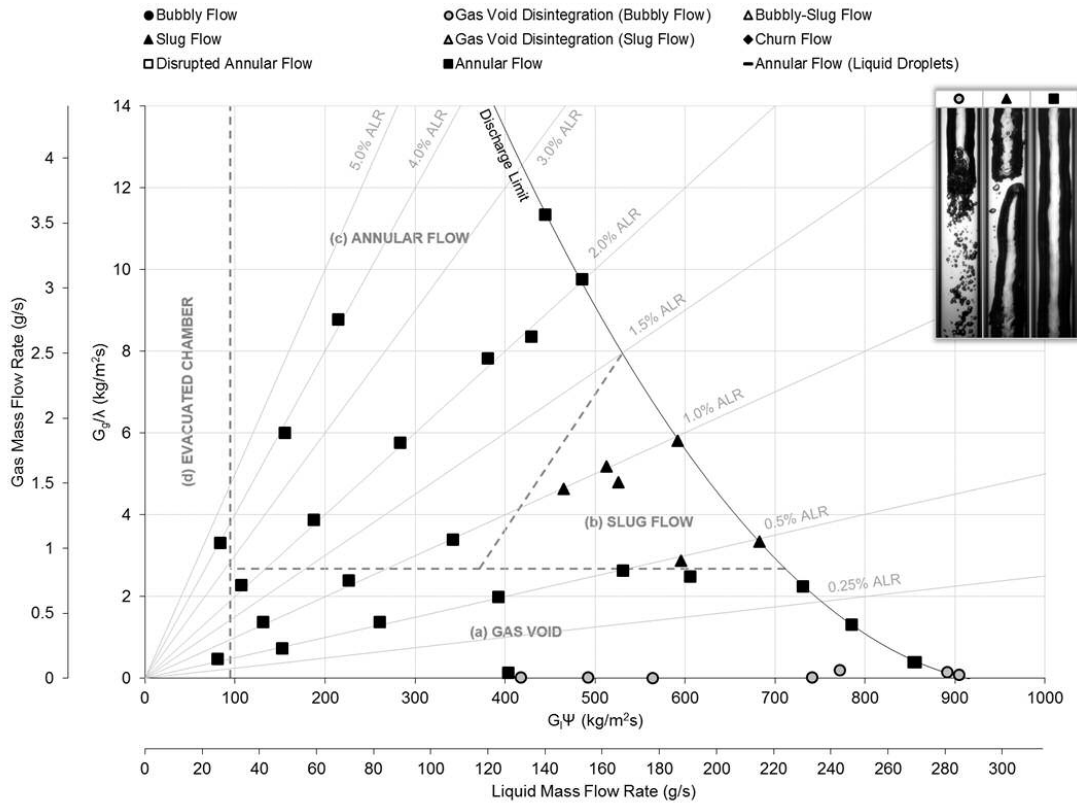


Figure A5.8 Flow regime map for aerator A1, with conventional flat-end body.

A conventional bubbly flow was not identified for any of the conditions tested, as bubbling at the aerator was not observed.

The formation of a gas void in the aerator wake was observed over a greater operating range compared to the benchmark configuration (Figure 5.8), which corresponded with all cases of cavity forming (Figure A5.8a). The gas void was seen to break up to form gas void disintegration (bubbly flow) at very low ALRs, whereas annular flow was formed under all other flow conditions. No instances of gas void disintegration (slug flow) were identified.

A region of slug flow was established at ALRs in excess of gas void formation and relatively high liquid flow rates (Figure A5.8b). The formation of this slug flow is thought to correspond to critical conditions in which large surface instabilities were formed, due to the action of internal gas shearing and liquid shearing – if two opposing instabilities have sufficient magnitude to meet, the gas core is severed into slugs. An annular flow was generated under all other conditions. The peripheral liquid flow was observed to be relatively thick but chaotic when corresponding with jetting (Figure A5.8c) and thin and smooth for conditions corresponding with evacuated chamber (Figure A5.8d).

A5.2.2 Porous Aerator (Aerator A6)

Figure A5.9 is the gas injection regime map of Aerator A6 (i.e. porous aeration insert in a liquid cross-flow). This shows the effect of varying the supply liquid mass flow rate up to 290 g/s, which corresponds to the discharge limit at 0% ALR with the discharge valve fully open and 5 bar_g operating pressure – this relates to a maximum liquid Bakers number of 923 kg/m²s in the 20 mm mixing chamber. The gas supply was varied up to the maximum achievable flow rate for the given aerator design (7 bar_g maximum gas supply pressure) or, if possible, 5% ALR. Analysis of the results enabled identification of four discrete gas injection regimes, which were categorised into three gas injection regions.

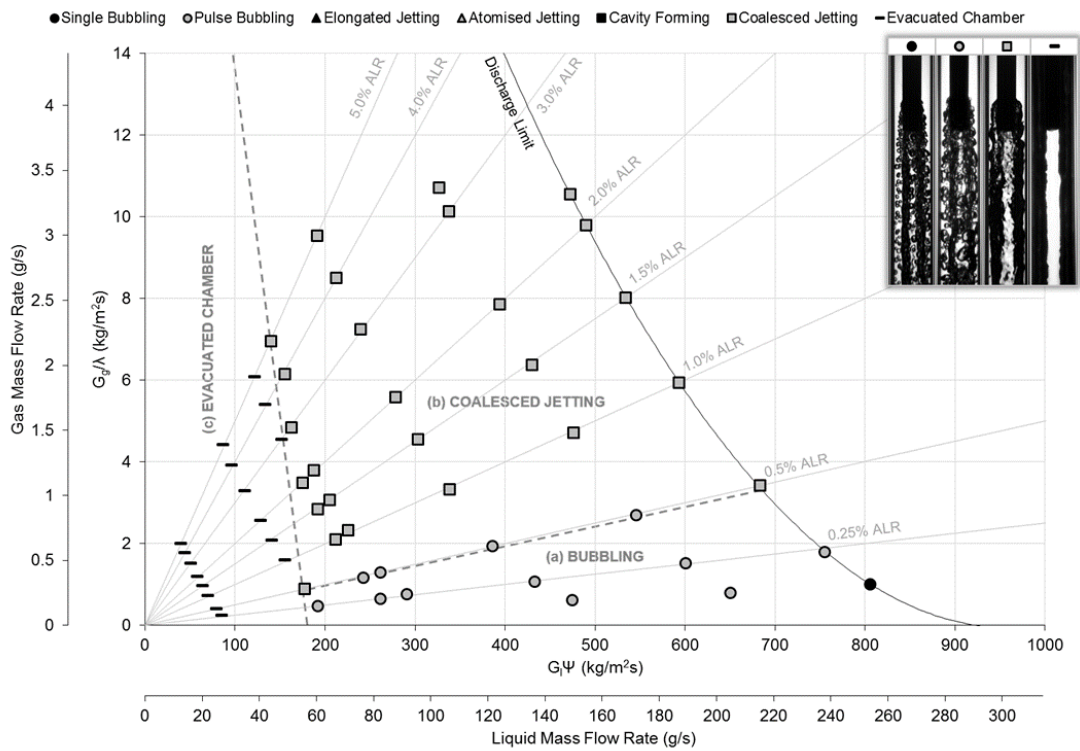


Figure A5.9 Gas injection regime map for aerator A6, with conventional flat-end body.

There appears to be an area within the aerator region which generates more bubbles than the other and therefore it is assumed there is discontinuities on the aeration area across the aerator – this is thought to be a function of this particular aerator, where difference in pore properties effect the resistance to gas flow.

The pore sizes for the porous aerator are substantially smaller than the aerator orifice diameter in the benchmark configuration – therefore, based on the previous results, it was expected that the bubbling region would be larger for the current case. However, the results

show a decreased bubbling region (Figure A5.9a) compared to the benchmark (Figure 5.7), due to the generation of coalesced jetting at higher ALRs. The occurrences of single bubbling at low ALRs are comparable to the benchmark case, whereas the majority of pulse bubbling cases are substituted by coalesced jetting. This implies that the pore spacing is insufficient to allow bubbles to fully expand without coalescing with neighbouring gas streams, thus forming a coalesced jet.

The gas injection map was dominated by coalesced jetting at high gas flow rates (Figure A5.9b). An evacuated chamber region was identified at low liquid velocities (Figure A5.9c), which was observed to be at a comparable level to the benchmark case. However, it appeared to be independent of the gas flow rate.

Figure A5.10 is the flow injection regime map of Aerator A6, which shows the effect of varying fluid flow rates on the flow regimes with areas of common regimes identified and marked. The five discrete flow regimes identified were grouped into four regions.

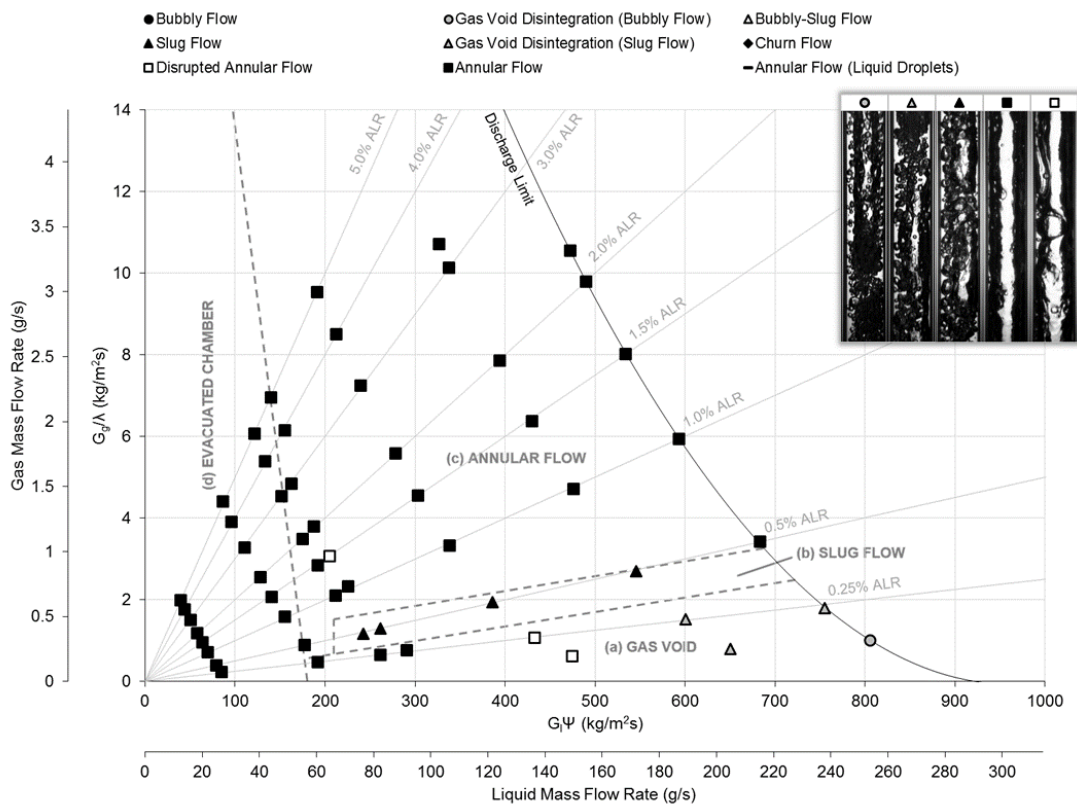


Figure A5.10 Flow regime map for aerator A6, with conventional flat-end body.

A conventional bubbly flow was not identified for any of the conditions tested due to the formation of a gas void in the aerator wake at low ALRs (Figure A5.10a), which displaced

any injected bubbles. The range of operating conditions for gas void formation was comparable with the benchmark configuration (Figure 5.8) and coincided with all instances of single bubbling and some low ALR cases of pulse bubbling.

Similarly, the gas void was seen to breakup under a limited range of conditions, forming gas void disintegration (bubbly flow) at the lowest ALR and highest liquid flow rates and gas void disintegration (slug flow) at higher ALRs. Under all other flow conditions, the gas void was observed to form an annular flow.

The operating range corresponding to intermittent regimes was significantly reduced compared the benchmark, with only a small slug flow region was established beyond the gas void region (Figure A5.10b) which in every case corresponded with pulse bubbling. The flow map was otherwise seen to be dominated by annular flow – this was achieved across a far greater range of conditions than the benchmark case. Annular flow was seen to correspond with coalesced jetting (Figure A5.10c) and the evacuated chamber gas injection regime (Figure A5.10d).

A5.3 Effect of Mixing Chamber Diameter

N.B. The figures presented in the current section feature differing axis scales than those presented previously.

A5.3.1 14 mm Diameter

Figure A5.11 is the gas injection regime map for a 14 mm diameter mixing chamber, using aerator A5 (i.e. 16 x 0.75 mm aerator orifice in a liquid cross-flow). This shows the effect of varying the supply liquid mass flow rate up to 290 g/s, which corresponds to the discharge limit at 0% ALR with the discharge valve fully open and 5 bar_g operating pressure. However, as the cross-section of the mixing chamber is reduced, the maximum liquid Bakers number has increased to 1880 kg/m²s to maintain continuity – this compares to the maximum of 923 kg/m²s in the benchmark case. The gas supply was varied up to the maximum achievable flow rate for the given aerator design (7 bar_g maximum gas supply pressure) or, if possible, 5% ALR – similarly, due to the reduced flow area, the corresponding gaseous Bakers numbers have also increased. Analysis of the results enabled identification of five discrete gas injection regimes, which were categorised into three gas injection regions.

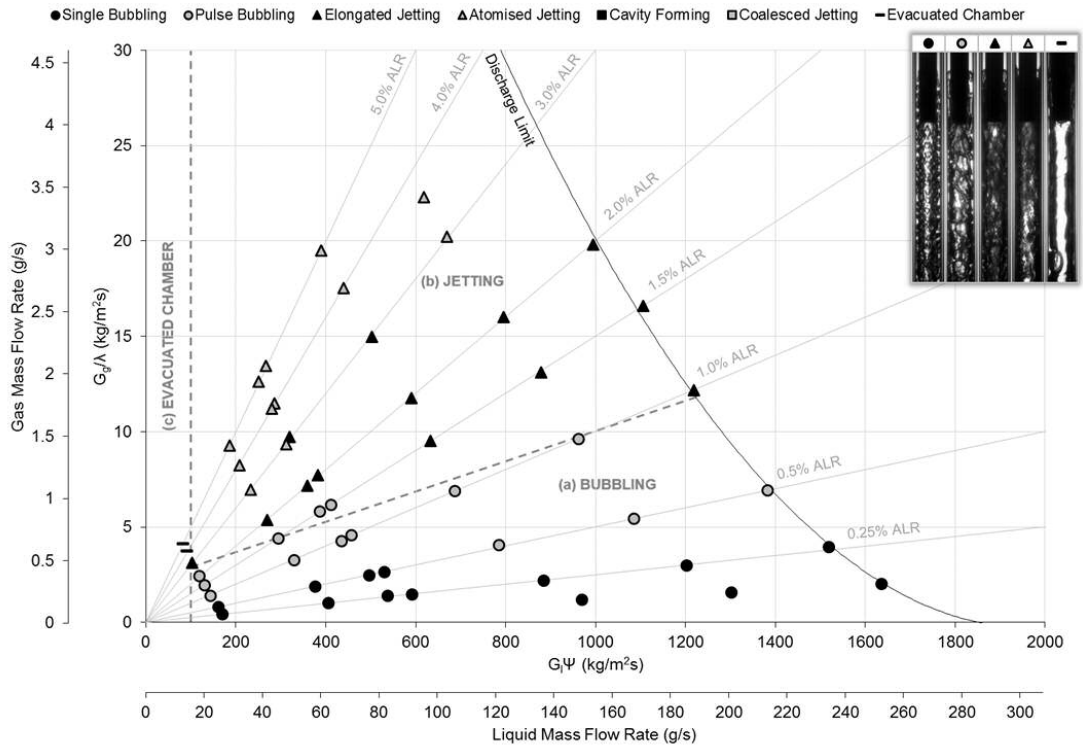


Figure A5.11 Gas injection regime map for 14mm mixing chamber diameter.

The bubbling region (Figure A5.11a) was identified at comparable flow rates to the benchmark case (Figure 5.7), however a greater number of single bubbling instances were observed at low ALRs, with some occurrences identified at 0.5% ALR. This implies that single bubbling is encouraged by increased liquid cross flow velocity (i.e. decreased mixing chamber diameters).

A large jetting regime was observed at high ALRs (Figure A5.11b). Compared to the benchmark case, increased ALRs were required to transition the flow regime from elongated jetting to atomised jetting – this could be due to the greater liquid cross-flow velocity providing greater drag on the emerging gas jet and preventing it from contacting with, and hence churning against, the mixing chamber wall. An evacuated chamber region (Figure A5.11c) was identified at a low liquid Bakers number of $100 \text{ kg/m}^2\text{s}$ – however, as the mixing chamber diameter is reduced, this corresponds to a much reduced liquid flow rate compared to the benchmark configuration and therefore conditions corresponding to evacuated chamber.

Figure A5.12 is the flow injection regime map of the 14 mm diameter mixing chamber, which shows the effect of varying fluid flow rates on the flow regimes with areas of common regimes identified and marked. As with the gas injection map, the maximum liquid and

gaseous Bakkers number have increased to maintain continuity in the reduced cross-section. The five discrete flow regimes identified were grouped into five regions.

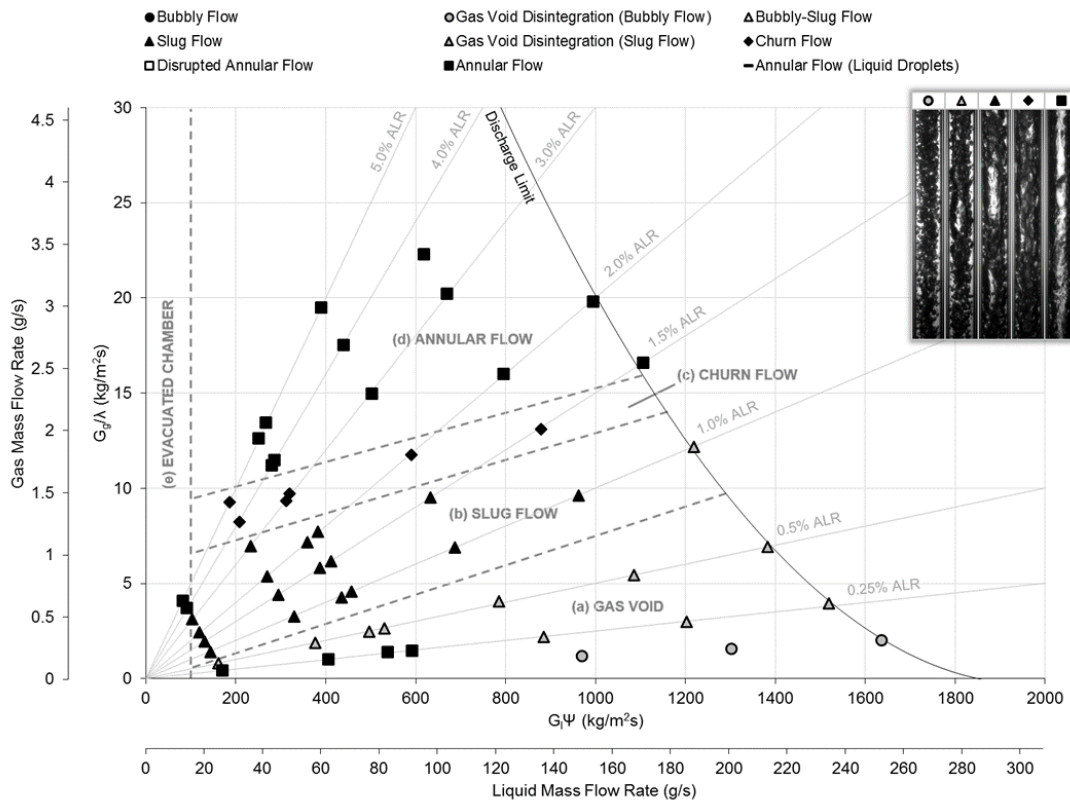


Figure A5.12 Flow regime map for 14mm mixing chamber diameter.

A conventional bubbly flow was not identified for any of the conditions tested due to the formation of a gas void in the aerator wake at low ALRs (Figure A5.12a). Gas void formation coincided with all instances of single bubbling and pulse bubbling at a low ALRs, whereby gas entities injected at the aerator were forced to flow around the gas void periphery. It was hypothesised that reducing the mixing chamber diameter would have the effect of suppressing gas void formation, due to the increased fluid velocities exerting greater detachment forces – however, conversely, gas void formation was observed across a greater number of flow rates with a decreased mixing chamber. Therefore, the results indicated that decreasing the mixing chamber results in a disproportionate increase in aerator wake effects.

Compared to the benchmark case (Figure 5.8), gas void disintegration (slug flow) dominated the gas void region, with gas void disintegration (bubbly flow) also achieved at lesser liquid flow rates – this is thought to be due the increased velocity exerting greater shear on the gas void and thus promoting breakup. All other flow conditions formed an annular flow.

A region of intermittent flow regimes were established beyond the gas void region – like the benchmark case, these were observed to transition from slug flow (Figure A5.12b) to churn flow (Figure A5.12c) with increasing ALR. Annular flow was achieved at the highest ALRs (Figure A5.12d). The transitional limits between regions were observed to have approximately the same relationship with respect to the Bakers numbers as the benchmark case. A thin annular flow was observed to correspond with the evacuated chamber region (Figure A5.12e).

A5.3.2 20 mm Diameter

This configuration is the benchmark case for the flat-end aerator body investigations. The gas injection and flow regime maps are presented in §5.2.

A5.4 Effect of Operating Pressure

N.B. The figures presented in the current section feature differing axis scales than those presented previously.

A5.4.1 5 bar_g

This configuration is the benchmark case for the flat-end aerator body investigations. The gas injection and flow regime maps are presented in §5.2.

A5.4.2 3 bar_g

Figure A5.13 is the gas injection regime map for 3 bar_g operating pressure, using aerator A5 (i.e. 16 x 0.75 mm aerator orifice in a liquid cross-flow). This shows the effect of varying the supply liquid mass flow rate up to 225 g/s, which corresponds to the discharge limit at 0% ALR with the discharge valve fully open and 3 bar_g operating pressure – this is reduced compared to the maximum flow of 290 g/s in the benchmark case. Consequently, the related maximum liquid Bakers number in the same 20 mm mixing chamber has also decreased to 717 kg/m²s, which compares to the maximum of 923 kg/m²s in the benchmark case. The gas supply was varied up to 5% ALR. Analysis of the gas injection map enabled identification of five discrete gas injection regimes, which were categorised into three gas injection regions.

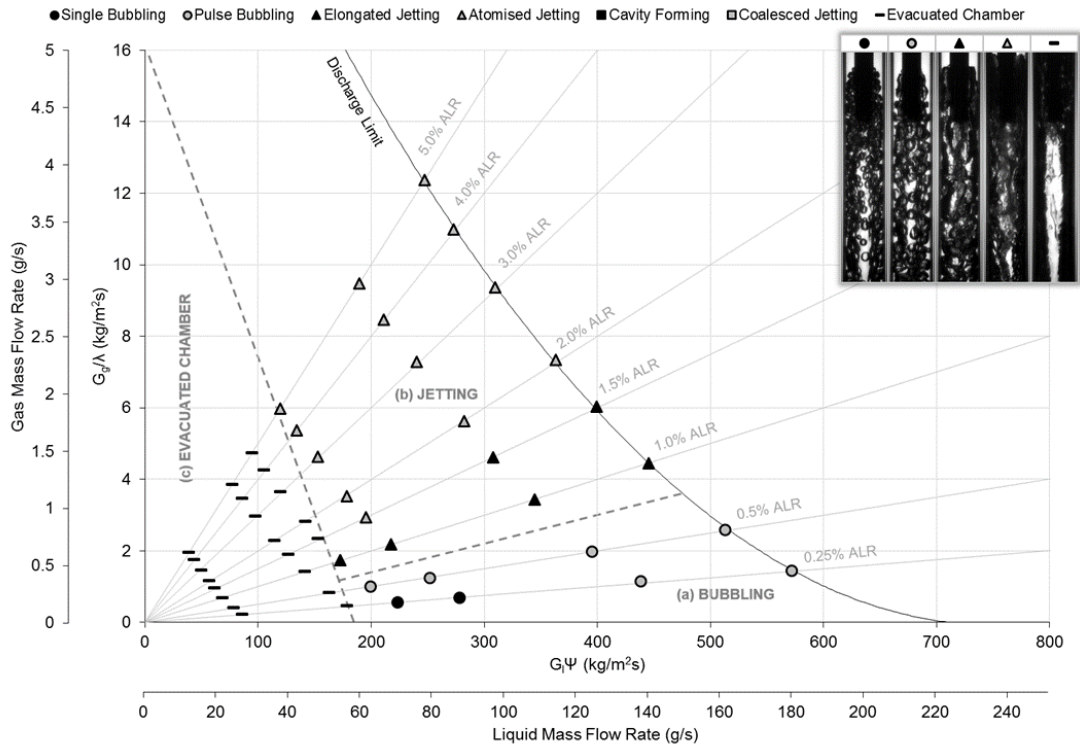


Figure A5.13 Gas injection regime map for 3 bar_g operating pressure.

The bubbling region (Figure A5.13a) was identified to be smaller than the benchmark case (Figure 5.7), but exhibited the same general trend with increasing ALR whereby single bubbling transitions to pulse bubbling. Single bubbling also appeared to be marginally suppressed.

Transition from the bubbling region to the jetting region (Figure A5.13b) was identified to occur at lower ALRs than the benchmark case, in which the general trend of elongated jetting transitioning to atomised jetting with increasing ALR was maintained. An evacuated chamber region (Figure A5.13c) was identified at comparably low liquid flow rates to the benchmark case, which also appeared to be suppressed with increasing ALR. As the maximum flow rate is reduced with reducing pressure, the evacuated chamber was observed to occupy a greater proportion of the operating range.

Figure A5.14 is the flow injection regime map for 3 bar_g operating pressure, which shows the effect of varying fluid flow rates on the flow regimes with areas of common regimes identified and marked. As with the gas injection map, the maximum liquid flow rate has reduced with the decreased operating pressure, which has resulted in a decreased maximum liquid Bakkers number. The six discrete flow regimes identified were grouped into five regions.

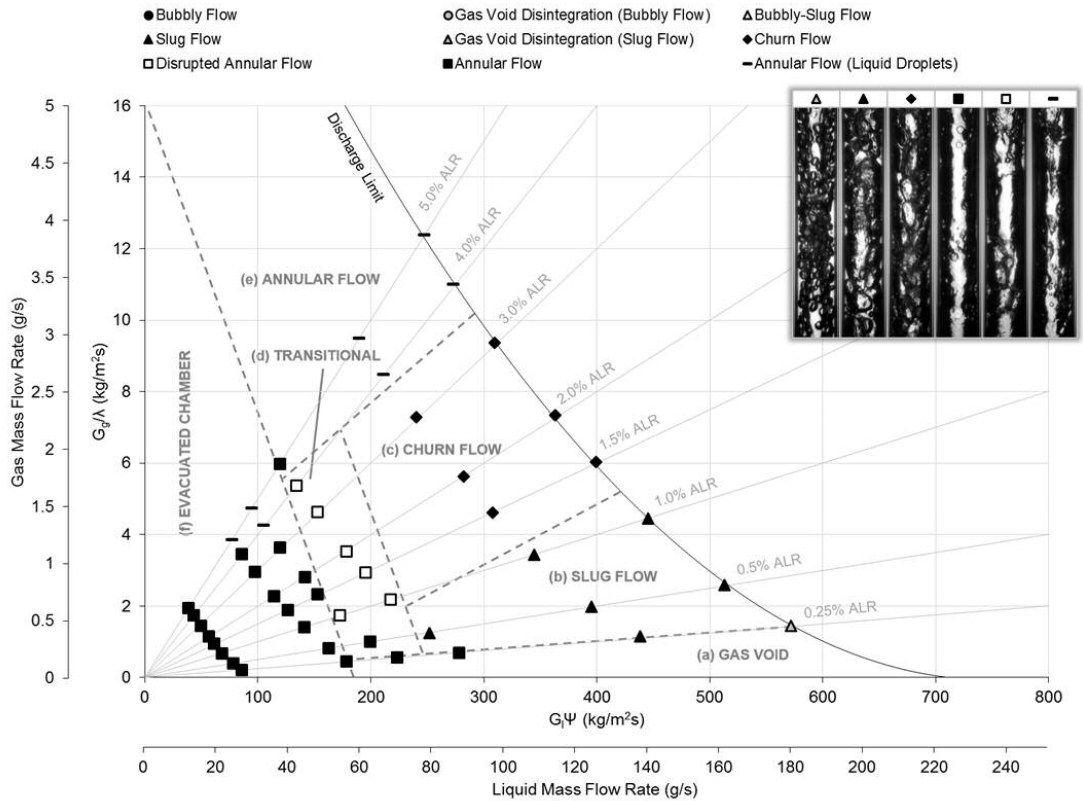


Figure A5.14 Flow regime map for 3 bar_g operating pressure.

A conventional bubbly flow was not identified for any of the conditions tested due to the formation of a gas void in the aerator wake at low ALRs (Figure A5.14a). This coincided with all instances of single bubbling, and some pulse bubbling at low ALRs. The gas void occurs at approximately same flow conditions as the benchmark case.

The gas void was only seen to break up in a single instance at the highest liquid flow rate and lowest ALR to form gas void disintegration (slug flow). All other observation of gas void formation resulted in an annular flow. Unlike the benchmark case, bubbly flow (through gas void shearing) was not observed.

A region of intermittent flow regimes were established at ALRs in excess of the gas void region – like the benchmark case (Figure 5.8), these were observed to transition from slug flow (Figure A5.14b) to churn flow (Figure A5.14c) with increasing ALR. Compared to the benchmark configuration, the transition between the intermittent regimes occurred at lower ALRs – therefore the effect of reducing operating pressure promotes the formation of intermittent flow regimes at lower ALRs. An annular flow occurs at high ALRs (Figure A5.14d), which commonly features liquid droplets within the gas core due to liquid running

off the aerator. A thin annular flow was identified for all conditions corresponding to the evacuated chamber gas injection regime (Figure A5.14e).

A5.4.3 1 bar_g

Figure A5.15 is the gas injection regime map for 1 bar_g operating pressure, using aerator A5 (i.e. 16 x 0.75 mm aerator orifice in a liquid cross-flow). This shows the effect of varying the supply liquid mass flow rate up to 130 g/s, which corresponds to the discharge limit at 0% ALR with the discharge valve fully open and 1 bar_g operating pressure – this is reduced compared to the maximum flow of 290 g/s in the benchmark case. Consequently, the related maximum liquid Bakers number in the same 20 mm mixing chamber has also decreased to 413 kg/m²s, which compares to the maximum of 923 kg/m²s in the benchmark case. The gas supply was varied up to 5% ALR. Analysis of the gas injection map enabled identification of five discrete gas injection regimes, which were categorised into three gas injection regions.

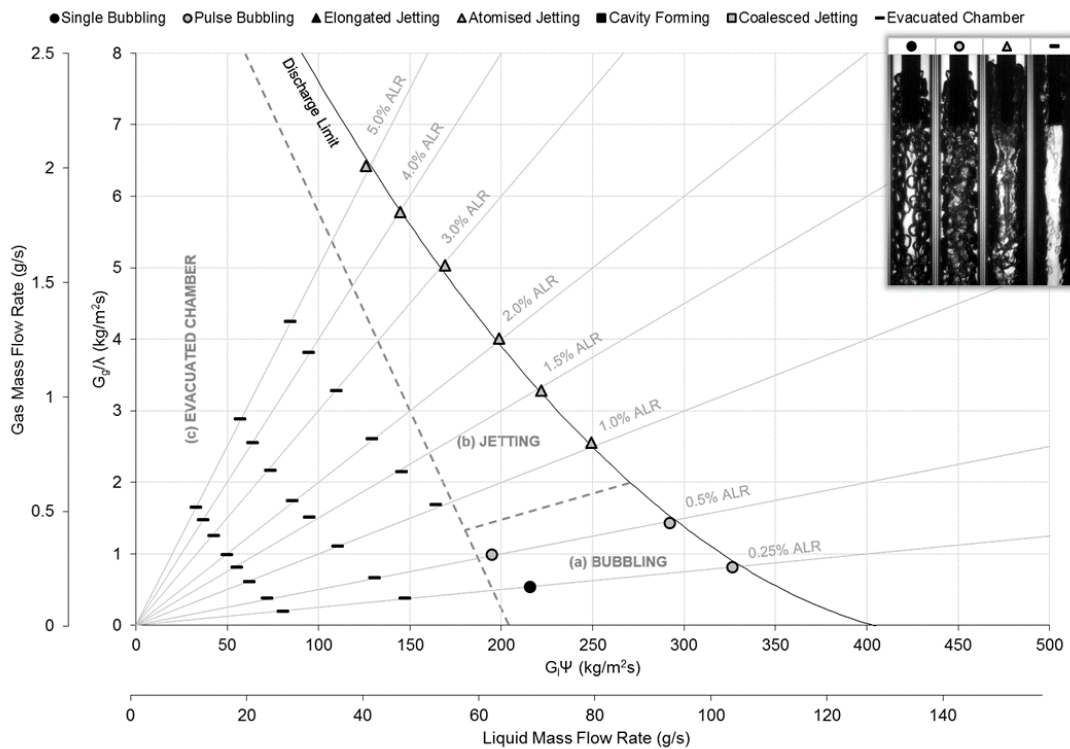


Figure A5.15 Gas injection regime map for 1 bar_g operating pressure.

The bubbling region (Figure A5.15a) was identified to be smaller than the benchmark case (Figure 5.7). Only a single observation of single bubbling was identified within this region.

Transition from the bubbling region to the jetting region (Figure A5.15b) was identified to occur at lower ALRs than the benchmark case, which was observed to consist solely of atomised jetting. An evacuated chamber region (Figure A5.15c) was identified at comparably low liquid flow rates to the benchmark case, which also appeared to be suppressed with increasing ALR. As the maximum flow rate is reduced with reducing pressure, the evacuated chamber was observed to occupy a greater proportion of the operating range.

Figure A5.16 is the flow injection regime map for 1 bar_g operating pressure, which shows the effect of varying fluid flow rates on the flow regimes with areas of common regimes identified and marked. As with the gas injection map, the maximum liquid flow rate has reduced with the decreased operating pressure, which has resulted in a decreased maximum liquid Bakers number. The five discrete flow regimes identified were grouped into five regions.

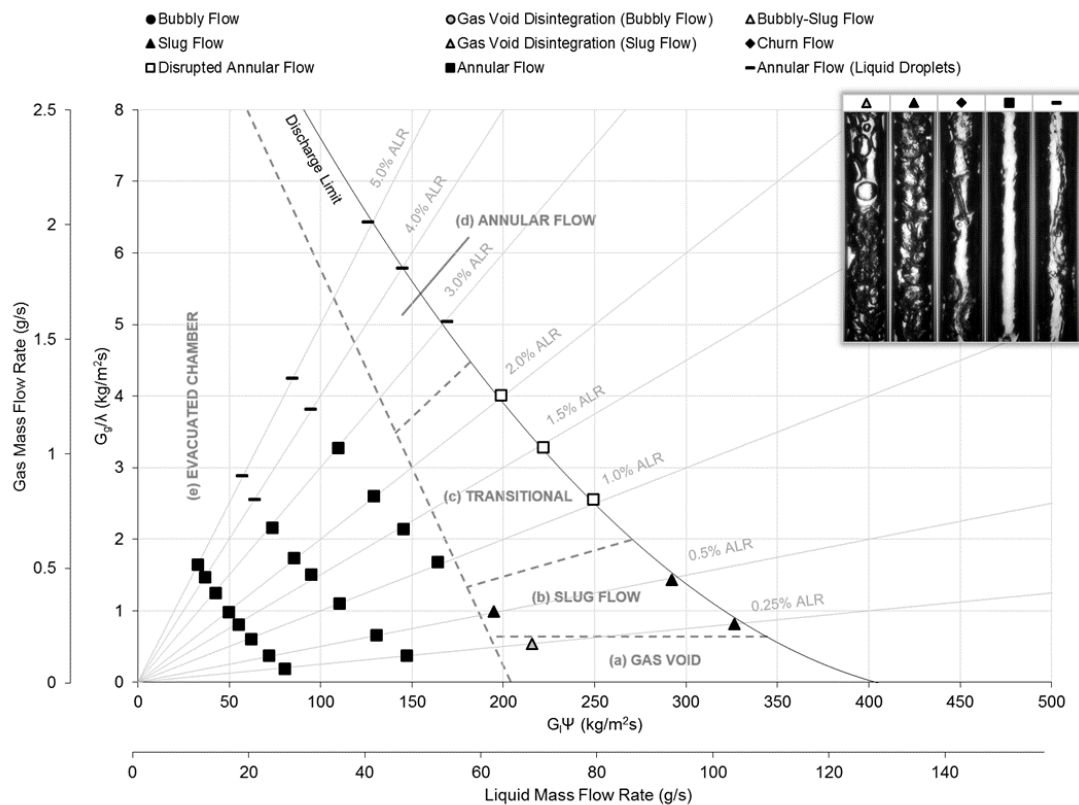


Figure A5.16 Flow regime map for 1 bar_g operating pressure.

A conventional bubbly flow was not identified for any of the conditions tested due to the formation of a gas void in the aerator wake at low ALRs (Figure A5.16a), which coincided

with the only instance of single bubbling. In this single case, the gas void was seen to break up to form gas void disintegration (slug flow).

A region of intermittent flow regimes were established at ALRs in excess of the gas void region – like the benchmark case (Figure 5.8), these were observed to transition from slug flow (Figure A5.16b) to churn flow (Figure A5.16c) with increasing ALR. Compared to the benchmark and previous case, the transition between the intermittent regimes occurred at lower ALRs – this supports the previous observation that a reducing operating pressure promotes the formation of intermittent flow regimes at lower ALRs. An annular flow occurs at high ALRs (Figure A5.16d), every case of which featured liquid droplets that run off the aerator and fall within the gas core. A thin annular flow was identified for all conditions corresponding to the evacuated chamber gas injection regime (Figure A5.16e), although some cases at high ALRs were also observed to feature liquid droplets within the gas core.

A5.5 Effect of Orientation

A5.5.1 Vertically Downwards

This configuration is the benchmark case for the flat-end aerator body investigations. The gas injection and flow regime maps are presented in §5.2.

A5.5.2 Vertically Upwards

Figure A5.17 is the gas injection regime map for a vertically upwards atomiser orientation, using aerator A5 (i.e. 16 x 0.75 mm aerator orifice in a liquid cross-flow). This shows the effect of varying the supply liquid mass flow rate up to 302 g/s, which corresponds to the discharge limit at 0% ALR with the discharge valve fully open and 5 bar_g operating pressure – this is marginally increased compared to the maximum flow of 290 g/s in the benchmark case. Consequently, the related maximum liquid Bakers number in the same 20 mm mixing chamber has also increased to 961 kg/m²s, which compares to the maximum of 923 kg/m²s in the benchmark case. The gas supply was varied up to 5% ALR. Analysis of the results enabled identification of four discrete gas injection regimes, which were categorised into two gas injection regions.

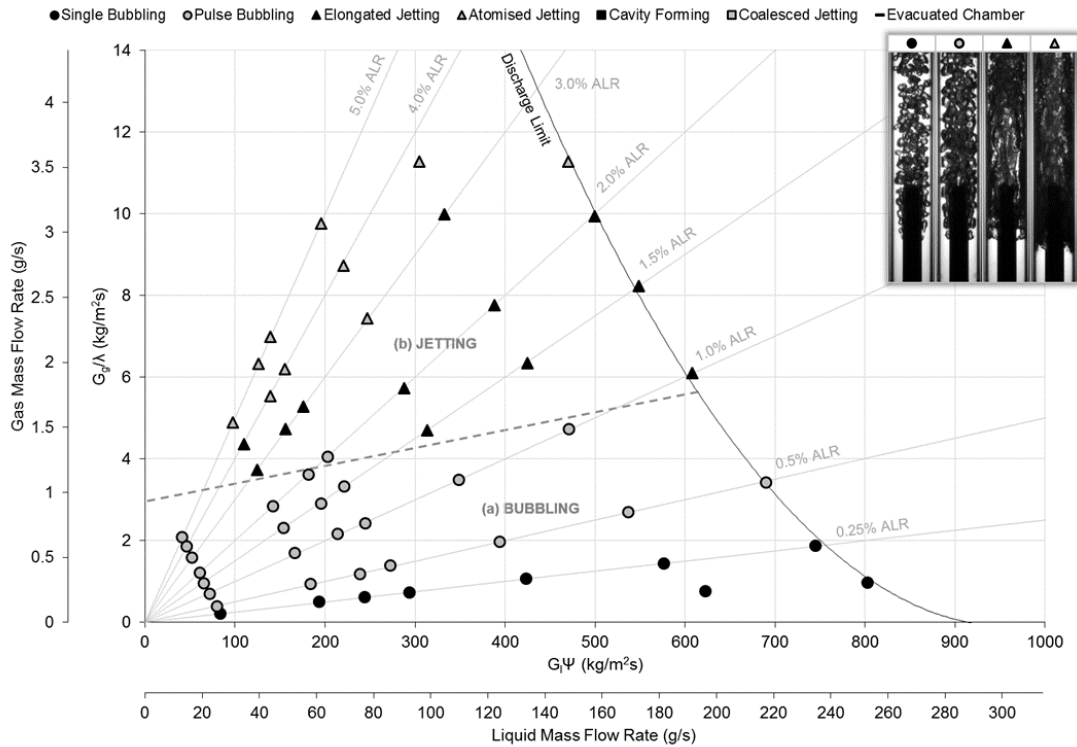


Figure A5.17 Gas injection regime map for vertically upwards orientation.

The bubbling region (Figure A5.17a) is seen to span a greater range of liquid flow rates compared to the benchmark (Figure 5.7). Single bubbling occurs at low ALRs and is marginally encouraged compared to the benchmark condition, particularly at low ALRs – this is thought to be due to the assistance of buoyancy in combination with other detachment mechanisms to separate bubbles from aerator.

Transition from pulse bubbling to the jetting region (Figure A5.17b) occurs with increasing ALR, which is marginally suppressed compared to the benchmark configuration. It is hypothesised that this is caused by pressure fluctuations within mixing chamber as ALR increases, which causes the gas injection to alternate between regimes – these fluctuations are thought to be caused as heterogeneous regimes pass through the exit orifice and is amplified in the vertically upwards orientation due to the hydrostatic head of liquid within the atomiser. Increasing ALR is seen to transition the jetting from elongated jetting to atomised jetting. The evacuated chamber regime, observed in the benchmark, is eliminated in vertically upward orientation – demonstrating that its formation is as a result of buoyancy effects. Its omission enables bubble and jetting formation at significantly reduced flow rates compared to the benchmark.

Figure A5.18 is the flow injection regime map of a vertically upwards atomiser orientation, which shows the effect of varying fluid flow rates on the flow regimes with areas of common regimes identified and marked. As with the gas injection map, the maximum liquid flow rate has been marginally increased with the orientation, which has resulted in an increased maximum liquid Bakers number. The three discrete flow regimes identified were grouped into three regions.

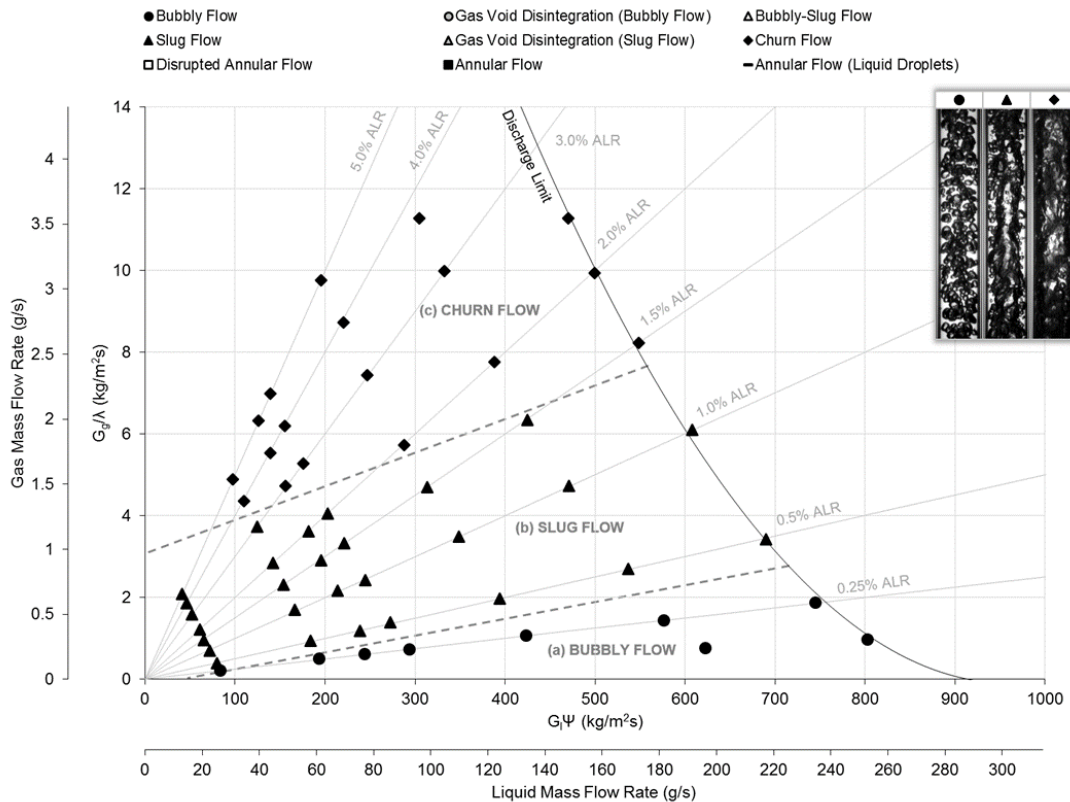


Figure A5.18 Flow regime map for vertically upwards orientation.

A gas void was not formed in the aerator wake for any flow condition, as the effect of buoyancy in a vertically upward orientation aids detachment from the aerator tip – this contrasts with the benchmark case, where buoyancy is an obstruction to gas void detachment. Consequently, injected bubbles were no longer displaced within the mixing chamber and hence a bubbly flow region was formed (Figure A5.18a) – every instance occurred at or under 0.25% ALR. All cases of bubbly flow for the current investigation coincided with single bubbling at the aerator.

A region of intermittent flow regimes were established at ALRs in excess of the bubbly region which, like the benchmark case (Figure 5.8), were observed to transition from slug flow (Figure A5.18b) to churn flow (Figure A5.18c) with increasing ALR. No instances of

annular flow observed, which is hypothesised to occur because the gas-phase rises at a greater velocity than liquid which generates shear on the gas-liquid interface and promotes churn flow.

APPENDIX 6: REGIME MAPS FOR STREAMLINED AERATOR DESIGNS

A6.1 Effect of Aerator Body Design

A6.1.1 Circular Arc

Figure A6.1 is the gas injection regime map for aerator A5 (i.e. 16 x 0.75 mm aerator orifice in a liquid cross-flow), with a circular arc streamlined aerator tip installed. This shows the effect of varying the supply liquid mass flow rate up to 290 g/s, which corresponds to the discharge limit at 0% ALR with the discharge valve fully open and 5 bar_g operating pressure, and relates to a maximum liquid Bakers number of 923 kg/m²s in the 20 mm mixing chamber. The gas supply was varied up to the maximum achievable flow rate for the given aerator design (7 bar_g maximum gas supply pressure) or, if possible, 5% ALR. Analysis of results enabled identification of six discrete gas injection regimes, which were categorised into three gas injection regions.

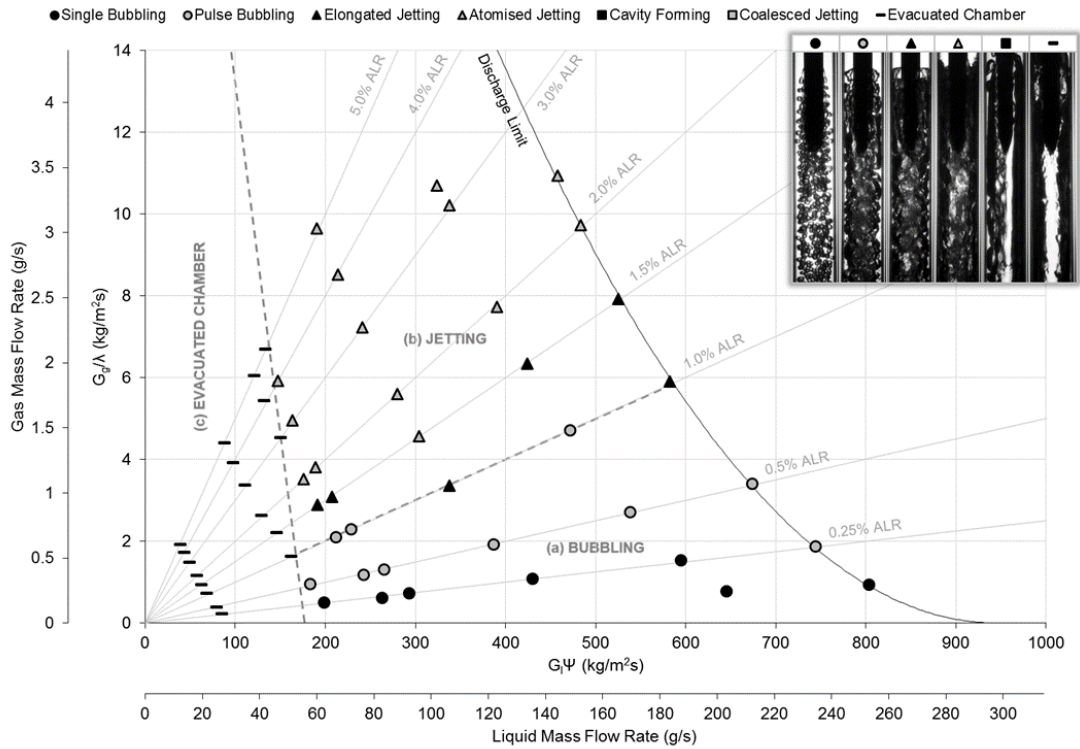


Figure A6.1 Gas injection regime map for aerator A5, with streamlined circular arc body.

A large region of bubbling (Figure A6.1a) was identified in a similar region to the ADARPA benchmark configuration (Figure 7.6) – albeit marginally smaller, owing to a greater presence of elongated jetting. Similarly, all instances of single bubbling were observed to occur at or below 0.25% ALR, with the region above this limit formed of pulse bubbling. In addition, the flow region was also observed to transition to jetting (Figure A6.1b) with increasing ALR, within which elongated jetting transitioned to atomised jetting at the highest ALRs. A region of evacuated chamber, where phase separation occurs prior to fluid injection, was identified at relatively low liquid flow rates (Figure A6.1c) in a comparable region to the benchmark case – this too appeared to be suppressed with high gas flow rates.

Figure A6.2 is the flow injection regime map for aerator A5, with a circular arc streamlined aerator tip installed. which shows the effect of varying fluid flow rates on the flow regimes with areas of common regimes identified and marked. The six discrete flow regimes identified were grouped into six regions.

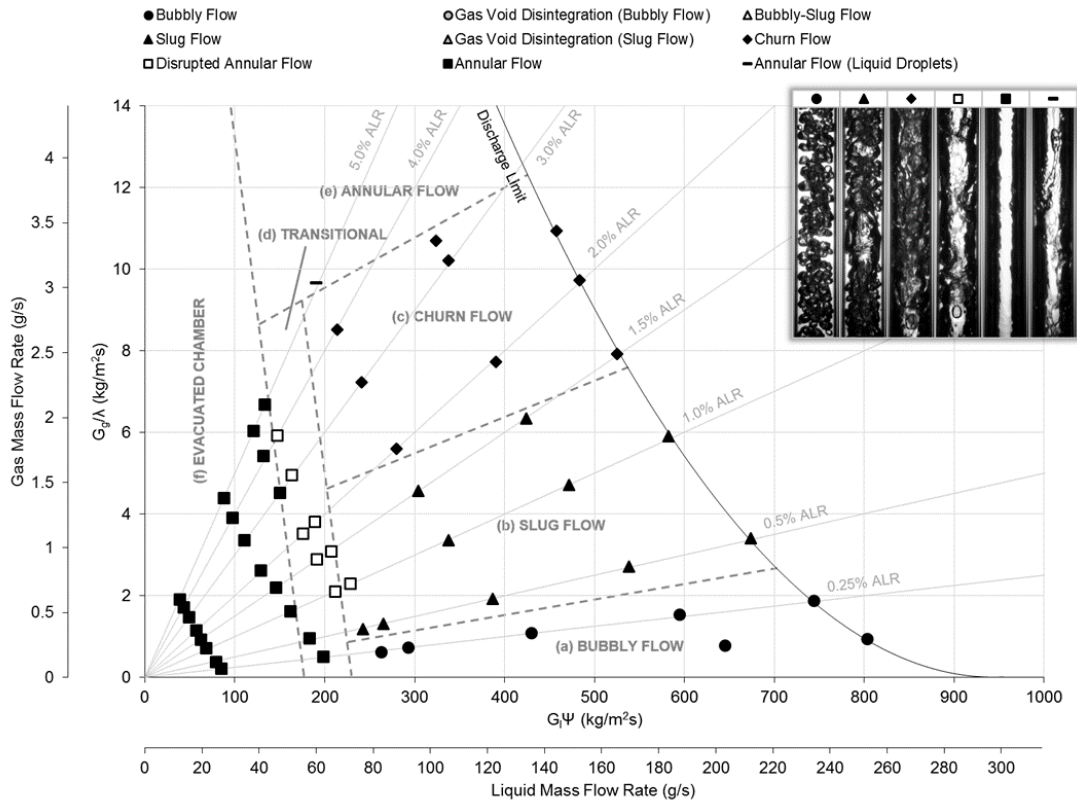


Figure A6.2 Flow regime map for aerator A5, with streamlined circular arc body.

Unlike with the conventional flat-end aerator (Figure 5.8), but similar to the ADARPA streamlined aerator tip (Figure 7.7), a bubbly flow region (Figure A6.2a) was observed at low ALRs with a circular arc aerator body. The majority of bubbly flow cases coincided with single bubbling at the aerator, although an isolated case of pulse bubbling at low ALR was also observed to form a bubbly flow. The internal flow performance in all other parts of the flow regime map were observed to be comparable with all other aerator body designs, in which flow was observed to transition from slug flow (Figure A6.2b) to churn flow (Figure A6.2c) with increasing ALR, before achieving an annular flow at the highest ALR (Figure A6.2e). A thin annular flow was also identified for all conditions corresponding to the evacuated chamber gas injection regime (Figure A6.2f). A transition region (Figure A6.2d) was also identified between the evacuated chamber and intermittent flow regions.

Irregular cases of annular flow were observed to develop from single bubble and pulse bubbling due to the formation of a buoyant gas void at very low liquid flow rates and ALRs, just beyond the limit of evacuated chamber. It is unknown if this void originates from partial bleeding of the mixing chamber upon start up, or due to the increased residence time and hence coalescence of the injected gas entities under these low flow conditions. Regardless, the void has sufficient buoyancy to overcome the liquid shear in the main mixing chamber

and does not become trapped in the aerator wake due to the reduced bluff body effect of the streamlined aerator tip. Equilibrium is satisfied just downstream of the aerator orifice, where the liquid shear and emerging gas momentum are sufficient to prevent it from rising and forming evacuated chamber. The void extends through the mixing chamber forming an annular flow.

A6.1.2 Hybrid

Figure A6.3 is the gas injection regime map for aerator A5, with a hybrid streamlined aerator tip installed. This shows the effect of varying the supply liquid mass flow rate up to 290 g/s, which corresponds to the discharge limit at 0% ALR with the discharge valve fully open and 5 bar_g operating pressure, and relates to a maximum liquid Bakers number of 923 kg/m²s in the 20 mm mixing chamber. The gas supply was varied up to the maximum achievable flow rate for the given aerator design (7 bar_g maximum gas supply pressure) or, if possible, 5% ALR. Analysis of results enabled identification of five discrete gas injection regimes, which were categorised into three gas injection regions.

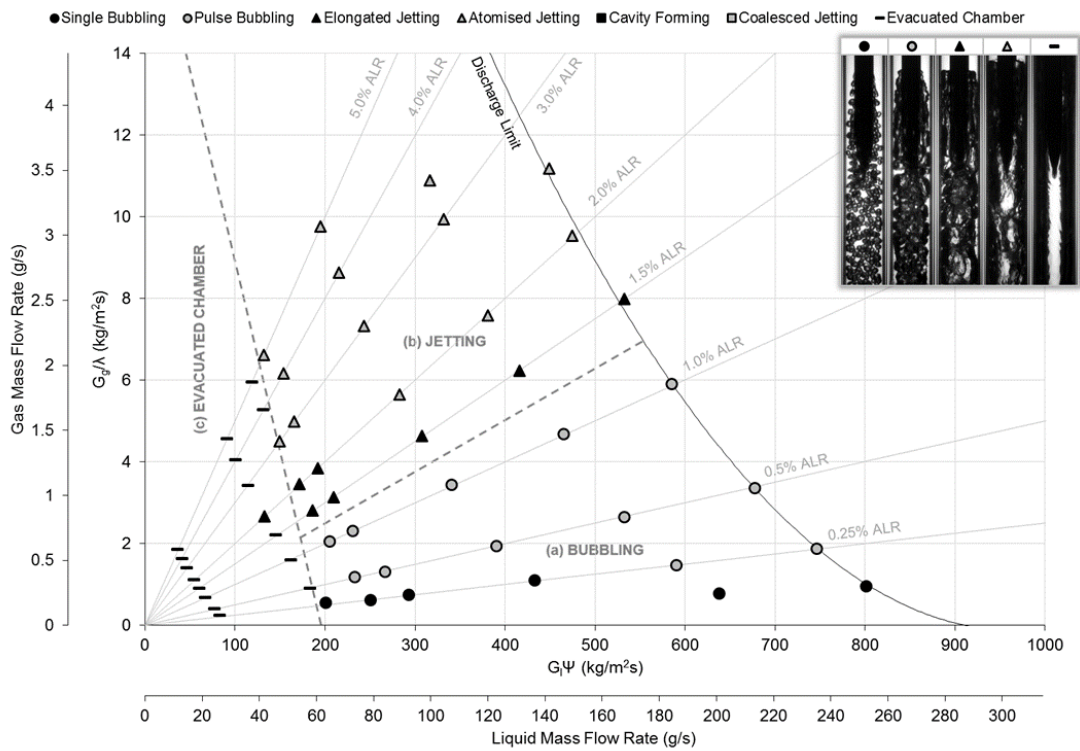


Figure A6.3 Gas injection regime map for aerator A5, with streamlined hybrid body.

A large region of bubbling (Figure A6.3a) was identified in a similar region to the ADARPA configuration (Figure 7.6) and the previously discussed streamlined aerator tips experiment

(Figure A6.1). Similarly, all instances of single bubbling were observed to occur at or below 0.25% ALR, with the region above this limit formed of pulse bubbling. In addition, the flow region was also observed to transition to jetting (Figure A6.3b) with increasing ALR, within which elongated jetting transitioned to atomised jetting at the highest ALRs. A region of evacuated chamber, where phase separation occurs prior to fluid injection, was identified at relatively low liquid flow rates (Figure A6.3c) in a comparable region to the benchmark case – this too appeared to be suppressed with high gas flow rates.

Figure A6.4 is the flow injection regime map for aerator A5, with a hybrid streamlined aerator tip installed, which shows the effect of varying fluid flow rates on the flow regimes with areas of common regimes identified and marked. The six discrete flow regimes identified were grouped into six regions.

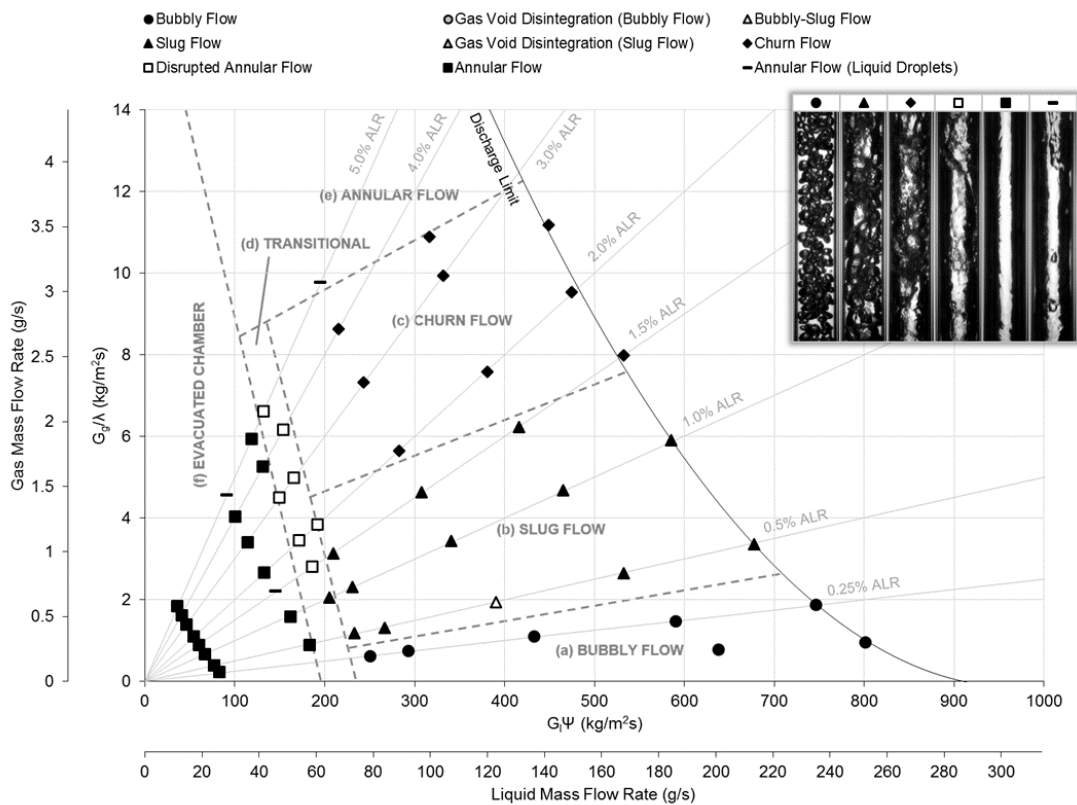


Figure A6.4 Flow regime map for aerator A5, with streamlined hybrid body.

Unlike with the conventional flat-end aerator (Figure 5.8), but similar to the previous streamlined aerator tip (Figure A6.2), a bubbly flow region (Figure A6.4a) was observed at low ALRs with a hybrid aerator body. The majority of bubbly flow cases coincided with single bubbling at the aerator, although an isolated case of pulse bubbling at low ALR was also observed to form a bubbly flow. The internal flow performance in all other parts of the

flow regime map were observed to be comparable with all other aerator body designs, in which flow was observed to transition from slug flow (Figure A6.4b) to churn flow (Figure A6.4c) with increasing ALR, before achieving an annular flow at the highest ALR (Figure A6.4e). A thin annular flow was also identified for all conditions corresponding to the evacuated chamber gas injection regime (Figure A6.4f). A transition region (Figure A6.4d) was also identified between the evacuated chamber and intermittent flow regions.

A6.1.3 Conical

Figure A6.5 is the gas injection regime map for aerator A5, with a conical streamlined aerator tip installed. This shows the effect of varying the supply liquid mass flow rate up to 290 g/s, which corresponds to the discharge limit at 0% ALR with the discharge valve fully open and 5 bar_g operating pressure, and relates to a maximum liquid Bakers number of 923 kg/m²s in the 20 mm mixing chamber. The gas supply was varied up to the maximum achievable flow rate for the given aerator design (7 bar_g maximum gas supply pressure) or, if possible, 5% ALR. Analysis of results enabled identification of five discrete gas injection regimes, which were categorised into three gas injection regions.

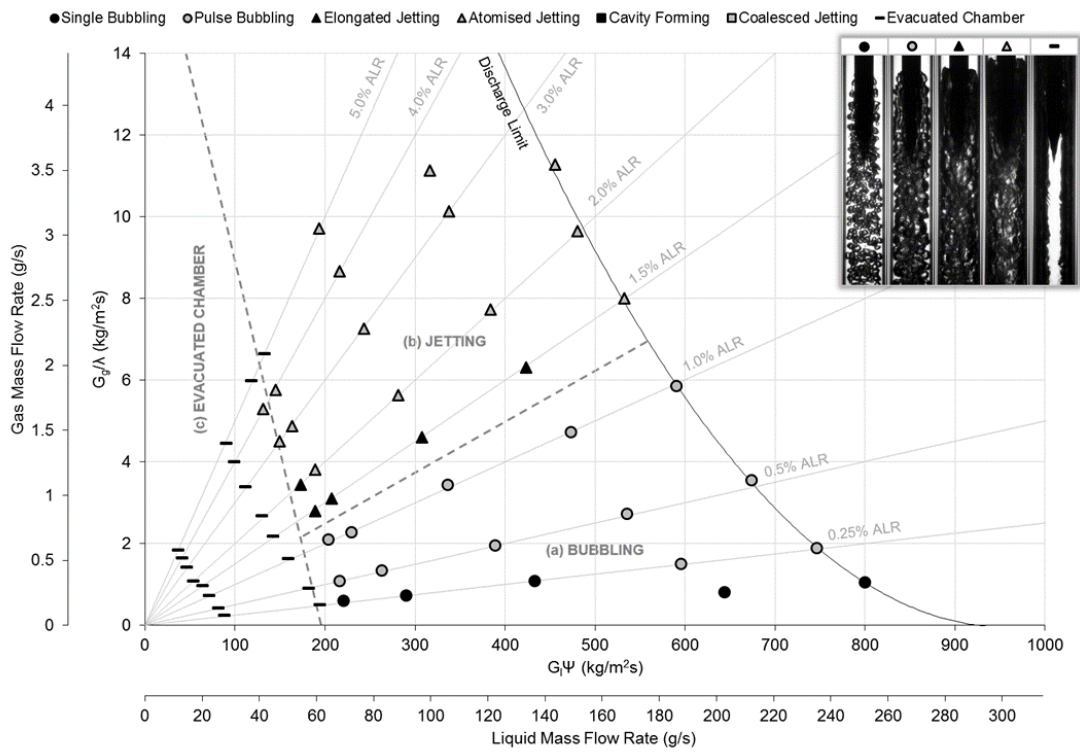


Figure A6.5 Gas injection regime map for aerator A5, with streamlined conical body.

A large region of bubbling (Figure A6.5a) was identified in a similar region to the ADARPA configuration (Figure 7.6) and the previously discussed streamlined aerator tips experiments (Figures A6.1 and A6.3). Similarly, all instances of single bubbling were observed to occur at or below 0.25% ALR, with the region above this limit formed of pulse bubbling. In addition, the flow region was also observed to transition to jetting (Figure A6.5b) with increasing ALR, within which elongated jetting transitioned to atomised jetting at the highest ALRs. A region of evacuated chamber, where phase separation occurs prior to fluid injection, was identified at relatively low liquid flow rates (Figure A6.5c) in a comparable region to the benchmark case – this too appeared to be suppressed with high gas flow rates.

Figure A6.6 is the flow injection regime map for aerator A5, with a conical streamlined aerator tip installed, which shows the effect of varying fluid flow rates on the flow regimes with areas of common regimes identified and marked. The seven discrete flow regimes identified were grouped into six regions.

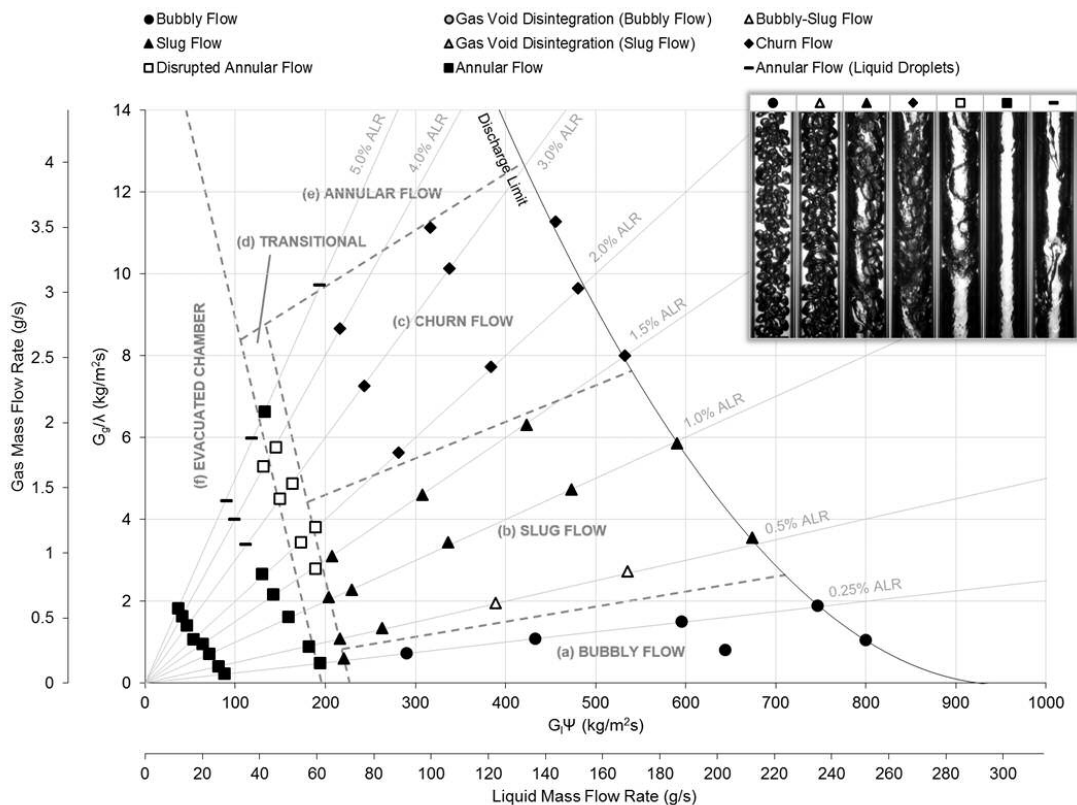


Figure A6.6 Flow regime map for aerator A5, with streamlined conical body.

Unlike with the conventional flat-end aerator (Figure 5.8), but similar to the previous streamlined aerator tips (Figures A6.2 and A6.5), a bubbly flow region (Figure A6.6a) was observed at low ALRs with a hybrid aerator body. The majority of bubbly flow cases

coincided with single bubbling at the aerator, although an isolated case of pulse bubbling at low ALR was also observed to form a bubbly flow. The internal flow performance in all other parts of the flow regime map were observed to be comparable with all other aerator body designs, in which flow was observed to transition from slug flow (Figure A6.6b) to churn flow (Figure A6.6c) with increasing ALR, before achieving an annular flow at the highest ALR (Figure A6.6e). A thin annular flow was also identified for all conditions corresponding to the evacuated chamber gas injection regime (Figure A6.6f). A transition region (Figure A6.6d) was also identified between the evacuated chamber and intermittent flow regions.

A6.1.4 ADARPA

The gas injection and flow regime maps for the equivalent ADARPA configuration are shown in §7.2.

A6.1.5 Flat-End

The gas injection and flow regime maps for the equivalent flat-end configuration are shown in §5.2.

APPENDIX 7: REGIME MAPS FOR ADARPA STREAMLINED AERATOR DESIGNS

A7.1 Effect of Aerator Orifice Diameter

A7.1.1 1 x 3.0 mm (Aerator A2)

Figure A7.1 is the gas injection regime map of Aerator A2 (i.e. 1 x 3.0 mm aerator orifice in a liquid cross-flow) with a streamlined ADARPA aerator body. This shows the effect of varying the supply liquid mass flow rate up to 290 g/s, which corresponds to the discharge limit at 0% ALR with the discharge valve fully open and 5 bar_g operating pressure, and relates to a maximum liquid Bakers number of 923 kg/m²s in the 20 mm mixing chamber. The gas supply was varied up to the maximum achievable flow rate for the given aerator design (7 bar_g maximum gas supply pressure) or, if possible, 5% ALR. Analysis of results enabled identification of four discrete gas injection regimes, which were categorised into three gas injection regions.

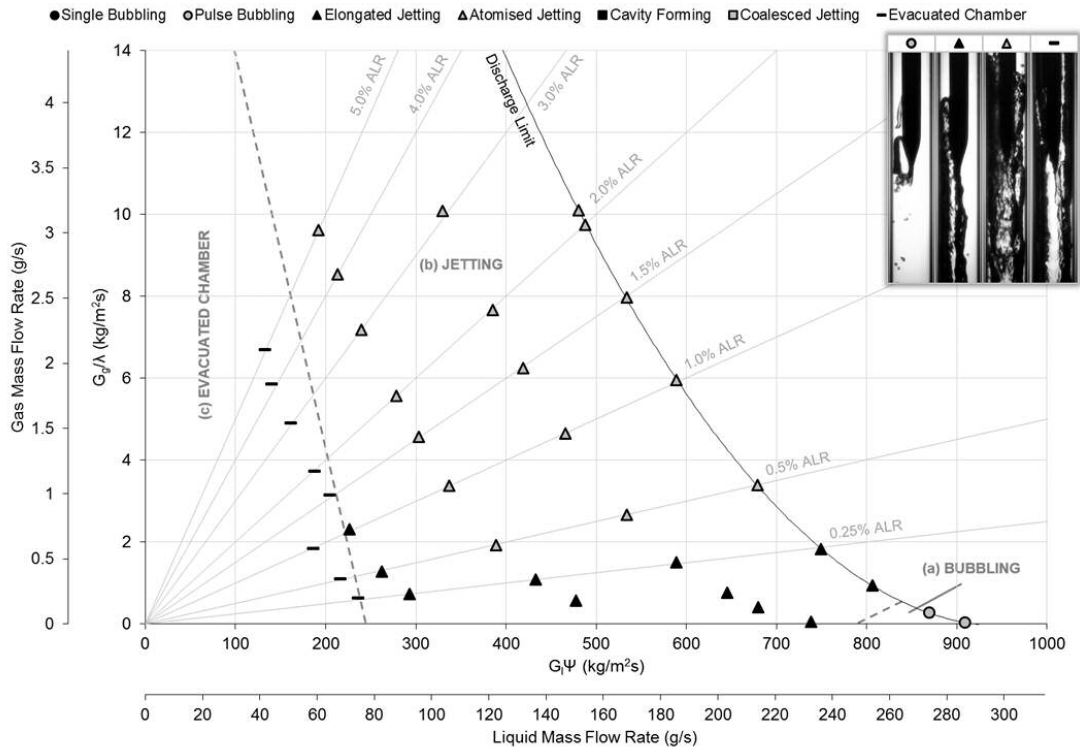


Figure A7.1 Gas injection regime map for aerator A2, with streamlined ADARPA body.

A significantly reduced bubbling region (Figure A7.1a) was identified compared to the benchmark case (Figure 7.6), which suggests that increasing the aerator orifice diameter acts to suppress bubbling. Unlike the benchmark configuration and equivalent flat-end aerator body case (Figure A5.1), single bubbling was not identified – instead pulse bubbling occurs, even at the lowest ALRs, in which formation of bubbles and large slugs (formed from the detachment of a growing gas void) alternate from the orifice.

Otherwise, the gas injection map is dominated by a jetting region (Figure A7.1b), with a general trend of elongated jetting transitioning to atomised jetting with increasing ALR. Unlike the equivalent flat-end aerator body case, no observations of cavity forming were identified as the gas void in the aerator wake was prevented. A region of evacuated chamber, where phase separation occurs prior to fluid injection, was identified at relatively low liquid flow rates (Figure A7.1c) in a comparable region to the previous cases – this too appeared to be marginally suppressed with high gas flow rates.

Figure A7.2 is the flow injection regime map for aerator A2, with an ADARPA streamlined aerator body, which shows the effect of varying fluid flow rates on the flow regimes with areas of common regimes identified and marked. The three discrete flow regimes identified were grouped into three regions.

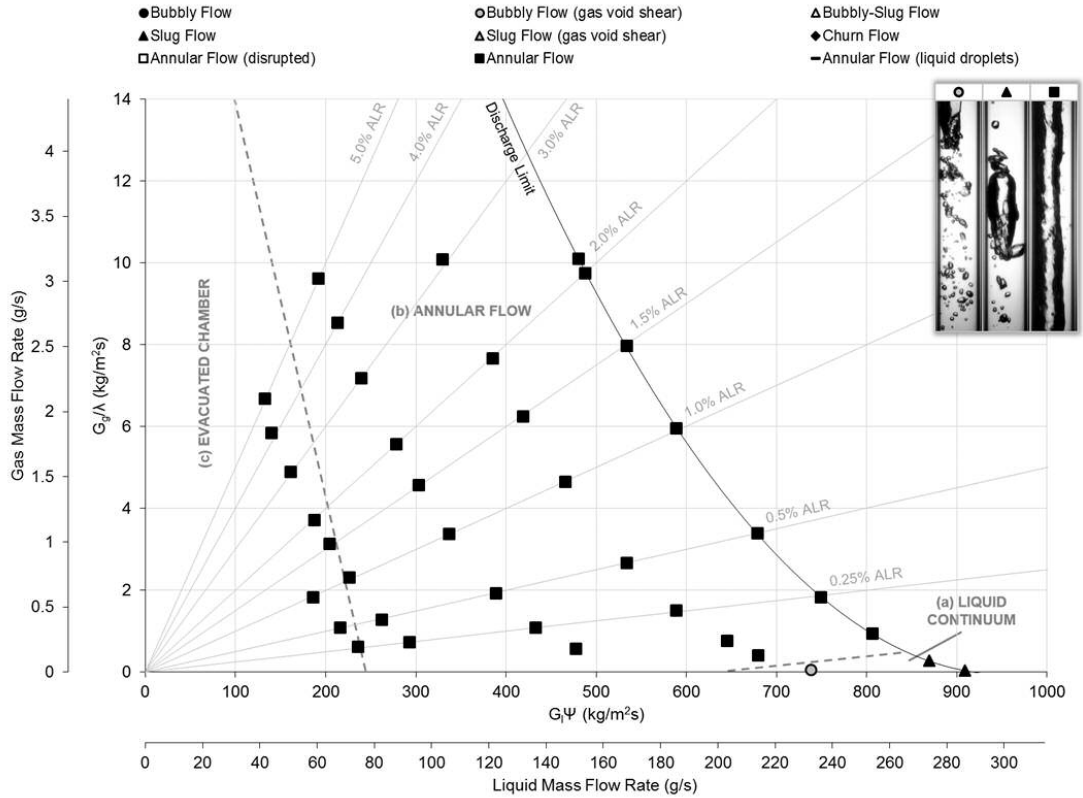


Figure A7.2 Flow regime map for aerator A2, with streamlined ADARPA body.

Unlike the equivalent flat-end configuration (Figure A5.2), a gas void was not observed to be formed in the aerator wake under all investigated configurations. In the benchmark case (Figure 7.7), this was seen to enable a large region of bubbly flow, however in the current experimentation no instances of bubbly flow were observed. Instead a small region of liquid continuum was identified at high liquid flow rates and low ALRs (Figure A7.2a), which consisted of slug flow formed by the injection of gas slugs at the aerator and, in an anomalous case, the gas entity was not observed to detach from the aerator, thus forming a continuous gas jet (i.e. elongated jetting) and bubbles were sheared from the base of the gas void in a gas void disintegration (bubbly flow) mechanism. Therefore, it is thought that the emerging gas jet is too stable to break up into uniformly sized bubbles, even at very low ALRs.

The internal flow performance of the current aerator was observed to be similar to the equivalent flat end aerator in all other regions of the flow regime map, whereby annular flow dominated the operating range. This correlated with every instance of jetting (in which an asymmetric gas core was formed that favoured the injection side of the aerator orifice) (Figure A7.2b) and evacuated chamber (in which a thin film of peripheral liquid was generated) (Figure A7.2c).

A7.1.2 4 x 2.0 mm (Aerator A3)

Figure A7.3 is the gas injection regime map of Aerator A3 (i.e. 4 x 2.0 mm aerator orifices in a liquid cross-flow) with a streamlined ADARPA aerator body. This shows the effect of varying the supply liquid mass flow rate up to 290 g/s, which corresponds to the discharge limit at 0% ALR with the discharge valve fully open and 5 bar_g operating pressure, and relates to a maximum liquid Bakers number of 923 kg/m²s in the 20 mm mixing chamber. The gas supply was varied up to the maximum achievable flow rate for the given aerator design (7 bar_g maximum gas supply pressure) or, if possible, 5% ALR. Analysis of results enabled identification of four discrete gas injection regimes, which were categorised into three gas injection regions.

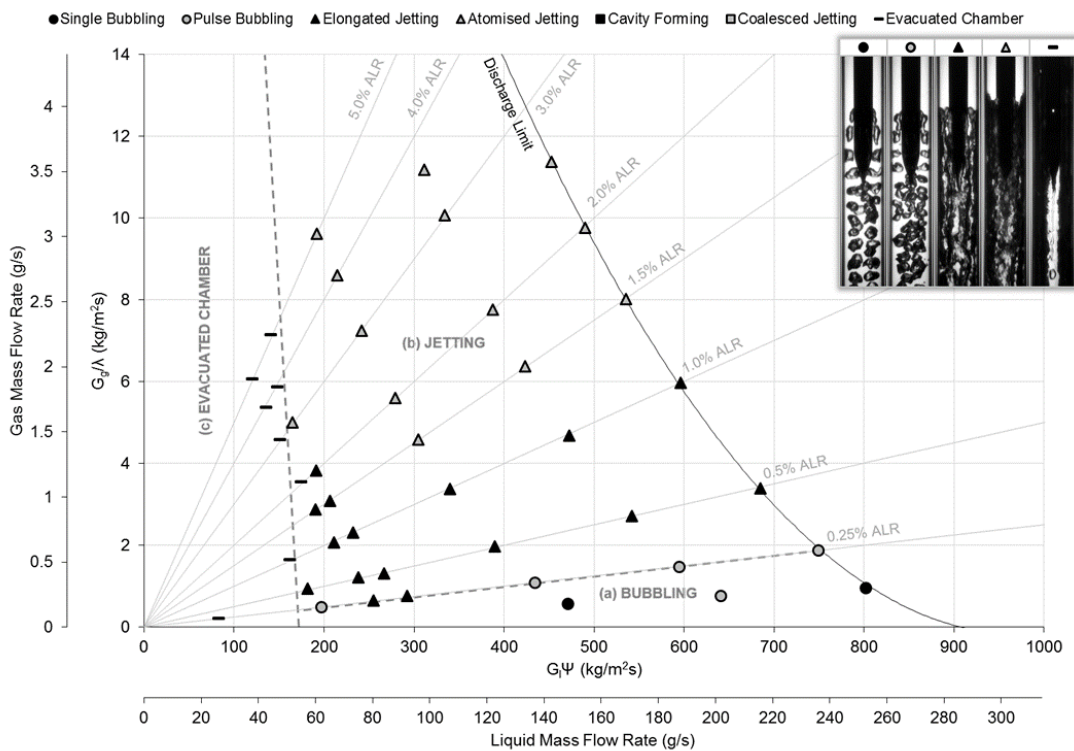


Figure A7.3 Gas injection regime map for aerator A3, with streamlined ADARPA body.

The gas injection regime map was seen to compare well with the equivalent flat-end aerator (Figure A5.3), which implies that the gas injection regimes are relatively unaffected by the aerator body design. The identified bubbling region (Figure A7.3a) was, however, seen to be significantly reduced compared to the benchmark configuration (Figure 7.6), with a greater dominance on jetting (Figure A7.3b) at high ALRs – this suggests that the emerging gas-phase has increased stability with increasing aerator orifice diameter and hence greater resilience to breakup into bubbles. A region of evacuated chamber, where phase separation

occurs prior to fluid injection, was identified at relatively low liquid flow rates (Figure A7.3c) in a comparable region to the previous cases – this too appeared to be marginally suppressed with high gas flow rates.

Figure A7.4 is the flow injection regime map for aerator A3, with an ADARPA streamlined aerator body, which shows the effect of varying fluid flow rates on the flow regimes with areas of common regimes identified and marked. The six discrete flow regimes identified were grouped into six regions.

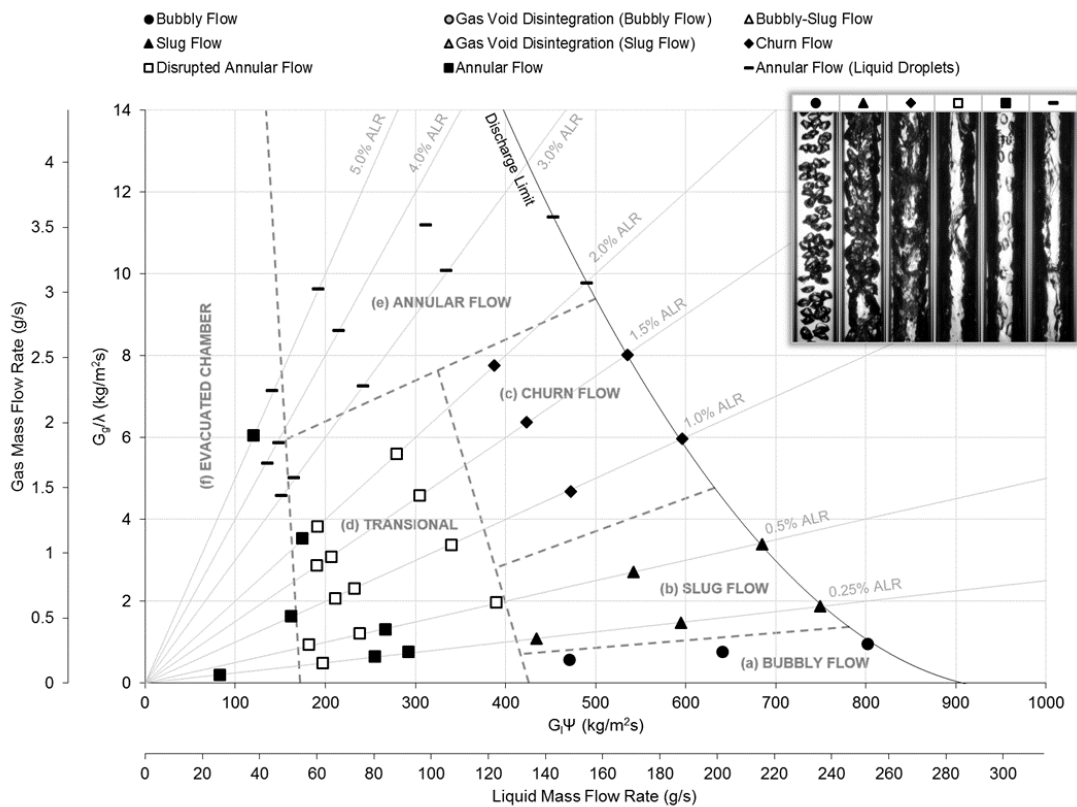


Figure A7.4 Flow regime map for aerator A3, with streamlined ADARPA body.

A bubbly flow region (Figure A7.4a) was enabled at low ALRs, which corresponds to the comparable conditions in which a gas void was formed in the aerator wake for the equivalent flat-end aerator design – these bubbly flow observations were observed to correspond with all single bubbling cases and some pulse bubbling at low ALRs. The bubbly flow region was, however, considerably smaller than the benchmark configuration (Figure 7.7) – further evidencing that reduced aerator orifice diameters aid preferable internal flow for effervescent atomisation.

Otherwise, the flow regime map was seen to compare well with the equivalent flat-end aerator, with flow transitioning to slug flow (Figure A7.4b), churn flow (Figure A7.4c) and annular flow (Figure A7.4e) with increasing ALR. Similarly, a thin annular flow was identified for all conditions corresponding to the evacuated chamber gas injection regime (Figure A7.4f) and a transition region (Figure A7.4d) was identified between the evacuated chamber and intermittent flow regions. This implies that the flow regimes unsuitable for effervescent atomisation are relatively unaffected by the aerator body design. The effect of an increased aerator orifice diameter was observed to decrease the transitional limits between the intermittent flow regimes and increasing the operating range corresponding to the transitional region.

A7.1.3 9 x 1.0 mm (Aerator A4)

Figure A7.5 is the gas injection regime map of Aerator A4 (i.e. 9 x 1.0 mm aerator orifice in a liquid cross-flow) with a streamlined ADARPA aerator body. This shows the effect of varying the supply liquid mass flow rate up to 290 g/s, which corresponds to the discharge limit at 0% ALR with the discharge valve fully open and 5 bar_g operating pressure, and relates to a maximum liquid Bakers number of 923 kg/m²s in the 20 mm mixing chamber. The gas supply was varied up to the maximum achievable flow rate for the given aerator design (7 bar_g maximum gas supply pressure) or, if possible, 5% ALR. Analysis of results enabled identification of four discrete gas injection regimes, which were categorised into three gas injection regions.

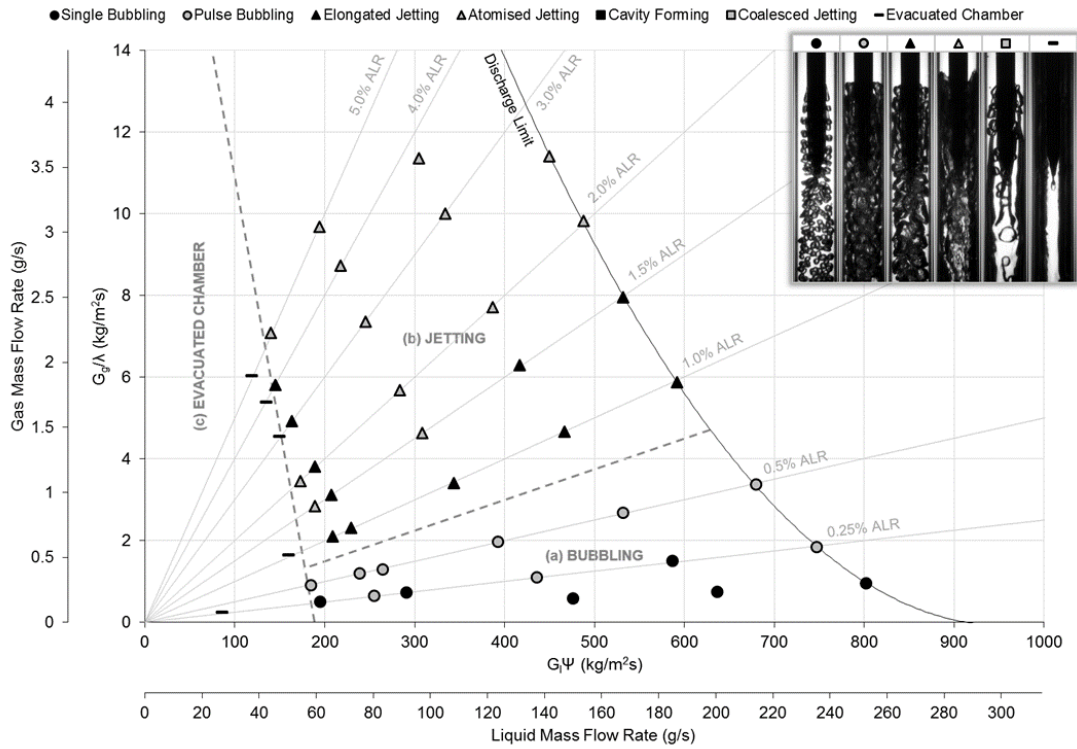


Figure A7.5 Gas injection regime map for aerator A4, with streamlined ADARPA body.

The gas injection regime map was seen to compare well with the equivalent flat-end aerator (Figure A5.5), which implies that the gas injection regimes are relatively unaffected by the aerator body design. The identified bubbling region (Figure A7.5a) was, however, seen to be marginally reduced compared to the benchmark configuration (Figure 7.6), with a greater proportion of observations at high ALRs identified as jetting (Figure A7.5b) – this further evidences that the emerging gas-phase has increased stability with increasing aerator orifice diameter and hence greater resilience to breakup into bubbles. A region of evacuated chamber, where phase separation occurs prior to fluid injection, was identified at relatively low liquid flow rates (Figure A7.5c) in a comparable region to the previous cases – this too appeared to be marginally suppressed with high gas flow rates.

Figure A7.6 is the flow injection regime map for aerator A4, with an ADARPA streamlined aerator body, which shows the effect of varying fluid flow rates on the flow regimes with areas of common regimes identified and marked. The six discrete flow regimes identified were grouped into six regions.

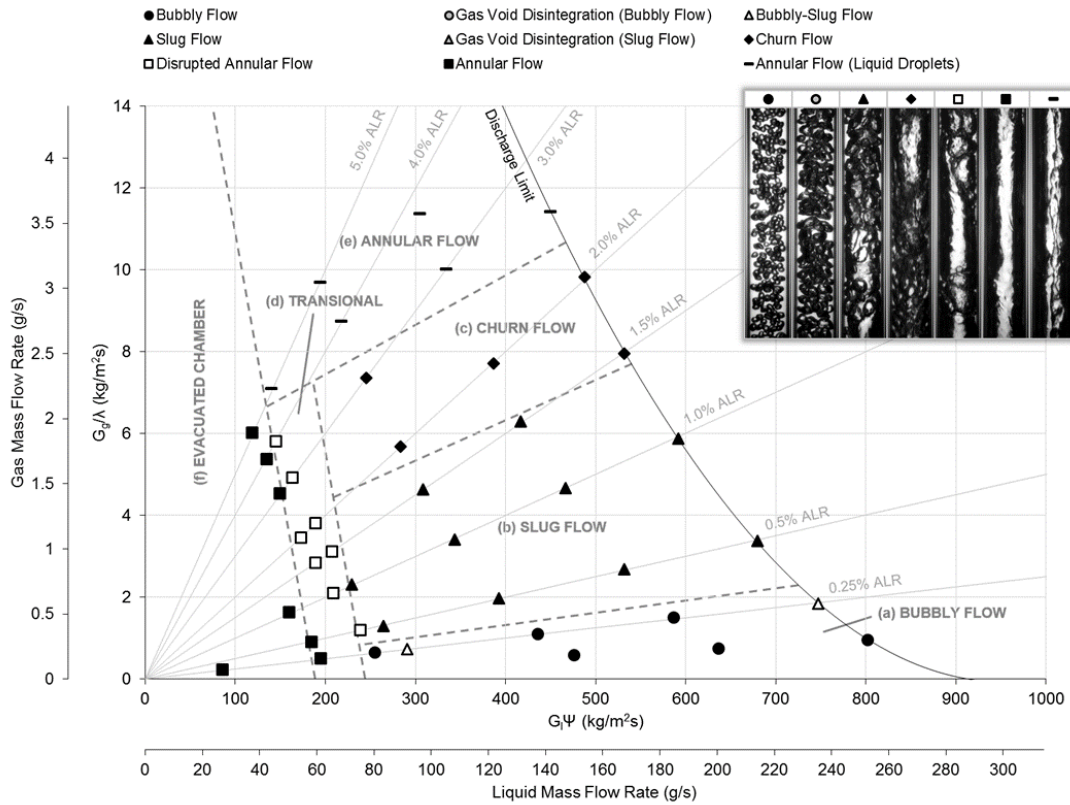


Figure A7.6 Flow regime map for aerator A4, with streamlined ADARPA body.

A bubbly flow region (Figure A7.6a) was enabled at low ALRs, which corresponds to the comparable conditions in which a gas void was formed in the aerator wake for the equivalent flat-end aerator design (Figure A5.6) – these bubbly flow observations were observed to correspond with all single bubbling cases and some pulse bubbling at low ALRs. The bubbly flow region was, however, marginally smaller than the benchmark configuration (Figure 7.7) – further evidencing that reduced aerator orifice diameters aid preferable internal flow for effervescent atomisation.

Otherwise, the flow regime map was seen to compare well with the equivalent flat-end aerator, with flow transitioning to slug flow (Figure A7.6b), churn flow (Figure A7.6c) and annular flow (Figure A7.6e) with increasing ALR. Similarly, a thin annular flow was identified for all conditions corresponding to the evacuated chamber gas injection regime (Figure A7.6f) and a transition region (Figure A7.6d) was identified between the evacuated chamber and intermittent flow regions. This implies that the flow regimes unsuitable for effervescent atomisation are relatively unaffected by the aerator body design. The effect of an increased aerator orifice diameter was observed to decrease the transitional limits between the intermittent flow regimes and increasing the operating range corresponding to the transitional region.

A7.1.4 16 x 0.75 mm (Aerator A5)

This configuration is the benchmark case for the ADARPA aerator body investigations. The gas injection and flow regime maps are presented in §7.2.

A7.2 Effect of Aeration Area

A7.2.1 1.77 mm² (Aerator A7)

Figure A7.7 is the gas injection regime map of Aerator A7 (i.e. 4 x 0.75 mm aerator orifice in a liquid cross-flow) with a streamlined ADARPA aerator body. This shows the effect of varying the supply liquid mass flow rate up to 290 g/s, which corresponds to the discharge limit at 0% ALR with the discharge valve fully open and 5 bar_g operating pressure, and relates to a maximum liquid Bakers number of 923 kg/m²s in the 20 mm mixing chamber. The gas supply was varied up to the maximum achievable flow rate for the given aerator design (7 bar_g maximum gas supply pressure) or, if possible, 5% ALR. As the aeration was considerably lower than the benchmark configuration, the restriction to gas flow was observed to be greater and, therefore, a reduced maximum gas flow was achieved. Analysis of results enabled identification of four discrete gas injection regimes, which were categorised into three gas injection regions.

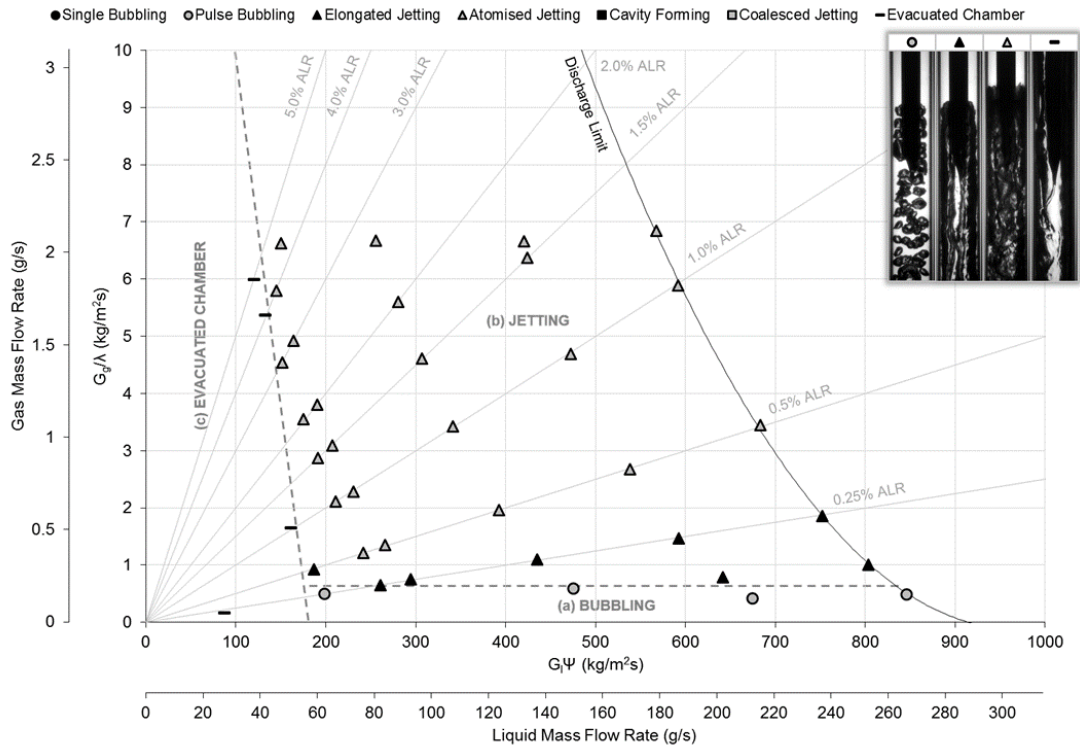


Figure A7.7 Gas injection regime map for aerator A7, with streamlined ADARPA body.

A significantly reduced bubbling region (Figure A7.7a) was identified compared to the benchmark case (Figure 7.6), which suggests that a decreased aeration area acts to suppress bubbling. Unlike the benchmark configuration, single bubbling was not identified as the gas velocity through each aerator orifice is sufficient to generate pulse bubbling even at the lowest ALRs in which bubbling alternates the formation of a gas jet which detaches from the orifice to form gas slugs.

Otherwise, the gas injection map is dominated by a large jetting region (Figure A7.7b), with a general trend of elongated jetting transitioning to atomised jetting with increasing ALR. A region of evacuated chamber, where phase separation occurs prior to fluid injection, was identified at relatively low liquid flow rates (Figure A7.7c) in a comparable region to the previous cases – this too appeared to be marginally suppressed with high gas flow rates.

Figure A7.8 is the flow injection regime map for aerator A7, with an ADARPA streamlined aerator body, which shows the effect of varying fluid flow rates on the flow regimes with areas of common regimes identified and marked. The four discrete flow regimes identified were grouped into three regions.

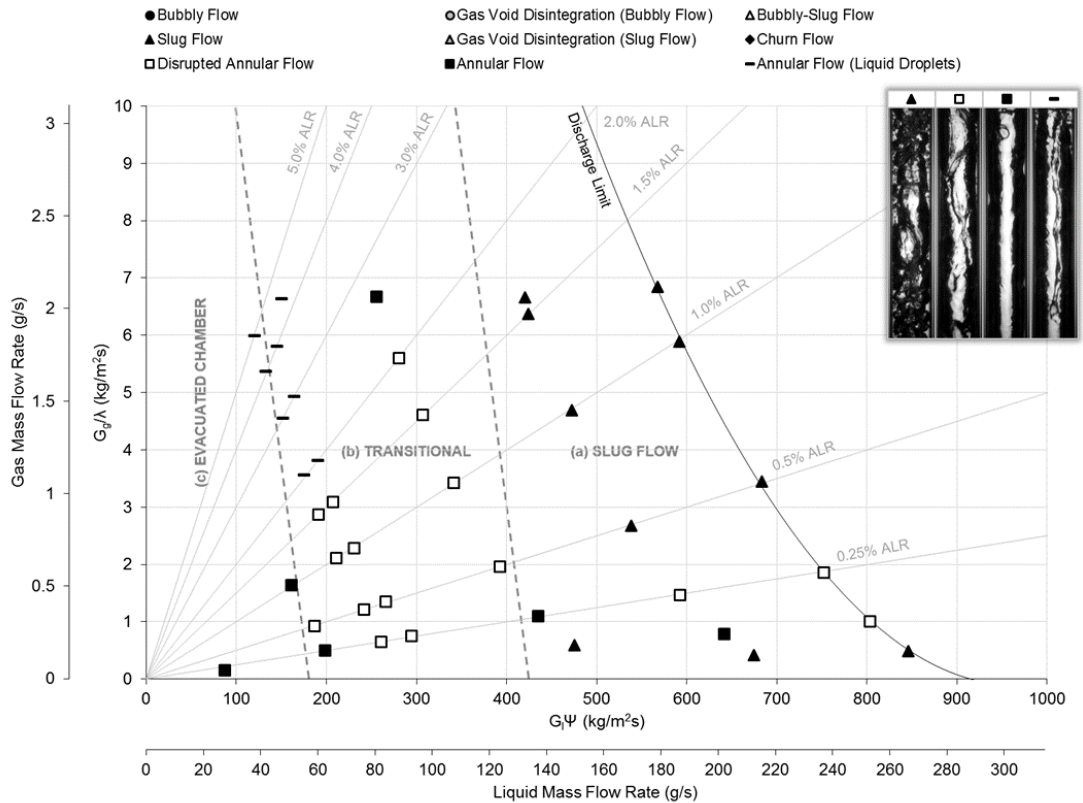


Figure A7.8 Flow regime map for aerator A7, with streamlined ADARPA body.

The flow map is distinctly different from the flow maps present previously. No bubbly flow region was identified, even at high liquid flow rates and low ALRs.

A slug region was identified at high liquid flow rates (Figure A7.8a), which was observed to transition to and from annular flow with increasing ALR. At low ALRs slugs are produced due to pulse bubbling at the aerator. At increased ALRs, the emerging gas jets (which previously detached to form gas slugs) now elongates into the mixing chamber – these either completely coalesce with each other within the mixing length to form an annular flow, or liquid ligaments exist between them to form a disturbed annular flow. With increasing ALRs, sufficient chaos is present within the jets for them to breakup into gas slugs prior to coalescing, thus forming a slug flow.

A thin annular flow was identified for all conditions corresponding to the evacuated chamber gas injection regime (Figure A7.8c) and a transition region (Figure A7.8b) was identified between the evacuated chamber and slug flow region.

A7.2.2 3.53 mm² (Aerator A8)

Figure A7.9 is the gas injection regime map of Aerator A8 (i.e. 8 x 0.75 mm aerator orifice in a liquid cross-flow) with a streamlined ADARPA aerator body. This shows the effect of varying the supply liquid mass flow rate up to 290 g/s, which corresponds to the discharge limit at 0% ALR with the discharge valve fully open and 5 bar_g operating pressure, and relates to a maximum liquid Bakers number of 923 kg/m²s in the 20 mm mixing chamber. The gas supply was varied up to the maximum achievable flow rate for the given aerator design (7 bar_g maximum gas supply pressure) or, if possible, 5% ALR. As the aeration was considerably lower than the benchmark configuration, the restriction to gas flow was observed to be greater and, therefore, a reduced maximum gas flow was achieved. Analysis of results enabled identification of five discrete gas injection regimes, which were categorised into three gas injection regions.

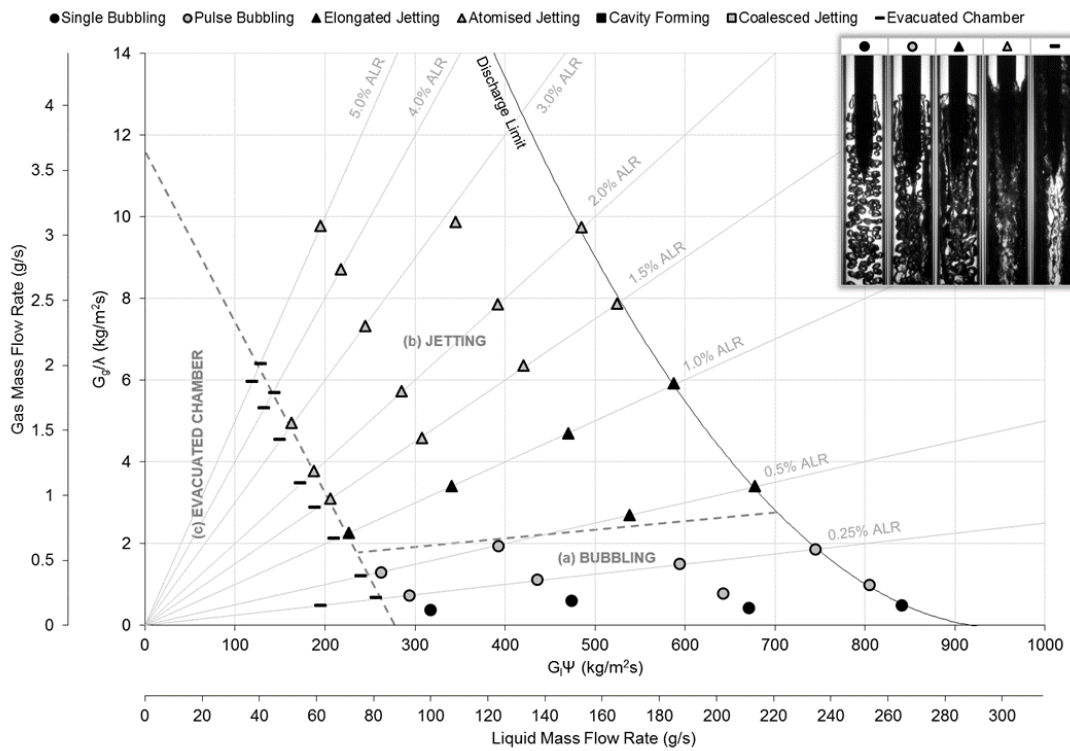


Figure A7.9 Gas injection regime map for aerator A8, with streamlined ADARPA body.

A bubbling region (Figure A7.9a) was identified at low ALRs, with single bubbling transitioning to pulse bubbling with increasing ALR. The bubbling region was seen to be smaller than the 7.07 mm² benchmark case (Figure 7.6) but significantly larger than the 1.77 mm² case (Figure A7.7) – this supports the previous findings that an increased aeration area promotes bubbling. At a critically high ALR, bubbling transitions to a jetting region (Figure

A7.9b), with a general trend of elongated jetting transitioning to atomised jetting with increasing ALR. A region of evacuated chamber, where phase separation occurs prior to fluid injection, was identified at relatively low liquid flow rates (Figure A7.9c) in a comparable region to the previous cases – this exhibited an unusually strong suppression with high gas flow rates.

Figure A7.10 is the flow injection regime map for aerator A8, with an ADARPA streamlined aerator body, which shows the effect of varying fluid flow rates on the flow regimes with areas of common regimes identified and marked. The six discrete flow regimes identified were grouped into five regions.

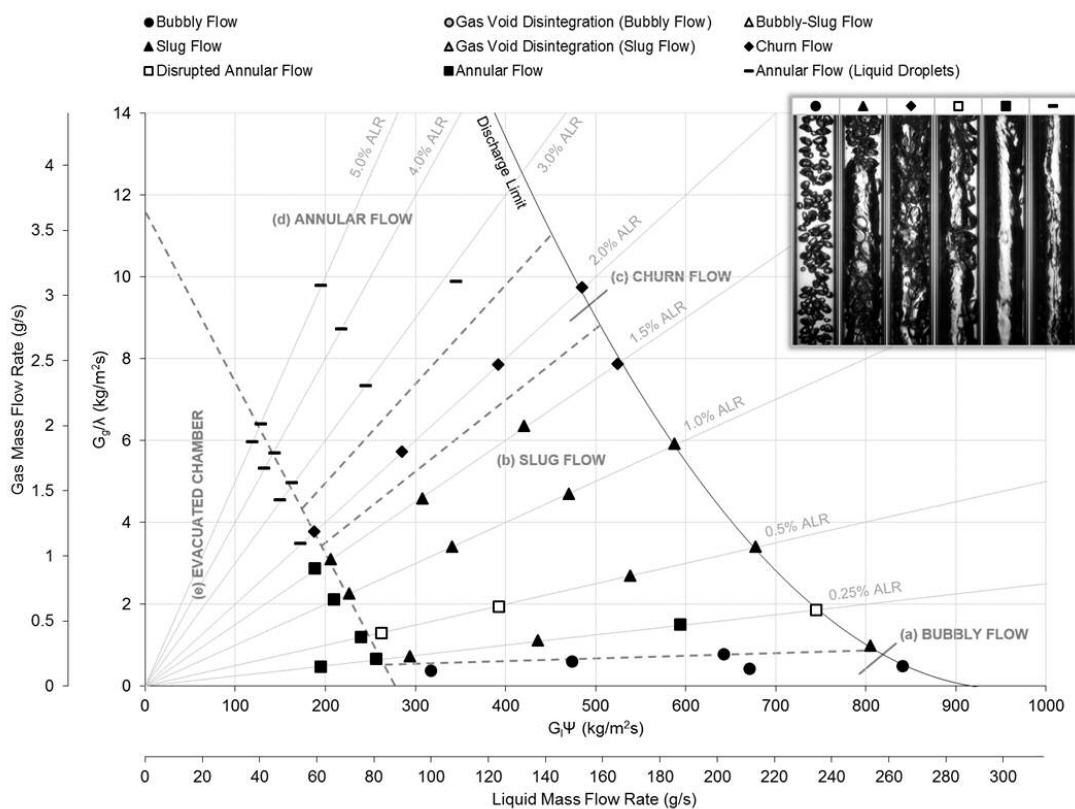


Figure A7.10 Flow regime map for aerator A8, with streamlined ADARPA body.

A region of bubbly flow exists at low ALR (Figure A7.10a), which corresponds with all cases of single bubbling at the aerator and a single low ALR case of pulse bubbling. The operating conditions corresponding with this regions were seen to be dramatically reduced compared to the benchmark configuration, where transition to the slug flow region (Figure A7.10b) occurred at lower ALRs – thus, further evidencing that decreased aeration area acts to suppress bubbly flow.

Similar to the 1.77 mm² case (Figure A7.8), the slug flow region has separating occurrences of annular flow, in the intermediate position between slug generation due to the injection of variably sized bubbles (i.e. pulse bubbling) and the chaotic breakup of injected gas jets (i.e. jetting). At further increased ALRs, the flow regimes was observed to transition to churn flow (Figure A7.10c) and finally annular flow (Figure A7.10d).

As with all other vertically downwards cases, a region of evacuated chamber was identified at relatively low liquid flow rates (Figure A7.10e) in a comparable region to the previous cases – this too appeared to be significantly suppressed with high gas flow rates.

A7.2.3 7.07 mm² (Aerator A5)

This configuration is the benchmark case for the ADARPA aerator body investigations. The gas injection and flow regime maps are presented in §7.2.

A7.2.4 14.14 mm² (Aerator A9)

Figure A7.11 is the gas injection regime map of Aerator A9 (i.e. 32 x 0.75 mm aerator orifice in a liquid cross-flow) with a streamlined ADARPA aerator body. This shows the effect of varying the supply liquid mass flow rate up to 290 g/s, which corresponds to the discharge limit at 0% ALR with the discharge valve fully open and 5 bar_g operating pressure, and relates to a maximum liquid Bakers number of 923 kg/m²s in the 20 mm mixing chamber. The gas supply was varied up to the maximum achievable flow rate for the given aerator design (7 bar_g maximum gas supply pressure) or, if possible, 5% ALR. As the aeration was larger than the benchmark configuration, the restriction to gas flow was observed to be reduced and, therefore, a greater maximum gas flow was achieved. Analysis of results enabled identification of five discrete gas injection regimes, which were categorised into three gas injection regions.

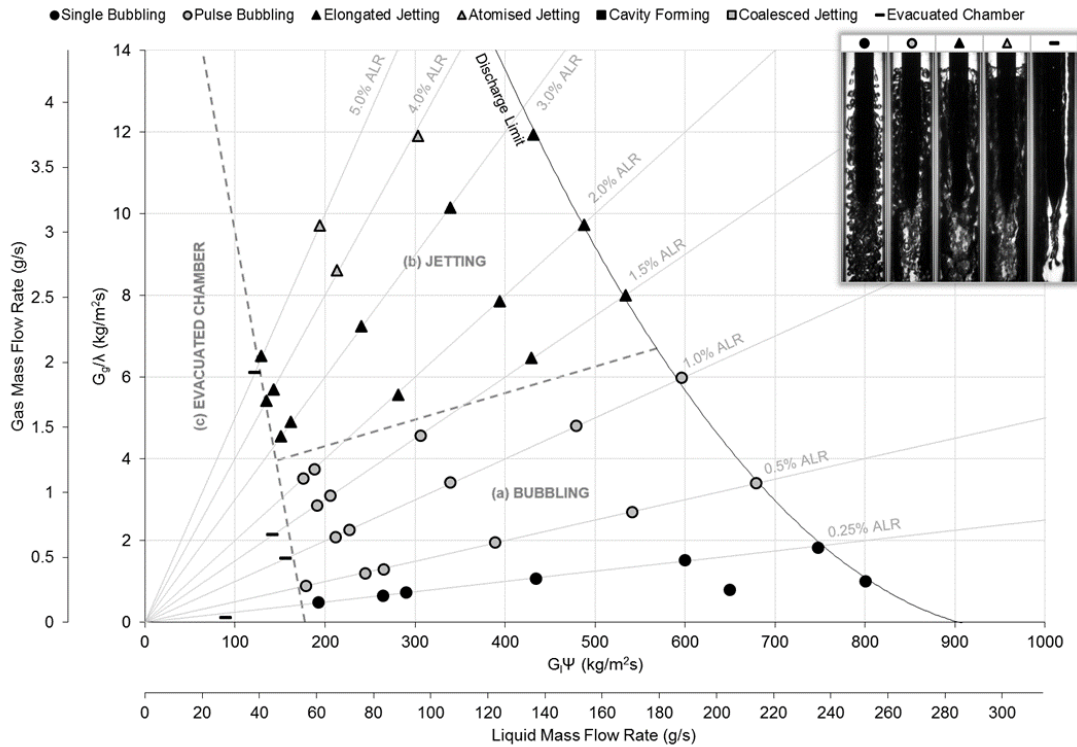


Figure A7.11 Gas injection regime map for aerator A9, with streamlined ADARPA body.

A large bubbling region (Figure A7.11a) was observed to dominate the gas injection map, with cases of single bubbling occurring at the lowest ALRs. This region was observed to be larger than all of the comparison cases (Figures A7.7, A7.9 and 7.6), which further evidences that increasing the aeration area yields a greater range of conditions in which bubbling can be achieved. As with all other cases, bubbling was observed to transition to jetting (Figure A7.11b) with increased ALRs, in which elongated jetting generally precedes atomised jetting. Similarly, evacuated chamber (Figure A7.11c) was observed at comparable low liquid flow rates, with a tendency to be suppressed with increasing gas flow rates.

Figure A7.12 is the flow injection regime map for aerator A9, with an ADARPA streamlined aerator body, which shows the effect of varying fluid flow rates on the flow regimes with areas of common regimes identified and marked. The seven discrete flow regimes identified were grouped into six regions.

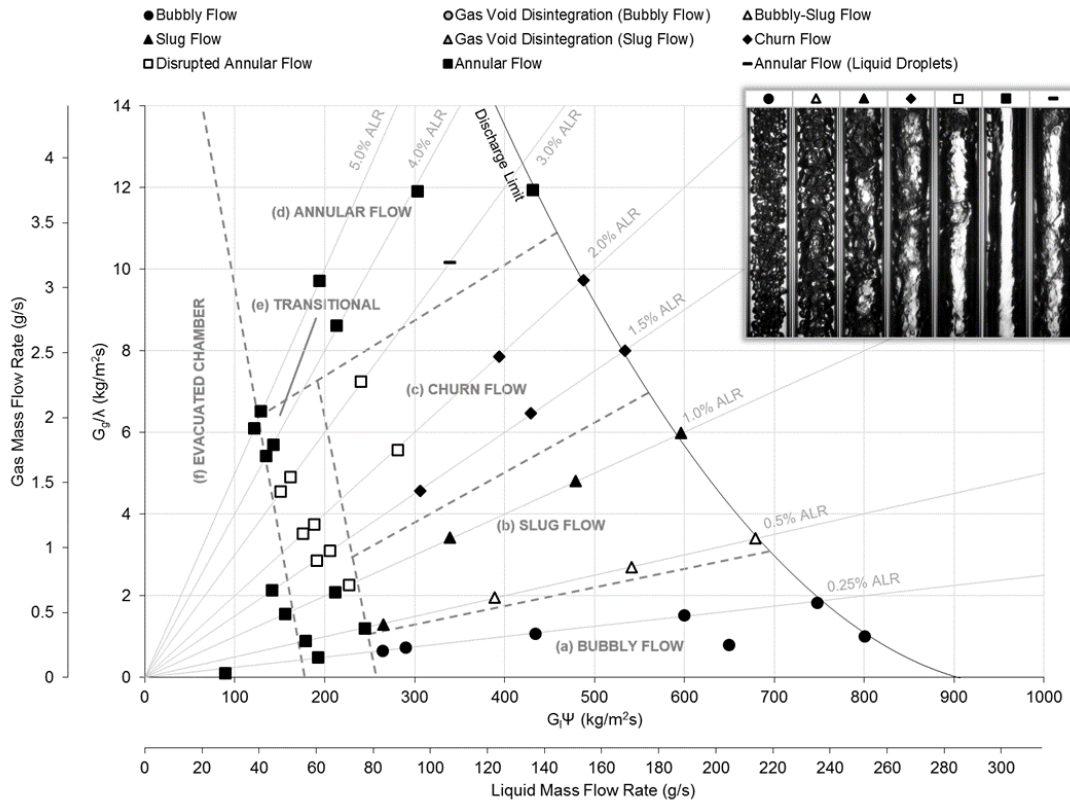


Figure A7.12 Flow regime map for aerator A9, with streamlined ADARPA body.

A large region of bubbly flow (Figure A7.12a) was observed at low ALRs, which corresponded with the majority of single bubbling cases and was observed over a comparable operating range to the benchmark case (Figure 7.7). However, at low liquid flow rates, bubbly flow was not observed despite bubbling at the aerator – this was due to the formation of a large gas void which found equilibrium just upstream of the aerator tip and thus an annular flow was formed.

The effect of increasing ALR, like the benchmark case, was generally observed to transition the internal flow from bubbly flow, to slug flow (Figure A7.12b), to churn flow (Figure A7.12d) and finally annular flow (Figure A7.12e). As with all other vertically downwards cases, a region of evacuated chamber was identified at relatively low liquid flow rates (Figure A7.12f) in a comparable region to the previous cases – this too appeared to be significantly suppressed with high gas flow rates. A regions of transitional flow exists between the evacuated chamber and intermittent regions (Figure A7.12e).

A7.3 Effect of Unconventional Aerator Designs

A7.3.1 Porous Aerator (Aerator A6)

Figure A7.7 is the gas injection regime map of Aerator A6 (i.e. porous aeration insert in a liquid cross-flow) with a streamlined ADARPA aerator body. This shows the effect of varying the supply liquid mass flow rate up to 290 g/s, which corresponds to the discharge limit at 0% ALR with the discharge valve fully open and 5 bar_g operating pressure, and relates to a maximum liquid Bakers number of 923 kg/m²s in the 20 mm mixing chamber. The gas supply was varied up to the maximum achievable flow rate for the given aerator design (7 bar_g maximum gas supply pressure) or, if possible, 5% ALR. Analysis of results enabled identification of four discrete gas injection regimes, which were categorised into three gas injection regions.

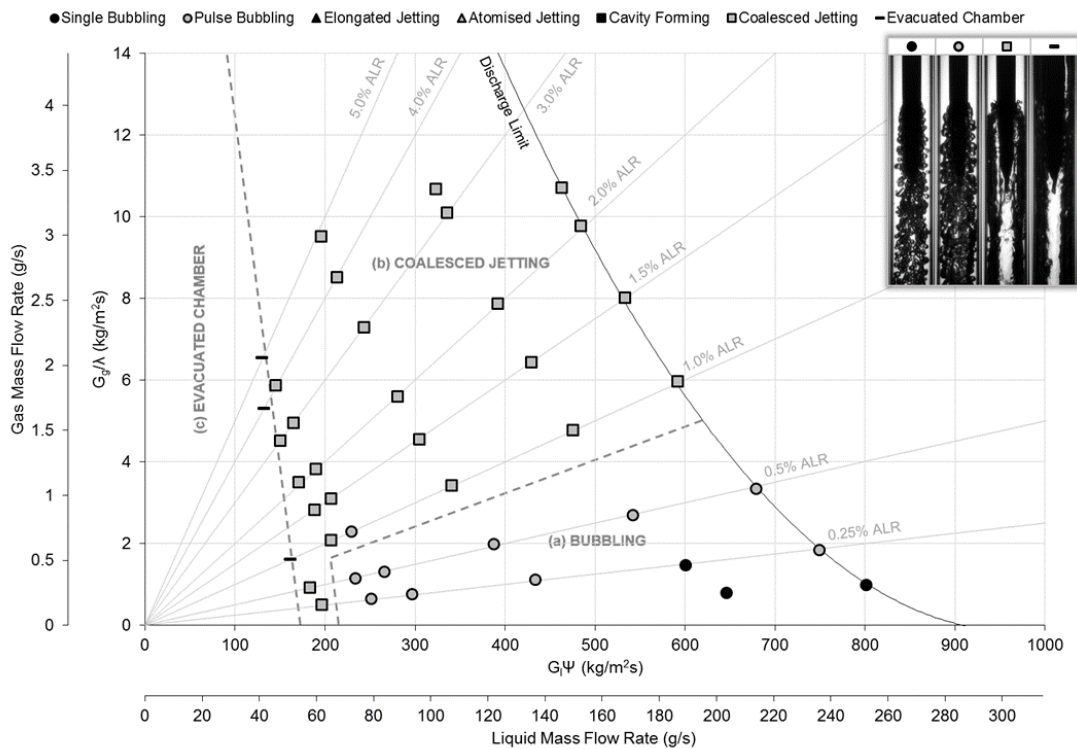


Figure A7.13 Gas injection regime map for aerator A6, with streamlined ADARPA body.

A large region of bubbling was identified at low ALRs (Figure A7.7a), whereby bubble formation was observed to be relatively chaotic and the porous medium did not appear to uniform (a localised area appeared to have greater flow rate) – this resulted in the formation of differing sized bubbles and thus promoted pulse bubbling. The few single bubbling cases

that were observed occurred at high liquid flow rates and low ALR. This chaotic nature of bubble formation is thought to explain the marginal differences between the gas injection performance between the streamlined and flat-end aerator designs. The bubbling region was observed to be of reduced size compared to the benchmark case (Figure 7.6), whereby gas injection tended towards coalesced jetting at high ALRs (Figure A7.7b) – observed to be due to the coalescence of emerging gas jets. As with all previous cases, a region of evacuated chamber was observed at low liquid flow rates and was marginally suppressed with increasing gas flow rate (Figure A7.7c).

Figure A7.8 is the flow injection regime map for aerator A6, with an ADARPA streamlined aerator body, which shows the effect of varying fluid flow rates on the flow regimes with areas of common regimes identified and marked. The six discrete flow regimes identified were grouped into four regions.

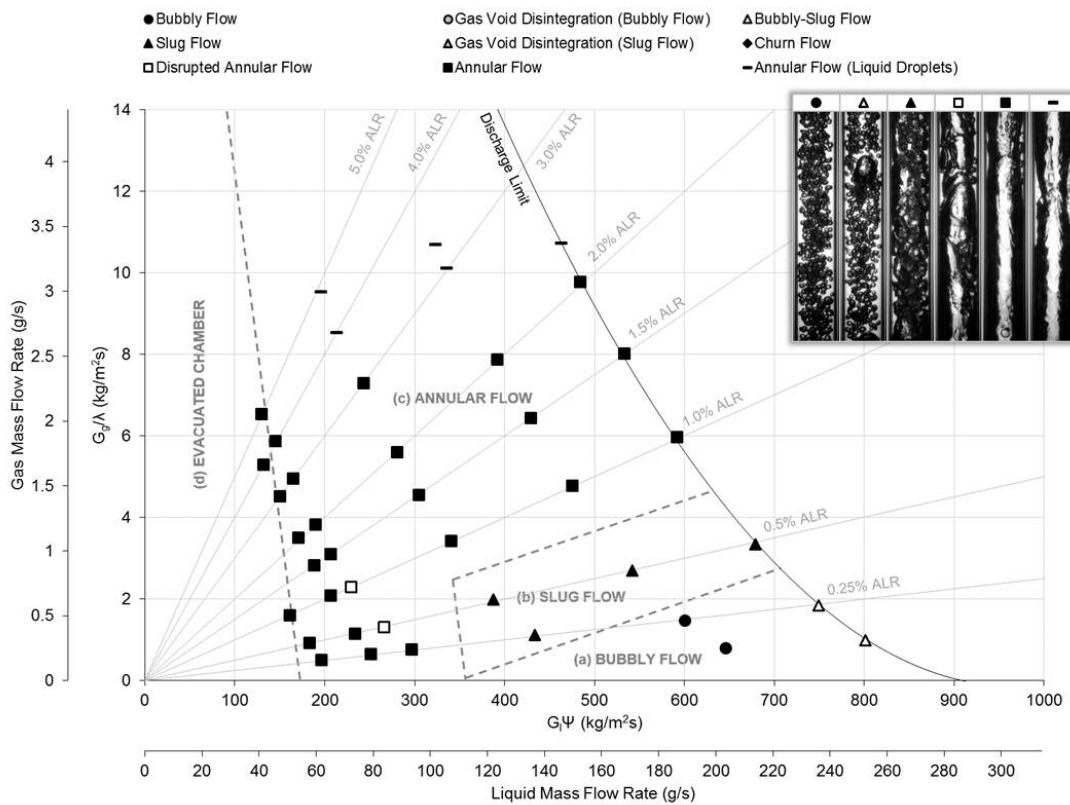


Figure A7.14 Flow regime map for aerator A3, with streamlined ADARPA body.

Compared to the equivalent flat-end aerator case (Figure A5.10), a bubbly flow region was enabled (Figure A7.8a) – however, this was observed to occur across significantly restricted operating conditions than the benchmark configuration (Figure 7.7). A number of bubbly-

slug occurrences were identified at high liquid flow rates, which appear to be caused by the injection of non-uniformly sized bubbles from the aerator.

The flow was observed to transition to slug flow with increasing ALR (Figure A7.8b), but a churn flow was not observed for this configuration – this is in keeping with the flat-end case. As before, this is hypothesised to occur as the emerging gas-phase coalesces with neighbouring pores to form coalesced jetting before a sufficiently stable individual jets are generated to enable churn flow. The flow regime map was dominated by annular flow (Figure A7.8c), either due to coalesced jetting, where a continuous gas core is injected directly from the aeration area, or evacuated chamber (Figure A7.8d), where a thin liquid film exist in the mixing chamber periphery.

A7.4 Effect of Mixing Chamber Diameter

A7.4.1 14 mm Diameter

Figure A7.15 is the gas injection regime map for a 14 mm diameter mixing chamber, using aerator A5 (i.e. 16 x 0.75 mm aerator orifice in a liquid cross-flow) with a streamlined ADARPA aerator body. This shows the effect of varying the supply liquid mass flow rate up to 290 g/s, which corresponds to the discharge limit at 0% ALR with the discharge valve fully open and 5 bar_g operating pressure. However, as the cross-section of the mixing chamber is reduced, the maximum liquid Bakers number has increased to 1880 kg/m²s to maintain continuity – this compares to the maximum of 923 kg/m²s in the benchmark case. The gas supply was varied up to the maximum achievable flow rate for the given aerator design (7 bar_g maximum gas supply pressure) or, if possible, 5% ALR – similarly, due to the reduced flow area, the corresponding gaseous Bakers numbers have also increased. Analysis of results enabled identification of five discrete gas injection regimes, which were categorised into three gas injection regions.

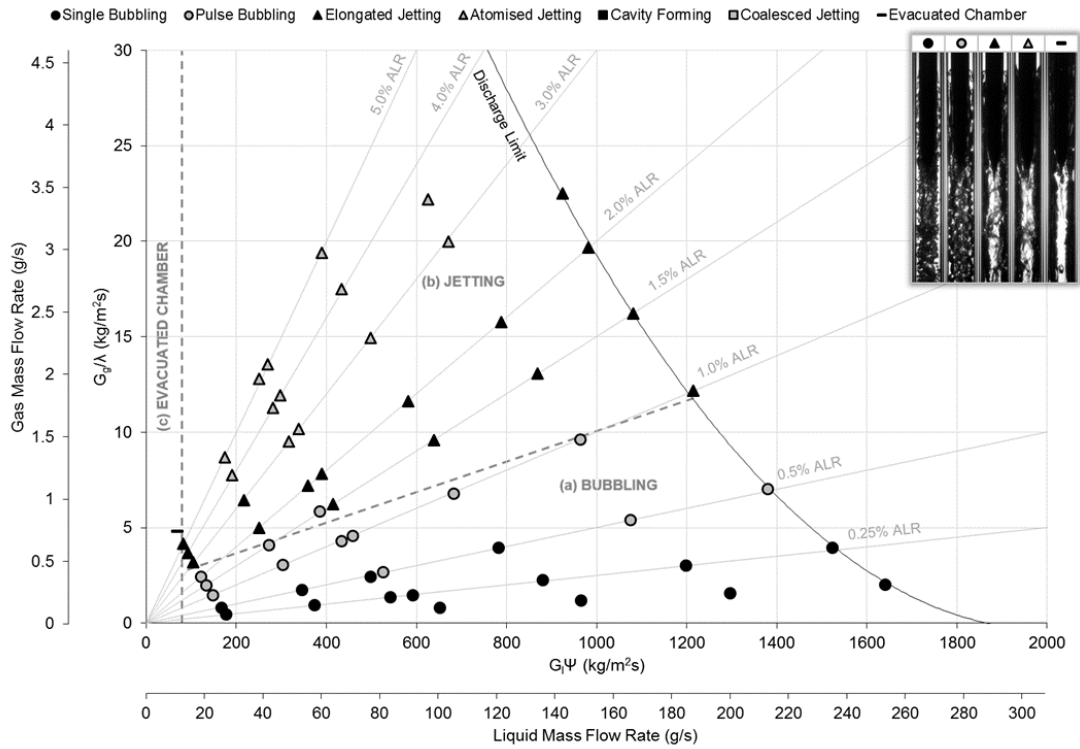


Figure A7.15 Gas injection regime map for 14 mm mixing chamber diameter.

The gas injection regimes were observed to occur at comparable operating conditions between the flat-end (Figure A5.11) and ADARPA aerator designs (Figure 7.6), with a large bubbling region was observed to exist at low ALRs (Figure A7.15a) – this indicates that the aerator body design does not have a significant effect on the performance at the aerator. Single bubbling was observed to be promoted at low ALRs compared to the larger 20 mm mixing chamber benchmark case, with transition to pulse bubbling at increasing gas flow rates.

Transition to jetting occurs at comparable ALRs regardless of mixing chamber diameter and aerator body design (Figure A7.15b), with elongated jetting transitioning to atomised jetting with increasing gas flow rate. An evacuated chamber region (Figure A7.15c) was identified at comparably low liquid Bakers numbers between the comparison cases – however, compared to the 20 mm mixing chamber diameter case, this corresponds to a much reduced liquid flow rate compared to the benchmark configuration and therefore conditions corresponding to evacuated chamber.

Figure A7.16 is the flow injection regime map of the 14 mm diameter mixing chamber with ADARPA aerator tip, which shows the effect of varying fluid flow rates on the flow regimes with areas of common regimes identified and marked. As with the gas injection map, the

maximum liquid and gaseous Bakers number have increased to maintain continuity in the reduced cross-section. The six discrete flow regimes identified were grouped into six regions.

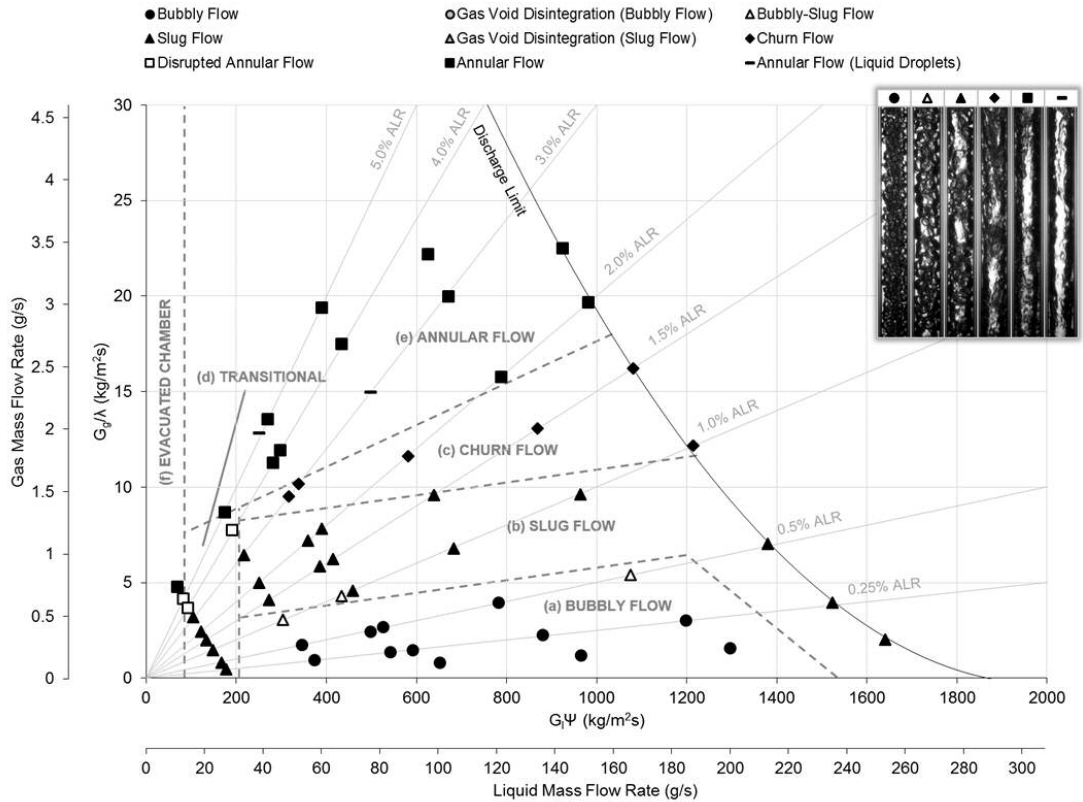


Figure A7.16 Flow regime map for 14 mm mixing chamber diameter.

Unlike the equivalent flat-end case (Figure A5.12), bubbly flow was established at low ALRs due to the prevention of gas void formation in the aerator wake (Figure A7.16a). This region was observed span a greater operating range than the 20 mm mixing chamber (Figure 7.7), due to suppression of the evacuated chamber (Figure A7.16f) and transitional regions (Figure A7.16d) at low liquid flow rates and marginally increased transitional ALR to slug flow (Figure A7.16b). In general the effect of increasing ALR was seen transition the flow regime from bubbly flow, to slug flow, to churn flow (Figure A7.16c) and finally annular flow (Figure A7.16e) at the highest ALR.

Interestingly, several slug flow observations were identified at the highest liquid flow rates and lowest ALRs, which are conditions typically corresponding to a bubbly flow. In these instances, slugs were observed to be formed as the two-phase flow passes the aerator tip and are, therefore, thought to be due critically high flow rates to generate bluff body effects for the ADARPA aerator tip.

A7.4.2 20 mm Diameter

This configuration is the benchmark case for the ADARPA aerator body investigations. The gas injection and flow regime maps are presented in §7.2.

A7.4.3 25 mm Diameter

Figure A7.17 is the gas injection regime map for a 25 mm diameter mixing chamber, using aerator A5 (i.e. 16 x 0.75 mm aerator orifice in a liquid cross-flow) with a streamlined ADARPA aerator body. This shows the effect of varying the supply liquid mass flow rate up to 290 g/s, which corresponds to the discharge limit at 0% ALR with the discharge valve fully open and 5 bar_g operating pressure. However, as the cross-section of the mixing chamber is increased, the maximum liquid Bakers number has decreased to 589 kg/m²s to maintain continuity – this compares to the maximum of 923 kg/m²s in the benchmark case. The gas supply was varied up to the maximum achievable flow rate for the given aerator design (7 bar_g maximum gas supply pressure) or, if possible, 5% ALR – similarly, due to the reduced flow area, the corresponding gaseous Bakers numbers have also decreased. Analysis of results enabled identification of five discrete gas injection regimes, which were categorised into three gas injection regions.

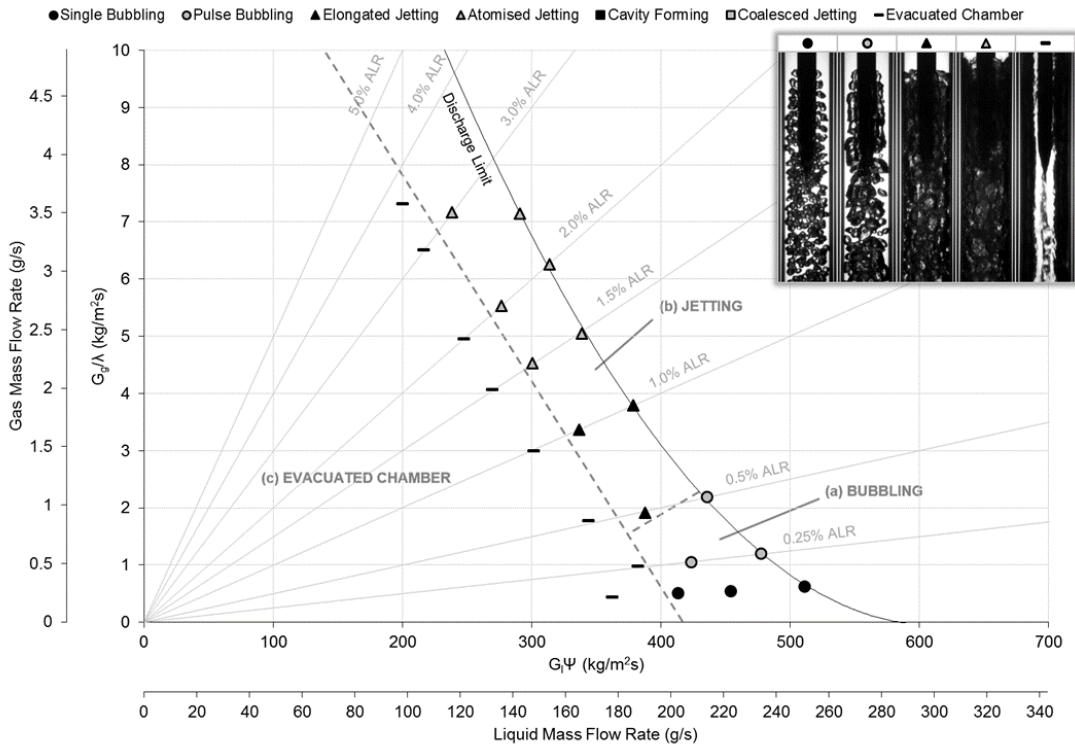


Figure A7.17 Gas injection regime map for 25 mm mixing chamber diameter.

A small region of bubbling was identified at low ALRs (Figure A7.17a), which transitioned between single bubbling and pulse bubbling with increasing ALR. The transition to elongated jetting was observed to occur at reduced ALRs compared to the previous cases (Figures A7.15 and 7.6), with atomised jetting occurring at the highest ALRs – these from a jetting region (Figure A7.17b). The gas injection regime map was, however, dominated by a large evacuated chamber region (Figure A7.17c) which occupied much of the operating range – this is due to buoyancy overcoming the reduced liquid shear around the aerator periphery. The liquid Baker’s numbers corresponding to this regime was seen to increase.

Figure A7.18 is the flow injection regime map of the 25 mm diameter mixing chamber with ADARPA aerator tip, which shows the effect of varying fluid flow rates on the flow regimes with areas of common regimes identified and marked. As with the gas injection map, the maximum liquid and gaseous Bakers number have decreased to maintain continuity in the reduced cross-section. The seven discrete flow regimes identified were grouped into four regions.

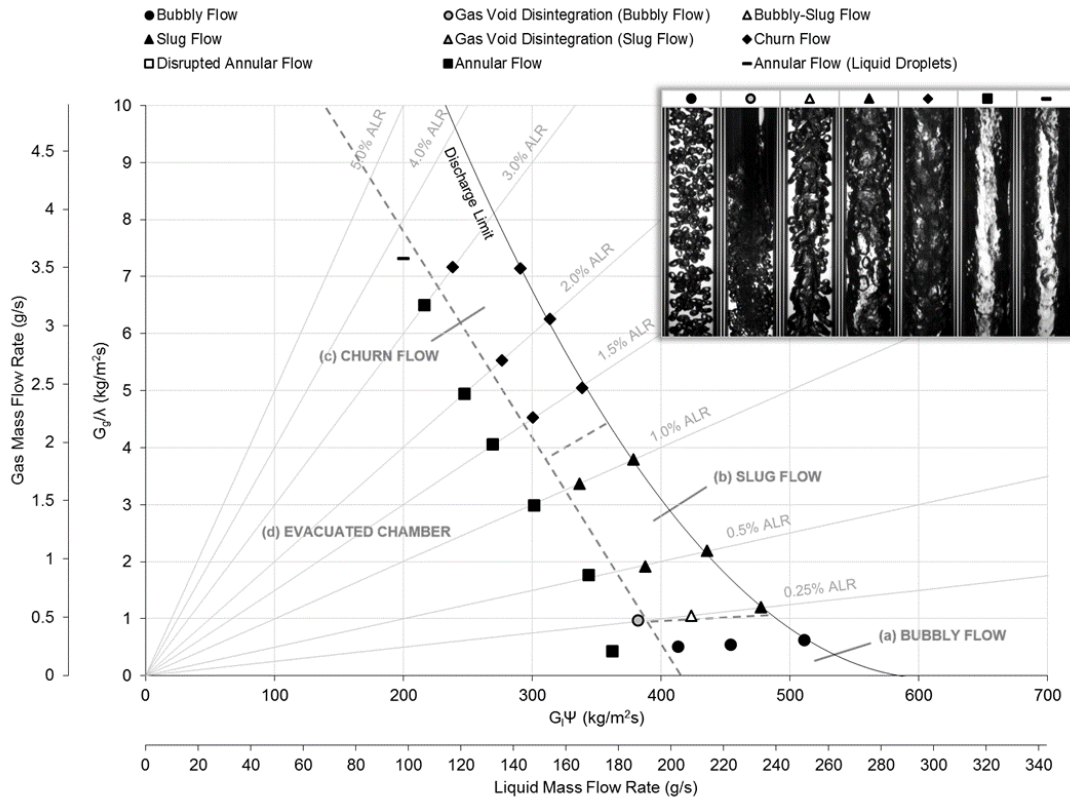


Figure A7.18 Gas injection regime map for 25 mm mixing chamber diameter.

Compared to the smaller mixing chamber diameters (Figures A7.16 and 7.7), a reduced region of bubbling was identified (Figure A7.18a) which, in all cases, correspond to single bubbling at the aerator. This was observed to be due an increase in the evacuated chamber region (Figure A7.18d), which typically generated a thin annular flow, and a transition to slug flow at reduced ALRs (Figure A7.18b). A churn flow region was observed at the highest ALRs (Figure A7.18c), without the observation of an annular flow within the testing limits. An isolated occurrence of gas void shearing (bubbly flow) was identified within the investigation, which was observed to occur due to evacuated chamber formation – in this case, the momentum of the liquid-phase upon start-up was not sufficient to bleed the atomiser of ambient air, however the subsequent breakup mechanisms acting on the remaining gas void were sufficient to shear bubbles off the leading edge.

A7.5 Effect of Operating Pressure

A7.5.1 5 bar_g

This configuration is the benchmark case for the ADARPA aerator body investigations. The gas injection and flow regime maps are presented in §7.2.

A7.5.2 3 bar_g

Figure A7.19 is the gas injection regime map for 3 bar_g operating pressure, using aerator A5 (i.e. 16 x 0.75 mm aerator orifice in a liquid cross-flow) using a streamlined ADARPA aerator body. This shows the effect of varying the supply liquid mass flow rate up to 225 g/s, which corresponds to the discharge limit at 0% ALR with the discharge valve fully open and 3 bar_g operating pressure – this is reduced compared to the maximum flow of 290 g/s in the benchmark case. Consequently, the related maximum liquid Bakers number in the same 20 mm mixing chamber has also decreased to 717 kg/m²s, which compares to the maximum of 923 kg/m²s in the benchmark case. The gas supply was varied up to 5% ALR. Analysis of the gas injection map enabled identification of five discrete gas injection regimes, which were categorised into three gas injection regions.

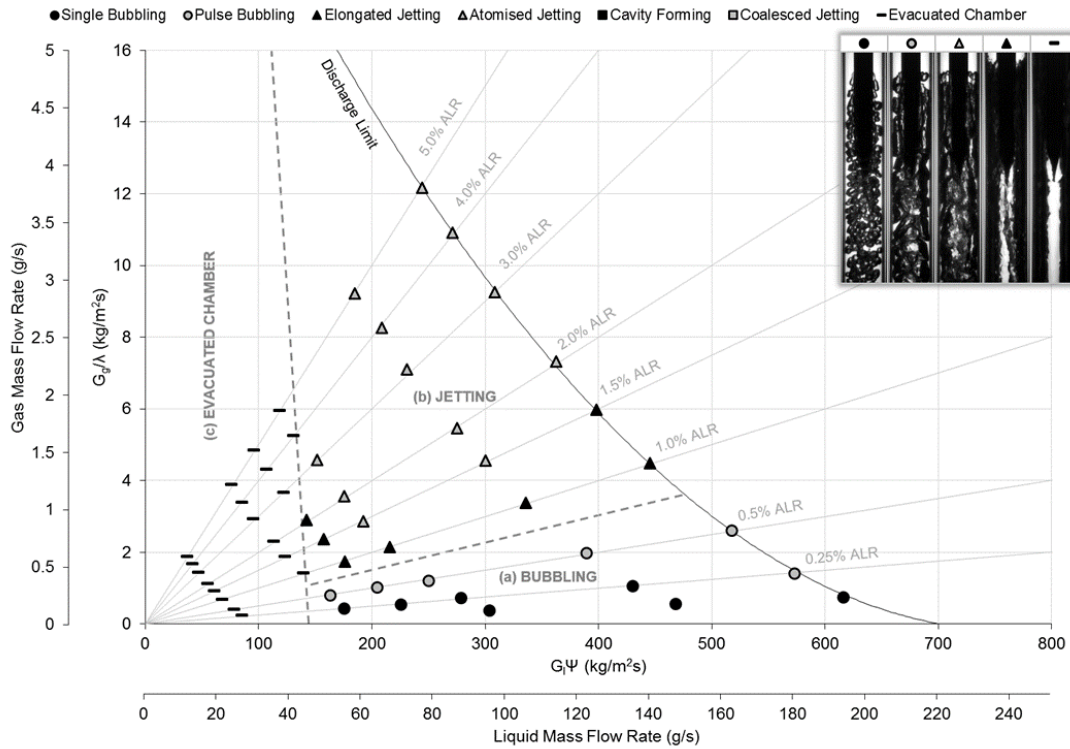


Figure A7.19 Gas injection regime map for 3 bar_g operating pressure.

A bubbling region was observed at low ALRs (Figure A7.19a), where single bubbling occurred at the lowest ALRs. The flow regime was observed to transition to jetting with increasing gas flow rate (Figure A7.19b), whereby elongated jetting precedes atomised jetting – this limit was observed to be marginally reduced with the decreased operating pressure, but was similar to the flat-end case (Figure A5.13). An evacuated chamber regime was observed at the lowest liquid flow rates (Figure A7.19c), at comparable liquid Bakers number to the comparison case (Figure 7.6) – this regime was observed to be marginally suppressed compared with increasing gas flow rate.

Figure A7.20 is the flow injection regime map for 3 bar_g operating pressure, which shows the effect of varying fluid flow rates on the flow regimes with areas of common regimes identified and marked. As with the gas injection map, the maximum liquid flow rate has reduced with the decreased operating pressure, which has resulted in a decreased maximum liquid Bakers number. The seven discrete flow regimes identified were grouped into six regions.

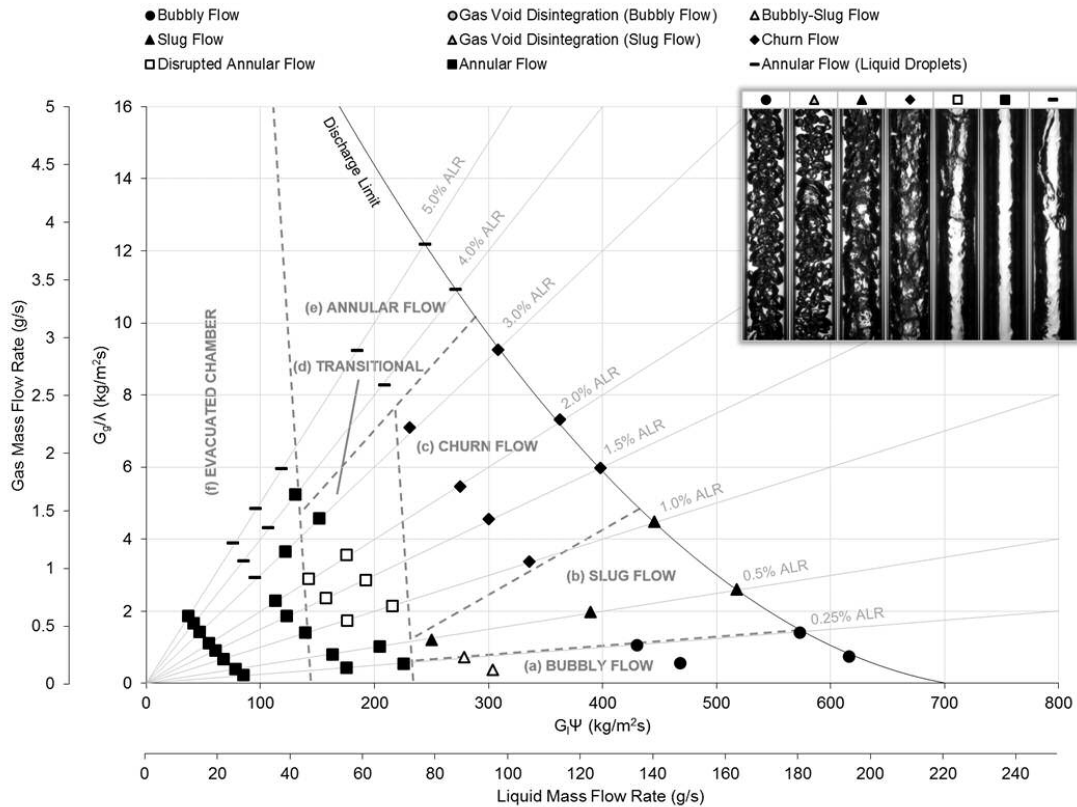


Figure A7.20 Flow regime map for 3 bar_g operating pressure.

A region of bubbly flow was observed at low ALRs (Figure A7.20a), which corresponded to single bubbling at the aerator and pulse bubbling at low ALRs. The general trend with increasing ALR was to transition flow to slug flow (Figure A7.20b), churn flow (Figure A7.20c) and finally annular flow (Figure A7.20e) – although the transitional limits were observed to be reduced compared to the higher operating pressure.

The effect of reducing liquid flow rate (i.e. exit orifice diameter) was observed to have a greater effect than with increased operating pressure. Bubbly-slug flow was observed at low liquid flow rates within the bubbly flow region, due to the injection of non-uniformly sized bubbles and, at the lowest ALR, aerator bluff body effects – this was observed to form a nucleation site within which bubbles could coalesce. A transitional region was formed at further reduced liquid flow rates (Figure A7.20d) whereby residence time within the mixing chamber increased and buoyancy played an increased role – at the lowest ALRs, this was observed to allow formation of a buoyant gas void just below the aerator orifices, and therefore an annular flow was formed despite bubbling at the aerator. At the lowest liquid flow rates, evacuated chamber was achieved, which formed a thin annular film (Figure

A7.20f) – this was observed at comparable liquid Bakers numbers to the comparisons case (Figure 7.7).

A7.5.3 1 bar_g

Figure A7.21 is the gas injection regime map for 1 bar_g operating pressure, using aerator A5 (i.e. 16 x 0.75 mm aerator orifice in a liquid cross-flow) using a streamlined ADARPA aerator body. This shows the effect of varying the supply liquid mass flow rate up 130 g/s, which corresponds to the discharge limit at 0% ALR with the discharge valve fully open and 1 bar_g operating pressure – this is reduced compared to the maximum flow of 290 g/s in the benchmark case. Consequently, the related maximum liquid Bakers number in the same 20 mm mixing chamber has also decreased to 413 kg/m²s, which compares to the maximum of 923 kg/m²s in the benchmark case. The gas supply was varied up to 5% ALR. Analysis of the gas injection map enabled identification of five discrete gas injection regimes, which were categorised into three gas injection regions.

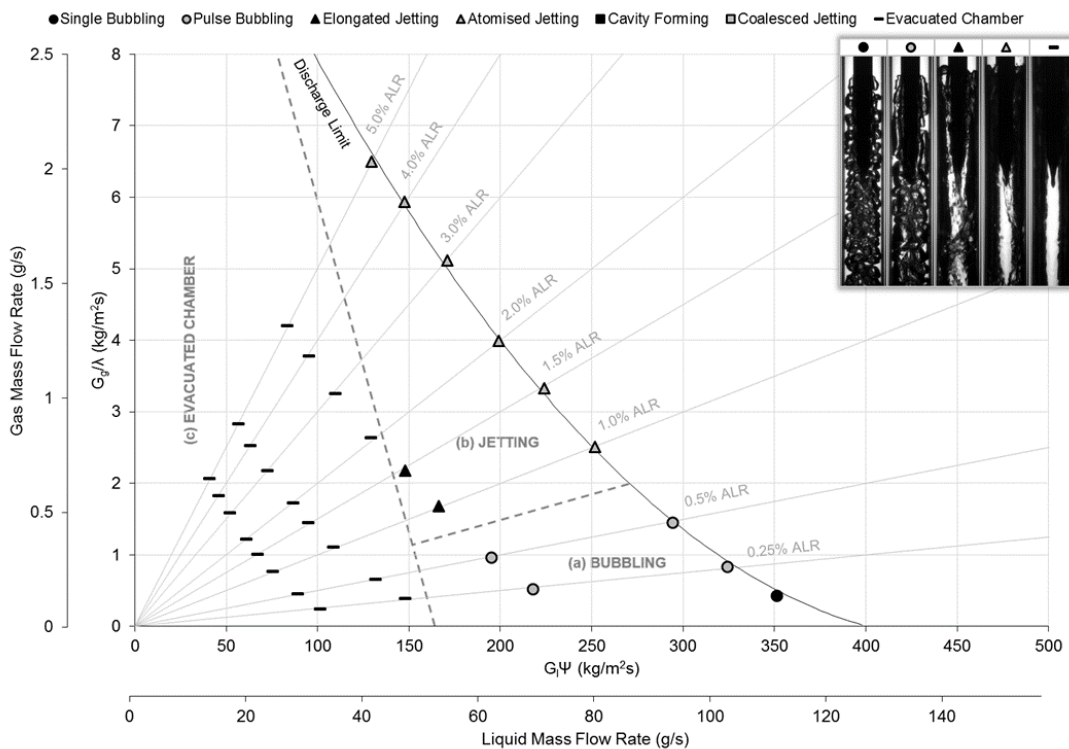


Figure A7.21 Gas injection regime map for 1 bar_g operating pressure.

The gas injection regime map was observed to be very similar to the flat-end equivalent case, with a small region of bubbling (Figure A7.21a) transitioning to jetting (Figure A7.21b) at increased ALRs – this transition was observed to occur at a reduced ALR than the 5 bar_g

benchmark case. An evacuated chamber region (Figure A7.21c) was identified at comparably low liquid flow rates to the benchmark case (Figure 7.6), which also appeared to be suppressed with increasing ALR. As the maximum flow rate is reduced with reducing pressure, the evacuated chamber was observed to occupy a greater proportion of the operating range.

Figure A7.22 is the flow injection regime map for 1 bar_g operating pressure, which shows the effect of varying fluid flow rates on the flow regimes with areas of common regimes identified and marked. As with the gas injection map, the maximum liquid flow rate has reduced with the decreased operating pressure, which has resulted in a decreased maximum liquid Bakkers number. The five discrete flow regimes identified were grouped into five regions.

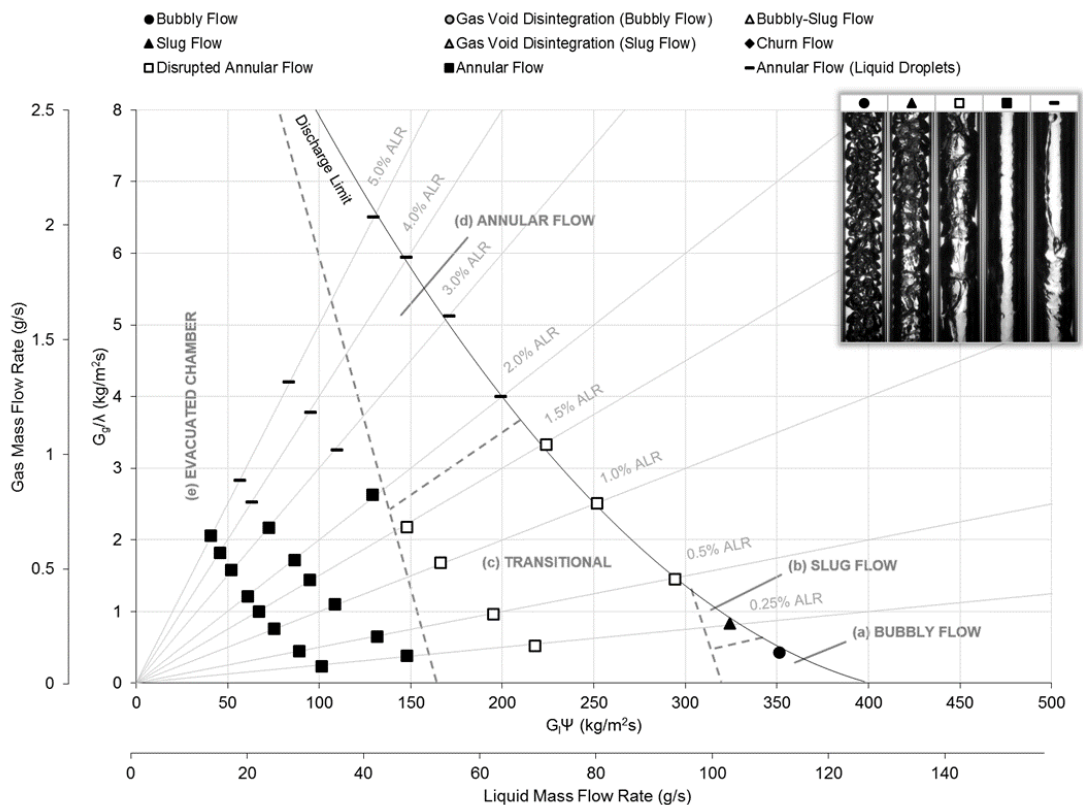


Figure A7.22 Gas injection regime map for 1 bar_g operating pressure.

An isolated occurrence of bubbly flow was identified at the greatest liquid flow and lowest ALR and, therefore, the bubbly flow region (Figure A7.22a) was significantly reduced compared to the 5 bar_g benchmark case (Figure 7.7). A single slug flow case was observed at an increased ALR (Figure A7.22b). Otherwise, the flow regime map was dominated by annular flow regimes: a disturbed annular flow (Figure A7.22c) was observed to transition to

annular flow at increased ALRs (Figure A7.22d), whereas a thin annular film was formed due to evacuated chamber at low liquid flow rates (Figure A7.22e) – this region was observed to be comparable to the comparison cases.

A7.6 Effect of Orientation

A7.6.1 Vertically Downwards

This configuration is the benchmark case for the ADARPA aerator body investigations. The gas injection and flow regime maps are presented in §7.2.

A7.6.2 Vertically Upwards

Figure A7.23 is the gas injection regime map for a vertically upwards atomiser orientation, using aerator A5 (i.e. 16 x 0.75 mm aerator orifice in a liquid cross-flow) with a streamlined ADARPA aerator body. This shows the effect of varying the supply liquid mass flow rate up to 290 g/s, which corresponds to the discharge limit at 0% ALR with the discharge valve fully open and 5 bar_g operating pressure, and relates to a maximum liquid Bakers number of 923 kg/m²s in the 20 mm mixing chamber. The gas supply was varied up to the maximum achievable flow rate for the given aerator design (7 bar_g maximum gas supply pressure) or, if possible, 5% ALR. Analysis of results enabled identification of four discrete gas injection regimes, which were categorised into two gas injection regions.

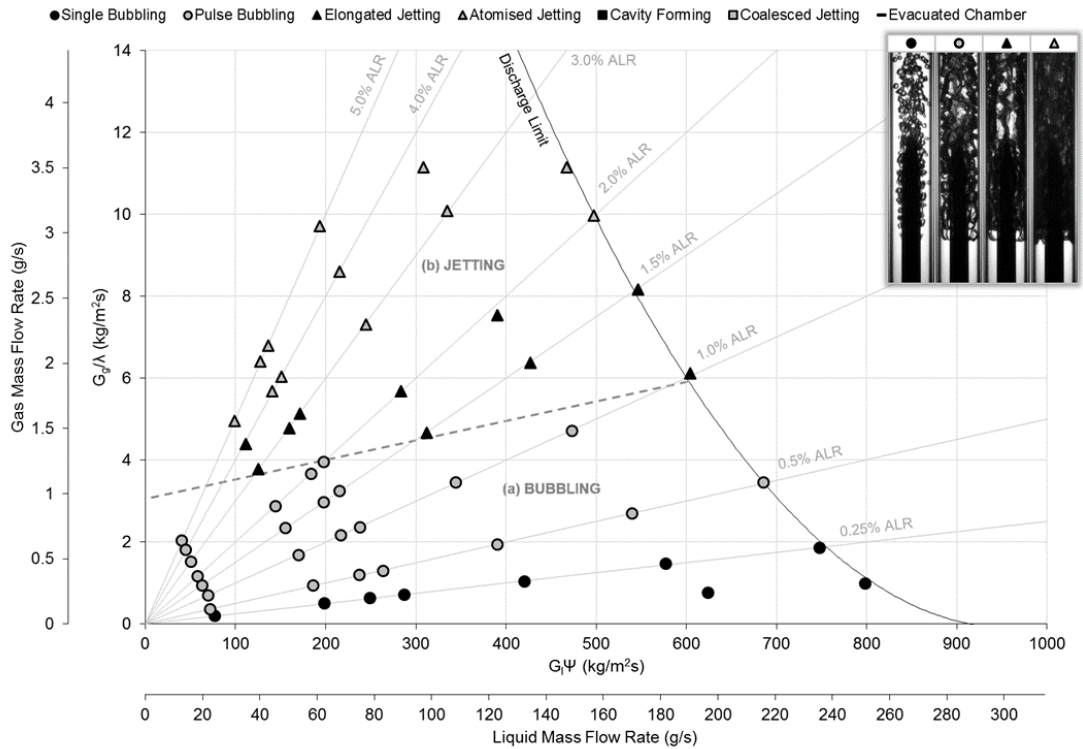


Figure A7.23 Gas injection regime map for vertically upwards orientation.

The gas injection regime map was seen to compare well with the equivalent flat-end aerator (Figure A5.17), which implies that the gas injection regimes are relatively unaffected by the aerator body design. The map features a larger bubbling region (Figure A7.23a) than the benchmark configuration (Figure 7.6) due to the assisted effects of buoyancy – this prevents an evacuated chamber region and also aids bubble detachment which delays transition to the jetting region (Figure A7.23b) at higher ALRs.

Figure A7.24 is the flow injection regime map for a vertically upwards orientation, with an ADARPA streamlined aerator body, which shows the effect of varying fluid flow rates on the flow regimes with areas of common regimes identified and marked. The three discrete flow regimes identified were grouped into three regions.

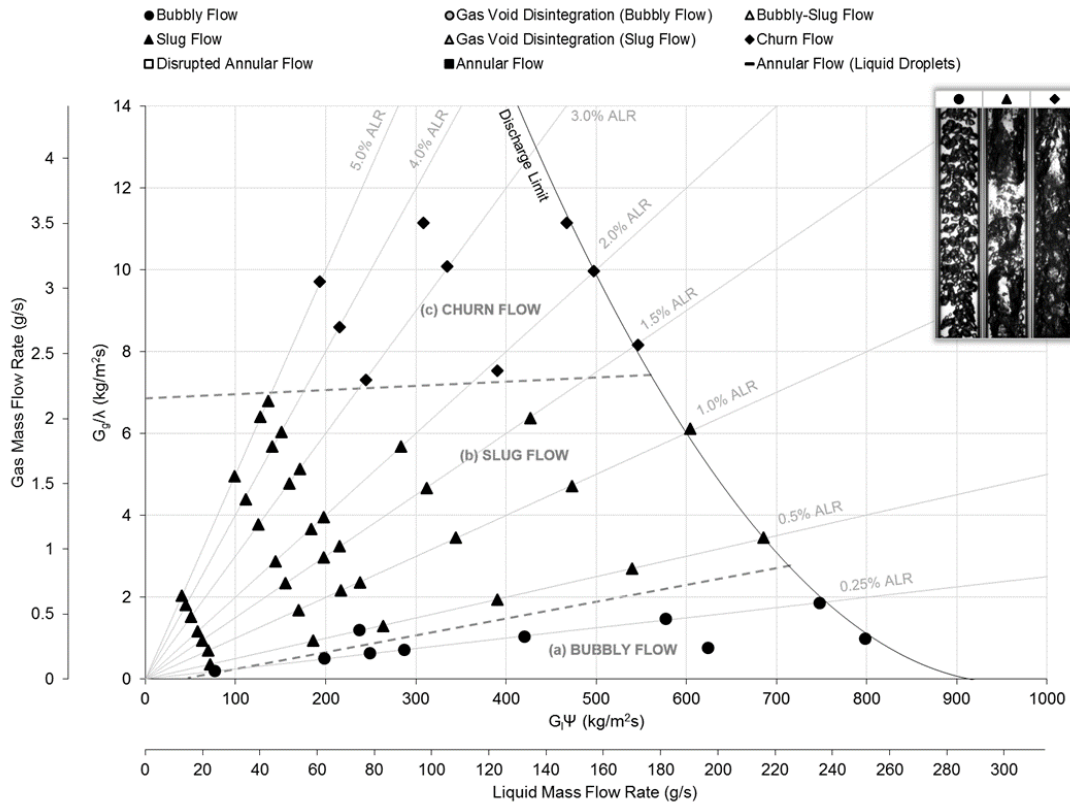


Figure A7.24 Flow injection regime map for vertically upwards orientation.

The flow regime map shows strong similarities to the flat-end case (Figure A5.18), which features a large bubbly flow region at low ALRs (Figure A7.24a). It has been shown throughout the results that the streamlined aerator tip acts to reduce the bluff-body effects of the aerator – in a vertically downwards orientation, this was seen to prevent formation of a gas void in the aerator wake, however in vertically upwards gas void formation was an issue with a flat end aerator and therefore the streamlined aerator had little effect.

A region of intermittent flow regimes were established at ALRs in excess of the bubbly region which, like the benchmark case (Figure 7.7), were observed to transition from slug flow (Figure A7.24b) to churn flow (Figure A7.24c) with increasing ALR. No instances of annular flow observed, which is hypothesised to occur because the gas-phase rises at a greater velocity than liquid which generates shear on the gas-liquid interface and promotes churn flow. In addition, evacuated chamber was prevented and hence annular flow due to this mechanism was prevented.